Transactions

Illinois of the U Library

ASME

Zero-Pressure Thermodynamic Properties of Some Monatomic Gases . . . . *J. A. Goff, Serge Gratch, and S. W. Van Voorhis* 725

Zero-Pressure Thermodynamic Properties of Carbon Monoxide and Nitrogen. . . . . . . *J. A. Goff and Serge Gratch* 741

The Thermodynamic Properties of Helium . . . . *S. W. Akin* 751

Some New Values of the Second Enthalpy Coefficient for Dry Air . . . . . . *J. R. Andersen* 759

New Measurements of the Heat Conductivity of Steam and Nitrogen . . . . *F. G. Keyes and D. J. Sandell, Jr.* 767

Compilation of Thermal Properties of Wind-Tunnel and Jet-Engine Gases at the National Bureau of Standards. . . . . *H. J. Hoge* 779

Pressure-Volume-Temperature Relationships of Gaseous Normal Hydrogen From Its Boiling Point to Room Temperature and From 0–200 Atmospheres . . . *H. L. Johnston and David White* 785

Heat Transfer to a Fluid Flowing Turbulently Between Parallel Walls With Asymmetric Wall Temperatures . . . . *R. A. Seban* 789

Heat-Transfer Rates in Centrifugal Compressors and the Effect of Internal Liquid Cooling on Performance . . . . *W. E. Trumpler, R. W. Frederick, and P. R. Trumpler* 797

The Hydrodynamic Lubrication of Cyclically Loaded Bearings . . . . *E. M. Simons* 805

The Mechanism of Lubrication Failure in High-Speed Ball Bearings . *F. C. Jones and D. F. Wilcock* 817

Turbulence in High-Speed Journal Bearings . . . . *D. F. Wilcock* 825

Closed-Cycle Gas Turbine . . . . *Curt Keller* 835

A Pyrometer for Measuring Total Temperature in Low-Density Gas Streams . . . . *Sidney Allen and J. R. Hamm* 851

Heat Transfer From an Air Jet to a Plane Plate With Entrainment of Water Vapor From the Environment . . . . *Max Jakob, R. L. Rose, and Maurice Spielman* 859

Pressure Drop and Convective Heat Transfer With Surface Boiling at High Heat Flux; Data for Aniline and n-Butyl Alcohol . . . . *Frank Kreith and Martin Summerfield* 869

Heat Transfer and Fluid Friction During Viscous Flow Across Banks of Tubes—III . . . . . *O. P. Bergelin, G. A. Brown, H. L. Hull, and F. W. Sullivan* 881

Experimental Evaluation of Human Shape Factors With Respect to Floor Areas . *F. W. Hutchinson* 889

AUGUST, 1950

VOL. 72, NO. 6

Transactions

of The American Society of Mechanical Engineers

Published on the tenth of every month, except March, June, September, and December

---

OFFICERS OF THE SOCIETY:

James D. Cunningham, *President*

Joseph L. Kopf, *Treasurer*   C. E. Davies, *Secretary*

COMMITTEE ON PUBLICATIONS:

Ronald B. Smith, *Chairman*

John Haydock   George R. Rich

C. B. Campbell   Paul T. Norton, Jr.

H. G. Wenig
D. R. Thomas } *Junior Advisory Members*

George A. Stetson, *Editor*   K. W. Clendinning, *Managing Editor*

REGIONAL ADVISORY BOARD OF THE PUBLICATIONS COMMITTEE

Kerr Atkinson—I
Otto de Lorenzi—II
W. E. Reaser—III
F. C. Smith—IV
Hendley Blackmon—V
R. E. Turner—VI
R. G. Roshong—VII
M. A. Durland—VIII

Published monthly by The American Society of Mechanical Engineers. Publication office at 20th and Northampton Streets, Easton, Pa. The editorial department is located at the headquarters of the Society, 29 West Thirty-Ninth Street, New York 18, N. Y. Cable address, "Dynamic," New York. Price $1.50 a copy, $12.00 a year for Transactions and the *Journal of Applied Mechanics;* to members and affiliates, $1.00 a copy, $6.00 a year. Changes of address must be received at Society headquarters three weeks before they are to be effective on the mailing list. Please send old as well as new address.... By-Law: The Society shall not be responsible for statements or opinions advanced in papers or . . . printed in its publications (B13, Par. 4).... Entered as second-class matter March 2, 1928, at the Post Office at Easton, Pa., under the Act of August 24, 1912.... Copyrighted, 1950, by The American Society of Mechanical Engineers. Reprints from this publication may be made on condition that full credit be given the Transactions of the ASME and the author and that date of publication be stated.

Zero-Pressure Thermodynamic Properties of Some Monatomic Gases

By J. A. GOFF,[1] SERGE GRATCH,[2] and S. W. VAN VOORHIS,[3] PHILADELPHIA, PA.

This paper presents definitive values of the zero-pressure thermodynamic properties of the stable naturally occurring isotopes and the normal isotopic mixtures of the following monatomic gases: Hydrogen (H), helium (He), carbon (C), nitrogen (N), oxygen (O), fluorine (F), sulphur (S), chlorine (Cl), argon (A), bromine (Br), iodine (I), mercury (Hg). These values cover the range 100 to 5000 deg R at the intervals indicated by the numbers in parentheses: 100(5)130(10)240(20)500(50)1000(100)2000(200)5000. They have been computed by the methods of quantum statistical mechanics from present best values of the relevant (a) general physical constants, (b) isotopic weights and fractional abundances, (c) spectroscopic data. Computational accuracy well beyond present physical accuracy has been maintained for practical reasons, final results being given to seven significant figures. Present physical accuracy is indicated by charts of estimated uncertainties. For some of the monatomic gases here considered, accurate values of their zero-pressure thermodynamic properties hitherto have been unavailable; for others the data presented are the first based upon recent spectroscopic and other input data to be made available at temperatures sufficiently close for convenient practical application.

INTRODUCTION

The engineer will readily recognize the need of accurate information regarding the thermodynamic properties of some of the monatomic gases considered in this paper. Monatomic hydrogen is formed in appreciable concentrations in the atomic-hydrogen welding flame; helium seems destined to play an important role in nuclear-engineering developments; welding techniques have been advanced significantly through the use of argon and helium which therefore must be produced in increasing quantities; mercury is one of the working substances of the modern mercury power plant.

The need for accurate information regarding the thermodynamic properties of other monatomic gases will be more and more strongly felt by the engineer as it becomes more and more necessary for him to take account of the limitations imposed by chemical equilibrium in combustion processes. In attempting to predict the composition of a gas mixture at chemical equilibrium, it is usual to assume no transmutation of atomic species. Under this assumption there are as many equations to be solved simultaneously, at a given pressure and temperature, as there are distinct atomic species. If the concentrations of the monatomic gases are used as unknowns, the equations for equilibrium take the same form regardless of the particular problem to which they are applied—only the terms to be included as making significant contributions to the pressure, volume, enthalpy, and entropy of the equilibrium mixture are different (1).[4] This suggests the importance of having suitable tables giving the thermodynamic properties of the monatomic gases for use in making chemical equilibrium calculations.

THEORY

The formulations on which modern tables giving the thermodynamic properties of gases are based rest firmly on the zero-pressure values of the product pv, of the enthalpy h, and of the reduced entropy $s + R\log_e p$ as calculated from spectroscopic data by the method of statistical mechanics; direct experimental measurements are used only to extend these values to higher pressures. The general principles of the method have been summarized by Herzberg (2, 3) who also has reviewed the present state of our knowledge of the spectroscopic data for various common gases. When this knowledge can be expressed by equations giving wave number E (cm^{-1}) as a function of certain quantum numbers which independently can take on all non-negative integral values within prescribed limits, the constants appearing in these equations are called "spectroscopic constants."

To each wave number E_i there is assigned a definite energy hcE_i, where h denotes Planck's constant, and c the velocity of light in vacuo. Both E_i and hcE_i are referred to alternatively as "energy levels." To each set of values of the various quantum numbers corresponds a distinct quantum state; but there may be more than one, say, p_i, distinct quantum states having the same energy hcE_i in the absence of an external electric or magnetic field. The first step in the calculations is to form the state sum or partition function Q, defined by

$$Q = \Sigma\, p_i\, e^{-hcE_i/kT} = \Sigma\, p_i\, e^{-c_2\tau E_i} \qquad \text{..........[1]}$$

where k is Boltzmann's constant, $c_2 = hc/k$ is the so-called second radiation constant, and τ denotes reciprocal absolute temperature T^{-1}. The summation is to extend over all accessible energy levels E_i. Values of the product pv, of the enthalpy h, and of the reduced entropy $s + R\log_e p$ are readily derivable from a knowledge of Q as a function of pressure p and temperature T.

In what follows it will be understood that the energy levels E_i are those that are strictly applicable only in the limiting case of "zero pressure" where the effects of intermolecular forces vanish. In some of the gases here considered, translation is the only mode of motion that contributes appreciably to the partition function Q up to 5000 deg R. As is well known, its contribution Q_{trans} is given by

$$Q_{\text{trans}}/nN_0 = [k(2\pi k/h^2N_0)^{3/2}]\,\frac{M^{3/2}T^{5/2}}{p} \qquad \text{.........[2]}$$

---

[1] Dean, Towne Scientific School and Director, University of Pennsylvania Thermodynamics Research Laboratory. Mem. ASME.

[2] Assistant Professor of Mechanical Engineering, Towne Scientific School, and Project Leader, University of Pennsylvania Thermodynamics Research Laboratory. Jun. ASME.

[3] Formerly Research Assistant, University of Pennsylvania Thermodynamics Research Laboratory; now with The Lummus Company, New York, N. Y.

Contributed by the Research Committee on Properties of Gases and Gas Mixtures, and the Heat Transfer and Applied Mechanics Divisions, and presented at the Annual Meeting, New York, N. Y., November 27–December 2, 1949, of The American Society of Mechanical Engineers.

Note: Statements and opinions advanced in papers are to be understood as individual expressions of their authors and not those of the Society. Paper No. 49—A-145.

[4] Numbers in parentheses refer to Bibliography at the end of the paper.

where n is the number of mols (on the chemical scale) of gas considered at absolute temperature T and absolute pressure p, and where M is the isotopic weight (also on the chemical scale) of the gas in question. The expression contains an additional general physical constant, namely, Avogadro's constant N_0. The quantity Q_{trans}/nN_0 must necessarily be dimensionless, which means that the right-hand member of Equation [2] may also contain one or more conversion factors, depending upon the units chosen for temperature T and pressure p.

At all accessible temperatures for any gas, the partition function Q splits into two independent factors, namely

$$Q = Q_{\text{trans}} \cdot Q_{\text{int}} \qquad [3]$$

where Q_{int} takes account of all internal energy levels. Possible contributions to Q_{int} from nuclear spin and other intranuclear levels will be excluded in accordance with usual practice because they are completely unaffected by ordinary chemical reactions not involving transmutation of atomic species. In the case of a monatomic gas the E_i contain only its electronic energy levels which, besides the second radiation constant $c_2 = hc/k$, are the only sources of uncertainty in the determination of its internal partition function Q_{int}.

The simplest procedure to follow in deriving the various thermodynamic properties of a gas from a knowledge of its partition function Q, as a function of pressure p and temperature T, is first to form its specific free enthalpy g, namely

$$g = -R\,T \log_e (Q/nN_0) \qquad [4]$$

where $R = kN_0$, except possibly for a conversion factor which may be regarded as exact by definition. Free enthalpy g is a characteristic function for the choice of pressure p and temperature T as independent variables; from it the volume v, the enthalpy h, and the entropy s can be derived by application of the following identical relations of thermodynamics: $v = \partial g/\partial p$, $h = \partial(\tau g)/\partial \tau$, and $s = -\partial g/\partial T$, respectively. It is clear therefore that no new constants subject to experimental error are introduced in the derivation.

1 CRITICAL EVALUATION OF INPUT DATA

General Physical Constants

In conformity with the practice of the authors' laboratory, the 1941 Birge (4) best values of the general physical constants have been used in all calculations of thermodynamic properties. While the present calculations were in progress, DuMond and Cohen (5) published a revision of some of the Birge values which they later (6) corrected for a slight error of their origin value of Planck's constant h. Fortunately, the DuMond-Cohen revisions as corrected leave all of the general physical constants here considered well within the Birge uncertainty limits. For this reason, and especially since DuMond and Cohen feel that experimental determinations currently under way in various laboratories will soon warrant a systematic re-evaluation of the data, we have decided to retain the Birge values for the time being. Table 1 shows a comparison of the 1941 Birge and the 1949 DuMond-Cohen values of the general physical constants involved in the present analysis.

As illustrated by the data in Table 1, DuMond and Cohen have been able substantially to diminish the estimated uncertainties of the best values of the general physical constants. It seems unlikely that these will be increased by the systematic re-evaluation of the data to be undertaken when experimental determinations currently under way in various laboratories will have been completed. Therefore we have decided to recalculate the uncertainties of our tabulated results in order to bring them more nearly into line with the DuMond-Cohen uncertainties of the general physical constants, at the same time retaining, however, the 1941 Birge best values.

TABLE 1 GENERAL PHYSICAL CONSTANTS

Constant	1941 Birge	1949 Dumond-Cohen
N_0 (1/gmol)	$(6.0228_3 \pm 0.0011)10^{23}$	$(6.0235 \pm 0.0004)10^{23}$
k (erg/°K)	$(1.38047_4 \pm 0.00026)10^{-16}$	$(1.38032 \pm 0.00011)10^{-16}$
c (cm/sec)	$(2.99776 \pm 0.00004)10^{10}$	$(2.99776 \pm 0.00004)10^{10}$
h (erg sec)	$(6.624_2 \pm 0.0024)10^{-27}$	$(6.6237 \pm 0.0011)10^{-27}$
c_2 (cm °K)	$1.4384_8 \pm 0.0003_4$	1.43853 ± 0.00019
R (erg/°K gmol)	$(8.31436 \pm 0.00038)10^7$	$(8.31436 \pm 0.00038)10^7$

NOTE: gmol denotes a unit of weight of M grams, where M is molecular weight on the "chemical" scale.

Isotopic Weights

As can be seen from Equations [3], [4], the correct expression for specific free enthalpy g contains the additive term $-(3/2)RT \log_e M$ where M denotes the isotopic weight of the gas in question. In engineering it is customary to express these weights as numbers on the so-called chemical scale on which the apparent molecular weight of the normal isotopic mixture of diatomic oxygen is arbitrarily assigned the value 32. In general, the most accurate determinations of isotopic weight are those based upon measurements of close doublet separations by means of modern linear-scale mass spectrographs of high resolution. The direct determinations are always expressed as numbers on the so-called "physical" scale on which the isotopic weight of monatomic oxygen O^{16} is arbitrarily assigned the value 16. A numeric on the physical scale bears a definite ratio to the corresponding numeric on the chemical scale, this ratio being a constant which has to be determined experimentally. Dumond and Cohen accept Birge's best value, namely

$$r = 1.000272 \pm 0.000005$$

as, of course, do we.

As mentioned previously, the most accurate determinations of isotopic weight are usually those made with the mass spectrograph. For the technically important monatomic gases here considered, except in the case of one or two of the less abundant isotopes, nuclear-reaction determinations serve only as checks. In the mass spectrograph a beam of molecular (or atomic) ions is focused on a photographic plate, the location of the point of focus depending on the ratio of the mass to the electric charge of the ion. Two different ions, having neighboring values of this ratio, form on the photographic plate a close doublet, the separation of which yields a determination of the mass difference between the two ions when proper account is taken of the fact that their electric charges can differ only by integral multiples of the unit electric charge. The very slight effects of ionization and compound formation per se are negligible and well beyond the ability of the mass spectrograph to detect.

In mass-spectrographic work, all masses are compared directly or indirectly with that of monatomic oxygen O^{16} which is taken to be exactly 16 by definition. The first step is a direct determination of the masses of monatomic hydrogen H^1, deuterium H^2, and carbon C^{12} to be used as substandards with which to compare the masses of other isotopes. Recent precision determinations of the masses of the isotopes of interest here have been carried out principally by Aston in 1936–1937, by Bainbridge and Jordan in 1936–1938, by Mattauch in 1936–1938, by Okuda, et al, in 1939–1941, and by Ewald in 1945–1946. In 1940–1941 Jordan reported preliminary results from a new mass spectrograph of greater resolving power and dispersion than were accessible to previous workers (7, 8).

The most recently published critical evaluations of existing data on isotopic masses are those of Livingston and Bethe (9) in 1937, of Birge (4) in 1941, of Flügge and Mattauch (10, 11) in 1942 and 1943, of Aston (12) in 1942, of Cohen and Hornyak (13) in 1947, and of Bainbridge (14) in 1948. These evaluations seem to justify retention of the 1941 Birge (4) best values of the isotopic masses, at any rate for H^1, H^2, He^4, C^{12}, C^{13}, N^{14}, N^{15}, O^{17}, O^{18}, I^{127}; at the same time they seem to allow substantial diminution of Birge's probable errors or uncertainties.

Another critical evaluation of existing data on isotopic masses not referred to in the foregoing, was published in Japanese by Okuda (15) in 1942. We have reason, however, to question the mass determinations of the Japanese workers (15, 16, 17, 18, 19, 20, 21, 22). For one thing, they claim less accuracy for some of their important determinations than do other workers, even though they used a mass spectrograph of higher resolving power. They made no check on the internal consistency of their ground-doublet separation determinations. Their values $(679.3 \pm 0.7)10^{-4}$ and $(693.0 \pm 2.3)10^{-4}$ for the mass-difference separations of the doublets $C_3^{12}H_4^1 — A^{40}$ and $C_3^{12}H_5^1 — H^1A^{40}$, respectively, are inconsistent. Their determinations of the masses of the two strongest nickel isotopes would assign to each an appreciably different packing fraction, which Aston (12) states " . . . is an unexpected result of great interest, if it is confirmed." Their values $(191.1 \pm 0.7)10^{-4}$, $(246.7 \pm 1.7)10^{-4}$, and $(421.7 \pm 0.9)10^{-4}$ for the mass-difference separations of the doublets $O_2^{16} — S^{32}$, $C_3^{12}H^1 — Cl^{35}$, and $C_3^{12}H^1 — Cl^{37}$, respectively, differ appreciably from those of Aston (12), namely, $(177 \pm 3.2)10^{-4}$, $(225 \pm 7)10^{-4}$, and $(412 \pm 7)10^{-4}$. Since we do have some question regarding the Japanese workers' determinations we feel obliged to disregard them and to disregard also the Flügge and Mattauch (10) values of the isotopic weights of S^{32}, S^{33}, S^{34}, S^{36}, Cl^{35}, Cl^{37} which have been based on these determinations. We will discuss in some detail the isotopic weight values that we have decided to accept for our present purposes.

Hydrogen. We accept the 1941 Birge values, namely

$$H^1 = 1.00813 \pm 0.000017$$
$$H^2 = 2.01473 \pm 0.000019$$

Helium. For He^3, Livingston and Bethe (9) have obtained the value 3.01707 ± 0.00012 from an analysis of the nuclear reaction $H^2(d,n)He^3$; Flügge and Mattauch (11) have obtained 3.016988 ± 0.000020 from an analysis of the nuclear reactions $H^2(d,n)He^3$ and $Li^6(p,\alpha)He^3$; Bainbridge (14) has obtained the value 3.017016 ± 0.000032 from an analysis of various nuclear-reaction and mass-spectrographic data. The last of these seems to us to be the best value available and we therefore accept it along with the 1941 Birge value of the He^4 mass; thus we accept

$$He^3 = 3.017016 \pm 0.000032$$
$$He^4 = 4.00389 \pm 0.00007$$

Carbon. We accept the 1941 Birge values, namely

$$C^{12} = 12.00386 \pm 0.00004$$
$$C^{13} = 13.00761 \pm 0.00015$$

Nitrogen. We accept the 1941 Birge values, namely

$$N^{14} = 14.00753 \pm 0.00005$$
$$N^{15} = 15.0049 \pm 0.0002$$

Oxygen. We accept the 1941 Birge values, namely

$$O^{17} = 17.0045$$

(no uncertainties given)

$$O^{18} = 18.0049$$

Fluorine. Aston (24) has obtained the value $(183.3 \pm 2.6)10^{-4}$ for the mass-difference separation of the doublet $O^{16}H^2H^1 — F^{19}$. Combined with mass values already accepted this gives

$$F^{19} = 19.00453 \pm 0.0003$$

which we regard as the best value presently available.

Sulphur. We accept Aston's value for S^{32}. Flügge and Mattauch (11) have determined the mass of S^{33} from an analysis of the nuclear reactions $S^{32}(d,p)S^{33}$ and $Cl^{35}(d,\alpha)S^{33}$ using the values of Okuda, et al (18), for S^{32} and Cl^{35}; we accept their value as the only one available at present, not bothering to correct it to strict consistency with our accepted values for S^{32} and Cl^{35} because the concentrations of S^{33} with which we have to deal are so very small. For S^{34} we accept the Livingston and Bethe (9) value, which happens to agree closely with that of Okuda and Ogata (16, 22), as corrected by Flügge and Mattauch (11). For S^{36} the best we can do is infer a value from Flügge and Mattauch's estimate of its packing fraction, namely, —6.5, since there are no mass-spectrographic or nuclear-reaction data to go on. Our accepted values are

$$S^{32} = 31.9823 \pm 0.0003$$
$$S^{33} = 32.98014 \pm 0.00040$$
$$S^{34} = 33.978 \pm 0.0020$$
$$S^{36} = 35.977 \pm 0.002$$

Chlorine. We accept Aston's (25, 33, 12) value for Cl^{35} which happens to be in good agreement with that of Okuda, et al (18), as corrected by Flügge and Mattauch (11), namely, 34.97884 ± 0.00019, with that of Livingston and Bethe (9) obtained from an analysis of the nuclear reaction $S^{32}(\alpha, p)Cl^{35}$, using Aston's value for S^{32}, namely, 34.9803 ± 0.00060, and especially with that of Gibert, Roggen, and Rossel (23), namely, 34.98054 (no uncertainty given). We also accept Aston's (25, 12) value for Cl^{37}, although it disagrees somewhat with that of Livingston and Bethe (9), namely, 36.9779 ± 0.0012, based upon his value for S^{32}; also with that of Okuda, et al (18), as corrected by Flügge and Mattauch (11), namely, 36.97769 ± 0.00010. Our accepted values for chlorine are

$$Cl^{35} = 34.9808 \pm 0.0007$$
$$Cl^{37} = 36.9785 \pm 0.0008$$

Argon. We accept Aston's (26, 12) value for A^{36} as determined from the mass-difference separations of the doublets $\frac{1}{2}A^{36} — O^{16}H_2^1$ and $A^{36} — C_3^{12}$ which happens to agree with that of Flügge and Mattauch (11) obtained in roundabout manner from nuclear-reaction data, namely, 35.97790 ± 0.00040. We accept Flügge and Mattauch's value for A^{38} which agrees well with that of Livingston and Bethe (9), namely, 37.974 ± 0.0025, but is based on more recent data. Following Aston (12), we accept Mattauch's 1938 value for A^{40} (27), even though the latter subsequently has revised his substandards somewhat (28) so that, strictly speaking, the 1938 value should be revised correspondingly, except that the original substandards were in closer agreement with the Birge values already accepted. Our accepted values for argon are

$$A^{36} = 35.9780 \pm 0.0010$$
$$A^{38} = 37.97461 \pm 0.00030$$
$$A^{40} = 39.97564 \pm 0.00015$$

Bromine. We accept Aston's (29, 30) values for Br^{79} and Br^{81} as the only ones presently available. His determinations were based upon the observed mass-difference separation of the doublet $\frac{1}{3}Br^{79} — \frac{1}{5}Xe^{132}$ and on the assumption of equal packing fractions for Br^{81} and Br^{79}. He had previously determined provisionally the mass value of Xe^{132} (31) from an unsatisfactory overlapping doublet and from comparison with the mass value of Xe^{129}. In 1942 he (12) brought his value up to date by correcting it for changes in his substandards. Our accepted values for bromine are

$$Br^{79} = 78.9415 \pm 0.0020$$
$$Br^{81} = 80.9401 \pm 0.0020$$

Iodine. Aston (32) reported in 1927 that he had found I^{127} to have the same packing fraction as Xe^{132}, namely, —4.1. This is the only mass-spectrographic evidence regarding the mass of I^{127}. Accepting his provisional value for Xe^{132} (31), a value of 126.948 would be computed for I^{127}. Birge (4) derives the value 126.915 ± 0.004 (on the chemical scale) from available chemical-reaction data; it is directly applicable to I^{127}, the only stable isotope of iodine. Mainly for the sake of consistency but also because Aston's value seems somewhat doubtful, we accept the Birge value, namely

$$I^{127} = 126.915 \pm 0.004 \text{ (chemical scale)}$$

Mercury. Published data on the masses of the mercury isotopes are meager and lacking in precision. In 1937 Aston (33) gave a provisional value of +1.4 for the packing fraction of Hg^{200}, based upon a somewhat doubtful comparison with the fundamental substandards through Xe^{132} and Xe^{129}; subsequently, he revised this value to +1.7 to accord with revisions in the substandards themselves (12). In his 1927 report, Aston (32) states that the mass intervals of the mercury isotopes can hardly be distinguished from unity. If we accept this statement and assume the same packing fraction +1.7 for all the isotopes, and if we accept the data on fractional abundances given in the "Fifth Report of the Committee on Atoms of the International Union of Chemistry," 1940 (34), we obtain the value 200.59 (on the chemical scale) for ordinary mercury which compares well with the value 200.61 given in the "Thirteenth Report on Atomic Weights of the International Union of Chemistry" (35), based on chemical-reaction data. While this favorable comparison is not convincing evidence of the accuracy of the mass-spectrographic determinations, still the Aston mass (12) values suffice for our purposes because larger errors can be tolerated in the case of mercury. We have used the following values:

$Hg^{196} = 196.033 \pm 0.02$
$Hg^{198} = 198.034 \pm 0.02$
$Hg^{199} = 199.034 \pm 0.02$
$Hg^{200} = 200.034 \pm 0.006$
$Hg^{201} = 201.034 \pm 0.02$
$Hg^{202} = 202.034 \pm 0.02$
$Hg^{204} = 204.035 \pm 0.02$

We conclude our discussion of isotopic weights by listing in Table 2 some recent values by Cohen and Hornyak (13), Bainbridge (14), and Ewald (36, 37) for some of the lighter elements. Undoubtedly, these are more precise than the ones we have accepted as just noted, but we have not attempted to use them because it would hardly be feasible for us to do so in a thoroughly consistent way.

Isotope Abundances

Ordinary oxygen, for example, is a mixture of the six different isotopic molecules that can be formed from the isotopes O^{16}, O^{17}, O^{18}. The atom fractions, or fractional abundances, of these isotopes in the mixture have been determined to be 0.99763, 0.00040, 0.00197, respectively. Using the isotopic weights previously adopted, namely, 16, 17.0045, 18.0049, respectively, we readily compute the value 32.00970 for the apparent molecular weight of ordinary oxygen on the physical scale. Its apparent molecular weight on the chemical scale is exactly 32 by definition, whence the value 1.000272 for the ratio between corresponding values on the two scales.

We require information regarding the isotope abundances of other normal isotopic mixtures. Existing data have been reviewed critically and evaluated by Livingston and Bethe (9) in 1937, by the Committee on Atoms of the International Union of Chemistry (34) in 1940, by Birge (4) in 1941, by Aston (12) in 1942, by Flügge and Mattauch (11) in 1943, and by Seaborg and Perlman (38) in 1948. We accept the 1941 Birge values for hydrogen, carbon, nitrogen, and oxygen. In this connection it may be well to mention that the isotope abundances of ordinary oxygen have been investigated recently by Thode and Smith (39) and by Urey (40), who have detected significant variations among samples obtained from various sources. For helium we accept the values of Aldrich and Nier (41, 42) applicable to well (natural-gas) helium. For fluorine, sulphur, chlorine, argon, iodine, and mercury, we accept the "Fifth Report of the Committee on Atoms of the International Union of Chemistry" (34) values with uncertainties estimated from the Seaborg and Perlman (38) data, and with Nier's (43) value of the fractional abundance of S^{36} in ordinary sulphur. The isotope abundances of argon have been investigated recently by Dibeler, Mohler, and Reese (44), whose results agree fairly well with those of Nier (45), which in turn do not dispute the values accepted here within the accuracy given. The isotope abundances of bromine have been investigated recently by Williams and Yuster (46) and by White and Cameron (47) with almost identical results; we accept those of the latter investigators because of their somewhat smaller uncertainties.

We conclude this brief discussion of isotope abundances by listing in Table 3 the values we have decided to accept for our present purposes.

TABLE 3 FRACTIONAL ABUNDANCES ACCEPTED FOR USE HERE

H^1	0.9998551	± 0.0000022	Cl^{35}	0.754	± 0.0018
H^2	0.0001449	± 0.0000022	Cl^{37}	0.246	± 0.0018
He^3	0.00000016	± 0.00000004	A^{36}	0.0031	± 0.000038
He^4	0.99999984	± 0.00000004	A^{38}	0.0006	± 0.000016
			A^{40}	0.9963	± 0.000054
C^{12}	0.98925	± 0.00024			
C^{13}	0.01075	± 0.00024	Br^{79}	0.5051	± 0.0006
			Br^{81}	0.4949	± 0.0006
N^{14}	0.99631	± 0.00008			
N^{15}	0.00369	± 0.00008	I^{127}	1.0000	
O^{16}	0.99762_6	± 0.00007	Hg^{196}	0.0015	± 0.000055
O^{17}	0.00040_2	± 0.00003	Hg^{198}	0.1011	± 0.0016
O^{18}	0.00197_2	± 0.00004	Hg^{199}	0.1703	± 0.0024
			Hg^{200}	0.2326	± 0.0029
F^{19}	1.00000		Hg^{201}	0.1317	± 0.0019
			Hg^{202}	0.2956	± 0.0021
S^{32}	0.951	± 0.0010	Hg^{204}	0.0672	± 0.0011
S^{33}	0.0074	± 0.00016			
S^{34}	0.042	± 0.0008			
S^{36}	0.00016	± 0.000016			

Spectroscopic Data

If in the expression $Q = \Sigma p_i e^{-c_2\tau E_i}$ we replace the E_i with the differences $E_i - E_0$, where E_0 is a constant for the gas in question, we merely augment Q by the factor $e^{c_2\tau E_0}$, diminish the free enthalpy g and the enthalpy h by a constant amount N_0hcE_0, but leave the entropy s unaltered. Furthermore, if for the mon-

TABLE 2 SOME NEWER VALUES OF ISOTOPIC WEIGHT

Isotope	Cohen-Hornyak	Bainbridge	Ewald
H^1	1.008128 ± 0.000003	1.0081283 ± 0.0000028	
H^2	2.014718 ± 0.000005	2.0147186 ± 0.0000055	
He^3		3.017016 ± 0.000032	
He^4		4.003880 ± 0.000032	
C^{12}	12.003847 ± 0.000016	12.003856 ± 0.000019	
C^{13}			13.007581 ± 0.000025
N^{14}	14.007539 ± 0.000015	14.007536 ± 0.000022	
N^{15}			15.004949 ± 0.000030

atomic gases here considered E_0 is understood to denote the energy of the ground electronic state so that $E_i > E_0$ for all other electronic levels, then N_0hcE_0 may be identified as the amount contributed by the electronic levels to the null-point ($T = 0$, $p = 0$) energy $\bar{u}$ of the gas in question. We have ascertained by preliminary calculations that for all gases considered here, separations $E_i - E_0$ exceeding 50,000 reciprocal centimeters (cm^{-1}) cannot affect our final results and therefore may be disregarded. In the case of hydrogen, for example, the next to the lowest electronic energy level lies some 82,000 cm^{-1} above the ground level so that we may, within the accuracy of our final results, take $Q_{\text{int}} = p_0e^{-c_2\tau E_0}$, where p_0 is the statistical weight of the ground level. It is well known that $p_0 = 2$ (exactly) for hydrogen, and we absorb the constant E_0 in the null-point energy $\bar{u}$; hence no detailed discussion of the spectroscopic data for hydrogen is necessary for our purposes.

Regarding the spectroscopic data for the other gases considered here, no general statement can be made at present. Among several excellent reviews of existing data are those of Bacher and Goudsmit (48) in 1932, of Robinson and Shortley (49) in 1937, of Shenstone (50) in 1938, of Moore (51) in 1945, of Meggers (52) in 1946, and of Moore (53) in 1948. These reviews serve as excellent guides to the literature, the first and last of them providing extremely useful tables of energy levels also. We proceed on the basis of this and other information separately to discuss each atom considered here.

Hydrogen. The ground state is a $1s:{}^2S_{1/2}$ state (48) with $p_0 = 2$, the next higher level lying some 82,000 cm^{-1} above it.

Helium. The ground state is a $1s^2:{}^1S_0$ state (48) with $p_0 = 1$, the next higher level lying some 160,000 cm^{-1} above it.

Carbon. The ground state is a $1s^22s^22p^2:{}^3P_0$ state (48) with $p_0 = 1$. The only low-lying levels are the $2s^22p^2:{}^3P,{}^1D,{}^1S$ and the $2s2p^3:{}^5S$ states, the next higher level having been rather definitely established as lying some 60,000 cm^{-1} above the ground level (54). Until recently the location of the ^5S state was in doubt, but Shenstone (55) has now obtained direct experimental evidence placing it at 33,735.2 ± 0.1 cm^{-1} above the ground state; he has also confirmed the findings of Chulanovskiĭ and Mokhnatkin (56) regarding the locations of the $^3P_1$ and the $^3P_2$ states. Edlén (54) has confirmed the values of Bacher and Goudsmit (48) for the locations of the $^1D_2$ and the $^1S_0$ states. We have based our calculations for carbon on the following data: 1(0.0); 3(16.56 ± 0.1); 5(43.47 ± 0.1); 5(10192 ± 1); 1(21647 ± 1); 5(33735.2 ± 0.1); 1(60331.3). The number before the parentheses is the statistical weight p_i of the level whose separation $E_i - E_0$ from the ground level is given within the parentheses in reciprocal centimeters (cm^{-1}).

Nitrogen. The ground state is a $1s^22s^22p^3:{}^4S^0{}_{3/2}$ state (48) with $p_0 = 4$. The only low-lying levels are the $2s^22p^3:{}^2D^0,{}^2P^0$ states, the next higher level lying some 83,000 cm^{-1} above the ground level. The most reliable data on the arc spectrum of nitrogen appear to be those of Ekefors (57), who was the first to detect the predicted splitting of the $^2D^0$ levels. Others (58, 59, 60) have confirmed his results (on the splitting of the $^2D^0$ levels) and, in addition, have confirmed the prediction that the splitting of the $^2P^0$ levels is quite small; it is of no interest to us here because it does not improve the accuracy of Ekefors' data. A brief analysis of the recent work of Kamiyama and others (61, 62, 63) suggests that their apparatus was incapable of resolving the $^2D^0$ levels and that, therefore, a detailed analysis would be unlikely to locate the low-lying levels more accurately than do the data of Ekefors. We have based our calculations for nitrogen upon the following data: 4(0.0); 6(19223 ± 2); 4(19231 ± 2); 6(28840 ± 2); 2(83285.5).

Oxygen. The ground state is a $1s^22s^22p^4:{}^3P_2$ state (48) with $p_0 = 5$. The only low-lying levels are the $2s^22p^4:{}^3P_1,{}^3P_0,{}^1D_2,{}^1D_0$ states, the next higher level lying some 74,000 cm^{-1} above the ground level. The latest and most reliable data on the arc spectrum of oxygen have been given by Edlén (64) in an excellent review article. We accept his values for the low-lying levels, assigning approximate uncertainties which we feel sure are of the right order of magnitude. Thus we have based our calculations for oxygen upon the following data: 5(0.0); 3(158.5 ± 0.1); 1(226.5 ± 0.1); 5(15867.7 ± 0.1); 1(33792.4 ± 0.2); 5(73767.8).

Fluorine. The ground state is a $1s^22s^22p^5:{}^2P_{3/2}{}^0$ state (48), with $p_0 = 4$. The only low-lying level is the $2s^22p^5:{}^2P_{1/2}{}^0$ state, the next higher lying some 102,000 cm^{-1} above the ground level. The most recent and probably the best data on the ultraviolet-arc spectrum of fluorine are those of Edlén (65) which we accept. It may be well to mention, however, that Edlén has redetermined the separation of the $2p^5:{}^2P^0{}_{3/2,\,1/2}$ levels to be 404.0 cm^{-1}, which differs slightly from Bacher and Goudsmit's (48) value of 407.0 cm^{-1}, obtained from Dingle's (66) evaluation of Bowen's (67) data. The very recent data of Lidén (68) are not concerned with the low-lying levels. We have based our calculations for fluorine on the following data: 4(0.0); 2(404.0 ± 0.5); 6(102406.50).

Sulphur. The ground level is a $1s^22s^22p^63s^23p^4:{}^3P_2$ state (48) with $p_0 = 5$. The only low-lying levels are the $3s^23p^4:{}^3P,{}^1D,{}^1S$ and the $3s^23p^34s:{}^5S_2{}^0$ levels, the next higher lying some 72,000 cm^{-1} above the ground level. Bacher and Goudsmit (48) give values for the $3p^4:{}^3P_{0,1,2}$ and the $3p^3({}^4S)4s:{}^5S_2{}^0$ levels based on the data of Hopfield (69), of Bungartz (70), and of Hopfield and Dieke (71). More recent investigations are those of Frerichs (72), of Meissner, Bartelt, and Eckstein (73), and of Ruedy (74, 75). In 1936, Bowen (76) revised Ruedy's (75) value of the $^1S_0$ level in order to align the p^4 configurations better with those of other similar atoms. Robinson and Shortley (49) disagree with this revision, but Edlén (77) has adduced rather convincing evidence in favor of it. We have decided to accept Ruedy's values as revised by Bowen, because they appear to be the most accurate direct determinations of the low-lying levels, and especially because they have been carefully checked by Edlén. We have based our calculations for sulphur upon the following data, the uncertainties given being only approximate: 5(0.0); 3(397.2 ± 1); 1(574.7 ± 0.5); 5(9239.8 ± 0.5); 1(22182.2 ± 1); 5(52623.8).

Chlorine. The ground state is a $1s^22s^22p^63s^23p^5:{}^2P_{3/2}{}^0$ state (48) with $p_0 = 4$. The only low-lying level is the $3s^23p^5:{}^2P_{1/2}{}^0$ level, the next higher lying some 72,000 cm^{-1} above the ground level. The latest reported work on chlorine is that of Kiess (78) which, however, does not evaluate the $^2P_{1/2}{}^0$ term; for this we must rely on Turner (79) even though his data are not as accurate as might be wished. We have based our calculations for chlorine upon the following data, the uncertainty given being only approximate: 4(0.0); 2(881 ± 3); 6(71954.00).

Argon. The ground state is a $1s^22s^22p^63s^23p^6:{}^1S_0$ state (48) with $p_0 = 1$. The next higher level almost certainly lies some 93,000 cm^{-1} above the ground level, such large separations being characteristic of the inert gases as remarked by Herzberg (80).

Bromine. The ground state is a $1s^22s^22p^63s^23p^63d^{10}4s^24p^5:{}^2P_{3/2}{}^0$ state (48) with $p_0 = 4$. The only low-lying level is the $4s^24p^5:{}^2P_{1/2}{}^0$ level, the next higher lying some 63,000 cm^{-1} above the ground level. The latest reported work on bromine is that of Kiess and de Bruin (81) which, however, does not evaluate the $^2P_{1/2}$ term; for this we must rely upon Turner (79). We have based our calculations for bromine upon the following data, the uncertainty given being only approximate: 4(0.0); 2(3685 ± 3); 6(63000).

Iodine. The ground state is a $1s^22s^22p^63s^23p^63d^{10}4s^24p^64d^{10}5s^25p^5:{}^2P_{3/2}{}^0$ state (82) with $p_0 = 4$. The only low-lying level is the $5s^25p^5:{}^2P_{1/2}{}^0$ level, the next higher lying some 54,000 cm^{-1} above the ground level according to what evidence is available.

The most recent and probably the best data on the arc spectrum of iodine are those of Murakawa (82) which are supported by the earlier work of Turner (79), of Evans (83), of McLeod (84), and of Hellerman (85). We have based our calculations for iodine on the following data, the uncertainty given being only approximate: 4(0.0); 2(7602.7 ± 1); 6(54630.0).

Mercury. The ground state is a $1s^2 2s^2 2p^6 3s^2 3p^6 3d^{10} 4s^2 4p^6 4d^{10}$-$4f^{14} 5s^2 5p^6 5d^{10} 6s^2 : {}^1S_0$ state (48) with $p_0 = 1$. The only low-lying levels are the $6s6p : {}^3P_{0,1,2}{}^0$ levels, the next higher lying some 54,000 cm^{-1} above the ground level. These low-lying levels have been very accurately located by Fukuda (86), by Stiles (87), and by Foote, et al (88), respectively, whose data we accept. Thus, we have based our calculations for mercury on the following data: 1(0.0); 1(37641.97 ± 0.7); 3(39412.25 ± 0.3); 5(44039.21 ± 2); 3(54065.7).

2 WORKING TABLES WITH ESTIMATED UNCERTAINTIES

Calculation of Thermodynamic Properties

From previous statements in this paper, it is clear that specific free enthalpy g is given by the expression

$$e^{-g/RT} = [k(2\pi k/h^2 N_0)^{3/2}]e^{-c_2\tau E_0} \Sigma p_i e^{-c_2\tau(E_i - E_0)} \frac{M^{3/2}T^{5/2}}{p} \quad \text{..[5]}$$

We replace the factor $e^{-c_2\tau E_0}$ with unity, knowing that we thereby merely diminish the free enthalpy g and the enthalpy h by the constant amount $N_0 hcE_0$, which we absorb in the null-point ($T = 0$, $p = 0$) energy $\bar{u}$, without affecting the entropy s. We introduce the so-called characteristic temperatures

$$\theta_i = c_2(E_i - E_0) \quad \text{..................[6]}$$

and define the dimensionless temperature functions

$$\begin{aligned} \alpha &= \Sigma p_i e^{-\theta_i \tau} \\ \beta &= \Sigma p_i(\theta_i \tau)e^{-\theta_i \tau} \quad \text{..................[7]} \\ \gamma &= \Sigma p_i(\theta_i \tau)^2 e^{-\theta_i \tau} \end{aligned}$$

Finally, using the 1941 Birge (4) values of the general physical constants, together with the conversion factors 1.8 °R/°K and 1,013,246 dyne/cm² atm, we derive

$$\log_e p - (g - \bar{u})/RT = -5.13397_5 + \frac{3}{2}\log_e M + \frac{5}{2}\log_e T + \log_e \alpha \quad \text{..........[8]}$$

in which pressure p is to be expressed in international atmospheres (atm) and temperature T in degrees Rankine (°R). In Equation [8] it is understood that M denotes isotopic weight on the chemical scale.

As mentioned previously, free enthalpy g is one of the characteristic functions of thermodynamics when expressed in terms of temperature T and pressure p as independent variables. Applying to Equation [8] the identical relations $v = \partial g/\partial p$, $s = -\partial g/\partial T$, $h = \partial(g\tau)/\partial\tau$, and the definition $c_p = \partial h/\partial T$, we easily derive

$$\left.\begin{aligned} (pv)_{p=0} &= RT \\ [s/R + \log_e p]_{p=0} &= -2.63397_5 + \frac{3}{2}\log_e M + \frac{5}{2}\log_e T \\ &\quad + \log_e \alpha + \beta/\alpha \\ [(h - \bar{u})/RT]_{p=0} &= 5/2 + \beta/\alpha \\ [c_p/R]_{p=0} &= 5/2 + \gamma/\alpha - (\beta/\alpha)^2 \end{aligned}\right\} \text{..[9]}$$

In each of Equations [9] the subscript $p = 0$ has been affixed to the left-hand member in order to emphasize that the expression is valid only in the absence of intermolecular forces, that is to say, it is valid only in the limiting case of zero pressure. The first contains the theory of the practical realization of absolute temperature, T. The quantity in brackets on the left of the second expression is what we call "reduced entropy," $s + R \log_e p$ divided by the gas constant R. The third is an expression for "mean isobaric specific heat" $(h - \bar{u})/T$ except that, strictly speaking, the null-point energy $\bar{u}$ should be replaced by the null-point enthalpy $\bar{h}$ which exceeds $\bar{u}$ by a finite, though for our purposes, negligibly small amount. The fourth is an expression for the "instantaneous isobaric specific heat," c_p. The fact that none of Equations [9] is valid at extremely low temperatures, say, below 0.01 °R does not concern us here.

To illustrate the use of Equations [9], we shall apply them to the case of monatomic hydrogen H^1 at 1000 °R. For H^1: $M = 1.00813/1.000272$; $p_0 = 2$; $\theta_0 = 0$; all other θ_i being negligibly high at the temperature in question, $\alpha = 2$ and $\beta = \gamma = 0$. We readily compute: $3/2 \log_e M = 0.01173_8$; $5/2 \log_e T = 17.26938_8$; $\log_e \alpha = 0.69314_7$. Accordingly, for the limiting case of zero pressure

$$\begin{aligned} s/R + \log_e p &= 15.34029_8 \\ (h - \bar{u})/RT &= 2.5 \\ c_p/R &= 2.5 \end{aligned}$$

Unit of Energy

There has been much discussion of late on the bothersome question of the calorie, which discussion Keenan (89) has summarized in a memorandum to members of the ASME Special Research Committee on Properties of Gases and Gas Mixtures. Prior to 1929, a large number of different kinds of calorie were in use, the circumstances surrounding the development of thermodynamics being intolerably confused thereby. At the First International Steam Tables Conference held in London, England, in 1929, the question of removing this confusion was discussed at length, and it was unanimously decided to adopt and promote the use of a single calorie, to be called the International Table calorie (IT cal), defined as 1/860 (mean) international watthour. This was the first unit of its kind to have international sanction. The conference which defined it included among its members: Prof. H. L. Callendar, the acknowledged British expert on the properties of steam; several representatives of the German Physikalisch-Technische Reichsanstalt; delegates from Czechoslovakia; and an American delegation including Dr. N. S. Osborne and Dr. H. C. Dickinson, both of the U. S. Bureau of Standards. In all subsequent publications dealing with the thermodynamic properties of steam, from virtually all sources throughout the world, including the U. S. Bureau of Standards, either the International Table calorie or the international electrical unit in terms of which it was defined, was used.

Unfortunately, the efforts of the First International Steam Tables Conference to promote the use of a single calorie have not been entirely successful. In 1930 Dr. E. W. Washburn of the U. S. Bureau of Standards proposed to the Commission on Thermochemistry of the International Union of Chemistry that the Commission agree to use a different calorie defined as 4.1833 international joules in order to preserve as many as possible of the numerical values given in International Critical Tables (90) in terms of a calorie defined as 4.185 absolute joules. This so-called artificial or thermochemical calorie (4.1833 international joules) was officially adopted by the Commission in 1934, and since has become firmly established. Thus, and mainly through lack of foresight, there has been erected an artificial barrier between the engineer on the one side and the thermochemist on the other. The two calories differ by as much as 1 part in approximately 1500.

Recently steps have been taken to abandon by international agreement the so-called international electrical units and to use instead the absolute or mechanical units. The 1941 Birge (4) value for the ratio between the two units is $1.00020 \pm 0.00004_5$ abs kwhr/(mean) int kwhr. DuMond and Cohen (91, 92) adopt the conversion factor 1.000165 abs kwhr/(NBS) int kwhr as exact by definition. Mueller and Rossini have proposed to redefine the thermochemical calorie as 4.1840 absolute joules, having previously (93) expressed the hope that "in the course of time physical scientists will become more and more familiar with the joule as the unit of energy, thermal and otherwise, and that the arbitrary conversion of joules to artificial (thermochemical) calories will become a chore that will gradually cease to be necessary."

We know of no completely satisfactory way out of the above dilemma but, being engineers, we have decided to adopt for the purpose of this paper a unit of energy called the International Tables Btu (IT Btu), defined by the conversion factors: 1 IT Btu g °K/IT cal lb °R; 860 IT cal/(mean) int whr; $1.00020 \pm 0.00004_5$ abs whr/(mean) int whr. Accordingly, we derive from the 1941 Birge (4) values of the general physical constants

$$R = 1.98581_{11} \pm 0.00018 \text{ IT Btu/°R mol} \ldots\ldots [10]$$

where the symbol "mol" denotes the pound-mol on the chemical scale. Thus our calculated values of the reduced entropy $s + R\log_e p$ (with pressure expressed in international atmospheres), mean isobaric specific heat $(h - \bar{u})/T$, and instantaneous isobaric specific heat c_p for monatomic hydrogen H^1 at 1000°R and, strictly speaking, zero pressure are: 30.46293_4 IT Btu/°R mol, 4.964528 IT Btu/°R mol, and 4.964528 IT Btu/°R mol, respectively.

ESTIMATED UNCERTAINTIES

In our calculations and subsequent interpolations we have tried to avoid any approximations that would affect our final results by more than ±2 in the eighth significant figure; before tabulating these results, however, we have rounded them off to seven significant figures. In this manner we have sought to achieve computational accuracy well beyond present physical accuracy for practical reasons. We wish now to give some indication of the limits of present physical accuracy and, for this purpose, shall compute what we call the estimated uncertainties of our final results.

In our calculations we have used the 1941 Birge (4) best values of the general physical constants consistently throughout. In estimating the uncertainties of our final results, however, we shall use the DuMond-Cohen (92) probable errors augmented by the differences, in absolute value, between the Birge and DuMond-Cohen best values. This procedure will tend to make our estimated uncertainties somewhat too conservative, but we believe it is the best one to use pending the systematic re-evaluation of all the data, which will surely be undertaken when experimental determinations currently under way in various laboratories have been completed.

From Equation [5] we see that the probable error of the quantity g/RT is to be derived in part from the probable errors of the constant $\log_e[k(2\pi k/h^2N_0)^{3/2}]$, the ratio 1.000272, the conversion factor 1,013,246 erg/cm³atm, and the isotopic weight M on the physical scale. We have calculated this constant or "translational" part of the uncertainty of g/RT for each of the isotopic monatomic gases here considered and have found it to lie between ± 0.00066 and ± 0.00069 in all cases.

The temperature function α is the only remaining source of uncertainty in our calculated values of g/RT. It makes what we may call the "electronic" contribution which arises jointly from the probable error of the second radiation constant c_2 and from those of the observed electronic-energy levels $E_i - E_0$. The corresponding electronic contributions to the uncertainties of the quantities $s/R + \log_e p$, $(h - \bar{u})/RT$, and c_p/R come from the functions $\log_e\alpha + \beta/\alpha$, β/α, and $\gamma/\alpha - (\beta/\alpha)^2$, respectively, in accordance with Equations [9]. We show these latter electronic uncertainties graphically in Figs. 1, 2, 3. To the electronic uncertainty of the quantity $s/R + \log_e p$ shown in Fig. 1, there must, of course, be added the constant amount 0.0007 (approximately) representing the translational uncertainty; the translational uncertainties of the quantities $(h - \bar{u})/RT$ and c_p/R are both nil in accordance with Equations [9].

Now we do not tabulate the dimensionless quantities just referred to, but rather the reduced entropy $s + R\log_e p$, the mean isobaric specific heat $(h - \bar{u})/T$, and the instantaneous isobaric specific heat c_p. To each of these tabulated quantities the relative probable error of the gas constant R contributes an additional uncertainty which we estimate to be 0.0091 per cent of the quantity tabulated. When the International Tables calorie was adopted in 1929, it was anticipated that the time would come when this calorie would have to be redefined in terms of the absolute or mechanical units. A move in this direction has been taken recently. When and if such a redefinition is adopted officially, it will be possible to state a relative probable error in the gas constant R only about one half as large as that just stated, that is, approximately 0.0046 per cent.

Returning to Figs. 1, 2, 3, it will be noticed that these cover only oxygen, carbon, sulphur, bromine, chlorine, fluorine, and iodine. In the cases of hydrogen, deuterium, helium, and argon, the electronic uncertainties are entirely negligible in the temperature range here considered. In the cases of nitrogen and mercury these uncertainties are not entirely negligible but are, nevertheless, too small to warrant complicating the figures to include them.

ISOTOPE EFFECTS

In general, each isotope of a particular atom possesses a slightly different set of electronic energy levels, $E_i - E_0$. It was through an investigation of these slight differences in the case of hydrogen that the existence of deuterium (heavy hydrogen) was first shown. Herzberg (94) states that the differences are only of the order of 2 cm⁻¹ and in many cases considerably smaller. Accordingly, we use the same spectroscopic data for each isotope (of a particular atom) and thereby assign to each the same mean isobaric specific heat $(h - \bar{u})/T$, the same instantaneous isobaric specific heat c_p, and, to within an additive constant amount $3/2R\log_e(M/M_0)$, the same reduced entropy $s + R\log_e p$. In this expression M_0 denotes the isotopic weight of a particular reference isotope. Thus it suffices to tabulate the thermodynamic properties of only one reference isotope of each monatomic gas if an auxiliary table is provided in which values of the quantity $(3/2)R\log_e(M/M_0)$ are listed. Table 4 is such an auxiliary table.

The reduced entropy $s + R\log_e p$ of the normal isotopic mixture of a given monatomic gas exceeds that of the reference isotope of isotopic weight M_0 by the constant amount $(3/2)R\Sigma x_i \log_e (M_i/M_0) - R\Sigma x_i \log_e x_i$, where the x_i are the fractional abundances (mol fractions) and the M_i are the isotopic weights of the various constituents of the mixture. Slight inaccuracies in the x_i do not appreciably affect the first sum if none of the M_i/M_0 differs much from unity, since in any event the x_i must add up to unity. The "mixing entropy," $-R\Sigma x_i \log_e x_i$ is, however, quite sensitive to inaccuracies in the x_i, and for this reason is listed separately in Table 4.

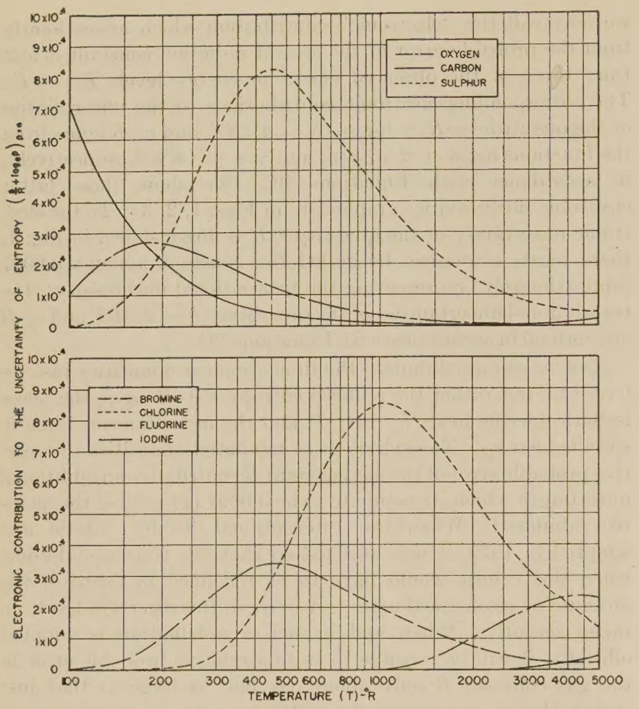

FIG. 1 ELECTRONIC UNCERTAINTY CONTRIBUTION

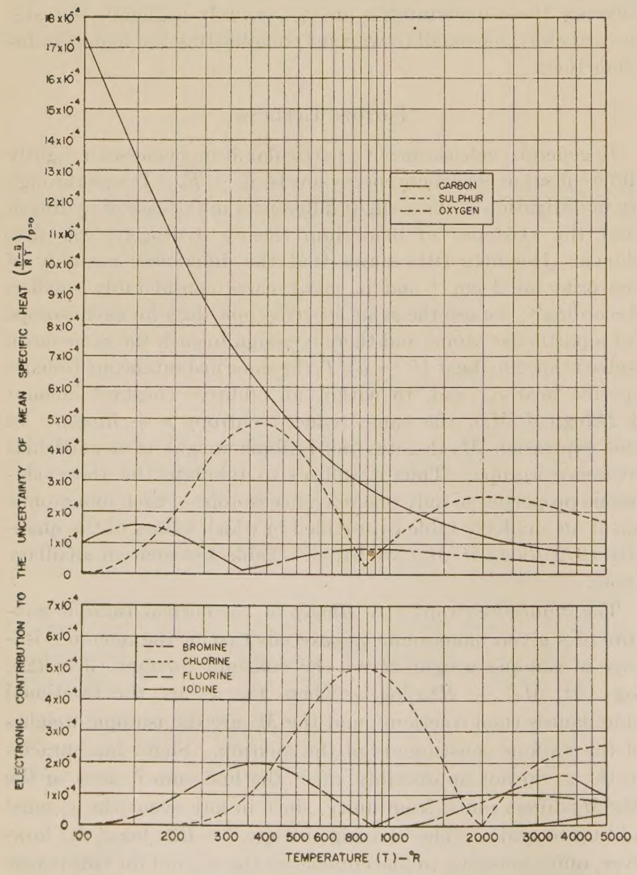

FIG. 2 ELECTRONIC UNCERTAINTY CONTRIBUTION

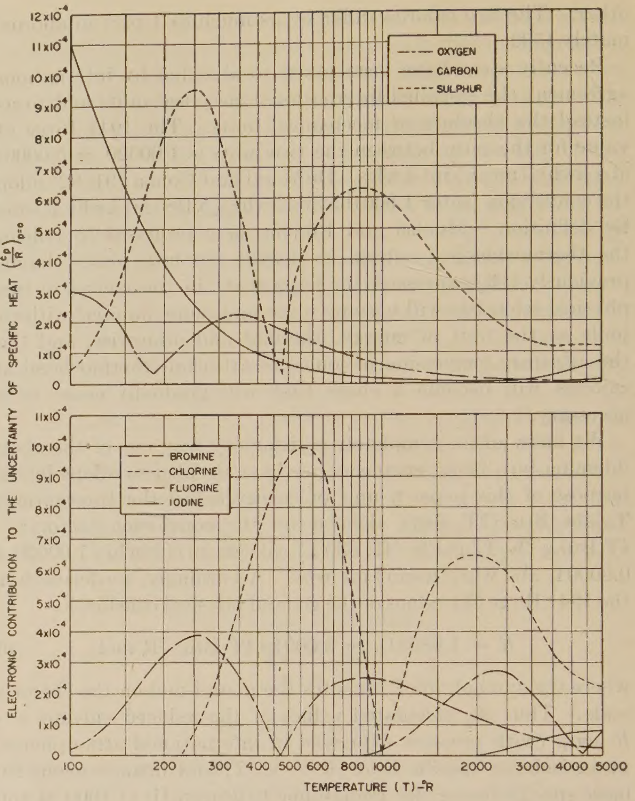

FIG. 3 ELECTRONIC UNCERTAINTY CONTRIBUTION

WORKING TABLES

The working tables here presented require little explanation beyond that already given. The original calculations were carried out with a precision of ±2 in the eighth significant figure; at 16°R intervals from 100 to 5220°R for hydrogen, helium, and argon; at the intervals shown in parentheses, namely, 76(8)-212(16)388(32)740(64)1580(128)5348°R for the other gases. The calculated values were then interpolated to the intervals, 100(5)130(10)240(20)500(50)1000(100)2000(200)5000°R for tab-

TABLE 4 REDUCED ENTROPY CORRECTIONS
(IT Btu/°R mol)

To get $s + R$ $\log_e p$ for	Add	And add mixing entropy	To $s + R$ $\log_e p$ for
H^2	+2.06243	...	H^1
Mixture	+0.00030	+0.00283	H^1
He^3	−0.84297	...	He^4
Mixture	0.00000	0.00000	He^4
C^{13}	+0.23919	...	C^{12}
Mixture	+0.02571	+0.11800	C^{12}
N^{15}	+0.20488	...	N^{14}
Mixture	+0.00076	+0.04817	N^{14}
O^{17}	+0.18137	...	O^{16}
O^{18}	+0.35165	...	O^{16}
Mixture	+0.00077	+0.03529	O^{16}
F^{19}	0.0	...	F^{19}
S^{33}	+0.09152	...	S^{32}
S^{34}	+0.18030	...	S^{32}
S^{36}	+0.35088	...	S^{32}
Mixture	+0.00831	+0.43416	S^{32}
Cl^{37}	+0.16543	...	Cl^{35}
Mixture	+0.04070	+1.10791	Cl^{35}
A^{36}	−0.31385	...	A^{40}
A^{38}	−0.17094	...	A^{40}
Mixture	−0.00983	+0.05173	A^{40}
Br^{81}	+0.07448	...	Br^{79}
Mixture	+0.03686	+1.38525	Br^{79}
I^{127}	0.0	...	I^{127}
Hg^{196}	−0.06018	...	Hg^{200}
Hg^{198}	−0.02993	...	Hg^{200}
Hg^{199}	−0.01493	...	Hg^{200}
Hg^{201}	+0.01485	...	Hg^{200}
Hg^{202}	+0.02963	...	Hg^{200}
Hg^{204}	+0.05911	...	Hg^{200}
Mixture	+0.00903	+3.35767	Hg^{200}

TABLE 5 ISOBARIC SPECIFIC HEAT $c_{p=0}$ FOR SOME SELECTED MONATOMIC GASES (IT Btu/mol °R)

T,°R	H^1	H^2	He^4	C^{12}	N^{14}	O^{16}	F^{19}	S^{32}	Cl^{35}	A^{40}	Br^{79}	I^{127}	Hg^{200}
100	4.964528	4.964528	4.964528	5.339415	4.964528	5.326954	4.967640	4.968862	4.964528	4.964528	4.964528	4.964528	4.964528
105	4.964528	4.964528	4.964528	5.305509	4.964528	5.366037	4.969173	4.970955	4.964528	4.964528	4.964528	4.964528	4.964528
110	4.964528	4.964528	4.964528	5.275833	4.964528	5.403196	4.971184	4.973685	4.964528	4.964528	4.964528	4.964528	4.964528
115	4.964528	4.964528	4.964528	5.249740	4.964528	5.438088	4.973735	4.977134	4.964529	4.964528	4.964528	4.964528	4.964528
120	4.964528	4.964528	4.964528	5.226694	4.964528	5.470475	4.976880	4.981371	4.964530	4.964528	4.964528	4.964528	4.964528
125	4.964528	4.964528	4.964528	5.206254	4.964528	5.500209	4.980660	4.986450	4.964532	4.964528	4.964528	4.964528	4.964528
130	4.964528	4.964528	4.964528	5.188052	4.964528	5.527218	4.985105	4.992411	4.964535	4.964528	4.964528	4.964528	4.964528
140	4.964528	4.964528	4.964528	5.157185	4.964528	5.573061	4.996043	5.007060	4.964550	4.964528	4.964528	4.964528	4.964528
150	4.964528	4.964528	4.964528	5.132181	4.964528	5.608429	5.009690	5.025336	4.964585	4.964528	4.964528	4.964528	4.964528
160	4.964528	4.964528	4.964528	5.111668	4.964528	5.634207	5.025874	5.047055	4.964658	4.964528	4.964528	4.964528	4.964528
170	4.964528	4.964528	4.964528	5.094648	4.964528	5.651507	5.044300	5.071872	4.964794	4.964528	4.964528	4.964528	4.964528
180	4.964528	4.964528	4.964528	5.080381	4.964528	5.661509	5.064596	5.099337	4.965028	4.964528	4.964528	4.964528	4.964528
190	4.964528	4.964528	4.964528	5.068311	4.964528	5.665363	5.086344	5.128942	4.965402	4.964528	4.964528	4.964528	4.964528
200	4.964528	4.964528	4.964528	5.058013	4.964528	5.664136	5.109120	5.160156	4.965966	4.964528	4.964528	4.964528	4.964528
210	4.964528	4.964528	4.964528	5.049161	4.964528	5.658781	5.132516	5.192454	4.966773	4.964528	4.964528	4.964528	4.964528
220	4.964528	4.964528	4.964528	5.041498	4.964528	5.650132	5.156152	5.225344	4.967879	4.964528	4.964528	4.964528	4.964528
230	4.964528	4.964528	4.964528	5.034823	4.964528	5.638903	5.179691	5.258371	4.969341	4.964528	4.964528	4.964528	4.964528
240	4.964528	4.964528	4.964528	5.028973	4.964528	5.625697	5.202841	5.291135	4.971210	4.964528	4.964528	4.964528	4.964528
260	4.964528	4.964528	4.964528	5.019255	4.964528	5.595281	5.247039	5.354533	4.976354	4.964528	4.964528	4.964528	4.964528
280	4.964528	4.964528	4.964528	5.011570	4.964528	5.561937	5.287312	5.413392	4.983609	4.964528	4.964528	4.964528	4.964528
300	4.964528	4.964528	4.964528	5.005389	4.964528	5.527684	5.322841	5.466341	4.993134	4.964528	4.964528	4.964528	4.964528
320	4.964528	4.964528	4.964528	5.000346	4.964528	5.493810	5.353277	5.512646	5.004954	4.964528	4.964528	4.964528	4.964528
340	4.964528	4.964528	4.964528	4.996179	4.964528	5.461102	5.378615	5.552063	5.018970	4.964528	4.964528	4.964528	4.964528
360	4.964528	4.964528	4.964528	4.992696	4.964528	5.430010	5.399073	5.584698	5.034986	4.964528	4.964528	4.964528	4.964528
380	4.964528	4.964528	4.964528	4.989757	4.964528	5.400760	5.415010	5.610889	5.052734	4.964528	4.964528	4.964528	4.964528
400	4.964528	4.964528	4.964528	4.987253	4.964528	5.373435	5.426857	5.631123	5.071908	4.964528	4.964528	4.964528	4.964528
420	4.964528	4.964528	4.964528	4.985104	4.964528	5.348027	5.435072	5.645962	5.092182	4.964528	4.964528	4.964528	4.964528
440	4.964528	4.964528	4.964528	4.983245	4.964528	5.324474	5.440113	5.655998	5.113229	4.964528	4.964528	4.964528	4.964528
460	4.964528	4.964528	4.964528	4.981626	4.964528	5.302680	5.442415	5.661818	5.134738	4.964528	4.964528	4.964528	4.964528
480	4.964528	4.964528	4.964528	4.980209	4.964528	5.282536	5.442382	5.663984	5.156420	4.964528	4.964529	4.964528	4.964528
500	4.964528	4.964528	4.964528	4.978960	4.964528	5.263924	5.440379	5.663019	5.178017	4.964528	4.964530	4.964528	4.964528
550	4.964528	4.964528	4.964528	4.976420	4.964528	5.223332	5.428801	5.649922	5.230234	4.964528	4.964536	4.964528	4.964528
600	4.964528	4.964528	4.964528	4.974494	4.964528	5.189895	5.410933	5.626259	5.277944	4.964528	4.964559	4.964528	4.964528
650	4.964528	4.964528	4.964528	4.973001	4.964528	5.162187	5.389617	5.596472	5.319633	4.964528	4.964618	4.964528	4.964528
700	4.964528	4.964528	4.964528	4.971820	4.964528	5.139063	5.366751	5.563621	5.354663	4.964528	4.964750	4.964528	4.964528
750	4.964528	4.964528	4.964528	4.970869	4.964528	5.119620	5.343560	5.529743	5.383008	4.964528	4.965007	4.964528	4.964528
800	4.964528	4.964528	4.964528	4.970093	4.964528	5.103150	5.320812	5.496145	5.405025	4.964528	4.965461	4.964528	4.964528
850	4.964528	4.964528	4.964528	4.969451	4.964528	5.089100	5.298961	5.463631	5.421289	4.964528	4.966196	4.964528	4.964528
900	4.964528	4.964528	4.964528	4.968913	4.964528	5.077031	5.278258	5.432667	5.432470	4.964528	4.967304	4.964528	4.964528
950	4.964528	4.964528	4.964528	4.968460	4.964528	5.066598	5.258823	5.403495	5.439262	4.964528	4.968881	4.964528	4.964528
1000	4.964528	4.964528	4.964528	4.968073	4.964528	5.057525	5.240688	5.376207	5.442333	4.964528	4.971019	4.964529	4.964528
1100	4.964528	4.964528	4.964528	4.967452	4.964528	5.042613	5.208210	5.327237	5.439703	4.964528	4.977298	4.964533	4.964528
1200	4.964528	4.964528	4.964528	4.966982	4.964528	5.030978	5.180373	5.285218	5.428714	4.964528	4.986631	4.964548	4.964528
1300	4.964528	4.964528	4.964528	4.966617	4.964528	5.021737	5.156564	5.249291	5.412465	4.964528	4.999236	4.964588	4.964528
1400	4.964528	4.964528	4.964528	4.966329	4.964528	5.014281	5.136174	5.218561	5.393173	4.964528	5.015058	4.964681	4.964528
1500	4.964528	4.964528	4.964528	4.966101	4.964528	5.008183	5.118658	5.192217	5.372373	4.964528	5.033818	4.964869	4.964528
1600	4.964528	4.964528	4.964528	4.965924	4.964528	5.003134	5.103549	5.169565	5.351096	4.964528	5.055082	4.965210	4.964528
1700	4.964528	4.964528	4.964528	4.965795	4.964528	4.998908	5.090457	5.150034	5.330019	4.964528	5.078324	4.965773	4.964528
1800	4.964528	4.964528	4.964528	4.965718	4.964528	4.995336	5.079058	5.133161	5.309568	4.964528	5.102986	4.966642	4.964528
1900	4.964528	4.964528	4.964528	4.965705	4.964528	4.992291	5.069088	5.118578	5.289999	4.964528	5.128521	4.967901	4.964528
2000	4.964528	4.964528	4.964528	4.965774	4.964528	4.989674	5.060327	5.105997	5.271450	4.964528	5.154420	4.969639	4.964528
2200	4.964528	4.964528	4.964528	4.966261	4.964528	4.985438	5.045738	5.085997	5.237611	4.964528	5.205567	4.974862	4.964528
2400	4.964528	4.964528	4.964528	4.967433	4.964530	4.982195	5.034184	5.071924	5.208040	4.964528	5.253609	4.982828	4.964528
2600	4.964528	4.964528	4.964528	4.969593	4.964537	4.979671	5.024893	5.063035	5.182370	4.964528	5.296748	4.993826	4.964528
2800	4.964528	4.964528	4.964528	4.973053	4.964558	4.977702	5.017321	5.058849	5.160129	4.964528	5.334039	5.007898	4.964528
3000	4.964528	4.964528	4.964528	4.978084	4.964613	4.976190	5.011073	5.058990	5.140843	4.964528	5.365175	5.024865	4.964528
3200	4.964528	4.964528	4.964528	4.984890	4.964738	4.975094	5.005862	5.063104	5.124079	4.964528	5.390276	5.044387	4.964528
3400	4.964528	4.964528	4.964528	4.993593	4.964994	4.974411	5.001472	5.070816	5.109459	4.964528	5.409733	5.066018	4.964528
3600	4.964528	4.964528	4.964528	5.004229	4.965466	4.974168	4.997740	5.081722	5.096661	4.964528	5.424080	5.089257	4.964528
3800	4.964528	4.964528	4.964528	5.016752	4.966273	4.974412	4.994543	5.095394	5.085415	4.964528	5.433915	5.113596	4.964528
4000	4.964528	4.964528	4.964528	5.031051	4.967562	4.975202	4.991784	5.111389	5.075492	4.964528	5.439842	5.138549	4.964528
4200	4.964528	4.964528	4.964528	5.046963	4.969510	4.976601	4.989386	5.129267	5.066703	4.964528	5.442439	5.163672	4.964528
4400	4.964528	4.964528	4.964528	5.064287	4.972317	4.978672	4.987290	5.148603	5.058887	4.964528	5.442240	5.188575	4.964528
4600	4.964528	4.964528	4.964528	5.082800	4.976198	4.981470	4.985447	5.168998	5.051912	4.964528	5.439721	5.212928	4.964529
4800	4.964528	4.964528	4.964528	5.102272	4.981377	4.985041	4.983818	5.190085	5.045665	4.964528	5.435305	5.236459	4.964531
5000	4.964528	4.964528	4.964528	5.122470	4.988079	4.989419	4.982372	5.211537	5.040050	4.964528	5.429357	5.258953	4.964534

TABLE 6 MEAN ISOBARIC SPECIFIC HEAT $[(h - \bar{u})/T]_{p=0}$ FOR SOME SELECTED MONATOMIC GASES (IT Btu/mol °R)

T, °R	H^1	H^2	He^4	C^{12}	N^{14}	O^{16}	F^{19}	S^{32}	Cl^{35}	A^{40}	Br^{79}	I^{127}	Hg^{200}
100	4.964528	4.964528	4.964528	6.120473	4.964528	5.050948	4.964825	4.964948	4.964528	4.964528	4.964528	4.964528	4.964528
105	4.964528	4.964528	4.964528	6.082454	4.964528	5.065029	4.964994	4.965182	4.964528	4.964528	4.964528	4.964528	4.964528
110	4.964528	4.964528	4.964528	6.046449	4.964528	5.079564	4.965228	4.965504	4.964528	4.964528	4.964528	4.964528	4.964528
115	4.964528	4.964528	4.964528	6.012365	4.964528	5.094402	4.965540	4.965932	4.964528	4.964528	4.964528	4.964528	4.964528
120	4.964528	4.964528	4.964528	5.980099	4.964528	5.109406	4.965945	4.966484	4.964528	4.964528	4.964528	4.964528	4.964528
125	4.964528	4.964528	4.964528	5.949546	4.964528	5.124452	4.966456	4.967178	4.964528	4.964528	4.964528	4.964528	4.964528
130	4.964528	4.964528	4.964528	5.920601	4.964528	5.139433	4.967085	4.968031	4.964528	4.964528	4.964528	4.964528	4.964528
140	4.964528	4.964528	4.964528	5.867134	4.964528	5.168833	4.968747	4.970274	4.964529	4.964528	4.964528	4.964528	4.964528
150	4.964528	4.964528	4.964528	5.818942	4.964528	5.197017	4.971007	4.973316	4.964531	4.964528	4.964528	4.964528	4.964528
160	4.964528	4.964528	4.964528	5.775358	4.964528	5.223583	4.973918	4.977229	4.964537	4.964528	4.964528	4.964528	4.964528
170	4.964528	4.964528	4.964528	5.735802	4.964528	5.248285	4.977506	4.982052	4.964548	4.964528	4.964528	4.964528	4.964528
180	4.964528	4.964528	4.964528	5.699774	4.964528	5.270995	4.981773	4.987794	4.964567	4.964528	4.964528	4.964528	4.964528
190	4.964528	4.964528	4.964528	5.666849	4.964528	5.291674	4.986699	4.994435	4.964601	4.964528	4.964528	4.964528	4.964528
200	4.964528	4.964528	4.964528	5.636658	4.964528	5.310347	4.992247	5.001935	4.964654	4.964528	4.964528	4.964528	4.964528
210	4.964528	4.964528	4.964528	5.608887	4.964528	5.327081	4.998368	5.010235	4.964734	4.964528	4.964528	4.964528	4.964528
220	4.964528	4.964528	4.964528	5.583267	4.964528	5.341973	5.005002	5.019264	4.964851	4.964528	4.964528	4.964528	4.964528
230	4.964528	4.964528	4.964528	5.559563	4.964528	5.355135	5.012087	5.028942	4.965013	4.964528	4.964528	4.964528	4.964528
240	4.964528	4.964528	4.964528	5.537575	4.964528	5.366690	5.019554	5.039186	4.965231	4.964528	4.964528	4.964528	4.964528
260	4.964528	4.964528	4.964528	5.498063	4.964528	5.385471	5.035374	5.061028	4.965876	4.964528	4.964528	4.964528	4.964528
280	4.964528	4.964528	4.964528	5.463577	4.964528	5.399277	5.051958	5.084127	4.966870	4.964528	4.964528	4.964528	4.964528
300	4.964528	4.964528	4.964528	5.433230	4.964528	5.408980	5.068860	5.107878	4.968291	4.964528	4.964528	4.964528	4.964528
320	4.964528	4.964528	4.964528	5.406327	4.964528	5.415336	5.085712	5.131765	4.970201	4.964528	4.964528	4.964528	4.964528
340	4.964528	4.964528	4.964528	5.382320	4.964528	5.418983	5.102221	5.155363	4.972647	4.964528	4.964528	4.964528	4.964528
360	4.964528	4.964528	4.964528	5.360768	4.964528	5.420451	5.118166	5.178339	4.975657	4.964528	4.964528	4.964528	4.964528
380	4.964528	4.964528	4.964528	5.341316	4.964528	5.420176	5.133389	5.200443	4.979240	4.964528	4.964528	4.964528	4.964528
400	4.964528	4.964528	4.964528	5.323674	4.964528	5.418514	5.147782	5.221495	4.983388	4.964528	4.964528	4.964528	4.964528
420	4.964528	4.964528	4.964528	5.307602	4.964528	5.415755	5.161281	5.241374	4.988083	4.964528	4.964528	4.964528	4.964528
440	4.964528	4.964528	4.964528	5.292899	4.964528	5.412134	5.173852	5.260010	4.993291	4.964528	4.964528	4.964528	4.964528
460	4.964528	4.964528	4.964528	5.279400	4.964528	5.407843	5.185487	5.277367	4.998972	4.964528	4.964528	4.964528	4.964528
480	4.964528	4.964528	4.964528	5.266963	4.964528	5.403036	5.196200	5.293443	5.005080	4.964528	4.964528	4.964528	4.964528
500	4.964528	4.964528	4.964528	5.255467	4.964528	5.397839	5.206013	5.308255	5.011566	4.964528	4.964528	4.964528	4.964528
550	4.964528	4.964528	4.964528	5.230209	4.964528	5.383759	5.226854	5.340012	5.029098	4.964528	4.964528	4.964528	4.964528
600	4.964528	4.964528	4.964528	5.208976	4.964528	5.368953	5.242971	5.364908	5.047885	4.964528	4.964530	4.964528	4.964528
650	4.964528	4.964528	4.964528	5.190879	4.964528	5.354081	5.255086	5.383894	5.067226	4.964528	4.964534	4.964528	4.964528
700	4.964528	4.964528	4.964528	5.175273	4.964528	5.339524	5.263884	5.397916	5.086547	4.964528	4.964544	4.964528	4.964528
750	4.964528	4.964528	4.964528	5.161676	4.964528	5.325493	5.269968	5.407835	5.105403	4.964528	4.964565	4.964528	4.964528
800	4.964528	4.964528	4.964528	5.149726	4.964528	5.312098	5.273853	5.414401	5.123472	4.964528	4.964606	4.964528	4.964528
850	4.964528	4.964528	4.964528	5.139140	4.964528	5.299383	5.275967	5.418246	5.140539	4.964528	4.964676	4.964528	4.964528
900	4.964528	4.964528	4.964528	5.129697	4.964528	5.287357	5.276664	5.419900	5.156469	4.964528	4.964790	4.964528	4.964528
950	4.964528	4.964528	4.964528	5.121223	4.964528	5.276006	5.276231	5.419796	5.171192	4.964528	4.964961	4.964528	4.964528
1000	4.964528	4.964528	4.964528	5.113575	4.964528	5.265304	5.274902	5.418290	5.184686	4.964528	4.965208	4.964528	4.964528
1100	4.964528	4.964528	4.964528	5.100318	4.964528	5.245708	5.270277	5.412183	5.208067	4.964528	4.966000	4.964528	4.964528
1200	4.964528	4.964528	4.964528	5.089225	4.964528	5.228279	5.263915	5.403308	5.226958	4.964528	4.967308	4.964529	4.964528
1300	4.964528	4.964528	4.964528	5.079807	4.964528	5.212733	5.256549	5.392806	5.241878	4.964528	4.969258	4.964532	4.964528
1400	4.964528	4.964528	4.964528	5.071712	4.964528	5.198815	5.248661	5.381429	5.253387	4.964528	4.971946	4.964539	4.964528
1500	4.964528	4.964528	4.964528	5.064678	4.964528	5.186303	5.240563	5.369671	5.262018	4.964528	4.975430	4.964554	4.964528
1600	4.964528	4.964528	4.964528	5.058511	4.964528	5.175008	5.232461	5.357855	5.268250	4.964528	4.979732	4.964583	4.964528
1700	4.964528	4.964528	4.964528	5.053061	4.964528	5.164770	5.224483	5.346190	5.272502	4.965428	4.984840	4.964635	4.964528
1800	4.964528	4.964528	4.964528	5.048210	4.964528	5.155454	5.216714	5.334813	5.275125	4.964528	4.990713	4.964721	4.964528
1900	4.964528	4.964528	4.964528	5.043868	4.964528	5.146944	5.209200	5.323806	5.276419	4.964528	4.997292	4.964854	4.964528
2000	4.964528	4.964528	4.964528	5.039961	4.964528	5.139144	5.201971	5.313223	5.276630	4.964528	5.004500	4.965047	4.964528
2200	4.964528	4.964528	4.964528	5.033235	4.964528	5.125355	5.188405	5.293426	5.274587	4.964528	5.020468	4.965683	4.964528
2400	4.964528	4.964528	4.964528	5.027697	4.964528	5.113554	5.176016	5.275516	5.270246	4.964528	5.037924	4.966759	4.964528
2600	4.964528	4.964528	4.964528	5.023137	4.964528	5.103349	5.164736	5.259482	5.264450	4.964528	5.056210	4.968398	4.964528
2800	4.964528	4.964528	4.964528	5.019427	4.964529	5.094441	5.154468	5.245273	5.257774	4.964528	5.074759	4.970699	4.964528
3000	4.964528	4.964528	4.964528	5.016494	4.964533	5.086606	5.145110	5.232827	5.250606	4.964528	5.093116	4.973730	4.964528
3200	4.964528	4.964528	4.964528	5.014296	4.964541	5.079668	5.136565	5.222071	5.243210	4.964528	5.110935	4.977523	4.964528
3400	4.964528	4.964528	4.964528	5.012813	4.964560	5.073495	5.128744	5.212930	5.235762	4.964528	5.127966	4.982084	4.964528
3600	4.964528	4.964528	4.964528	5.012032	4.964596	5.067981	5.121567	5.205324	5.228382	4.964528	5.144040	4.987386	4.964528
3800	4.964528	4.964528	4.964528	5.011943	4.964661	5.063048	5.114964	5.199167	5.221147	4.964528	5.159056	4.993384	4.964528
4000	4.964528	4.964528	4.964528	5.012534	4.964771	5.058634	5.108872	5.194370	5.214107	4.964528	5.172962	5.000017	4.964528
4200	4.964528	4.964528	4.964528	5.013788	4.964948	5.054691	5.103238	5.190837	5.207293	4.964528	5.185745	5.007212	4.964528
4400	4.964528	4.964528	4.964528	5.015685	4.965215	5.051186	5.098014	5.188473	5.200722	4.964528	5.197418	5.014891	4.964528
4600	4.964528	4.964528	4.964528	5.018197	4.965604	5.048092	5.093159	5.187180	5.194401	4.964528	5.208015	5.022975	4.964528
4800	4.964528	4.964528	4.964528	5.021291	4.966148	5.045387	5.088637	5.186860	5.188331	4.964528	5.217584	5.031383	4.964528
5000	4.964528	4.964528	4.964528	5.024932	4.966886	5.043058	5.084414	5.187417	5.182510	4.964528	5.226178	5.040040	4.964528

TABLE 7 REDUCED ENTROPY $(s + R\log_e p)_{p=0}$ FOR SOME SELECTED MONATOMIC GASES (IT Btu/mol °R)

T, °R	H^1	H^2	He^4	C^{12}	N^{14}	O^{16}	F^{19}	S^{32}	Cl^{35}	A^{40}	Br^{79}	I^{127}	Hg^{200}
100	19.03169	21.09411	21.76338	29.21003	28.24663	29.19301	29.15571	31.14941	30.97277	28.61742	33.39717	34.81230	33.41380
105	19.27391	21.33633	22.00560	29.46971	28.48885	29.45387	29.39812	31.39189	31.21499	28.85964	33.63939	35.05452	33.65602
110	19.50486	21.56728	22.23655	29.71582	28.71980	29.70436	29.62933	31.62320	31.44594	29.09059	33.87034	35.28547	33.88697
115	19.72554	21.78797	22.45723	29.94975	28.94048	29.94532	29.85036	31.84436	31.66662	29.31127	34.09102	35.50616	34.10765
120	19.93683	21.99926	22.66852	30.17268	29.15177	30.17746	30.06211	32.05627	31.87791	29.52256	34.30231	35.71744	34.31894
125	20.13949	22.20192	22.87118	30.38562	29.35443	30.40139	30.26535	32.25972	32.08057	29.72522	34.50497	35.92011	34.52160
130	20.33420	22.39663	23.06590	30.58945	29.54915	30.61764	30.46078	32.45540	32.27528	29.91994	34.69968	36.11482	34.71632
140	20.70211	22.76454	23.43381	30.97276	29.91706	31.02900	30.83060	32.82589	32.64319	30.28785	35.06759	36.48273	35.08423
150	21.04463	23.10706	23.77632	31.32768	30.25957	31.41476	31.17574	33.17195	32.98571	30.63036	35.41011	36.82525	35.42674
160	21.36503	23.42746	24.09673	31.65823	30.57998	31.77759	31.49956	33.49695	33.30612	30.95077	35.73051	37.14565	35.74715
170	21.66601	23.72843	24.39770	31.96760	30.88095	32.11973	31.80479	33.80366	33.60711	31.25174	36.03149	37.44662	36.04812
180	21.94977	24.01220	24.68147	32.25838	31.16472	32.44307	32.09368	34.09433	33.89089	31.53550	36.31525	37.73039	36.33188
190	22.21819	24.28062	24.94988	32.53274	31.43313	32.74930	32.36809	34.37802	34.15935	31.80392	36.58367	37.99880	36.60030
200	22.47284	24.53526	25.20453	32.79244	31.68778	33.03989	32.62956	34.63468	34.41405	32.05857	36.83831	38.25345	36.85495
210	22.71506	24.77748	25.44675	33.03900	31.93000	33.31612	32.87940	34.88723	34.65636	32.30079	37.08054	38.49567	37.09717
220	22.94601	25.00843	25.67770	33.27370	32.16095	33.57918	33.11871	35.12954	34.88744	32.53174	37.31149	38.72662	37.32812
230	23.16669	25.22912	25.89838	33.49766	32.38163	33.83010	33.34843	35.36254	35.10830	32.75242	37.53217	38.94730	37.54880
240	23.37798	25.44040	26.10967	33.71181	32.59292	34.06982	33.56937	35.58703	35.31983	32.96371	37.74346	39.15859	37.76009
260	23.77535	25.83778	26.50705	34.11394	32.99030	34.51894	33.98758	36.01308	35.71793	33.36108	38.14083	39.55597	38.15746
280	24.14326	26.20569	26.87496	34.48562	33.35821	34.93239	34.37793	36.41208	36.08697	33.72899	38.50874	39.92388	38.52538
300	24.48578	26.54821	27.21747	34.83116	33.70072	35.31495	34.74396	36.78740	36.43111	34.07151	38.85126	40.26639	38.86789
320	24.80618	26.86861	27.53788	35.15404	34.02113	35.67062	35.08849	37.14171	36.75373	34.39191	39.17166	40.58680	39.18830
340	25.10715	27.16958	27.83885	35.45705	34.32210	36.00269	35.41381	37.47713	37.05756	34.69289	39.47263	40.88777	39.48927
360	25.39092	27.45335	28.12261	35.74253	34.60586	36.31395	35.72185	37.79543	37.34488	34.97665	39.75640	41.17153	39.77303
380	25.65934	27.72176	28.39103	36.01239	34.87428	36.60674	36.01421	38.09811	37.61758	35.24507	40.02482	41.43995	40.04145
400	25.91398	27.97641	28.64568	36.26826	35.12893	36.88306	36.29228	38.38645	37.87723	35.49972	40.27946	41.69460	40.29610
420	26.15620	28.21863	28.88790	36.51154	35.37115	37.14461	36.55727	38.66157	38.12518	35.74194	40.52168	41.93682	40.53832
440	26.38715	28.44958	29.11885	36.74340	35.60210	37.39285	36.81023	38.92447	38.36255	35.97289	40.75263	42.16777	40.76927
460	26.60784	28.67026	29.33953	36.96488	35.82278	37.62904	37.05212	39.17603	38.59032	36.19357	40.97332	42.38845	40.98995
480	26.81912	28.88155	29.55082	37.17686	36.03407	37.85429	37.28375	39.41706	38.80931	36.40486	41.18460	42.59974	41.20124
500	27.02179	29.08421	29.75348	37.38014	36.23673	38.06956	37.50589	39.64826	39.02024	36.60752	41.38727	42.80240	41.40390
550	27.49496	29.55738	30.22665	37.85456	36.70990	38.56929	38.02393	40.18750	39.51623	37.08069	41.86044	43.27557	41.87707
600	27.92693	29.98935	30.65862	38.28748	37.14187	39.02230	38.49556	40.67815	39.97341	37.51266	42.29241	43.70754	42.30904
650	28.32430	30.38673	31.05600	38.68559	37.53925	39.43659	38.92784	41.12734	40.39756	37.91003	42.68979	44.10492	42.70641
700	28.69221	30.75464	31.42391	39.05408	37.90716	39.81828	39.32643	41.54089	40.79311	38.27795	43.05771	44.47283	43.07433
750	29.03473	31.09716	31.76642	39.39707	38.24968	40.17215	39.69590	41.92359	41.16355	38.62046	43.40025	44.81535	43.41684
800	29.35513	31.41756	32.08683	39.71786	38.57008	40.50202	40.04004	42.27940	41.51170	38.94087	43.72070	45.13575	43.73725
850	29.65610	31.71853	32.38780	40.01915	38.87105	40.81097	40.36195	42.61162	41.83989	39.24184	44.02175	45.43672	44.03822
900	29.93987	32.00230	32.67156	40.30318	39.15482	41.10150	40.66424	42.92302	42.15010	39.52560	44.30564	45.72049	44.32198
950	30.20829	32.27072	32.93998	40.57182	39.42323	41.37572	40.94909	43.21596	42.44402	39.79402	44.57424	45.98890	44.59040
1000	30.46293	32.52536	33.19463	40.82666	39.67788	41.63536	41.21837	43.49242	42.72311	40.04867	44.82917	46.24355	44.84505
1100	30.93610	32.99853	33.66780	41.30014	40.15105	42.11667	41.71630	44.00247	43.24178	40.52184	45.30323	46.71672	45.31822
1200	31.36808	33.43050	34.09977	41.73234	40.58302	42.55491	42.16824	44.46416	43.71467	40.95381	45.73668	47.14869	45.75019
1300	31.76545	33.82788	34.49714	42.12990	40.98039	42.95723	42.58193	44.88574	44.14858	41.35118	46.13630	47.54607	46.14756
1400	32.13336	34.19579	34.86506	42.49795	41.34831	43.32910	42.96331	45.27360	44.54900	41.71909	46.50735	47.91399	46.51547
1500	32.47588	34.53831	35.20757	42.84058	41.69082	43.67483	43.31706	45.63273	44.92039	42.06161	46.85398	48.25652	46.85799
1600	32.79628	34.85871	35.52798	43.16108	42.01123	43.99789	43.64691	45.96708	45.26643	42.38201	47.17952	48.57696	47.17839
1700	33.09725	35.15968	35.82895	43.46214	42.31220	44.30107	43.95591	46.27988	45.59020	42.68299	47.48667	48.87799	47.47937
1800	33.38102	35.44345	36.11271	43.74597	42.59596	44.58670	44.24654	46.57376	45.89428	42.96675	47.77763	49.16184	47.76313
1900	33.64944	35.71186	36.38113	44.01445	42.86438	44.85670	44.52088	46.85090	46.18082	43.23517	48.05421	49.43041	48.03155
2000	33.90408	35.96651	36.63578	44.26916	43.11903	45.11270	44.78066	47.11312	46.45169	43.48982	48.31793	49.68527	48.28620
2200	34.37725	36.43968	37.10895	44.74247	43.59220	45.58806	45.26225	47.59878	46.95249	43.96299	48.81161	50.15915	48.75937
2400	34.80922	36.87165	37.54092	45.17463	44.02417	46.02170	45.70077	48.04068	47.40692	44.39496	49.26665	50.59234	49.19134
2600	35.20660	37.26903	37.93829	45.57232	44.42154	46.42039	46.10334	48.44627	47.82275	44.79233	49.68890	50.99160	49.58871
2800	35.57451	37.63694	38.30620	45.94072	44.78946	46.78934	46.47544	48.82130	48.20597	45.16024	50.08283	51.36217	49.95662
3000	35.91703	37.97945	38.64872	46.28399	45.13198	47.13272	46.82138	49.17030	48.56131	45.50276	50.45194	51.70825	50.29914
3200	36.23743	38.29986	38.96912	46.60547	45.45239	47.45383	47.14462	49.49691	48.89255	45.82316	50.79904	52.03315	50.61954
3400	36.53840	38.60083	39.27010	46.90793	45.75338	47.75543	47.44796	49.80408	49.20274	46.12414	51.12643	52.33961	50.92052
3600	36.82217	38.88459	39.55386	47.19365	46.03718	48.03975	47.73373	50.09421	49.49442	46.40790	51.43607	52.62983	51.20428
3800	37.09058	39.15301	39.82228	47.46454	46.30567	48.30869	48.00385	50.36932	49.76968	46.67632	51.72962	52.90564	51.47270
4000	37.34523	39.40766	40.07693	47.72222	46.56044	48.56386	48.25997	50.63108	50.03026	46.93097	52.00851	53.16856	51.72735
4200	37.58745	39.64988	40.31915	47.96807	46.80285	48.80663	48.50346	50.88089	50.27768	47.17319	52.27399	53.41988	51.96957
4400	37.81840	39.88083	40.55010	48.20325	47.03409	49.03819	48.73552	51.11994	50.51320	47.40414	52.52718	53.60667	52.20052
4600	38.03908	40.10151	40.77078	48.42877	47.25520	49.25956	48.95717	51.34926	50.73792	47.62482	52.76905	53.89185	52.42120
4800	38.25037	40.31280	40.98207	48.64550	47.46709	49.47164	49.16931	51.56969	50.95279	47.83611	53.00048	54.11421	52.63249
5000	38.45303	40.51546	41.18473	48.85419	47.67057	49.67523	49.37273	51.78199	51.15865	48.03877	53.22224	54.32844	52.83515

TABLE 8 ENTHALPY $(h - \bar{u})_{p=0}$ FOR SOME SELECTED MONATOMIC GASES (IT Btu/mol)

T, °R	H^1	H^2	He^4	C^{12}	N^{14}	O^{16}	F^{19}	S^{32}	Cl^{35}	A^{40}	Br^{79}	I^{127}	Hg^{200}
100	496.4528	496.4528	496.4528	612.0473	496.4528	5050948	496.4825	496.4948	496.4528	496.4528	496.4528	496.4528	496.4528
105	521.2754	521.2754	521.2754	638.6577	521.2754	531.8280	521.3244	521.3441	5212754	521.2754	521.2754	521.2754	521.2754
110	546.0981	546.0981	546.0981	665.1094	546.0981	558.7520	546.1750	546.2055	546.0981	546.0981	546.0981	546.0981	546.0981
115	570.9207	570.9207	570.9207	691.4220	570.9207	585.8562	571.0371	571.0822	570.9207	570.9207	570.9207	570.9207	570.9207
120	595.7433	595.7433	595.7433	717.6119	595.7433	613.1287	595.9134	595.9781	595.7433	595.7433	595.7433	595.7433	595.7433
125	620.5660	620.5660	620.5660	743.6933	620.5660	640.5566	620.8070	620.8973	620.5660	620.5660	620.5660	620.5660	620.5660
130	645.3886	645.3886	645.3886	769.6782	645.3886	668.1263	645.7211	645.8441	645.3887	645.3886	645.3886	645.3886	645.3886
140	695.0339	695.0339	695.0339	821.3988	695.0339	723.6367	695.6246	695.8384	695.0341	695.0339	695.0339	695.0339	695.0339
150	744.6792	744.6972	744.6972	872.8413	744.6792	779.5525	745.6510	745.9974	744.6797	744.6792	744.6792	744.6792	744.6792
160	794.3244	794.3244	794.3244	924.0573	794.3244	835.7733	795.8268	796.3566	794.3259	794.3244	794.3244	794.3244	794.3244
170	843.9697	843.9697	843.9697	975.0863	843.9697	892.2084	846.1760	846.9488	843.9731	843.9697	843.9697	843.9697	843.9697
180	893.6150	893.6150	893.6150	1025.959	893.6150	948.7791	896.7191	897.8029	893.6221	893.6150	893.6150	893.6150	893.6150
190	943.2603	943.2603	943.2603	1076.701	943.2603	1005.418	947.4727	948.9427	943.2741	943.2603	9432603	943.2603	943.2603
200	992.9056	992.9056	992.9056	1127.332	992.9056	1062.069	998.4494	1000.387	992.9308	992.9056	992.9056	992.9056	992.9056
210	1042.551	1042.551	1042.551	1177.866	1042.551	1118.687	1049.657	1052.149	1042.594	1042.551	1042.551	1042.551	1042.551
220	1092.196	1092.196	1092.196	1228.319	1092.196	1175.234	1101.100	1104.238	1092.267	1092.196	1092.196	1092.196	1092.196
230	1141.841	1141.841	1141.841	1278.700	1141.841	1231.681	1152.780	1156.657	1141.953	1141.841	1141.841	1141.841	1141.841
240	1191.487	1191.487	1191.487	1329.018	1191.487	1288.006	1204.693	1209.405	1191.655	1191.487	1191.487	1191.487	1191.487
260	1290.777	1290.777	1290.777	1429.496	1290.777	1400.222	1309.197	1315.867	1291.128	1290.777	1290.777	1290.777	1290.777
280	1390.068	1390.068	1390.068	1529.802	1390.068	1511.797	1414.548	1423.556	1390.724	1390.068	1390.068	1390.068	1390.068
300	1489.358	1489.358	1489.358	1629.969	1489.358	1622.694	1520.658	1532.364	1490.487	1489.358	1489.358	1489.358	1489.358
320	1588.649	1588.649	1588.649	1730.025	1588.649	1732.907	1627.428	1642.165	1590.464	1588.649	1588.649	1588.649	1588.649
340	1687.939	1687.939	1687.939	1829.989	1687.939	1842.454	1734.755	1752.823	1690.700	1687.939	1687.939	1687.939	1687.939
360	1787.230	1787.230	1787.230	1929.876	1787.230	1951.362	1842.540	1864.202	1791.236	1787.230	1787.230	1787.230	1787.230
380	1886.521	1886.521	1886.521	2029.700	1886.521	2059.667	1950.688	1976.168	1892.111	1886.521	1886521	1886.521	1886521
400	1985.811	1985.811	1985.811	2129.470	1985.811	2167.406	2059.113	2088.598	1993.355	1985.811	1985.811	1985.811	1985.811
420	2085.102	2085.102	2085.102	2229.193	2085.102	2274.617	2167.738	2201.377	2094.995	2085.102	2085.102	2085.102	2085.102
440	2184.392	2184.392	2184.392	2328.876	2184.392	2381.339	2276.495	2314.404	2197.048	2184.392	2184.392	2184.392	2184.392
460	2283.683	2283.683	2283.683	2428.524	2283.683	2487.608	2385.324	2427.589	2299.527	2283.683	2283.683	2283.683	2283.683
480	2382.973	2382.973	2382.973	2528.142	2382.973	2593.457	2494.176	2540.853	2402.438	2382.973	2382.973	2382.973	2382.973
500	2482.264	2482.264	2482.264	2627.734	2482.264	2698.919	2603.006	2654.128	2505.783	2482.264	2482.264	2482.264	2482.264
550	2730.490	2730.490	2730.490	2876.615	2730.490	2961.068	2874.770	2937.007	2766.004	2730.490	2730.491	2730.490	2730.490
600	2978.717	2978.717	2978.717	3125.386	2978.717	3221.372	3145.782	3218.945	3028.731	2978.717	2978.718	2978.717	2978.717
650	3226.943	3226.943	3226.943	3374.072	3226.943	3480.152	3415.806	3499.531	3293.697	3226.943	3226.947	3226.943	3226.943
700	3475.169	3475.169	3475.169	3622.691	3475.169	3737.667	3684.719	3778.541	3560.583	3475.169	3475.181	3475.169	3475.169
750	3723.396	3723.396	3723.396	3871.257	3723.396	3994.120	3952.476	4055.876	3829.052	3723.396	3723.424	3723.396	3723.396
800	3971.622	3971.622	3971.622	4119.781	3971.622	4249.678	4219.082	4331.520	4098.778	3971.622	3971.685	3971.622	3971.622
850	4219.849	4219.849	4219.849	4368.269	4219.849	4504.475	4484.572	4605.509	4369.458	4219.849	4219.975	4219.849	4219.849
900	4468.075	4468.075	4468.075	4616.728	4468.075	4758.621	4748.997	4877.910	4640.822	4468.075	4468.311	4468.075	4468.075
950	4716.301	4716.301	4716.301	4865.162	4716.301	5012.206	5012.419	5148.806	4912.632	4716.301	4716.713	4716.301	4716.301
1000	4964.528	4964.528	4964.528	5113.575	4964.528	5265.304	5274.902	5418290	5184.686	4964.528	4965.528	4964.528	4964.528
1100	5460.981	5460.981	5460.981	5610.350	5460.981	5770.278	5797.305	5953.401	5728.874	5460.981	5462600	5460.981	5460.981
1200	5957.433	5957.433	5957.433	6107.070	5957.433	6273.935	6316.698	6483.970	6272.350	5957.433	5960.770	5957.435	5957.433
1300	6453.886	6453.886	6453.886	6603.749	6453.886	6776.554	6833.514	7010.648	6814.442	6453.886	6460.036	6453.891	6453.886
1400	6950.339	6950.339	6950.339	7100.396	6950.339	7278.342	7348.125	7534.001	7354.742	6950.339	6960.725	6950.354	6950.339
1500	7446.792	7446.792	7446.792	7597.017	7446.792	7779.455	7860.845	8054.507	7893.027	7446.792	7463.145	7446.831	7446.792
1600	7943.244	7943.244	7943.244	8093.618	7943.244	8280.013	8371.937	8572568	8429.201	7943.244	7967.572	7943.333	7943.244
1700	8439.697	8439.697	8439.697	8590.204	8439.697	8780.109	8881.622	9088.524	8963.253	8439.697	8474228	8439.880	8439.697
1800	8936.150	8936.150	8936.150	9086.779	8936.150	9279.816	9390.085	9602.663	9495.226	8936.150	8983.284	8936.498	8936.150
1900	9432.603	9432.603	9432.603	9583.349	9432.603	9779.194	9897.481	10115.23	10025.20	9432.603	9494.854	9433.223	9432.603
2000	9929.056	9929.056	9929.056	10079.92	9929.056	10278.29	10403.94	10626.45	10553.26	9929.056	10009.00	9930.094	9929.056
2200	10921.96	10921.96	10921.96	11073.12	10921.96	11275.78	11414.49	11645.54	11604.09	10921.96	11045.03	10924.50	10921.96
2400	11914.87	11914.87	11914.87	12066.47	11914.87	12272.53	12422.44	12661.24	12648.59	11914.87	12091.02	11920.22	11914.87
2600	12907.77	12907.77	12907.77	13060.16	12907.77	13268.71	13428.31	13674.65	13687.57	12907.77	13146.14	12917.84	12907.77
2800	13900.68	13900.68	13900.68	14054.40	13900.68	14264.44	14432.51	14686.77	14721.77	13900.68	14209.33	13917.96	13900.68
3000	14893.58	14893.58	14893.58	15049.48	14893.60	15259.82	15435.33	15698.48	15751.82	14893.58	15279.35	14921.19	14893.58
3200	15886.49	15886.49	15886.49	16045.75	15886.53	16254.94	16437.01	16710.63	16778.27	15886.49	16354.99	15928.07	15886.49
3400	16879.39	16879.39	16879.39	17043.56	16879.50	17249.88	17437.73	1772396	17801.59	16879.39	17435.08	16939.08	16879.39
3600	17872.30	17872.30	17872.30	18043.31	17872.54	18244.73	18437.64	18739.17	18822.18	17872.30	18518.54	17954.59	17872.30
3800	18865.21	18865.21	18865.21	19045.38	18865.71	19239.58	19436.86	19756.83	19840.36	18865.21	19604.41	18974.86	18865.21
4000	19858.11	19858.11	19858.11	20050.13	19859.09	20234.53	20435.49	20777.48	20856.43	19858.11	20691.85	20000.07	19858.11
4200	20851.02	20851.02	20851.02	21057.91	20852.78	21229.70	21433.60	21801.52	21870.63	20851.02	21780.13	21030.29	20851.02
4400	21843.92	21843.92	21843.92	22069.01	21846.95	22225.22	22431.26	22829.28	22883.18	21843.92	22868.64	22065.52	21843.92
4600	22836.83	22836.83	22836.83	23083.70	22841.78	23221.22	23428.53	23861.03	23894.24	22836.83	23956.87	23105.68	22836.83
4800	23829.73	23829.73	23829.73	24102.20	23837.51	24217.86	24425.46	24896.93	24903.99	23829.73	25044.40	24150.64	23829.73
5000	24822.64	24822.64	24822.64	25124.66	24834.43	25215.29	25422.07	25937.09	25912.55	24822.64	26130.89	25200.20	24822.64

ulation. Before final tabulation, however, they were rounded off to seven significant figures.

Table 5 lists values of isobaric specific heat c_p for all isotopic gases considered; Table 6 lists values of mean isobaric specific heat $(h - \bar{u})/T$; Table 7 lists values of reduced entropy $s + R \log_e p$ (with pressure expressed in international atmospheres); Table 8 lists values of enthalpy $h - \bar{u}$ for all isotopic gases considered. Strictly speaking, the data listed in these tables are valid only in the limiting case of zero pressure where the effects of intermolecular forces vanish. The unit of energy is the International Tables Btu (IT Btu) in terms of which the universal gas constant takes the value $R = 1.98581_{11}$ IT Btu/°R mol, the symbol "mol" being understood to denote the "pound-mol" on the *chemical* scale.

COMPARISON WITH OTHER DATA

The principles and procedures for calculating zero-pressure thermodynamic properties from spectroscopic and other data by the methods of quantum statistical mechanics have been well understood for some time. It appears, nevertheless, that only six papers of any consequence dealing with the zero-pressure thermodynamic properties of the monatomic gases here considered have hitherto been published. The only tables previously available are (*a*) various skeleton tables giving values of free enthalpy—actually the quantity $(g - \bar{u})/T - R \log_e p$—for the monatomic gases, hydrogen, nitrogen, oxygen, sulphur, chlorine, and iodine; (*b*) the familiar skeleton tables of the U. S. Bureau of Standards (95) for hydrogen, carbon, nitrogen, and oxygen; (*c*) a skeleton table of reduced free enthalpy for carbon (96) at intervals of 1000° K from 2000 to 6000° K. Except in the Bureau of Standards table (95), the published data have been based on the now obsolete values of the general physical constants and atomic weights given in International Critical Tables (90) and, in some cases, on obsolete spectroscopic data.

In Table 9 we compare our results with those of previous authors. The data in this table are values of the quantity $(g - \bar{u})/T - R \log_e p$ or $(h - \bar{u})/T - (s + R \log_e p)$ for some normal isotopic mixtures, mixing entropy excluded in accordance with the practice followed by previous authors. Before listing the data of previous authors in Table 9, we have corrected them to the value of the gas constant R used in this paper, in order to make them comparable with our data. The comparison shows that most of the discrepancies between our values and those of previous authors can be ascribed to the use of different values of the general physical constants. Only in a few cases have recent changes in spectroscopic data produced significant changes in the thermodynamic properties. It is especially interesting to note that the agreement between our values and those of the Bureau of Standards (95) is quite good except in the case of carbon.

ACKNOWLEDGMENT

It is a pleasure to acknowledge the generous support and active co-operation of the Navy Department, Bureau of Ships, and Office of Naval Research, in sponsoring our work through our University of Pennsylvania Thermodynamics Research Laboratory. We wish especially to thank Dr. G. Herzberg of the National Research Council of Canada, a member of our Laboratory's Advisory Committee, for his very valuable suggestions and criticisms, not only on the subject of atomic spectra but on the work of this project as a whole. We wish also to thank Miss Helen Tulloch, Miss Eleanor Smith, and Mrs. Jean Okada of the Laboratory's computing staff, for their painstaking efforts to achieve computational accuracy in the results presented in this paper.

BIBLIOGRAPHY

1 "Thermodynamics of Gas Mixtures," by J. A. Goff—a lecture delivered at the Brown University Course of Advanced Instruction in Research in Mechanics during the summer of 1945, Brown University, Providence, R. I., 1945.

2 "Infrared and Raman Spectra of Polyatomic Molecules," by G. Herzberg, D. Van Nostrand Company, Inc., New York, N. Y. 1945, pp. 501–530.

3 "Molecular Constants From Spectroscopic Data," by G. Herzberg, Trans. ASME, vol. 70, 1948, pp. 623–624.

4 "A New Table of Values of the General Physical Constants," by R. T. Birge, *Reviews of Modern Physics*, vol. 13, 1941, pp. 233–239.

5 "Our Knowledge of the Atomic Constants F, N, m, h in 1947 and of Other Constants Derivable Therefrom," by J. W. M. DuMond and E. R. Cohen, *Reviews of Modern Physics*, vol. 20, 1948, pp. 82–108.

6 "Erratum: Our Knowledge of the Atomic Constants F, N, m, h in 1947 and of Other Constants Derivable Therefrom," by J. W. M. DuMond and E. R. Cohen, received April 23, 1949.

7 "The $C^{12}H_2$—N^{14} Mass Difference," by E. B. Jordan, *Physical Review*, vol. 58, 1940, pp. 1009–1010.

8 "The Mass Differences of the Fundamental Doublets Used in the Determination of the Isotopic Weights of C^{12} and N^{14}," by E. B. Jordan, *Physical Review*, vol. 60, 1941, pp. 710–713.

9 "Nuclear Physics. C. Nuclear Dynamics, Experimental," by M. S. Livingston and H. A. Bethe, *Reviews of Modern Physics*, vol. 9, 1937, pp. 245–390.

10 "Nuclear Physics Tables and an Introduction to Nuclear Physics," by J. Mattauch and S. Flügge, 1942; translated by E. P. Gross and S. Bargman, Interscience Publishers, Inc., New York, N. Y., 1946.

11 "Isotopenbericht 1942," by S. Flügge and J. Mattauch, *Physikalische Zeitschrift*, vol. 44, 1943, pp. 181–201; ibid., p, 391.

12 "Mass Spectra and Isotopes," by F. W. Aston, second edition, Longmans, Green and Co., New York, N. Y., 1942.

13 "Least Squares Fit of the Fundamental Mass Doublets," by E. R. Cohen and W. F. Hornyak, *Physical Review*, vol. 72, 1947, p. 1127.

14 "Isotopic Weights of the Fundamental Isotopes," by K. T. Bainbridge, National Research Council, Division of Mathematical and Physical Sciences, Nuclear Science Series, Preliminary Report No. 1, June, 1948.

TABLE 9 COMPARISON WITH OTHER DATA

The function $(g - \bar{u})/T - R \log_e p$ for some normal isotopic mixtures
(IT Btu/°R mol; mixing entropy excluded)

Gas	Reference	900°R	1800°R	2700°R	3600°R	4500°R
Hydrogen...	(97)	—24.995	—28.436	—30.449	—31.878	—32.985
	(95)	—24.976	—28.416	—30.430	—31.858	—32.966
	GGV[a]	—24.97564	—28.41679	—30.42973	—31.85794	—32.96574
Carbon.....	(95)	—35.183	—38.703	—40.744	—42.186	—43.304
	GGV	—35.19919	—38.72347	—40.76443	—42.20733	—43.32600
Nitrogen....	(98)	—34.205	—37.646	—39.659	—41.087	—42.196
	(95)	—34.191	—37.632	—39.646	—41.074	—42.181
	GGV	—34.19104	—37.63219	—39.64514	—41.07341	—42.18208
Oxygen.....	(99)	—35.832	—39.448	—41.526	—42.988	—44.117
	(95)	—35.815	—39.433	—41.510	—42.972	—44.102
	GGV	—35.81491	—39.43201	—41.51032	—42.97253	—44.10127
Sulphur....	(100)	—37.526	—41.261	—43.407	—44.909	—46.064
	GGV	—37.51143	—41.24726	—43.39345	—44.89719	—46.05637
Chlorine....	(101)	—37.050	—40.665	—42.813	—44.322	—45.485
	GGV	—37.03437	—40.65989	—42.79753	—44.30648	—45.46968
Iodine......	(102)	—40.772	—44.213	—46.225	...	...
	GGV	—40.75596	—44.19712	—46.21073	...	...

---

[a] The initials GGV (Goff, Gratch, Van Voorhis) refer to this paper.

15 "Determination of Masses of Atoms by Mass Spectra," by T. Okuda, *Bulletin of the Institute of Physical and Chemical Research* (Tokyo), vol. 21, 1942, pp. 1–17. (see *Chemical Abstracts*, vol. 41, 1947, p. 5389f)

16 "Isotopic Weights of Sulfur and Titanium," by T. Okuda and K. Ogata, *Proceedings of the Physico-Mathematical Society of Japan*, vol. 25, 1943, pp. 374–375. (see *Chemical Abstracts*, vol. 41, 1947, p. 6142g)

17 "Preliminary Report on the Mass of ^{12}C and ^{14}N," by T. Asada, T. Okuda, K. Ogata, and S. Yoshimoto, *Nature*, vol. 143, 1939, p. 797.

18 "On the Isotopic Weights of Chlorine, Argon, and Iron by the Doublet Method," by T. Okuda, K. Ogata, K. Aoki, and Y. Sugawara, *Physical Review*, vol. 58, 1940, pp. 578–579.

19 "On the Isotopic Weight of C^{12}," by K. Ogata, *Proceedings of the Physico-Mathematical Society of Japan*, series 3, vol. 22, 1940, pp. 486–491.

20 "On the Isotopic Weights of Carbon and Nitrogen by the Doublet Method," by T. Asada, T. Okuda, K. Ogata, and S. Yoshimoto, *Proceedings of the Physico-Mathematical Society of Japan*, (3) vol. 22, 1940, pp. 41–45.

21 "Isotopic Weights of Ni Isotopes by the Doublet Method," by T. Okuda, K. Ogata, H. Kuroda, S. Shima, and S. Shindo, *Physical Review*, vol. 59, 1941, p. 104.

22 "Isotopic Weights of Sulfur and Titanium," by T. Okuda and K. Ogata, *Physical Review*, vol. 60, 1941, p. 690.

23 "Sur les Masses de Cl^{35} et Cl^{37}," by A. Gibert, F. Roggen, and J. Rossel, *Portugaliae Physica*, vol. 1, 1944, pp. 43–46.

24 "New Data on Isotopes. Isotopic Weights by the Doublet Method," by F. W. Aston, *Nature*, vol. 137, 1936, p. 613.

25 "Isotopic Weights by the Doublet Method," by F. W. Aston, *Nature*, vol. 138, 1936, p. 1094.

26 "Isotopic Weight of ^{12}C," by F. W. Aston, *Nature*, vol. 139, 1937, p. 922.

27 "Die Substandards in der Massenspektrographie," by J. Mattauch, *Zeitschrift für technische Physik*, vol. 19, 1938, pp. 578–582.

28 "Discussion on the Isotopic Weight of C^{12}," by J. Mattauch, *Physical Review*, vol. 57, 1940, pp. 1155–1159.

29 "Packing Fractions of Bromine, Chromium, Nickel, and Titanium," by F. W. Aston, *Nature*, vol. 141, 1938, p. 1096.

30 "Masses of Some Light Atoms Measured by Means of New Mass Spectrograph," by F. W. Aston, *Nature*, vol. 137, 1936, pp. 357–358.

31 "Packing Fractions of Krypton and Xenon," by F. W. Aston, *Nature*, vol. 140, 1937, p. 149.

32 "A New Mass Spectrograph and the Whole Number Rule," by F. W. Aston, Proceedings of the Royal Society of London, series A, vol. 115, 1927, pp. 487–514.

33 "A Second-Order Focusing Mass Spectrograph and Isotopic Weights by the Doublet Method," by F. W. Aston, Proceedings of the Royal Society of London, series A, vol. 163, 1937, pp. 391–404.

34 "Fifth Report of the Committee on Atoms of the International Union of Chemistry," by F. W. Aston, N. Boer, O. Hahn, W. D. Harkins, F. Joliot, R. S. Mulliken, and M. L. Oliphant, *Journal of the Chemical Society*, London, 1940, pp. 1416–1417.

35 "Thirteenth Report of the Committee on Atomic Weights of the International Union of Chemistry," by G. P. Baxter, M. Guichard, and R. Whytlaw-Gray, *Journal of the American Chemical Society*, vol. 69, 1947, pp. 731–736.

36 "Eine Neukonstruktion des Mattauch-Herzog'schen doppelfokussierenden Massenspektrographen. Die Massen von ^{13}C und ^{15}N," by H. Ewald, *Zeitschrift für Naturforschung*, vol. 1, 1946, pp. 131–136.

37 "Massenspektroskopische Atomgewichtbestimmungen," by H. Ewald, FIAT Rev. German Sci., 1939–1946, Inorg. Chem. Part I, 1948, pp. 12–25.

38 "Table of Isotopes," by G. T. Seaborg and I. Perlman, *Reviews of Modern Physics*, vol. 20, 1948, pp. 585–667.

39 "The Natural Abundances of the Oxygen Isotopes," by H. G. Thode and H. R. Smith, National Research Council of Canada, Atomic Energy Project Report MX-129, April, 1945.

40 "Oxygen Isotopes in Nature and in the Laboratory," by H. C. Urey, *Science*, vol. 108, 1948, pp. 489–496.

41 "The Abundance of He^{3} in Atmosphere and Well Helium," by L. T. Aldrich and A. O. Nier, *Physical Review*, vol. 70, 1946, pp. 983–984.

42 "The Concentration of He^{3} in the Liquid and Vapor Phases of He^{4}," by H. A. Fairbank, C. T. Lane, L. T. Aldrich, and A. O. Nier, *Physical Review*, vol. 71, 1947, pp. 911–913.

43 "The Isotopic Constitution of Calcium, Titanium, Sulfur, and Argon," by A. O. Nier, *Physical Review*, vol. 53, 1938, pp. 282–286.

44 "Mass-Spectrometer Study of the Rare Gases," by V. H. Dibeler, F. L. Mohler, and R. M. Reese, *Journal of Research of the National Bureau of Standards*, vol. 38, 1947, pp. 617–620, Research Paper RP1799.

45 "A Mass-Spectrographic Study of the Isotopes of Argon, Potassium, Rubidium, Zinc, and Cadmium," by A. O. Nier, *Physical Review*, vol. 50, 1936, pp. 1041–1045.

46 "Isotopic Constitution of Tellurium, Silicon, Tungsten, Molybdenum, and Bromine," by D. Williams and P. Yuster, *Physical Review*, vol. 69, 1946, pp. 556–567.

47 "Natural Abundance of Isotopes of Stable Elements," by J. R. White and A. E. Cameron, *Physical Review*, vol. 74, 1948, pp. 991–1000.

48 "Atomic Energy States," by R. F. Bacher and S. Goudsmit, McGraw-Hill Book Co., New York, N. Y., 1932.

49 "The Coupling of p-Electron Configurations," by H. A. Robinson and G. H. Shortley, *Physical Review*, vol. 52, 1937, pp. 713–723.

50 "Atomic Spectra," by A. G. Shenstone, *Reports on Progress in Physics*, Physical Society of London, England, vol. 5, 1938, pp. 210–227.

51 "A Multiplet Table of Astrophysical Interest," by C. E. Moore, Princeton University Observatory, Princeton, N. J., 1945.

52 "Spectroscopy, Past, Present, and Future," by W. F. Meggers, *Journal of the Optical Society of America*, vol. 36, 1946, pp. 431–448.

53 "Atomic Energy Levels as Derived From the Analyses of Optical Spectra," by C. E. Moore, Circular of the National Bureau of Standards 467, vol. 1, sec. 1, 1948.

54 "Wellenlängen und Termsysteme zu den Atomspektren der Elemente Lithium, Beryllium, Bor, Kohlenstoff, Stickstoff, und Sauerstoff," by B. Edlén, *Nova Acta Regiae Societatis Scientiarum Upsaliensis*, series IV, vol. 9, No. 6, 1934, pp. 1–153.

55 "The ^5S State of Carbon," by A. G. Shenstone, *Physical Review*, vol. 72, 1947, pp. 411–414.

56 "The Fine Structure of the Triplet $(2s^2)\ (2p)\ (3s)\,^3P \rightarrow (2s^2)\ (2p^2)\,^3P$ of the Carbon Atom," by V. M. Chulanovskiĭ and M. P. Mokhnatkin, Comptes rendus de l'academie des sciences de l'URSS. (N.S.), vol. 2, 1934, pp. 18–19.

57 "Das Bogenspektrum von Stickstoff," by E. Ekefors, *Zeitschrift für Physik*, vol. 63, 1930, pp. 437–443.

58 "Die Feinstruktur des metastabilen $^2D_{5/2,3/2}$-Terms des Stickstoffatoms," by W. Tschulanovsky, *Zeitschrift für Physik*, vol. 82, 1933, pp. 134–145.

59 "The Metastable ^2D-Level of the Nitrogen Atom," by H. Stücklen and E. P. Carr, *Physical Review*, vol. 43, 1933, pp. 944–945.

60 "The Fine Structure of the Metastable Levels of Nitrogen," by B. Stepanov, *Physikalische Zeitschrift der Sowietunion*, vol. 8, 1935, pp. 352–353.

61 "The Arc Spectrum of Nitrogen (N I). Part II-A. Extreme Ultraviolet Region," by M. Kamiyama, *Scientific Papers of the Institute of Physical and Chemical Research*, Tokyo, Japan, vol. 36, 1939, pp. 375–384.

62 "The Arc Spectrum of Nitrogen (N I). Part I. Historical, and Part IIB. Near-Infra-Red Region," by M. Kamiyama and T. Sugiura, *Scientific Papers of the Institute of Physical and Chemical Research*, Tokyo, Japan, vol. 37, 1940, pp. 479–487.

63 "The Arc Spectrum of Nitrogen (N I). Part III. The Intermediate Region," by M. Kamiyama and H. Noguchi, *Scientific Papers of the Institute of Physical and Chemical Research*, Tokyo, Japan, vol. 39, 1942, pp. 475–483.

64 "The Arc Spectrum of Oxygen, O I," by Bengt Edlén, *Kungliga Svenska Vetanskapsakademiens Handlingar*, series III, vol. 20, No. 10, 1943, 31 pp.

65 "Beitrag zu den Spektren F III, F II, und F I," by B. Edlén, *Zeitschrift für Physik*, vol. 93, 1934, pp. 433–449.

66 "The Spectrum of Fluorine (F I) Part II," by H. Dingle, Proceedings of the Royal Society of London, series A, vol. 117, 1927, pp. 407–416.

67 "Series Spectra of Boron, Carbon, Nitrogen, Oxygen, and Fluorine," by I. S. Bowen, *Physical Review*, vol. 29, 1927, pp. 231–247.

68 "Wave-Length Measurements and New Energy Levels in the Arc Spectrum of Fluorine, F I," by K. Lidén, Arkiv för Matematik, Astronomi och Fysik, vol. 35A, No. 24, 1948, 13 pp.

69 "Series Spectra in Oxygen and Sulfur," by J. J. Hopfield, *Nature*, vol. 112, 1923, pp. 437–438.

70 "Beitrag zur Kenntnis des Sauerstoff- und Schwefelspektrums," by E. Bungartz, *Annalen der Physik*, series 4, vol. 76, 1925, pp. 709–728.

71 "PP′ Groups in the Elements S(I) to K(IV)," by J. J. Hopfield and G. H. Dieke, *Physical Review*, vol. 27, 1926, p. 638.

72 "Zum Bogenspektrum des Schwefels," by R. Frerichs, *Zeitschrift für Physik*, vol. 80, 1933, pp. 150–160.

73 "Zur Kenntnis des Schwefel-Bogenspektrums," by K. W. Meissner, O. Bartelt, and L. Eckstein, *Zeitschrift für Physik*, vol. 86, 1933, pp. 54–81.

74 "The Arc Spectrum of Sulfur in the Ultraviolet," by J. E. Ruedy, *Physical Review*, vol. 43, 1933, p. 1045.

75 "The Arc Spectrum of Sulfur in the Ultraviolet," by J. E. Ruedy, *Physical Review*, vol. 44, 1933, pp. 757–760.

76 "Forbidden Lines," by I. S. Bowen, *Reviews of Modern Physics*, vol. 8, 1936, pp. 55–81.

77 "On $s^2p^4\ {}^1S$ and $sp^5\ {}^1P$ in the S I Isoelectronic Sequence," by B. Edlén, *Physical Review*, vol. 62, 1942, pp. 434–437.

78 "A New Description and Analysis of the Arc Spectrum of Chlorine," by C. C. Kiess, *Journal of Research of the National Bureau of Standards*, vol. 10, 1933, pp. 827–839, Research Paper RP570.

79 "The Arc Spectra of Iodine, Bromine, and Chlorine in the Schumann Region," by L. A. Turner, *Physical Review*, vol. 27, 1926, pp. 397–406.

80 "Atomic Spectra and Atomic Structure," by G. Herzberg, Dover Publications, New York, N. Y., 1944, pp. 146–147.

81 "The Arc Spectrum of Bromine and Its Structure," by C. C. Kiess and T. L. de Bruin, *Journal of Research of the National Bureau of Standards*, vol. 4, 1930, pp. 667–692.

82 "Ueber die Spektren J II, J I, und Cl II," by K. Murakawa, *Zeitschrift für Physik*, vol. 109, 1938, pp. 162–174.

83 "The Arc Spectrum of Iodine," by S. F. Evans, Proceedings of the Royal Society of London, England, series A, vol. 133, 1931, pp. 417–430.

84 "New Lines in the Ultraviolet Spectrum of Atomic Iodine," by J. H. McLeod, *Physical Review*, vol. 49, 1936, pp. 804–807.

85 "Ueber die Hochfrequenz- (Kurzwellen-) anregung einiger Spektren in fernen Ultraviolet," by M. Hellerman, *Zeitschrift für Physik*, vol. 104, 1937, pp. 417–429.

86 "The New Lines ($1s$-$2p_{1,3}$) of Zinc, Cadmium, and Mercury," by M. Fukuda, *Scientific Papers of the Institute of Physical and Chemical Research*, Tokyo, Japan, vol. 4, 1926, pp. 171–175.

87 "A Determination of the Wave Lengths (International System) for the Arc and Spark Spectrum of Mercury," by H. Stiles, *Astrophysical Journal*, vol. 30, 1909, pp. 48–61.

88 "The Excitation of Forbidden Spectral Lines," by P. D. Foote, T. Takamine, and R. L. Chenault, *Physical Review*, vol. 26, 1925, pp. 165–175.

89 "Memorandum on the Definition of the Calorie," by J. H. Keenan, an unpublished memorandum sent in April, 1949, to members of the ASME Special Research Committee on properties of Gases and Gas Mixtures.

90 "International Critical Tables," National Research Council, McGraw-Hill Book Company, Inc., New York, N. Y., vol. 1, 1926, p. 16 ff.

91 "Our Knowledge of the Atomic Constants F,N,m,h in 1947 and of Other Constants Derivable Therefrom," by J. W. M. DuMond and E. R. Cohen, *Reviews of Modern Physics*, vol. 20, 1948, pp. 82–108.

92 "Erratum: Our Knowledge of the Atomic Constants F,N, m,h in 1947 and of Other Constants Derivable Therefrom," by J. W. M. DuMond and E. R. Cohen, received April 23, 1949.

93 "The Calory and the Joule in Thermodynamics and Thermochemistry," by E. F. Mueller and F. D. Rossini, *American Journal of Physics*, vol. 12, 1944, pp. 1–7.

94 "Atomic Spectra and Atomic Structure," by G. Herzberg, Dover Publications, New York, N. Y., 1944, pp. 182–185.

95 "Selected Values of Properties of Hydrocarbons," by F. D. Rossini, K. S. Pitzer, W. J. Taylor, J. P. Ebert, J. E. Kilpatrick, C. W. Beckett, M. G. Williams, and H. G. Werner, Circular of the National Bureau of Standards C461, November, 1947, pp. 173, 191, 209, 227, and 280.

96 "The Free Energy of Diatomic Carbon Vapor," by A. R. Gordon, *Journal of Chemical Physics*, vol. 5, 1937, pp. 350–352.

97 "The Entropy of Hydrogen and the Third Law of Thermodynamics. The Free Energy and Dissociation of Hydrogen," by W. F. Giauque, *Journal of the American Chemical Society*, vol. 52, 1930, pp. 4816–4831.

98 "The Heat Capacity and Entropy of Nitrogen. Heat of Vaporization. Vapor Pressures of Solid and Liquid. The Reaction ${}^1/_2N_2 + {}^1/_2O_2 = NO$ From Spectroscopic Data," by W. F. Giauque and J. O. Clayton, *Journal of the American Chemical Society*, vol. 55, 1933, pp. 4875–4889.

99 "The Dissociation of Oxygen to 5000°K. The Free Energy of Atomic Oxygen," by H. L. Johnston and M. K. Walker, *Journal of the American Chemical Society*, vol. 55, 1933, pp. 187–193.

100 "The Free Energy of Sulfur Monoxide and the Dissociation Constants of S_2," by G. W. Montgomery and L. S. Kassel, *Journal of Chemical Physics*, vol. 2, 1934, pp. 417–418.

101 "The Hydrogen, Chlorine, Hydrogen Chloride Equilibrium at High Temperatures," by W. F. Giauque and R. Overstreet, *Journal of the American Chemical Society*, vol. 54, 1932, pp. 1731–1744.

102 "The Free Energy of Iodine and Hydrogen Iodide From Spectroscopic Data," by G. M. Murphy, *Journal of Chemical Physics*, vol. 4, 1936, pp. 344–350.

Zero-Pressure Thermodynamic Properties of Carbon Monoxide and Nitrogen

By J. A. GOFF[1] and SERGE GRATCH,[2] PHILADELPHIA, PA.

In this report are presented tables of the principal thermodynamic properties of carbon monoxide and of nitrogen along the zero-pressure isobar in the range 100 to 5000 deg R at the intervals indicated by the numbers in parentheses as follows: 100[5]130[10]240[20]500[50]1000[100]2000[200]5000. The data have been computed by the method of quantum statistical mechanics in the University of Pennsylvania Thermodynamics Research Laboratory under Project G-3. Computational accuracy well beyond present physical accuracy has been maintained for practical reasons. It is believed that the tables given herein should supersede all previous ones. The calculated values are in satisfactory agreement with those obtained from calorimetric and acoustic velocity measurements.

Introduction and Theory

THIS is the third of a series of reports on the calculation of thermodynamic properties of gases along the zero-pressure isobar by the methods of quantum statistical mechanics. These calculations were carried out at the University of Pennsylvania Thermodynamics Research Laboratory under the sponsorship of the United States Navy, Bureau of Ships, as an essential part of an extensive program for the determination of the thermodynamic properties of some technically important gases. The general aims of this program and the theoretical basis for the calculations have been outlined in the first two reports (1, 2).[3] Only as much of the theory will be reviewed in the present report as is necessary for an understanding of the special results obtained in the case of carbon monoxide and nitrogen.

The spectroscopic data are usually expressed by an equation giving wave number E (cm^{-1}) as a function of certain quantum numbers which independently can take on all non-negative integral values within prescribed limits; the constants appearing in this equation are called spectroscopic constants. To each wave number E_i there is assigned a definite energy $\epsilon_i = hcE_i$, where h denotes Planck's constant, and c the velocity of light in vacuo. To each set of values of the various quantum numbers there corresponds a distinct quantum state; but there may be more than one, say, p_i distinct quantum states having the same energy ϵ_i in the absence of an external electric or magnetic field.

The first step in the calculation is to form the state sum or partition function Q defined by

$$Q = \Sigma p_i e^{-\epsilon_i/kT} = \Sigma p_i e^{-c_2 \tau E_i} \ldots\ldots\ldots\ldots [1]$$

where k is Boltzmann's constant, c_2 is the so-called second radiation constant hc/k, and τ denotes reciprocal absolute temperature T^{-1}. The summation is to be extended over all accessible energy levels ϵ_i. Now the specific free enthalpy g of the gas in question is given by

$$g = -RT \log_e (Q/nN_0) \ldots\ldots\ldots\ldots [2]$$

where n is the number of mols of gas with state sum Q and N_0 is Avogadro's number. This is subject to augmentation by an arbitrary constant $\bar{u}$, which can be identified as the null-point ($p = 0$, $T = 0$) energy of the gas in question, since the numerical value to be assigned to the energy ϵ_0 of the lowest level is arbitrary.[4] Since free enthalpy g is a characteristic function of pressure p and temperature T, the enthalpy h, reduced entropy $s + R \log_e p$, and product pv can be derived from it in a simple manner by application of well-known identical relations of thermodynamics, namely, $h = \partial(\tau g)/\partial\tau$, $s = -\partial g/\partial T$, and $v = \partial g/\partial p$, if the state sum Q in Equation [2] is expressed as function of p and T. From the first of these relations it is to be noticed that enthalpy h, like free enthalpy g, is subject to augmentation by a constant amount $\bar{u}$; the second shows that such augmentation does not affect the entropy s.

In a previous report (1) it was explained that the contributions to the state sum from translation can be evaluated separately from those for internal motions (rotation, vibration, etc.). If the effect of intermolecular forces is neglected, the following result is obtained

$$[\log_e p - g/RT]_{p=0} = \frac{5}{2} \log_e T + \log_e [(2\pi Mk/h^2N_0)^{3/2}k] + \log_e Q_{\text{int}} \ldots\ldots [3]$$

where M denotes the molecular weight, and Q_{int} is the contribution to the state sum from internal motions only. Consistent units must be used in the arguments of the logarithms. The subscript $p = 0$ is affixed to the quantity on the left to emphasize that Equation [3] is strictly valid only in the absence of intermolecular forces, that is, it is valid only in the limiting case of zero pressure. At not too low temperatures the effects of intermolecular forces remain small until fairly high pressures are reached; therefore the zero-pressure properties can be used without correction in ordinary engineering calculations not involving too-high pressures.

Internal State Sum

The energy levels ϵ_i entering the internal state sum Q_{int} represent the rotational, vibrational, electronic, and nuclear contributions. It has been shown that the contribution from nuclear spin may be disregarded if the resulting properties are to be used only in the analysis of processes which involve no transmutation of atomic species, provided, of course, that the practice is followed consistently for all molecules. In the case of carbon monoxide and nitrogen the electronic contributions are negligible in the temperature range here considered. In this

---

[1] Dean, Towne Scientific School; Director, University of Pennsylvania Thermodynamics Research Laboratory. Mem. ASME.

[2] Assistant Professor of Mechanical Engineering, Towne Scientific School; Project Leader, University of Pennsylvania Thermodynamics Research Laboratory. Jun. ASME.

[3] Numbers in parentheses refer to the Bibliography at the end of the paper.

Contributed by the Research Committee on Properties of Gases and Gas Mixtures, and the Heat Transfer and Applied Mechanics Divisions, and presented at the Annual Meeting, New York, N. Y., November 27–December 2, 1949, of The American Society of Mechanical Engineers.

Note: Statements and opinions advanced in papers are to be understood as individual expressions of their authors and not those of the Society. Paper No. 49—A-50.

[4] Not completely arbitrary, because the null-point energy of a molecular gas is definitely related to the null-point energies of the associated monatomic gases.

range, therefore, it is only necessary to take account of the rotational-vibrational energy levels for the ground electronic state, which is the $X^1\Sigma_g{}^+$ state in the case of nitrogen (N_2) and the $X^1\Sigma^+$ state in the case of carbon monoxide (CO) (3). For these states the rotational-vibrational energy levels can be expressed by the following equation for the corresponding wave numbers E_i measured from the lowest level

$$E_i = \omega_0 v - \omega_0 x_0 v^2 + \omega_0 y_0 v^3 - \ldots + B_v J(J+1) - D_v J^2 (J+1)^2 + F_v J^3 (J+1)^3 - \ldots \quad \ldots\ldots [4]$$

with

$$B_v = B_0 - \alpha_0 v + \ldots; \quad B_0 = B_e - \frac{1}{2}\alpha_0 + \ldots \quad \ldots\ldots [4a]$$

$$D_v = D_0 - \beta_0 v + \ldots; \quad D_0 = D_e - \frac{1}{2}\beta_0 + \ldots \quad \ldots\ldots [4b]$$

$$F_v = F_0 - \gamma_0 v + \ldots; \quad F_0 = F_e - \frac{1}{2}\gamma_0 + \ldots \quad \ldots\ldots [4c]$$

$$\omega_0 = \omega_e - \omega_e x_e + \frac{3}{4}\omega_e y_e - \ldots \quad \ldots\ldots [4d]$$

$$\omega_0 x_0 = \omega_e x_e - \frac{3}{2}\omega_e y_e + \ldots \quad \ldots\ldots [4e]$$

$$\omega_0 y_0 = \omega_e y_e - \ldots \quad \ldots\ldots [4f]$$

where

ω_e = zero-order vibrational frequencies
$x_e, y_e, \ldots$ = anharmonicity constants
B_e = rotational constant[5]
$D_e, F_e, \ldots$ = rotational stretching constants
$\alpha_0, \beta_0, \gamma_0, \ldots$ = rotation-vibration coupling constants
v, J = quantum numbers

In the case of $^1\Sigma$ states, such as the ones here considered, the statistical weights p_i (neglecting the contribution from nuclear spin) are given for heteronuclear molecules, such as CO, by

$$p_i = 2J + 1$$

In the case of homonuclear molecules, such as $N_2{}^{14}$, these statistical weights must be multiplied by additional factors which are different according to whether J is even or odd. At not too-low temperatures it may be shown (4) that the internal state sum over the even values of J differs from that over the odd values of J by only a negligible amount and that, as a result, the effect of the additional factor in the statistical weights is equivalent to dividing all the statistical weights $(2J + 1)$ by a symmetry number σ, which has the value 2 for homonuclear molecules, and of course has the value unity for heteronuclear molecules. At very low temperatures this is not the case and as a result a homonuclear gas like $N_2{}^{14}$ must be considered as a mixture of two different species, the so-called ortho and para modifications. In the case of nitrogen at 100 deg R and higher temperatures, the difference between the two modifications is entirely negligible; the method of calculating the properties of the ortho and para modifications, of the equilibrium mixture, and of the normal mixture at lower temperatures is discussed in general terms in many references, e.g. (4), and its application to the case of nitrogen is treated in a previous report from this laboratory (5). Of course, if the two atoms of the nitrogen molecule are different isotopes, as in the case of $N^{14}N^{15}$, the molecule is heteronuclear, and therefore its symmetry number is unity.

MATHEMATICAL REARRANGEMENT[6]

The first step in the evaluation of the internal state sum Q_{int} for the set of energy levels given by Equation [4] is to evaluate the sum over J for arbitrarily fixed values of the vibrational quantum number v. This can easily be done by application of the Euler-Maclaurin formula. The result is

$$\Sigma(2J+1)e^{[-b_1(1-s_1 v)J(J+1)+b_2(1-s_2 v)J^2(J+1)^2-\ldots]} = (\Sigma y_i v^i)/b_1 \ldots\ldots [5]$$

where the y_i are simple functions of $b_1 = c_2\tau B_0$, $b_2 = c_2\tau D_0$, $b_3 = c_2\tau F_0, \ldots.$, $s_1 = \alpha_0/B_0$, $s_2 = \beta_0/D_0, \ldots.$ which have been listed elsewhere (5) and need not be reproduced here. The summation on the left extends over all nonnegative, integral values of the rotational quantum number J. Strictly speaking, that on the right extends over all nonnegative, integral values of the index i. However, in the case of nitrogen and carbon monoxide the sum over i is very rapidly convergent, and in the temperature range here considered it is sufficient to include in the sum only the first seven terms.

Substitution of Equations [4] and [5] into Equation [1] yields

$$\sigma b_1 Q_{\text{int}} = \Sigma y_i v^i e^{[-c_2\tau(\omega_0 v - \omega_0 x_0 v^2 + \omega_0 y_0 v^3 - \ldots)]} \ldots\ldots [6]$$

The summation extends over i and v. The latter should cover all non-negative, integral values up to the dissociation limit. For nitrogen and carbon monoxide up to at most 5000 deg R, as long as only the first seven values of i are considered, no significant error is introduced by extending the summation over v to infinity.

The contribution to the exponential in Equation [6] from the quadratic and cubic terms in v can be reduced to a power series in v by expansion in a Taylor series. This reduction facilitates evaluation of the quantities Y_i defined by

$$Y_i = (1-x)\sum_{v=0}^{\infty} v^i x^v e^{c_2\tau(\omega_0 x_0 v^2 - \omega_0 y_0 v^3 + \ldots)}$$

where $x = e^{-c_2\tau\omega_0}$. Each Y_i is a combination of sums of the form

$$A_n = (1-x)\sum_{v=0}^{\infty} v^n x^v$$

These sums can be expressed as simple functions of $y = x/(1 - x)$, which have been listed elsewhere (1, 5).

After having evaluated the y_i and Y_i, it is a straightforward matter to calculate Q_{int} from

$$\sigma b_1(1-x)Q_{\text{int}} = \Sigma y_i Y_i = \alpha \ldots\ldots\ldots\ldots [7]$$

Algebraic expressions for the first and second derivatives of α are obtained easily (5) from the results just given and need not be reproduced here.

ZERO-PRESSURE PROPERTIES

Having evaluated the sum α in Equation [7] it is possible to write down convenient expressions for the various zero-pressure thermodynamic properties of particular interest. This part of the mathematical rearrangement is completely analogous to the corresponding part previously published for carbon dioxide

---

[5] B_e is inversely proportional to the largest principal moment of inertia I_e at the equilibrium internuclear separation, that is, $B_e = h/8\pi^2 c I_e$.

[6] A more detailed derivation of the working equations has been given elsewhere (5). It must be noted that the notation used in previous reports was slightly different from that used in this paper.

(1), and therefore only the final results will be given here. These are

$$[\log_e p - (g - \bar{u})/RT]_{p=0} = \frac{7}{2}\log_e T - \log_e(1 - e^{-\theta\tau}) + \log_e \alpha + \log_e[(2\pi Mk/h^2N_0)^{3/2}(k/\sigma c_2 B_0)\} \quad \ldots\ldots [8]$$

$$[(h - \bar{u})/RT]_{p=0} = \frac{7}{2} + \frac{\theta\tau}{e^{\theta\tau} - 1} + T\frac{d\log_e \alpha}{dT} \quad \ldots\ldots [8a]$$

$$[s/R + \log_e p]_{p=0} = [\log_e p - (g - \bar{u})/RT]_{p=0} + [(h - \bar{u})/RT]_{p=0} \quad \ldots\ldots [8b]$$

$$[c_p/R]_{p=0} = \frac{7}{2} + \frac{(\theta\tau)^2 e^{\theta\tau}}{(e^{\theta\tau} - 1)^2} + T\frac{d^2(T\log_e \alpha)}{dT^2} \quad \ldots\ldots [8c]$$

where again it is noted (*a*) that the free enthalpy g and the enthalpy h are subject to augmentation by a constant amount $\bar{u}$ representing the null-point energy, and (*b*) that the arguments of the logarithms in Equation [8] must be expressed in consistent units. The quantity $\theta = c_2\omega_0$ is the so-called characteristic temperature of the gas considered.

The terms containing $\log_e \alpha$ essentially represent the combined corrections for anharmonicity, rotational stretching, and rotation-vibration coupling. Approximate expressions for $\log_e \alpha$ have been obtained (5) and may be useful for rapid calculations of the properties of other similar gases. Formulas for correcting $\log_e \alpha$ and its derivatives for small changes in the spectroscopic constants have also been obtained (5). These formulas may be useful for future revisions of the tables, as well as for the calculation of the properties of other than the most abundant isotopes, in which case the tabulated values have to be corrected for small isotopic effects on the spectroscopic constants.

Physical Constants and Conversion Factors

In conformity with the practice of this laboratory the 1941 Birge (6) values of the general physical constants have been used consistently. As explained in another report (2), the probable errors given by Birge have been revised on the basis of the analysis of DuMond and Cohen (7). The adopted constants are

$$R = (8.31436 \pm 0.00038) \times 10^7 \text{ erg deg K}^{-1}\text{ g-mol}^{-1}$$

$$c_2 = 1.43848 \pm 0.00024 \text{ cm deg K}$$

$$\log_e[(2\pi k/h^2N_0)^{3/2}k] = -5.13397_5 \pm 0.00065 \text{ (with argument in g-mol}^{3/2}\text{ atm deg R}^{-5/2}\text{g}^{-3/2})$$

ratio of physical to chemical atomic weights = 1.000272 ± 0.000005

Following usual steam-table practice, the Btu has been used as unit of energy in preparing the tables presented in this report. The particular Btu used is defined by the following conversion factors: 1.8 Btu g/ITcal lb and 860/1.00020 ITcal/abs kwhr.[7] Temperature on the Rankine scale (deg R) is used as independent argument and the pound-mol (mol) is used as unit of weight, in order to simplify the analysis of problems involving gas mixtures. In the case of reduced entropy $s + R\log_e p$, it is to be understood that pressure is expressed in international atmospheres (atm).

Atomic Weights

The available data on the weights of the various isotopes of carbon, oxygen, and nitrogen have been reviewed in a previous report (2). The values used in the present calculations are those recommended by Birge (6), for consistency with previous calculations from this laboratory. The changes indicated by more recent data are altogether negligible. The adopted values of the isotopic weights and of the relevant abundance ratios are listed in Table 1.

TABLE 1 ISOTOPIC WEIGHTS OF CARBON, OXYGEN, AND NITROGEN (PHYSICAL SCALE)

Isotope	Weight	Abundance
C^{12}	12.00386	92
C^{13}	13.00761	1
N^{14}	14.00753	270
N^{15}	15.0049	1
O^{16}	16.0000	506
O^{17}	17.0045	0.204
O^{18}	18.0049	1

The molecular weights of the various possible carbon monoxide and nitrogen molecules can be computed directly from the data in Table 1, converting them to the chemical scale by division by 1.000272. The following are of particular interest:

$C^{12}O^{16}$: M = 27.99625 (chemical scale)
CO : M = 28.01139 (normal isotopic mixture, chemical scale)
N_2^{14} : M = 28.00744 (chemical scale)
N_2 : M = 28.01480 (normal isotopic mixture, chemical scale)

The values for the normal isotopic mixtures are in excellent agreement with those adopted by the Committee on Atomic Weights of the International Union of Chemistry (8).

Spectroscopic Constants for Nitrogen

The best complete analysis of the vibrational structure of the ground electronic level ($X^1\Sigma^+_g$) of diatomic nitrogen is that given by Birge and Hopfield (9) in 1928; they give for the vibrational contribution to the wave numbers

$$2345.16\, v - 14.445\, v^2 \text{ (cm}^{-1})$$

The constants in this expression are subject to a relatively large uncertainty since they were obtained from the band heads rather than the band origins. Several new bands have been analyzed since 1928 (10, 11, 12, etc.). All these newer results indicate that there should be no revision of the first two vibrational constants, even though R. Herman (12), on the basis of her own measurements as well as those of Wulf and Melvin and of Janin, proposes the addition of cubic and quartic terms, obtaining the following expression for the vibrational contribution

$$2345.16\, v - 14.445\, v^2 + 0.0064958\, v^3 - 0.000509\, v^4 \text{ (cm}^{-1})$$

The contribution from the last two constants to the thermodynamic properties up to 5000 deg R is not significant. Therefore, since these two constants appear to have a rather large probable error, it was decided not to include them in the present calculations. Available data do not permit a reliable estimate of the uncertainties of the vibrational constants just quoted. More or less arbitrarily we have assumed a probable error of ±0.1 cm^{-1} for the first constant 2345.16, and a probable error of ±0.01 cm^{-1} for the second constant 14.445.

The earlier rotational analyses have been revised by Watson and Koontz (13), whose results have been confirmed by Spinks (14). According to their analysis, the rotational constants for the ground electronic state of nitrogen are

$$B_0 = 1.998 \pm 0.002 \text{ cm}^{-1}; \quad \alpha_0 = 0.018 \text{ cm}^{-1}$$

It appears safe to assume that the probable error of α_0 is at most ±0.001 cm^{-1}. These values are in excellent agreement with the somewhat less accurate values obtained by Rasetti (15) from the Raman spectrum, and by Janin (10) from the Vegard-Kaplan bands. Other rotational constants have not been determined from direct measurements but may be calculated from approximate theoretical equations which are reviewed by Jevons (16) and Birge (17). Spinks (14) lists values of D_e and β_0 calculated from these formulas; however, his values are only preliminary and are not correct. From the constants adopted for these calculations and the quoted formulas, we obtain

---

[7] In the previous report on the properties of carbon dioxide (1) the conversion factor 860/1.00019 ITcal/abs kwhr was given by mistake. Actually the value 860/1.00020 had been used in the calculations, with the corresponding value R = 1.98581 Btu/mol deg R.

$$D_0 = 5.808 \times 10^{-6}\ \mathrm{cm}^{-1};\quad F_0 = 4 \times 10^{-12}\ \mathrm{cm}^{-1}$$

The calculated values of β_0 and of other rotational constants are negligible. While it is not possible to state the probable error of the constants thus obtained, it seems safe to assume that the probable error of the value of D_0 given in the foregoing does not exceed 0.1×10^{-6} cm^{-1}, and that the probable error of F_0 has no significant effect on the accuracy of the thermodynamic properties herein presented.

In conclusion the constants adopted for the ground electronic state of diatomic nitrogen (N_2^{14}) are those listed in Table 2. Constants not listed there are assumed to be negligibly small. The first excited electronic state is the $A^3\Sigma^+_u$ state, which is about 50,000 cm^{-1} above the ground state (3), and therefore does not make a significant contribution to the thermodynamic properties in the temperature range here considered.

TABLE 2 SPECTROSCOPIC CONSTANTS FOR NITROGEN (N_2^{14}) IN THE GROUND ELECTRONIC STATE

$\omega_0 = 2345.16 \pm 0.1\ \mathrm{cm}^{-1}$
$\omega_0 x_0 = 14.445 \pm 0.01\ \mathrm{cm}^{-1}$
$B_0 = 1.998 \pm 0.002\ \mathrm{cm}^{-1}$
$\alpha_0 = 0.018 \pm 0.001\ \mathrm{cm}^{-1}$
$D_0 = (5.808 \pm 0.1) \times 10^{-6}\ \mathrm{cm}^{-1}$
$F_0 = 4 \times 10^{-12}\ \mathrm{cm}^{-1}$

The data given in Table 2 suffice also for the calculation of the constants for N_2^{15} and $N^{14}N^{15}$. Indeed, the vibrational and rotational constants of isotopes are related through the following theoretical equations (18)

$$\left.\begin{array}{ll} \omega_e^i = \rho\omega_e & \omega_e^i x_e^i = \rho^2\omega_e x_e \\ B_e^i = \rho^2 B_e & \alpha_e^i = \rho^3\alpha_e \\ D_e^i = \rho^4 D_e & \rho = \sqrt{\mu/\mu^i} \end{array}\right\} \ldots\ldots\ldots [9]$$

where superscript i indicates the heavier isotope and μ is reduced mass. It must be noted again that $N^{14}N^{15}$ is heteronuclear and therefore has a symmetry number $\sigma = 1$.

Spectroscopic Constants for Carbon Monoxide

Until recently the best available analysis of the vibrational structure of the ground electronic level ($X^1\Sigma^+$) of carbon monoxide was that given by Read (19), and the most reliable set of rotational constants was that of Gerö, Herzberg, and Schmid (20). A tabulation of the thermodynamic properties of carbon monoxide based upon those constants has been issued by this laboratory (21). Recently, new data have been obtained and a more accurate analysis has been completed by associates of G. Herzberg. Dr. Herzberg has very kindly communicated to us the new spectroscopic constants in advance of publication. These constants, which have been adopted for the calculation of the tables of properties herein presented, are listed in Table 3. The probable error in each constant will be assumed to be five units in the last tabulated figure, except in the case of B_e and α_0, in which case the probable error will be assumed to be five units in the penultimate figure. This assignment of probable errors is quite arbitrary, but sufficient data are not available to the authors for a more rational assignment. The additional constant $F_0 = 6.5 \times 10^{-12}$ has been calculated from previously mentioned, theoretical formulas (16, 17). Other constants are considered to be negligible. The first excited electronic state of carbon monoxide is the $a^3\Pi$ state, which is about 48,000 cm^{-1} above the ground state (3, 22), and therefore makes no significant contribution to the tabulated properties in the temperature range here considered. The properties of other isotopes may be obtained easily by means of Equation [9].

TABLE 3 SPECTROSCOPIC CONSTANTS FOR CARBON MONOXIDE ($C^{12}O^{16}$) IN THE GROUND ELECTRONIC STATE

$\omega_e = 2170.21\ \mathrm{cm}^{-1}$
$\omega_e x_e = 13.461\ \mathrm{cm}^{-1}$
$\omega_e y_e = 0.0308\ \mathrm{cm}^{-1}$
$B_e = 1.9313_9\ \mathrm{cm}^{-1}$
$\alpha_e = 0.01748_5\ \mathrm{cm}^{-1}$
$D_e = 6.43 \times 10^{-6}\ \mathrm{cm}^{-1}$
$\beta_e = -0.04 \times 10^{-6}\ \mathrm{cm}^{-1}$

Final Results

The final results of the present calculations are given in Table 4. It might be well to repeat that the data listed in this table are characterized by computational accuracy well beyond present physical accuracy. The unit of energy used is the (International Steam Tables) Btu in terms of which the universal gas constant R has the value 1.98581 Btu/mol deg R. The usual practice of excluding the contribution to the reduced entropy from nuclear spin has been followed.

The probable errors of the tabulated data arise from several separate factors. All the properties contain as a factor the universal gas constant R, and therefore have at least a relative error equal to the relative error of R. The latter depends on the choice of units. If the units chosen can be defined directly in terms of the absolute units of energy, then the relative error contributed by R is ± 0.000046 or ± 0.0046 per cent. If the units chosen are defined in terms of the international electrical units, then the relative error contributed by R is about twice as much, namely, ± 0.000091 or ± 0.0091 per cent.

In order to discuss the other sources of error independently of R, we shall consider next the errors in the dimensionless quantities obtained by dividing by R the following tabulated properties: reduced entropy, mean isobaric specific heat, and specific heat. In the case of the last two named quantities, the probable error originates only from errors in the rotational-vibrational contributions. This probable error is shown in Fig. 1. In the case of the entropy, an additional probable error of about ± 0.0007 (dimensionless) arises from the translational contribution. In this case most of the error in the rotational contribution arises from the classical term $\log_e(c_2 B_0 \tau)$. The probable error of this term has the value ± 0.0012 in the case of nitrogen, and ± 0.00043 in the case of carbon monoxide. Since these errors are constant, they cancel in calculations for processes not involving chemical changes. Therefore, only the probable errors in the rotational-vibrational contributions exclusive of the classical term $\log_e (c_2 B_0 \tau)$ are of general interest. These are shown graphically in Fig. 1.

The zero-pressure properties presented in this paper apply to the most abundant isotopes, namely, carbon monoxide $C^{12}O^{16}$ and nitrogen N_2^{14}. All the data necessary to obtain the properties of molecules containing other isotopes have been given in this report, and these properties may be obtained easily by applying small corrections to the values listed in Table 4. Detailed tables for each isotope are not given here because of space limitations.

Regarding the thermodynamic properties of the normal isotopic mixture of nitrogen (N_2), the following statements may be made: Its enthalpy and isobaric specific heat are almost identical with those of the most abundant isotope N_2^{14}; its reduced entropy exceeds that of N_2^{14} by about 0.00078 Btu/mol deg R because it contains some isotopes of higher molecular weight M than that of N_2^{14}, by about 0. 0102 Btu/mol deg R because the statistical weights p_i of $N^{14}N^{15}$ differ from those of N_2^{14}, and by a mixing entropy of about 0.086 Btu/mol deg R.

TABLE 4 ZERO-PRESSURE PROPERTIES OF DIATOMIC NITROGEN (N_2^{14}) AND OF CARBON MONOXIDE ($C^{12}O^{16}$)

T degR	Reduced Entropy $(s + R\log_e p)_{p=0}$ Btu/mol degR		Mean Isobaric Specific Heat $[(h-\bar{u})/T]_{p=0}$ Btu/mol degR		Enthalpy $(h-\bar{u})_{p=0}$ Btu/mol		Isobaric Specific Heat $c_{p=0}$ Btu/mol degR	
	N_2	CO	N_2	CO	N_2	CO	N_2	CO
100	34.04942	35.50111	6.91620	6.91754	691.620	691.754	6.95091	6.95099
105	34.38855	35.84025	6.91785	6.91913	726.374	726.509	6.95092	6.95100
110	34.71191	36.16361	6.91935	6.92058	761.129	761.264	6.95093	6.95102
115	35.02089	36.47260	6.92073	6.92191	795.884	796.019	6.95095	6.95104
120	35.31672	36.76343	6.92199	6.92312	830.638	830.774	6.95096	6.95106
125	35.60047	37.05219	6.92315	6.92424	865.393	865.530	6.95097	6.95108
130	35.87309	37.32482	6.92422	6.92527	900.148	900.285	6.95099	6.95110
140	36.38822	37.83995	6.92613	6.92712	969.658	969.796	6.95103	6.95114
150	36.86779	38.31953	6.92779	6.92872	1039.17	1039.31	6.95106	6.95119
160	37.31640	38.76815	6.92925	6.93013	1108.68	1108.82	6.95110	6.95123
170	37.73781	39.18957	6.93053	6.93137	1178.19	1178.33	6.95114	6.95128
180	38.13513	39.58690	6.93168	6.93248	1247.70	1247.85	6.95118	6.95133
190	38.51096	39.96274	6.93271	6.93347	1317.21	1317.36	6.95122	6.95138
200	38.86751	40.31930	6.93363	6.93437	1386.73	1386.87	6.95126	6.95143
210	39.20667	40.65846	6.93447	6.93518	1456.24	1456.39	6.95131	6.95148
220	39.53004	40.98184	6.93524	6.93592	1525.75	1525.90	6.95135	6.95153
230	39.83905	41.29085	6.93594	6.93660	1595.27	1595.42	6.95139	6.95159
240	40.13489	41.58671	6.93659	6.93723	1664.78	1664.94	6.95143	6.95164
260	40.69131	42.14314	6.93773	6.93834	1803.81	1803.97	6.95152	6.95174
280	41.20648	42.65833	6.93872	6.93930	1942.84	1943.00	6.95161	6.95185
300	41.68609	43.13796	6.93958	6.94014	2081.87	2082.04	6.95170	6.95196
320	42.13474	43.58663	6.94034	6.94088	2220.91	2221.08	6.95179	6.95207
340	42.55620	44.00810	6.94102	6.94155	2359.95	2360.13	6.95188	6.95220
360	42.95356	44.40548	6.94162	6.94214	2498.98	2499.17	6.95199	6.95236
380	43.32944	44.78138	6.94217	6.94268	2638.03	2638.22	6.95211	6.95257
400	43.68604	45.13801	6.94267	6.94319	2777.07	2777.27	6.95227	6.95284
420	44.02524	45.47725	6.94313	6.94365	2916.12	2916.34	6.95247	6.95322
440	44.34868	45.80072	6.94356	6.94410	3055.17	3055.40	6.95273	6.95375
460	44.65775	46.10984	6.94397	6.94453	3194.23	3194.49	6.95310	6.95448
480	44.95368	46.40584	6.94436	6.94497	3333.29	3333.59	6.95359	6.95545
500	45.23755	46.68980	6.94474	6.94541	3472.37	3472.71	6.95425	6.95674
550	45.90048	47.35306	6.94572	6.94665	3820.14	3820.66	6.95695	6.96174
600	46.50599	47.95914	6.94683	6.94823	4168.10	4168.94	6.96171	6.97003
650	47.06351	48.51750	6.94825	6.95035	4516.36	4517.73	6.96930	6.98244
700	47.58037	49.03555	6.95012	6.95322	4865.09	4867.26	6.98034	6.99952
750	48.06245	49.51919	6.95262	6.95702	5214.46	5217.76	6.99529	7.02153
800	48.51450	49.97318	6.95586	6.96167	5564.69	5569.49	7.01440	7.04847
850	48.94043	50.40142	6.95997	6.96787	5915.97	5922.69	7.03768	7.08005
900	49.34344	50.80710	6.96502	6.97507	6268.52	6277.57	7.06500	7.11584
950	49.72624	51.19288	6.97109	6.98351	6622.53	6634.33	7.09607	7.15530
1000	50.09109	51.56096	6.97818	6.99315	6978.18	6993.15	7.13050	7.19780
1100	50.77423	52.25123	6.99546	7.01587	7695.01	7717.45	7.20755	7.28949
1200	51.40496	52.88963	7.01663	7.04268	8419.95	8451.22	7.29235	7.38631
1300	51.99216	53.48472	7.04124	7.07289	9153.62	9194.76	7.38135	7.48447
1400	52.54248	54.04294	7.06876	7.10576	9896.26	9948.06	7.47161	7.58119
1500	53.06102	54.56919	7.09860	7.14059	10647.9	10710.9	7.56087	7.67453
1600	53.55178	55.06736	7.13022	7.17676	11408.4	11482.8	7.64757	7.76330
1700	54.01792	55.54054	7.16312	7.21375	12177.3	12263.4	7.73063	7.84685
1800	54.46204	55.99129	7.19685	7.25111	12954.3	13052.0	7.80942	7.92490
1900	54.88629	56.42173	7.23107	7.28851	13739.0	13848.2	7.88363	7.99745
2000	55.29245	56.83368	7.26546	7.32566	14530.9	14651.3	7.95317	8.06464
2200	56.05649	57.60807	7.33381	7.39841	16134.4	16276.5	8.07854	8.18409
2400	56.76418	58.32466	7.40050	7.46824	17761.2	17923.8	8.18697	8.28584
2600	57.42327	58.99140	7.46468	7.53455	19408.2	19589.8	8.28053	8.37260
2800	58.03995	59.61467	7.52591	7.59713	21072.5	21272.0	8.36132	8.44687
3000	58.61927	60.19967	7.58399	7.65597	22752.0	22967.9	8.43130	8.51079
3200	59.16540	60.75076	7.63890	7.71116	24444.5	24675.7	8.49219	8.56614
3400	59.68187	61.27156	7.69069	7.76291	26148.3	26393.9	8.54543	8.61438
3600	60.17167	61.76516	7.73950	7.81141	27862.2	28121.1	8.59225	8.65671
3800	60.63736	62.23423	7.78550	7.85690	29584.9	29856.2	8.63366	8.69412
4000	61.08116	62.68104	7.82884	7.89961	31315.4	31598.4	8.67049	8.72738
4200	61.50501	63.10759	7.86972	7.93975	33052.8	33347.0	8.70345	8.75717
4400	61.91059	63.51560	7.90830	7.97753	34796.5	35101.1	8.73308	8.78400
4600	62.29939	63.90661	7.94475	8.01313	36545.9	36860.4	8.75990	8.80832
4800	62.85398	64.28196	7.97924	8.04673	38300.3	38624.3	8.78429	8.83050
5000	63.03178	64.64286	8.01189	8.07849	40059.4	40392.5	8.80659	8.85083

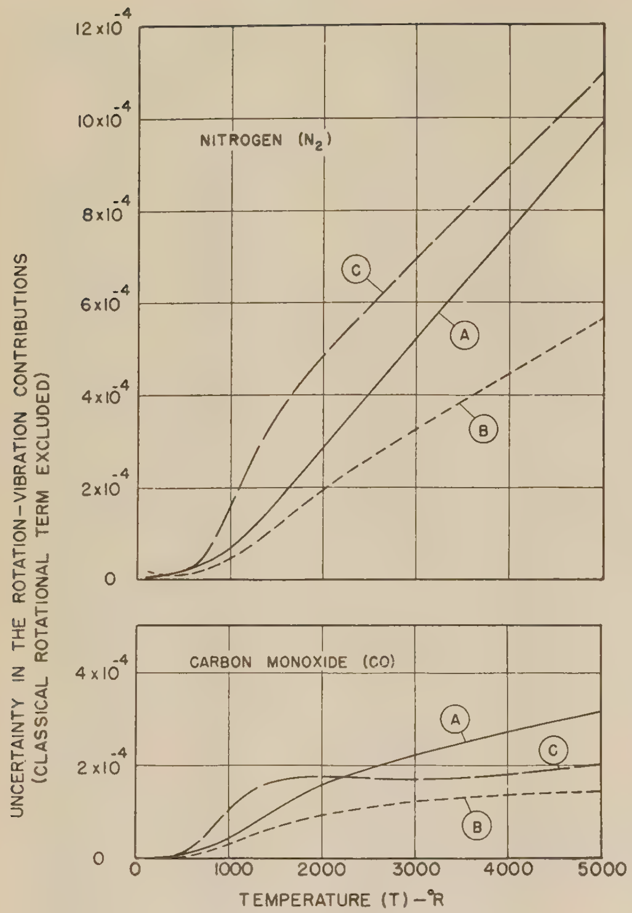

Fig. 1 Uncertainty in Thermodynamic Properties

(A, Reduced entropy; B, mean isobaric specific heat; C, isobaric specific heat.)

The mixing entropy has been estimated on the assumption that the mixture contains in significant concentration only N_2^{14} and $N^{14}N^{15}$.

Regarding the thermodynamic properties of the normal isotopic mixture of carbon monoxide (CO), the following statements may be made: Its enthalpy and isobaric specific heat are almost identical with those of the most abundant isotopes $C^{12}O^{16}$; its reduced entropy exceeds that of $C^{12}O^{16}$ by about 0.00161 Btu/mol deg R because it contains some isotopes of higher molecular weight M than that of $C^{12}O^{16}$, and by a mixing entropy of about 0.153 Btu/mol deg R. The mixing entropy has been estimated on the assumption that the mixture contains in significant concentration only $C^{12}O^{16}$, $C^{12}O^{17}$, $C^{12}O^{18}$, $C^{13}O^{16}$.

In addition to the foregoing corrections there are, strictly speaking, some temperature-dependent corrections to account for the isotopic effect on the rotational and vibrational constants. These, however, can reasonably be expected not to exceed the uncertainties in the calculated properties, and therefore may be ignored.

Comparison With Other Data

The first extensive tabulation of the zero-pressure thermodynamic properties of nitrogen is that of Giauque and Clayton (23), who published tables of the free enthalpy of this gas. Trautz and Adler (24) published tables of the specific heat of nitrogen and other gases, but their tables were rather inaccurate. Johnston and Davis (25) reviewed the available data on the spectroscopic constants and calculated tables of the entropy and of the specific heat of nitrogen. Wagman, et al (26) corrected the Johnston and Davis tables for recent changes in the accepted values of the general physical constants and atomic weights, but not for some significant changes in the rotational constants. Woolley (27) in 1944, prepared an unpublished tabulation of the principal thermodynamic properties of nitrogen by correcting the Johnston and Davis tables for changes in the rotational constants as well as in the general physical constants and atomic weights. In 1944, Woolley used essentially the same constants as those herein adopted, except that he apparently used the incorrect values of D_e and β_0 given by Spinks (14). In 1947 Woolley revised and extended his earlier tables, presumably using the spectroscopic constants adopted for the calculations of tables previously issued from this laboratory (5).

The results of the present calculations for nitrogen are compared with those of previous authors in Table 5, the comparison being based on the isobaric specific heat $c_{p=0}$. In the second column are listed the original Johnston and Davis (25) values converted to Btu/mol deg R by multiplication by 1.98581/1.9869 = 0.99945. In the third column are listed the Wagman, et al, (26) revisions of the Johnston and Davis values converted to Btu/mol deg R by multiplication by 1.98581/1.98718 = 0.99931. In the fourth column are listed values interpolated from our final tables rounded off to the number of figures used by the other authors for greater ease of comparison. No comparison with the 1947 Woolley (27) unpublished tables is shown, since his tables are essentially equivalent to ours, except for the fact that we maintained greater computational accuracy.

TABLE 5 ZERO-PRESSURE ISOBARIC SPECIFIC HEAT OF NITROGEN

(Values in Btu/mol deg R)

T, deg R	Johnston and Davis	Wagman	Goff and Gratch
180	6.951	...	6.951
900	7.067	7.065	7.065
1800	7.817	7.811	7.809
2700	8.329	8.324	8.322
3600	8.599	8.596	8.592
4500	8.756	8.753	8.747

While the differences between the three sets of values listed in Table 5 are small, they are significant, since they definitely exceed the probable error of our values. The conclusions to be drawn from comparisons of the other properties are similar; these comparisons are not shown here because of space limitations. It should be noted that most of the previous tabulations are for the normal isotopic mixture, but they do not include the mixing entropy and the effect of the heteronuclearity of $N^{14}N^{15}$. Therefore the values of reduced entropy given by the other authors should exceed our values for N_2^{14} by about 0.0015 Btu /mol deg R because of differences in molecular weights.

The first extensive tabulation of the zero-pressure thermodynamic properties of carbon monoxide is that of Clayton and Giauque (28), who published tables of the free enthalpy of this gas. Kassel (29) tabulated the specific heat of carbon monoxide. Gordon and Barnes (30) calculated a single set of values of the thermodynamic properties of carbon monoxide at 3000 deg K. Johnston and Davis (25) reviewed the available data on the spectroscopic constants and calculated tables of the entropy and of the specific heat of carbon monoxide. Wagman, et al (26) corrected the Johnston and Davis tables for recent changes in the accepted values of the general physical constants and atomic weights, but not for some significant changes in the spectroscopic constants.

The results of the present calculations for carbon monoxide are compared with those of previous authors in Table 6, the comparison being based on the isobaric specific heat $c_{p=0}$. In the second column are listed the Kassel (29) values converted to

TABLE 6 ZERO-PRESSURE ISOBARIC SPECIFIC HEAT OF CARBON MONOXIDE

(Values in Btu/mol deg R)

T, deg R	Kassel	Johnston and Davis	Wagman	Goff and Gratch
180	6.949	6.950	...	6.951
900	7.111	7.118	7.115	7.116
1800	7.914	7.932	7.927	7.925
2700	8.390	8.417	8.413	8.411
3600	8.626	8.662	8.659	8.657
4500	8.758	8.802	8.800	8.796

Btu/mol deg R by multiplication by 0.99945. In the third column are listed the Johnston and Davis (25) values similarly converted to Btu/mol deg R. In the fourth column are listed the Wagman, et al (26) revisions of the Johnston and Davis values converted to Btu/mol deg R by multiplication by 0.99931. In the fifth column are listed values interpolated from our final tables rounded off to the number of figures used by the other authors for greater ease of comparison.

The differences between the four sets of values listed in Table 6 are small but significant, since they definitely exceed the probable error of our values. The differences of our tables from the previous tabulations are due primarily to the recent revision of the vibrational and rotational constants. As in the case of nitrogen, no comparison of the other properties is given here because of space limitations. In the case of the entropy, since the tables by other authors are for the normal isotopic mixture (mixing entropy excluded), the values given by the other authors should exceed our values for $C^{12}O^{16}$ by about 0.0032 Btu/mol deg R because of differences in molecular weights.

As has been previously pointed out by Johnston and Davis (25), the available results from calorimetric adiabatic expansion, velocity of sound, and explosion measurements are much less accurate than those from spectroscopic data, at least in the case of carbon monoxide and nitrogen. Anyway a partial comparison with those data (based on isobaric specific heat) is shown in Fig. 2. The older data, in particular those from acoustic velocity measurements, have been omitted since they are too inaccurate. Also several recent results near room temperature have been omitted to avoid overcrowding the graph. The two points credited to Fenning and Whiffin (35) were calculated from their formulation, which supposedly is valid from 2370 to 3060 deg K. The points credited to Henry (31) are Henry's smoothed values, and not the original experimental values. The most accurate values used for this comparison are probably those obtained by Eucken and Lüde (32) and by Eucken and Mücke (33) by means of an adiabatic expansion experiment; these values are reported to be accurate to about 0.1 per cent. The Eucken and Lüde (32) results for nitrogen, which are in excellent agreement with the spectroscopic values, could not be shown in Fig. 2 because of overcrowding.

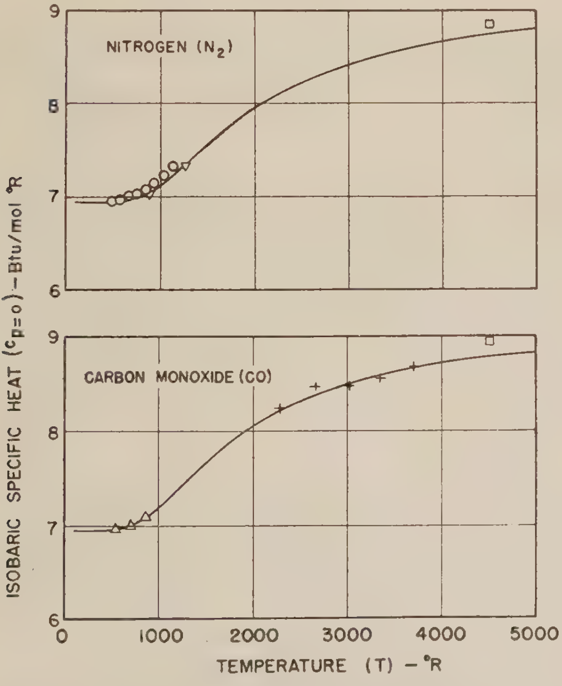

FIG. 2 COMPARISON WITH OTHER DATA
(—Goff-Gratch; ○ Henry (31); △ Eucken-Lüde (32); ▽ Eucken-Mücke (33); + Sherratt-Griffiths (34); □ Fenning-Whiffin (35).)

Taking account of the relative lack of accuracy of the experimental values, their agreement with the spectroscopic values is quite satisfactory.

ACKNOWLEDGMENT

It is a pleasure for the authors to acknowledge the extremely valuable advice and suggestions of Dr. Gerhard Herzberg, Director, Division of Physics, National Research Council of Canada. It is also a pleasure to acknowledge the substantial co-operation of the Navy Department, Bureau of Ships, which sponsored the project leading to the preparation of the tables presented in this report. The co-operation of the computational staff of the Thermodynamics Research Laboratory is also gratefully acknowledged.

BIBLIOGRAPHY

1 "Zero-Pressure Thermodynamic Properties of Carbon Dioxide," by Serge Gratch, Trans. ASME, vol. 71, 1949, pp. 897–902.

2 "Zero-Pressure Thermodynamic Properties of Some Monatomic Gases," by J. A. Goff, Serge Gratch, and S. W. Van Voorhis, Trans. ASME, vol. 72, 1950, pp. 725–739.

3 "Molekülspektren," by H. Sponer, Julius Springer, Berlin, vol. 1, 1935 (Tabellen), pp. 14, 32.

4 "Statistical Thermodynamics," by R. H. Fowler and E. A. Guggenheim, Cambridge University Press, London, 1939, p. 187.

5 "Zero-Pressure Properties of Diatomic Gases. I. Nitrogen," by Serge Gratch, Annual Report From the Thermodynamics Research Laboratory, University of Pennsylvania, July, 1946, Project G-3.

6 "A New Table of Values of the General Physical Constants," by R. T. Birge, *Reviews of Modern Physics*, vol. 13, 1941, pp. 233–239.

7 "Our Knowledge of the Atomic Constants F, N, m, and h in 1947, and of Other Constants Derivable Therefrom," by J. W. M. DuMond and E. R. Cohen, *Reviews of Modern Physics*, vol. 20, 1948, pp. 82–108; see also "Erratum," privately communicated, received April 23, 1949.

8 "Thirteenth Report of the Committee on Atomic Weights of the International Union of Chemistry," by G. P. Baxter, M. Guichard, and R. Whytlaw-Gray, *Journal of the American Chemical Society*, vol. 69, 1947, pp. 731–736.

9 "The Ultra-Violet Band Spectrum of Nitrogen," by R. T. Birge and J. J. Hopfield, *Astrophysical Journal*, vol. 68, 1928, pp. 257–278.

10 "Le spectre d'émission de l'azote sous la pression atmosphérique. Analyse des bandes du système de Vegard-Kaplan," by J. Janin, *Cahiers de physique*, vol. 18, Dec., 1943, pp. 48–54.

11 "Extension of the A-X System of Nitrogen," by R. Herman, *Nature*, vol. 157, 1946, p. 843; see also Comptes rendus des séances de l'Académie des sciences, vol. 222, 1946, pp. 1226–1227.

12 "Contribution a l'étude des spectre de la molécule d'azote," by R. Herman, *Annales de physique*, vol. 20, 1945, pp. 241–291.

13 "Nitrogen Molecular Spectra in the Vacuum Ultraviolet," by W. W. Watson and P. G. Koontz, *Physical Review*, vol. 45, 1934, p. 561; ibid., vol. 46, 1934, pp. 32–37.

14 "Rotational Structure of the Birge-Hopfield Bands of N_2," by J. W. T. Spinks, *Canadian Journal of Research*, vol. 20, sect. A, 1942, pp. 1–5.

15 "Incoherent Scattered Radiation in Diatomic Molecules," by F. Rasetti, *Physical Review*, vol. 34, 1929, pp. 367–371.

16 "Band-Spectra of Diatomic Molecules," by W. Jevons, The Physical Society, London, Cambridge University Press, 1932, p. 27.

17 "Molecular Spectra in Gases," by E. C. Kemble, R. T. Birge, W. F. Colby, F. W. Loomis, and L. Page, *Bulletin of the National Research Council*, vol. 11, part 3, December, 1926, p. 237.

18 "Molecular Spectra and Molecular Structure. I. Diatomic Molecules," by G. Herzberg, Prentice-Hall, Inc., New York, N. Y., 1939, pp. 151–155.

19 "Rotational and Vibrational Structure of the Fourth Positive Bands of Carbon Monoxide," by D. N. Read, *Physical Review*, vol. 46, 1934, pp. 571–575.

20 "On the Cameron Bands ($^3\Pi$ — $^1\Sigma$) of Carbon Monoxide," by L. Gerö, G. Herzberg, and R. Schmid, *Physical Review*, vol. 52, 1937, pp. 467–471.

21 "Zero-Pressure Properties of Diatomic Gases. II. Carbon Monoxide," by Serge Gratch, Annual Report From the Thermodynamics Research Laboratory, University of Pennsylvania, July, 1947, Project G-3.

22 "Zur Vervollständingung des Termschemas von Kohlenoxyd. II," by R. Schmid and L. Gerö, *Zeit. für Physik*, vol. 106, 1937, pp. 205–211.

23 "The Heat Capacity and Entropy of Nitrogen. Heat of Vaporization. Vapor Pressure of Solid and Liquid. The reaction $^1/_2\,N_2 + {}^1/_2\,O_2 = NO$ from Spectroscopic Data," by W. F. Giauque and J O. Clayton, *Journal of the American Chemical Society*, vol. 55, 1933, pp. 4875–4889.

24 "Spektroskopische Berechnung der Molwärmen von Luft, O_2, N_2," by M. Trautz and H. Adler, *Zeit. für Physik*, vol. 89, 1934, pp. 1–11.

25 "Heat Capacity Curves of the Simpler Gases. IV. Extension of the 'Free Energy' Formula of Giauque and Overstreet to Yield Reliable Approximation Formulas for the Calculation of Entropy and of Heat Capacity From Spectroscopic Data. Entropy and Heat Capacity of Carbon Monoxide and of Nitrogen From Near Zero Absolute to 5000°K," by H. L. Johnston and C. O. Davis, *Journal cf the American Chemical Society*, vol. 56, 1934, pp. 271–276.

26 "Heats, Free Energies, and Equilibrium Constants of Some Reactions Involving O_2, H_2, H_2O, C, CO, CO_2," by D. D. Wagman, J. E. Kilpatrick, W. J. Taylor, K. S. Pitzer, and F. D. Rossini, *Journal of Research* of the National Bureau of Standards, vol. 34, 1945, pp. 143–161, Research Paper RP1634.

27 "Thermodynamic Functions for Molecular Nitrogen in the Ideal Gas State," by H. W. Woolley, National Bureau of Standards, private communication, unpublished, 1944; revised, 1947.

28 "The Heat Capacity and Entropy of Carbon Monoxide. Heat of Vaporization. Vapor Pressures of Solid and Liquid. Free Energy to 5000°K From Spectroscopic Data," by J. O. Clayton and W. F. Giauque, *Journal of the American Chemical Society*, vol. 54, 1932, pp. 2610–2626; ibid., vol. 55, 1933, pp. 5071–5073.

29 "Mathematical Methods for Computing Thermodynamic Functions from Spectroscopic Data," by L. S. Kassel, *Journal of Chemical Physics*, vol. 1, 1933, pp. 576–585.

30 "Evaluation of the Series Which Arise in the Calculation of Thermodynamic Quantities from Spectroscopic Data," by A. R. Gordon and C. Barnes, *Journal of Chemical Physics*, vol. 1, 1933, pp. 297–307.

31 "Specific Heats of Air, Oxygen, Nitrogen From 20°C to 370°C," by P. S. H. Henry, Proceedings of the Royal Society of London, part A, vol. 133, 1931, pp. 492–506.

32 "Die spezifische Wärme der Gase bei mittleren und hohen Temperaturen. I. Die spezifische Wärme der Gase; Luft, Stickstoff, Sauerstoff, Kohlenoxyd, Kohlensäure, Stickoxydul und Methan zwischen 0° und 220°C," by A. Eucken and K. v. Lüde, *Zeit. für Physikalische Chemie*, part B, vol. 5, 1929, pp. 413–441.

33 "Die Bestimmung der wahren spezifischen Wärme einiger Gase bei hohen Temperaturen nach der Lummer-Pringsheimschen Methode," by A. Eucken, and O. Mücke, *Zeit. für Physikalische Chemie*, part B, vol. 18, 1932, pp. 167–188.

34 "The Determination of the Specific Heat of Gases at High Temperatures by the Sound Velocity Method. I. Carbon Monoxide," by G. G. Sherratt and E. Griffiths, Proceedings of the Royal Society of London, series A, vol. 147, 1934, pp. 292–308.

35 "The Specific Heat of Gases at High Temperatures," by R. W. Fenning and A. C. Whiffin, Philosophical Transactions of the Royal Society of London, series A, vol. 238, 1939, pp. 149–212.

Discussion

H. W. Woolley.[8] The computations described in this paper seem to have been made carefully and to show considerable ingenuity in the arrangement of the method of calculation.

In regard to nitrogen, the writer wishes to apologize for some ambiguity in his private communication of 1944 (27),[9] which must have led to the statement that for one of his tables incorrect spectroscopic constants D_e and β_0, given by Spinks (14), apparently were used. Spinks' constants were not used, but instead computed constants which were essentially identical with those used in the present paper. Before accepting the statement that the constants by Spinks are incorrect, one might consider a deviation plot of divided differences of vibrational term values, according to actual observational data (9, 15),[10] as shown in Fig. 3 of this discussion. The sloping straight line represents the equation given by Birge and Hopfield, drawn with a half-width equal to 0.1 cm,$^{-1}$ the uncertainty assigned to ω by the authors of the present paper. The scattering of the data of Birge and Hopfield are regarded by the writer as consistent with careful measurement, since they had to measure their photographic film to $^1/_{1000}$ mm to determine a line to one wave number. The uncertainty of 2 cm,$^{-1}$ given by Rasetti for his 1929 Raman value, is shown on the diagram. The 1938 Raman value of Miller is 2.4 cm^{-1} below the value of Rasetti. If one takes the uncertainty in ω from that for the Raman data, and the uncertainty in α as assigned by the authors, then the values of Spinks for D and β are covered by their uncertainties.

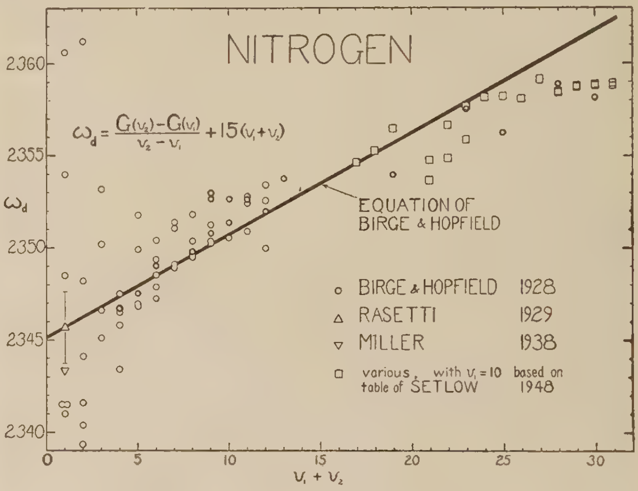

Fig. 3 Vibrational Data for Nitrogen

In spite of the possibility of further improvement in the spectroscopic constants, the writer has considered the new table for nitrogen to be a satisfactory basis for a table in the NBS-NACA series of "Thermal Properties of Gases." This table, Table 11.10 of that series, extends on upward in temperature to 5000 K, using the writer's 1947 results, which were obtained quite simply by using the tables of Gordon and Barnes with a small corrective addition appropriate for higher temperature. His results were in excellent agreement with the results presented in this paper, but were based on four-decimal-place tables so there was no thought of five-decimal-place accuracy.

A year ago Professor Gratch presented values of zero-pressure thermodynamic properties of carbon dioxide at a meeting of the Society (1).[9] His results for the specific heat are shown in a deviation plot in Fig. 4 of this discussion. The writer has been quite puzzled about their behavior in the temperature range above 2000 K. Comparison with an admittedly uncertain extrapolation

---

[8] Thermodynamics Section, National Bureau of Standards, U. S. Department of Commerce, Washington, D.C.

[9] Reference is to authors' bibliography.

[10] Authors' bibliography (9,15) and the following:
"A Note on the Raman Spectra of Nitrogen," by C. E. Miller, *Journal of Chemical Physics*, vol. 6, 1938, pp. 902–904.
"High Energy States of N_2^+ and N_2," by R. B. Setlow, *Physical Review*, vol. 74, 1948, pp. 153–162.

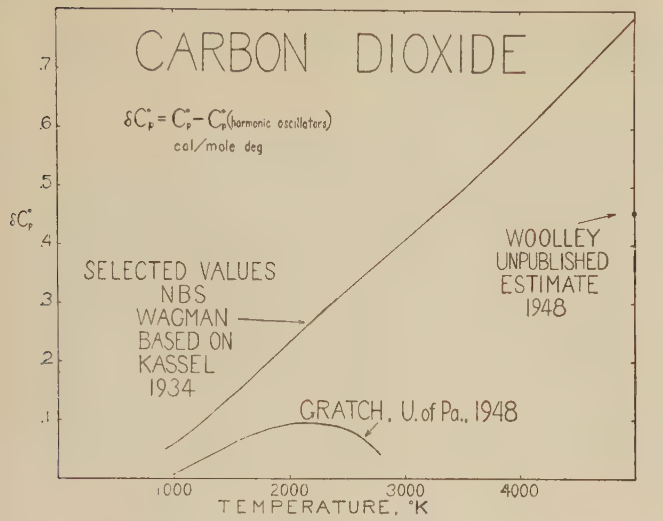

Fig. 4 Comparison of Estimates for Specific Heat for Carbon Dioxide

based on Kassel's results, and with an estimate which was made for 5000 K have led the writer to think that there might be something in the results which should be investigated further. In spite of this, the results presented by Professor Gratch for carbon dioxide have been included in the NBS-NACA tables as the only recently computed table available. It is the writer's private impression, however, that if any rocket researchers or others are interested in very accurate values for calculations at elevated temperatures, they should take Fig. 4 of this discussion into account and be aware that values obtained by a wrong extrapolation might possibly be in error by several units in the first decimal place in such a function as the specific heat, with corresponding errors in the other thermodynamic functions.

Authors' Closure

We regret that we must disagree with most of Mr. Woolley's criticisms of our paper. Consider first his criticism of the standard error (± 0.1 cm^{-1}) we have assigned to the Birge-Hopfield best value (2345.16 cm^{-1}) of the vibrational constant ω_0. His plot of the observed vibrational data, Fig. 3, is entirely misleading because it gives undue weight to the low-quantum-number data. After all, it is the quantity $G(v) = \omega_e(v + {}^1/_2) + \ldots$ that is important for the determination of zero-pressure thermodynamic properties; hence the problem is to determine those values of ω_e, $\omega_e x_e$, etc. which, when inserted in the Birge-Hopfield-Herman equation, give the best values of $G(v)$ from the least squares point of view. If he had plotted observed values of $G(v_2) - G(v_1)$ as deviations from the corresponding values calculated from the Birge-Hopfield-Herman equation and then analyzed these deviations by the method of least squares after weighting them properly, he would have found that ± 0.1 cm^{-1} is indeed a reasonable estimate of the standard error of ω_0 despite the fact that individual wave-length measurements may be uncertain by as much as several reciprocal centimeters, especially at low quantum numbers.

Next, consider Mr. Woolley's comments on the rotational constants D_e and β_0. Theoretically, D_e should be approximately equal to the quantity $4B_e^3/\omega_e^2$. From this it is clear that the disagreement between us regarding the uncertainty of ω_0 is entirely irrelevant to the discussion of D_e; Fig. 3 has no bearing on the matter whatsoever. The largest observed rotational quantum number J is about 20; D_e is of order of magnitude 6×10^{-6}; the corresponding value of $D_e J^2(J+1)^2$ is about 1 cm^{-1}; this is probably well within the uncertainty of the rotational wave-length measurements which cannot, therefore, yield reliable values of D_e and β_0. But, in order to calculate reliable values of the zero-pressure thermodynamic properties of nitrogen even up to temperatures as high as 5000 deg R we must take account of rotational levels up to $J = 100$; therefore we are practically forced to rely on the theoretical values of D_e and β_0. When we found that our calculated values of these rotational constants differed appreciably from those of Spinks we consulted Professor Herzberg who assured us that ours were correct and that those of Spinks were definitely in error. We can admit no ambiguity in Mr. Woolley's statement to one of us (SG) that his original (1944) calculations of the zero-pressure thermodynamic properties of nitrogen were based on Spinks' incorrect values of D_e and β_0; furthermore, we note that the results of Mr. Woolley's subsequent (1947) calculations differ from those of his original calculations by amounts that are accurately accounted for by an assumed change from the Spinks to the theoretical values of D_e and β_0.

Mr. Woolley has been good enough to comment upon a previous paper by one of us (SG) entitled, "Zero-Pressure Thermodynamic Properties of Carbon Dioxide." We heartily agree with him that the results presented therein may not stand extrapolation to temperatures as high as 5000 deg K and we second his warning to rocket researchers and others against placing reliance on any rule-of-thumb extrapolation. In our opinion Mr. Woolley's Fig. 4 is an excellent example of the kind of extrapolation to be avoided especially since it starts away down at 1000 deg K, the highest temperature for which Kassel made accurate calculations. It is our impression that Mr. Woolley made a number of rather drastic approximations in arriving at his unpublished estimate of the value of zero-pressure isobaric specific heat at 5000 deg K and that, therefore, accurate calculations may or may not confirm it. We see no reason to conclude that the downward concavity of the Gratch curve below 2700 deg K (Fig. 4) must persist above that temperature. In short, we are inclined to think that the comparison of Fig. 4 is entirely meaningless.

The Thermodynamic Properties of Helium

By S. W. AKIN,[1] SCHENECTADY, N. Y.

Evaluation has been made of the density, enthalpy, entropy, viscosity, and thermal conductivity of helium in the range of pressures from atmospheric to 6000 psia and at temperatures from —440 F to 600 F. These data are composed of observed values published prior to 1945, and of extrapolations based upon the Beattie-Bridgeman equation of state and kinetic theory. The results evaluated to four significant figures are tabulated for particular values of pressure and temperature. Graphic plots of the same information are also presented, with an accuracy sufficient for investigations of flow and heat-transfer processes involving high-pressure helium.

INTRODUCTION

THE properties of helium for engineering use presented in this paper are based upon the most acceptable values of experimental data as reviewed and evaluated by Keesom (1).[2] The range of these observed data was extended where necessary by extrapolation procedures which are described under headings for each of the properties. In summary, the respective range of pressures and temperatures included by experimental data and extrapolation is shown in Table 1. For the density data, this information is shown in Fig. 1.

TABLE 1 RANGE OF PRESSURES AND TEMPERATURES STUDIED

	Observed range		Extrapolated range	
	Pressure, psia	Temperature, deg F	Pressure, psia	Temperature, deg F
Viscosity	Independent	—435 to 1525	None	None
Thermal conductivity	Independent	—424 to 212	None	212 to 1100
Enthalpy	14.7 to 900	—440	900 to 6000	—440 to 600
Entropy	14.7 to 900	—440	900 to 6000	—440 to 600

To maintain consistency in the thermodynamic properties, two independent equations were used in the evaluations. The numerical results were in agreement within 0.5 per cent. Where graphical solutions were necessary, plotting was arranged to permit the reading of values to a corresponding degree of accuracy.

DENSITY

To determine the densities at the temperatures and pressures selected in this report, the reciprocal of density (specific volume) was evaluated from the Beattie-Bridgeman equation of state (2). For convenience, the values of the constant terms given in reference (2) were converted to the engineering units indicated.

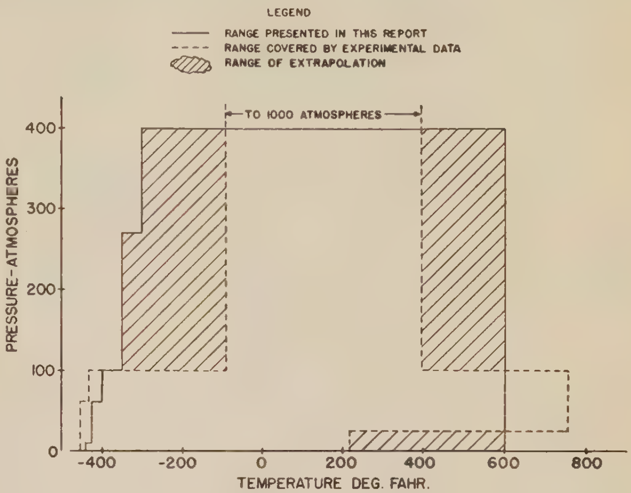

FIG. 1 PLOT COMPARING RANGE OF TEMPERATURES AND PRESSURES COVERED BY OBSERVED VALUES OF DENSITY FROM REFERENCE (1) AND DENSITIES PRESENTED IN PAPER

(Shaded portion indicates the range of extrapolation.)

$$p = \frac{RT\,(1-\alpha)\,(v+B)}{v^2} - \frac{A}{v^2} \qquad [1]$$

where

p = absolute pressure, psia

T = absolute temperature, deg R

$T°R = t°F + 459.69$

v = specific volume, ft^3/lb

$R = 2.6829, \dfrac{\text{ft}^3 - \text{lb}}{°\text{R} - \text{lb} - \text{in.}^2}$

$\alpha = \dfrac{C}{v\,T^3}$, dimensionless

$A = A_1\left(1 - \dfrac{a}{v}\right)$

$A_1 = 5.0906$, (ft^3/lb)^2 × (lb/in.^{2})

$a = 0.23963$, ft^3/lb

$B = B_1\left(1 - \dfrac{b}{v}\right)$

$B_1 = 0.056063$, ft^3/lb

$b = 0$

$C = 934.17, \dfrac{\text{ft}^3\,T^3}{\text{lb}}$

The specific volumes are given in Table 2.

At several pressures and temperatures throughout the range of calculations, the specific volumes computed from Equation [1] were compared with values determined from the equation of state in the virial form, as follows

$$p = \frac{RT}{(v - B_0)} \qquad [2]$$

The second virial coefficient B_0 was evaluated using the relation

---

[1] General Engineering and Consulting Laboratory, General Electric Company. Jun. ASME.

[2] Numbers in parentheses refer to the Bibliography at the end of the paper.

Contributed by the Special Research Committee on Properties of Gases and Gas Mixtures and the Heat Transfer and Applied Mechanics Divisions and presented at the Annual Meeting, New York, N. Y., November 27–December 2, 1949, of THE AMERICAN SOCIETY OF MECHANICAL ENGINEERS.

NOTE: Statements and opinions advanced in papers are to be understood as individual expressions of their authors and not those of the Society. Manuscript received at ASME Headquarters, October 10, 1949. Paper No. 49—A-96.

TABLE 2 PROPERTIES OF HELIUM

v, Specific volume, cu ft per lb
h, Enthlapy, Btu per lb

s, Entropy, Btu per lb, deg F
Total temperature, deg F

Absolute Pressure Lbs. per sq. in.		-440	-425	-400	-350	-300	-250	-200	-150	-100	0	100	200	300	400	500	600
14.696	v	3.431	6.315	10.92	20.06	29.20	38.33	47.46	56.59	65.72	83.97	102.2	120.5	138.7	157.0	175.3	193.5
	h	26.5	46.2	76.9	138.8	200.9	263.0	325.1	387.1	449.2	573.3	697.4	821.5	945.6	1070	1194	1318
	s	2.602	3.364	4.045	4.807	5.276	5.616	5.883	6.103	6.290	6.597	6.842	7.047	7.223	7.378	7.515	7.639
30	v	0.8847	1.847	3.225	5.925	8.613	11.30	13.98	16.67	19.35	24.72	30.09	35.45	40.82	46.18	51.55	56.92
	h	24.9	45.4	76.7	139.0	201.1	263.2	325.4	387.4	449.5	573.6	697.7	821.8	946.0	1070	1194	1318
	s	1.987	2.749	3.435	4.197	4.667	5.008	5.275	5.495	5.682	5.989	6.234	6.439	6.615	6.770	6.907	7.031
150	v	0.209	0.6188	1.094	2.001	2.901	3.797	4.693	5.589	6.484	8.274	10.06	11.85	13.64	15.43	17.22	19.01
	h	21.3	43.5	75.9	139.3	201.8	264.0	362.2	388.3	450.4	574.6	698.7	822.8	946.9	1071	1195	1319
	s	1.269	2.198	2.884	3.649	4.121	4.462	4.729	4.949	5.137	5.443	5.689	5.894	6.070	6.224	6.361	6.485
400	v		0.2558	0.4344	0.7768	1.116	1.453	1.790	2.127	2.463	3.135	3.806	4.478	5.149	5.820	6.491	7.162
	h		41.5	75.7	140.3	203.4	266.0	328.3	390.5	452.7	576.9	701.1	825.2	949.3	1073	1197	1322
	s		1.618	2.380	3.158	3.631	3.973	4.241	4.461	4.649	4.956	5.201	5.407	5.583	5.737	5.874	5.998
600	v		0.189	0.3054	0.5327	0.7590	0.9844	1.209	1.434	1.658	2.107	2.555	3.002	3.450	3.897	4.345	4.792
	h		41.3	75.4	141.0	204.7	267.5	330.0	392.3	454.5	578.8	703.0	827.1	951.2	1075	1199	1323
	s		1.396	2.176	2.955	3.428	3.770	4.039	4.259	4.448	4.754	5.000	5.205	5.381	5.536	5.673	5.797
900	v		0.146	0.221	0.3704	0.5212	0.6717	0.8060	0.9720	1.122	1.421	1.720	2.019	2.317	2.616	2.914	3.212
	h		43.0	75.0	142.1	206.6	269.8	332.5	395.0	457.3	581.7	705.9	830.0	954.1	1078	1202	1326
	s		1.176	1.984	2.750	3.224	3.567	3.836	4.057	4.245	4.552	4.798	5.004	5.180	5.334	5.472	5.595
1500	v		0.11	0.154	0.2410	0.3310	0.4214	0.5118	0.6021	0.6922	0.8722	1.052	1.231	1.411	1.590	1.769	1.948
	h			75.2	144.3	210.5	274.5	337.6	400.4	462.8	588.0	711.7	835.8	959.9	1084	1208	1332
	s			1.752	2.498	2.968	3.311	3.580	3.801	3.990	4.297	4.544	4.748	4.926	5.080	5.218	5.341
2500	v		0.09	0.11	0.163	0.2165	0.2707	0.3251	0.3795	0.4338	0.5422	0.6504	0.7585	0.8664	0.9741	1.082	1.189
	h				148	217	282.2	346.1	409.0	472.0	596.9	721.3	845.5	969.6	1094	1218	1342
					2.255	2.712	3.054	3.324	3.545	3.734	4.042	4.289	4.493	4.671	4.826	4.963	5.087
4000	v		0.07	0.09	0.119	0.151	0.185	0.219	0.253	0.288	0.356	0.424	0.492	0.559	0.627	0.694	0.762
	h				154	227	293.9	358.9	422.7	485.9	611.2	735.8	860.1	984.2	1108	1232	1356
	s				2.036	2.479	2.818	3.087	3.308	3.497	3.806	4.053	4.258	4.436	4.591	4.729	4.853
6000	v		0.06	0.07	0.09	0.114	0.137	0.160	0.183	0.205	0.251	0.297	0.343	0.388	0.433	0.479	0.524
	h					240	309.4	375.9	440.6	504.4	630.3	755.2	879.5	1004	1127	1251	1375
	s					2.279	2.614	2.881	3.102	3.292	3.602	3.839	4.054	4.233	4.388	4.526	4.650

from reference (3) with the constants converted to engineering units

$$B_0 = 0.305937\,\tau^{1/4} - 1.845\,\tau^{3/4} - 0.822\,\tau^{5/4}\ldots\ldots [3]$$

where

B_0 is expressed in ft³/lb
τ = reciprocal temperature ($1/T\,°R$)
$T\,°R = (t\,°F + 459.69)$

Calculations showed that the coefficients given by this equation were in substantial agreement with the values adopted by Keesom (1).

The comparison indicates that for pressure less than 2500 psia and for densities less than 4.32 lb per cu ft (critical density), good agreement exists between the two equations. At higher pressures, the values determined from Equation [1] were from 3 to 10 per cent larger. However, Keesom (1) points out that no equation had been proposed which agrees exactly with observed facts. On the strength of his remarks, densities determined which were larger than 10 lb per cu ft have been reported to only one significant figure in order to show possible trends.

Another comparison was made at 30 C with the equation for the isotherm observed by C. A. Johnson (4). The greatest difference was about 1 per cent at 6000 psia. The equation is

$$pv = 1462.391 + 0.047232\,p - 2.98 \times 10^{-7}\,p^2\ldots\ldots [4]$$

where

p = absolute pressure, psi
v = specific volume, ft³/lb

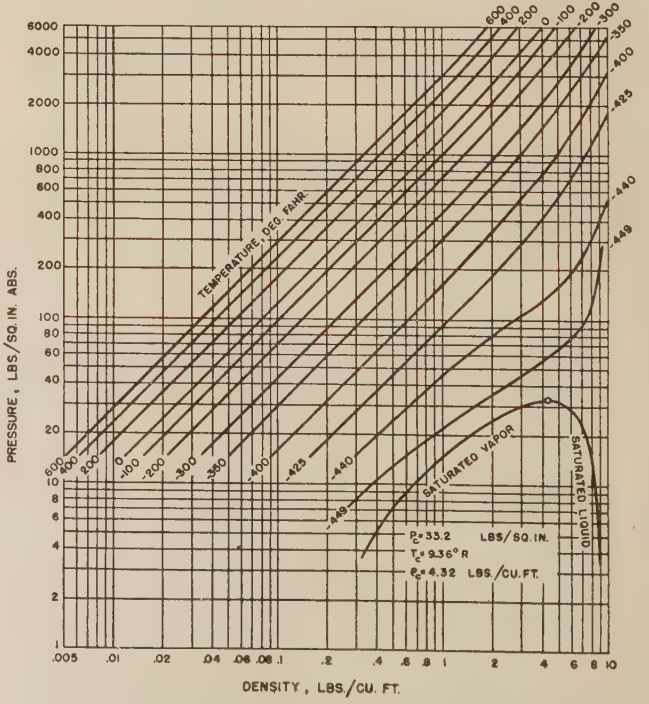

FIG. 2 DENSITY OF HELIUM PLOTTED AS FUNCTION OF ABSOLUTE PRESSURE FOR SELECTED RANGE OF TEMPERATURES

Fig. 2 shows a plot of the pressure, density, and temperature relations calculated from Equation [1]. Values for the saturated liquid and saturated vapor were taken directly from Zelmanov's data (5).

VISCOSITY

The following equation (1) was used to determine the viscosity of helium as plotted in Fig. 3

$$\eta = 8.315\,(T)^{0.647} \times 10^{-4} \ldots\ldots\ldots\ldots\ldots [5]$$

where

η = viscosity, lb (mass)/hr ft
T = absolute temperature, deg R
T°R = (t°F + 459.69)

The values found by this equation represent the true viscosity with an accuracy of 1 per cent in the range of —450 F to 2000 F and independent of pressure.[3]

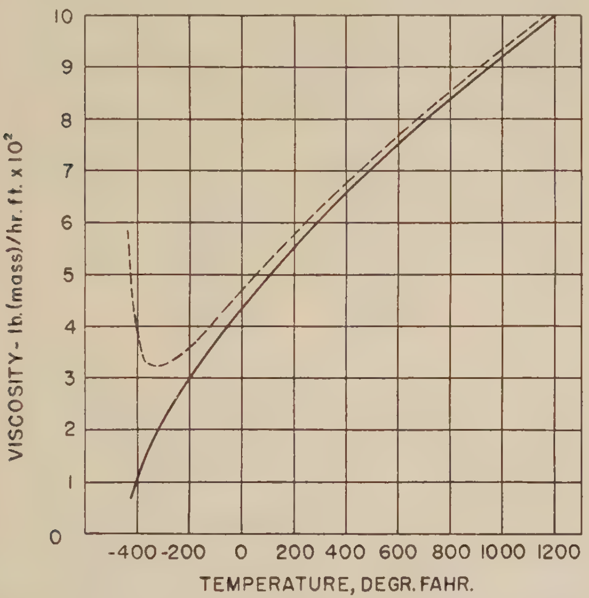

FIG. 3 VISCOSITY OF HELIUM PLOTTED AS FUNCTION OF TEMPERATURE
(Dashed line indicates estimated values for 6000 psia.[3])

Values determined in Equation [5] were compared with two separate equations covering the full temperature range. The first equation valid from —258 C to —22 C is (7)

$$\log_{10}(\eta) = 6.90595 - 10 + 0.650 \log_{10} T\,^{\circ}\mathrm{R} \ldots\ldots [6]$$

The second equation is a form of Sutherland's formula with constants suggested by Keyes (4), and is valid above —100 C

$$\eta = \frac{249.67 \times 10^{-7}\sqrt{T}}{1 + \dfrac{100.4}{T}} \ldots\ldots\ldots\ldots\ldots [7]$$

where for both equations

η = viscosity, lb (mass)/hr ft
T = temperature, deg R
T°R = (t°F + 459.69)

Agreement was within plus and minus 2 per cent from —432 F to 700 F, and within 3½ per cent up to 1200 F.

THERMAL CONDUCTIVITY

The thermal-conductivity values given in Fig. 4 and listed in Table 3 combine three sources of information. In the range 3 R to 161 R, recent data published by Ubbink and de Haas (8) were used. In the range 161 R to 672 R, values were taken from a smoothed curve based upon an evaluation of the observed data by several experimenters (1). In the range 672 R to 1572 R, extrapolation was made by use of the following kinetic-theory (9) relation

TABLE 3 INTERCEPT VALUES OF THERMAL CONDUCTIVITY AS A FUNCTION OF TEMPERATURE TAKEN FROM FIG. 4

k expressed as Btu/hr-ft² (°F/ft)

T°F	$k \times 10^4$	T°F	$k \times 10^4$
—456	22	—100	673
—450	63	0	792
—440	106	200	1000
—430	133	400	1191
—420	160	600	1365
—410	186	800	1524
—400	210	1000	1675
—300	400	1100	1750
—200	550		

$$k = \eta\, c_v \epsilon \ldots\ldots\ldots\ldots\ldots\ldots\ldots [8]$$

in which

k = thermal conductivity, Btu/hr-ft²(°F/ft)

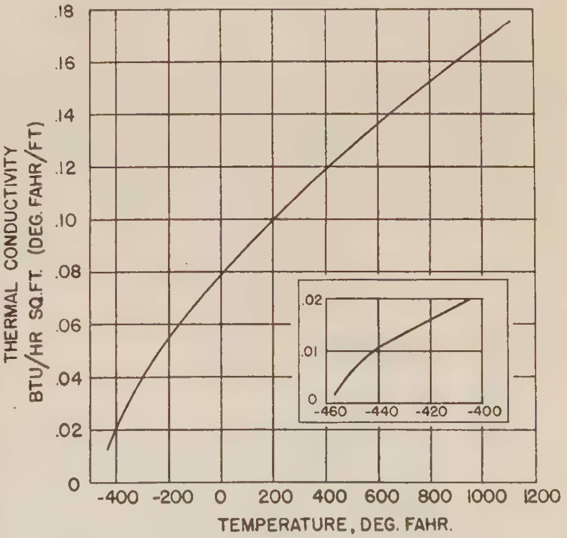

FIG. 4 THERMAL CONDUCTIVITY OF HELIUM PLOTTED AS FUNCTION OF TEMPERATURE

---

[3] From consideration of kinetic theory, it is expected that viscosity should be independent of pressure (4). But at 6000 psia, the volume of the molecules is an appreciable part of the volume occupied by the gas, and therefore we might suppose helium would display the properties of a "dense" gas. To check this possibility, the variation of viscosity at high density was determined from the equation (6)

$$\frac{\eta'}{\eta} = b\rho\left(\frac{1}{b\rho x} + \frac{4}{5} + 0.7614\, b\rho x\right)$$

where at a given temperature using any consistent set of units
η' is viscosity at high pressure
η is viscosity at atmospheric pressure
$b = \frac{2}{3}\pi\frac{\sigma^3}{m}$
σ = molecular radius
m = mass of helium atom
ρ = mass density
$x = 1 + \frac{5}{8} b\rho + 0.2869\,(b\rho)^2$

The results of this computation are shown as the dashed line in Fig. 3, and indicate that at normal temperatures, the effect of increased pressure is not great. However, until data on the viscosity of helium at high pressures are available, these calculations should be considered only as an estimate of the possible variation.

η = viscosity, lb/hr-ft
c_v = specific heat at constant volume, 0.7445 Btu/lb-°F
ϵ = proportionality constant

A value for the proportionality constant, which could be used with reasonable certainty above 672 R, was obtained as follows: Equation [8] was solved for ϵ in the range 60 R to 672 R, using observed values of thermal conductivity, viscosity, and constant-volume specific heat. Above 540 R, ϵ had a constant value of 2.44. This value was then used in Equation [8] with the observed values of viscosity to determine the conductivity up to 1572 R. Table 3 gives the intercept values taken graphically from the smoothed curve in Fig. 4, with temperatures converted to the Fahrenheit scale.

ENTHALPY-ENTROPY

In order that the extrapolated enthalpy and entropy values presented in this paper would be consistent with recently published data, the following values (5 and 10) were taken as the datum[4] for computation

T_0 = absolute temperature, 19.69 R (—440 F)
P_0 = absolute pressure, 14.7 psia
h_0 = enthalpy, 26.56 Btu per lb
S_0 = entropy, 2.602 Btu per lb-deg F

Evaluation of the enthalpies given in Table 2 proceeded as follows: Changes in enthalpy with increasing temperature at constant pressure were found from Equation [4]

$$h_T = h_0 + \int_{T_0}^{T} c_{p_0}\, dt + \int_{T_0}^{T} \left(\frac{\partial B_0\, \tau}{\partial \tau}\right)_p dp \ldots\ldots [9]$$

in which

h_T = enthalpy at temperature T, Btu per lb
h_0 = enthalpy at —440° F, 26.56 Btu per lb
c_{p_0} = specific heat at constant pressure as $p \rightarrow 0$, 1.241 Btu per lb-°F
p = absolute pressure, atm

The expression

$$\left(\frac{\partial B_0\, \tau}{\partial \tau}\right)_p$$

obtained by operating on Equation [3], using the same notation is

$$\left(\frac{\partial B_0\, \tau}{\partial \tau}\right)_p = 0.38242\, \tau^{1/4} - 3.229\, \tau^{3/4} - 1.850\, \tau^{5/4} \ldots [10]$$

The enthalpies at atmospheric pressure for the selected temperatures were calculated by substituting Equation [10] in Equation [9]. Letting these enthalpies at atmospheric pressure be the datum, the Joule-Kelvin coefficients were used to find the changes in temperature with increasing pressure. At the chosen enthalpies

$$\Delta T = \mu \Delta P \ldots\ldots\ldots\ldots\ldots\ldots\ldots [11]$$

where, by definition

$$\mu = \left(\frac{\partial T}{\partial P}\right)_h = \text{deg R/psia}$$

T = absolute temperature, deg R

The Joule-Kelvin coefficients have been determined experimentally from 15 psia to 2930 psia in the range 572 F to —310 F (11). Down to —248 F, the coefficient is independent of pressure, but at lower temperatures it increases with increasing pressure.

To establish a reasonable basis for extrapolation to higher pressures, values of μ were calculated from 15 psia to 6000 psia in the range of 600 F to —300 F, using the well-known equation

$$\mu = -\frac{1}{c_p}\left[V - T\left(\frac{\partial V}{\partial T}\right)_p\right] \ldots\ldots\ldots\ldots [12]$$

where $[(\partial V)/(\partial T)]_p$ was obtained by operation on the Beattie-Bridgeman equation of state.

The calculated coefficients showed a dependence on pressure at all temperatures which amounted to a variation of plus or minus 8 per cent from the average of the calculated values. Further, these average values were from 2 to 5 per cent less than the experimental values. The observation can be made that overall discrepancies of this magnitude in μ can cause errors in the enthalpies at 6000 psia of only about 1 per cent at —300 F, and even less at higher temperatures. On this basis, use of the experimental values listed in Table 4 for the entire range of pressures was concluded to be sufficiently accurate for this work.[5]

TABLE 4 JOULE-KELVIN COEFFICIENTS USED IN THE DETERMINATION OF ISENTHALPS FROM 15 PSIA TO 600 PSIA

Temp, deg F	°R/psia
600	0.00759
400	0.00759
200	0.00759
0	0.00735
—100	0.00710
—200	0.00655
—300	0.00480

It was possible to show a consistency in the variation of μ with temperature by checking the enthalpies for a given pressure found through Equation [11] by use of Equation [9]. At selected temperatures down to —300 F, the enthalpies were in disagreement by no more than 0.5 per cent.

Below —300 F, a temperature-enthalpy chart was constructed using Zelmanov's data below —425 F, and the previously calculated data above —300 F. Graphical interpolation with a readable accuracy of 0.1 Btu was used to determine the enthalpies listed in Table 2.

Additional auxiliary temperature-enthalpy curves were made to large scale from which the values for the isenthalps in Figs. 5, 6, and 7 were found. The accuracy of this graphical plot was within plus or minus 1 deg and one Btu.[6]

Using the values at atmospheric pressure given by Zelmanov, changes in the entropy with increasing temperature were made using the following equation

$$s_T = S_0 + c_p \ln\left(\frac{T}{T_0}\right) \ldots\ldots\ldots\ldots\ldots [13]$$

When entropies had been calculated for the selected temperature, the entropies at higher pressures at these same temperatures were then determined, using the values at atmospheric pressure as the datum, and the following equation

$$s_p = S_0 + \int_{V_0}^{V} \left[\left(\frac{\partial p}{\partial T}\right)_V dv\right]_T \ldots\ldots\ldots\ldots [14]$$

---

[4] The datum for these values was chosen by the original investigator so that the enthalpy and entropy of liquid helium at 14.7 psia were equal to zero. The values given were obtained by graphical interpolation after suitable unit conversion.

[5] It is well to point out that the coefficients adopted by this procedure may not truly represent the actual phenomenon, and that experimental data at higher pressures would be desirable for checking the data given here.

[6] Subsequent to the preparation of Figs. 5, 6, and 7, a slight error was found in checking the calculations. This error amounts to no more than 0.5 per cent at any temperature or pressure; this did not justify replotting the data. This accounts for the obvious discrepancies between Table 2 and Figs. 5, 6, and 7.

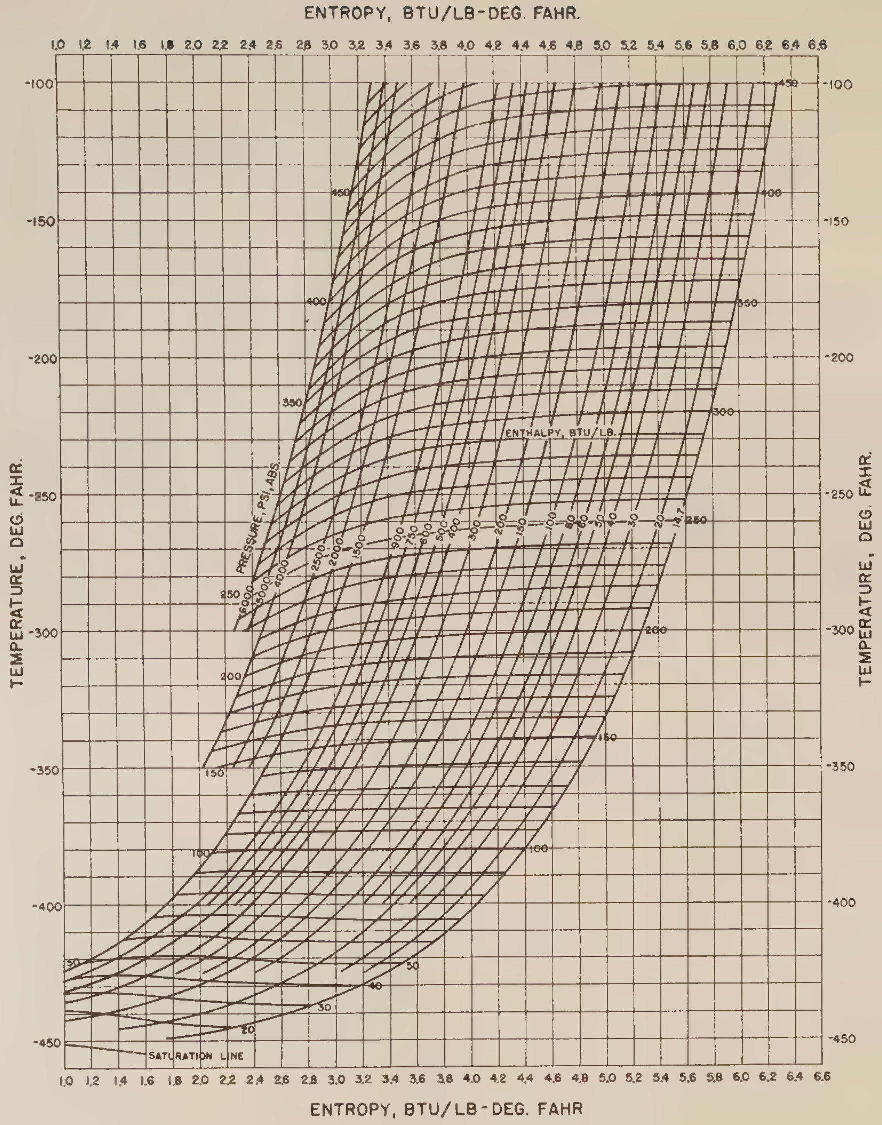

Fig. 5 Temperature-Entropy Diagram for Helium in Range —450 F to —100 F for Selected Series of Pressures and Showing Lines of Constant Enthalpy

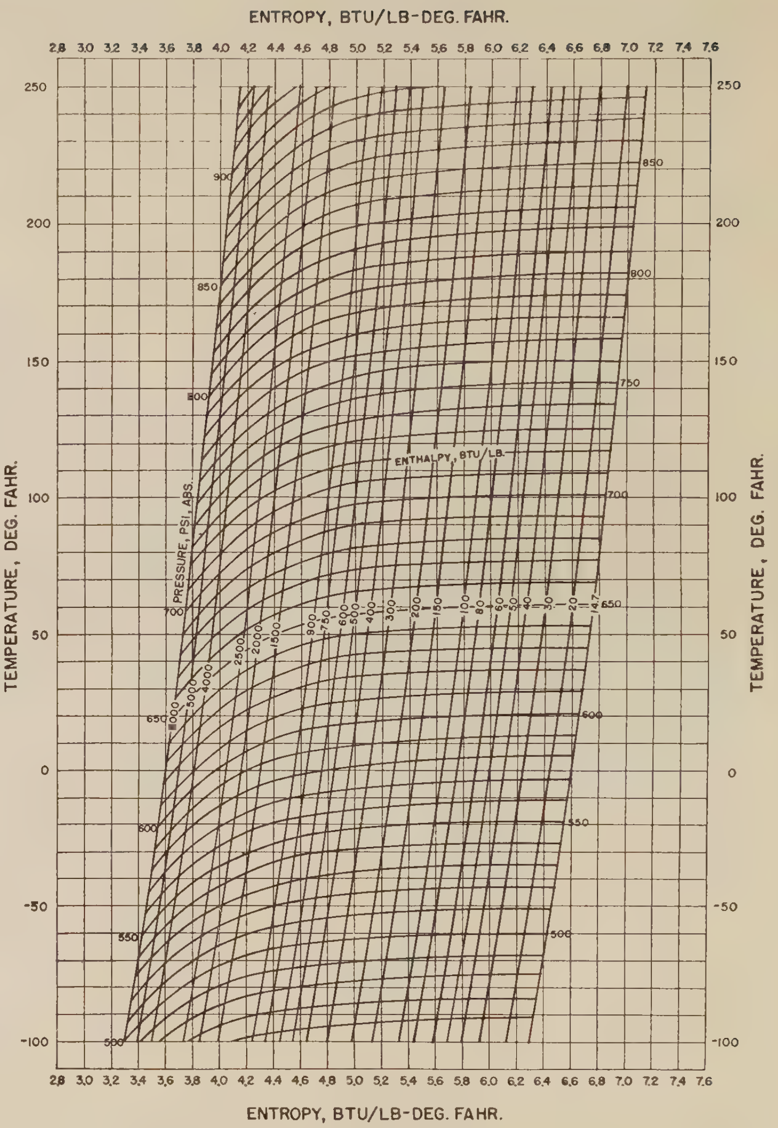

Fig. 6 Temperature-Entropy Diagram for Helium in Range —100 F to 250 F for Selected Series of Pressures and Showing Lines of Constant Enthalpy

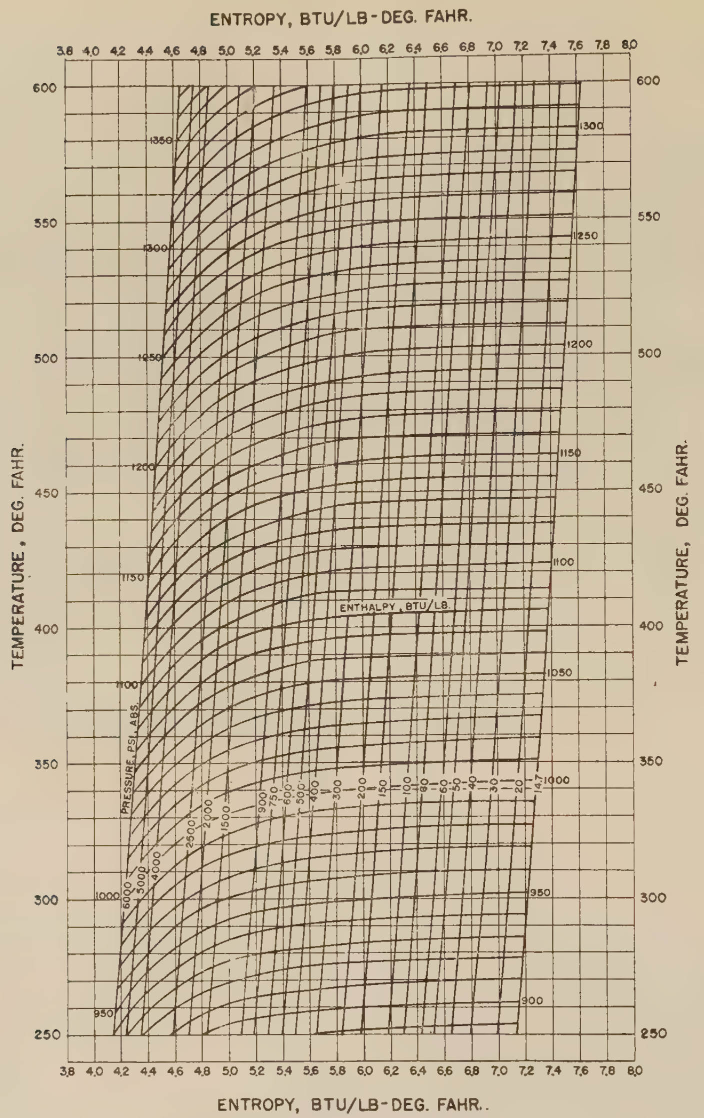

Fig. 7 Temperature-Entropy Diagram for Helium in Range 250 F to 600 F for Selected Series of Pressures and Showing Lines of Constant Enthalpy

The function $[(\partial p)/(\partial T)]_V$ was calculated by operating on the Beattie-Bridgeman equation. Again at the higher pressure, the entropy differences corresponding to selected temperatures were checked by use of Equation [13]. In no case were the entropies in disagreement by more than $^1/_3$ per cent.

The values of entropy have been entered in Table 2 and plotted in Figs. 5, 6, and 7. Entropies for the intermediate pressures were obtained by graphical interpolation with an accuracy of 0.5 per cent.

Acknowledgments

Appreciation is expressed for the valuable information supplied by Prof. Frederick G. Keyes of the Massachusetts Institute of Technology, and for the instructive assistance by Mr. R. H. Norris of the General Electric Company. The author is indebted to Mr. R. M. Woody and Miss V. Demeo who performed the calculations, and to Mr. F. T. Rohrs who prepared the curve plots.

BIBLIOGRAPHY

1 "Helium," by W. H. Keesom, Elsevier, Amsterdam, Holland, 1942, pp. 27–142.

2 "Equations of State," by J. A. Beattie and W. H. Stockmayer, Reports on Progress in Physics, vol. 7, 1940, p. 207.

3 "Temperature," published by American Institute of Physics, Reinhold Publishing Corporation, New York, N. Y., 1941, p. 55.

4 "Personal Letter to Author," from Frederick G. Keyes, Massachusetts Institute of Technology, October, 1946.

5 "The Entropy Diagram for Helium at Low Temperatures," by J. Zelmanov, *Journal of Physics*, USSR, vol. 8, 1944, pp. 135–141.

6 "The Mathematical Theory of Non-Uniform Gases," by S. Chapman and T. G. Cowlings, Cambridge University Press, London, England, 1939, pp. 274–286.

7 "Chemical Engineers Handbook," by John H. Perry, McGraw-Hill Book Company, Inc., New York, N. Y., second edition, 1941, p. 792.

8 "Thermal Conductivity of Gases," by J. B. Ubbink and W. J. de Haas, *Physics*, vol. 10, 1943, pp. 465–470.

9 "Kinetic Theory of Gases," by E. H. Kennard, McGraw-Hill Book Company, Inc., New York, N. Y., first edition, 1938, pp. 178–180.

10 "Specific Heat and Enthalpy of Helium at Low Temperatures," by J. Zelmanov, *Journal of Physics*, USSR, vol. 8, 1944, pp. 129–134.

11 "Joule-Thomson Effect in Helium," by J. R. Roebuck and H. Osterberg, *Physical Review* (2), vol. 43, 1933, p. 60.

Discussion

F. G. Keyes.[7] The author gives a comprehensive survey of the factual data upon which his tables are based, and Fig. 1 of the paper, leads quickly to a grasp of the extrapolation required because of the limitations in range of measurements of the p-v-T properties.

The present tables are believed to be the most exact that can be compiled at this time, and cover the entire superheat from a few degrees above the critical temperature to a temperature (600 F or 315.5 C) reached by a restricted amount of the experimental data. However, the analytic functions used to represent the basic observational data are of a form known to be reliable for extrapolation.

The basic data for viscosity are fairly complete, that for heat conductivity less so, and no pressure effects, which are small, have been measured.

Author's Closure

The author wishes to thank Prof. F. G. Keyes for his instructive remarks. It is gratifying to learn that the data presented here should be useful in commercial design work. Realizing many of the inevitable shortcomings inherent in the preparation of extrapolated information, the author hopes that additional experimental work will be undertaken on the properties of this gas.

---

[7] Department of Chemistry, Massachusetts Institute of Technology, Cambridge, Mass.

Some New Values of the Second Enthalpy Coefficient for Dry Air

By J. R. Andersen,[1] Philadelphia, Pa.

Measurements of the second enthalpy coefficient for dry CO_2-free air are reported for three temperatures: 0 C, 10 C, and 30 C. These values, which are in excellent agreement with the best data on air in the literature, were formulated, together with the data of Eucken, Clusius, and Berger by the equation

$$\beta = -0.05442G(0.01244\, T),\ \text{ft}^3/\text{lb}$$

The second virial coefficient was then calculated by means of the equation

$$B = 0.05442\, F(0.01244\, T) - 2.33 \times 10^{-5}T,\ \text{ft}^3/\text{lb}$$

where the value of the constant of integration was adjusted to give the best fit with the Holborn and Schultze compressibility data. These equations represent adequately all reliable data on air in the temperature range —80 C to 200 C. The functions F and G are the well-known Lennard-Jones functions, abridged tables of which are given in the Appendix.

Introduction

This report presents the results so far obtained in an experimental program for the determination of the thermodynamic properties of gases and gas mixtures at low pressures. The preference for low pressures is of course due to the interesting inferences which may be drawn as to the intermolecular force potential through the application of statistical mechanics. The method used, which is called by us the "Isothermal Joule-Thomson Experiment," consists of the measurement of the change in enthalpy with pressure at various constant temperatures. The method is generally similar to the Joule-Thomson experiment in that a steady flow of gas at constant inlet and exit pressures flows through a calorimeter in which there is an orifice or other constriction to induce a drop in pressure, but differs from it by the introduction of a heater to restore the outlet temperature to its inlet value. Our choice of this type of experiment was dictated mainly by the following considerations: (*a*) the low-pressure data are determined directly, that is, without the necessity for extrapolation or differentiation of high-pressure data; and (*b*) certain design problems inherent in Joule-Thomson or specific-heat calorimeters are less onerous in this experiment, because it is not necessary to maintain temperature differences at the two ends of the calorimeter.

In order not to complicate the development of the calorimeter by the necessity for solving other difficult problems concurrently, it was decided at the outset to use air as the experimental fluid and to limit the range of physical conditions accessible to the apparatus. The upper limit of pressure was set at 4 atm, and the temperature range selected was 0 C to 30 C.

Measurements of the second enthalpy coefficient for dry CO_2-free air are reported for three temperatures: 0 C, 10 C, and 30 C. These values are in excellent agreement with the best data on air available in the literature and serve to indicate that the apparatus in its present form is capable of producing reliable data on the low-pressure properties of gases and gas mixtures in the range of physical conditions accessible to it.

Theory and Practical Realization of Experiment

The equation of state of a gas is conveniently expressed as a power series in pressure

$$pv = (pv)^0 + Bp + Cp^2 + \ldots \qquad [1]$$

where $(pv)^0$ is the zero pressure value of pv, and $B, C, \ldots$ are called virial coefficients. $(pv)^0$ and $B, C, \ldots$ are temperature functions. The enthalpy of a gas can also be expressed as a power series in pressure

$$h = h^0 + \beta p + \gamma p^2 + \ldots \qquad [2]$$

where h^0 is the zero pressure enthalpy and $\beta, \gamma, \ldots$ are herein called enthalpy coefficients. h^0 and $\beta, \gamma, \ldots$ are temperature functions. If $(pv)^0$ and h^0 are finite the second law of thermodynamics asserts that $(pv)^0$ is proportional to a universal temperature function called absolute temperature, i.e., $(pv)^0 = RT$.

The virial coefficients $B, C, \ldots$ and the enthalpy coefficients $\beta, \gamma, \ldots$ are related. Consider the identical relation of thermodynamics

$$(\partial h/\partial p)_T = v - T(\partial v/\partial T)_p \qquad [3]$$

It follows that

$$\beta = d(B\tau)/d\tau;\quad \gamma = {}^1/_2\, d(C\tau)/d\tau \qquad [4]$$

where the reciprocal temperature $\tau = 1/T$ is used. Numerical values of the virial coefficients can be obtained from the enthalpy coefficients by integration of these equations

$$\left.\begin{aligned} B &= (1/\tau)\left[\int_{\tau_0}^{\tau} \beta\, d\xi + C_1\right] \\ C &= (2/\tau)\left[\int_{\tau_0}^{\tau} \gamma\, d\xi + C_2\right] \end{aligned}\right\} \qquad [5]$$

provided that some means of evaluating the constants of integration are available.

A steady-flow calorimeter suitable for the determination of the enthalpy coefficients consists of the following elements: (*a*) An entrance section for measurement of the inlet pressure and temperature; (*b*) an orifice or other constriction to induce a drop in pressure; (*c*) an electric heater; and (*d*) an exit section for measurement of the exit pressure and temperature. Furthermore, in order to eliminate the need for making difficult and uncertain corrections to the data, it is desirable to have the kinetic energy of flow of the experimental fluid negligibly small in the entrance and exit sections, and to establish adiabatic conditions along the walls of the calorimeter between the entrance and exit sections so that the rate of heat absorption between these sections is just that

---

[1] Assistant Professor of Mechanical Engineering, Towne Scientific School, University of Pennsylvania; Project Leader, University of Pennsylvania Thermodynamics Research Laboratory. Jun. ASME.

Contributed by the Research Committee on Properties of Gases and Gas Mixtures and the Heat Transfer and Applied Mechanics Divisions and presented at the Annual Meeting, New York, N. Y., November 27–December 2, 1949, of The American Society of Mechanical Engineers.

Note: Statements and opinions advanced in papers are to be understood as individual expressions of their authors and not those of the Society. Paper No. 49—A-40.

deliberately introduced by the electric heater. In addition, it is necessary to provide (*a*) accurate control of the inlet and exit pressures; (*b*) a thermostat to establish the temperature level of the apparatus; and (*c*) means for measurement of the rate of flow of the experimental fluid.

Under steady-flow conditions, with negligible kinetic energy of flow in the inlet and exit sections, conservation of energy requires that

$$h_2 - h_1 = {}_1Q_2/G \ldots\ldots\ldots\ldots [6]$$

where h_2 and h_1 are the enthalpies of the experimental fluid at the exit and entrance sections, respectively, ${}_1Q_2$ is the rate of heat absorption between these sections, and G is the rate of flow of the experimental fluid. If the rate of heat input is adjusted to restore the exit temperature to its inlet value, there is obtained

$$(h_2 - h_1)_T = ({}_1Q_2)_T/G \ldots\ldots\ldots\ldots [7]$$

The pressure drop $p_2 - p_1$ is also determined. These measurements yield numerical values of the ratio

$$[(h_2 - h_1)/(p_2 - p_1)]_T = ({}_1Q_2)_T/(p_2 - p_1)G \ldots\ldots [8]$$

that is, values of the change in enthalpy with pressure at constant temperature are determined.

The enthalpy coefficients are obtained readily from these data since

$$[(h_2 - h_1)/(p_2 - p_1)]_T = \beta + \gamma(p_1 + p_2) + \ldots\ldots [9]$$

If the measurements are carried out at a sufficiently low pressure (strictly zero pressure), the second enthalpy coefficient β is determined directly.

Statistical mechanics predicts that for molecules whose intermolecular force potential $E(r)$ is independent of orientation, the second virial coefficient B is related to it by the expression

$$B = 2\pi N_0 \int_0^\infty (1 - e^{-E(r)\tau/k})\, r^2\, dr \ldots\ldots [10]$$

in which r is the separation of any pair of molecules, N_0 is Avogadro's number, and k is the Boltzmann constant. This relation results from two basic assumptions, both of which are very nearly fulfilled at sufficiently high temperatures. It is assumed that a Maxwellian velocity distribution prevails and, further, that the kinetic and potential energies of the molecules are completely independent of each other and continuously variable. It follows that the second enthalpy coefficient β is related to the intermolecular force potential by the expression

$$\beta = 2\pi N_0 \int_0^\infty \{1 + [E(r)\tau/k - 1]e^{-E(r)\tau/k}\} r^2\, dr \ldots [11]$$

Thus accurate values of the second enthalpy coefficient can give important information on the intermolecular force potential. Furthermore, Equations [10] and [11] with a plausible empirical form for the intermolecular force potential $E(r)$ can be used effectively in the formulation of experimental data.

One widely used empirical form for the intermolecular force potential is that of Lennard-Jones

$$E(r) = 4\epsilon\, [(r_0/r)^{12} - (r_0/r)^6] \ldots\ldots\ldots\ldots [12]$$

In this expression ϵ and r_0 can be regarded as parameters for empirical adjustment. The Lennard-Jones potential is shown graphically in Fig. 1. Using the Lennard-Jones form for the intermolecular force potential in Equations [10] and [11], the necessary integrations can be carried out. The results are

$$B = (2\pi N_0 r_0^3/3)\, F(kT/\epsilon) \ldots\ldots\ldots\ldots [13]$$

$$\beta = -(2\pi N_0 r_0^3/3)\, G(kT/\epsilon) \ldots\ldots\ldots\ldots [14]$$

The functions F and G have been tabulated by J. O. Hirschfelder, R. B. Bird, and E. L. Spotz (1)[2] and others. An abridged table of these functions is given in the Appendix.

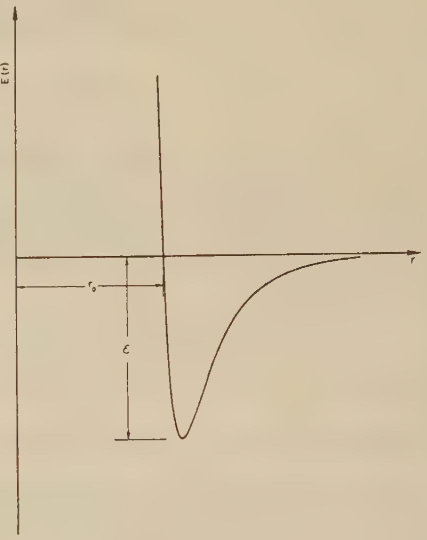

Fig. 1 Lennard-Jones Intermolecular Force Potential

Description of Apparatus

The arrangement of the apparatus used is shown schematically in Fig. 2.

The thermostat temperature-regulation system was of conventional construction and operation. The temperature range selected for experimentation permitted the use of water as thermostat fluid. The temperature of the thermostat was controlled by the circulation of an auxiliary fluid through coils immersed in the thermostat. The circulation of the auxiliary fluid was controlled by a conventional mercury-alcohol thermoregulator operating a circulating pump through a thyratron circuit. The temperature of the auxiliary fluid was maintained at the proper value by either an electric heater or a refrigeration machine as required. The auxiliary fluid was a mixture of water and ethylene glycol. The temperature regulation obtained with this system was of the order of ±0.005 deg C as ordinarily operated. The regulation could have been improved by the utilization of a more careful operating technique, but this was not thought to be necessary, since the temperature fluctuations were effectively damped by the heavy vacuum jacket surrounding the calorimeter. The inlet air to the calorimeter passed through a thermal ballast chamber to reduce its temperature fluctuation to negligible proportions.

The air was supplied during a test by a small compressed-air cylinder suspended from one arm of a sensitive balance. The rate of flow was determined by recording the time required for a certain weight of air to flow from this cylinder. The weight of air withdrawn was determined by the replacement method, the weights being placed directly over the center of gravity of the cylinder. Since weighing under flow conditions was necessary, a flexible take-off tube was provided. Balance was indicated by a balance signal and timing device, operated by a needle and mercury thimble mounted on the balance. The rate-of-flow determination as made with this system was the least reliable of the measurements. The reproducibility of the flow-rate measurement under identical flow conditions was seldom better than 1 part in 1000 and often not better than 1 part in 500. The difficulty

---

[2] Numbers in parentheses refer to Bibliography at the end of the paper.

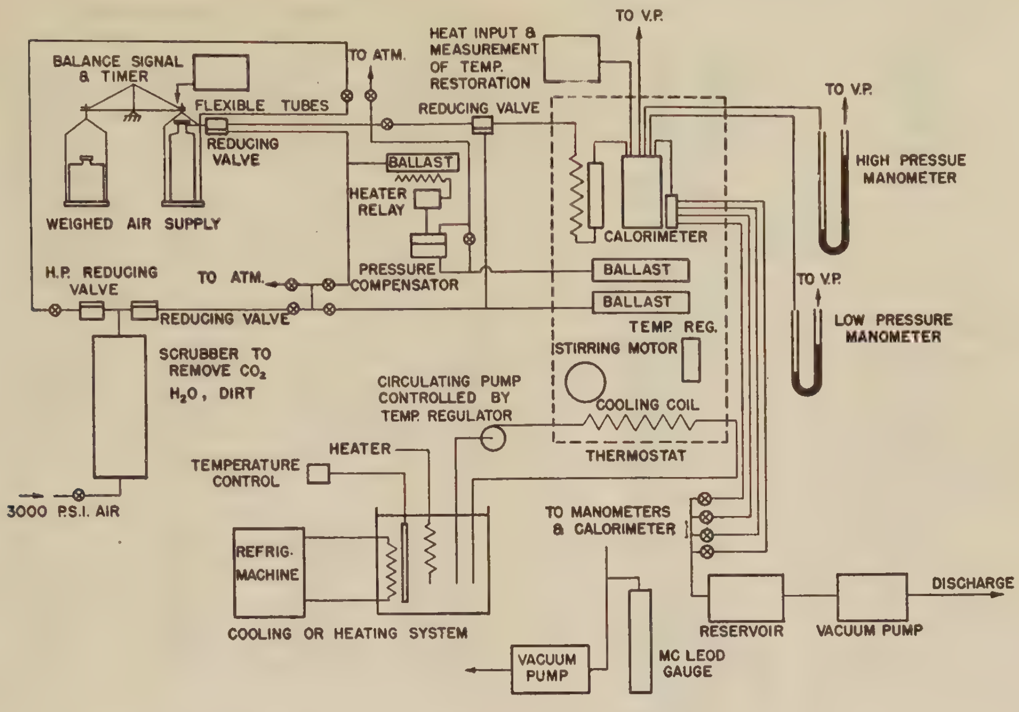

Fig. 2 Schematic Diagram of Apparatus

seemed to be due to vibrations transmitted to the balance from other machinery in the laboratory.

The rate of flow and inlet pressure were controlled by the calorimeter orifice in conjunction with two reducing valves in series.

For convenience of operation and to make the reducing-valve settings independent of room temperature and barometric pressure, both of these reducing valves were arranged for pneumatic operation. The first reducing valve was compensated for drift in its discharge pressure by an electric heater wound around the ballast cylinder in its pneumatic system. This heater was actuated by a diaphragm pressure-compensating device which compared the discharge pressure of the reducing valve with a reference pressure maintained by a ballast cylinder submerged in the thermostat. The second reducing valve had its pneumatic system pressure maintained by another ballast cylinder submerged in the thermostat. The pressure regulation obtained with this system was of the order of ±0.002 in. Hg.

The back pressure in the calorimeter was controlled by a bank of four orifices in parallel so arranged that any one or a combination of them could be opened to give the desired back pressure. This bank of orifices was thermostated to eliminate the effect of room-temperature changes. All orifices were operated with their back pressures less than the corresponding critical back pressure to make the flow through them depend only on the upstream temperature and pressure so that the settings of the pressures and the rate of flow were separated from any influence arising from adjustment of the heat input.

The pressures were measured by mercury manometers. The manometers had one leg evacuated to eliminate the effect of barometric pressure variation and also in order to give the absolute pressure directly. The absolute pressure in the vacuum system was measured with a McLeod gage. The manometers were of one-piece glass construction, the tubes having a bore of about $^1/_2$ in. to minimize the effect of capillary depression. The meniscuses were located by means of small telescopes mounted on micrometer screws whose settings were established by comparison with a steel scale mounted on the manometer frame.

The essential features of the calorimeter in its final form are shown in Fig. 3. In use this device was mounted inside a heavy evacuated submarine which was in turn submerged in the thermostat. The experimental fluid entered the calorimeter through tube 1 after being brought to the thermostat temperature by passing through a cooling coil submerged in the thermostat and the thermal ballast. The inlet conditions were measured at section 2.

The high-pressure manometer was connected to tube 3. A five-junction copper-constantan differential thermocouple 4 was used to indicate temperature restoration between the inlet and outlet sections. The remainder of the calorimeter consisted of an inlet labyrinth 5, orifice 6, heater 7, outlet labyrinth 8, mixing screens 9, and radiation shields 10 and 11. The heater wires were brought out through the capillary tubes 12 and the packing glands 13. The low-pressure manometer was connected to tube 14.

The design of the inlet labyrinth may seem to be unnecessarily elaborate but this design was evolved after extensive experimentation with simpler arrangements clearly demonstrated their inadequacy in respect to heat leakage to the orifice by conduction along its inlet pipe. The orifice consisted of a thin brass disk cemented to the end of a long, thin-walled, lucite tube. The outlet labyrinth served to provide additional radiation shielding for the heater and helped to promote uniform flow conditions at the outlet section. The mixing screens served also to promote uniform flow conditions.

The entire calorimeter was constructed of brass with the exception of the orifice mounting tube and the form on which the heater element was wound which were of lucite. Demountable connections had neoprene gaskets coated with shellac on assembly. The electrical energy to the heater was supplied by Willard DD-5-1 storage batteries which had excellent voltage stability for the low discharge rates used in this application. The heat-input circuit consisted of the batteries, voltage dividers for adjustment, the heater element, and a standard resistance. The potentials across the heater and the standard resistance were measured with a Leeds and Northrup type K-2 potentiometer making use of a volt box

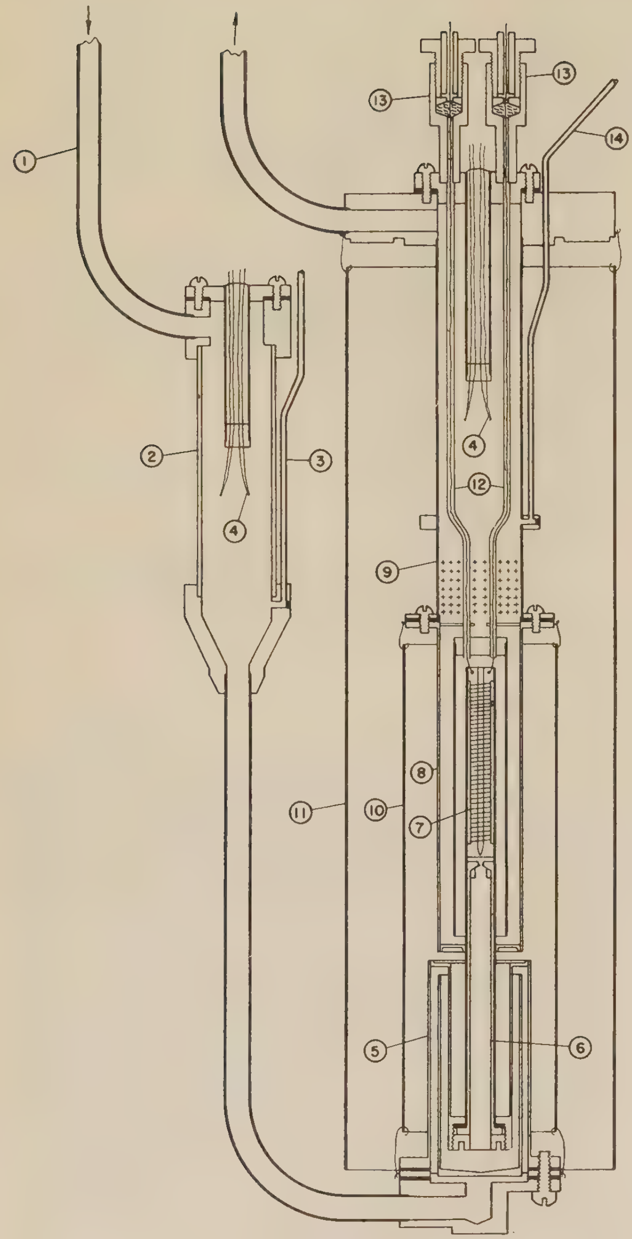

FIG. 3 THE CALORIMETER

when necessary. Temperature restoration was indicated by a high-sensitivity galvanometer connected directly to the differential thermocouple. The sensitivity of the indication of temperature restoration was about ±0.0005 deg C.

EXPERIMENTAL MEASUREMENTS

The measurements made on dry CO_2-free air with the apparatus in its final form are given in Table 1. It will be noted that at each temperature, measurements were made at two different pressure drops. Since the same orifice was used, this resulted in two different rates of flow. These two series of measurements served to show (*a*) that the results were not sensitive to the rate of flow, and (*b*) that $[(h_2 - h_1)/(p_2 - p_1)]_T$ was not a function of pressure within the sensitivity of the apparatus. Dependence of the results on the rate of flow was taken as evidence of heat leakage to the orifice in the calorimeter. In the earlier arrangements used, the results had a pronounced sensitivity to the rate of flow, but successive improvements made in the thermal isolation of the orifice to reduce its heat leak reduced this sensitivity. Since the final measurements had a negligible dependence on the rate of flow, it was concluded that heat leakage to the orifice in the final design was negligible. The range of pressures used was not sufficient to reveal any dependence of $[(h_2 - h_1)/(p_2 - p_1)]_T$ on pressure, so these values were taken as a direct measure of the second enthalpy coefficient, β.

TABLE 1 MEASUREMENTS ON AIR

Run	t (°C)	$p_1 - p_2$ (lb/ft²)	G x 10^5 (lb/sec)	$h_2 - h_1$ (ft-lb/lb)	- β (ft³/lb)
34	10	3857.30	3.2069	158.120	0.04099
35	10	3845.27	3.2120	157.854	0.04105
36	10	3849.35	3.2074	156.728	0.04072
37	10	3855.34	3.2168	157.888	0.04095
39	10	6651.79	4.7403	274.970	0.04070*
40	10	6621.50	4.7361	273.470	0.04066*
41	10	6632.05	4.6882	275.511	0.04090*
42	10	6629.76	4.6926	271.214	0.04091
43	10	6632.40	4.6837	272.875	0.04114
44	10	3764.17	3.0071	150.943	0.04010
45	10	3784.44	3.0313	154.039	0.04070
Av.	10				0.04080
58	0	4716.04	3.7983	212.654	0.04509
59	0	4716.81	3.8051	212.118	0.04497
60	0	6701.83	4.7700	300.968	0.04491
61	0	6710.00	4.7968	299.782	0.04468
62	0	6714.34	4.7861	300.660	0.04478
63	0	6709.24	4.7913	299.923	0.04470
64	0	4734.15	3.8190	210.379	0.04444
65	0	4738.36	3.7782	214.186	0.04520
Av.	0				0.04485
66	30	4694.57	3.6955	164.978	0.03514
67	30	4696.13	3.6928	165.437	0.03523
68	30	4700.05	3.6887	164.536	0.03501
69	30	4695.59	3.7002	163.715	0.03487
70	30	6674.81	4.6418	232.611	0.03485
71	30	6676.33	4.6501	232.117	0.03477
72	30	6669.68	4.6574	233.423	0.03500
73	30	6672.00	4.6328	234.644	0.03517
Av.	30				0.03500

* These values were corrected for the presence of water.

There was evidence that in runs 39, 40, and 41, water was present in the calorimeter. This was attributed to adsorption of water on the walls of the calorimeter as a result of exposure to the atmosphere when the calorimeter was disassembled for repair just prior to run 39. These runs were corrected for the presence of water on the assumption that the inlet air to the calorimeter was saturated with water at 10 C. This correction was calculated from the data by J. A. Goff (2) and had the magnitude 0.00064 ft³/lb.

FORMULATION OF DATA

The data were formulated, using Equation [14], with the constants $2\pi N_0 r_0^3/3$ and k/ϵ, adjusted by the method of least squares to fit the three average values of β at 0 C, 10 C, and 30 C. The results were

$$2\pi N_0 r_0^3/3 = 0.0525_6 \pm 0.0062, \text{ ft}^3/\text{lb}$$

$$k/\epsilon = 0.01226 \pm 0.00056, \text{ deg K}^{-1}$$

The standard error of each of the three experimental values based on this formulation is ±0.00039 ft³/lb. Of course, the use of statistical methods with so few experimental values does not lead to reliable conclusions, but may be used as an indication of the goodness of fit. Values calculated from this formulation are compared with the experimental values in Table 2.

TABLE 2 COMPARISON WITH FIRST FORMULATION

T (deg K)	β (ft³/lb) Observed	 Calculated	 Deviation
273.16	0.04485	0.04466	—0.00019
283.16	0.04080	0.04112	0.00032
303.16	0.03500	0.03487	—0.00013

It was felt that the only other reliable values of β for air in the literature were those of A. Eucken, K. Clusius, and W. Berger (3). Therefore the least-squares adjustment of the constants in Equation [14] was repeated using their values as well. Their values were given a weight of one third as compared with the values from the present investigation. The results of this formulation were

$$2\,\pi\,N_0 r_0^3/3 = 0.05442 \pm 0.00187,\ \mathrm{ft^3/lb}$$

$$k/\epsilon = 0.01244 \pm 0.00019,\ \mathrm{deg\ K^{-1}}$$

The standard error of each of our experimental values based on this formulation is $\pm$0.00027 ft³/lb. Thus the results of this investigation can be formulated together with the Eucken, Clusius, and Berger data by means of Equation [14] with no significant change in the constants. A comparison of values calculated from this formulation and the experimental values is given in Table 3 and shown graphically in Fig. 4.

TABLE 3 COMPARISON WITH SECOND FORMULATION

T (deg K)	Observers	β (ft³/lb) Observed	Calculated	Deviation
273.16	Andersen	0.04485	0.04473	−0.00012
283.16		0.04080	0.04115	0.00035
303.16		0.03500	0.03483	−0.00017
193.0	Eucken Clusius Berger	0.08994	0.08947	−0.00047
249.5		0.05335	0.05452	0.00117
273.2		0.04509	0.04474	−0.00035
289.8		0.03919	0.03892	−0.00027

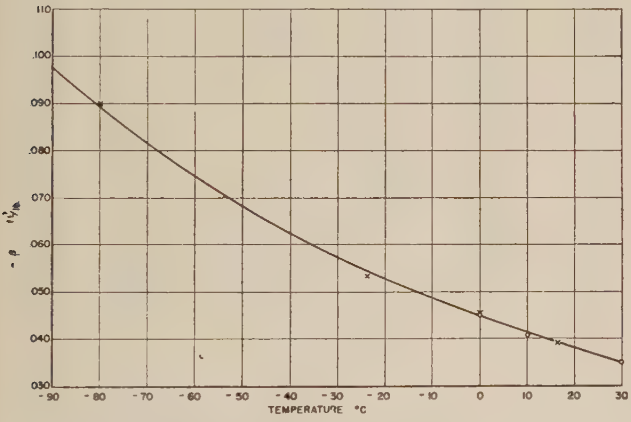

FIG. 4 THE SECOND ENTHALPY COEFFICIENT FOR AIR
(O, Andersen; ×, Eucken, Clusius, Berger; —β=—0.05442 G[0.01244 T].)

The agreement shown in Table 3 is excellent; therefore it is felt that Equation [14] with the second set of constants represents adequately the best available data on the second enthalpy coefficient for air in the temperature range —80 C to 30 C. This formulation, however, must be considered an empirical one since (*a*) air is a mixture of gases so that β should be represented by a linear combination of integrals of the type given in Equation [11] rather than by a single such integral; and (*b*) the Lennard-Jones form for the intermolecular force potential only approximates the correct potential. Therefore to deduce values of the second virial coefficient B, one would expect to modify Equation [13] to

$$B = (2\pi N_0 r_0^3/3)\ F(kT/\epsilon) + C_1 T \ldots\ldots\ldots\ldots [15]$$

in accordance with Equations [5] since there would be no good reason to expect the constant of integration to be zero.

A comparison of Equation [15], using the constants of the second formulation with the values of B obtained from the Holborn and Schultze compressibility data, quoted by Curtiss and Hirschfelder (4), and with a single unpublished value obtained in this laboratory by W. Pfefferle, is given in Table 4.

TABLE 4 COMPARISON OF B WITH OBSERVED DATA

t (deg C)	B (ft³/lb) Observed	Calculated	Deviation
0	−0.00653	−0.00665	−0.00012
30*	−0.00300*	−0.00301	−0.00001
50	−0.00126	−0.00112	0.00014
100	0.00209	0.00243	0.00034
150	0.00475	0.00474	−0.00001
200	0.00669	0.00713	0.00044

* This value is due to W. Pfefferle.

TABLE 5 COMPARISON OF FORMULATIONS OF β

t (°C)	- β (ft³/lb) (a)	(b)	(c)	(d)	(e)	(f)
100	0.01821	0.02147	0.02335	0.02258	0.02202	0.02199
75	0.02344	0.02544	0.02715	0.02633	0.02604	0.02614
50	0.02931	0.03023	0.03161	0.03073	0.03017	0.03116
25	0.03671	0.03614	0.03694	0.03601	0.03648	0.03739
0	0.04473	0.04360	0.04341	0.04245	0.04346	0.04379
- 25	0.05514	0.05329	0.05145	0.05051	0.05215	0.05183
- 50	0.06828	0.06634	0.06173	0.06093	0.0630	0.06146
- 75	0.08530	0.08475	0.07534	0.07501	0.0770	0.07549
- 100	0.10830	0.11231	0.09427	0.09525	0.0966	0.09377

(a) Present formulation (Equation (15))	
(b) Bridgeman (1929)	(7)
(c) Beattie-Bridgeman (1928)	(9)
(d) Claitor-Crawford (1948)	(8)
(e) Curtiss-Hirschfelder (1948)	(4)
(f) Roebuck-Murrell (1941)	(5)

The agreement is excellent, showing that Equations [14] and [15] with the constants $2\pi N_0 r_0^3/3 = 0.05442$ ft³/lb, $k/\epsilon = 0.01244$ deg K⁻¹, $C_1 = -2.33 \times 10^{-5}$ ft³/lb-deg K represent all existing extensive information on air [except the Roebuck Joule-Thomson data, reference (5)] adequately over the temperature interval—80 C to 200 C. This seems to show that the Roebuck data are systematically in error. This conclusion is in agreement with the observations of de Groot and Michels (6) on the Roebuck Joule-Thomson data for CO_2.

A comparison of the present formulation of the second enthalpy coefficient for air with several other current ones is given in Table 5. All of the quoted formulations except the present one and that of Bridgeman (7) have apparently given too much weight to the Roebuck data in the temperature range considered.

It may be remarked that the agreement of the present formulation and that of Claitor and Crawford (8) improves at lower temperatures and is quite good at —150 C to —180 C. This is encouraging, since the Claitor and Crawford formulation gives much weight to the accurate velocity-of-sound data available at these low temperatures.

CONCLUSIONS

Some new experimental values of the second enthalpy coefficient for dry, CO_2-free air are reported. These values were formulated together with the data of Eucken, Clusius, and Berger (3) by the equation

$$\beta = -0.05442\ G(0.01244\ T),\ \mathrm{ft^3/lb} \ldots\ldots\ldots [16]$$

The second virial coefficient was then calculated by means of the equation

$$B = 0.05442\ F(0.01244\ T) - 2.33 \times 10^{-5}T,\ \mathrm{ft^3/lb} \ldots [17]$$

in which the value of the constant of integration was adjusted to give the best fit with the Holborn and Schultz compressibility data for air. The conclusion is that Equations [16] and [17] represent adequately all reliable data on air in the temperature range —80 C to 200 C.

Acknowledgment

It is a pleasure for the author to acknowledge the aid of Dean John A. Goff, under whose direction this investigation was carried out. It is also a pleasure to acknowledge the aid of the Bureau of Ships and the Office of Naval Research, both of the United States Navy, who sponsored the project through the University of Pennsylvania Thermodynamics Research Laboratory. The aid of the members of the laboratory staff, particularly in the matter of construction of parts of the apparatus, is greatly appreciated. The helpful suggestions of Mr. Serge Gratch, particularly in regard to methods of formulating the data, were invaluable.

BIBLIOGRAPHY

1 "Viscosity and Other Physical Properties of Gases and Gas Mixtures," by J. O. Hirschfelder, R. B. Bird, and E. L. Spotz, paper presented at the Annual Meeting, New York, N. Y., November 28–December 3, 1948, of The American Society of Mechanical Engineers. (Preprints available from the Towne Scientific School, University of Pennsylvania.)

2 "Final Report of the Working Subcommittee of the International Joint Committee on Psychrometric Data," by J. A. Goff, paper presented at the Annual Meeting, New York, N. Y., November 28–December 3, 1948, of The American Society of Mechanical Engineers. (Preprints available from the Towne Scientific School, University of Pennsylvania.)

3 "Eine Apparaten zur exacten Messung des isothermen Drosseleffektes bei verschiedenen Temperaturen und Drucken," by A. Eucken, K. Clusius, and W. Berger, *Zeitschrift für Technische Physik*, vol. 13, 1932, pp. 267–270.

4 "Thermodynamic Properties of Air," by C. F. Curtiss and J. O. Hirschfelder, Navy Bureau of Ordnance Report, University of Wisconsin, CM-472, June 1, 1948.

5 "The Kelvin Scale From the Gas Scales by Use of Joule-Thomson Data," by J. R. Roebuck and T. A. Murrell, *Temperature*, Reinhold Publishing Corporation, New York, N. Y., 1941, pp. 60–73.

6 "The Joule-Thomson Effect and the Specific Heat at Constant Pressure of Carbon Dioxide," by S. R. de Groot and A. Michels, *Physica*, vol. 14, 1948, pp. 218–227.

7 "The Joule-Thomson Effect and Heat Capacity at Constant Pressure for Air," by O. C. Bridgeman, *Physical Review*, vol. 34, 1929, pp. 527–533.

8 "Thermodynamic Properties of Oxygen, Nitrogen, and Air at Low Temperatures," by L. C. Claitor and D. B. Crawford, paper presented at the Annual Meeting, New York, N. Y., November 28–December 3, 1948, of The American Society of Mechanical Engineers. (Preprints available from the Towne Scientific School, University of Pennsylvania.)

9 "A New Equation of State for Fluids," by J. A. Beattie and O. C. Bridgeman, Proceedings of the American Academy of Arts and Sciences, vol. 63, 1928, pp. 229–308.

Appendix

LENNARD-JONES FUNCTIONS *F* AND *G*

kT/ε	F	G	kT/ε	F	G
0.30	-27.878	104.47	2.60	- 0.2664	1.4211
0.40	-13.797	44.046	2.70	- 0.2236	1.3235
0.50	- 8.7204	25.637	2.80	- 0.1845	1.2339
			2.90	- 0.1483	1.1513
0.60	- 6.1978	17.450	3.00	- 0.1150	1.0750
0.70	- 4.7102	12.965			
0.80	- 3.7338	10.189	3.10	- 0.0843	1.0043
0.90	- 3.0474	8.3100	3.20	- 0.0559	0.9387
1.00	- 2.5380	6.9663	3.30	- 0.0292	0.8776
			3.40	- 0.0048	0.8207
1.10	- 2.1450	5.9555	3.50	0.0185	0.7674
1.20	- 1.8352	5.1728			
1.30	- 1.5842	4.5476	3.60	0.0403	0.7176
1.40	- 1.3755	4.0420	3.70	0.0608	0.6707
1.50	- 1.2008	3.6146	3.80	0.0800	0.6267
			3.90	0.0983	0.5852
1.60	- 1.0515	3.2577	4.00	0.1154	0.5461
1.70	- 0.9232	2.9523			
1.80	- 0.8119	2.6887	4.10	0.1315	0.5089
1.90	- 0.7141	2.4591	4.20	0.1465	0.4738
2.00	- 0.6277	2.2572	4.30	0.1606	0.4405
			4.40	0.1743	0.4089
2.10	- 0.5505	2.0781	4.50	0.1871	0.3788
2.20	- 0.4820	1.9180			
2.30	- 0.4200	1.7744	4.60	0.1995	0.3503
2.40	- 0.3638	1.6450	4.70	0.2112	0.3232
2.50	- 0.3129	1.5278	4.80	0.2228	0.2972
			4.90	0.2332	0.2725
			5.00	0.2435	0.2489

Discussion

F. G. Keyes.[3] The measurement of an isothermal property is always to be preferred to a nonisothermal one because of the great difficulty of controlling heat flow. Thus in the case of the Joule-Thomson effect, for example, a sharp fall or rise of temperature is produced in a length of tube through which a fluid passes a constriction in the tube, and the quantity desired is the ratio of temperature change to the pressure difference across the construction or expansion plug. The long history of the efforts to secure accuracy in the measurements of the Joule-Thomson effect is largely an account of successive improvements to control heat flow caused by the temperature difference being measured, and also kinetic effects induced in the gas by expansion at the "plug."

Professor Andersen's measurements of the enthalpy pressure coefficient of air

$$(\partial h/\partial p)_T = v - T(\partial v/\partial T)_r = (\partial v\tau/\partial\tau)_p,\ \tau = T^{-1}$$

are most encouraging, not only because they are made by a method which is, in principle, of the isothermal type, but also because the results lead directly to a quantity representative of the departure of a gas from the ideal state. The Joule-Thomson effect (μ) is, however, an involved function of "gas imperfection" as the equation

$$\mu = [T(\partial v/\partial T) - v]/[C_p{}^0 - \int T(\partial^2 v/\partial T^2)dp]$$

indicates. Indeed it is possible to design the apparatus for the measurement of both $(\partial h/\partial p)_T$ and $(\partial h/\partial T)_p$, $[C_p{}^0 + \int T(\partial^2 v/\partial T^2)dp]$, thus obtaining complete factual information on the equation of state and thermal properties in the equilibrium state. Moreover, by the use of this method the adverse effects of adsorption are avoided since a "flow" method is employed and measurements may be extended to temperatures practically inaccessible to apparatus employed for measuring p-v-T properties directly.[4]

The first exposition of the importance of measuring the quantity $(\partial h/\partial p)_T$ is due to Edgar Buckingham[5] and a full discussion of the significance and uses of both the enthalpy coefficient and the Joule-Thomson coefficient was published twelve years later by Harvey N. Davis.[6] The development of the required experimental procedures took place independently (1932) in Germany[7] and in the United States.[8] The methods used differed, however, in an important particular. In Germany the investigator allowed the gas to expand as in a Joule-Thomson measurement with subsequent warming to the initial temperature, thereby foregoing entirely any attempt to conduct an isothermal measurement. The United States workers expanded the gas in a uniform-bore platinum-iridium capillary tube in the walls of which an electric current was flowing sufficient to produce the heat needed to compensate for the Joule-Thomson cooling of the gas; a condition indicated by the equality of the temperature of the gas entering and leaving the capillary.[9,10]

---

[3] Department of Chemistry, Massachusetts Institute of Technology, Cambridge, Mass.

[4] Measurements of the p-v-T properties of helium have recently been reported by W. G. Schneider to 600° C; a remarkable achievement. "Compressibility of Gases at High Temperatures. II. The Second Virial Coefficient of Helium in the Temperature Range 0 to 600° C, by W. G. Schneider and J. A. H. Duffie, *Journal of Chemical Physics*, vol. 17, 1949, p. 751.

[5] "On a Modification of the Plug Experiment," by Edgar Buckingham, *Philosophical Magazine*, vol. 6, 1903, p. 519.

It will be observed that the flowing gas experiences a sharp change of velocity within the restriction and the attendant increase in kinetic energy of the gas will be compensated at the expense of the sensible heat of the fluid. There will also be energy amounts due to the friction of the fluid in the constriction besides entrance and exit effects. Accordingly $(\partial h/\partial p)_T$ cannot be made a rigorously isothermal experiment throughout the path of flow except in the limit of zero mass movement. However, the temperature changes due to the kinetic effects in the constriction are small relative to the Joule-Thomson effect, excluding the special region of inversion where $(\partial h/\partial p)_T$ tends to zero. Above the inversion temperature heat must be abstracted from the expanding gas and this cooling could be applied with precision by making use of the Peltier effect that occurs in proportion to electric-current flow at one of a pair of junctions formed by two metallic wires of differing substance.

The author employs for the correlation of his measurements the intermolecular potential, Equation [12] which is a convenient special form of the so-called Lennard-Jones formula for the potential energy of intermolecular interaction, namely, $E = \gamma r^{-n} - \mu r^{-m}$, where n/m is taken to be 2, and m is 6 in accord with the first approximation for the negative part of the potential based on the quantum theory. Equation [12] has been widely used, as the author states. The writer's colleague, Prof. I. Amdur,[11] has succeeded in measuring the repulsive or positive part of the potential in the case of He-He and He-H_2, and finds for the first and second pair of particles the following potential forms

$$\text{He-He, } V_+ \ (r) = 11.3 \exp{(-4.63\, r^{1/2})} \times 10^{-10} \text{ ergs } (r \text{ range } 0.55 - 1.05A)$$

$$\text{He-H}_2\text{, } V_+(r) = 0.846 \exp{(-24.9\, r^2)} + 0.211 \exp{(-2.40\, r^2)} \times 10^{-10} \text{ erg } (r \text{ range } 0.28 - 0.70A)$$

The foregoing equations are illustrative of the complexity of the analytical forms required to represent within experimental accuracy the positive potential. For the negative part of the potential it has long been known that where accuracy of knowledge of the potential is required, the following type of expression is to be used

$$V_- \ (r) = - \mu r^{-6}(1 + \mu_1 r^{-2} + \ldots\ldots \mu_n r^{-2n})$$

It is therefore clear that Equation [12] must be regarded as a rough expedient sufficient for exploratory purposes or as a first approximation, provided the ranges of representation are restricted. In the present case the range from —90 to 30 C is accurately represented and it is hoped measurements may be extended to temperatures of perhaps 500 C, or higher if possible.

AUTHOR'S CLOSURE

The remarks by Professor Keyes are greatly appreciated. To have Professor Keyes give a short history of the "Isothermal Joule-Thomson Experiment" is a welcome supplement to the paper since the author had not been willing to take the space for it and further since Professor Keyes has personally contributed such a great deal to it.

Professor Keyes' further remarks on the proper representation of the intermolecular force potential are very interesting and point up the difficulty in obtaining accurate analytical expressions for any thermodynamic property over an extended range of physical conditions. The interesting feature of the formulation presented in the paper is not that any particular virtue is associated with the use of the Lennard-Jones form for the intermolecular force potential but rather, that this crude approximation to the correct form for the intermolecular force potential represents the data so well.

---

[6] "Note on the Value of Joule-Thomson Observations for Computing Steam Tables," by Harvey N. Davis, *Physical Review*, vol. 5, 1915, p. 359.

[7] "An Apparatus for Exact Measurement of the Isothermal Porous Plug Effects at Various Temperatures and Pressures," by A. Eucken, K. Clusius, and W. Berger, Zeitschrift für Technische Physik, vol. 13, 1932, p. 267.

[8] "The Pressure Variation of the Heat Function as a Direct Measure of the van der Waals Forces," by F. G. Keyes and S. C. Collins, Proceedings of the National Academy of Science, vol. 18, 1932, p. 328.

[9] The further development of the method is reported in a paper, "The Heat Capacity and Pressure Variation of the Enthalpy for Steam From 38 to 125 C, Part V, Steam Research Program," by S. C. Collins and F. G. Keyes, Proceedings of the American Academy of Arts and Sciences, vol. 72, 1938, p. 72. This method can also be used to determine the heat of a chemical reaction for gaseous dissociations of the type $A_2 \rightarrow 2\ A_1$.

[10] "Note on the Year's Progress on the Precise Measurement of the Effects of Intermolecular Potential in Gases," by S. C. Collins and F. G. Keyes, *Journal of Physical Chemistry*, vol. 43, 1939, p. 5.

[11] "Repulsive Interaction Potentials at Small Interaction Distances: He-He and H_2-H_2 Systems," by I. Amdur, *Journal of Chemical Physics*, vol. 17, 1949, p. 844.

New Measurements of the Heat Conductivity of Steam and Nitrogen[1]

By F. G. KEYES[2] and D. J. SANDELL, JR.,[3] CAMBRIDGE, MASS.

The heat conductivity of steam has been measured by Timroth and Vargaftig (1940) from approximately 100 to 550 C and to pressures of 250 atm, using the hot-wire type of conductivity cell, wherein the wire of pure platinum serves as thermal emitter, and its electrical-resistance change provides the temperature indication. The new measurements in the present paper were obtained using a concentric cylinder type of conductivity cell in which the heater and thermometric parts were isolated from contact with the material whose conductivity was being measured. Vargaftig had published (1937) measurements of the heat conductivity of nitrogen in substantially the same cell used for steam. The new measurements on nitrogen are in tolerable agreement with the Vargaftig measurements, but in the case of steam the new measurements are considerably lower in magnitude. A comparison of the two sets of steam data indicates some peculiarities of temperature trend in the Timroth and Vargaftig data which find no correspondence in the data of any other substance, and also differs from the trend relative to the new data. A formulation of the steam and nitrogen data is given in terms of pressure and temperature as independent variables.

Measurements of the heat conductivity of steam for pressures of about 1 kg per cm^2 were published in 1937 by Vargaftig (1)[4] for the temperature range 69 to 550 C. A few years later, however (1940), data appeared by Timroth and Vargaftig (2) for the temperature range 250 to 550 C and to pressures of 250 kg per cm^2. These later data were correlated by one of the authors and a table of the values given in the Keenan and Keyes Steam Tables (3) beginning with the 1943 printing.

The only earlier measurements for steam are those of Moser (4) who gave values relative to air at 100 C and somewhat less. The most comprehensive earlier data, however, were published by Milverton (5) who carried out a painstaking investigation in the temperature region just below 100 C. Milverton detected a pressure effect; roughly, one tenth of that deducible by extrapolation from the data of Timroth and Vargaftig. Milverton's formulated data give a value for the heat conductivity of steam at 100 C at zero pressure,[5] in fair agreement with Vargaftig's 1937 value: $5.77 \cdot 10^{-5}$ and $5.63 \cdot 10^{-5}$, respectively, in cgs units. Moser's values are now mainly of historic interest.

The present measurements of the heat conductivity of nitrogen are associated with those of steam for several reasons, as follows:

1 All the measurements on steam have been obtained using the "hot-wire" method originally due to Schleiermacher (6); a method which makes use of a wire of pure platinum stretched axially within a tube containing the fluid of interest. The wire serves as an electrical heater for measured heat losses and also as a resistance thermometer. The method during the past 25 years has been brought to a high state of perfection for the measurement of heat conductivities of gases at low pressures. The Timroth and Vargaftig (2) measurements on steam represent an attempt to adapt the hot-wire method to measurements with steam and nitrogen [Vargaftig (1)] under pressure. It is desirable, however, to confirm the accuracy of the existing results through the use of a different method, and the alternate measurements of nitrogen and steam in the steam cell constitute a control which has proved highly desirable.

2 The case of steam presents difficulties of a fundamental nature in interpreting the apparent heat conductivities due to its highly polar character,[6] namely, its property of absorbing and emitting radiation. All metals emit radiation when heated and in varying degrees depending upon the state of the emitting surface. Thus silver under the most favorable conditions will reflect close to 99 per cent of radiant energy, while platinum wire in practice may, as shown by Milverton, reflect only 90 per cent or less. The use of nitrogen, which is transparent to radiation, served as a means of controlling the behavior of the steam cell.

The effect of radiation absorption on the heat conductivity (the latter defined as proportional to the temperature gradient) may be described by noting that the gradient, when determined by measuring the surface temperatures of the metal, or other material, walls of the conductivity cell between which the steam is confined, does not correspond to the actual gradient since a part of the radiant energy emitted by the hotter surface is absorbed depending on the

---

[1] Results recorded in this article are from a thesis submitted as partial fulfillment of the requirements for the degree of Doctor of Philosophy in Chemistry at the Massachusetts Institute of Technology.

This paper is a summary of part of the results obtained in the course of a program of research supported by the Office of Naval Research.

[2] Professor of Physical Chemistry, Massachusetts Institute of Technology. Mem. ASME.

[3] Graduate Student, Massachusetts Institute of Technology.

[4] Numbers in parentheses refer to the Bibliography at the end of the paper.

Contributed by the Research Committee on Properties of Gases and Gas Mixtures, Heat Transfer, and Applied Mechanics Divisions and presented at the Annual Meeting, New York, N. Y., November 27–December 2, 1949, of The American Society of Mechanical Engineers.

Note: Statements and opinions advanced in papers are to be understood as individual expressions of their authors and not those of the Society. Paper No. 49—A-43.

[5] The meaning to be attached to the phrase, "heat conductivity at zero pressure, λ_0," in the case of gases, is similar to "specific heat at zero pressure, $C_p{}^0$." The concept relates to the fact of experience that on extrapolation of the quantities measured at finite pressures to lower pressures, the "pressure effect" becomes linear to an increasing degree as the limit zero is approached, and λ_0 is the limiting value in the sense of this ultimate extrapolation. Experience shows, however, that at very low pressures, beginning at about 0.1 mm (about 0.002 psia), gases begin to exhibit properties in containers of finite size in contrast to the properties manifest when the distance interval between molecular collisions is microscopic relative to the dimensions of the container. Thus in the heat-conductivity cell used in the present investigation at a pressure of 0.0000002 psia, the number of molecules between the walls has become so small that the amount of heat transferred by them is not measurable in comparison to the heat transferred by radiation. It follows also that the quantities λ_0 and $C_p{}^0$ are functions of temperature only as $(pv)^0$ is solely temperature-dependent.

[6] The term "polar" refers to the fact that the water molecule, due to its structure and in complete contrast to nitrogen, possesses a permanent electric dipole of large magnitude. The presence of the dipole is responsible for the strong energy radiation absorption and emission characteristics of steam.

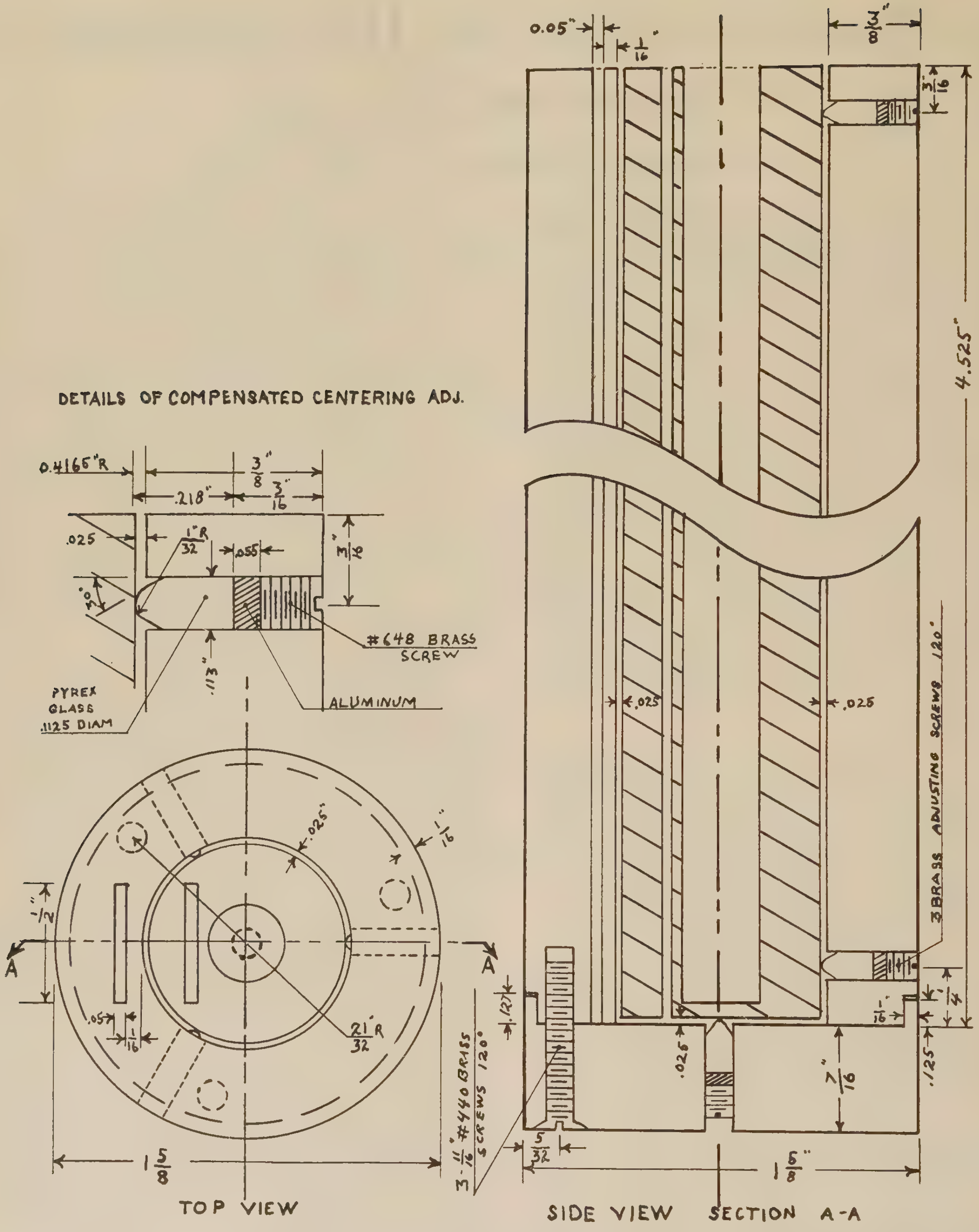

Fig. 1 Conductivity Cell and Heating Cylinder
Material—silver.)

geometry and distance of separation of the surfaces and the detailed structure of the emission spectrum of the steam. The usual procedure of subtracting the total amount of the radiation due to the hotter surface from the total energy input to the cell is permissible in the case of a radiation-transparent gas like nitrogen, but evidently not in the case of the polar substance water vapor, unless the radiation effect is of the same order of magnitude as the experimental error of the conductivity measurement or less. In so far as is known, the rational adjustment of measurements of heat conductivity of polar substances to allow for radiation-absorption characteristics has never been made or discussed.

Finally, the choice of cell design in the case of steam must be governed by the finite electrical conductivity which is a property of water and adsorbed water vapor on surfaces. The disturbing effects of moisture, for example, on the behavior of platinum-resistance thermometers has long been known.

The leads from the cell used by Timroth and Vargaftig were in contact at room temperature with liquid water at the point of exit from the cell case. This circumstance along with possible disturbance to the functioning of the platinum wire as a resistance thermometer because of adsorbed water vapor and the Thomson effect[7] was not discussed in their paper and the question of radiation "corrections" was referred to without sufficient detail for critical judgment. Since Vargaftig in the 1937 paper gives tests of a steam cell using nitrogen as well as steam, a comparison of the results using nitrogen and steam in our steam cell proves interesting.

The Strain-Free and the Steam Cell

There has been in use during the past year a silver "strain-free" cell and also the steam cell whose heaters and thermocouples and all leads were encased to prevent contact with steam or water. The encasement predisposed the cell to thermal strains which were absent in the strain-free type where the heater and thermocouples were in direct contact with the substance under measurement. The leads from the strain-free cell parts were, however, so delicate (0.003-in. × 0.0155-in. ribbon) that no strain or distortion of recognizable amount could occur through temperature or pressure change.

The general form of cell employed, Fig. 1, was the concentric cylinder type of fine silver with an axial heater throughout the length of the inner cylinder, and thermocouples in the cylinder walls of the inner or emitter cylinder and the outer or receiver cylinder. A bottom portion of silver was attached, adjusted in distance of its inner surface from the lower face of the emitter by an amount (0.025 in. ± 0.0001 in.) equal to the annulus formed by the emitter and receiver. Thermal contact of the bottom piece to the receiver was secured by means of three screws holding the surfaces at the receiver piece in contact.

Above the cell there is a "heat station" or heat guard to intercept the flow of heat to or from the emitter along the electrical leads.[8] The heat station contains a heater and a thermocouple along with means for bringing about good thermal contact of the leads with the body of the heat station. The temperature of the heat station, as indicated by its thermocouple, was maintained the same as that of the emitter as recorded by its thermocouples.

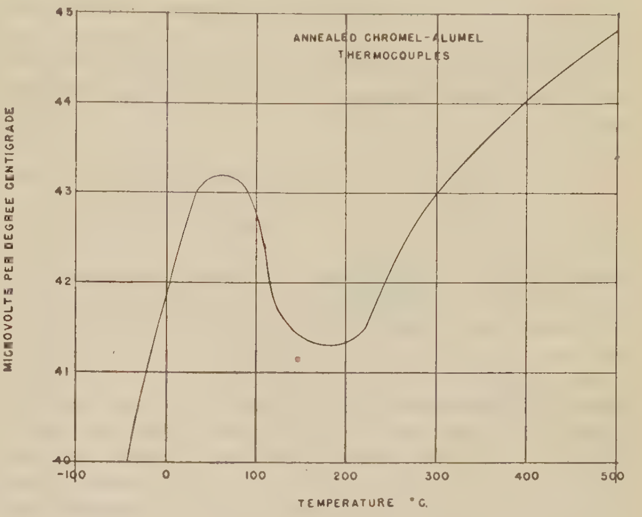

Fig. 2 Annealed Chromel-Alumel Thermocouples

The thermocouple wire employed was chromel-P and alumel, chosen because of its adaptability to high temperatures, its large and moderately constant value of dE/dt over the temperature range of the measurements.

It was necessary to develop means for measuring $\Delta E/\Delta t$, where E is the electromotive force (emf) of the couple, and Δt, the temperature difference between hot and cold junction, was 2 to 5 deg C. The course of the $\Delta E/\Delta t$ values is represented in Fig. 2 and a confirmation of the accuracy of the values was obtained by comparing the graphically obtained integral values from the $\partial E/\partial t$, t-plot from zero to various temperatures with measured integral values between the ice point and corresponding temperatures. For example, the 0-deg to 100-deg-C measured value of the emf is 4289 μv, while the integrated value 4290 was found by graphical integration under the dE/dt, t-curve. All thermocouple wire used was in ribbon form 0.003 in. thick and 0.0155 in. wide, annealed to 500 deg C for 205 hr in the presence of carbon dioxide. The potentiometer was sensitive enough for readings to 0.1 μv, equivalent to 0.0025 deg C for a single junction. For the 25-ohm platinum-resistance thermometers a Mueller bridge of Wolff manufacture was employed.

The Cell Constant

The dimensions of the silver emitter and receiver were obtained through the use of the length-measuring facilities and standard gages of the mechanical engineering department (M.I.T). However, to obtain the mean diameter of the inside cylindrical surface of the receiver, it was first measured for length and outer diameter prior to drilling the thermocouple and centering holes. From the weight of the receiver in air and water, using Archimedes' principle, it accordingly became possible to deduce the mean inner diameter. The dimensions, Fig. 1, of the steam cell were approximately as follows: Length of annulus, 4.5 in.; smaller diameter of annulus, 0.8512 in.; larger 0.9012 in.; annular width 0.025 deg. The strain-free cell was very closely of the same dimensions.

The Fourier theory of heat conduction leads to the following equation for a steady state of heat flow in the case of an infinite cylindrical annulus where λ is the heat conductivity of the material in the annulus; r_2 its larger and r_1 its smaller radius; L the length; t_2 and t_1 the temperatures corresponding to the surfaces of radii r_2, r_1; and q_c the heat flow per sec in the steady state

$$q_c/(t_2 - t_1) = \lambda \frac{2\pi L}{\ln r_2/r_1} \quad \ldots\ldots\ldots\ldots\ldots [1]$$

---

[7] The Thomson effect is a measure of the amount of distortion of a temperature gradient due to an electric-current flow. If σ denotes the Thomson coefficient, q the heat absorbed or evolved depending upon the direction of current flow, then $q = \sigma\, i(dt/dx)dx$. The effect has never been given consideration in interpreting the data from "hot-wire" conductivity cells.

[8] The intercepting of heat flow along the leads is necessarily imperfect in the case of the heater leads because of the higher temperature which the heater wire must have to effect heat transfer to the body of the emitter. This heater-wire temperature will be greater as the energy imparted to the heater is increased.

The heat-temperature difference ratio for the circular bottom of the emitter is $q_b/(t_2 - t_1) = \lambda(\pi r_1^2)/(\Delta r)$ where Δr is $r_2 - r_1$. There will also be a small additional flow of heat at the corners of this bottom disk, an item, $q_c/(t_2 - t_1) = (c\lambda)/(\Delta r)$, approximately $^1/_{300}$ of the whole. We have then

$$\lambda = \Sigma q/\Delta t \left(\frac{1}{\dfrac{2\pi L}{\ln r_2/r_1} + \dfrac{\pi r_1^2}{\Delta r} + \dfrac{c}{\Delta r}} \right) = \Sigma q/\Delta t \times C \ldots [2]$$

where C is the cell constant equal to the quantity in parentheses, a function only of the cell dimensions.

A question arises regarding the degree of approximation to infinite length for the actual cell described. The ratio of length to annular width is 180. However, the material silver has a conductivity 17,000 times that of air at 0 deg C and 1 atm, and while toward the bottom heat is actually flowing axially as well as radially, the proportion is only 1 in 22 of the whole for the entire emitter surface, while at the top heat is largely prevented from flowing axially owing to the presence of the heat station at the same temperature as the emitter. However, the main reliance justifying the use of the infinite cylinder formula rests on the fact of the enormously greater heat conductivity of the silver tending to prevent to a good approximation any variation of temperature at points on the radius of the emitter near the bottom. Tests with a brass cell at the outset of the investigation indicated no "measurable" differences in temperature at the ends of the emitter relative to temperatures at the middle.

Using the computed cell constant in the case of the strain-free cell, the following values were obtained for the heat conductivity of air at 0 deg C.

Strain-free brass cell $\lambda \cdot 10^5$ = 5.83 (steam calories per cm per sec per deg C)
Strain-free silver cell $\lambda \cdot 10^5$ = 5.80
Correlation value $\lambda \cdot 10^5$ = 5.77

The "correlation" value quoted is obtained from a consideration of all the published data to 1947, for the heat conductivity of air. The smoothing equation found to be satisfactory follows

$$\text{(Air) } \lambda_0 \cdot 10^5 = \frac{0.6302\sqrt{T}}{1 + 245.1\tau/10^{12\tau}}, \text{ IT cal per cm per sec per deg C} \ldots\ldots [3]$$

where λ_0 signifies the conductivity for the limiting pressure zero, T denotes Kelvin scale temperature, and τ its reciprocal T^{-1}. The large amount of data for air extending over the temperature range about 100 deg to 600 deg K lies for the greater part in a deviation band of width ± 3 per cent.

Mode of Taking and Treating Observational Data

It is a well-known fact that the amount of energy which is radiated from the surface of a solid surface is very sensitive to the state of the surface. The presence of a film of oil, oxide, or even in some instances vapors, is known to increase markedly the radiation absorbed or emitted. The experimental arrangement in the present measurements permitted the cell case to be highly exhausted to the point where residual gas made no measurable contribution to the loss of heat from the emitter. The measured losses in vacuo were then due to conduction at the points of support of the emitter at the pyrex cone contact, Fig. 1, along the copper leads of the heater and to radiation from the emitter surface.[9] At each temperature of observation in the strain-free cell used for the nitrogen measurements, a determination of the in-vacuo heat loss was made. In the case of the steam cell, in-vacuo heat-loss determinations were made at 100 C and the cell constant determined using the control gas nitrogen. At higher temperatures the in-vacuo heat loss was determined through the use of nitrogen.

The quantities measured are the heat input to the emitter in joules of electrical energy, the temperature of the emitter at a point about 1 mm from the emitter surface, and similarly the temperature of the receiver. The temperature of the surface of the emitter and the receiver is not the same as the temperature of these elements at a finite distance from the surface, except for infinitely small energy rates to the emitter. Also, only in the limit of small energy input will the lead loss along the heater leads, due to the unavoidable higher heater-wire temperature, become negligible. Turbulence or natural heat convection, while allowed for in the design, can be regarded as rigorously absent only when the temperature difference approaches zero.[10] Therefore at least three complete sets of observations of the steady-state values for increasing energy input with corresponding readings of the temperatures of the cell elements were made for each constant temperature of the surrounding environment of the cell case and constant pressure of the substance under measurement. By graphical treatment the value of $q/\Delta t$, the energy input divided by the corresponding temperature difference, was obtained for $q^2/\Delta t$ approaching zero. The following considerations indicate the reason for using the latter variable:

The total heat input q is assumed given by the following equation

$$q = \lambda C\,\Delta t + C_r(\bar{T})^3\,\Delta t + G\,\Delta t + C_e\,q^2 \ldots\ldots\ldots [4]$$

where λ is the heat conductivity of the gas within the cell in a fixed state, C is the cell constant, and Δt the temperature difference corresponding to the energy input q. C_r is the radiation constant for the cylindrical silver emitter, $\bar{T}$ the mean temperature of emitter and receiver, G the constant appropriate to the conduction of heat along the centering supports maintaining the emitter in an axial position within the receiver, while C_e is a constant of proportionality relating to the elevation of temperature at the heater-copper lead junction above the mean temperature of the heat station.[11] Dividing the left-hand member of Equation [4] by Δt leads to the justification for the choice of variables.

An equation similar to Equation [4] results for the in vacuo situation with the term containing λ absent. Therefore, by determining the limiting value of $q/\Delta t$ for the in-vacuo condition, it becomes possible to compute λ. All the heat conductivities listed were obtained by this procedure of multiple observations, and their graphical extrapolation to obtain $(q/\Delta t)\ q \rightarrow 0$.

---

[9] The radiation loss from the silver surface may be assumed related to temperature according to the fourth power of the Kelvin temperature. It has been found that the emissivity of silver formulated by this relationship is a function of temperature. Evidently the radiation loss of heat becomes very great at high temperatures and for this reason the accuracy of measurements of heat conductivity becomes progressively impaired with advancing temperature. It will also be observed as mentioned earlier that the difficulty of interpreting the observational data becomes greatly enhanced in the case of polar substances among which steam is an outstanding example.

[10] H. Kraussold (7) has shown that the criterion for negligible convection requires that the annulus width δ in the concentric cylinders be given by the following relationship

$$\delta \gtreqless 10 \left(\frac{\mu k}{\rho^2 \cdot g \cdot \beta \cdot \Delta t \cdot c} \right)^{1/3}$$

where c is the specific heat, μ the viscosity, ρ the density, g the gravitational acceleration, β the volume exhaustivity with temperature, and Δt the temperature difference.

[11] The temperature elevation of the heater wire above the mean temperature of the emitter necessarily required to effect heat transfer may be assumed to vary with energy transferred as the energy input for small inputs, or $\partial\epsilon/\partial q \sim q$, which leads to the relation ϵ, the elevation of junction temperature, proportional to q^2. The latter relationship follows from the empirical finding of a linear relation between $q/\Delta t$ and $q^2/\Delta t$.

TABLE 1 HEAT CONDUCTIVITY OF STEAM
(IT cal per sec per cm per deg C)

t °C	p atm	$10^5 \lambda$ obs	$10^5 \lambda$ calc *	Dev. **
102.86	0.03	5.666 a	5.665	0.0
102.82	0.47	5.734 a	5.719	+ 0.3
199.84	4.67	8.064 c	7.773	+ 3.6
199.80	12.52	8.650 c	8.310	+ 3.9
202.30	0.03	7.391 a	7.580	- 2.6
202.34	4.70	7.580 a	7.819	- 3.2
202.40	9.26	7.973 a	8.102	- 1.6
202.30	12.52	8.264 a	8.340	- 0.9
297.85	4.71	9.668 c	9.584	+ 0.9
297.77	12.52	9.887 c	9.792	+ 1.0
297.91	21.97	10.144 c	10.090	+ 0.5
297.21	43.49	10.712 c	11.024	- 2.9
300.40	73.87	12.517 c	13.187	- 5.3
306.64	39.98	10.752 b	10.894	- 1.3
306.40	63.92	11.333 b	12.249	- 8.1
306.82	21.54	10.325 b	10.199	+ 1.2
307.52	4.57	9.938 b	9.759	+ 1.8
307.39	4.57	9.915 b	9.759	+ 1.6
307.76	12.70	10.205 b	9.958	+ 2.4
307.33	12.70	10.171 b	9.958	+ 2.1
351.18	12.52	10.560 c	10.741	- 1.7
350.53	43.71	11.470 c	11.473	0.0
350.76	72.86	13.032 c	12.522	- 3.9
349.01	103.77	13.925 c	14.229	- 2.2
350.40	149.93	18.681 c	18.686	0.0

* Computed from the following equation

$$10^5 \lambda_p = 10^5 \lambda_o + 1.096\,(10^{0.934 \times 10^9 \tau^4 p} - 1)$$

where $\tau = T^{-1}$ and p is in atm.

and $$10^5 \lambda_o = \frac{1.5456 \sqrt{T}}{1 + 1737.3\tau/10^{12\tau}}$$

** The deviation is given by the expression

$$\frac{\lambda_{obs} - \lambda_{calc}}{\lambda_{obs}} \times 100$$

a represents values of heat conductivity in steam cell No. 1

b represents values of heat conductivity in revision No. 1 of steam cell No. 1

c represents values of heat conductivity in revision No. 2 of steam cell No. 1

The Steam Data

The value of λ, the heat conductivity for steam, deduced from the observations taken to August, 1949, are assembled in Table 1.

The basis for correlating the data requires λ_0, the heat conductivity corresponding to zero pressure, since the quantity is a function of temperature only, and it is convenient in the absence of any adequate theory of the effect of pressure on heat conductivity to assume that λ generally may be represented by the following form of relationship

$$\lambda = \lambda_0 + f(\tau_1 p) \qquad [5]$$

It is likely that when more complete data for a variety of substances become available the pressure dependence can be more simply expressed in terms of density and temperature as independent variables, but convenience at present is served by a pressure-temperature function.

It may be supposed that the pressure effect will diminish as T increases ($T^{-1} = \tau$ small), and this indeed proved to be the case when, some years ago, the Timroth and Vargaftig data were correlated. The form of function $f(\tau,p)$ found to represent the Russian data most satisfactorily was as follows

$$f(p,\tau) = C\,[e^{a\tau^4 p} - 1\} \qquad [6]$$

a relationship which vanishes as p approaches zero and also as T becomes very large for any finite pressure. Also, for small pressures at all finite temperatures the pressure effect of $f(\tau, p)$ becomes $(Ca)\tau^4 p$, on expanding the exponential in Equation [6], a linear dependence.

At constant pressure λ_0, as has long been known, increases indefinitely and regularly with temperature while $f(\tau, p)$ of Equation [6] decreases. Therefore, for a particular value of the temperature along the isopiestic heat conductivity-temperature course, there will be a minimum in λ, the minima for increasing isopiestics occurring at progressively higher temperatures. This is exactly what the Timroth and Vargaftig data show with λ falling from the saturation-pressure value, reaching the minimum and again increasing. Therefore, for the isopiestic above the minimum there are two temperatures with numerically equal λ-values.

The value of C in Equation [6] was taken to be 1.096 for the new steam data with $0.934 \cdot 10^9$ ($2.151 \cdot 10^9$ nat logs) for a. The λ_0 values employed in computing the values in Table 1 were obtained from the following equation based on the 1-atm measurements

$$10^5 \lambda_0 = \frac{1.5456 \sqrt{T}}{1 + 1737.3\tau/10^{12\tau}}, \text{ IT cal per sec per cm per deg C} \qquad [7]$$

The fifth column of Table 1 lists the deviations of the observed conductivities from those computed and there appears to be no pronounced trend in sign except the tendency to negative values around 200 deg and positive at about 307 deg C. It will be observed that the $f(\tau,p)$ chosen is a two-constant form and, when additional data are available, it may be found that a less simple correlative equation is required.

The Timroth and Vargaftig data were represented some years ago (3) by the form of Equation [6], with, however, the constants $c = 2.486$ and $a = 1.832 \cdot 10^9$ (nat logs) for pressure in atmospheres, τ in reciprocal Kelvin degrees, and $10^5\lambda$ in IT cal per sec per cm per deg C. Accordingly, the pressure effect is considerably larger for the Timroth and Vargaftig observations. It was also found that the λ_0, or more accurately, the λ_1 values for 1 kg per cm² exhibited an exponential rise with temperature beginning at about 250 C, and extending to 550 C. The equation obtained for the Timroth and Vargaftig λ_1 data (1 kg per cm) follows

$$10^5 \lambda_1 = 0.3191 \sqrt{T}\, e^{1.5234 \cdot 10^{-9} T^3}, \text{ cal per sec per cm per deg C} \qquad [8]$$

However, taking the ensemble of low-pressure data published in the 1937 paper of Vargaftig (1), and the 1940 paper of Timroth and Vargaftig (2), it is possible to correlate the data from below 100 to 550 C with the following form

$$10^5 \lambda_1 = \frac{1.0446 \sqrt{T}}{(2.191 \cdot 10^3 \tau / 10^{1.59 \cdot 10^4 \tau^2} - 1)} \qquad [9]$$

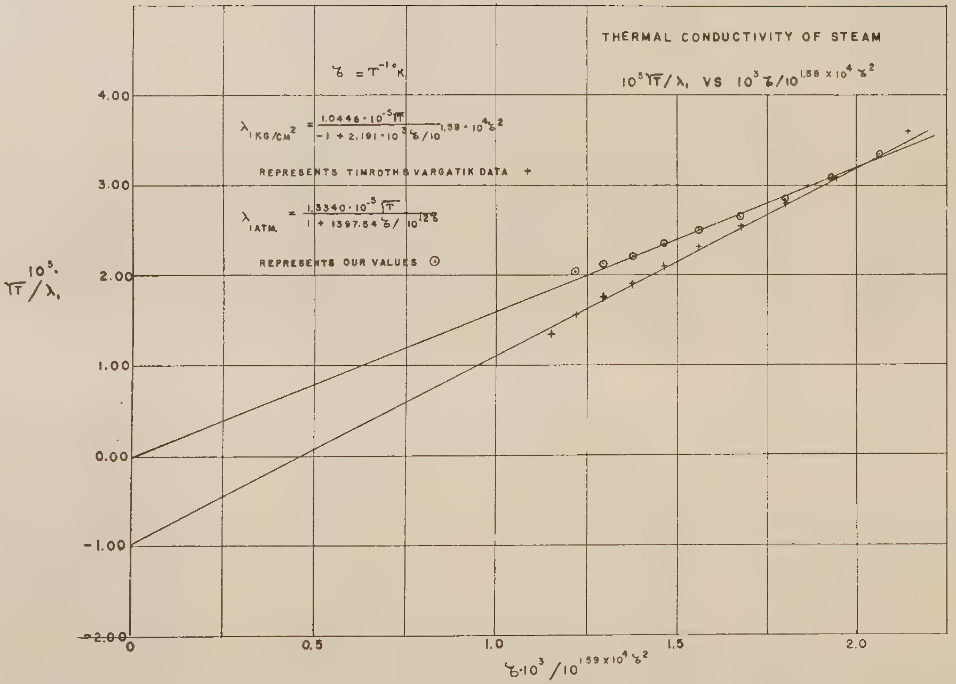

Fig. 3 Thermal Conductivity of Steam $10^5\sqrt{T}/\lambda_1$ Versus $10^3\tau/10^{1.59\times10^4\tau^2}$

TABLE 2 HEAT CONDUCTIVITY OF STEAM

($10^5\lambda$ in IT cal per sec per cm per deg C)

t	$10^5\lambda$ (TV)calc (a)	$10^5\lambda$ (TV)obs (b)	$10^5\lambda$ (KS) (c)
		20 kg per cm²	
250	10.58	10.97 (+3.5)	9.33 (+13.4)
300	11.14	11.33 (+1.7)	10.04 (+11.0)
350	12.18	12.11 (-0.5)	10.87 (+12.0)
400	13.65	13.61 (-0.3)	11.78 (+15.9)
500	18.20	18.55 (+2.0)	13.70 (+32.8)
		40 kg per cm²	
300	12.49	12.22 (-2.2)	10.80 (+15.7)
350	13.01	12.67 (-2.6)	11.33 (+14.9)
400	14.20	14.11 (-0.6)	12.08 (+17.6)
500	18.49	19.03 (+2.9)	13.84 (+33.6)
		60 kg per cm²	
300	14.35	13.89 (-3.2)	11.91 (+20.5)
350	14.06	13.39 (-4.8)	11.93 (+17.8)
400	14.86	14.94 (+0.5)	12.45 (+19.4)
500	18.80	19.50 (+3.7)	14.02 (+34.0)
		100 kg per cm²	
350	17.09	15.83 (-7.3)	13.78 (+24.0)
400	16.59	16.28 (-1.9)	13.46 (+25.3)
500	19.54	20.22 (+3.5)	14.43 (+35.4)
		150 kg per cm²	
350	23.53	21.67 (-7.9)	18.11 (+30.0)
400	19.77	18.61 (-5.9)	15.45 (+27.3)
500	20.69	20.83 (+0.7)	15.09 (+38.1)

(a) Correlation values computed from the following equations based on Timroth and Vargaftig's values reported in 1940:

$$10^5\lambda_0 = 0.3191\sqrt{T}\,10^{0.6616\cdot10^{-9}T^3} \;:\; 10^5\lambda = 10^5\lambda_0 + 2.486(10^{0.77\cdot10^9\tau^4 p} - 1);$$

pressure in kg per cm²

(b) Timroth and Vargaftig's reported values. The bracketed number is the quantity $\frac{\lambda_{obs} - \lambda_{calc}}{\lambda_{obs}} \times 100$.

(c) Values computed from the following equations based on the new observations of the heat conductivity reported in Table I. The bracketed adjacent numbers are the deviations in percent relative to the TV computed value.

$$10^5\lambda_0 = \frac{1.5456\sqrt{T}}{1 + 1737.3\tau/10^{12\tau}} \;;\; 10^5\lambda = 10^5\lambda_0 + 1.096(10^{0.934\cdot10^9\tau^4 p} - 1);$$

pressures in atm.

Note: The equation designated $10^5\lambda_0$ in the Steam Tables and based upon the Timroth and Vargaftig observations is actually formulated from their one kilogram per cm² values. Accordingly the $10^5\lambda_0$ equation should be labeled $10^5\lambda_1$ and (p - 1) substituted for p in the $f(\tau,p)$ part of the $10^5\lambda$ equation. However the error introduced by assuming $10^5\lambda_1$ equal to $10^5\lambda_0$ is inconsequential in the temperature range 250° to 500° C.

The implications contained in the form Equation [9] are made evident by considering Fig. 3 where $10^5\sqrt{T}/\lambda_1$ is plotted versus $\tau\cdot10^3/10^{1.59\cdot10^4\tau^2}$. In the figure the observed Vargaftig, and Timroth and Vargaftig data are represented and also the authors' data for 1 atm. The Russian λ_1, $\sqrt{T}$ data in the variable $\sqrt{T}/\lambda_1$ decrease so rapidly with increasing temperature (declining τ) that the extrapolation to higher temperatures than 550 C is moving to negative values in contrast to the trend of the new data. Extrapolation of λ_1 by means of either Equation [8] or Equation [9] to 2000 K would cause λ_1 to assume very large values; literally infinite values for temperatures which would cause the denominator of Equation [9] to vanish. Actually, however, the new data (λ_0 instead of λ_1) are best represented by Equation [7]; an equation of the form which correlates satisfactorily the λ_0 values for a number of other gases from low (—200 C) temperatures to about 300 C (air, nitrogen, oxygen, hydrogen, helium, carbon monoxide, and carbon dioxide).

TABLE 3 HEAT CONDUCTIVITIES OF STEAM FOR PRESSURES APPROACHING ZERO

t °C	$10^5\lambda_1$(T.V.)[a]	$10^5\lambda_0$(T.V.)[b]	$10^5\lambda_0$(K.S.)[c]	Dev.[d]
250	9.078	9.046	8.518	6.1
300	10.178	10.156	9.522	6.7
350	11.517	11.502	10.522	9.3
400	13.177	13.166	11.533	14.2
500	17.941	17.934	13.566	32.2

a Computed from the equation $10^5\lambda_1 = 0.3191\sqrt{T}\ 10^{0.6616\cdot10^{-9}T^3}$ see "Note" at foot of Table 2.

b The values in column three are the λ_1 values (1 kg per cm^2) of Timroth and Vargaftig corrected by using the Keyes and Sandell f(τ,p) relation. See "c" at foot of Table 2.

c These values are computed from the $10^5\lambda_0$ equation based on the new observations.

d $\dfrac{\lambda_0\,\text{T.V.} - \lambda_0\,\text{K.S.}}{\lambda_0\,\text{K.S.}} \times 100$

The data of Timroth and Vargaftig are compared with the new data on heat conductivity in Table 2 for temperatures from 250 to 500 C at pressures from 20 kg per cm². The comparison is made of the computed Timroth and Vargaftig values with computed values using the correlative equations based upon the new data and given at the bottom of the table. The corresponding observed values of Timroth and Vargaftig are also listed in the table to supply an impression of their accord with the computed values. In every case the new values as represented by the correlative equations are less than the Timroth and Vargaftig values. However, the temperatures of the new observations do not extend above 350 C.

It is of interest to compare the low pressure λ_0, or λ_1, values from the Timroth and Vargaftig measurements with the similar new values. For this purpose Table 3 is given for the range 250 to 500 C. Below 250 C the agreement between the two groups of low-pressure data is more satisfactory, although the Timroth and Vargaftig data are the larger. From Table 3 it appears that a considerable part of the difference between the Timroth and Vargaftig data and the new data is caused by the larger λ_0-value.

TABLE 4 NEW DATA FOR HEAT CONDUCTIVITY OF NITROGEN

t °C	p atm	$10^5\lambda$ obs	$10^5\lambda$ calc *	Dev.
0.57	1	5.857 a	5.824	+ 0.6
0.70	1	5.790 b	5.824	- 0.6
0.69	45.5	6.370 b	6.388	- 0.3
0.48	93.7	7.106 b	7.105	+ 0.0
0.64	140.7	7.958 b	7.963	- 0.1
27.21	1	6.257 a	6.234	+ 0.4
29.40	26.0	6.609 a	6.527	+ 1.2
25.54	60.9	7.065 a	6.891	+ 2.5
24.38	91.2	7.340 a	7.291	+ 0.7
24.05	122.6	7.787 a	7.829	- 0.5
25.14	151.7	8.286 a	8.290	- 0.1
104.46	1	7.293 d	7.264	+ 0.4
104.15	1	7.292 a	7.264	+ 0.4
101.58	1	7.241 c	7.229	+ 0.2
104.12	44.7	7.781 a	7.637	+ 1.9
101.24	49.6	7.759 c	7.646	+ 1.5
101.63	100.7	8.328 c	8.170	+ 1.8
104.11	101.0	8.294 a	8.197	+ 1.2
200.55	1	8.394 d	8.410	- 0.2
202.29	1	8.402 a	8.430	- 0.3
199.80	1	8.374 c	8.402	- 0.3
202.49	24.9	8.813 a	8.588	+ 2.6
200.25	49.6	8.796 c	8.729	+ 0.8
202.61	91.0	9.344 a	9.070	+ 2.7
202.25	100.7	9.219 c	9.116	+ 1.1
202.69	146.9	9.772 a	9.547	+ 2.4
308.56	1	9.210 b	9.560	- 3.8
301.20	1	9.183 d	9.485	- 3.3
307.18	1	9.419 b	9.545	- 1.3
297.85	1	9.199 c	9.428	- 2.5
310.08	45.5	9.641 b	9.815	- 1.9
297.73	49.6	9.611 c	9.697	- 0.9
310.12	93.7	9.932 b	10.100	- 1.7
307.17	93.7	9.906 b	10.073	- 1.7
297.85	100.7	9.938 c	10.011	- 0.7
309.80	142.6	10.598 b	10.423	+ 1.7
348.88	1	9.753 c	9.960	- 2.1
351.76	1	9.801 d	9.985	- 1.9
349.13	49.6	10.010 c	10.208	- 2.0
347.11	100.7	10.268 c	10.475	- 2.0
401.13	1	10.455 d	10.459	0.0
		Brass Cell		
0	1	5.74	5.84	- 1.7
0	25.3	6.13	6.11	+ 0.1
0	50.1	6.52	6.44	+ 1.4
0	76.7	6.95	6.83	+ 1.8
0	101.4	7.14	7.33	- 2.7
0	126.3	7.82	7.68	+ 1.8

a signifies measurements in Steam Cell No. 1.

b " " " " " No. 1, Revision 1.

c " " " " " No. 1, Revision 2.

d " " " Strain-Free Cell.

* Computed from Equation [10].

NITROGEN HEAT-CONDUCTIVITY DATA

The data for 1 atm pressure in the case of gaseous nitrogen were taken in the silver strain-free cell, as were those for air, and used to determine the cell constant of the steam cell. Heat-conductivity values for nitrogen under pressure have not been completed but it is expected that a complete series of measurements will be made to at least 450 C. The data available are collected in Table 4 in which the computed values appear using the following equations

$$10^5\lambda = 10^5\lambda_0 + 2.5\,(10^{0.52\tau p} - 1)\ldots\ldots\ldots[10]$$

$$10^5\lambda_0 = \frac{0.4508\sqrt{T}}{1 + 84.07\tau/10^{12\tau}}$$

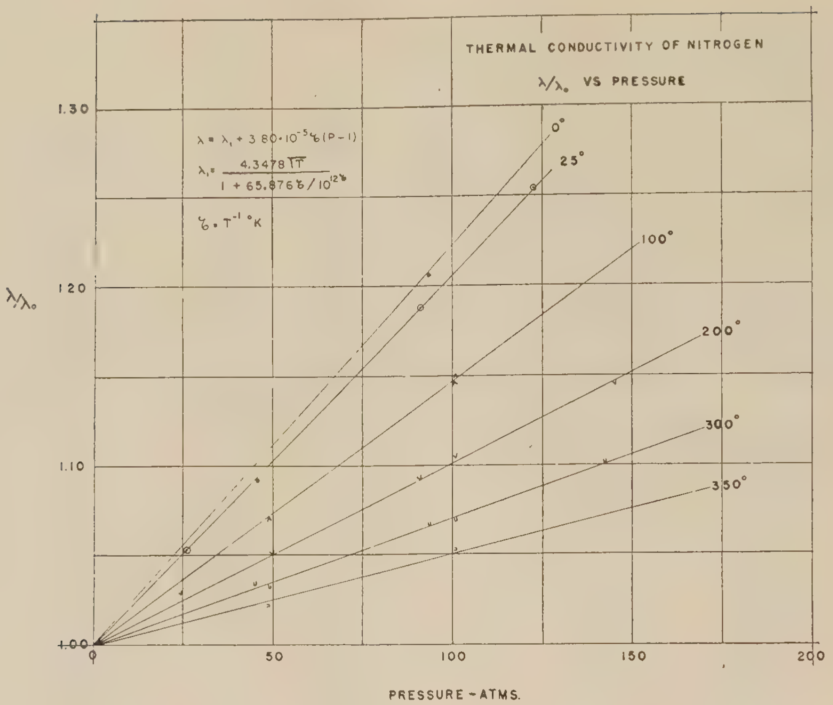

Fig. 4 Thermal Conductivity of Nitrogen λ/λ_0 Versus Pressure

TABLE 5 COMPARISON OF HEAT-CONDUCTIVITY VALUES GIVEN BY VARGAFTIG FOR NITROGEN WITH NEW VALUES

t °C	P(atm)	$10^5\lambda$ (V)	$10^5\lambda$ (K.S.)	Deviation
40.3	0.968	6.444	6.455	+ 0.155
62.1	0.968	6.806	6.741	- 0.964
41.8	2.904	6.472	6.498	+ 0.400
63.0	2.904	6.833	6.775	- 0.856
41.7	6.775	6.500	6.544	+ 0.672
61.3	6.775	6.861	6.797	- 0.972
41.1	14.518	6.611	6.629	+ 0.272
60.9	14.518	6.944	6.880	- 0.930
40.9	19.357	6.667	6.686	+ 0.284
59.4	19.357	6.944	6.916	- 0.405
40.4	30.972	6.833	6.820	- 0.190
58.1	30.972	6.944	7.034	+ 1.279
40.0	46.458	6.972	7.004	+ 0.457
56.7	46.458	7.278	7.195	- 1.154
39.5	62.911	7.139	7.197	+ 0.806
55.2	62.911	7.417	7.368	- 0.665
38.9	87.108	7.556	7.486	- 0.935
53.4	87.108	7.778	7.630	- 1.940

(V) Refers to Vargaftig (1)

(K.S.) $\lambda_p = \lambda_1 + 3.8 \times 10^{-5}\tau(p - 1)$

$$\lambda_1 = \frac{4.3478 \times 10^{-6}\sqrt{T}}{1 + 65.8761\tau/10^{12\tau}}$$

representing nitrogen thermal conductivity values of the present investigation.

$$\text{Deviation} = \frac{\lambda(V) - \lambda(\text{calc})\ (K.S.)}{\lambda\ (\text{calc})\ (K.S.)} \times 100$$

The $f(\tau,p)$ of Equation [6] can also be assumed to be linear or of the following form which represents the data with tolerable accuracy to 100 atm

TABLE 6 NEW NITROGEN λ_0-VALUES COMPARED WITH OLDER DATA

t, deg C	λ_0(obs)	λ_0(calc eq [10])	λ (eq [12])
−200	...	2.160[a]	2.198
0	5.816	5.829	5.825
25	6.219	6.192	6.170
100	7.224	7.201	7.168
200	8.382	8.398	8.338
300	9.178	9.468	9.384
350	9.786	9.966	9.870
400	10.457	10.443	10.310

[a] Extrapolated from 0 deg C by means of Equation [10]. Equation [12] is based upon all the older published observational data in the —200 C region and those extending to 400 C.

$$10^5\lambda = 10^5\lambda_1 + 3.8\tau(p - 1) \qquad [11]$$

$$10^5\lambda_1 = \frac{0.4348\sqrt{T}}{1 + 65.88\tau/10^{12\tau}}$$

Fig. 4 represents the new nitrogen data using the variable λ/λ_0 in relation to the linear isotherm for λ/λ_0 taken from Equation [11].

A comparison of the nitrogen heat-conductivity data of Vargaftig (1) in the range 40 to 63 C and to pressure of 87 atm with the new data (Equation [11]) is given in Table 5.

Table 6 gives a comparison of the $10^5\lambda_0$ values for N_2 with the new observations for 1 atm reduced to zero pressure and round temperatures from the data of Table 4. In the fourth column the values obtained from a correlation of all the published data for nitrogen to 1947, are listed as computed from the following equation

$$10^5\lambda_0 = \frac{0.442\sqrt{T}}{1 + 76.92\tau/10^{12\tau}} \qquad [12]$$

No theoretical explanation of the pronounced difference between $f(\tau,p)$ for steam, $c(e^{a\tau^4p} - 1)$, as compared with nitrogen, $c(e^{a\tau p} - 1)$, is offered. The status of the theory of the pressure effect has been greatly affected by the absence of factual information on substances until recently. However, Enskog (8) has deduced a first-order form on the basis of a van der Waal's molecular model; a relationship which has been tested recently by E. W. Comings and M. F. Nathan (9).

Acknowledgment

We take pleasure in acknowledging the continued general assistance of Miss Mildred Levin who took charge of the thermocouple and platinum-resistance thermometry.

BIBLIOGRAPHY

1 "The Dependence of the Coefficients of Thermoconductivity of Gases and Vapours on the Pressure," by N. Vargaftig, *Technical Physics* (USSR), vol. 4, 1937, p. 343.

2 "Thermal Thermoconductivity and Viscosity of Steam at High Temperatures and Pressures," by D. L. Timroth and N. Vargaftig, *Journal of Physics*, (USSR), vol. 2, 1940, pp. 101–111.

3 "Thermodynamic Properties of Steam," by J. H. Keenan and F. G. Keyes, John Wiley & Sons, Inc., New York, N. Y., table 7, 1943, and subsequent printings.

4 "Über die Wärmeleitfahigkeit der Gasen und Dampfen bei hohern Temperaturen," by E. Moser, Dissertation, Berlin, Germany, 1913.

5 "An Experimental Investigation of Thermal Conduction Through Vapors," by S. W. Milverton, Proceedings of the Royal Society of London, series A, vol. 150, 1935, pp. 287–308.

6 "Über die Wärmeleitungs der Gasen und Dampfen bei hohern Temperaturen des Quecksilberdampfes," by A. Schleiermacher, *Annalen der Physik*, vol. 36, 1889, pp. 346–357.

7 *Mitteilung über Forschungsarbeiten auf dem Gebiete des Ingenieurwesens*, Julius Springer, Berlin, Germany, Heft 21, 1905.

8 "Mathematical Theory of Non-Uniform Gases," by S. Chapman and T. G. Cowling, The Macmillan Company, New York, N. Y.; Cambridge, University Press, London, England, 1939, chapt. 16.

9 "Thermal Conduction of Gases at High Pressures," by E. W. Comings and M. F. Nathan, *Industrial and Engineering Chemistry*, vol. 39, 1947, pp. 964–970.

Discussion

Irving Granet[12] and R. M. Gould.[13] The authors are to be congratulated for having completed successfully an accurate and extremely difficult experimental determination of the heat conductivity of steam. The need for an accurate determination of this property recently has been emphasized by the practical realization of units generating steam at 1000 F and 1350 psia.[14] The data presented in the paper will aid the designer in better predicting the performance of such units and the researcher in correlating his data on a sounder basis.

Some time ago the writers had occasion to use the data of Timroth and Vargaftig as correlated and reported by Professor Keyes in the later printings of the "Steam Tables." At that time it was noted that the values of λ_0 (actually λ_1 for a pressure of 1 kg per cm^2) listed in the Steam Tables exhibited a peculiar reverse curvature. These values were recomputed using the original correlation equation of Professor Keyes (Equation [8] of the present paper), and it was found that all of the 800 deg F values were incorrect as well as the values for saturated vapor at 32 F, 500 psia, and 1750 psia. The writers then differentiated this function twice and determined that a point of inflection does exist in the original Keyes equation. In Fig. 5 of this discussion is shown the original data of the Russian investigators and also a plot of the Keyes values as given in the "Steam Tables" for a pressure of 1 kg per cm^2. It will be noted that the error gives rise to a deviation from the original data of 11 per cent. The inflection gives rise to no substantial deviation from the original Russian data.

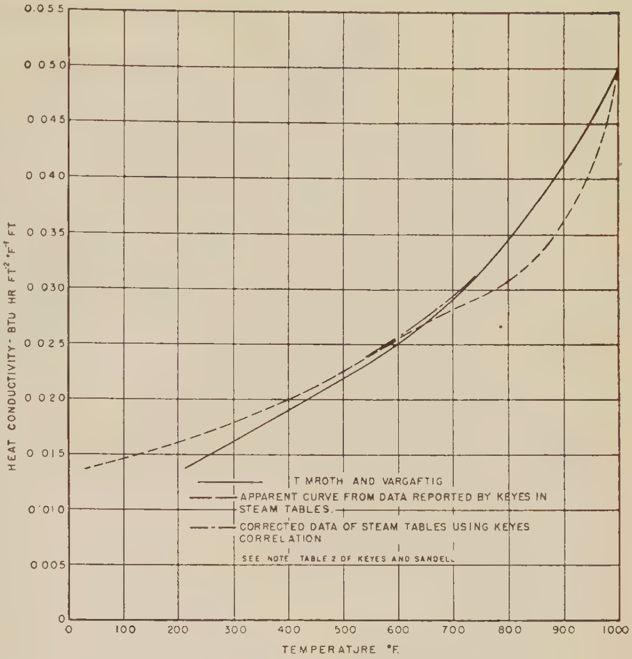

Fig. 5 Comparison of Keyes Correlation, Data Reported in Steam Tables, and Original Timroth and Vargaftig Values at a Pressure of 1 Kg Per Cm^2

In the present paper, Equation [7] is used to correlate the values of heat conductivity of steam at zero pressure. The writers felt that in view of certain similarities in Equations [7] and [8], and the discrepancies just noted, similar points might be exhibited by the present correlation. In order to test for such a condition, two devices were used. The values of λ_0 were calculated over a wide range of temperature using Equation [7], and a large-scale plot of these values was then made. This showed, in the range for which the plot was made, that while the reverse curvature was of such an order as to cause a negligible defection in the correlation, two points of inflection seemed to exist—at about 200 F and at 1100 F. Since, to the writers' knowledge, the only other gas which exhibits such a reversal of curvature to any marked extent is hydrogen,[15] it was felt that a further investigation of this point was justified. By a similar mathematical analysis it was determined tentatively that a point of inflection exists in this function between 1000 F and 1200 F. While it is puzzling to the writers to find such a phenomenon in an equation used to represent λ_0 which ". . . . increases indefinitely and regularly with temperature. . .," it is noted that this phenomenon is of a negligible order.

In order to substantiate the present correlation some particular values of pressure and temperature were chosen, and the heat-conductivity values were calculated on the basis of the authors' correlation. For the values of temperature and pressure chosen, exact agreement was found with the corresponding values of heat conductivity listed in Table 2 of the paper.

It is understood that in the near future the values of heat conductivity of steam, as determined and correlated in this paper, will be incorporated in a new printing of the Steam Tables. To facilitate the use of this information in the interim, the writers have prepared Table 7 and Fig. 6 of this discussion. All values in Table 7 were determined by utilizing Equation [7] of the paper,

---

[12] Engineer, Research Department, Foster Wheeler Corporation, New York, N. Y. Jun. ASME.

[13] Engineer, Research Department, Foster Wheeler Corporation, New York, N. Y.

[14] "One Thousand Degrees F. . . . . A New High in Steam Temperature," by Philip Sporn, *Electrical World*, vol. 126, Aug, 17, 1946, pp. 60–67. Reprinted as Bulletin B-46-20, Foster Wheeler Corporation, New York, N. Y.

[15] "An Investigation of Aircraft Heaters; II Properties of Gases," by M. Tribus and L. M. K. Boelter, NACA, October, 1942.

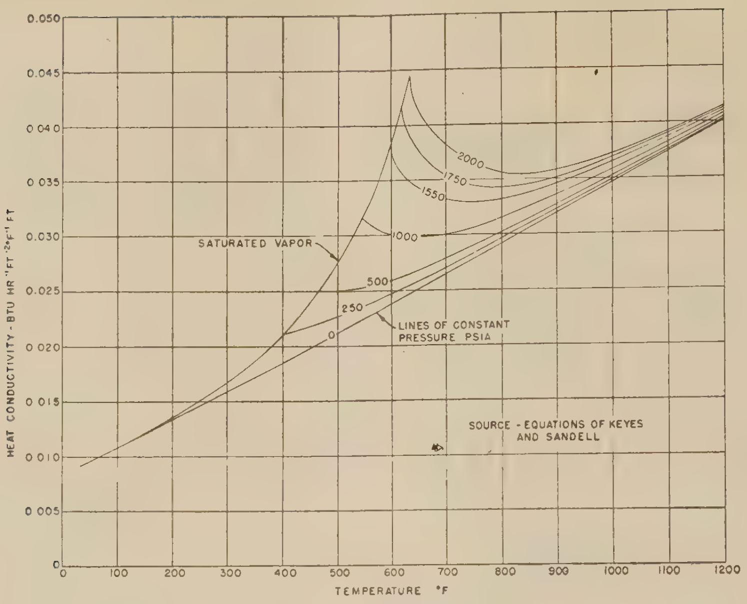

Fig. 6 Heat Conductivity of Steam

TABLE 7 HEAT CONDUCTIVITY × 10^3 (Btu hr^{-1} ft^{-2} deg F^{-1} ft)

	Temperature, deg F							
	Sat. vapor	32	200	400	600	800	1000	1200
Sat. vapor		9.16	13.5	21.1	38.5			
psia								
0	...	9.16	13.3	18.4	23.8	29.2	34.7	40.1
250	21.2				24.7	29.7	34.9	40.3
500	25.0				26.0	30.2	35.2	40.4
1000	31.6				30.1	31.4	35.7	40.7
1500	38.0				37.6	33.2	36.4	41.1
1750	41.2				...	34.3	36.8	41.3
2000	44.5				...	35.5	37.2	41.5

and the $f(p, \tau)$ as given by the authors. These values were determined to four significant places, but only three significant places are given in Table 7, since the writers feel that with the present data more than three places would not be warranted.

A word of caution must be noted at this time. When new accurate determinations of thermodynamic properties are made available, there is a tendency to use them in conjunction with the general heat-transfer relationships and equations made prior to the existence of the new data. For example, in the design of superheaters, the maximum tube temperature is a limiting factor. Using the present data for the heat conductivity of steam in the Poensgen[16] correlation will indicate a temperature differential between the tube and the steam 30 per cent higher than that obtained using the data of Timroth and Vargaftig with the same heat-flux density. This would indicate erroneously a maximum heat-flux density, lower than that which could be used. Therefore the user of such equations should, where possible, determine the sources of the physical properties used by the correlator or investigator, as the case may be, and use the same sources in order to obtain reasonably accurate and correct predictions. If it is warranted, the user should recorrelate previous data using the new physical properties.

Serge Gratch.[17] These new data are certainly very accurate and reliable, and should supersede the older, apparently incorrect data by Timroth and Vargaftig.

The main value of the paper lies in the presentation of a greatly improved technique for the measurement of heat conductivity of gases. In this connection engineers and scientists owe a great debt of gratitude to the senior author, Dr. F. G. Keyes, who for nearly half a century has been the leader in the development of new techniques for the accurate determination of properties of fluids. For resourcefulness and ingenuity in solving experimental problems Dr. Keyes is unequaled in his field, and stands high as guide and inspiration to the younger scientists.

R. L. Scorah.[18] The authors state clearly that the interpretation of the apparent heat conductivity measured for steam is complicated by the effect of radiation emitted and absorbed by the steam itself; and further, in so far as is known, the adjustment of heat-conductivity measurements to allow for radiation emission and absorption within the test material has never been made or discussed. This is a point of fundamental importance.

From the authors' description of their mode of taking and treating observational data, it appears that no allowance was made for the effect of radiation emitted and absorbed by the steam. When $(q/\Delta t)$ for $q = 0$ is obtained by graphical extrapolation, Equation [4] of the paper becomes

$$\left(\frac{q}{\Delta t}\right)_{q=0} = \lambda C + C_r(\overline{T})^3 + G + H$$

which is solved for λ. In general, the "radiation constant" C_r, is a function of the surface temperature, emissivity, and shape, and the steam-film thickness and density. The new term H on the right-hand side of the foregoing equation has been added here to account for the effect of radiation emitted and absorbed within the film. The term C is fixed by the dimensions of the test cell, and the term G compensates for conduction within the emitter supports. The terms C_r and H, however, depend in part upon the emissivity of the test-cell surface material. The authors used silver and obtained lower values of conductivity than did the Russian experimenters who used platinum. This difference in results may be due in part to the difference in the emissivity of silver and platinum. Since engineering materials ordinarily show a much higher emissivity than polished silver, an emissivity correction would appear to be in order for applying heat-conductivity data measured by silver surfaces. This question must be clarified be-

---

[16] "Heat Transmission," by W. H. McAdams, second edition, McGraw-Hill Book Company, Inc., New York, N. Y., 1942, p. 172.

[17] University of Pennsylvania, Philadelphia, Pa. Jun. ASME.

[18] University of Missouri, Columbia, Mo. Mem. ASME.

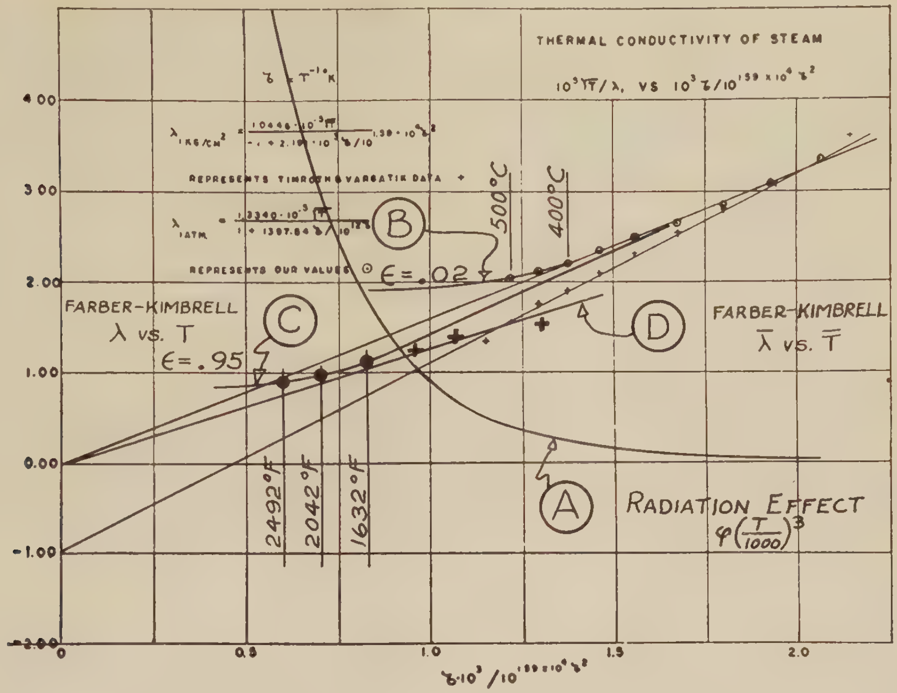

Fig. 7 Thermal Conductivity of Steam $10^5\sqrt{T}/\lambda_1$ Versus $10^3\tau^2/10^{1.59\times10^4\tau^2}$

fore much confidence can be attached to any interpretation of heat-conductivity measurements for materials which absorb and emit radiation. It appears that with multiple observations at different emissivities, the heat conductivity with zero surface emission or absorption could be obtained by graphical extrapolation. The required emissivity correction could then be established.

Radiation becomes increasingly important at temperatures above 500 C, which is the limiting value of the authors' present paper. Our students have obtained rough values of the heat conductivity of steam at somewhat higher temperatures and at a pressure of 1 atm. For example, in the data of Farber[19] for his April 25 tests, the last three runs were made with fully developed stable film boiling. From the optical measurements of J. T. Kimbrell,[20] the film was found to be 0.015 in. thick, as compared with the value of 0.025 in. in the authors' apparatus. Convection within this thin film was neglected. The radiation flux was estimated by the Stefan-Boltzmann equation, the temperatures being that of the wire surface and the saturation temperature of water; the emissivities, 0.95 for the wire and 0.963 for water. The remaining heat flux was considered as steady conduction, and the mean heat conductivity of the steam film was computed with the Fourier equation. No radiation correction of the type H was applied. The results are given in Table 8 of this discussion. Since the available data on the heat conductivity of steam is nearly linear at low pressures (the present paper included), the following linear relation passing through the saturated-vapor line at 1 atm was considered to represent the Farber-Kimbrell experiments

TABLE 8

t, deg F	k_m, Btu hr^{-1} ft^{-2} F^{-1} ft
1632	0.0465
2042	0.0492
2492	0.0640

$$k = 0.014 + 0.000043\,(t\text{-}212) \ldots\ldots\ldots\ldots [13]$$

At 500 C (932 F), this expression gives a value for the heat conductivity about 37 per cent greater than the zero-pressure value reported by the authors. Farber's experiments were never intended to measure the heat conductivity of steam, and while no high order of precision can be assigned to the numerical values, these data were obtained from steam films subjected to an intense radiation flux from a high-emissivity emitter. These data suggest an emissivity correction of considerable magnitude.

The correlation and extrapolation of steam-conductivity data is complicated when radiation phenomena are considered. As the temperature increases, the magnitude of the radiation flux increases very rapidly. Curve A in Fig. 7 herewith, is similar to the authors' C_r term and is shown here only as a first approximation of the whole radiation effect. At high temperatures, the authors' data for an emissivity of about 0.02 departs from their straight line, as shown by Curve B. The departure begins at about 400 C. Since the radiation flux is increased approximately 50 per cent in the next 100 deg, the upward trend of Curve B may be due in part to this radiation increase. The fact that the trend of the authors' data is upward may be of special interest.

Curve C represents our student data. The instantaneous heat conductivity was computed for the test temperatures of the emitter by means of Equation [13] of this discussion. Considering the emissivity of about 0.95, these results do not appear to be completely inconsistent with those of the paper. The comparison of Curve B with Curve C suggests the possible range of the emissivity effect. Curve D represents the student data when using the mean heat conductivity calculated from Equation [13], and the arithmetic-mean film temperature. This plot enters the high-temperature region of the Russian data. Since at this writing we do not have the Russian papers, it is not clear what significance if any should be attached to this coincidence.

---

[19] "Heat Transfer to Water Boiling Under Pressure," by F. A. Farber and R. L. Scorah, Trans. ASME, vol. 70, 1948, pp. 369–384.

[20] Graduate Student, University of Missouri, Columbia, Mo.

Authors' Closure

The authors appreciate the careful discussion of the paper by Mr. Granet and Mr. Gould, who are correct in stating that the 800 F values in the Steam Tables are not in accord with the equations given in the text, section 7, page 23. The lambda-zero pressure value should be 34.42 instead of 30.55, and the pressure increments are correct. The new value is 29.2 as given in Table 7.

The authors had not been aware of the inflection feature of the correlating equation until it was brought to their attention by the commentators at the time of the meeting. The effect is small, however, as stated, and it does not invalidate the use of the correlative form which is in substantial accord with the kinetic-gas theory based on a van der Waals' molecular field. There is a qualification to this statement, however, due to the presence of the exponential term in Equation [7], a term which was found to be necessary if a long range of temperature is to be represented. Actually the Sutherland type formula is given in the classical kinetic-gas theory for the viscosity, and not for the heat conductivity,[21] the latter coming out of the theory in the form: lambda proportional to the viscosity times the specific heat at constant volume.

The classical kinetic-gas theory gives no accounting of the temperature dependence of the specific heat, and since the specific heat for all except monatomic gases is a function of the temperature, it would be expected that the heat conductivity would involve a stronger temperature dependence as compared with the viscosity alone. The authors regard Equation [7] as a semi-empirical equation which appears to be of value in representing the observations on heat conductivity over considerable ranges of temperature. Reference should be made in this connection to the paper by J. O. Hirschfelder, R. B. Bird, and E. L. Spotz, a report on the transport properties of gases and gas mixtures.[22]

Substitute tables 6 and 7, of the Steam Tables have already been sent to the printers, and the commentators' Table 7 is in exact agreement with the authors' table.

Professor Scorah's values given in Table 8 can be represented by a linear equation. It is important to observe, relative to Professor Scorah's representation of the Table 8 values, that a linear equation is not suitable for long ranges of temperature. The Equation [7] is of the Sutherland type modified on the basis of a critical consideration of all the available heat conductivity data for the gases: air, helium, hydrogen, oxygen, nitrogen, CO, CO_2, as well as H_2O.[23]

The difference in the emissivity of the wire used by Professor Scorah's collaborators and that of silver used in the steam-heat conductivity work is very large, and there is insufficient data on the absorption spectrum and emissivity of steam to make the required correction of the apparent conductivity when the emissivity from the wire is as large as 0.95. Indeed under present circumstances the best that can be done is to use materials in the measurements that have as low an emissivity as possible, and silver appears to be better than any other metal.

As remarked in the text, the trend of the Russian data as given in Fig. 7 leads to an extrapolation impasse, namely, it tends progressively to very large values with increasing temperatures. This could be due in part to the high emissivity of the platinum wire which under operating conditions has been shown by Timroth and Vargaftig to be the order of 0.11; a figure in substantial agreement with Milverton's results for the platinum wire of his apparatus.

The authors thank the commentators for their encouraging and helpful comments.

---

[21] "Mathematical Theory of Non-Uniform Gases," by S. Chapman and T. G. Cowling, The Macmillan Company, Cambridge, Mass., 1939, p. 184.

[22] "Viscosity and Other Physical Properties of Gases and Gas Mixtures," by J. O. Hirschfelder, R. B. Bird, and E. L. Spotz, Trans. ASME, vol. 71, 1949, p. 921

[23] Final Report, Office of Naval Research, Task Order XI, M.I.T. Contract N5ori-78, Project Designation No. NR-059-037, October 1, 1949.

Compilation of Thermal Properties of Wind-Tunnel and Jet-Engine Gases at the National Bureau of Standards

By HAROLD J. HOGE,[1] WASHINGTON, D. C.

A project for the preparation of a series of tables of thermal properties of gases is described. This project was undertaken by the National Bureau of Standards at the suggestion and with the co-operation of the National Advisory Committee for Aeronautics. The scope of the project, tables now available, work in progress, and plans for the future are described. The lack of adequate data at high temperatures and also at high pressures is pointed out.

INTRODUCTION

RESEARCH involving wind tunnels, jet engines, and missiles requires good thermal data on the gases which flow through the tunnels or jets, or which the missile encounters in its flight. The following are typical examples of the problems encountered:

1 Compressed gas in a tank at a known temperature and pressure expands to a low pressure as it passes through a wind tunnel. How do the temperature and velocity change along the tunnel? If water is present, at what temperature will it be precipitated, and will ice or liquid water be formed? Will the major constituents of the gas condense? Will condensation shock interfere with the measurements?

2 A missile flies through the earth's atmosphere, compressing and heating a layer of air in front of it. How much heat will be conducted to the missile and how hot will it get? How much deceleration will it experience?

3 Fuel is burned in a jet engine. What is the composition of the products of combustion? How does the efficiency of the engine depend on the operating temperature? Will the walls of the engine get too hot?

These questions and many others cannot be answered unless reasonably accurate thermal data are available.

Thermal data for the region near room temperature are available, although they are not always easy to locate or in convenient form for use. But as the interval from room temperature increases the data become more scarce, to the extent that above 900 or 1000 deg K data are practically nonexistent. A similar situation exists with regard to pressure. Near a pressure of 1 atm the data are fairly plentiful, but at high and low pressures they are scarce. This is especially true of the nonequilibrium properties such as viscosity and thermal conductivity.

A project for the compilation of tables of thermal data on wind-tunnel and jet-engine gases has been established at the National Bureau of Standards with the co-operation of the National Advisory Committee for Aeronautics. This project was initiated by Dr. F. G. Brickwedde, chief, Heat and Power Division, who prepared a plan for the tables. This plan was sent to a large number of laboratories and individuals for comments and suggestions. After these had been received and considered, the program described in this paper was evolved. Several individuals have contributed to this program during the past year, and 16 tables have been published.

THE PROJECT

The program as it exists at present calls for the critical evaluation of available data, and the preparation of conveniently usable tables of thermal properties of the following gases:

- Dry air
- Moist air
- Steam
- Hydrogen
- Oxygen
- Nitrogen
- Carbon dioxide
- Carbon monoxide
- Nitrogen dioxide (NO_2)
- Nitric oxide (NO)
- Helium
- Freon 12 (CF_2Cl_2)
- Argon

The following properties are to be tabulated, in general, as functions of both temperature and pressure:

- Heat capacity (C_p)
- Enthalpy (total heat)
- Entropy
- Gibbs free energy
- Compressibility factor
- Density
- Ratio of specific heats
- Velocity of sound
- Relaxation parameters
- Viscosity
- Thermal conductivity
- Prandtl number
- Vapor pressure

Additions both to the list of gases and to the list of properties are anticipated as the project continues. For example, it is already evident that atoms and molecules formed by dissociation of certain gases in the list will have to be considered. The temperature and pressure ranges to be covered are almost always limited by the available data. At pressures below 1 or 2 atm, data are needed from the condensation temperature (vapor-pressure curve) to 3000 deg K. Throughout part of this temperature range, from room temperature to about 700 deg K, low-pressure data are not enough, and the aim is, where practical, to extend the tables to a pressure of 100 atm.

A few of the properties in the tabulation call for explanations or comment. Gibbs free energies are needed when equilibria are to be computed between products of combustion. Compressibility factor is the dimensionless quantity $Z = pV/nRT$, which equals unity for an ideal gas. The ratio of specific heats is of course C_p/C_v, the specific heat at constant pressure divided by the specific heat at constant volume. Relaxation is the process of distribution of energy among the various degrees of freedom of the molecule. When a gas is suddenly heated or cooled, the vibrational degrees of freedom do not gain or lose energy as fast as the translational or rotational degrees of freedom. This effect has often been neglected, but it can become quite important in

---

[1] Member, Thermodynamics Section, National Bureau of Standards.

Contributed by the Research Committee on Properties of Gases and Gas Mixtures and the Heat Transfer and Applied Mechanics Divisions, and presented at the Annual Meeting, New York, N. Y., November 27–December 2, 1949, of THE AMERICAN SOCIETY OF MECHANICAL ENGINEERS.

NOTE: Statements and opinions advanced in papers are to be understood as individual expressions of their authors and not those of the Society. Paper No. 49—A-86.

aerodynamic processes. The relaxation parameters to be tabulated are the relaxation time, the relaxation distance, and the specific heat (vibrational) associated with the relaxation. The Prandtl number $\eta C_p/k$ is the product of the viscosity and the specific heat at constant pressure divided by the thermal conductivity. It is particularly useful in heat-transfer problems at the surfaces of missiles.

In the preparation of the tables, emphasis is placed on convenience in use, and upon the inclusion of a brief summary of the more important questions involved in the critical evaluation. Suitably qualified estimates of the accuracy of the tables are given, even though these are sometimes very rough and approximate. In the present stages of the program we have thought it wise not to place extreme emphasis on accuracy, but simply to select the best data available and tell how good we think they are. When this has been done, so that the tables give a fairly good coverage of the selected field, we hope to begin to issue replacements for the less reliable tables. In most cases this will require new experimental work, or computations of an original nature. Some of this original work we expect to undertake ourselves, but for much of it we will have to depend on others. One of the minor functions of the project will be to show where there is greatest need for new experimental work.

In order to make the tables equally convenient regardless of the units to be employed, they are, wherever practical, expressed in dimensionless form. Then, on the same page with a given table, clearly labeled conversion factors are given which permit a quantity obtained from the table to be expressed in any units likely to be desired. This applies to the entries in the tables rather than to the argument or arguments (independent variables) of the tables. For example, a table giving the thermal conductivity of a gas at specified values of temperature and pressure will have as entries values of k/k_0 where k_0 is the thermal conductivity at some standard condition, such as 0 deg C and 1 atm. The arguments T and p, however, will normally be dimensional (T both in deg K and deg R, and p in atm, psia, or mm Hg). These have been left in dimensional form because it was felt that the use of too many dimensionless quantities might cause confusion.

The ease with which interpolations may be made is one of the most important factors in the practical use of a table. Seldom is it possible to avoid interpolation altogether. But linear interpolation is relatively simple and rapid as compared with higher-order interpolation, even when tables of interpolation coefficients[2] are at hand. Our goal has been to subtabulate to the point where linear interpolation can be used everywhere. Unfortunately, this has not always been practical, because in some cases it would have led to very large tables. In these cases care has been taken to indicate clearly where linear interpolation is not adequate.

One of the published tables is shown in Fig. 1. This table, No. 2.10, gives specific heat, enthalpy, and entropy of dry air as calculated from spectroscopic data (ideal gas state). The full-sized table consists of four 8 × 10 $^1/_2$-in. pages printed by a photo-offset process. The original tables of the data proper were printed by International Business Machine typewriters actuated directly by punch cards, with rules and headings put in by hand. This procedure has been used whenever the data were already available on punch cards as a result of subtabulation or other operations performed on IBM equipment. It may be mentioned in passing that where IBM equipment has been used the tables can be furnished on punch cards.

The brief text accompanying a table contains a description of the table and how to use it, and an evaluation of the data upon which the table is based. In some cases a graph can be included which shows the agreement between the table and the principal experimental data. Such a graph can quickly give the user of a table an idea of its accuracy that he could otherwise get only from hours of study of the original papers.

WORK ACCOMPLISHED AND IN PROGRESS

The tables now available for distribution are listed as follows (as of September, 1949):

2.10	Dry Air (Ideal Gas State), Specific Heat, Enthalpy, Entropy
2.42	Dry Air, Thermal Conductivity
5.42	Steam, Thermal Conductivity
7.10	Molecular Hydrogen (Ideal Gas State) Specific Heat, Enthalpy, Entropy
7.42	Molecular Hydrogen, Thermal Conductivity
9.10	Molecular Oxygen (Ideal Gas State), Specific Heat, Enthalpy, Entropy
9.42	Molecular Oxygen, Thermal Conductivity
9.50	Vapor Pressure of Oxygen
11.10	Molecular Nitrogen (Ideal Gas State), Specific Heat, Enthalpy, Entropy
11.42	Molecular Nitrogen, Thermal Conductivity
13.42	Carbon Dioxide, Thermal Conductivity
14.42	Carbon Monoxide, Thermal Conductivity
15.42	Nitrogen Dioxide, Thermal Conductivity
16.42	Nitric Oxide, Thermal Conductivity
18.42	Freon 12, Thermal Conductivity
19.42	Argon, Thermal Conductivity

So far it has been possible to keep each publication to a length of 4 pages or less. Undoubtedly, some will have to be longer, but it is planned to keep them as compact as is consistent with good legibility. A numbering scheme for the tables has been adopted which identifies both the substance and the properties treated in a table. For example, in table 9.50, the 9 shows that the substance is oxygen and the 50 shows that the property tabulated is vapor pressure.

Of the tables now issued, a large fraction gives ideal gas properties. These are computed from spectroscopic data. They furnish limiting values which should be approached by the real gas at low pressures, and they are virtually the only type of data available in the higher temperature ranges.

A large number of calculations of ideal gas properties have been published in the last 10 or 15 years. Many of these have become obsolete because of the subsequent publication of better molecular data. The process of selection of an ideal gas table is begun by checking the more recent tables at various temperatures. The table which appears to be most accurate is more carefully checked, sometimes by spot calculations starting from the molecular constants themselves. When the most adequate basic calculation of ideal gas properties has been accepted, it is generally necessary to subtabulate it. It is also converted to dimensionless units in such a way that the final table will be consistent with the latest values of the fundamental constants. Most of the tables of ideal gas properties published by the project to date have been prepared under the supervision of Harold W. Woolley.

In the field of real gas properties a considerable amount of effort has been put on the properties of dry and moist air. Curtiss and Hirschfelder[3,4] have published two sets of tables that have served as the basis of this work. These have been retabulated with pressure rather than density as an independent variable, and some new intermediate values have been computed. Subtabulation has been performed; the tables have been made dimensionless and modified in some other respects. This work has been

---

[2] "Tables of Lagrangian Interpolation Coefficients," prepared by Mathematical Tables Project, WPA, Columbia University Press, New York, N. Y., 1944.

[3] "Thermodynamic Properties of Air," by C. F. Curtiss and J. O. Hirschfelder, University of Wisconsin Naval Research Laboratory Report CM-472, June 1, 1948.

[4] "Thermodynamic Properties of Air—II," by J. O. Hirschfelder and C. F. Curtiss, University of Wisconsin Naval Research Laboratory Report CM-518, December 21, 1948.

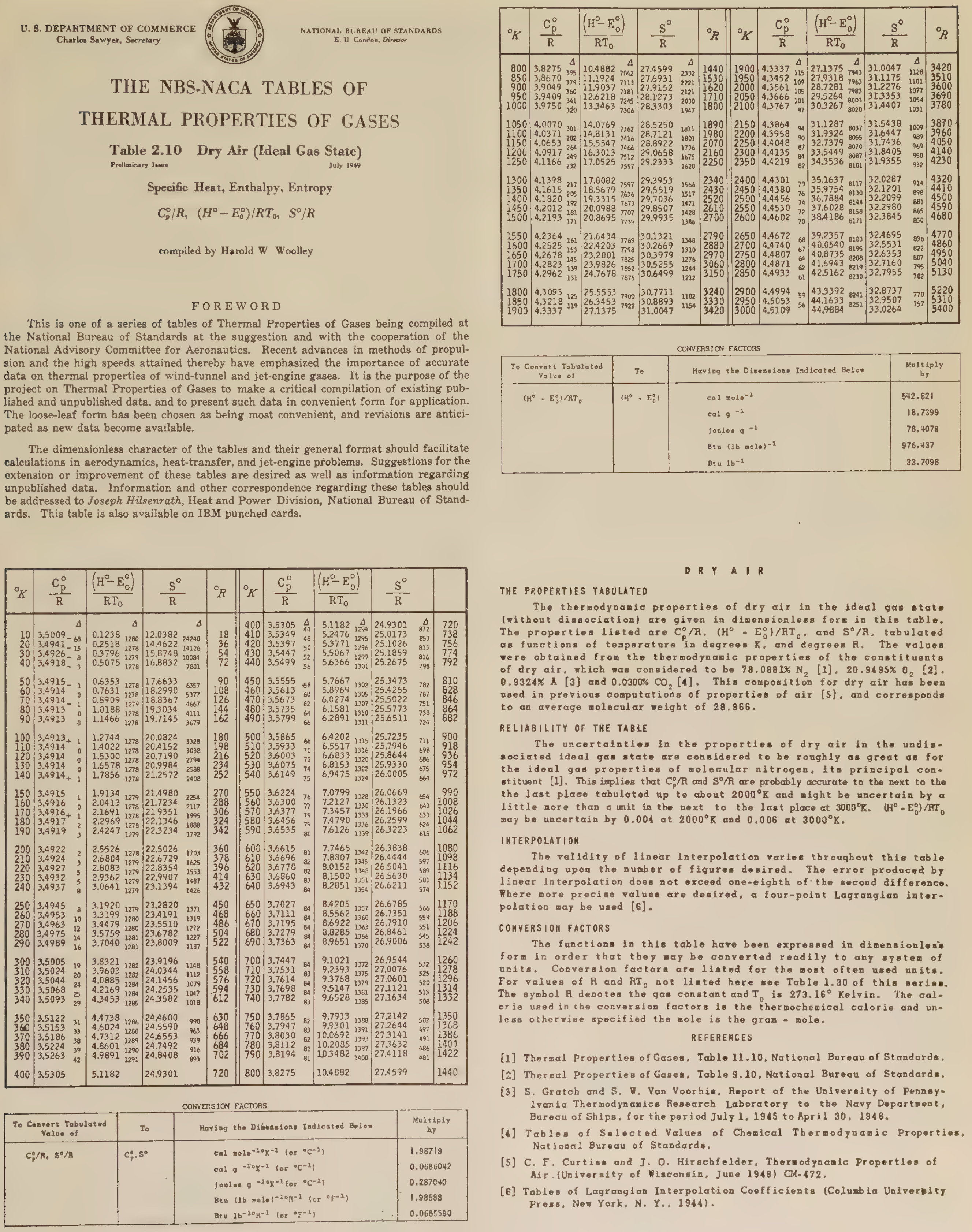

U. S. DEPARTMENT OF COMMERCE
Charles Sawyer, *Secretary*

NATIONAL BUREAU OF STANDARDS
E. U Condon, *Director*

THE NBS-NACA TABLES OF THERMAL PROPERTIES OF GASES

Table 2.10 Dry Air (Ideal Gas State)

Preliminary Issue
July 1949

Specific Heat, Enthalpy, Entropy

$C_p^\circ/R,\ (H^\circ-E_0^\circ)/RT_0,\ S^\circ/R$

compiled by Harold W Woolley

FOREWORD

This is one of a series of tables of Thermal Properties of Gases being compiled at the National Bureau of Standards at the suggestion and with the cooperation of the National Advisory Committee for Aeronautics. Recent advances in methods of propulsion and the high speeds attained thereby have emphasized the importance of accurate data on thermal properties of wind-tunnel and jet-engine gases. It is the purpose of the project on Thermal Properties of Gases to make a critical compilation of existing published and unpublished data, and to present such data in convenient form for application. The loose-leaf form has been chosen as being most convenient, and revisions are anticipated as new data become available.

The dimensionless character of the tables and their general format should facilitate calculations in aerodynamics, heat-transfer, and jet-engine problems. Suggestions for the extension or improvement of these tables are desired as well as information regarding unpublished data. Information and other correspondence regarding these tables should be addressed to *Joseph Hilsenrath*, Heat and Power Division, National Bureau of Standards. This table is also available on IBM punched cards.

°K	C_p°/R	Δ	$(H^\circ-E_0^\circ)/RT_0$	Δ	S°/R	Δ	°R
10	3.5009−	68	0.1238	1280	12.0382	24240	18
20	3.4941−	15	0.2518	1278	14.4622	14126	36
30	3.4926−	8	0.3796	1279	15.8748	10084	54
40	3.4918−	3	0.5075	1278	16.8832	7801	72
50	3.4915−	1	0.6353	1278	17.6633	6357	90
60	3.4914	0	0.7631	1278	18.2990	5377	108
70	3.4914−	1	0.8909	1279	18.8367	4667	126
80	3.4913	0	1.0188	1278	19.3034	4111	144
90	3.4913	0	1.1466	1278	19.7145	3679	162
100	3.4913+	1	1.2744	1278	20.0824	3328	180
110	3.4914	0	1.4022	1278	20.4152	3038	198
120	3.4914	0	1.5300	1278	20.7190	2794	216
130	3.4914	0	1.6578	1278	20.9984	2588	234
140	3.4914+	1	1.7856	1278	21.2572	2408	252
150	3.4915	1	1.9134	1279	21.4980	2254	270
160	3.4916	0	2.0413	1278	21.7234	2117	288
170	3.4916+	1	2.1691	1278	21.9351	1995	306
180	3.4917	2	2.2969	1278	22.1346	1888	324
190	3.4919	3	2.4247	1279	22.3234	1792	342
200	3.4922	2	2.5526	1278	22.5026	1703	360
210	3.4924	3	2.6804	1279	22.6729	1625	378
220	3.4927	5	2.8083	1279	22.8354	1553	396
230	3.4932	5	2.9362	1279	22.9907	1487	414
240	3.4937	8	3.0641	1279	23.1394	1426	432
250	3.4945	8	3.1920	1279	23.2820	1371	450
260	3.4953	10	3.3199	1280	23.4191	1319	468
270	3.4963	12	3.4479	1280	23.5510	1272	486
280	3.4975	14	3.5759	1281	23.6782	1227	504
290	3.4989	16	3.7040	1281	23.8009	1187	522
300	3.5005	19	3.8321	1282	23.9196	1148	540
310	3.5024	20	3.9603	1282	24.0344	1112	558
320	3.5044	24	4.0885	1284	24.1456	1079	576
330	3.5068	25	4.2169	1284	24.2535	1047	594
340	3.5093	29	4.3453	1285	24.3582	1018	612
350	3.5122	31	4.4738	1286	24.4600	990	630
360	3.5153	33	4.6024	1288	24.5590	963	648
370	3.5186	38	4.7312	1289	24.6553	939	666
380	3.5224	39	4.8601	1290	24.7492	916	684
390	3.5263	42	4.9891	1291	24.8408	893	702
400	3.5305		5.1182		24.9301		720
400	3.5305	44	5.1182	1294	24.9301	872	720
410	3.5349	48	5.2476	1295	25.0173	853	738
420	3.5397	50	5.3771	1296	25.1026	833	756
430	3.5447	52	5.5067	1299	25.1859	816	774
440	3.5499	56	5.6366	1301	25.2675	798	792
450	3.5555	58	5.7667	1302	25.3473	782	810
460	3.5613	60	5.8969	1305	25.4255	767	828
470	3.5673	62	6.0274	1307	25.5022	751	846
480	3.5735	64	6.1581	1310	25.5773	738	864
490	3.5799	66	6.2891	1311	25.6511	724	882
500	3.5865	68	6.4202	1315	25.7235	711	900
510	3.5933	70	6.5517	1316	25.7946	698	918
520	3.6003	72	6.6833	1320	25.8644	686	936
530	3.6075	74	6.8153	1322	25.9330	675	954
540	3.6149	75	6.9475	1324	26.0005	664	972
550	3.6224	76	7.0799	1328	26.0669	654	990
560	3.6300	77	7.2127	1330	26.1323	643	1008
570	3.6377	79	7.3457	1333	26.1966	633	1026
580	3.6456	79	7.4790	1336	26.2599	624	1044
590	3.6535	80	7.6126	1339	26.3223	615	1062
600	3.6615	81	7.7465	1342	26.3838	606	1080
610	3.6696	82	7.8807	1345	26.4444	597	1098
620	3.6778	82	8.0152	1348	26.5041	589	1116
630	3.6860	83	8.1500	1351	26.5630	581	1134
640	3.6943	84	8.2851	1354	26.6211	574	1152
650	3.7027	84	8.4205	1357	26.6785	566	1170
660	3.7111	84	8.5562	1360	26.7351	559	1188
670	3.7195	84	8.6922	1363	26.7910	551	1206
680	3.7279	84	8.8285	1366	26.8461	545	1224
690	3.7363	84	8.9651	1370	26.9006	538	1242
700	3.7447	84	9.1021	1372	26.9544	532	1260
710	3.7531	83	9.2393	1375	27.0076	525	1278
720	3.7614	84	9.3768	1379	27.0601	520	1296
730	3.7698	84	9.5147	1381	27.1121	513	1314
740	3.7782	83	9.6528	1385	27.1634	508	1332
750	3.7865	82	9.7913	1388	27.2142	502	1350
760	3.7947	83	9.9301	1391	27.2644	497	1368
770	3.8030	82	10.0692	1393	27.3141	491	1386
780	3.8112	82	10.2085	1397	27.3632	486	1404
790	3.8194	81	10.3482	1400	27.4118	481	1422
800	3.8275		10.4882		27.4599		1440

CONVERSION FACTORS

To Convert Tabulated Value of	To	Having the Dimensions Indicated Below	Multiply by
C_p°/R, S°/R	C_p°, S°	cal mole^{-1}°K^{-1} (or °C^{-1})	1.98719
		cal g^{-1}°K^{-1} (or °C^{-1})	0.0686042
		joules g^{-1}°K^{-1}(or °C^{-1})	0.287040
		Btu (lb mole)$^{-1}$°R^{-1} (or °F^{-1})	1.98588
		Btu lb^{-1}°R^{-1} (or °F^{-1})	0.0685590

°K	C_p°/R	Δ	$(H^\circ-E_0^\circ)/RT_0$	Δ	S°/R	Δ	°R
800	3.8275	395	10.4882	7042	27.4599	2332	1440
850	3.8670	379	11.1924	7113	27.6931	2221	1530
900	3.9049	360	11.9037	7181	27.9152	2121	1620
950	3.9409	341	12.6218	7245	28.1273	2030	1710
1000	3.9750	320	13.3463	7306	28.3303	1947	1800
1050	4.0070	301	14.0769	7362	28.5250	1871	1890
1100	4.0371	282	14.8131	7416	28.7121	1801	1980
1150	4.0653	264	15.5547	7466	28.8922	1736	2070
1200	4.0917	249	16.3013	7512	29.0658	1675	2160
1250	4.1166	232	17.0525	7557	29.2333	1620	2250
1300	4.1398	217	17.8082	7597	29.3953	1566	2340
1350	4.1615	205	18.5679	7636	29.5519	1517	2430
1400	4.1820	192	19.3315	7673	29.7036	1471	2520
1450	4.2012	181	20.0988	7707	29.8507	1428	2610
1500	4.2193	171	20.8695	7739	29.9935	1386	2700
1550	4.2364	161	21.6434	7769	30.1321	1348	2790
1600	4.2525	153	22.4203	7798	30.2669	1310	2880
1650	4.2678	145	23.2001	7825	30.3979	1276	2970
1700	4.2823	139	23.9826	7852	30.5255	1244	3060
1750	4.2962	131	24.7678	7875	30.6499	1212	3150
1800	4.3093	125	25.5553	7900	30.7711	1182	3240
1850	4.3218	119	26.3453	7922	30.8893	1154	3330
1900	4.3337		27.1375		31.0047		3420
1900	4.3337	115	27.1375	7943	31.0047	1128	3420
1950	4.3452	109	27.9318	7963	31.1175	1101	3510
2000	4.3561	105	28.7281	7983	31.2276	1077	3600
2050	4.3666	101	29.5264	8003	31.3353	1054	3690
2100	4.3767	97	30.3267	8020	31.4407	1031	3780
2150	4.3864	94	31.1287	8037	31.5438	1009	3870
2200	4.3958	90	31.9324	8055	31.6447	989	3960
2250	4.4048	87	32.7379	8070	31.7436	969	4050
2300	4.4135	84	33.5449	8087	31.8405	950	4140
2350	4.4219	82	34.3536	8101	31.9355	932	4230
2400	4.4301	79	35.1637	8117	32.0287	914	4320
2450	4.4380	76	35.9754	8130	32.1201	898	4410
2500	4.4456	74	36.7884	8144	32.2099	881	4500
2550	4.4530	72	37.6028	8158	32.2980	865	4590
2600	4.4602	70	38.4186	8171	32.3845	850	4680
2650	4.4672	68	39.2357	8183	32.4695	836	4770
2700	4.4740	67	40.0540	8195	32.5531	822	4860
2750	4.4807	64	40.8735	8208	32.6353	807	4950
2800	4.4871	62	41.6943	8219	32.7160	795	5040
2850	4.4933	61	42.5162	8230	32.7955	782	5130
2900	4.4994	59	43.3392	8241	32.8737	770	5220
2950	4.5053	56	44.1633	8251	32.9507	757	5310
3000	4.5109		44.9884		33.0264		5400

CONVERSION FACTORS

To Convert Tabulated Value of	To	Having the Dimensions Indicated Below	Multiply by
$(H^\circ - E_0^\circ)/RT_0$	$(H^\circ - E_0^\circ)$	cal mole^{-1}	542.821
		cal g^{-1}	18.7399
		joules g^{-1}	78.4079
		Btu (lb mole)$^{-1}$	976.437
		Btu lb^{-1}	33.7098

DRY AIR

THE PROPERTIES TABULATED

The thermodynamic properties of dry air in the ideal gas state (without dissociation) are given in dimensionless form in this table. The properties listed are C_p°/R, $(H^\circ - E_0^\circ)/RT_0$, and S°/R, tabulated as functions of temperature in degrees K, and degrees R. The values were obtained from the thermodynamic properties of the constituents of dry air, which was considered to be 78.0881% N_2 [1], 20.9495% O_2 [2], 0.9324% A [3] and 0.0300% CO_2 [4]. This composition for dry air has been used in previous computations of properties of air [5], and corresponds to an average molecular weight of 28.966.

RELIABILITY OF THE TABLE

The uncertainties in the properties of dry air in the undissociated ideal gas state are considered to be roughly as great as for the ideal gas properties of molecular nitrogen, its principal constituent [1]. This implies that C_p°/R and S°/R are probably accurate to the next to the the last place tabulated up to about 2000°K and might be uncertain by a little more than a unit in the next to the last place at 3000°K. $(H^\circ - E_0^\circ)/RT_0$ may be uncertain by 0.004 at 2000°K and 0.006 at 3000°K.

INTERPOLATION

The validity of linear interpolation varies throughout this table depending upon the number of figures desired. The error produced by linear interpolation does not exceed one-eighth of the second difference. Where more precise values are desired, a four-point Lagrangian interpolation may be used [6].

CONVERSION FACTORS

The functions in this table have been expressed in dimensionless form in order that they may be converted readily to any system of units. Conversion factors are listed for the most often used units. For values of R and RT_0 not listed here see Table 1.30 of this series. The symbol R denotes the gas constant and T_0 is 273.16° Kelvin. The calorie used in the conversion factors is the thermochemical calorie and unless otherwise specified the mole is the gram - mole.

REFERENCES

[1] Thermal Properties of Gases, Table 11.10, National Bureau of Standards.

[2] Thermal Properties of Gases, Table 9.10, National Bureau of Standards.

[3] S. Gratch and S. W. Van Voorhis, Report of the University of Pennsylvania Thermodynamics Research Laboratory to the Navy Department, Bureau of Ships, for the period July 1, 1945 to April 30, 1946.

[4] Tables of Selected Values of Chemical Thermodynamic Properties, National Bureau of Standards.

[5] C. F. Curtiss and J. O. Hirschfelder, Thermodynamic Properties of Air (University of Wisconsin, June 1948) CM-472.

[6] Tables of Lagrangian Interpolation Coefficients (Columbia University Press, New York, N. Y., 1944).

Fig. 1 Reproduction of One of the Tables in the NBS Series on "Thermal Properties of Gases"
(Actual size of each of the 4 pages is 8 × 10½ in.)

under the supervision of William S. Benedict. The available data on thermal conductivities of gases have been evaluated and tabulated by Ralph L. Nuttall, and some viscosity data have been furnished by Francis C. Morey.

Several experimental investigations for the determination of thermal data are in progress in the Heat and Power Division of the NBS. Among these are measurements of the heat capacities C_p, of carbon dioxide, water vapor, and freon 12 by Joseph F. Masi; measurements of thermal conductivities at high pressures and temperatures, by Ralph L. Nuttall; and measurements of vapor pressures by the author. Some of these investigations were undertaken simultaneously with the project for the compilation of data, to fill in gaps where data were urgently needed.

As a preliminary step in the compilation of the tables a card file of over 1000 references was prepared, primarily by a search of Chemical Abstracts back to 1926, but also by consulting survey articles and reports such as the group of papers on gas properties published by this Society.[5] This file of references is gradually being processed as the tables are prepared, and in proportion as the references are read and evaluated, the file becomes more and more valuable. It is planned to maintain this file not only to promote the preparation of the tables, but also to aid in answering inquiries for thermodynamic data. The NBS receives a large number of such inquiries each year. These are welcomed, for it is one of the functions of this Bureau to supply or indicate sources of scientific information when these are known to members of its staff. Letters of inquiry are very useful to us as an aid in planning our future program.

Plans for the Future

In the immediate future we expect to devote a large part of our effort to the tabulation of real gas properties. Ideal gas tables have been more readily available and our progress with them has been more rapid, but the properties of the real gases are necessary for accurate calculations. In addition to the tables, we plan to prepare charts and diagrams such as Mollier charts and entropy-temperature diagrams that will be more convenient than tables for problems where graphic accuracy is adequate. When most of the data in the field of the project have been tabulated, emphasis will be placed on filling in the gaps with new experimental work, and on revising tables that are out of date. We know already that there will be more gaps than filled places in our outline, and we hope that much new experimental work will be undertaken.

The most urgent needs for new data appear to be in the fields of high temperature and high pressure. Measurements are especially needed of heat capacities and thermal conductivities. A few of these are under way at NBS but much more work is needed.

In several instances unpublished work or work in process of publication has been brought to our attention, and this has been extremely helpful to us. Communications of work in progress will be welcomed by any member of our group. If sufficient information becomes available the project will, if requested, act as a clearing house for information on work in progress in various laboratories. Those who have suggestions or comments concerning the tables, or who wish to obtain copies, should write to Joseph Hilsenrath, Thermodynamics Section, NBS, who is in charge of the project. At present the tables are being issued without charge.

Discussion

J. A. Goff.[6] It is gratifying to note from the paper that excellent progress is being made at the National Bureau of Standards with the preparation of working tables and diagrams of the properties of technically important gases. This is an essential part of any really comprehensive program of gas-properties research and as such is of particular interest to the ASME Gas Properties Committee. Of no less interest to the committee are the Bureau's offer to act as a clearing house for information on work in progress in various laboratories and its plan to maintain a relatively complete file of gas-properties references. These are tasks that the committee hardly can hope to do itself in view of the difficulty it has encountered in obtaining financial support. The NBS-NACA Tables of Thermal Properties of Gases project, which the author describes, is sure to reveal serious gaps in existing knowledge regarding gas properties, and in so doing will render a valuable service.

Although the Bureau claims not to have placed extreme emphasis on accuracy in the present stage of its program, it is obvious that it has exercised great care in the selection and appraisal of the data it has so far tabulated. At the same time, its selection of units in terms of which to express the data seems ill-advised. Its claim that convenience in use is gained by selecting R as the unit of entropy and RT_0 as that of energy is difficult to allow. It is true of course that the probable error of the ratio $c_p°/R$, for example, is slightly less than that of $c_p°$ itself, but this has nothing to do with convenience. In the opinion of the discusser, tables of $c_p°$ itself with suitable conversion factors would have been a good deal more convenient and only very slightly less accurate than tables of $c_p°/R$ with suitable conversion factors.

The writer also wonders why the Bureau proposes to tabulate the specific-heat ratio c_p/c_v since this cannot be substituted for k in the familiar expressions $pv^k = \text{const}$, and $a^2 = kgpv$, for the isentropes and the acoustic velocity, respectively, of a perfect gas with constant specific heats, to determine the isentropes and acoustic velocity of an actual gas with variable specific heats. There is considerable confusion on this point which tables of c_p/c_v would only serve to perpetuate.

In the auxiliary tables of conversion factors the symbol "cal" is understood to designate the thermochemical calorie which has recently been redefined as equal to 4.184 absolute joules exactly. The Btu referred to in these auxiliary tables is defined in terms of this calorie by the conversion factor 0.99934 Btu·g·°C/cal·lb·deg F. It is unfortunate that the simple numeric unity, has been lost in the struggle for individuality; perhaps something can yet be done to restore it.

C. N. Warfield.[7] The compilation of thermal properties of wind-tunnel and jet-engine gases as described in the paper is a valuable contribution in that it presents the results of an extensive search for existing data and makes available to the engineer and scientist in convenient form what appears at the present time to be the best available values. The NBS staff is to be commended especially for the convenient form in which these data are made available, and for the expeditious manner in which the results have been released.

An examination of the 16 tables that are listed in the paper gives rise to comments on a number of specific topics as follows:

Nomenclature. Neither symbols, subscripts, nor superscripts are defined in the tables. A convenient reference, or list of such definitions, would be useful.

Ideal Gas State. A comparison of Table 2.10 with the tables of reference 5 thereto (Curtiss and Hirschfelder, U. Wis. Report, APL No. CM-472) reveals that the values listed for specific heat and for enthalpy correspond to the ideal zero-pressure state, whereas the values listed for entropy correspond to a pressure of 1 atm.. A statement of this fact would avoid confusion in regard to the use of the entropy values tabulated.

---

[5] Symposium on Gas Properties, Trans. ASME, vol. 70, 1948, pp. 621 ff.

[6] Dean, Towne Scientific School, University of Pennsylvania, Philadelphia, Pa. Mem. ASME.

[7] Applied Physics Laboratory, The Johns Hopkins University, Silver Spring, Md.

Although Report No. CM-472 is not listed as a reference for Table 11.10, a similar comparison indicates that the values of entropy for molecular nitrogen have been treated as in the case of dry air.

However, in Table 7.10 (for molecular hydrogen), it is conveniently stated that all values are for the "ideal gas state for a pressure of 1 atmosphere."

Thermal Conductivities. Table 2.42 lists values of thermal conductivity of dry air at various temperatures, but fails to give any indication concerning variation with pressure. Presumably the values listed are for a pressure of 1 atm, and a statement to this effect would be helpful. This comment is also applicable to the other tables for thermal conductivity, excepting only Table 5.42 (for steam) in which thermal conductivities are listed for 11 pressures (from 1 atm to 300 atm), as well as for various temperatures.

It is important to call attention at this time to the fact that some of the values listed may not be valid for direct use in those applications involving very rapid changes in pressure, temperature, etc., such as occur in shock waves and possibly in other applications in supersonic aerodynamics. In this connection the NBS tables on relaxation phenomena are awaited with considerable interest.

AUTHOR'S CLOSURE

Dean Goff raised a question as to the advisability of the choice of dimensionless units. We wish it were possible to find a set of units with dimensions acceptable in all fields where our tables will find use. We are sympathetic with Dean Goff's point of view, but his selection of units would not have universal acceptance. Dimensionless variables were chosen because aerodynamic physicists and engineers, for whom these tables were undertaken, showed a greater preference for them than for any set of dimensional units. This may be so because dimensionless variables and properties are in general use in aerodynamics. From the NBS-NACA tables that are now in dimensionless units, tables in any other units may be prepared with little trouble.

Our conversion factors are so chosen that those who wish to work with calories will obtain values in terms of the thermochemical calorie, while those who prefer Btu's will obtain the kind of Btu that they are accustomed to. We believe that this is the way each group wants it. The thermochemical calorie = 4.1840 abs joules, and the Btu = 1055.040 abs joules. These are independent definitions. In these units, specific heats in calories per gram degree C are nearly, but not exactly, equal to specific heats in Btu per pound degree F.. If the I.T. calorie is used, the equality becomes exact. Such a relationship has some advantage, but will probably not induce the users of either the thermochemical calorie or the present Btu to change their accustomed units.

With regard to Dr. Warfield's suggestion that symbols, subscripts, and superscripts be defined, it may be of interest that an introductory table for the series is being prepared. This table is to contain the definitions referred to and also lists of basic constants and conversion factors. Dr. Warfield's other comments are also well taken and we expect to adopt his suggestions in the preparation of future tables.

The careful consideration that the discussers have given to the NBS-NACA tables is much appreciated.

Pressure-Volume-Temperature Relationships of Gaseous Normal Hydrogen From Its Boiling Point to Room Temperature and From 0-200 Atmospheres

By H. L. JOHNSTON[1] and DAVID WHITE,[2] COLUMBUS, OHIO

This paper presents a summary of accurate measurements on data of state for normal hydrogen gathered over a period of years by a group of investigators in The Ohio State University Cryogenic Laboratories. Results cover a wide range of temperature and pressure.

INTRODUCTION

ACCURATE measurements of data of state for normal hydrogen have been carried out by a group of investigators, in The Ohio State University Cryogenic Laboratories over a period of years. The purpose of the present paper is to present a summary derived from the results obtained over a wide range of temperature and pressure. A detailed description of the work will be published in a series of papers which will appear shortly. A survey of the P-V-T properties of hydrogen made by the Bureau of Standards[3] summarizes existing data which cover this range of temperature and pressure. However, this is the first work to cover the entire range with a high degree of precision and accuracy throughout.

APPARATUS

A drawing of the apparatus in which the gas was compressed is shown in Fig. 1. The pipette *H* is surrounded by a series of blocks *E*, *F*, and *G* and enclosed in an evacuated can *J* to prevent heat leak. The pipette can be maintained to within a few thousandths of a degree of a specified temperature, at all temperatures, for at least $^1/_2$ hr.

Briefly, the operation of the apparatus is as follows:

Gas is introduced into a pipette which has already been cooled to the desired temperature and compressed to the desired pressure. After thermal equilibrium has been established, the pressure is measured on an M.I.T. type dead-weight gage.[4] The precision of this gage varies from 1 part in 10,000 to 1 part in 100,000 with increasing pressure. In some of the earlier work at high pressures, an American instrument-type gage was used with a precision of 1 part in 3000 or 4000. Both types of gages were calibrated using the vapor pressure of carbon dioxide at the ice point as a primary standard.[5] The temperature of the gas is measured simultaneously with the pressure by means of thermocouples standardized with a helium thermometer. Temperatures can be read with a precision of 0.0005 deg C at room temperatures and of 0.003 deg at 20 deg K. The accuracy of the temperature scale is probably not better than 0.02 deg C at the lower temperatures, but is slightly better at the higher temperatures.

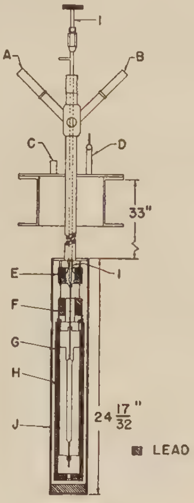

A High-pressure gas inlet
B Thermocouple tubes
C Transfer-tube inlet for coolant
D Safety T-tube and evacuation line for dewar in which apparatus is immersed
E, *F*, *G* Auxiliary upper and lower blocks
H Calibrated pipette connected to auxiliary block by means of small capillary
I Pipette valve and stem which shuts pipette off from dead space
J Evacuated outer can

FIG. 1 (*left*) THE P-V-T APPARATUS

After first closing the valve above the pipette *I* (see Fig. 1), and pumping out the gas held in the dead space above this valve, the number of moles of gas is obtained by expanding the gas in the pipette into calibrated cylinders maintained at constant temperature. The expansions are generally carried out in two or three steps so that the pressures in the calibrated cylinders never significantly exceed 1 atm. Pressures are read on a constant-volume mercury manometer to within 0.03 mm Hg with the aid of a cathetometer.

The hydrogen used in this work was extremely pure. Impurities never exceeded 0.001 to 0.002 mole per cent. The gas was prepared by triple distillation of electrolytic hydrogen.

P-V-T DATA

A few sample isotherms, with experimental points, are shown in Figs. 2, 3, 4, and 5, to indicate the precision of the data. Figs. 2 and 3 show the low-pressure data, while Figs. 4 and 5 show the isotherms over the complete pressure range from 0 to 200 atm.

---

[1] Director, Cryogenic Laboratory, Department of Chemistry, The Ohio State University.

[2] Post-Doctorate Research Fellow, Cryogenic Laboratory, Department of Chemistry, The Ohio State University.

[3] "Compilation of Thermal Properties of Hydrogen and Its Various Isotopic Ortho-Para Modifications," by H. W. Woolley, R. B. Scott, and F. G. Brickwedde.

[4] "High-Pressure Technique," by F. G. Keyes, *Industrial and Engineering Chemistry*, vol. 23, 1931, p. 1375.

[5] "A Fixed Point for Calibration of Pressure Gauges. The Vapor Pressure of Liquid Carbon Dioxide at 0°," by O. C. Bridgeman, *Journal of the American Chemical Society*, vol. 49, 1927, p. 1174.

Contributed by the Research Committee on Properties of Gases and Gas Mixtures, Heat Transfer and Applied Mechanics Divisions, and presented at the Annual Meeting, New York, N. Y., November 27–December 2, 1949, of THE AMERICAN SOCIETY OF MECHANICAL ENGINEERS.

NOTE: Statements and opinions advanced in papers are to be understood as individual expressions of their authors and not those of the Society. Paper No. 49—A-149.

TABLE 1 SMOOTHED PV/RT VALUES FROM BOILING POINT OF HYDROGEN TO ROOM TEMPERATURE AND FROM 0–200 ATM

Temp. °K.	1 atm	2 atm	5 atm	10 atm	15 atm	20 atm	25 atm	30 atm	35 atm	40 atm	45 atm
300	1.000528	1.001137	1.003047	1.006134	1.009221	1.012268	1.015355	1.018483	1.021570	1.024658	1.027786
250	1.000674	1.001308	1.003258	1.006572	1.009837	1.013202	1.016517	1.019832	1.023146	1.026412	1.029776
200	1.001686	1.002356	1.004550	1.008084	1.011679	1.015274	1.018869	1.022464	1.026120	1.029959	1.033737
175	1.000777	1.001473	1.003561	1.007181	1.010801	1.014491	1.018041	1.021522	1.025142	1.028831	1.032660
150	1.000453	1.001103	1.002970	1.006219	1.009467	1.012716	1.016046	1.019375	1.022949	1.026684	1.030583
125	1.000240	1.000629	1.002092	1.004431	1.006770	1.009109	1.011351	1.013690	1.016030	1.018954	1.022170
100	0.999719	0.999597	0.999109	0.998622	0.998500	0.998622	0.998866	0.999475	1.000450	1.002034	1.004227
90	1.000123	0.999311	0.997280	0.994166	0.991457	0.989426	0.988072	0.987260	0.987260	0.987937	0.989426
80	0.998397	0.997026	0.993065	0.986820	0.981336	0.976309	0.972043	0.968540	0.966102	0.964884	0.964579
75	0.998007	0.996058	0.990208	0.981271	0.973147	0.965997	0.960148	0.955273	0.951373	0.948773	0.946823
60	0.995452	0.991390	0.978391	0.957673	0.936346	0.916035	0.898161	0.882928	0.869929	0.859773	0.852461
50	0.991387	0.982627	0.958049	0.917410	0.876042	0.835890	0.796225	0.764346	0.743419	0.725898	0.717137
40	0.983327	0.967516	0.918258	0.830993	0.732174	0.619976	0.523590	0.490599	0.498049	0.523590	0.556732
35	0.974104	0.949439	0.873706	0.725367	0.472461	0.316480	0.350872	0.395686	0.443975	0.491568	0.538120

Temp. °K.	50 atm	60 atm	70 atm	80 atm	90 atm	100 atm	125 atm	150 atm	175 atm	200 atm
300	1.030873	1.037048	1.043303	1.049437	1.055612	1.061827	1.077304	1.092903	1.108746	1.124589
250	1.033139	1.039818	1.046691	1.053711	1.060925	1.068335	1.086907	1.105528	1.124150	1.142527
200	1.037576	1.045436	1.053296	1.061401	1.069505	1.077609	1.098326	1.119531	1.141467	- ------
175	1.036489	1.044494	1.052918	1.061620	1.070600	1.079650	1.103040	1.127475	1.152954	1.179616
150	1.034643	1.042683	1.051210	1.059819	1.069077	1.078579	1.104729	1.132585	1.162065	1.192763
125	1.025679	1.033769	1.042542	1.052191	1.062133	1.072952	1.102778	1.135723	1.170910	1.209411
100	1.006785	1.013365	1.021285	1.030788	1.041267	1.053086	1.089760	1.133014	1.179802	1.227930
90	0.991322	0.996738	1.004592	1.014206	1.025445	1.038850	1.081368	1.131469	1.185768	1.243045
80	0.964884	0.968083	0.975090	0.985449	0.998549	1.015611	1.067861	1.127576	1.192471	1.262087
75	0:945848	0.946173	0.952673	0.965347	0.982408	1.001582	1.059591	1.129624	1.201281	1.275701
60	0.848399	0.849617	0.863429	0.885975	0.914613	0.947517	1.042980	1.145349	1.250967	1.360850
50	0.718354	0.740499	0.777730	0.825183	0.874095	0.926414	1.062931	1.198230	1.332557	1.466833
40	0.591395	0.665585	0.741904	0.818527	0.893021	0.965995	1.149039	1.325697	1.495666	1.664115
35	0.583976	0.674647	0.765318	0.854252	0.940059	1.025171	1.235347	1.436143	1.637287	- ------

TABLE 2 SMOOTHED PV/RT BELOW SATURATION CURVE OF HYDROGEN

Temp, deg K	0.2 atm	0.4 atm	0.6 atm	0.8 atm	1 atm	2 atm	3 atm	4 atm	5 atm	6 atm
30	0.993975	0.986571	0.978970	0.971567	0.964163	0.926037	0.886088	0.842840	0.794831	0.737993
25	0.989520	0.977901	0.966283	0.954418	0.942305	0.877046				
20	0.984540	0.965573	0.946901	0.928230						

TABLE 3 SMOOTHED PV/RT AT MINIMUM IN PV/RT VERSUS PLOT

Temp	Pressure at minimum	PV/RT at minimum
100	17	0.998500
90	32	0.987260
80	45	0.964579
75	54	0.945686
60	54	0.847383
50	46.8	0.716407
40	30.6	0.490295
35	19	0.315090

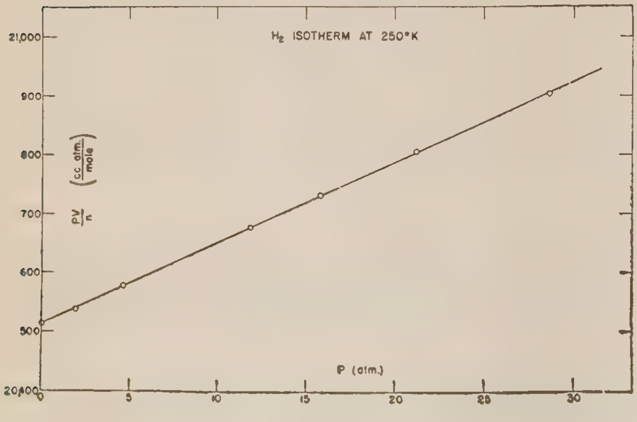

FIG. 2

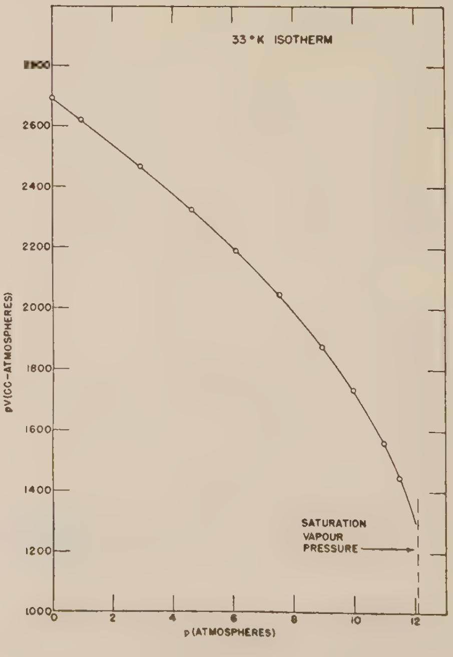

FIG. 3

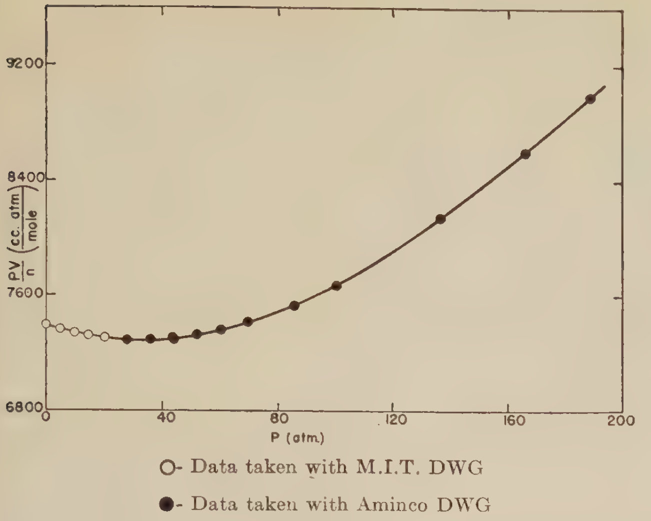

FIG. 4 HYDROGEN ISOTHERM AT 90 DEG K

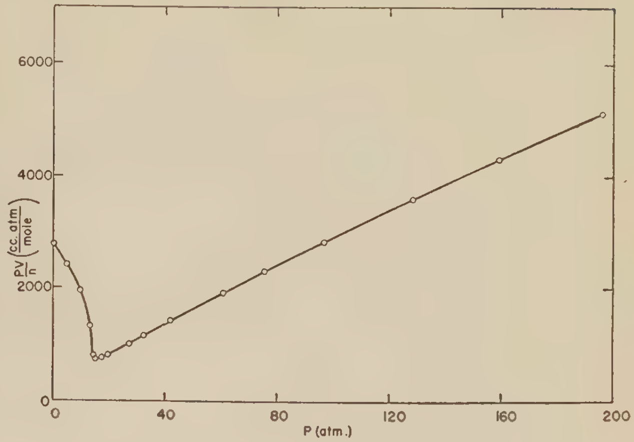

FIG. 5 HYDROGEN ISOTHERM AT 34 DEG K

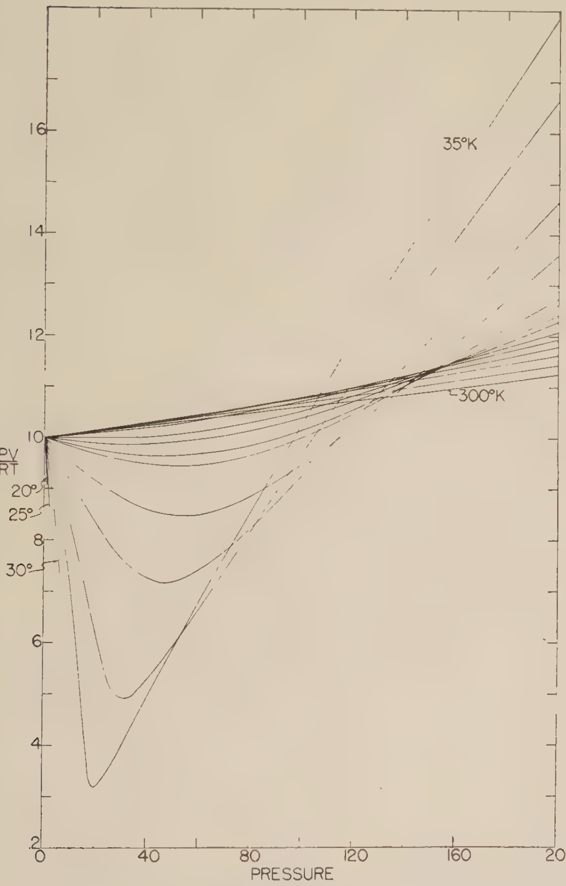

FIG. 6 RELATIVE ISOTHERMS FOR HYDROGEN

(Temperature of isotherms reading from top left-hand side down are 35, 40, 50, 60, 75, 80, 90, 100, 125, 150, 175, 200, 250, 300 deg Kelvin. Short isotherms at left represent data below critical temperature, 20, 25, 30 deg Kelvin, and extend only to vapor-pressure curve.)

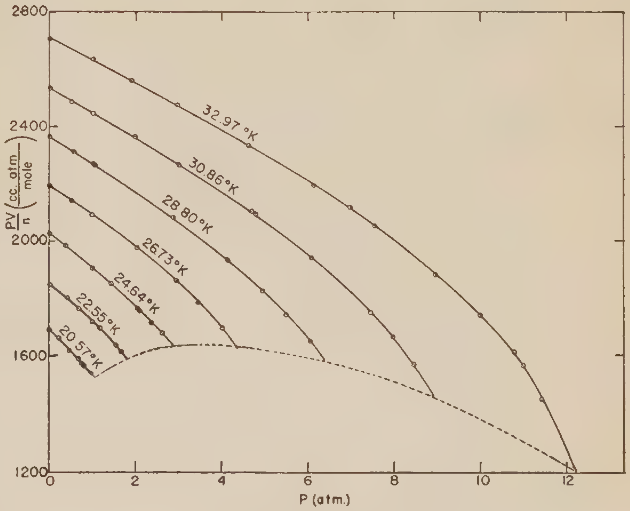

FIG. 7 P-V-T DATA OF HYDROGEN BETWEEN BOILING POINT AND CRITICAL TEMPERATURE

(Dotted line represents vapor-pressure curve of hydrogen between normal boiling point and critical temperature.)

Tables 1, 2, and 3 present a summary of the smoothed PV/RT values at integral values of the pressure and temperature. Isotherms below the "critical point" extend only to the saturation curve.

Analytical expressions are now being obtained for the individual isotherms by means of IBM machines using a virial form of equation. The constants of these equations will be correlated with temperature to give analytical expressions for all isotherms. These analytical expressions will be used to construct a Mollier diagram, which will be submitted for publication in the future.

Fig. 6 shows a plot of the data given in Tables 1, 2, and 3. Fig. 7 shows the experimental data taken below the critical temperature up to the saturation curve.

Heat Transfer to a Fluid Flowing Turbulently Between Parallel Walls With Asymmetric Wall Temperatures

By R. A. SEBAN,[1] BERKELEY, CALIF.

The case of heat transfer to a fluid of constant properties flowing turbulently between parallel walls having arbitrary but uniform temperatures is considered on an analytical basis, which is an extension of the work of Martinelli and of Harrison and Menke. Therefore, only conditions for a flow fully developed from the hydrodynamic and thermal standpoint are considered. It is shown that the existence of solutions for the case of one adiabatic wall enables the specification of the temperature distribution and heat-transfer coefficients for cases in which the walls have any uniform temperature values. The effect of inequality in the wall temperatures is shown to be small for Prandtl numbers greater than unity but significant for fluids of low Prandtl number, such as molten metals. To facilitate its use in the present applications, the existing solution for one adiabatic wall is extended.

NOMENCLATURE

CERTAIN temperatures are defined in Fig. 1 and these are not repeated in the following nomenclature which is used throughout the paper:

a = thermal diffusivity, sq ft per sec
c = heat capacity, Btu/(lb mass) (deg F)
D = distance between the plates, ft
h = heat-transfer coefficient Btu/(hr) (ft²) (deg F)
k = thermal conductivity, Btu/(hr) (ft²) (deg F/ft)
p = pressure, (lb force)/ft²
q_O = heat-transfer rate per unit area at wall, Btu/(hr) (ft²)
T = temperature, deg F
U = velocity, fps
U_τ = friction velocity, $U_m \sqrt{\dfrac{c_f}{2}}$ fps
x = direction of flow, ft
X = temperature-difference ratio, defined in Equation [8]
y = direction normal to flow, ft
ϵ = eddy diffusivity, sq ft per sec
ν = kinematic viscosity, sq ft per sec
ρ = fluid density, lb mass/ft³
τ_O = shear stress at wall, lb force/ft²

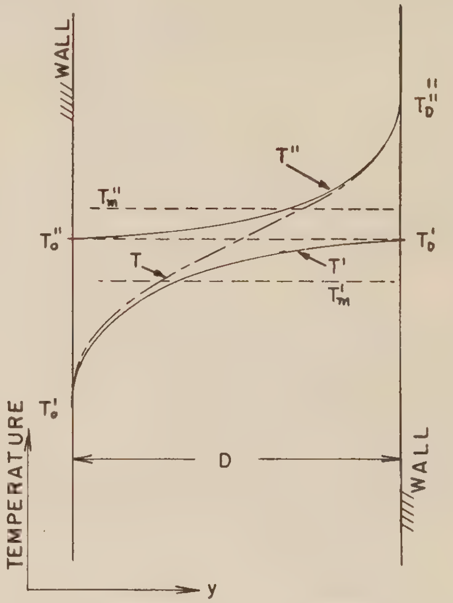

FIG. 1 SCHEMATIC REPRESENTATION OF COMPOSITION OF ADIABATIC-WALL SOLUTIONS

DIMENSIONLESS NUMBERS

c_f = skin friction coefficient $\dfrac{2g\tau_O}{\rho U_m^2}$
$\dfrac{2hD}{k}$ = Nusselt number
ν/a = Prandtl number
$\dfrac{2U_mD}{\nu}$ = Reynolds number
$\dfrac{h}{\rho U_m c}$ = Stanton number
D^+ = dimensionless channel width $\dfrac{DU_\tau}{\nu}$

SUBSCRIPTS

m = mean value
O, D = wall value
30 = value at point where $\dfrac{yU_\tau}{\nu} = 30$

INTRODUCTION

In a recent paper Harrison and Menke (1)[2] have extended the method of Martinelli (2) to the specification of the temperature distribution in the turbulent flow of a molten metal between parallel walls, one wall being adiabatic. It is the purpose of this paper to demonstrate that the existence of a solution for the case of one adiabatic wall enables the specification of the temperature distribution and, consequently, of the heat-transfer co-

---

[1] Lecturer in Mechanical Engineering, University of California. Jun. ASME.

Contributed by the Heat Transfer Division and presented at the Annual Meeting, New York, N. Y., November 27–December 2, 1949, of THE AMERICAN SOCIETY OF MECHANICAL ENGINEERS.

NOTE: Statements and opinions advanced in papers are to be understood as individual expressions of their authors and not those of the Society. Paper No. 49—A-18.

[2] Numbers in parentheses refer to the Bibliography at end of paper.

efficients for the more general case in which the heat transfer takes place through both walls, the walls having any uniform temperatures. The solution for the case of one adiabatic wall has been extended so as to yield the quantities necessary for such a specification.

Specification of Temperature Distribution

The problem considered herein involves the turbulent flow of a fluid of constant properties between two parallel walls, the temperatures of the walls having any uniform value. The flow is fully developed from a hydrodynamic and thermal standpoint, that is, the generalized velocity and temperature distributions in the flow cross section are assumed to be independent of the distance in the direction of flow.

The energy and momentum equations can be written as follows (neglecting any thermal effects of flow energy dissipation)

$$U\frac{\partial T}{\partial x} = \frac{\partial}{\partial y}\left[(\epsilon + a)\frac{\partial T}{\partial y}\right] \qquad [1]$$

$$\frac{1}{\rho}\frac{\partial p}{\partial x} = \frac{\partial}{\partial y}\left[(\epsilon + \nu)\frac{\partial U}{\partial y}\right] \qquad [2]$$

For the problem considered, the boundary conditions applying to the energy equation are at

$$y = 0 \qquad T = T_O$$
$$y = D \qquad T = T_D$$

The usual method of solution of Equation [1] involves assumptions of the following type:

(*a*) Separation of molar and molecular transfer effects into separate regions, after von Kármán.

(*b*) The neglect of changes in stream thermal-energy content in those regions in which molecular transfer effects are appreciable.

(*c*) The assumption that

$$U\frac{\partial T}{\partial x} = U_m\frac{\partial T_m}{\partial x}$$

Except for the assumption of constant velocity, this is correct for the case of constant wall heat-transfer rate and has yielded satisfactory results for cases of constant wall temperatures in previous applications of this type of analysis.

(*d*) Integration of Equation [1] in terms of the diffusivity as calculated from Equation [2] and a specified velocity distribution.

The problem can be solved in this way, but a simpler development is realized by use of the available solution for one adiabatic wall. This solution satisfies Equation [1] under the restrictions just specified, for boundary conditions which are at

$$y = 0 \qquad T = T_O'$$
$$y = D \qquad \frac{dT'}{dy} = 0$$

and the solution may be specified as[3]

$$f'(y) = \frac{T' - T_O'}{T_D' - T_O'} \quad \text{so that} \quad \left.\begin{aligned} f'(0) &= 0 \\ f'(D) &= 1 \end{aligned}\right\} \qquad [3]$$

Evidently the same solution is applicable if the heated and adiabatic walls are interchanged, so that the boundary conditions become at

$$y = D \qquad T = T_D''$$
$$y = 0 \qquad \frac{dT''}{dy} = 0$$

and this solution may be specified as

$$f''(D - y) = \frac{T'' - T_D''}{T_O'' - T_D''} \quad \text{so that} \quad \left.\begin{aligned} f''(0) &= 0 \\ f''(D) &= 1 \end{aligned}\right\} \qquad [4]$$

Because of the linearity of Equation [1], any sum of solutions is also a solution, and a proper addition of the solutions represented by Equations [3] and [4] will yield a temperature distribution satisfying the boundary conditions of the present problem. Fig. 1 reveals such a combination of solutions, which can be stated in the following way

$$T = T' + T'' - T_O'' \qquad [5]$$

Then, in terms of the two adiabatic wall solutions given by Equations [3] and [4]

$$T = T_O' + (T_D' - T_O')f'(y) + T_D'' - T_O'' + (T_O'' - T_D'')f''(D - y) \qquad [6]$$

The temperature distribution given by Equation [6] satisfies the energy equation in virtue of the fact that the solutions $f'(y)$ and $f''(y)$ satisfy that equation. Agreement with the boundary conditions of the present problem is demonstrated as follows:

At $y = 0$

$$T = T_O' + (T_D' - T_O')(0) + T_D'' - T_O'' + (T_O'' - T_D'')(1)$$
$$T = T_O'$$

At $y = D$

$$T = T_O' + (T_D' - T_O')(1) + T_D'' - T_O'' + (T_O'' - T_D'')(0)$$
$$T = T_D' + T_D'' - T_O''$$

and since the solutions are so combined that $T_D' = T_O''$, therefore $T = T_D'$ and the boundary condition at this point is fulfilled.

The determination of the temperature distribution specified by Equation [6] requires knowledge of the differences $T_D' - T_O'$ and $T_D'' - T_O''$, which are in turn related to the mean temperature of the fluid. This relation is determined by the use of Equation [6] in the specification of the mixed mean fluid temperature. This mean fluid temperature is defined as

$$T_m = \int_O^D \frac{1}{D}\frac{U}{U_m}T\,dy$$

and in consequence, from Equation [6]

$$T_m = T_O' + T_D'' - T_O'' + (T_D' - T_O')\frac{1}{D}\int_O^D \frac{U}{U_m}f'(y)dy + (T_O'' - T_D'')\frac{1}{D}\int_O^D \frac{U}{U_m}f''(D - y)dy \qquad [7]$$

Because of the assumed symmetry of the velocity distribution, U/U_m, about the flow center line, $y = D/2$, the two integrals occurring in the right side of the Equation [7] have the same value. Further, these integrals also express the ratio of the difference between wall and mean temperatures to the difference between the two wall temperatures for the solutions applying to the adiabatic wall cases as given by Equations [3] and [4]. Thus for the case of wall *D* being adiabatic

$$\frac{1}{D}\int_O^D \frac{U}{U_m}f'(y)dy = \frac{T_m' - T_O'}{T_D' - T_O'} \qquad [8]$$

For convenience in what follows this temperature ratio is designated by the symbol *X*.

For the case of wall *O* being adiabatic

---

[3] The prime superscripts as used herein are merely discriminating symbols, and do not indicate differentiation.

$$\frac{1}{D}\int_0^D \frac{U}{U_m} f''(D-y)dy = \frac{T_m'' - T_D''}{T_O'' - T_D''} = X \quad \text{.....} [9]$$

Introduction of these relations into Equation [7] yields the final expression

$$T_m = T_m' + T_m'' - T_O'' \quad \text{.............} [10]$$

or the alternative form

$$T_m = T_D'' + X(T_O'' - T_D'') + T_O' + X(T_D' - T_O') - T_O'' \quad \text{..........} [11]$$

It has been noted that the temperature distribution obtaining for wall temperatures T_O and T_D can be obtained from Equation [6] once the temperature T_O'', $(T_O'' = T_D')$ is known. This temperature is obtained from Equation [11] in terms of the mean fluid temperature, T_m, and the temperature-difference ratio X. The ratio X is obtained from the solution for one adiabatic wall and some magnitudes are indicated in the Appendix of this paper.

HEAT-TRANSFER COEFFICIENTS

Knowledge of the temperature distribution enables the specification of the heat-transfer coefficient in terms of the temperature gradient at the wall under consideration. Thus at the wall $y = 0$

$$h = \frac{-k \left.\frac{\partial T}{\partial y}\right|_{y = 0}}{T_O - T_m} \quad \text{................} [12a]$$

and at the wall $y = D$

$$h = \frac{+k \left.\frac{\partial T}{\partial y}\right|_{y = D}}{T_D - T_m} \quad \text{..............} [12b]$$

Differentiation of Equation [5] so as to form $\partial T/\partial y$ and evaluation of this quantity at $y = 0$ and at $y = D$ reveals that the magnitude of the temperature gradient at the walls remains the same as for the adiabatic-wall solution for the wall considered. The heat-transfer coefficient given by Equation [12] is consequently different from that obtaining for one adiabatic wall only in so far as the prevailing wall temperatures affect the difference between the temperature of the wall considered and the mixed mean fluid temperature.

Thus at $y = 0$, the ratio of the heat-transfer coefficient obtaining for one adiabatic wall to that for the more general case here considered can be stated as

$$\frac{h'}{h} = \frac{T_O - T_m}{T_O' - T_m'} = 1 + \frac{T_O'' - T_m''}{T_O' - T_m'} \quad \text{........} [13a]$$

and at $y = D$

$$\frac{h''}{h} = 1 + \frac{T_O'' - T_m'}{T_O'' - T_m''} \quad \text{..............} [13b]$$

As given by Equations [13a] and [13b], the heat-transfer coefficients are, in general, different for each wall, and they are the same for both walls only when the wall temperatures are the same or are equally above and below the mean fluid temperature.

Consideration of the definitions of the Nusselt and Stanton numbers indicates that Equations [13a] and [13b] can also be considered as ratios of these numbers, as well as ratios of the heat-transfer coefficients.

DISCUSSION

An immediate application of the foregoing theory is the specification of the maximum variation of the heat-transfer coefficient due to changes in the wall-temperature values. Already it has been noted that the heat-transfer coefficient differs from that obtaining for the system with one adiabatic wall only in so far as the difference between the wall and mean fluid temperatures differs from that in the adiabatic-wall solution. Thus the extremes of variation occur for the case of equal wall temperatures ($T_O - T_m = T_D - T_m$), on one hand, and for wall temperatures equally above and below the mean fluid temperature ($T_O - T_m = T_m - T_D$) on the other. If Equations [13a] and [13b] are evaluated for these conditions, it is found that the ratio of heat-transfer coefficients specified by these equations depends only upon the temperature-difference ratio X. This ratio can be evaluated from the known adiabatic-wall solution and the ratio of the heat-transfer coefficient h, obtaining for one of the cases just considered, to the coefficient h', obtaining for the adiabatic-wall solution, can then be determined. This ratio of heat-transfer coefficients is shown in Fig. 2 as a function of the Prandtl and Reynolds numbers.

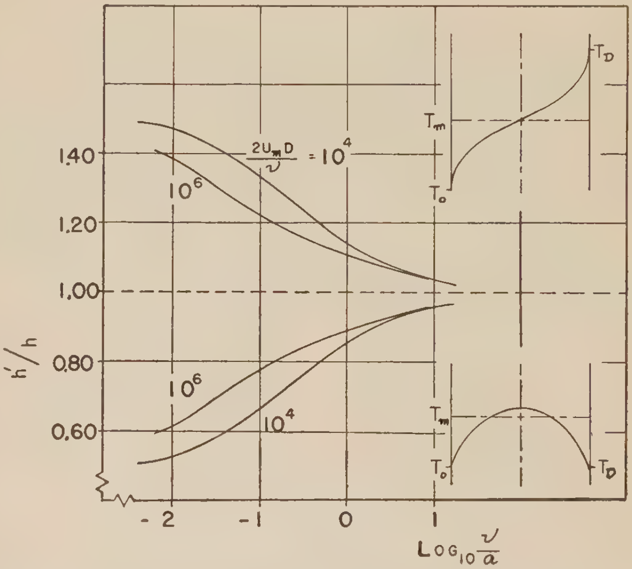

FIG. 2 VARIATION IN HEAT-TRANSFER COEFFICIENT DUE TO CHANGES IN MAGNITUDES OF WALL TEMPERATURES

(The two extreme cases are shown in reference to the case of one adiabatic wall. Temperature distributions are shown schematically adjacent to the curves depicting variation. The heat-transfer coefficient for one adiabatic wall is h'.)

The effect of variation in the wall-temperature values on the heat-transfer coefficient is seen to be significant only for fluids of relatively small Prandtl numbers. For fluids of high Prandtl number, the preponderant portion of the difference between wall and mean fluid temperatures occurs in the flow sublayers, and in consequence, the magnitude of the difference is not affected substantially by the relative wall-temperature magnitudes. Fig. 2 reveals that the variation in the heat-transfer coefficient is quite small for fluids having a Prandtl number greater than 10.

A specific example of the combination of two adiabatic wall solutions to obtain the temperature distribution for a case in which the wall temperatures are not equal consists in the comparison of this theory with the data of Corcoran (3), et al. These experimenters determined temperature distributions across the stream, and heat-transfer coefficients for air flowing turbulently in a rectangular duct having an aspect ratio of 16, the wall temperatures being uniform with respect to length. The data and the prediction according to the present theory are presented in Fig. 3, the prediction being obtained as follows:

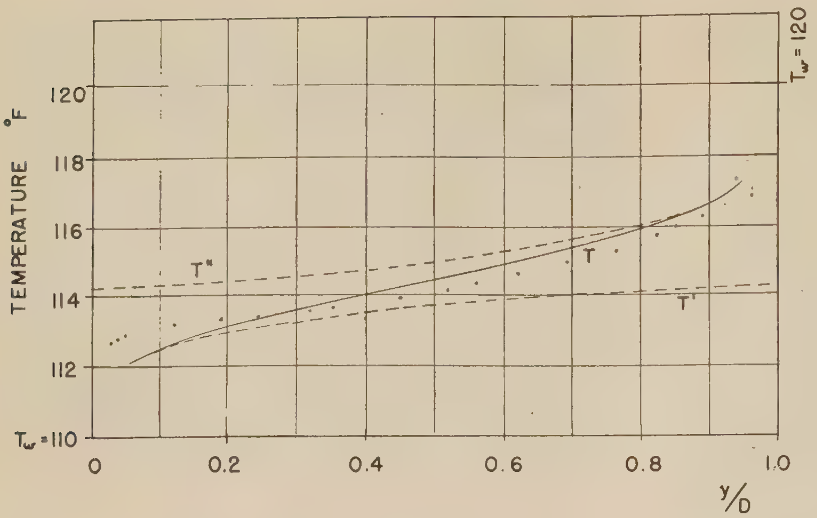

Wall temperatures...	110 and 120 F
Mean air temperature.	114.5 F
Reynolds number....	30,500
Measured Nusselt number: 120 F side......	70
Predicted Nusselt number:	
120 F side...........	53
110 F side...........	48

Fig. 3 (*left*) Predicted and Experimental Temperature Distribution for Air Flow in a Rectangular Channel

Given: Mean air temperature 114.5 F; wall temperature T_O = 110 F; T_D = 120 F; Reynolds number = 30,500.

Solution: It is first necessary to determine the temperature-difference ratio X, obtaining for the Prandtl and Reynolds numbers of the flow. The use of Equation [18] (see Appendix) for the determination of $(T_O' - T_m')$ and of Equation [14] through [17] for the determination of $(T_O' - T_D')$ yields $X = 0.85$ for a Prandtl number of 0.72, and the given Reynolds number. (Linear interpolation of Fig. 4 yields $X = 0.84$.) The values associated with the two adiabatic-wall solutions from which the desired result is obtained are now determined as follows:

From Equation [8] From Equation [9]

$$0.85 = \frac{T_m' - 110.0}{T_D' - 110.0} \qquad 0.85 = \frac{T_m'' - 120.0}{T_O'' - 120.0}$$

and from Equation [10]

$$114.5 = T_m' + T_m'' - T_D''$$

Solution of these equations yields

$$T_D' = T_O'' = 114.2; \; T_m' = 113.6; \; T_m'' = 115.1$$

The temperature distribution is specified by Equation [6], the necessary "adiabatic-wall" temperature distributions being obtained from Equations [14] through [17] (see Appendix). This distribution already has been calculated in the process of evaluating the ratio X.

The determination of the heat-transfer coefficients does not require the determination of the temperature distribution, but knowledge only of the temperature quantities just noted. Thus the process is somewhat shortened if an approximate value of X is obtained from Fig. 4.

The Nusselt number for the adiabatic-wall case has been calculated as 60.2. (A magnitude can be approximated from Fig. 5.) Application of Equations [13a] and [13b] yields the Nusselt numbers for the case under consideration:

For the 110 deg F wall

$$\frac{h'}{h} = 1 + \frac{114.2 - 115.1}{110.0 - 113.6}, \qquad \frac{2hD}{k} = \frac{60.2}{1.25} = 48$$

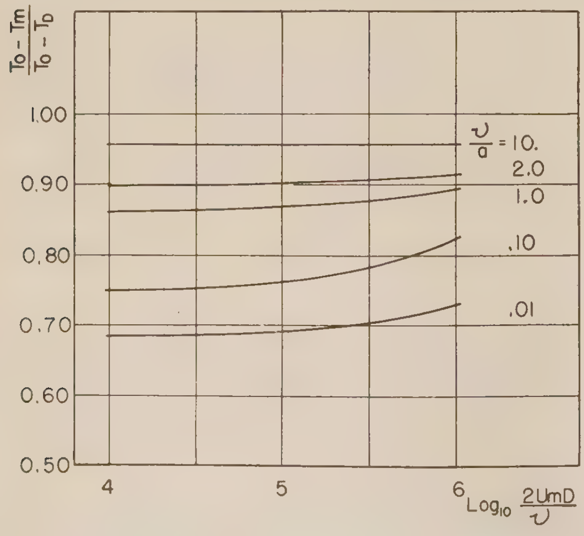

Fig. 4 Temperature-Difference Ratio as a Function of Reynolds and Prandtl Numbers

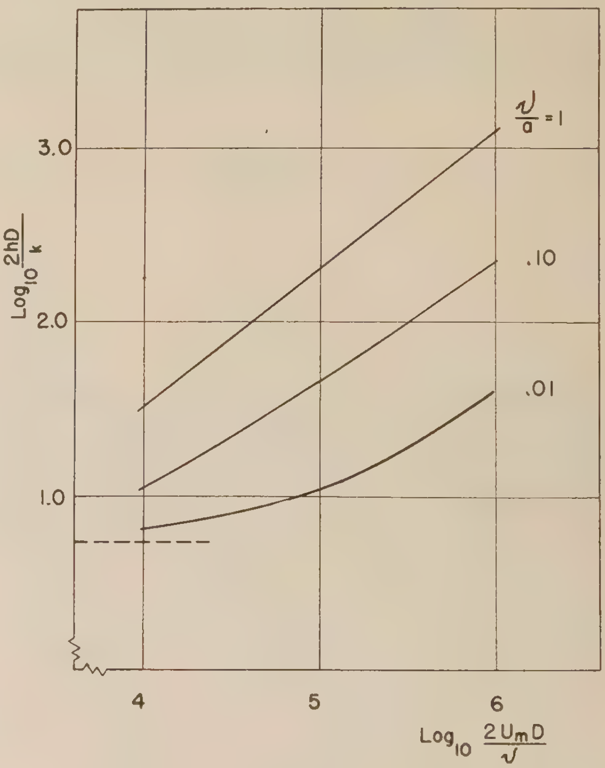

Fig. 5 Nusselt Number as a Function of Reynolds and Prandtl Numbers

For the 120 deg F wall

$$\frac{h''}{h} = 1 + \frac{114.2 - 113.6}{120.0 - 115.1}, \qquad \frac{2hD}{k} = \frac{60.2}{1.12} = 53$$

The predicted Nusselt number is seen to be substantially less than the experimental value at the 120 deg F wall. A similar discrepancy can be noted between the measured and predicted temperature distribution. This might be ascribable to an inadequate starting length, except that the experimental apparatus had a 75-width length upstream from the measuring section.

CONCLUSIONS

The case of heat transfer to an incompressible fluid flowing turbulently between parallel walls has been considered for the case of arbitrary uniform wall-temperature values. A technique of calculating the heat-transfer coefficients and the temperature distribution has been indicated.

Variations in the magnitude of the heat-transfer coefficient due to the relative values of the wall temperatures have been shown to reside in variation of the difference between wall and mean fluid temperatures. Such variations are shown to be substantial only for fluids of low Prandtl number.

Presently available data are not sufficiently extensive to establish the accuracy of the solution for the general case. For the case of equal wall temperatures, the solution can be shown to coincide with existing solutions (2) for the case of equal wall temperatures, and these solutions are in accord with experimental data for the flow of air in ducts of large aspect ratio.

The extension of these concepts to the case of a fluid flowing turbulently in an annulus depends upon the radius of curvature involved. It is complicated by the dissimilarity of the two adiabatic-wall solutions necessary to a general solution, and the adiabatic-wall solutions are in turn complicated by the inequality of the skin-friction coefficients on the inner and outer cylindrical surfaces.

BIBLIOGRAPHY

1 "Heat Transfer to Liquid Metals Flowing in Asymmetrically Heated Channels," by W. B. Harrison and J. R. Menke, Trans. ASME, vol. 71, October, 1949, pp. 797–803.

2 "Heat Transfer to Molten Metals," by R. C. Martinelli, Trans. ASME, vol. 69, 1947, pp. 947–960.

3 "Temperature Gradients in Turbulent Gas Streams," by W. A. Corcoran, B. Roudebush, and B. H. Sage, *Chemical Engineering Progress*, vol. 43, March, 1947, pp. 135–142.

4 "Measurements of the True Temperature and Heat Exchange in a Catalytic Reaction," by M. Jakob, Trans. AIChE, vol. 35, 1939, pp. 563–586.

Appendix

TEMPERATURE DISTRIBUTION AND HEAT-TRANSFER COEFFICIENTS FOR THE CASE OF ONE ADIABATIC WALL

The basis of the method proposed for the calculation of the heat-transfer coefficient for the more general wall-temperature conditions is the availability of results for the heat-transfer coefficient and for the temperature ratio X for the case of heat transfer to a fluid flowing between parallel plates, one plate being adiabatic. Harrison and Menke (1) have outlined the method of solution for this case and have presented Nusselt numbers for fluids of low Prandtl number. In these results the temperature ratio X is not given. The solution is here extended by giving expressions for the temperature distribution and by a general result for the Nusselt number for cases of fluids of large Prandtl number. Values of the temperature ratio X are presented for some Prandtl numbers.

The assumptions necessary for a solution have been indicated in the body of the paper. On such bases and upon the assumption of an eddy diffusivity, the temperature distribution across the channel can be obtained. In accord with the assumptions of Harrison and Menke, the diffusivity for heat has been presumed the same as for momentum transfer, and that diffusivity is obtained from the presumed linear shear distribution and the Prandtl-Nikuradse velocity distribution, except in the central region of the channel. In this region, from $y/D = 1/4$ to $y/D = 3/4$ the diffusivity has been assumed constant at its maximum value, which obtains at $y/D = 1/4$ in the basic calculation. The calculations of Harrison and Menke reveal this to be a plausible assumption.

The temperature distribution obtained from the integration of Equation [1] can be specified in terms of the following equations

$$\text{Region } 0 < \frac{y}{D} < \left.\frac{y}{D}\right|_{30}$$

$$\frac{T_O - T_{30}}{\dfrac{2.5\, q_O}{\rho c U_\tau}} = 2\frac{\nu}{a} + 2\log\left(5\frac{\nu}{a} + 1\right) \quad \text{.......[14]}$$

$$\text{Region } \left.\frac{y}{D}\right|_{30} < \frac{y}{D} < \frac{1}{4}$$

$$\frac{T_{30} - T_{y/D}}{2.5\dfrac{q_O}{\rho c U_\tau}} = \left[\frac{1}{4} - \frac{3}{8}\frac{1}{(m-n)}\right]\log\frac{\dfrac{y}{D} - m}{\left.\dfrac{y}{D}\right|_{30} - m}$$

$$+ \left[\frac{1}{4} + \frac{3}{8}\frac{1}{(n-m)}\right]\log\frac{\dfrac{y}{D} - n}{\left.\dfrac{y}{D}\right|_{30} - n} \quad \text{.........[15]}$$

where in this particular equation

$$m = \frac{-1 + \sqrt{1 + \dfrac{20}{D^{+}\nu/a}}}{-4} \qquad n = \frac{-1 - \sqrt{1 + \dfrac{20}{D^{+}\nu/a}}}{-4}$$

$$\text{Region } \frac{1}{4} < \frac{y}{D} < \frac{3}{4}$$

$$\frac{T_{1/4} - T}{2.5\dfrac{q_O}{\rho c U_\tau}} = \frac{1}{2.5}\frac{1}{\left(0.05 + \dfrac{1}{D^{+}\nu/a}\right)}\left[\frac{y}{D} - \frac{y^2}{2D^2} - \frac{7}{32}\right] \text{[16]}$$

$$\text{Region } \frac{3}{4} < \frac{y}{D} < \frac{y}{D} \text{ at } (D-y)\frac{U_\tau}{\nu} = 30$$

$$\frac{T_{3/4} - T}{2.5\dfrac{q_O}{\rho c U_\tau}} = \left[\frac{1}{4} - \frac{1}{8}\frac{1}{(m-n)}\right]\log\frac{y/D - m}{3/4 - m}$$

$$+ \left[\frac{1}{4} + \frac{1}{8}\frac{1}{(m-n)}\right]\log\frac{y/D - n}{3/4 - n} \quad \text{.......[17]}$$

where in this particular equation

$$m = \frac{-3 + \sqrt{1 + \dfrac{20}{D^{+}\nu/a}}}{-4} \qquad n = \frac{-3 - \sqrt{1 + \dfrac{20}{D^{+}\nu/a}}}{-4}$$

For fluids with Prandtl numbers greater than unity, the effect of molecular conduction in the turbulent region of the flow becomes small. In such cases those terms in the foregoing expressions which involve the Prandtl number can be eliminated and substantially simpler expressions obtained.

The specification of the temperature distribution, together with the assumed velocity distribution, enables the evaluation of the mixed mean temperature of the fluid. This is expressed conveniently in the form of the difference between wall and mean fluid temperatures as

$$\frac{T_O - T_m}{2.5\,\dfrac{q_O}{\rho c U_\tau}} = \frac{1}{U_m}\int_O^D U\,\frac{T_O - T}{2.5\,\dfrac{q_O}{\rho c U_\tau}}\,dy \ldots\ldots\ [18]$$

The integral in Equation [18] is evaluated graphically or numerically by means of the temperature distribution as given in the previous equations. It is apparent that the evaluation of Equation [18] immediately yields an expression for the heat-transfer coefficient

$$h = \frac{q_O}{T_O - T_m}$$

Combination of Equation [18] with the expression for the difference between the wall temperatures yields an expression for the ratio

$$X = \frac{T_O - T_m}{T_O - T_D}$$

Fig. 4 reveals the general variation of this ratio with the Reynolds and Prandtl numbers. Consideration of the problems on the basis of the neglect of all turbulent diffusion effects on the heat transfer reveals a lower limit of about 0.66 on the value of X and reference to the figure indicates that conditions at $\nu/a = 0.01$ begin to approach this extreme.

The heat-transfer coefficient, expressed as a Nusselt number, is shown in Fig. 5. There the minimum value of the Nusselt number as derived by Jakob (4) for laminar flow is shown as a dashed line. A similar consideration, assuming heat transfer by conduction only and a uniform velocity for the entire flow, yields a Nusselt number only slightly higher, so that the dashed line indicates an approximate limit for all Reynolds-number values. The entrance effect under such conditions would be expected to be considerable.

For Prandtl numbers greater than unity, the negligible effect of molecular conduction in the turbulent core enables a specification of the mixed mean temperature which is independent of the Prandtl number if it is assumed that the mixed mean temperature of the fluid in the turbulent region of the flow is equal to the mixed mean temperature of the entire flow. This is a reasonable approximation even at low Reynolds numbers. It is found that for these cases the quantity

$$\frac{T_{30} - T_m}{2.5\, q_O/\rho c u_\tau}$$

is a substantially linear function of the friction Reynolds number, $2U_\tau D/\nu$. This enables a convenient specification of the heat-transfer coefficient in the form

$$\frac{h}{U_m \rho c} = \frac{\sqrt{\dfrac{c_f}{2}}}{5\,\dfrac{\nu}{a} + 5\log\left(5\,\dfrac{\nu}{a} + 1\right) + 2.38\log\dfrac{U_\tau D}{29\nu}} \ldots [19]$$

It has been noted by R. Lyon (1) that the increased effect of the Prandtl number, when the Prandtl number becomes small, can be accounted for in an empirical expression of the Nusselt number of the type

$$\frac{2hD}{k} = A + B\left(\frac{2U_m D}{a}\right)^n$$

where A, B, and n are constants. Constant A serves to rationalize conditions at small Peclet numbers where the "limiting" value of the Nusselt number is approached. The Nusselt numbers presented in Fig. 5 can be expressed by the equation

$$\frac{2hD}{k} = 5.8 + 0.020\left(\frac{2U_m D}{a}\right)^{0.8}$$

in the range

$$10^2 < \frac{2U_m D}{a} < 10^5$$

$$0.01 < \nu/a < 1.0$$

with an accuracy of ±5 per cent.

Discussion

J. R. Menke.[4] The author has provided a worth-while extension to our understanding of heat transfer at low Prandtl number. He has noted the utility of superposition of the earlier solutions (1, 2),[5] and he has extended and refined the calculations. The former result, the summation of solutions, is not altogether surprising, possible, as he of course points out, because of the linearity of the fundamental differential equations. The latter results, the calculations, are more complete (extending over the full range of 10^4 to 10^6 for Reynolds number, and 0.01 to 1.0 for Prandtl number) and probably more accurate than those given in (1).[5] The results given in (1) and (2)[5] have been subjected to a first experimental test with rather reasonable agreement and are reported in a paper by Dr. R. N. Lyon[6] needing citation here.

We have, however, no new experimental information[7] on the behavior of the eddy diffusivity near the center line of flow. The author, therefore, has used the earlier (and imperfect) assumptions of (1)[5] with consequent limitations to accurate results. Powerful tools have been given to the experimenter to test these assumptions; measured traverses of temperature, t, and temperature derivative, $(\partial t)/(\partial y)$, will yield much information in fluids with low Prandtl numbers. One might, perhaps, suggest these measurements in a liquid metal flowing between plane parallel walls with almost all the heat flowing into one wall and out the other, i.e., heat flow "straight" across the channel. This approach is perhaps the most sensitive method for obtaining the differential description of the processes at work in the stream. A simplified method for measuring the integral result (the heat-transfer coefficient itself) is suggested in (1).[5] Techniques for handling the liquid metals are rather well developed today; further studies with gases are also worth while.

Moreover, the question of the ratios of the eddy transports of heat, mass, and momentum is subject to more powerful attack with the availability of radioactive isotopes to compare measured mass transports with the foregoing measured heat transports.

Richard N. Lyon.[8] Dr. Seban has presented a powerful concept in his method for superimposing the heat flow from two walls of a flat channel to enable calculation of the over-all heat-transfer effects. It will undoubtedly find wide application in the design of heat exchangers, as well as in future investigation of forced-convection heat transfer. The use of three relationships implied or stated by Dr. Seban in his paper, but not stressed by him, enable the usefulness of his concept to be shown clearly.

---

[4] Nuclear Development Associates, Inc., New York, N. Y. Jun. ASME.

[5] Author's Bibliography.

[6] "Heat Transfer at High Fluxes in Confined Spaces," by R. N. Lyon, Dissertation, Doctor of Philosophy, University of Michigan, Ann Arbor, Mich., 1949.

[7] Dr. B. H. Sage, California Institute of Technology, Pasadena, Calif., has indicated several forthcoming papers.

[8] Oak Ridge National Laboratory, Oak Ridge, Tenn.

These are

$$h' = h'' \qquad \ldots\ldots\ldots\ldots [20]$$

$$T_D' = T_O'' \qquad \ldots\ldots\ldots\ldots [21]$$

$$T_m = T_m' + T_m'' - T_O'' \ldots\ldots\ldots\ldots [10]$$

In most heat-transfer problems, the calculation of the actual heat-transfer coefficient at the two walls is not the ultimate objective. Usually one is interested in determining T_O, T_m, T_D, q_O, and q_D. Any three of these variables plus the values of the Reynolds number and of D for the system, together with the thermal conductivity of the fluid and its Prandtl number, will completely define the isothermal forced-convection system with smooth walls, as postulated by Dr. Seban. The value of h' or h'' can be calculated by the usual relationships for ordinary fluids, or by the last equation in the appendix of Dr. Seban's paper for the case of liquid metals. The value of X can be obtained from Fig. 4 with a knowledge of the Reynolds and Prandtl numbers. Any two of the five temperature and heat-flow variables listed herein can be calculated easily using a simple extension of Dr. Seban's paper as follows

$$T_m = T_m' + T_m'' - T_O'' \ldots\ldots\ldots\ldots [10]$$

or

$$T_m = \frac{q_O}{h'} - \frac{q_D}{h''} + T_O + T_D - T_O''$$

Since $h' = h''$ and $T_O'' = T_D'$, this may be written

$$h'(T_m - T_O) = \frac{q_D}{X} + q_O - q_D \ldots\ldots\ldots\ldots [22]$$

or alternately as

$$h'(T_D - T_m) = \frac{q_O}{X} - q_O + q_D \ldots\ldots\ldots\ldots [23]$$

Adding Equation [22] to Equation [23] gives

$$h'X(T_D - T_O) = q_O + q_D \ldots\ldots\ldots\ldots [24]$$

Solving for q_o in Equation [22] and in Equation [24], and equating the solutions

$$h'(T_m - T_O) - q_D\left(\frac{1}{X} - 1\right) = h'X(T_D - T_O) - q_D \,. \, [25]$$

Solving for q_D in Equation [23] and in Equation [24] and equating the solutions

$$h'(T_D - T_m) - q_O\left(\frac{1}{X} - 1\right) = h'X(T_D - T_O) - q_O \,. \, [26]$$

Calculation of any of the five variables in terms of any three of the remaining variables plus h' and X may be accomplished by means of the appropriate equation from the following rearrangement of Equations [23], [24], [22], [25], and [26]

$$h'T_m - h'T_D + \left(\frac{1}{X} - 1\right) q_O + q_D = 0 \ldots\ldots\ldots [27]$$

$$h'XT_O - h'XT_D + q_O + q_D = 0 \ldots\ldots\ldots [28]$$

$$h'T_O - h'T_m + q_O + \left(\frac{1}{X}\right) q_D = 0 \ldots\ldots\ldots [29]$$

$$(1 - X)h'T_O - h'T_m + h'XT_D - \left(2 - \frac{1}{X}\right) q_D = 0 \ldots\ldots\ldots [30]$$

$$h'XT_O - h'T_m + (1 - X)h'T_D + \left(2 - \frac{1}{X}\right) q_O = 0 \ldots\ldots\ldots [31]$$

The symbol q_O represents the heat flux entering one wall from the fluid, while q_D represents the heat entering the fluid from the opposite wall. Negative values of q_O and q_D merely indicate heat flow in the opposite directions.

Values of h_O and h_D can be obtained if desired from the definitive equations

$$h_O = \frac{q_O}{T_m - T_O}; \qquad h_D = \frac{q_D}{T_D - T_m}$$

The writer hopes the foregoing comments will stimulate more rapid utilization of Dr. Seban's important contribution to the field of forced-convection heat transfer.

AUTHOR'S CLOSURE

Mr. Menke has appropriately emphasized the uncertainty concerning the magnitude of the eddy diffusivities for heat and momentum near the center line of the flow. In the present analysis, as in that of Harrison and Menke, a uniform diffusivity corresponding to the maximum value indicated by use of the Prandtl-Nikuradse expression for the velocity distribution in the turbulent region of the flow has been employed for the entire central half of the flow. Actual diffusivities are expected to be somewhat lower, and thus the heat-transfer rates predicted by the present analysis are somewhat too high. This discrepancy depends both upon the amount of heat flowing across the center line and upon the Prandtl number of the fluid. At the low Prandtl numbers typical of molten metals, particularly at low Reynolds numbers, the relative effect of molecular conduction is so great that the contribution of turbulent diffusion to the heat transfer is quite small.

There is a further question regarding the relation between the diffusion coefficients for heat and momentum transfer, which might be determined from measurements of the velocity and temperature and gradients thereof. Fig. 3 of the paper indicates experimental measurements on a system designed to realize such an objective and similar experimentation with fluids of low Prandtl number would be useful in indicating if there is any dependence of the eddy diffusivity for heat upon the Prandtl number.

Dr. Lyon's examination has produced a valuable generalization of the problem, expressed finally in the last five equations of his discussion. The flexibility of that expression of the results has there been noted, and one important point can be emphasized therefrom because these equations enable the specification of the wall temperatures in terms of the heat rates q_O and q_D. It can be shown that if the heat rates q_O and q_D are constant with respect to x, then the assumption "c" which follows Equation [2] is most precisely fulfilled. For such a case Equations [27] to [31] enable the relation of T_O and T_D to the mean fluid temperature T_m, the variation of which is linear with x because of the constant heat input to the fluid. Thus the linear variation of the wall temperatures corresponding to the constant-heat-rate case can be determined.

Heat-Transfer Rates in Centrifugal Compressors and the Effect of Internal Liquid Cooling on Performance

By W. E. TRUMPLER,[1] R. W. FREDERICK,[2] and P. R. TRUMPLER[3]

This paper makes a preliminary exploration of the cooling rates which may be obtained in the internal passages of a centrifugal compressor. A mechanism for such calculations is proposed, data are given and correlated, and the results are used for prediction of performance of a compressor pumping 7500 cfm air to 100 psi, assuming various cooling arrangements.

NOMENCLATURE

The following nomenclature is used in the paper:

A = area, sq ft; A_0 refers to diffuser wall, A_1 to diffuser side of plate, A_2 to return channel side of plate, A_3 to diaphragm wall in return channel
c_p = specific heat of gas at constant pressure Btu/(lb_m) (deg F)
D = hydraulic diameter, ft, equal to $\frac{4 \times \text{flow area}}{\text{wetted perimeter}}$
g = acceleration of gravity, ft/sec²
G = mass velocity, lb_m/(hr) (sq ft)
h = heat-transfer film coefficient, Btu/(hr) (sq ft) (deg F)
k = thermal conductivity of gas, Btu/(hr)(sq ft) (deg F/ft)
K = thermal conductivity of diaphragm metal, Btu/(hr) (sq ft) (deg F/ft)
n = exponent in polytropic change of state
N = rotative speed, rpm
p = absolute pressure, lb_f per sq ft; subscripts 1 and 2 refer to beginning and end of a succession of states.
q = heat flow rate, Btu per hr; subscripts 0 to 3 have same meaning as for areas A
Q = volume rate of fluid flow, cfm
R = gas constant in $pv = RT$
T = absolute temperature, deg F abs
u = peripheral velocity of impeller, fps
U = over-all conductance, Btu/(hr) (sq ft) (deg F)
$(UA)_\infty$ = value of UA, assuming water film coefficient infinite
v = specific volume, cu ft per lb_m
V = fluid velocity, fps
w = flow rate of gas, lb_m per hr
Z = absolute viscosity lb_m/(hr) (ft)

β is defined as $\dfrac{1}{\dfrac{n-1}{n}}\left[\left(\dfrac{p_2}{p_1}\right)^{\frac{n-1}{n}} - 1\right]$

γ = ratio of specific heats, c_p/c_v
η = efficiency; subscript H refers to hydraulic efficiency
μ = pressure coefficient
ρ = density, lb_m per cu ft

Subscripts:

d refers to diffuser
r refers to return channel
w refers to water

INTRODUCTION

For many applications the advantages resulting from cooling a gas during compression have been clearly established. Usually this cooling is obtained by withdrawing the gas from the machine at one or more intermediate points in the compression and passing it through heat exchangers. The construction of a centrifugal compressor is such that, without much added expense, the gas may be cooled as it flows through the fixed passages. Because of the high velocities in these passages the heat-transfer film coefficients are high. The questions may well be asked, what is the magnitude of these coefficients? how can one calculate the cooling effect which may be obtained in present commercial designs? and what is the effect of such cooling on over-all performance and other economic factors affecting users of centrifugal compressors?

It is the purpose of this paper to provide limited answers to these three questions. The answers are limited first in scope, concerning themselves only with one commercial centrifugal design, that manufactured by the authors' company, and applying the results to a study of only one process condition, namely, compression of 7500 cfm air at 68 F and 14.7 psia to 114.7 psia.

A second limitation is inherent in our method. As with most industrial research, the need for results was urgent and the man power limited. Therefore it was not possible to examine critically many of the assumptions upon which the theory is based.

FILM COEFFICIENTS IN COMPRESSOR PASSAGES

In Fig. 1 is shown an assembly of a commercial four-stage centrifugal compressor of the type used in the investigation. Outer diameter of all impellers is 18 in., and operating speeds vary from 7300 to 9800 rpm, depending on the application.

A detailed view of an intermediate stage is shown in Fig. 2. The gas first enters guide vanes, which direct the flow at the desired angle into the impeller. At the impeller periphery the gas leaves the wheel at a velocity near the acoustic. Conversion of velocity to pressure is accomplished in the diffuser, which, except for inlet and outlet, consists of two smooth parallel surfaces. At the return bend, the gas velocity is of the order of 300 fps. The gas approaches the next stage through the return channel which has integrally cast ribs, or return vanes, to direct the flow into the next stage. The casting, which encloses the return channel and the cooling-water passage, is known as the "diaphragm." Both diaphragms and inlet guide vanes are split on a horizontal diameter.

---

[1] Chief Engineer, Centrifugal Engineering Department, Clark Brothers Company, Inc., Olean, N. Y. Mem. ASME.

[2] Turtle Creek, Pa. Jun. ASME.

[3] Professor of Mechanical Engineering, Illinois Institute of Technology, Chicago, Ill.; Consultant, Clark Brothers Company, Inc. Mem. ASME.

Contributed by the Heat Transfer Division and presented at the Annual Meeting, New York, N. Y., November 27–December 2, 1949, of THE SOCIETY OF MECHANICAL ENGINEERS.

NOTE: Statements and opinions advanced in papers are to be understood as individual expressions of their authors and not those of the Society. Paper No. 49—A-93.

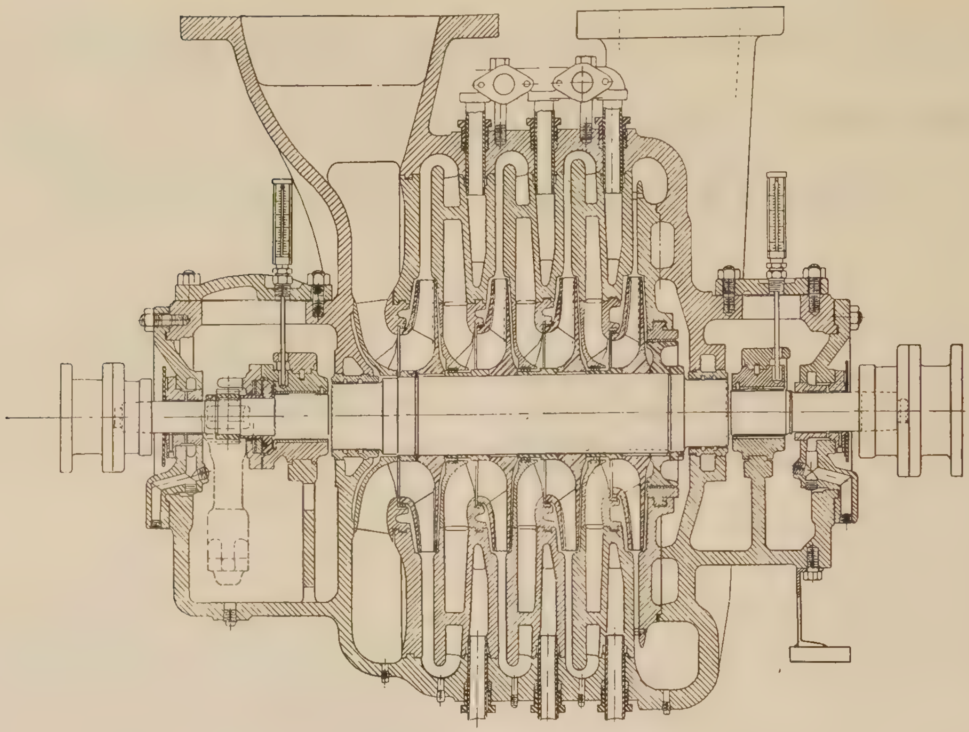

Fig. 1 Section Through Typical Four-Stage Centrifugal Compressors

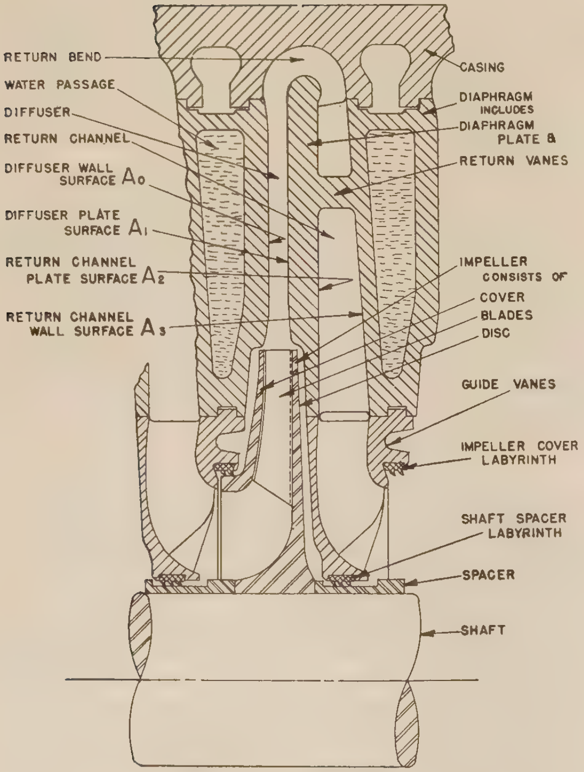

Fig. 2 Representative Intermediate-Stage Construction

Guide-vane sections may be either cast or fabricated by welding, with the latter method preferred. Three types of guide vanes are used in the standard design and provide for a gas flow approaching the impeller with an angular velocity in the direction of rotation (With), against rotation (Ag), or straight radial (Rad), with zero rotation. By changing the guide-vane selection the capacity of a given stage may be changed as much as ± 15 per cent without loss of efficiency, and without change in any other physical element or change in speed. By capacity is meant the actual volume per unit time flowing through the stage inlet.

Fig. 3 shows the design of an AB-diaphragm inserted between stages A and B. Two other designs are used for smaller-capacity stages, namely, B-diaphragm for insertion between B-stages and between B and C-stages, and C-diaphragms for all lower-capacity stages. Diffuser widths, which are specified to maintain the same velocity in each stage, may be controlled by different finishing dimensions on otherwise identical castings.

Each half-diaphragm has its own external water connections, thus eliminating internal connections at the split. The coring of the water passages is designed to obtain maximum water film coefficients with passages of reasonable size, and to minimize entrainment of air. Plugs around the diaphragm periphery permit some degree of mechanical cleaning of water passages, although chemical cleaning is recommended. The water-flow directions are indicated in Fig. 3. Normal flow rate for this size (No. 2) case is 100 gpm, divided equally between top and bottom halves, and 50 gpm flows through the half-diaphragms in series from one end of the machine to the other.

The diaphragms are cast iron or a high-conductivity bronze.

It will be clear that analysis of the heat transfer from the compressed gas through the irregular diaphragm wall to the water is a complex matter. Assuming that the water film resistance is small compared with the total thermal resistance, the heat-transfer problem may be divided into three parts, namely, gas film coefficient in diffuser, gas film coefficient in return channel, and resistance of metal wall. The effect of heat flow between casing and gas at the return bend, along the shaft, through the guide vanes and at the impeller walls was assumed sufficiently small that it could be taken into account adequately by the ex-

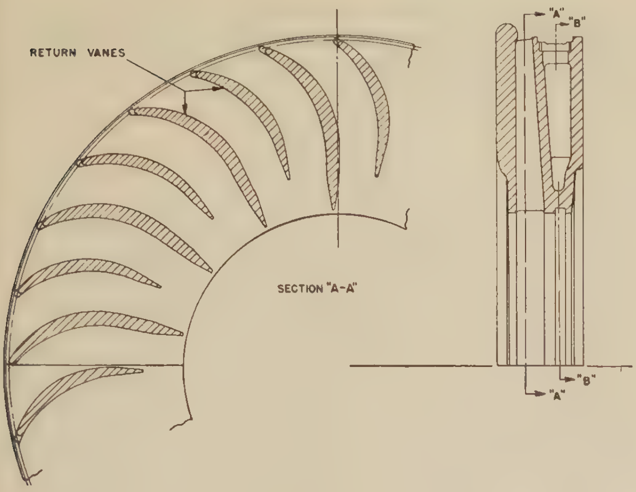

FIG. 3(*a*) SECTION THROUGH RETURN-CHANNEL VANES

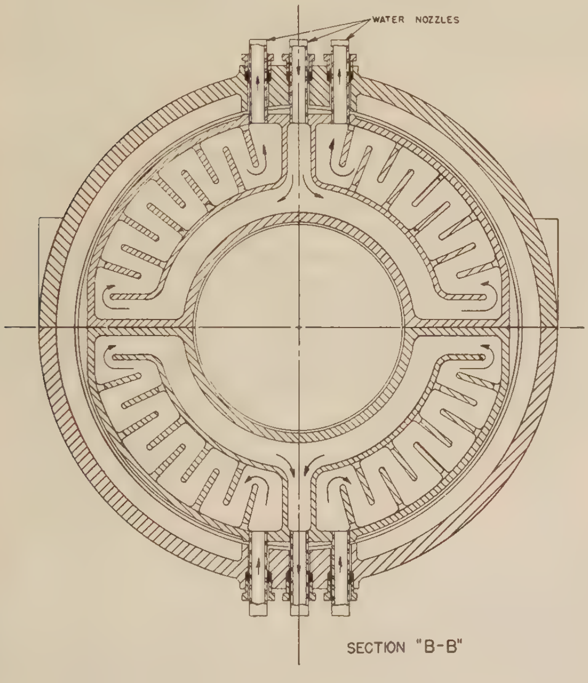

FIG. 3(*b*) SECTION THROUGH DIAPHRAGM COOLING-WATER PASSAGES

perimentally determined constant in the diffuser film-coefficient equation.

Three important assumptions are made in calculating the gas film coefficient in the diffuser, as follows:

1 Although there is a large variation in gas velocity, an average value of the coefficient is applied to the entire surface.

2 The value of h_d varies in accordance with an equation of the same form as that generally used for turbulent-flow film coefficients inside pipes or ducts[4]

$$\frac{h_d D}{k} = \text{const} \left(\frac{VD\rho}{Z}\right)^{0.8} \left(\frac{c_p Z}{k}\right)^{0.4} \quad \ldots\ldots\ldots\ldots [1]$$

with D taken as the diffuser width, and V directly proportional to the gas velocity entering the diffuser. Diffuser dimensions other than D are identical for a given size of machine.

3 The velocity V is independent of the capacity and directly proportional to the peripheral velocity of the impeller. Since impeller diameter is uniform for each compressor size, this implies that V is proportional to rpm. The justification for this simplification is indicated in Fig. 4 which shows velocity diagrams at various loads at a given peripheral velocity, for the particular type of impeller used in the centrifugal being investigated.

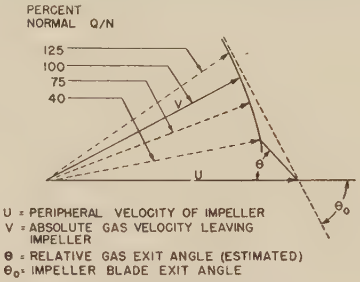
PERCENT
NORMAL Q/N
125
100
75
40
V
U
θ
θ₀
U = PERIPHERAL VELOCITY OF IMPELLER
V = ABSOLUTE GAS VELOCITY LEAVING IMPELLER
θ = RELATIVE GAS EXIT ANGLE (ESTIMATED)
θ₀ = IMPELLER BLADE EXIT ANGLE

FIG. 4 VELOCITIES AT IMPELLER EXIT

As a consequence of these assumptions, and neglecting variation of the Prandtl modulus with gases, the equation for diffuser film coefficient becomes

$$h_d = 2.0\, c_p (N\rho)^{0.8} \left(\frac{Z}{D}\right)^{0.2} \quad \ldots\ldots\ldots\ldots\ldots [2]$$

where the constant was determined by trial and error to fit a wide range of performance data on two size No. 2 (18-in-diameter impeller) machines.

Gas properties were evaluated at total (stagnation) temperature and total pressure at the return bend. The stagnation temperature was used as the effective gas temperature for determining heat-flow potential between gas and surface.

The effective wall area A_0 in the diffuser was taken from the outer impeller diameter to the outer edge of the diaphragm, and the diffuser-plate area A_1 was taken from the outer impeller diameter to the maximum plate diameter.

It was assumed that the coefficient in the return channel could also be calculated by Equation [1] which, with a constant of 0.023 as recommended by McAdams and a Prandtl modulus of 0.78, becomes

$$h_r = 0.027\, c_p\, G^{0.8} \left(\frac{Z}{D_r}\right)^{0.2} \quad \ldots\ldots\ldots\ldots\ldots [3]$$

In determining the gas-flow area through the return channels, the arithmetic average of the areas at the outer and inner edges of the diaphragm was used. The gas flow per unit time was taken as its value at the compressor discharge, thus neglecting leakage effects. The hydraulic diameter D_r was found for entrance and exit of the return channels, and the arithmetic average of their two-tenths power taken to evaluate $(D_r)^{0.2}$. Thermal properties were evaluated from stagnation temperature and total pressure at the adjacent return bend.

In the return channels, the plate area A_2 was equal to the diffuser side plate area A_1 minus the cross-sectional area of the vanes plus one half the surface area of the vanes. The area of the diaphragm wall A_3 was taken to be the area from the outer edge of the diaphragm to the point of contact with the inserted vanes minus the cross-sectional area of the integral return vanes plus one half the surface area of the integral vanes. The reason for the separation of the return-channel surface into plate area and diaphragm wall area will become clear with discussion of the wall resistance calculation.

---

[4] "Heat Transmission," by W. H. McAdams, second edition, McGraw-Hill Book Company, Inc., New York, N. Y., 1942.

Heat flow through the walls is calculated on the basis of the following assumptions:

1 The gas contacts four isothermal surfaces: namely, diffuser wall, diffuser plate, return-channel plate, and diaphragm wall, the effective surface areas of which have been previously defined.

2 The temperature difference between the two plate surfaces is the temperature drop calculated to conduct the heat flowing into the diffuser plate surface through the thickness of the plate.

3 Heat flow into the water takes place by three independent parallel paths: namely, (1) from the two plate surfaces through the return vanes, which have an effective length equal to the average width of the return channel, plus the thickness of the wall between the return channel and water passage, an effective heat-flow area equal to the total cross-sectional area of the vanes, and a temperature drop from the return-channel plate surface to the water surface, (2) from the diaphragm wall surface to surface on the water side of the wall from which return-vane cross-sectional area has been subtracted, and (3) from diffuser wall surface to water surface on the other side of the wall.

The water surfaces used for the three parallel heat-flow paths were the total return-vane cross-sectional area, the diaphragm wall surface A_3, and the diffuser wall surface A_0. A water conductance of 2000 based on these surfaces was assumed unless otherwise noted.

It should be understood clearly that the method here used for calculating heat flow through the complex diaphragm walls may limit seriously the generality of the conclusions. Solution by successive numerical approximation was attempted, but convergence was too slow.

Based on the heat-transfer mechanism just described, and with a knowledge of fundamental stage characteristics used to calculate the performance of uncooled machines, the performance of a cooled compressor may be established. The stage characteristics are the pressure coefficient μ and the hydraulic efficiency η_H, both as functions of the independent variable Q/N at the entrance to the stage. The definition of μ for one stage is

$$\mu = \frac{\int_{p_1}^{p_2} v\,dp}{\dfrac{u^2}{g}} \qquad \text{[4]}$$

which for air as a perfect gas following the compression process pv^n constant, may be written

$$\mu = \frac{1725\,T_1\,\beta}{u^2} \qquad \text{[5]}$$

where

$$\beta = \frac{1}{\dfrac{n-1}{n}}\left[\left(\frac{p_2}{p_1}\right)^{\frac{n-1}{n}} - 1\right] \qquad \text{[6]}$$

The definition of hydraulic efficiency is

$$\eta_H = \frac{\int_{p_1}^{p_2} v\,dp}{Wk_f} \qquad \text{[7]}$$

where Wk_f represents the total mechanical work into the fluid being compressed. For a perfect gas following the process pv^n constant, with no heat transferred to the fluid, it may be verified that

$$\eta_H = \frac{\dfrac{\gamma-1}{\gamma}}{\dfrac{n-1}{n}} \qquad \text{[8]}$$

For air, a commonly used value for $(\gamma - 1)/\gamma$ is 0.283, which will be used in all calculations given in the paper. Temperatures and pressures at stage entrance and exit are related by the equation

$$\frac{T_2}{T_1} = \left(\frac{p_2}{p_1}\right)^{\frac{n-1}{n}} \qquad \text{[9]}$$

Knowing the temperature T_1, pressure p_1, and volumetric gas flow Q at stage entrance, plus the impeller rpm, the values of μ and η_H are first determined at the given Q/N from characteristic curves determined from previous experiments on uncooled machines. Pressure p_2 at entrance to the next stage, and T_2, the total temperature at impeller exit (same as temperature entering next stage in an uncooled machine) are then calculated. The gas temperature entering the next stage is determined on the basis of film coefficients and metal conductances as previously outlined. The calculation is a trial-and-error procedure. The temperature of the diffuser-plate surface must be such that the heat transferred to both sides of the plate is equal to the heat flowing through the return vanes.

The constant in Equation [2] was set to obtain agreement between calculated and observed performance of two different commercial machines.

Tests of Water-Cooled Compressors

Important physical data on the two machines tested are given in Tables 1 and 2. Both were four-stage size No. 2 compressors, similar in design to the machine in Fig. 1. Both had 18-in-diam impellers and were designed for operation at 9600 rpm. The first machine was designed for full-load volumetric suction flow of 7500 cfm air at 68 F and 14.7 psia, the second for 2700 cfm air at 85 F and 42 psia. Each machine was operated over the entire volumetric capacity range both with and without cooling water. Since the available power for these tests was limited, suction pressures at or below atmospheric were used. Speeds ranged from 9060 to 10,070 rpm.

TABLE 1 DIAPHRAGM DIMENSIONS

	Diaphragm type		
	AB	B	C
A_0, sq ft	3.53	3.53	3.53
A_1, sq ft	3.98	3.98	3.98
A_2, sq ft	4.69	4.83	4.96
A_3, sq ft	4.89	5.03	5.16
Return-channel $(D_r)^{0.2}$	0.637	0.633	0.625
Return-channel flow area, sq ft	0.346	0.319	0.291
Return-channel wall thickness, ft	0.0365	0.0365	0.0365
Return-vane cross-sectional area, sq ft	0.844	0.945	1.06
Return-vane axial length, ft	0.083	0.083	0.083
Plate thickness, ft	0.0704	0.0650	0.0650 0.0704
Diffuser-wall thickness, ft	0.0442	0.0495	0.0650

TABLE 2 DIFFUSER WIDTHS

Impeller	Guide vane	Diffuser width, D, ft
A	Ag	0.0573
B	Ag	0.0469
B	Rad	0.0443
D	Ag	0.0312
D	Rad	0.0312
E	Ag	0.0312
E	Rad	0.0312

Standard ASME long-radius low-ratio nozzles of 5 and 6 in. throat diam, installed in accordance with the ASME Code, measured air flow out of the compressors. Speed was measured with a stop watch and a revolution counter geared to the shaft. All pressures were measured with impact tubes adjusted at each run to point directly into the air stream. Gas temperatures were measured with bare mercury-in-glass thermometers, except within compressor passages, where calibrated bare copper-constantan thermocouples were used. Since gas velocities were not over approximately 300 fps, all recovery factors were taken as unity, that is, temperatures were considered as stagnation values. Each gas temperature was the average reading of at least two probes, and all pressures, except those inside the compressor case, were the average of at least two independent impact-tube readings.

Pressure and temperature readings were taken at the following locations: Upstream from the inlet flange, downstream from the discharge flange, and at the three return bends. One pressure point and two temperature points were located around the machine at each return bend.

It should be noted that instrumentation at the return bends was not adequate for the desired accuracy. Pressures, and particularly temperatures, varied around the circumference. Two temperature readings at a return bend usually were within 2 deg F, but differences up to 13 deg F were noted. Since each thermocouple was made of specially selected wire and checked with the assembled probe in a special hot-air calibration apparatus to read within 0.5 deg F of the standard Leeds and Northrup calibration curve, it was concluded that the readings reflected nonuniform conditions within the compressor. Differences would vary with change in load. It was not considered desirable to insert more probes into the machine in order to obtain a better average.

For many runs the suction flow to the compressor was throttled by means of two flat contiguous perforated plates which could be moved with respect to each other. Thus the flow was throttled without setting up irregular velocity distribution at the compressor inlet. To insure an even better velocity distribution, three 12-in-diam plates with $^{1}/_{8}$-in-diam holes on $^{5}/_{16}$-in. pitch were inserted about six inches apart in the duct section between throttle plate and inlet flange. A gate valve in the compressor discharge line was used for control purposes.

In the cooling runs, water flow through the diaphragms (separate for the upper and lower casing halves) was measured with weighing tanks and platform scales. Temperature rise of the cooling water did not exceed 10 deg, and therefore thermometers with 0.1-deg divisions were used.

In all runs except a few in the surge region, data were taken at approximately 15-min intervals until two successive readings showed no appreciable difference. The average of these two readings was taken for calculation. Data on the various runs are presented in Tables 3 and 4.

In Figs. 5 and 6 are given the stage characteristic curves calculated from data on the test compressors operated without cooling. Since it was not convenient to obtain data at entrance to the guide vanes, the return-bend measurements were used instead. The first stage, therefore, extends from inlet flange to first return bend, the second stage from first to second return bend, the third stage from second to third return bend, and the fourth stage from third return bend to discharge flange. It will be seen that corrections were made for heat gain or loss in first and fourth stages

TABLE 3(*a*) TEST DATA, HIGH-CAPACITY COMPRESSOR, UNCOOLED

Calculations	Run 123-1	Run 123-2	Run 123-3	Run 123-4	Run 123-5	Run 123-6	Run 123-7	Run 123-8	Run 123-9	Run 123-10	Run 123-11
Nozzle diameter, in.	6.00	6.00	6.00	6.00	6.00	6.00	6.00	6.00	6.00	6.00	6.00
Nozzle coefficient	0.995	0.995	0.995	0.995	0.995	0.995	0.995	0.995	0.995	0.995	0.995
Nozzle-inlet temp, deg F	325.0	323.5	313.1	325.9	335.9	337.0	339.5	334.5	330.5	331.8	332.5
ΔP nozzle, in. water	31.58	32.02	35.26	30.84	28.25	24.34	16.94	14.19	10.50	8.20	3.74
Barometer, in. Hg	28.51	28.50	28.50	28.50	28.52	28.52	28.52	28.52	28.52	28.52	28.52
Air temp, suction, deg F	77.0	79.2	71.7	72.2	72.8	74.6	75.1	74.3	76.0	78.3	78.0
Air temp, 2nd stage (in), deg F	147.2	148.4	138.5	146.3	154.2	155.1	158.0	160.6	162.4	165.2	188.4
Air temp, 3rd stage (in), deg F	221.1	218.5	206.1	218.7	227.6	230.2	237.6	235.5	234.6	240.3	270.3
Air temp, 4th stage (in), deg F	289.9	289.5	278.0	289.5	303.6	305.4	314.8	312.5	311.6	317.3	342.8
Air temp, discharge, deg F	351.6	350.5	335.7	353.8	367.4	370.3	380.0	375.7	377.0	384.0	409.3
Pressure, suction, in. Hg	—11.15	—13.07	—14.66	—9.07	—6.02	—2.94	—4.88	—4.96	—4.67	—4.84	—4.75
Pressure, 2nd stage (in), in. Hg	—6.10	—7.29	—10.97	—3.50	2.90	7.42	4.72	4.31	3.87	3.42	2.75
Pressure, 3rd stage (in), in. Hg	1.57	—.92	—6.40	6.37	12.92	19.06	15.41	14.46	13.51	12.80	11.12
Pressure, 4th stage (in), in. Hg	10.20	6.49	1.16	16.38	24.99	32.53	27.75	26.29	24.30	23.30	20.54
Pressure, discharge, in. Hg	19.67	14.72	6.87	27.50	38.39	47.46	41.11	39.19	36.45	34.95	30.79
Time 14,400 blower rev, min	1.527	1.525	1.515	1.532	1.533	1.545	1.522	1.520	1.528	1.520	1.520
Rpm, *N*	9440	9450	9500	9400	9390	9320	9450	9470	9430	9470	9470
Inlet-air flow, cfm, *Q*	6190	6875	8180	5400	4450	3635	3280	3020	2575	2305	1555
Q/*N* inlet	0.656	0.728	0.861	0.575	0.475	0.390	0.347	0.319	0.273	0.243	0.164

TABLE 3(*b*) TEST DATA, HIGH-CAPACITY COMPRESSOR, COOLED

Calculations	Run 122-1	Run 122-2	Run 122-3	Run 122-4	Run 122-5	Run 122-6	Run 122-7	Run 122-8	Run 122-9	Run 122-10	Run 122-11	Run 122-12
Nozzle diameter, in.	6.00	6.00	6.00	6.00	6.00	6.00	6.00	6.00	6.00	6.00	6.00	6.00
Nozzle coefficient	0.995	0.995	0.995	0.995	0.995	0.995	0.995	0.995	0.995	0.995	0.995	0.995
Nozzle-inlet temp, deg F	260.0	257.6	255.6	263.8	260.0	258.5	257.0	257.8	245.0	244.0	244.0	227.0
ΔP nozzle, in. water	27.51	31.38	26.98	26.44	21.16	33.29	32.10	32.21	15.32	12.06	9.51	5
Barometer, in. Hg	28.45	28.46	28.48	28.49	28.52	28.55	28.55	28.55	28.58	28.58	28.59	28.59
Air temp, suction, deg F	76.4	76.1	76.5	76.7	72.9	72.5	69.8	69.6	67.5	71.3	73.3	73.5
Air temp, 2nd stage (in), deg F	140.4	140.3	145.5	146.6	149.9	131.6	134.2	133.8	143.3	148.4	151.1	152.3
Air temp, 3rd stage (in), deg F	192.2	192.0	194.2	198.6	202.3	182.8	187.0	187.7	195.3	194.1	196.8	195.5
Air temp, 4th stage (in), deg F	232.9	230.7	234.0	240.3	241.0	227.0	227.6	228.1	227.1	228.6	231.7	223.2
Air temp, discharge, deg F.	279.2	274.2	274.3	285.2	282.7	274.8	273.4	274.3	268.6	268.6	270.8	258.5
Pressure, suction, in. Hg	—11.69	—8.70	—4.24	—8.10	—4.21	—14.22	—12.18	—12.15	—5.30	—5.18	—4.98	—5.32
Pressure, 2nd stage (in), in. Hg	—6.72	—3.63	4.54	—0.78	5.57	—9.62	—6.43	—6.21	3.98	3.47	3.66	2.29
Pressure, 3rd stage (in), in. Hg	0.22	5.32	14.86	8.32	16.94	—3.67	0.52	0.64	14.63	13.64	13.86	11.20
Pressure, 4th stage (in), in. Hg	8.73	15.03	27.60	19.43	30.97	3.12	8.84	9.13	27.50	25.91	26.28	22.01
Pressure, discharge, in. Hg	18.76	26.35	42.28	32.67	47.43	10.96	18.80	19.25	43.26	40.90	41.29	35.10
Time 14,400 blower rev, min	1.538	1.568	1.590	1.535	1.536	1.531	1.552	1.549	1.539	1.517	1.500	1.532
Water flow, top, min/200 lb	0.629	0.642	0.675	0.571	0.573	0.572	0.568	0.577	0.467	0.475	0.489	0.440
Water flow, bot, min/200 lb	0.679	0.653	0.728	0.608	0.617	0.612	0.653	0.632	0.506	0.510	0.530	0.474
Water temp (in), deg F	71.4	71.6	71.6	71.8	71.6	71.2	70.95	70.75	68.5	68.45	68.3	68.2
Water temp (out) top, deg F	78.6	78.8	80.3	78.95	79.4	77.1	77.1	77.2	74.4	74.2	74.4	72.95
Water temp (out) bot, deg F	79.1	79.4	81.0	79.5	80.0	77.65	77.65	77.7	74.9	74.6	74.8	73.5
Rpm, *N*	9370	9190	9060	9380	9380	9400	9270	9300	9360	9500	9600	9400
Inlet-air flow, cfm, *Q*	6250	5660	4260	5020	3730	7960	6835	6815	3330	2970	2620	1982
Q/*N* inlet	0.667	0.616	0.4705	0.535	0.398	0.847	0.736	0.733	0.356	0.3125	0.273	0.211

TABLE 4(*a*) TEST DATA, LOW-CAPACITY COMPRESSOR, UNCOOLED

Calculations	Run 120-1	Run 120-2	Run 120-3	Run 120-4	Run 120-5	Run 120-6	Run 121-1	Run 121-2	Run 121-3	Run 121-4	Run 121-5	Run 121-6
Nozzle diameter, in....	5.00	5.00	5.00	5.00	5.00	5.00	5.00	5.00	5.00	5.00	5.00	5.00
Nozzle coefficient.....	0.990	0.990	0.990	0.990	0.990	0.990	0.990	0.990	0.990	0.990	0.990	0.990
Nozzle-inlet temp., deg F..................	261.7	310.1	339.4	292.4	348.3	273.5	335.9	337.2	336.2	333.5	332.8	348.6
ΔP nozzle, in. water...	35.69	21.43	12.58	27.17	3.69	31.68	4.00	5.96	8.22	10.70	1.77	2.04
Barometer, in. Hg.....	28.63	28.62	28.60	28.60	28.61	28.62	28.59	28.59	28.59	28.59	28.59	28.59
Air temp suction, deg F	76.9	80.0	80.2	80.2	78.5	74.2	76.8	78.5	76.2	75.0	76.6	86.8
Air temp, 2nd stage (in), deg F..............	131.2	145.8	158.7	140.5	171.9	133.8	164.0	159.2	154.7	151.1	177.2	189
Air temp, 3rd stage (in), deg F..............	176.7	204.4	229.1	192.3	252.7	183.2	240.9	231.5	228	223.8	259.8	276.4
Air temp, 4th stage (in), deg F..............	225.8	270.5	303.7	252.8	334.8	238.3	318.3	308.8	304.8	298.1	338.9	359.4
Air temp, discharge, deg F..............	269.8	326.5	362.6	304.1	394.2	283.0	376.7	368.3	363.2	357.0	394.6	407
Pressure, suction, in. Hg................	—4.94	—4.94	—4.72	—5.11	—4.79	—5.01	—6.86	—6.98	—7.18	—6.93	—6.20	—0.89
Pressure, 2nd stage (in), in. Hg.............	0.92	3.27	4.90	2.08	3.83	1.59	1.06	0.99	1.20	1.62	1.58	8.45
Pressure, 3rd stage (in), in. Hg.............	7.44	13.13	16.27	10.50	13.93	9.14	10.24	10.32	11.10	11.88	10.85	19.62
Pressure, 4th stage (in), in. Hg.............	14.82	25.12	30.25	20.49	25.81	18.01	21.37	21.42	23.16	24.31	21.60	31.82
Pressure, discharge, in. Hg................	22.21	38.42	45.39	31.73	38.78	27.81	33.67	33.97	36.50	38.13	33.20	45.45
Time 17,500 blower rev, min...........	1.847	1.832	1.799	1.841	1.751	1.855	1.764	1.782	1.784	1.811	1.747	1.749
Rpm, *N*..............	9480	9550	9740	9500	10000	9440	9910	9820	9800	9660	10020	10000
Inlet-air flow, cfm, *Q*..	3480	2622	1955	3010	1054	3245	1207	1488	1760	1980	784	685
Q/*N*, inlet...........	0.367	0.275	0.203	0.317	0.105	0.344	0.1218	0.1515	0.1795	0.205	0.0784	0.0685

TABLE 4(*b*) TEST DATA, LOW-CAPACITY COMPRESSOR, COOLED

Calculations	Run 118-1	Run 118-2	Run 118-3	Run 118-4	Run 118-5	Run 118-6	Run 119-1	Run 119-2	Run 119-3	Run 119-4	Run 119-5
Nozzle diameter, in..............	5.00	5.00	5.00	5.00	5.00	5.00	5.00	5.00	5.00	5.00	5.00
Nozzle coefficient................	0.990	0.990	0.990	0.990	0.990	0.990	0.990	0.990	0.990	0.990	0.990
Nozzle-inlet temp, deg F.........	209.5	219.5	220.0	216.5	203	210.1	201.9	208.4	216.5	195.4	194.6
ΔP nozzle, in. water..............	31.44	18.45	11.32	25.11	4.32	28.62	3.73	6.30	8.59	1.51	1.82
Barometer, in. Hg................	28.63	28.62	28.63	28.63	28.63	28.63	28.63	28.63	28.63	28.64	28.64
Air temp suction, deg F...........	71.4	69.8	68.8	68.1	70.4	67.7	72.3	75.4	74.7	76.8	76.6
Air temp, 2nd stage (in), deg F....	121.2	128.5	133.7	123.6	137.0	119.8	139.6	139.8	141.3	145.4	148.1
Air temp, 3rd stage (in), deg F....	151.9	165.2	171.7	157.6	169.0	151.5	169.7	169.3	174.8	170.6	174.3
Air temp, 4th stage (in), deg F.....	182.4	196.8	202.2	190.3	190.0	183.3	190.2	193.9	202.6	184.6	187.6
Air temp, discharge, deg F........	215.0	229.5	230.5	224.4	218.6	216.7	217.4	222.1	229.2	211.7	214.2
Pressure, suction, in. Hg.........	—4.98	—4.92	—5.93	—4.90	—4.30	—4.76	—6.99	—6.82	—6.83	—6.88	—4.09
Pressure, 2nd stage (in), in. Hg...	1.26	3.39	3.39	2.50	4.73	1.96	0.99	1.34	1.80	0.88	4.63
Pressure, 3rd stage (in), in. Hg....	8.73	13.97	15.00	11.68	16.29	10.17	11.33	11.56	12.72	11.27	16.13
Pressure, 4th stage (in), in. Hg....	17.99	27.81	30.41	23.44	31.11	20.42	24.60	24.80	27.15	24.66	30.94
Pressure, discharge, in. Hg........	29.23	44.38	48.27	37.80	48.96	32.87	40.80	41.34	44.17	40.66	48.78
Time 17,500 blower rev, min......	1.856	1.8405	1.812	1.851	1.764	1.872	1.753	1.772	1.790	1.739	1.756
Water flow, top, min/200 lb.......	0.602	0.620	0.610	0.614	0.641	0.671	0.920	0.875	0.873	0.924	1.00
Water flow, bot, min/200 lb.......	0.607	0.600	0.610	0.622	0.695	0.685	0.940	0.895	0.890	0.954	1.026
Water temp (in), deg F.........	71.4	71.4	71.35	71.3	70.95	70.55	67.8	68.0	68.1	68.1	68.2
Water temp (out) (top), deg F.....	76.05	76.9	77.1	76.45	76.75	75.75	75.6	75.75	76.55	75.35	76.9
Water temp (out (bot), deg F.....	76.05	76.9	77.1	76.45	76.75	75.75	75.7	75.75	76.65	75.45	77.0
Rpm, *N*.......................	9430	9510	9660	9450	9910	9340	9980	9860	9770	10070	9960
Inlet-air flow, cfm, *Q*............	3360	2540	2073	2956	1214	3155	1344	1647	1906	819	794
Q/*N*, inlet.....................	0.356	0.267	0.2147	0.3125	0.1224	0.338	0.135	0.167	0.195	0.0814	0.0796

for the low-capacity compressor. These corrected curves were used in subsequent analysis.

In Figs. 7 and 8 are shown the measured temperatures in each machine and those calculated on the basis of the method described in the previous section. The specific heat of air at constant pressure and the thermal conductivity of cast iron were treated as constants with values of 0.24 Btu/(lb) (deg F) and 27.0 Btu/(hr) (sq ft) (deg F/ft), respectively. The water temperature of any one diaphragm was considered constant and, for purposes of determining wall temperature, all diaphragms in one compressor were assumed to cause equal temperature rise of cooling water.

The agreement between observed and calculated temperature was considered satisfactory for general engineering use. At the lowest Q/N-values shown in Figs. 7 and 8, the machines were either in or close to surge. Under these conditions the assumption implicit in Equation [2] could hardly be expected to hold.

The results indicate that average gas-film coefficients in centrifugal compressors are quite high, varying in our tests from 54 to 180 Btu/(hr) (sq ft) (deg F) for the diffuser and 24 to 36 for the return channel. These values apply of course to the low absolute pressures of the tests.

For a machine of the same type, compressing from atmosphere to 100 psia, diffuser average film coefficients as high as 300 will be obtained. A test was actually made on a water-cooled two-casing machine compressing to 100 psia. Only one load condition was run, however, but the calculated terminal temperatures checked the observed within the limits of experimental error.

Predicted Performance of Cooled Machines

The calculation procedure previously outlined was used to study five cooling arrangements for a centrifugal compressor designed to compress 7500 cfm air at 68 F and 14.7 psia to 114.7 psia with cooling water at 75 F. The compressor size and operating conditions were so selected because of general interest in utility air for large process or manufacturing plants. The five cooling arrangements considered were: (1) two four-stage cases with an intercooler, no diaphragm cooling, (2) two four-stage cases with an intercooler and cooled iron diaphragms, (3) one eight-stage compressor with cooled iron diaphragms, (4) one eight-stage compressor with cooled high-conductivity ($K = 154$) bronze diaphragms,[5] and (5) one eight-stage compressor with cooled diaphragms of infinite conductivity. The intercooler pressure drop, including that for interconnecting piping, was taken as 2 psi at full load, and air cooling to 100 F was assumed.

The characteristic curves in Fig. 9 were used, taking Q/N for each stage as 100 per cent for compressor operation at rated load, 7500 inlet cfm. Each arrangement was calculated on this basis for performance at 3750, 5000, 6250, and 7500 cfm inlet flow.

---

[5] Material specifications supplied by P. R. Mallory and Company, Inc., Indianapolis, Ind.

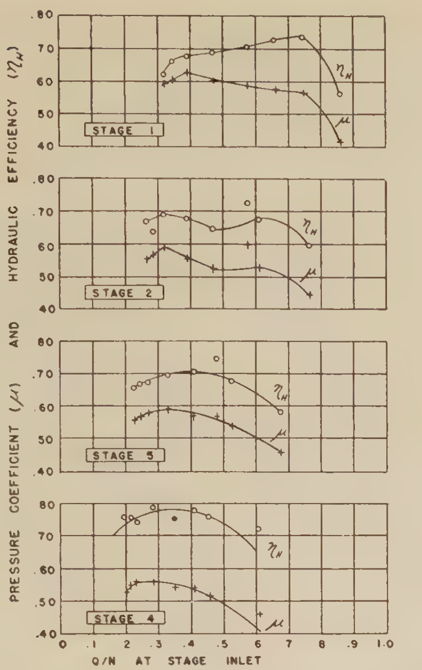

Fig. 5 High-Capacity Compressor Uncooled-Stage Characteristics

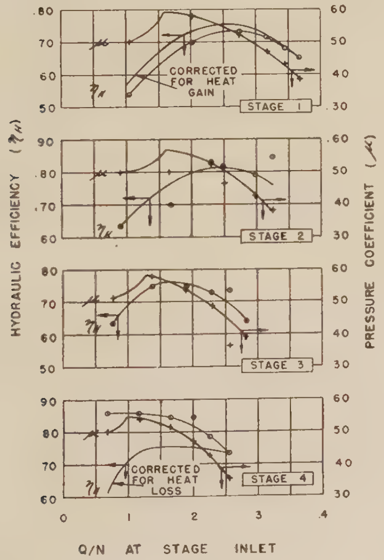

Fig. 6 Low-Capacity Compressor Uncooled-Stage Characteristics

At part loads the Q/N-value for any stage differs from its value at rated load, and the ratio of the two multiplied by 100 is the "per cent Q/N" used as abscissa in Fig. 9.

It should be noted that Fig. 9 does not give maximum values for the type of compressor here described, and probably not average values. They are reasonable values, not uncommon in industrial practice, and were considered satisfactory for the purpose of this study.

The cooling-water flow was held constant for all loads. For the two cooled four-stage cases, a flow of 80 gpm parallel to the air flow was used for each case. For the eight-stage cases 80 gpm flowed through the first four diaphragms parallel to the air flow, and another 80 gpm flowed through the last three diaphragms counter to the air flow.

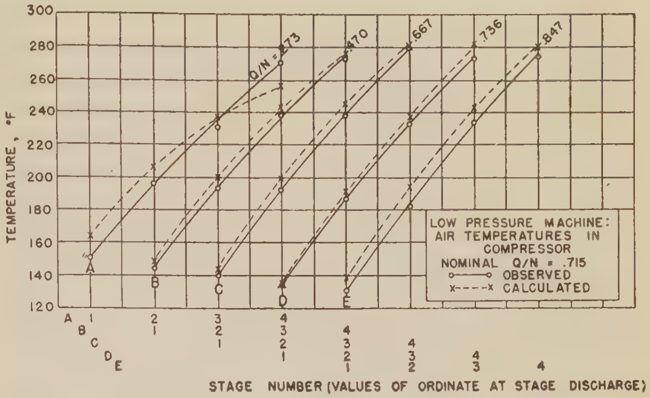

Fig. 7 High-Capacity Compressor Air-Temperature Correlations

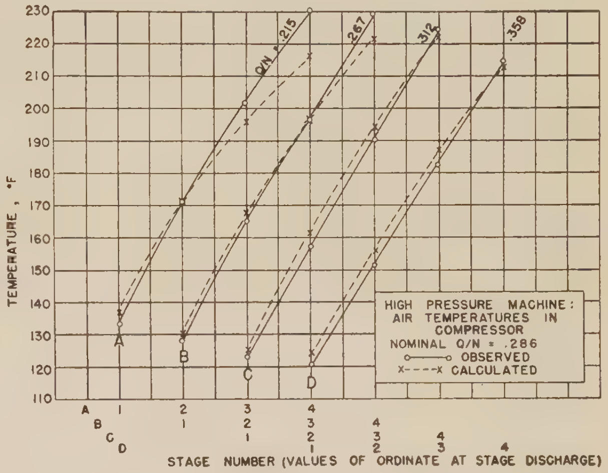

Fig. 8 Low-Capacity Compressor Air-Temperature Correlations

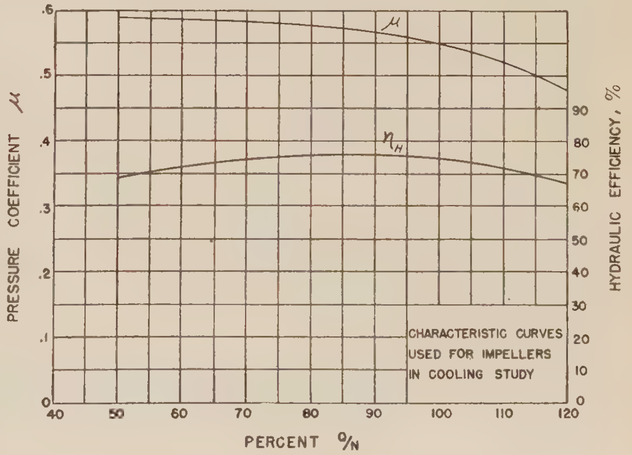

Fig. 9 Characteristic Curves of Compressor Stages in Cooling Study

The interstage operating temperatures calculated for the maximum and minimum inlet volumes are plotted in Fig. 10, and the over-all adiabatic and isothermal efficiencies and speeds for the complete range of inlet volumes in Fig. 11.

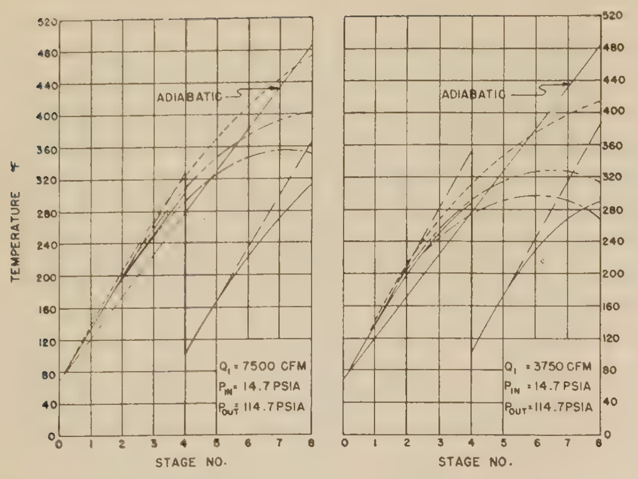

—— Two uncooled four-stage cases and intercooler.

·—— ·- Two four-stage cases with cooled cast-iron diaphragms and intercooler.

— — — — One eight-stage case with cooled cast-iron diaphragms.

— · — One eight-stage case with cooled high-conductivity bronze diaphragms.

—— – —— One eight-stage case with cooled diaphragms of infinite-conductivity material.

Fig. 10 Operating Temperature With Various Cooling Arrangements

Three important conclusions may be noted from Fig. 10, as follows:

1 The air discharge temperature of the water-cooled machine with high-conductivity bronze diaphragms is approximately that of the uncooled machine with two casings and intercooling.

2 The air temperature in a diaphragm-cooled machine appears to reach a maximum and then decrease in further compression stages. A study of the heat-transfer mechanism will confirm the existence of this maximum. Furthermore, the maximum temperature with high-conductivity bronze is in the neighborhood of 400 F, which is well within the range of existing gas operating temperatures in centrifugal compressors. It also insures reasonable adiabatic efficiencies, even at high compression ratios.

3 At half capacity, the air temperature in the diaphragm-cooled machines is actually lower than at full load, while the temperature in intercooled machines has risen. Relatively better part-load performance of diaphragm-cooled machines, therefore, may be anticipated. This is a consequence of the high velocity maintained in the diffuser at light loads, which maintains high heat-transfer rates, and thus tends to counteract the effect of lower hydraulic efficiency.

Fig. 11 will verify the relatively better part-load performance of diaphragm-cooled machines. Other conclusions which may be drawn from Fig. 11 are as follows:

1 The diaphragm-cooled machine (using high-conductivity bronze) has an adiabatic efficiency about 3 percentage points lower than the standard arrangement of two uncooled cases with intercooler.

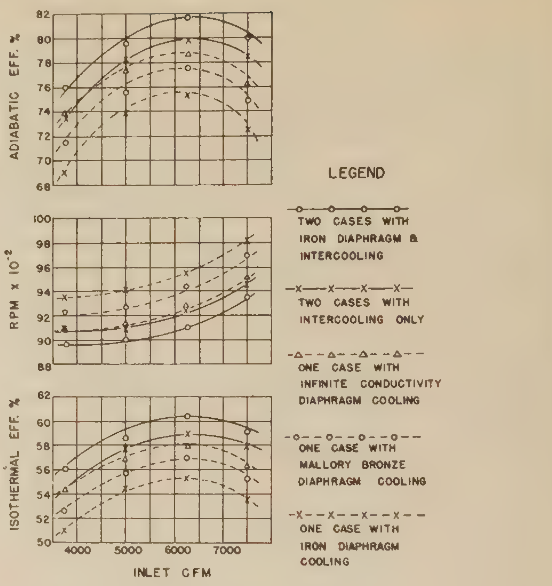

Fig. 11 Efficiencies and Speeds With Various Cooling Arrangements

2 The use of high-conductivity bronze is probably justified, although not much can be gained by using a still higher-conductivity material. This conclusion is of course limited to the specific process application and to the geometry of the diaphragm.

3 If high efficiency is desired, diaphragm cooling will be a considerable aid to the intercooler in raising efficiency.

The relative desirability of each type of cooling is clearly a complex problem, involving such factors as space requirements, initial cost, maintenance, cost of power, availability and quality of cooling water, properties of the gas, and the gas process. From a study of a number of industrial applications it appears that diaphragm cooling should be considered seriously.

Conclusion

To many manufacturers and users, perhaps the most important conclusion to be reached from the findings of this investigation is that internal cooling makes possible low-cost, compact, multistage centrifugals for compression to relatively high pressures. In the past it has been general practice to supply air-compressor cases of only four or five stages, since more stages in a case would involve gas temperatures too high for economical compression. Thus the average 100-psig air compressor consists of two cases plus intercooler. Based on the study here presented, this arrangement can, with only a small loss in operating efficiency, be reduced to a compact single case containing all the stages without any external cooling.

Acknowledgment

The authors express their appreciation to Clark Brothers Company for permission to publish this paper.

The Hydrodynamic Lubrication of Cyclically Loaded Bearings

By E. M. Simons,[1] Columbus, Ohio

The results of an experimental investigation of lubricating-film thicknesses in a journal bearing subjected to various loading conditions are presented and compared with theoretical predictions. General agreement with the theory has been found, except in the important cases of rotating and sinusoidally alternating loads applied at one half the frequency of shaft rotation. Here, instead of the theoretical eccentricity ratio of unity, finite film thicknesses have been observed. Free whirling in an unloaded bearing has been found to occur at slightly *less* than one half the shaft speed. High steady loads, high shaft speeds, and low lubricant viscosities have been found to inhibit journal whirl. The dependence of eccentricity ratio upon the extent of film rupture has been demonstrated for steady loads.

Nomenclature

The following nomenclature is used in the paper:

r = radius of journal or bearing
w = axial width of bearing
c = radial clearance, or difference between radii of bearing and journal
e = distance between center of journal and center of bearing, called eccentricity
η = e/c, called eccentricity ratio
μ = absolute viscosity of lubricant
N_j = average rotational frequency of journal in revolutions per unit time
N_p = average frequency of rotation or oscillation of load, in revolutions or cycles per unit time
N_e = mean frequency of rotation of journal center in its orbit, revolutions per unit time
F = external load applied to bearing
$P = \dfrac{F}{2rw}$ = load per unit projected area of bearing
$S = \left(\dfrac{r}{c}\right)^2 \dfrac{\mu N_j}{P}$ = dimensionless parameter, often called Sommerfeld variable or Sommerfeld number
Line of centers = line determined by center of journal and center of bearing
Clearance circle = locus of journal center for $\eta = 1$; this is a circle whose radius is c

Introduction

Sleeve bearings subjected to rotating or fluctuating loads are commonly encountered in practice. Although a number of theoretical studies (1, 2, 3, 4, 5, 6, 7)[2] of the behavior of such bearings have been published, little experimental work has been reported to prove or disprove the conclusions of these studies. Analytical treatments of even the simplest cases of cyclic loading require a number of questionable assumptions in order to reduce the mathematical complexity. Such studies indicate that there are certain speed and load conditions under which it is impossible for hydrodynamic lubrication to exist.

To check the validity of the mathematical investigations and to extend the knowledge of the effect of loading conditions on hydrodynamic lubrication, the National Advisory Committee for Aeronautics authorized an experimental study of the subject at Battelle Memorial Institute.

The plan of this investigation was to construct a testing machine in which constant or varying unidirectional, or constant rotating loads could be applied, singly or together, to a precision test bearing. The effect of the load diagram on hydrodynamic lubrication could be determined from the motions of the journal in the bearing.

Initially, simple loading conditions were studied, and then successively more complicated ones as the simpler conditions were understood. The loading conditions which are of interest are as follows:

1 Unloaded.
2 Constant unidirectional loads.
3 Constant rotating loads.
4 Unidirectional loads, varying in magnitude.
5 Combinations of the foregoing.

This study is by no means completed. Current work is aimed toward determining the sources of the discrepancies between theory and experiment and finding what modifications are required in the theory to bring the two into agreement.

Apparatus

Spindle and Bearings. The testing machine designed and constructed for this study is presented in Fig. 1. The machine employs a ring-lapped 4-in-diam spindle mounted in a support bearing (left), and a test bearing (right), both of which are precision-bored by a technique developed at Battelle (8).

The support bearing is a nonwhirling pivoted-pad type (9), consisting of four steel-backed babbitt shoes, bored to provide 0.002-in. diametral clearance. The relatively large spindle length (28 in.), and the high stability of the support bearing make it possible to measure journal motions in the test bearing with a minimum contribution by motions excited in the support bearing.

The test bearing consists of a silver-plated steel shell pressed into the cast-iron housing and finish-bored in position. The diametral clearance is 0.004 in. The bearing has a 2-in. test length between two circumferential oil grooves and a $^1/_4$-in. sealing section beyond each groove. Since the stiff pivoted-pad support bearing holds the shaft center line essentially fixed at one end of the shaft, the test bearing was bored tapered in order to keep the shaft surface approximately parallel to the test bearing along the line of nearest approach. The taper was made linear, the end farthest from the support bearing being 0.0003 in. larger in diameter.

Loading Systems. Loads are applied, by means of calibrated

---

[1] Battelle Memorial Institute. Mem. ASME.

[2] Numbers in parentheses refer to the Bibliography at the end of the paper.

Contributed by the Special Research Committee on Lubrication and the Petroleum Division and presented at the Annual Meeting, New York, N. Y., November 27–December 2, 1949, of The American Society of Mechanical Engineers.

Note: Statements and opinions advanced in papers are to be understood as individual expressions of their authors and not those of the Society. Paper No. 49—A-41.

compression springs, through two pressure-lubricated babbitt loading bearings, one for unidirectional loads and the other for rotating loads. The loading mechanisms are visible at the right of the test-bearing housing in Fig. 1. The small spring seen at the top removes the weight of the shaft from the test bearing, enabling true no-load tests to be run. Sinusoidally alternating loads are applied by an adjustable cam which cyclically compresses the loading spring. Rotating loads are applied through a bell crank, one arm of which is attached to the loading bearing and the other to the loading spring. The bell crank pivots on a pin through the rotating-load jackshaft. The ranges of loads attainable are as follows:

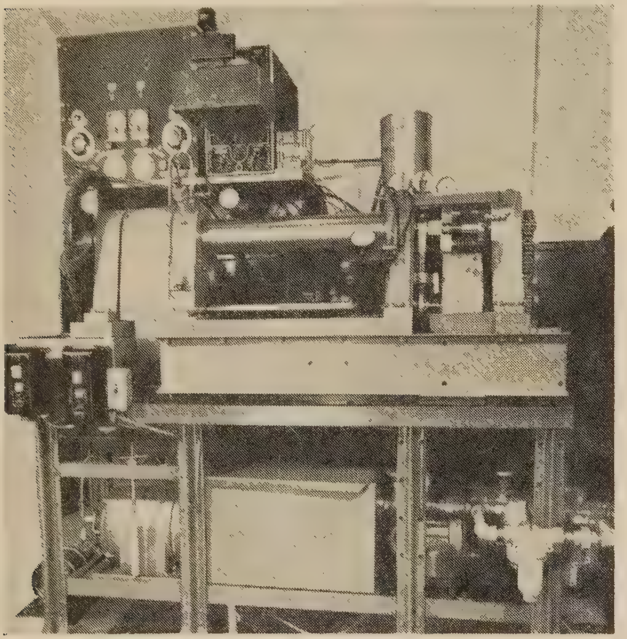

Fig. 1 Machine for Testing Hydrodynamically Lubricated Sleeve Bearings Under Various Loading Conditions

Steady vertical load	0 to 500 lb ($62^1/_2$ psi)
Sinusoidally varying vertical load	±0 to ±250 lb (±$31^1/_4$ psi)
Constant rotating load	0 to 500 lb ($62^1/_2$ psi)

Drive Arrangement. A 3-hp, 1740-rpm motor drives a jackshaft, through a Toledo Timer speed changer, with V-belts. The jackshaft is coupled to the independently mounted test spindle by a Lord bonded-rubber coupling to minimize the transmission of vibration. Spindle speeds of 25 to 2500 rpm can be obtained.

The camshaft is driven through change gears from the spindle, with the following ratios of spindle speed to camshaft speed available: 10:1, 6:1, 4:1, 2.80:1, 2.43:1, 2.11:1, 2.06.1, 2:1, 1.95:1, 1.89:1, 1.65:1, 1.43:1, 1:1, 0:67:1, 0.40:1. The flywheel on the camshaft tends to maintain uniform spindle speed during alternating-load tests.

The rotating-load jackshaft is driven through a gear-and-chain arrangement from the camshaft, and may be driven in either direction with respect to the spindle rotation.

Lubrication. All journal bearings are pressure-fed by a 12-gpm, 100-psi pump with by-pass pressure control. The two circumferential oil grooves in the test bearing have separate feed lines with independent control valves and gages. This arrangement provides good control of lubricant flow through the test bearing, while maintaining positive pressures at the ends. The lubricant is continuously filtered by micronic filters, and is maintained near room temperature by cooling coils in the sump. An oil reservoir is provided above the test bearing to permit operation with flood lubrication, if desired.

Radio-Frequency Micrometer. The instrument used to reveal the effectiveness of hydrodynamic lubrication is a specially built radio-frequency micrometer, the components of which are visible in Fig. 1. These consist of the receiver and power supply on the shelf at the upper left, the cathode-ray oscillograph to the right of the receiver, and the two probes, one of which is hidden from view, fastened to the left face of the test-bearing housing at an angle of 45 deg with the horizontal.

A description of the electrical circuits and the operation of the micrometer has been published (10). Briefly, minute displacements of the spindle are measured as a function of changes in electrical capacitance between the spindle and the micrometer probes. This capacitance is made part of the resonant circuit of a high-frequency radio oscillator, and variations cause sufficient changes in oscillator frequency to be readily measured by techniques developed for frequency-modulation broadcasting.

Journal Whirl

Types of Whirl. In general, the motion of a journal in a sleeve bearing is composed of two parts, i.e., a pure rotation about its own axis, and a combined rotation and translation of this axis with respect to the axis of the bearing. This latter motion is known as "whirling." Whirling may be self-excited, as in the case of oil whip, discussed by Newkirk, Taylor, and Grobel (11, 12), or it may be induced by external dynamic loads. It can be stable, with the journal center moving in a closed orbit with regular periodicity, or it may be transient.

In certain machines, such as high-speed turbine compressors and steam turbines, serious vibration difficulties have been traced to journal whirl in sleeve-type bearings. This is particularly true where centrifugal forces resulting from journal eccentricity are large. Whirling could be troublesome in many other applications. For example, in machine-tool spindles, shaft whirl causes inaccuracies in machining and undesirable surface roughness. Whirling in sleeve-type propeller-shaft bearings, such as aircraft and marine shaft bearings, could easily contribute to fatigue-induced failures.

Frequency of No-Load Whirling. Robertson (2) has demonstrated mathematically that, neglecting oil-drag forces, the resultant oil-pressure force caused by journal rotation in an ideal bearing is at right angles to the line of centers and produces stable whirling at one half the rotational frequency of the journal. Swift (3) has shown analytically that an unloaded ideal bearing whirls in a circular orbit at any eccentricity whatsoever, with an angular velocity of exactly half of the journal speed.

To check these conclusions, precise measurements were made of the frequency of no-load transient whirling just after the journal had come up to speed from a standstill. It was necessary to use starting transients for these tests because sustained no-load whirling could not be obtained in the test bearing, regardless of the combination of speed, lubricant viscosity, and feed pressure employed. It was found that the natural whirl during no-load starting occurred at slightly less than one half the shaft speed, as seen in Table 1.

TABLE 1 FREQUENCY OF NO-LOAD SHAFT WHIRL, WITH SAE 10 OIL

Spindle speed, N_j, rpm	N_e/N_j, flood lubrication	N_e/N_j, 50 psig feed pressure
154	0.4980	0.4971
380	0.4968	...

These observations agree with the conclusions of Hagg (9), who states that one half the rotational frequency is the upper limit of whirling frequency for an unloaded ideal bearing, but that, "in reality, this upper limit is reduced because of fluid friction and bearing leakage." However, Taylor (13), in discussing Hagg's paper, points out that this was usually, but not always, the case in his own experiments, where frequency ratios as high as 0.6 were observed. In any case, it is difficult to see how fluid friction and side leakage alter the simple theory which demonstrates that an unloaded journal should whirl at one half the shaft speed.

Factors Influencing Shaft Whirl. Swift's work (3) would indicate that, in general, the journal center would not be stationary under no load, nor even under a constant load. On the contrary, the experiments have shown that in the absence of external periodic excitation, the ultimate equilibrium position of the journal center was always a stationary spot. For example, Fig. 2 shows that when the shaft was started from rest under no load, it moved in a spiral path which invariably ended in a steady position at the center of the bearing. However, the conditions of the particular test determined how quickly this equilibrium position was reached. Similarly, when the shaft was started from rest under a steady unidirectional load, the transient motion of the journal center never failed to die out at some fixed eccentricity ratio.

Obviously, the physical characteristics of the test setup were such that sufficient damping forces were present, over a wide range of operating variables, to prevent the journal center from moving continually in an orbit. Such damping forces are generally not considered in the theory. Experimentally, it was found that the most rapid damping of journal whirl was obtained with high steady loads, high shaft speeds, high lubricant feed pressures, or low-viscosity lubricants. The damping effect of higher lubricant pressure on whirling can be seen by comparing (*a*) and (*b*) in Fig. 2; the damping effect of high speed is strikingly shown by comparison of (*b*) with (*c*); while the steadying influence of low viscosity is evident from the fact that it always took much longer to reach equilibrium when higher-viscosity lubricants were used at the same speed and lubricant feed pressure.

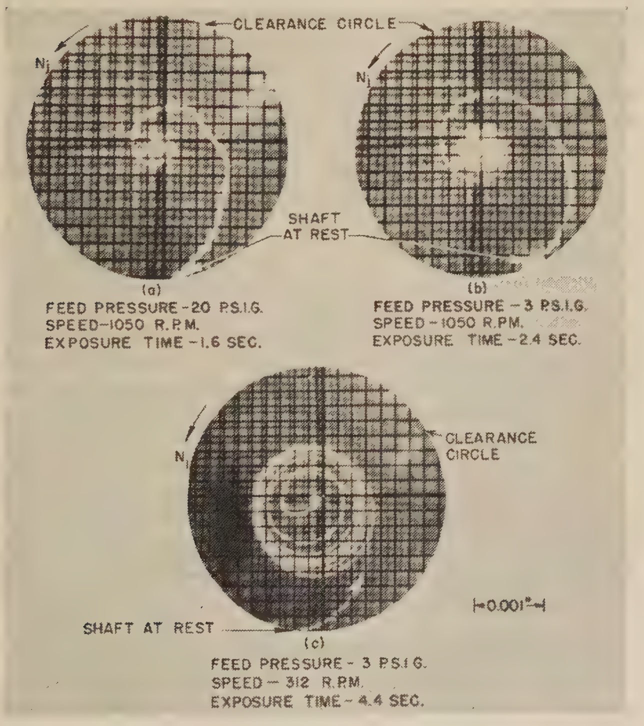

Fig. 2 Transient Motions of Journal Center During No-Load Starting, Using Kerosene at 80 F as Lubricant

(μ = 1.52 centipoises.)

Unidirectional Steady Loads

Starting and Stopping Under Steady Load. Fig. 3 shows the motion of the spindle center when started from rest under an upward load of 50 psi. It is commonly thought that, upon starting from rest, the shaft crawls along the bearing wall in a direction opposite to that shown, until solid friction is reduced sufficiently by the formation of an oil film for hydrodynamic forces to take over. This effect was not observable in Fig. 3, indicating that a load-carrying oil film was generated much more rapidly than is usually assumed and that the rolling motion, if present at all, was too small to be detected in the photograph.

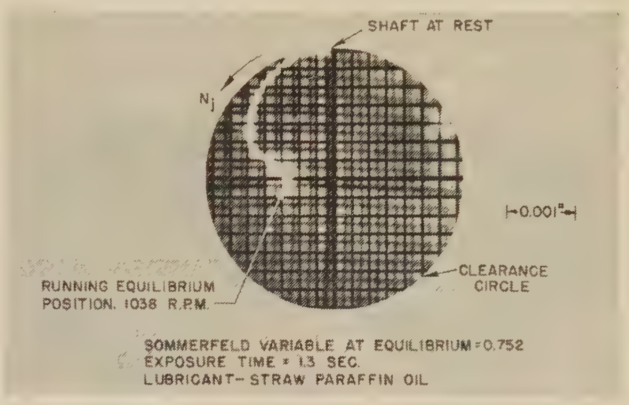
SHAFT AT REST
N_j
0.001"
CLEARANCE CIRCLE
RUNNING EQUILIBRIUM POSITION. 1038 R.P.M.
SOMMERFELD VARIABLE AT EQUILIBRIUM = 0.752
EXPOSURE TIME = 1.3 SEC.
LUBRICANT - STRAW PARAFFIN OIL

Fig. 3 Transient Motion of Journal Center When Started From Rest Under 50-Psi Upward Load

Starting at the top of the clearance space, the shaft movement appeared to be first to the left and then downward as it came up to speed and the load-carrying capacity of the bearing increased. It then moved toward the center of the clearance circle, finally stabilizing at an eccentricity ratio of 0.27, which agrees with the theoretical predictions of Muskat and Morgan (14).

The absence of full spiraling motions like those obtained with no-load starting is apparent. Indeed, it has been found that free whirling of the journal is strongly damped by the application of an external load.

When the shaft was stopped under 50-psi upward load, its center retraced exactly the path in Fig. 3, moving to the left and then upward as the rotational motion slowed down and the load-carrying capacity of the oil film decreased.

Oil-Film Tension. In a flooded full journal bearing, the theoretical pressure distribution over the semicylinder on one side of the line of centers is the exact negative reflection of that on the semicylinder on the other side of the line of centers. This condition implies that the integrated pressure-area product in the film can have no component along the line of centers, so that the displacement of the journal in the bearing must be normal to the direction of load application. It also indicates that when a flooded full journal bearing is operated with an unbroken oil film, one half the external load is supported by hydrodynamic pressures above atmospheric on the loaded side, and the other half by equal pressures below atmospheric on the unloaded side. For example, if the external load is 10 psi, the average negative pressure on the unloaded side will be 5 psi, and the peak negative pressure may be in the vicinity of 3 times the average, say, 15 psi.

If this peak negative pressure exceeded 1 atm, the oil film would rupture in the region of theoretical pressures below absolute zero, unless the film were capable of carrying a tensile load. In the latter case, the rupture would occur when the negative pressures exceeded the tensile strength of the oil film. Any such break in the film will require that the journal move in the direction of loading and generally result in higher eccentricities than those predicted by hydrodynamic theory for ideal bearings. This implies that a flooded bearing would operate with a continuous film only when the external loads were very low. However, the application of feed pressures in the circumferential oil grooves of the test bearing makes it possible to support higher loads without film rupture, because the feed pressure helps to prevent a tensile stress in the oil film.

Studies of the behavior of a unidirectionally loaded bearing were conducted by running the bearing at no load, and photographing the spindle motions as an upward load was applied gradually enough to maintain equilibrium at all times. Some views taken in this way are presented in Fig. 4. In (*a*), the shaft moved horizontally (normal to the direction of loading), in accordance with the theory, until the external load reached about 20 psi. At this point the negative pressures became too great, the oil film ruptured, and the shaft moved upward, in the direction of the load. As the feed pressures were increased [(*b*) and (*c*)], the rupture occurred at higher and higher loads, until, at a feed pressure of about 15 psig, the film remained apparently intact under the total load of 50 psi [cf, Fig. 4(*d*)], and no upward motion of the shaft took place. The rupture occurs suddenly in some cases, as evidenced by a sharp break from horizontal to upward motion, such as in Fig. 4(*a*) and (*c*).

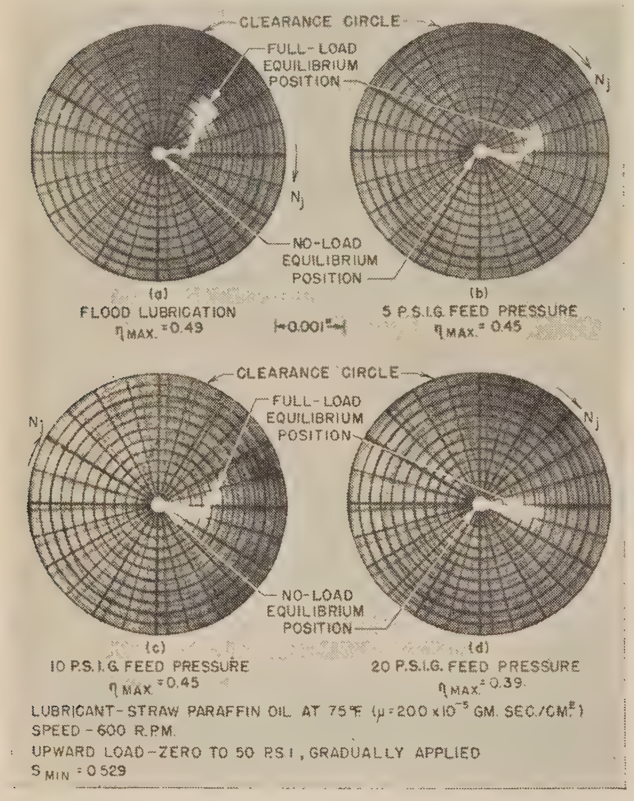
CLEARANCE CIRCLE
FULL-LOAD EQUILIBRIUM POSITION
N_j
NO-LOAD EQUILIBRIUM POSITION
0.001"
CLEARANCE CIRCLE
FULL-LOAD EQUILIBRIUM POSITION
N_j
N_j
NO-LOAD EQUILIBRIUM POSITION

(a) FLOOD LUBRICATION $\eta_{MAX.} = 0.49$

(b) 5 P.S.I.G. FEED PRESSURE $\eta_{MAX.} = 0.45$

(c) 10 P.S.I.G. FEED PRESSURE $\eta_{MAX} = 0.45$

(d) 20 P.S.I.G. FEED PRESSURE $\eta_{MAX} = 0.39$

LUBRICANT-STRAW PARAFFIN OIL AT 75°F ($\mu = 200 \times 10^{-5}$ GM. SEC./CM.²)
SPEED - 600 R.P.M.
UPWARD LOAD-ZERO TO 50 P.S.I., GRADUALLY APPLIED
$S_{MIN} = 0.529$

Fig. 4 Effect of Lubricant Feed Pressure on Shaft Position During Gradual Load Application

Rough calculations of the magnitude of the negative film pressures indicate that the oil film is withstanding a small tensile stress, from a few to 50 psi. It is known that liquids can withstand tension under some circumstances and conditions in a bearing appear to be favorable.

Effect of Film Rupture on Eccentricity. Since the circumferential pressure distribution in a full journal bearing has rather sharp positive and negative peaks, it would be expected that, with a gradual increase in load, incipient film rupture would occur in a highly localized region of peak negative pressure, spreading over a larger and larger fraction of the bearing area as the load was further increased. The dependence of eccentricity ratio upon the extent of such film rupture is demonstrated by the experimental results shown in Fig. 5 which is a plot of eccentricity ratio as a function of Sommerfeld number for steady, unidirectional loading.

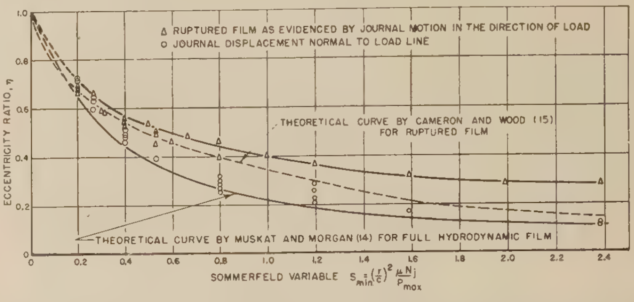

Fig. 5 Observed and Theoretical Eccentricities of Test Bearing Under Steady Unidirectional Loading

The lowest circled points agree, within experimental accuracy, with the theoretical curve from Muskat and Morgan (14), based upon a continuous oil film. The upper curve, drawn through the points showing the greatest departure from the curve of Muskat and Morgan, represents the cases where the oil feed pressure was low (flood lubrication), and film rupture had occurred to the greatest extent. Between these two curves are eccentricities which result from various degrees of film rupture, the points lying closest to the lower curve representing very small localized areas of rupture, and those lying near the upper curve representing rupture over more extensive areas. This range of eccentricity ratios was produced, at a given Sommerfeld number, by varying the oil feed pressure in the circumferential grooves, as illustrated in Fig. 4.

The curve of Cameron and Wood (15) in Fig. 5 is based upon numerically calculated results for what is essentially a ruptured film. The film is assumed to start at the large film-thickness end of the line of centers and extend to a point beyond the minimum film-thickness end where both the pressure and pressure gradient drop simultaneously to zero. The discrepancy between the curve of Cameron and Wood and the experimental curve for the ruptured film is very likely the result of this stringent restriction upon the extent of rupture.

Most theoretical treatments of journal bearings assume continuity of the oil film around the bearing arc. Fig. 5 demonstrates that these theories cannot be used to predict the behavior of bearings in practice unless the application involves high enough lubricant feed pressures or low enough external loads to preclude rupture at any point in the oil film.

Constant Load Rotating at Constant Speed

Fig. 6 shows the eccentricities resulting from the application of a 7.8-psi load rotating at various frequencies. For all ratios of N_p/N_j greater than about 0.25, the orbits were circular, and the eccentricity ratio was taken as the ratio of the radius of the orbit to the radius of the clearance circle. However, when N_p/N_j was 0.25 or less, the orbits were stable and closed in one cycle of load application, but they were not circular. In such cases, the maximum value of eccentricity ratio was plotted in Fig. 6. This explains why the points at $N_p/N_j = 0.25$ and 0.167 fall above the curve drawn.

$N_p/N_j = 0$ represents a constant unidirectional load, and the measured value of η here agrees with Muskat's prediction (14) for a flooded full journal bearing under these conditions. As N_p/N_j is

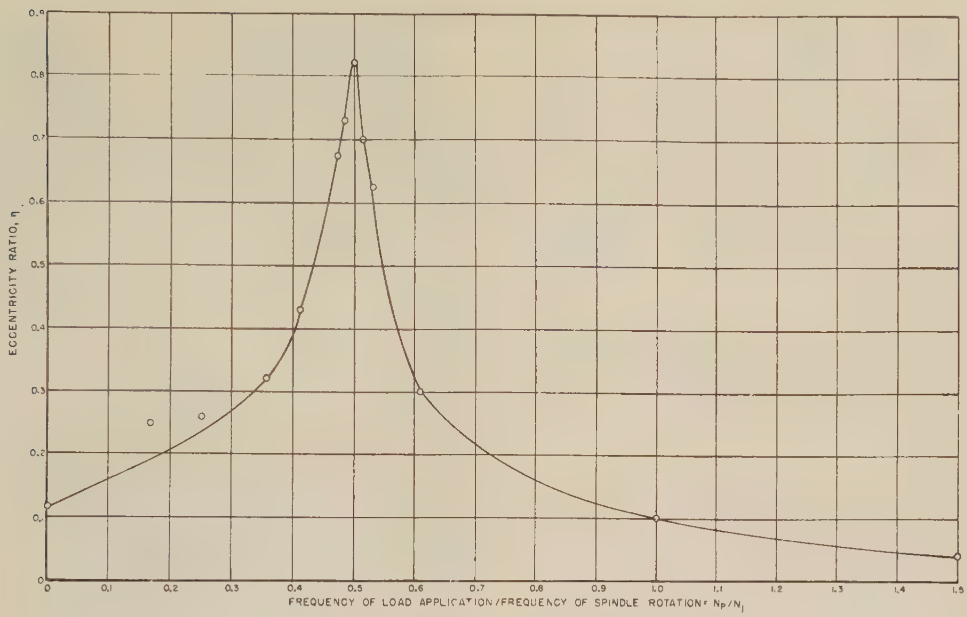

Fig. 6 Effect of Relative Frequency of Load Application on Eccentricity Ratio for Constant Load of 7.8 Psi Rotating at Constant Speed

(S = 2.38; lubricant, kerosene.)

increased, η increases also, peaking sharply at $N_p/N_j = 0.5$. Further increase in N_p/N_j is accompanied by a drop in η, which has about the same value at $N_p/N_j = 1.0$ as at $N_p/N_j = 0$. This agrees with the findings of Burwell (17) and Underwood and Stone (16), viz., that a bearing subjected to a constant rotating load applied at the frequency of shaft rotation has a load capacity (as defined by eccentricity) numerically the same as if the load were stationary. Frequency ratios greater than 1.0 yield eccentricities lower than those obtained by constant unidirectional loading.

Robertson (2), Swift (3), Burwell (7), and others have demonstrated mathematically that when the load is rotating at one half the shaft speed, the bearing is unable to carry any load with an eccentricity ratio other than unity. Before this conclusion could be drawn, however, the following assumptions had to be made:

1 No end leakage.
2 Continuous oil film around the bearing.
3 No local changes in viscosity.
4 The oil has no inertia.
5 Oil pressure is constant along a radius.
6 The orbit is circular and concentric with the clearance circle ($d\eta/dt = 0$)
7 The angle between the line of centers and the load direction is constant. If so, its value is 90 deg.

In all the experiments run with $N_p/N_j = 0.5$, it was found that the eccentricity ratio was less than unity, decreasing slowly with decreasing load and decreasing rapidly with increasing speed. These effects are apparent in Fig. 7. Nevertheless, it is true that the eccentricity rises to a sharp peak when $N_p/N_j = 0.5$, Fig. 6, and that it is best to avoid such conditions in practice whenever possible. A knowledge of the factors which are favorable to the existence of an oil film under these conditions could provide valuable aid in the design of sleeve bearings for applications where cyclic load components at or near one half the frequency of shaft rotation are unavoidable.

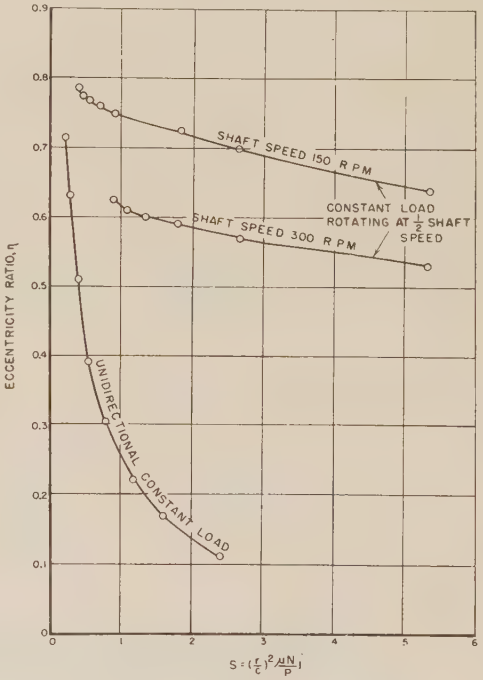

Fig. 7 Eccentricity Measurements for Load Rotating at ½ Shaft Speed

(Flood lubrication with straw paraffin oil.)

One possible explanation for the presence of a load-carrying oil film, in violation of theoretical predictions when $N_p/N_j = 0.5$, lies in the discarding of higher-order terms in the development of the theory (2). However, when this was investigated by substituting test conditions into the discarded terms, it was found that these terms were truly negligible, causing theoretical changes in eccentricity which were considerably smaller than the error in experimental measurements.

Another likely source of the discrepancy was the possibility of a dynamic stiffening effect in the pivoted-pad support bearing, which might prevent the journal from attaining the maximum eccentricity in the test bearing. The stiffening effect would have to stem from dynamic forces, since it was possible to maintain contact between journal and bearing while rotating the load a full revolution slowly by hand. To ascertain the role of support-bearing hydrodynamic forces in stiffening, test-bearing motions were studied first with SAE 10 oil in the support bearing and then with kerosene in the support bearing, while maintaining constant conditions at the test bearing. The tests showed that the viscosity of the lubricant in the support bearing had no effect on the eccentricity in the test bearing. This and other considerations proved that support-bearing stiffness did not limit journal motions in the test bearing.

A third explanation proposed for the nonunit eccentricity ratios obtained with $N_p/N_j = 0.5$ was that gyroscopic forces might oppose the hydrodynamic effects. However, simple computations showed that, because of the low journal speeds used in the tests, gyroscopic forces were much too small to have any noticeable effect on eccentricity.

Burwell has suggested (17) that thermal expansion of the oil in the minimum-film-thickness region might give rise to pressure development. He points out that the local rate of heat production, and hence of local temperature rise, will vary along the film inversely as the film thickness, being greatest at the point of minimum film thickness. Hence cooler oil will be dragged into the region of minimum film thickness, and the subsequently heated oil will be carried away. This plausible explanation has not been investigated as yet.

In an effort to obtain some clue from the appearance of the test bearing, the shaft was removed and the bearing studied. Burnish marks near both ends of the bearing gave strong indication that the shaft and bearing axes had somehow become misaligned. Very careful measurements revealed the fact that the axes diverged by 0.0006 in. in the 3-in. housing length. This misalignment was reduced to 0.00015 in. by straining the machine bed with short lengths of arc weld, which contracted the parent metal, causing the housings to move in the proper directions.

Table 2 shows that this improvement in alignment resulted in a closer approach to the theoretical eccentricity ratio of unity when $N_p/N_j = 0.5$, indicating that misalignment is probably a contributing factor in the discrepancy between theory and experiments.

TABLE 2 EFFECT OF BEARING MISALIGNMENT ON ECCENTRICITY, WITH ROTATING LOAD AT ONE-HALF SHAFT SPEED

Shaft speed, rpm	Eccentricity ratios	
	0.0006 in. misalignment	0.00015 in. misalignment
150	0.72	0.83
300	0.61	0.66

NOTE: Rotating load, 12.5 psi at one-half shaft speed; SAE 10 oil, flood lubrication.

That misalignment might prevent a zero oil-film thickness when $N_p/N_j = 0.5$ can be seen from the qualitative discussion which follows. Assuming that center A, Fig. 8, whirls in a circular orbit, B and C are forced to rotate in circular orbits also (since one end of the shaft is essentially fixed), but the centers of the latter orbits will be displaced, respectively, below and above the center line of the bearing. This nonconcentric whirling of the shaft at every section except A will produce varying hydrodynamic forces F_1 and F_2, equivalent to external loads superimposed on the applied rotating load. As will be discussed in a later section of this paper, such combined loads may reduce the eccentricity below that which would result from the rotating load alone, applied at one half the shaft speed. Furthermore, an increase in shaft speed would increase the hydrodynamic forces F_1 and F_2 and further reduce the eccentricity. This agrees with the results in Fig. 7 and in Table 2. Additional experimental effort along these lines is in progress.

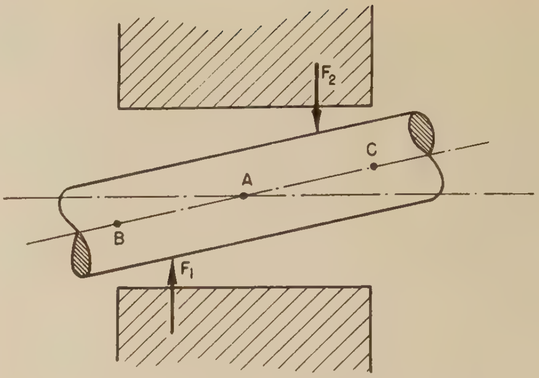

FIG. 8 EFFECT OF MISALIGNMENT ON SHAFT WHIRL

SINUSOIDAL ALTERNATING LOAD IN VERTICAL DIRECTION

Burwell (7) has extended the hydrodynamic theory of lubrication to the general case of a periodic load and has applied his findings to the solution of the problem of a sinusoidal reciprocating load with a journal rotating at constant speed. Since no analytical solution to his differential equations could be found, he carried out the solution by a step-by-step numerical integration, using trial-and-error methods to obtain closed-path solutions in one cycle of load application. Dick (4) studied the case of simple sinusoidal loading by assuming that the journal-center path was an ellipse and that the hydrodynamic load along one axis of the ellipse was zero. He then compared the hydrodynamic load along the other axis with a sinusoidal load.

Burwell's calculations produced orbits which resemble ellipses for sinusoidal alternating loads. He and Dick both found that the long axis was in the direction of loading when N_p/N_j was greater than 0.5, and that the long axis was perpendicular to the load line when N_p/N_j was less than 0.5. At $N_p/N_j = 0.5$, the orbit was the clearance circle. These shapes agree rather well, in general, with experimental findings, as may be seen from the examples in Fig. 9.

Furthermore, as Burwell pointed out, the paths become more complicated for values of N_p/N_j less than about 0.25. His orbit for $N_p/N_j = 0.25$ did not exhibit the extra loop shown in Fig. 10 (*a*), but this discrepancy can perhaps be attributed to the wide divergence between his value of $S_{\min}$ (0.01) and that used in the experiment (2.38). Fig. 10 (*b*) shows an interesting symmetric double-loop pattern obtained with $N_p/N_j = {}^1/_6$. The complicated gyrations of the shaft center before finally settling down to an equilibrium orbit are illustrated in Fig. 10 (*c*), which was photographed $1^1/_2$ min after the shaft had been started from rest. It took an additional $1^1/_2$ min to reach an equilibrium orbit similar in shape to Fig. 9 (*a*).

Most of the frequency ratios tested produced equilibrium orbits which closed in 1 cycle of load application. The exception to this was $N_p/N_j = 0.7$, in which case the path was an oscillating spiral between a larger and a smaller orbit. The time required to reach equilibrium, the complex transient patterns traced by the shaft center before equlibrium was reached, and the character of the ultimate equilibrium orbit indicate that certain N_p/N_j ratios produce equilibrium orbits which close in 1 cycle of loading only as a result of external damping conditions, or the fact that particular initial conditions existed. The behavior is analogous to the forced vibrations of a resonant system, in which the equations of motion contain terms dependent upon the initial conditions, and upon the resonant frequency. These terms can be neglected only after damping has eliminated the effect of initial conditions. There is a great deal of room for further work in correlating the theory with experiments.

Since the orbits were not circular, except when $N_p/N_j = 0.5$, it

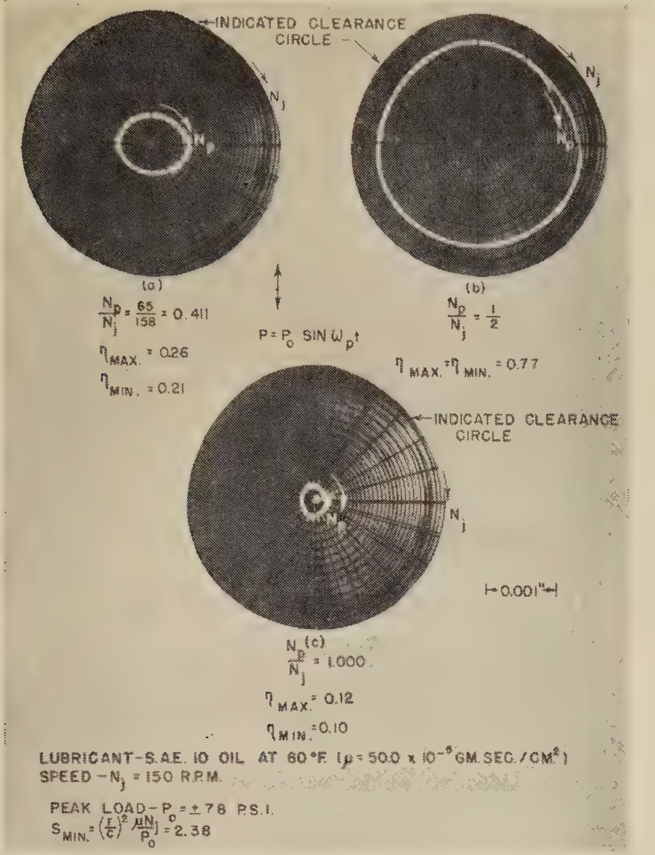
INDICATED CLEARANCE CIRCLE
N_j
(a)
$\frac{N_p}{N_j} = \frac{65}{158} = 0.411$
$\eta_{MAX.} = 0.26$
$\eta_{MIN.} = 0.21$
$P = P_0 \sin \omega_p t$
(b)
$\frac{N_p}{N_j} = \frac{1}{2}$
$\eta_{MAX.} = \eta_{MIN.} = 0.77$
INDICATED CLEARANCE CIRCLE
N_j
⊢0.001"⊣
(c)
$\frac{N_p}{N_j} = 1.000$
$\eta_{MAX.} = 0.12$
$\eta_{MIN.} = 0.10$
LUBRICANT–S.A.E. 10 OIL AT 80°F ($\mu = 50.0 \times 10^{-5}$ GM. SEC./CM.^{2})
SPEED – N_j = 150 R.P.M.
PEAK LOAD – P_0 = ± 78 P.S.I.
$S_{MIN.} = \left(\frac{r}{c}\right)^2 \frac{\mu N_j}{P_0} = 2.38$

Fig. 9 Journal Center Orbits Under Sinusoidal Alternating Load

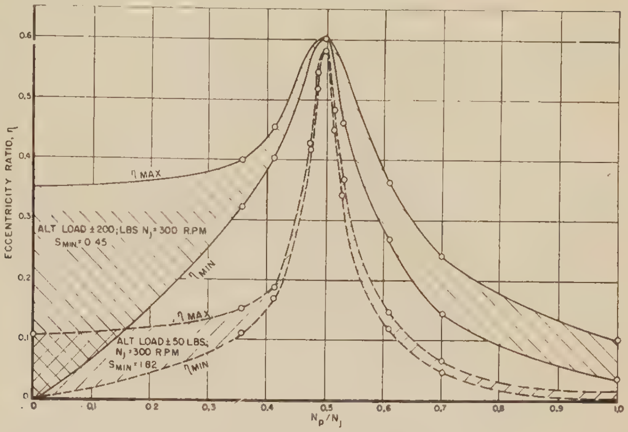

Fig. 11 Shaft Motions in Journal Bearing With Sinusoidal Loads at Various Frequencies

was possible to measure a maximum and a minimum eccentricity. Plots of these values for two different values of $S_{\min}$ are shown in Fig. 11. When the load was applied at very low frequency ($N_p/N_j = 0$), the eccentricity varied from zero, when the load was zero, to a maximum which corresponded to the peak load applied continuously. As N_p/N_j was increased, both $\eta_{\max}$ and $\eta_{\min}$ increased, $\eta_{\min}$ increasing faster than $\eta_{\max}$ until N_p/N_j reached 0.5, at which point $\eta_{\min} = \eta_{\max}$, and the orbit was circular. Further increase in N_p/N_j resulted in a rapid drop in eccentricity, with $\eta_{\max}$ falling considerably below that for the constant unidirectional load, at values of N_p/N_j above about 0.65. These observations correspond generally to the relative load-capacity curves presented by Burwell (7) and Underwood and Stone (16).

The outstanding discrepancy between the results of the experiments and the theoretical work was the fact that, just as with a rotating load, the observed eccentricity ratios were not unity for sinusoidal loading at $N_p/N_j = 0.5$. A careful study was made of the effects of the various operating variables on eccentricity under this condition of loading. It was soon discovered that, above a certain very light load, the magnitude of the load had little influence on eccentricity. For example, as may be seen from Fig. 11, increasing the load by a factor of 4 raised the eccentricity ratio from 0.58 to only 0.60. The effects of speed and viscosity are apparent in Fig. 12 which shows that varying the viscosity in a given test seemed to have a small effect on the eccentricity when $N_p/N_j = 0.5$, while changing the speed had a pronounced effect. Under these conditions of loading, the Sommerfeld variable, which is a parameter of true hydrodynamic lubrication, provided no correlation between eccentricity and the operating variables.

The origin of load-supporting pressures in the lubricant film, with $N_p/N_j = 0.5$, is not known. It seems not unlikely that the explanation is the same for the case of the sinusoidal load as for a rotating load. Efforts to solve this problem are continuing.

Combined Rotating and Alternating Loads

Tests were run with a combination of rotating and alternating loads. The rotating load was applied at the frequency of shaft rotation to simulate centrifugal loading. The sinusoidal alternating load was applied at one half the spindle speed to represent, for example, gas-pressure loading in a four-stroke-cycle engine crankshaft bearing.

Fig. 13 shows the effect of increasing the rotating load while holding the alternating load constant. It is highly significant

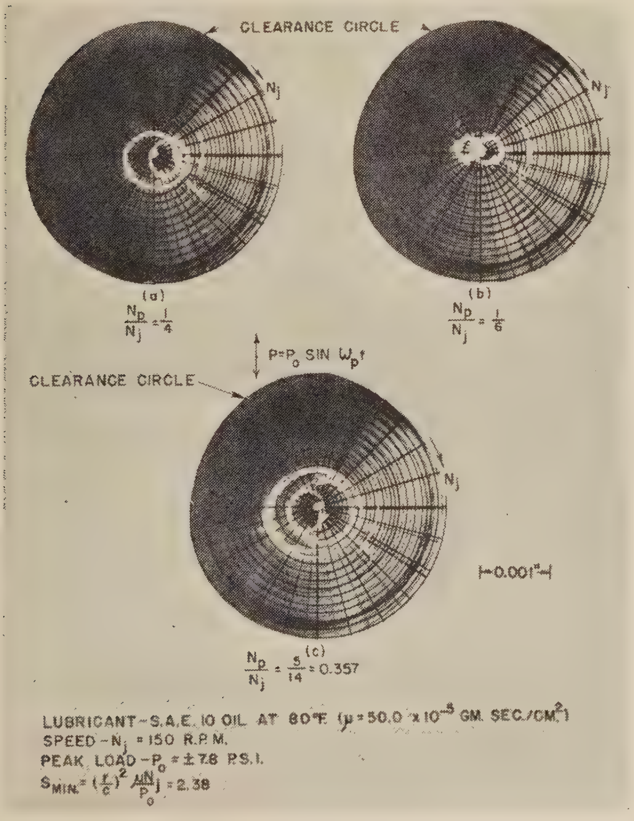
CLEARANCE CIRCLE
N_j
N_j
(a)
$\frac{N_p}{N_j} = \frac{1}{4}$
(b)
$\frac{N_p}{N_j} = \frac{1}{6}$
$P = P_0 \sin \omega_p t$
CLEARANCE CIRCLE
N_j
⊢0.001"⊣
(c)
$\frac{N_p}{N_j} = \frac{5}{14} = 0.357$
LUBRICANT–S.A.E. 10 OIL AT 80°F ($\mu = 50.0 \times 10^{-5}$ GM. SEC./CM.^{2})
SPEED – N_j = 150 R.P.M.
PEAK LOAD – P_0 = ± 78 P.S.I.
$S_{MIN.} = \left(\frac{r}{c}\right)^2 \frac{\mu N_j}{P_0} = 2.38$

Fig. 10 (*left*) Journal Center Paths Under Sinusoidal Alternating Load

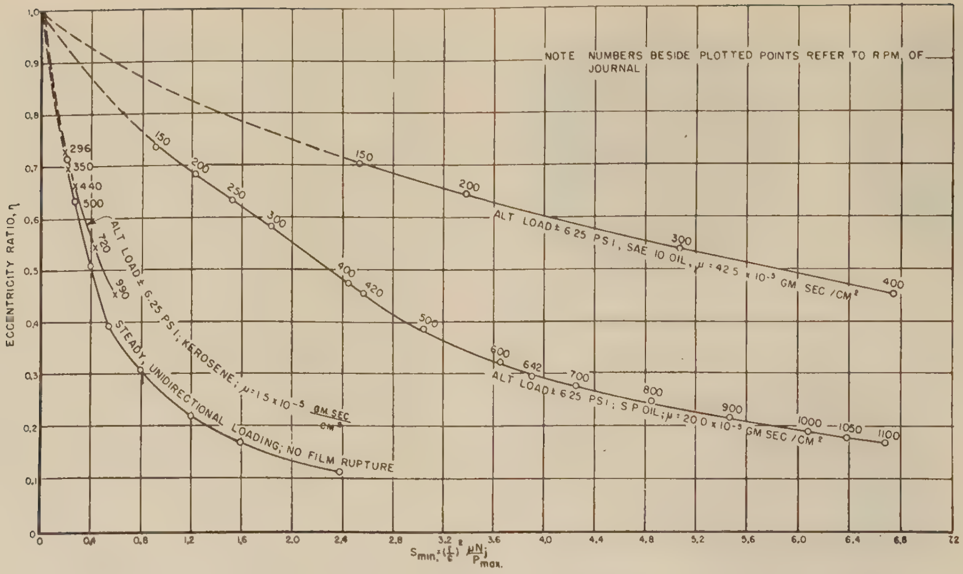

Fig. 12 Eccentricity With Sinusoidal Loading at One-Half Frequency of Journal Rotation ($N_p = {}^1/_2\ N_j$)

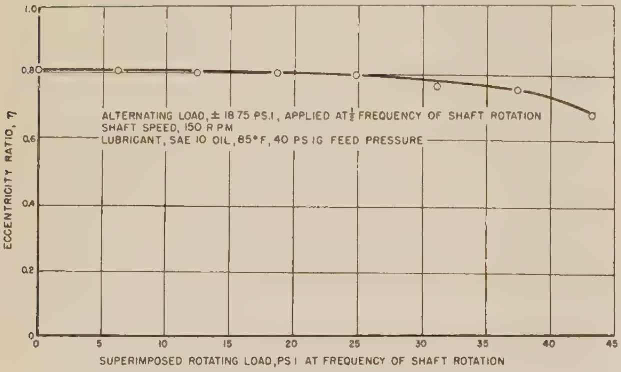

Fig. 13 Eccentricity Under Combined Periodic Loads

that the alternating load alone, applied at one half the shaft frequency, produced eccentricity ratios which were greater than those resulting from the combined loads. Furthermore, it may be seen that the higher the superimposed rotating load, the thicker the operating oil film. This phenomenon helps to explain why four-stroke-cycle engine crankshaft bearings can operate with complete film lubrication, in spite of the gas-pressure loading at the critical frequency of one half the shaft speed. The inertia and centrifugal-load components tend to reduce the eccentricity in the same manner as was found in the experiments.

In view of the foregoing, it is entirely possible that troublesome whirling in sleeve bearings, subjected to alternating loads at one half the shaft speed, can be reduced to a safe operating level by the addition of a rotating load at the frequency of shaft rotation. This could be accomplished by purposely introducing some unbalance in the rotating members and damping the resulting vibration.

Acknowledgment

The author is indebted to the National Advisory Committee for Aeronautics for permission to present this paper.

Grateful acknowledgment is due Dr. R. W. Dayton for his able advice in carrying out this work.

BIBLIOGRAPHY

1 "The Hydrodynamical Théory of the Lubrication of a Cylindrical Bearing Under Variable Load, and of a Pivot Bearing," by W. J. Harrison, Trans. Cambridge Philosophical Society, London, England, vol. 22, 1919, pp. 373–388.

2 "Whirling of a Journal in a Sleeve Bearing," by D. Robertson, *Philosophical Magazine*, vol. 15, 1933, pp. 113–130.

3 "Fluctuating Loads in Sleeve Bearings," by H. W. Swift, *Journal of the Institution of Civil Engineers*, vol. 5, 1936–1937, pp. 161–195.

4 "Alternating Loads on Sleeve Bearings," by J. Dick, *Philosophical Magazine*, vol. 35, 1944, pp. 841–848.

5 "Note on the Hydrodynamic Theory of Journal Bearings," by J. C. Bell, *Physical Review*, vol. 68, 1945 (abstract), pp. 101–102.

6 "Calculation of the Performance Characteristics of Plain Bearings," by A. Frankel (from *Mitteilungen aus dem Institut für Thermodynamik und Verbrennungsmotorenbau*, Eidgenossische Technische Hochschule, Zurich, Switzerland), *Engineers' Digest*, vol. 3, 1946, (*a*) pp. 223–228; (*b*) pp. 287–290; (*c*) pp. 400–403, and (*d*), pp. 465–468.

7 "The Calculated Performance of Dynamically Loaded Sleeve Bearings," by J. T. Burwell, Journal of Applied Mechanics, Trans. ASME, vol. 69, 1947, p. A-231.

8 "Lathe Fixture Bores to Exceptional Tolerances," by R. W. Dayton and C. M. Allen, *American Machinist*, vol. 93, Feb. 10, 1949, pp. 89–91.

9 "The Influence of Oil-Film Journal Bearings on the Stability of Rotating Machines," by A. C. Hagg, Journal of Applied Mechanics, Trans. ASME, vol. 68, 1946, p. A-211.

10 "Capacitive Micrometer," by R. W. Dayton and G. M. Foley, *Electronics*, vol. 19, 1946, pp. 106–111.

11 "Shaft Whipping Due to Oil Action in Journal Bearings," by B. L. Newkirk and H. D. Taylor, *General Electric Review*, vol. 28, 1925, pp. 559–568.

12 "Oil-Film Whirl—A Nonwhirling Bearing," by B. L. Newkirk and L. P. Grobel, Trans. ASME, vol. 56, 1934, pp. 607–615.

13 "The Influence of Oil-Film Journal Bearings on the Stability of Rotating Machines," by H. D. Taylor, Journal of Applied Mechanics, Trans. ASME, vol. 69, 1947, p. A-77.

14 "The Thick-Film Lubrication of Full Journal Bearings of Finite Width," by M. Muskat and F. Morgan, Journal of Applied Mechanics, Trans. ASME, vol. 61, 1939, p. A-117.

15 "The Full Journal Bearing," by A. Cameron and Mrs. W. L. Wood, paper presented to The Institution of Mechanical Engineers, May 2, 1947.

16 "Load-Carrying Capacity of Journal Bearings," by A. F. Underwood and J. M. Stone, SAE Quarterly. Trans. vol. 1, January, 1947, pp. 56–57.

17 "Personal Communication to the National Advisory Committee for Aeronautics," by J. T. Burwell, Nov. 29, 1948.

Discussion

J. T. **Burwell.**[3] The author is to be congratulated on having developed a most ingenious method for observing the instantaneous position of a journal inside a bearing and of using the method to study the performance of the journal bearing under various loading conditions. This information has been badly needed in order to provide a check on the theory of hydrodynamic lubrication upon which we are beginning to base design calculations for dynamically loaded bearings. It is interesting that a good many of the results of the simple theory such as the position of the journal under loads, its path under alternating loads, and oil-film rupture are now confirmed experimentally by this work. This gives us confidence that the theory can be used safely for the design of bearings subjected to varying loads. In this connection it is even more fortunate that the deviations from the simple theory that are found in the present work appear to be on the conservative side.

There appear to be five main discrepancies between the present experimental results and the predictions of the simple theory, as follows:

1 The shaft does not whirl in this apparatus under no-load conditions.

2 The transient whirl upon starting has a frequency slightly less than one half the shaft speed.

3 The shaft does not move in a periodic orbit under a constant unidirectional load.

4 The eccentricity ratio does not become unity under a constant load rotating at one half the shaft speed.

5 The eccentricity ratio does not become unity under a sinusoidal alternating load having a frequency of one half the shaft speed.

It is possible that all these discrepancies can be ascribed to a single cause. For instance, regardless of the exact nature of the cause, all five discrepancies are consistent with the single conclusion that a journal center rotation N_e equal to one half the shaft speed N_j is not for this bearing a natural or critical frequency. However, the explanation of this conclusion is not at all obvious.

It has been suggested that the absence of the periodic motions under no-load and under constant-load conditions must be due to damping forces not taken into account in the theory. For this reason the oil-drag forces on the whirling shaft have been reexamined to see whether they could be the source of the damping. It is found that their resultants parallel to and perpendicular to the line of centers are of the order of c/r times the corresponding resultants of the film pressures. This makes them equal to about 0.1 per cent of the film-pressure forces in the present experiments. More importantly it is difficult to understand how any forces of this nature can damp out these motions, since energy is being continually fed in by the rotating shaft. Rather, it would appear that positive forces directed radially inward are required to drive the journal center to the center of the clearance circle under no-load conditions as shown in Fig. 2 of the paper. The source of such radial forces, in the absence of oil-film rupture, is difficult to see unless it is a stiffness caused by the support bearing.

The oil-drag forces were found to give rise to a whirling speed very slightly less than one half the shaft speed, but unfortunately not in good agreement with the speed actually found. The expression for the ratio of the two speeds is

$$\frac{N_e}{N_j} = \frac{1}{2} - \frac{1}{12} \cdot \frac{c}{r} \cdot \frac{2+\eta^2}{\eta^2} \left(1 - (1-\eta^2)^{1/2}\right) \ldots\ldots [1]$$

where the symbols are as defined in the original paper. For a value of η near unity this becomes approximately

$$\frac{N_e}{N_j} \simeq \frac{1}{2} - \frac{1}{4} \cdot \frac{c}{r} \ldots\ldots [2]$$

With the dimensions of the present apparatus, this would lead to a value of N_e/N_j of approximately 0.4998 instead of 0.4980, as actually observed. The difference from $^1/_2$ becomes even less as η decreases. Furthermore, Equation [1], herewith, predicts no dependence of this ratio on shaft speed as shown by the data in Table 1 of the paper.

Since many lightly loaded shafts do show oil whip in practice, the conclusion of its absence in the present case cannot be entirely general. Possibly it is due to the absence of dynamic unbalance forces owing to the simple structure and the great accuracy with which the present shaft was made.

Turning to the last two disagreements with the theory, it seems most likely, as the author suggests, that the explanation of the two is the same. This is because the sinusoidal loading was found to induce a circular orbit having half the shaft speed, which is just the same orbit as that induced by the constant load rotating at this speed. The orbit, rather than the applied load, directly determines the pressure distribution in the oil film.

The writer has suggested that the explanation for these two discrepancies is probably to be found in the thermal expansion of the oil which was first suggested by Fogg[4] to explain the load capacity observed in certain high-speed thrust bearings. This seems to be borne out by the strong dependence of the discrepancy on speed, since one would expect the amount of expansion which determines the load capacity to be dependent on the power consumption which is proportional to μN^2 rather than to μN for a purely hydrodynamic effect.

Furthermore, the resultant oil-film pressure due to thermal expansion will probably have a component parallel to the line of centers which can drive the journal toward the center of the clearance space. As discussed previously, this seems to be necessary to suppress its periodic motions under constant and no-load conditions.

It might be interesting to see whether there is some interrelation between the five discrepancies. For instance, the results in Table I of the paper indicate that while the journal will not whirl indefinitely, yet it does prefer a frequency slightly less than one half the shaft speed. This suggests that under a constant load rotating at one of the speed ratios given in Table 1, the eccentricity ratio might approach unity more closely than it does for the load rotating at exactly one half the shaft speed. Has the author tried this?

Nevertheless, in spite of the absence of any very satisfactory explanation the absence of the whirling and periodic motions under constant or no load is reassuring when using the theory to calculate the journal center path under sinusoidal and more complicated forms of loading such as occur on actual connecting-rod bearings. The solutions were obtained on the assumption[5] that all transients arising from such motions would be absent and that only a steady-state motion, having the frequency of the applied load, would exist. The general agreement of the shape of the orbits shown in Figs. 9 and 10 of the paper, for a sinusoidal alternating load with those calculated under this assumption,[6] give us confidence that calculations of more complicated types of loading on this assumption will be correct. In the absence of this assumption the calculating problem becomes so complicated as to be well nigh impossible of solution.

---

[3] Massachusetts Institute of Technology, Cambridge, Mass.

[4] "Film Lubrication of Parallel Thrust Surfaces," by A. Fogg, *Engineering*, vol. 159, 1945, p. 138.

[5] Reference (7), author's bibliography.

[6] Ibid., Fig. 6.

E. F. Macks.[7] In 1946 the paper by Underwood and Stone[8] verified experimentally the theory that a sleeve bearing would fail if subjected to a rotating load at one-half shaft speed, and to quote from the paper:

"It should be especially noted that the critical speed for zero load capacity is reached when the journal is twice the load speed. This proportion was proved for all journal speeds."

Now, however, another apparently very carefully prepared experimental paper appears which presents results some of which differ significantly from those of Underwood and Stone.

There are many very valuable experimental contributions given in this paper, but we feel the main thing in this report is the fact that an attitude of one was not obtained either with constant rotating load or sinusoidally alternating load at the theoretically critical speed; and the dependence of the attitude particularly upon speed but also upon viscosity and load. Since there is such a wide difference from theory, this work indicates either (*a*) that the theory must be revised to include terms which have been previously considered negligible or which have been entirely omitted, or (*b*) to find out what unique feature of the test machine contributes to the development of a hydrodynamic film in the test bearing.

Regarding possible changes in theory, the author's suggestion of thermal expansion may be a partial answer, but it should be recalled that in the equivalent system, that is, with respect to a fixed point on the load vector, there is no net flow circumferentially in the region of minimum film thickness, and therefore for any hot oil to be continually replaced, it must depend upon adherence to the moving members and upon side leakage. Also, inasmuch as the flow varies as the cube of the clearance, there will be little end flow in the region of the minimum film thickness.

Regarding the test machine, misalignment has been shown to be important, but we do not feel that it is the whole story. There may be something either in the test bearing or inherent in the test machine which prevents an attitude of one from being obtained under the critical conditions. We would like to ask the author if there is any possibility that the loading system—say, the loading springs involved or the manner in which the load is applied, or anything else—might contribute to a vibration conducive to the generation of a squeeze film or an unknown superimposed load on the test bearing. Also, any movement of the test-bearing housing is extremely critical, since the micrometer probes are attached to the housing. Is this a possibility? May we also ask if the author has found during operation that changes of speed or load affect the alignment and to what extent; and if he feels that such alignment changes may invalidate any of the results obtained or reported before it was discovered how sensitive the machine was to misalignment?

We feel that it would be well for the author to explain the care which was required to obtain a true clearance circle and the effect of a film on either the bearing or journal during this calibration, and also to mention how the oil-film temperature was determined to obtain the value of viscosity used in the calculation of the Sommerfeld number.

S. M. Marco.[9] Bearing theory has advanced through many stages from the time of Petroff and Osborne Reynolds to the present. Although many papers have been written concerning both theoretical and experimental investigations of bearings, nevertheless the agreement between theory and experiment remains qualitative rather than quantitative. The true purpose of both theoretical and experimental investigations of bearings is to supply information to the designer so that he may arrive at bearing designs which are better. In general the situation at present is that the designer of bearings cannot rely too heavily on theory or experiment. He is forced to design bearings largely by trial and error, relying on his own experience and that of other designers to guide him in his selection of the various factors which affect the operation of a real bearing. The plain fact is that real bearings do not act in the way which theory predicts except in a qualitative sense. It is for this reason that those of us who are interested in the design field welcome all investigations which will lead eventually to a better understanding of the factors which affect the operation of a real bearing.

It seems to the writer that the investigation reported in this paper could well be the beginning of a long-time investigation which would lead eventually to an understanding of the relative importance of deviations of actual bearing conditions from those which we are forced to assume in theoretical bearings. Such things as the effect of shaft deflection, the effect of restraints caused by adjacent bearings, the effect of complex periodic loading, and numerous other similar factors must be investigated if the designer is to be supplied with reliable quantitative information.

That the investigation reported by the author shows some of the discrepancies between bearing theory and experimental bearings is brought out in a number of instances. For example, this work shows that for the conditions of this test bearing, whirl in the absence of a periodic disturbing force is always damped out, whereas theory predicts that a steady-state whirl should be produced. Undoubtedly, this is due to the neglect in the theory of such damping forces as oil drag, shaft stiffness, constraints imposed by adjacent bearings, and the like. In this connection, would the author explain some of the factors which might be inferred from the paper but which are not explicitly stated? For example, in Fig. 2 does the exposure time indicate accurately the total length of time for damping to reduce the amplitude of whirl to zero? It would be of interest to know if the frequency of whirl is constant for a given set of conditions, i.e., does the frequency of whirl remain constant while the amplitude is decreasing? If it is, it would indicate a common type of damped vibration—a conclusion that might give a clue as to the type of damping involved. Apparently higher speed reduces the time required for damping but does it reduce the number of cycles required to bring the amplitude to zero? This is not quite clear from Fig. 2(*b*) and (*c*). The effects of load, lubricant viscosity, and feed pressure on damping are somewhat obscure. Also, it would be of interest to have the author explain the method of measuring the speed of whirl with the precision indicated in his Table 1.

In describing the unidirectional steady-load tests, the author states that upon starting from rest, this journal did not start to roll along the bearing wall as is commonly assumed. This is the action which is usually assumed when the journal has squeezed out sufficient oil so that dry friction exists. This paper does not indicate how fully this matter was explored. Fig. 3 of the paper indicates a bearing pressure of 50 psi which is a fairly low pressure. It is possible that because of the low pressures involved, the oil was never squeezed out completely, and therefore no dry friction resulted. Would heavier loads have resulted in the journal rolling along the bearing wall until a film had been built up? Since this is an important factor in bearing wear, this matter should be investigated thoroughly.

The work on oil-film rupture, as affected by feed pressure, is of great interest. The results of this work would indicate that most practical bearings, with the exception of a very few using extremely high lubricant feed pressures, operate with a partial film only. Since the theory of film lubrication predicts friction coefficient and load-carrying capacity on an assumed continuous film, it would appear again that the theoretical bearing is so different from the practical bearing that predictions based upon theory may well be completely unsafe for design purposes.

---

[7] Flight Propulsion Research Laboratory, NACA, Cleveland Airport, Cleveland, Ohio. Jun. ASME.

[8] Reference (16), Author's bibliography.

[9] Professor of Mechanical Engineering, The Ohio State University, Columbus, Ohio. Jun. ASME.

The investigation of rotating and sinusoidally varying loads brings out some interesting facts. Figs. 6 and 11 of the paper show that while a ratio of load frequency to shaft frequency of one half is serious, it does not result in a complete breakdown of the supporting film. Fig. 13 shows that a rotating load at shaft frequency, superimposed on a sinusoidal load at one-half shaft frequency, results in a lower eccentricity than for the case of the alternating load alone. The author states that this may be the reason that four-stroke-cycle engine crankshaft bearings can operate with complete film lubrication. It would take considerably more investigation with higher specific loads to prove this.

However, the writer feels that the fact that a thin film exists with sinusoidal load, i.e., the eccentricity ratio is not unity, is the reason that such bearings operate. The work of Needs[10] would indicate that for a given bearing geometry, a larger eccentricity will support greater loads than will smaller eccentricities for the same oil viscosity and peripheral speed.

In the writer's opinion, Figs. 7 and 12 of the paper are of extreme importance since they show definitely that the Sommerfeld number is not an adequate parameter for describing the eccentricity of a bearing subjected to nonstatic loading.

It is to be hoped that the author of this paper can be encouraged and supported in a continuation and extension of this important piece of research.

B. L. Newkirk.[11] One item of especial interest in the paper is the indication of tensile stress in the liquid in the top of a full bearing. Under laboratory conditions, liquids have shown very considerable tensile strength. There has been doubt about the development of such strength in the lubricating film in apparatus under operating conditions. The presence of minute bubbles in the oil, or impurities which might promote the formation of bubbles, might inhibit the development of tensile stress in the liquid. In these experiments such tensile stresses amounting to perhaps 45 psi seem to have developed when a load of 50 psi was carried with a feed pressure of 15 psig. This is on the assumption that the peak negative pressure in the upper half is 3 times the average negative pressure of 25 psi. It would be interesting to know whether bearings in service could be counted on to behave reliably in this manner, what the effect of impurities in the oil would be, and whether higher feed pressures would produce higher tensile stress in the film. Theoretical values of tensile strength of liquids are very high. Possibly they may be realized in bearings.

The whirling shown in Fig. 2 of the paper is not the "oil-film whirl" which sometimes appears as a disturbing factor in the operation of machines. Such whirling develops when a machine runs at some speed that is approximately twice the shaft critical speed, or at some higher speed. There is an interaction between the elastic behavior of the shaft, and the oil film, and the shaft whirls at a frequency determined by its stiffness and the load it carries, while rotating at a much higher frequency. This model has a very stiff shaft carrying no load except its own weight. The critical speed would be far above the speeds of these tests.

The possibility that a journal might whirl with a whirl speed equal to one-half running speed was pointed out in 1925.[12] The studies made at that time indicate that such a tendency did exist in an unloaded bearing during continuous operation, at all speeds up to as high as 2250 rpm, but that it is feeble and easily suppressed.

H. Poritsky.[13] This writer was particularly impressed by the verification loads of the predictions of the complete journal theory at low loads, where the displacement is perpendicular to the load, and the discrepancy between theory and tests at higher loads where the displacement has a component perpendicular to and one in the direction of the load. The explanation, as pointed out by the author, surely lies in the fact that the generally available theory requires the existence of negative pressures in the oil. While negative pressures up to a certain point might be sustained by oil, beyond that point the oil will foam, and the theory has to be modified correspondingly. When that is done, no doubt some of the discrepancies between existing "theory" and experiment will be eliminated.

In regard to the amplitudes of vibration or whirl in case of rotating and sinusoidally alternating loads, the writer's unpublished studies of some 10 years ago have shown that here, too, the discrepancy may be ascribed to negative pressures. Most of the published analytical studies of oil whirl show that a rotor should be unstable at all speeds, whereas, as has been discovered by Dr. B. L. Newkirk,[12] instability exists only at speeds above double the critical speed. When one takes into account the component of displacement in the direction of the load (due to the failure of the negative oil pressures required by theory), it is possible to show that this discrepancy may be largely explained. No doubt the displacement under sinusoidal loads can similarly be explained.

A. F. Underwood.[14] This paper is helpful in bringing further attention to dynamically loaded bearings by contributing experimental results. It has become clear that no longer can we treat such bearings as statically loaded bearings.

The author points out that the study is not complete, and that further work is being done to investigate the existence of an oil film at the critical speed. The machine used to conduct the tests is extremely rigid in relation to the very light loads imposed on it, compared to most commercial machines. The highest eccentricity reported is 0.8 whereas many dynamically loaded bearings operate above 0.95. Although no failures caused by zero oil-film thickness were found by the author, we have had failure of bearings under 25 psi when operating at the critical speed. Other cases have come to our attention, in which bearing failure occurred when running at critical speeds, and we feel it is highly desirable to design bearings well outside of such conditions until the reasons for the results reported in this paper are understood thoroughly.

It is interesting to note the damping effect of higher lubricant pressure demonstrated in Fig. 2 of the paper. In tests reported previously,[15] it was necessary to reduce the supply pressure to a very low value to stop the damping. Probably the effect would be less important if the bearing pressures were raised.

We are wondering how accurately the gas pressure on the bearings of a four-cycle engine can be considered a true critically applied load. It is applied every other revolution, but each alternate revolution has practically no "half-speed" load during which time the oil film can be re-established.

---

[10] "Effect of Side Leakage in 120-Degree Centrally Supported Journal Bearings," by S. J. Needs, Trans. ASME, vol. 56, 1934, p. 721.

[11] Professor of Vibration, Practice and Theory, Rensselaer Polytechnic Institute, Troy, N. Y. Mem. ASME.

[12] "Shaft Whipping Due to Oil Action in Journal Bearings," by B. L. Newkirk and H. D. Taylor, *General Electric Review*, vol. 28, August, 1925, p. 559.

[13] Consulting Engineer, General Electric Company, Schenectady, N.Y. Mem. ASME.

[14] General Motors Research Laboratory, Detroit, Mich.

[15] Reference (16), author's bibliography.

The author suggests the use of an unbalance to reduce whirl when alternating loads are imposed at one half the shaft speed, and then damp the resulting vibrations. Another solution, when three or more bearings are in a machine, is to unbalance each one individually to apply a stabilizing load. However, by applying these loads so as to give an over-all balance to the machine, there will be very little resulting vibration transmitted to the mountings.

AUTHOR'S CLOSURE

Dr. Burwell raises the interesting point that, since the natural whirl frequency of this journal is slightly less than one half the shaft speed, a constant load rotating at this natural frequency might produce an eccentricity ratio closer to unity than does a load rotating at exactly one half the shaft speed. Unfortunately, no experiments of this nature have been tried, since the camshaft change gears do not permit the required frequency ratio of 0.498 or 0.497. However, the author feels that this idea has sufficient merit to warrant the installation of a separate variable-speed camshaft drive to check this point. This will be done at an early date.

With regard to Mr. Macks' question concerning the possibility that some phenomenon associated with the loading system might be responsible for eccentricity ratios less than unity when $N_p/N_j = 0.5$, recent efforts have been directed toward resolving this question. The natural frequencies of the loading springs are well outside the operating-speed range. However, preliminary measurements indicate that there is a small amount of relative motion between the test-bearing housing and the support-bearing housing, when the machine is running with a rotating load. This motion appears to occur at the loading frequency and amounts to several ten-thousandths of an inch in the axial direction at the shaft center line. No transverse motions were observed. The significance and exact mechanism of this movement are not yet known.

The only precaution which was necessary to obtain a good clearance circle was to be sure that the manual rotation of the load was accomplished slowly. Approximately 1 min for a complete revolution was found to give a maximum clearance circle. It is felt that any surface films remaining on the bearing or journal would be too thin to affect the pattern at the micrometer magnifications used. The oil temperature was measured by thermocouples in the feed lines just before the oil entered the bearing.

In response to Professor Marco's questions concerning Fig. 2 of the paper, the exposure times represent the actual periods during which the camera shutter was open. They are thus somewhat longer than the exact duration of the whirling motion. Unfortunately, little quantitative information concerning damping can be derived from Fig. 2 because of this and because the periods of acceleration from rest to the whirl frequency are not known. Considerably more work is needed to ascertain precisely why high load, low viscosity, and high feed pressure produce the whirl-damping effects observed.

In the method used for determining the very exact ratios of N_e/N_j listed in Table 1 of the paper, only the departures from a precise 1:2 ratio were measured. The technique consisted of attaching a narrow piece of adhesive tape axially on the shaft at a point where it passed under the area of measurement of the probes. Because of the different dielectric constant of the tape compared to air, there was a distinct kick on the oscilloscope screen each time the tape passed under a probe. Since the spindle rotated approximately twice for each orbital revolution, and a kick was registered by each of the two probes, the pattern on the oscilloscope screen consisted of a circle with four distinct kicks. If the speed of orbital rotation were precisely one half the speed of shaft rotation, this pattern would remain stationary. Any departure from this precise 1:2 ratio was indicated by a slow rotation of the pattern, which could be timed easily. From the frequency and direction of this rotation, a very accurate value of N_e/N_j could be calculated.

Another point raised by Professor Marco concerns the fact that Fig. 3 shows no evidence that this journal started to roll along the bearing wall, when started from rest. It is possible that, in the tests, the loads were too light to squeeze out the oil film and permit dry friction. This matter was not explored fully.

The author agrees with Professor Newkirk that the matter of tensile stresses in journal-bearing oil films merits further consideration. Some qualitative studies were made with a lucite bearing on a steel shaft, observing the film conditions with ultraviolet light. The lubricant was introduced at a point source in the unloaded region of the bearing. It was found that film rupture started in localized areas on both sides of the oil hole, the evacuated areas extending, at times, for some distance circumferentially, but seldom reaching axially to the outside edges of the bearing. These observations led to the belief that film rupture, originating in a highly localized region of peak negative pressure and extending over only a small fraction of the bearing length, results in a redistribution of pressures on the unloaded side of the journal. Only when the load becomes high enough to rupture the film over a sizable fraction of the bearing area does the shaft move in the direction of the load, the amount of motion, and, hence the eccentricity, depending upon the extent of the rupture. The observations were only qualitative, since the lucite distorted under the influence of load and temperature. A glass bearing has been made to permit more exact tests, but no experiments have been run with it as yet.

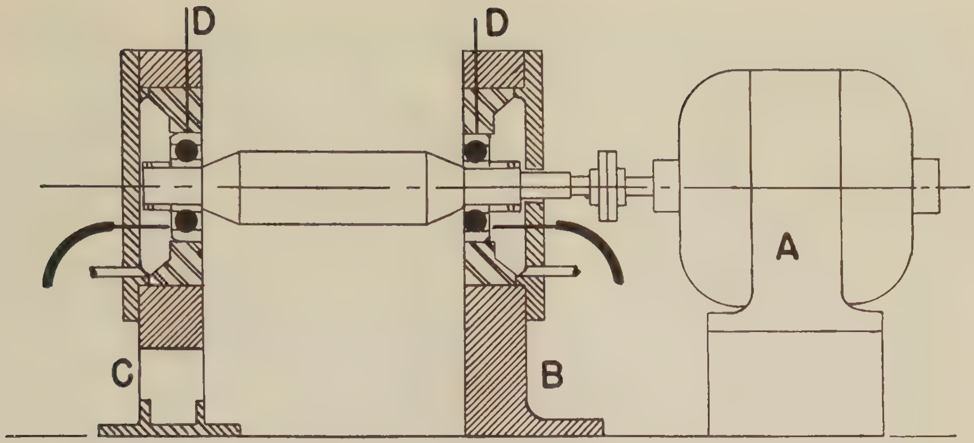

Fig. 1 Diagram of Test Equipment
(A, motor; B, fixed pedestal; C, flexible pedestal; D, thermocouples.)

The Mechanism of Lubrication Failure in High-Speed Ball Bearings

By F. C. JONES[1] and D. F. WILCOCK,[2] WEST LYNN, MASS.

When lubrication fails, the first point of distress in a high-speed ball bearing occurs at the rolling contact between a ball and a race. Because of the curvature of the race, sliding as well as rolling must occur in the contact area. Hence the absence of an oil film results in friction and heat. The localized heating and resultant differential expansion of the parts cause preloading of the bearing owing to loss of internal clearance. This process progresses rapidly to cause spalling or pitting of the races and balls, skidding balls, broken ball separators, and a jammed bearing.

Introduction

Operating conditions for antifriction bearings are becoming severe in certain applications; and today large bearings are being operated at high temperatures, high loads, and relatively high speeds. To meet these conditions, forced oil lubrication of the bearings has been necessary, particularly in order to help keep the bearings cool and to provide positive assurance of lubrication.

In machines with direct-connected oil pumps, there may be a short period during starting in which no oil will flow to the bearing, and therefore it becomes important to determine whether this situation might prove dangerous to the bearing. In a recent study,[3] an improvement in roller bearings was described which permits operation for extended periods without fluid lubrication. Three factors in addition to the material improvement make this type of operation possible, namely, (1) the pure rolling nature of the contact between rollers and races, (2) the light loading on the sliding surfaces between rollers and roll separator, and (3) the relatively large internal clearance. It was felt that the ball bearing, because of the nature of the rolling contact, would be much more marginal in its lubrication requirements.

Tests on high-speed ball bearings were arranged, under various conditions of lubrication. Examination of bearings after partial failure has provided interesting information as to the route by which failure occurs. Despite the opinion which is sometimes expressed,[4] that the oil film is unimportant between balls and races because of the high pressures generated beneath the ball, these experiments have shown that it is precisely in the area between ball and race that the initial distress appears when the lubricant is depleted.

Test Apparatus

The ball bearings used in these tests are 50-mm-bore medium-series precision ball bearings, No. 310. Each bearing contains a complement of eight $^3/_4$-in. balls, separated by a two-piece riveted retainer of laminated cloth-base phenolic material. The retainer is guided by the inner-race shoulders. The total radial internal clearance of the test bearings varies from 0.0013 to 0.0018 in.

The test equipment is shown in Fig. 1. It consists of a shaft carried by two of the No. 310 bearings and direct-coupled to a two-pole high-frequency motor. Motor power is furnished by a frequency changer. Motor speed is 13,200 rpm. A radial load of 19 lb is applied to each bearing due to the weight of the shaft. A thrust load of 300 lb is applied by adjusting the position of the bearing carrier in the flexibly mounted housing, in order to obtain the necessary deflection of the supporting reeds, as measured by a dial indicator.

---

[1] Thomson Laboratory, General Electric Company.

[2] Thomson Laboratory, General Electric Company. Mem. ASME.

[3] "Improved High-Speed Roller Bearings," by D. F. Wilcock and F. C. Jones, *Lubrication Engineering*, vol. 5, June, 1949, p. 129.

Contributed by the Research Committee on Lubrication and the Petroleum Division and presented at the Annual Meeting, New York, N.Y., November 27–December 2, 1949, of The American Society of Mechanical Engineers.

Note: Statements and opinions advanced in papers are to be understood as individual expressions of their authors and not those of the Society. Paper No. 49—A-36.

[4] "Methods of Lubricating High-Speed Ball Bearings," by A. F. Brewer, *Machinery Magazine*, vol. 55, 1948, pp. 172–178.

The bearing in the fixed coupling end housing is lubricated with 0.5 gpm of AN-O-8 grade 1065 oil, and functions as a guide bearing. The test bearing is located in the flexibly mounted housing and is lubricated as desired for each test. The test-bearing outer-race temperature is measured with an iron-Copnic thermocouple which is spring-loaded against the outer race.[5] A high-speed G-E potentiometer-type photoelectric recorder is used to record the temperature-time curve during testing. A very rapid rise in temperature signals the depletion of the lubricant supply after which the test shaft usually is stopped as quickly as possible. After removal from the test shaft, the failed bearing is cut open for examination.

EXPERIMENTAL RESULTS

As part of the study of the amount of lubrication necessary in the ball bearing, a series of bearings were prepared with varying amounts of oil on the surfaces; and the length of time before a lubrication failure occurred was noted. Minute amounts of oil were added by immersing each bearing in oil solutions of varying concentrations. Because of slight oil absorption in the separator material, accurate determinations of the weight of oil added were not possible. The following schedule was followed in oil-coating the bearings:

1 Cleaned and soaked in solvent.
2 Air and furnace dried.
3 Cooled in a desiccator.
4 Soaked in a dilute oil-solvent solution.
5 Air and furnace dried.
6 Cooled in a desiccator.
7 Installed in the testing machine.

The running time to failure was found to be roughly proportional to the concentration of oil in which the bearing had been dipped, as shown in Fig. 2. By dipping an outer and inner race separately in a 5 per cent solution, the weight of oil added to the steel parts is estimated to be 13.5×10^{-6} gm per sq cm, which corresponds to a layer 12 Ångstroms thick, or about one molecular layer. Additional oil undoubtedly is absorbed at the separator surface and transferred to the balls in the actual bearing tests. No separator failures occurred during this testing.

The tests were stopped as soon as temperature rise of the outer race was noted. Fig. 3 shows a typical temperature record for the final portion of the test. The appearance of a bearing outer race after a partial failure is shown in Fig. 4. Three pitted areas in which sliding has occurred separated by two narrow shiny bands where only rolling took place are clearly visible. All the bearing

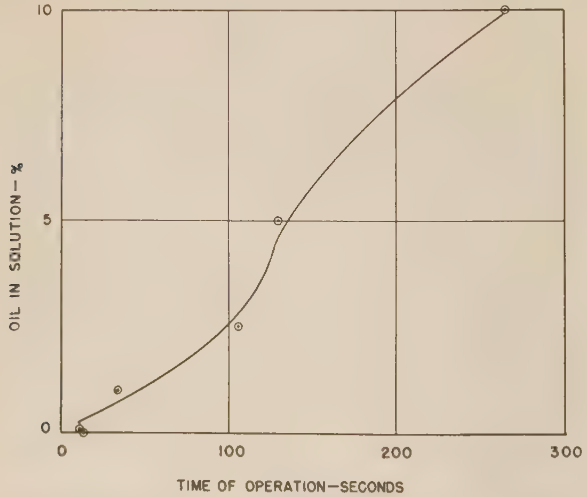

Fig. 2 Variation in Running Time With Concentration of Oil Solution in Which Bearing Was Dipped

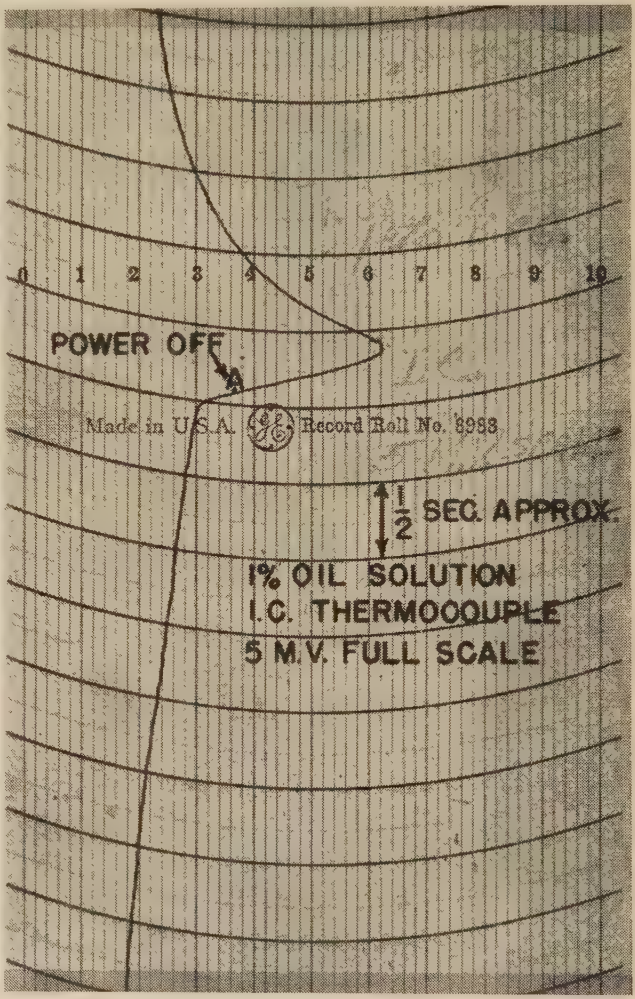

Fig. 3 Typical Chart Showing Rapid Temperature Rise at Beginning of Unlubricated Period

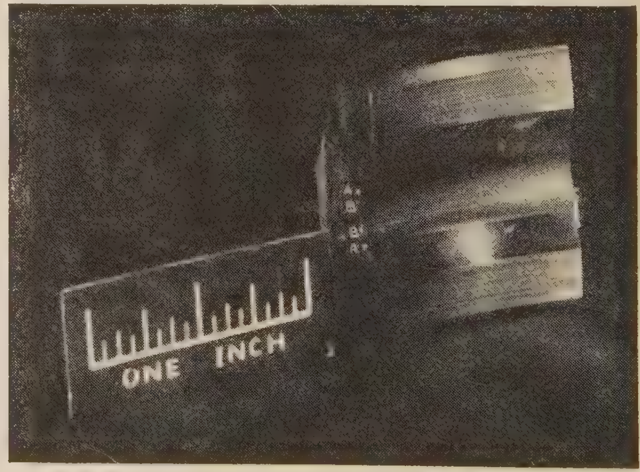

Fig. 4 Close-Up of Portion of Bearing Outer Race After Partial Failure, Showing Alternating Bands of Sliding and Rolling Contact

(A-A edges of track; B-B lines of rolling contact.)

---

[5] "Grease—An Oil Storehouse for Bearings," by D. F. Wilcock and M. Anderson, Special Technical Publication No. 84, ASTM, 1948, see p. 36.

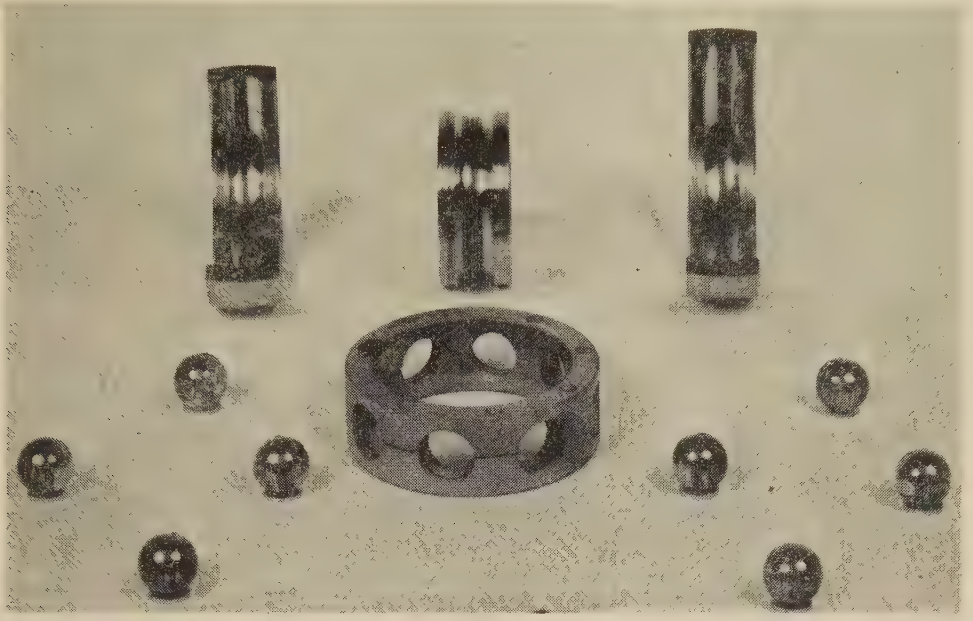

FIG. 5 BEARING PARTS AFTER PARTIAL FAILURE

parts are shown in Fig. 5 which illustrates the tracking which occurs on the balls and inner race, as well as on the outer race. Three other tests were made which are of interest. These are as follows:

1 A run using a large mass on the shaft to increase the radial load to 100 lb. A dry bearing was used, and no time could be recorded, since the bearing had not come up to speed before failure. The races and balls were darkened and covered with steel flakes. The separator broke during this failure, probably because of the greatly increased inertia of the weighted shaft which prevented the usual rapid stop.

2 A run was made in which the bearing was partially failed and then run with jet-oil lubrication. No complete failure occurred; and, although noisy, the operation was satisfactory during a 2-hr run.

3 A run was made carrying the failure beyond the point of rapid temperature rise. In this case the bearing seized without separator failure. There were steel flakes rolled onto the races and balls.

To investigate the possibility that the initial lubrication failure occurred between ball and race and not at the separator because of the better bearing characteristics of the phenolic separator, some tests have been made on standard No. 306 bearings with pressed-steel separators at speeds of 900 to 3600 rpm. These bearings also were lubricated with very small quantities of oil, of the order of 1 mg, applied from a 2 per cent solution in benzene. They were stopped at the first sign of distress, either noise or temperature rise. When the bearings were cut open, tracks were observed on the races similar to those in Fig. 4, but they were too faint to photograph readily. No marking or evidence of wear could be found on the steel surfaces of the separator, indicating again that the area of initial lubrication failure is between the ball and the race. When the bearings were not stopped immediately at the first sign of distress, very pronounced tracks were produced on the races together with brown iron-oxide powder. At this stage, some marking of the separator had taken place also.

DISCUSSION OF FAILURE CONDITIONS

The tracking observed on the races and balls after a partial failure is an interesting verification of the conditions beneath a loaded ball which are predicted mathematically. The two shiny bands separating the three pitted strips in each track correspond to the lines where pure rolling motion occurs, sliding occurring over the balance of the area of contact.

A section of a ball bearing is shown in Fig. 6, indicating the loaded area between a ball and the outer race. Because of the differences in radii between the axis of rotation of the ball and the contact point with the outer race, the surface travel for a given angular rotation will vary from point to point, and, in general, will not agree with the corresponding portion of the outer-race circumference traversed by the ball. Thus if

r = the maximum distance from the axis of rotation of the ball to a point in the contact area

$r_1 = r - \Delta$ is distance to some other point in contact area

R = maximum radius of outer race

$R_1 = R - \Delta$ is outer-race radius corresponding to r_1

then the number of revolutions of the ball per revolution around the outer race is

$$n = \frac{2\pi R}{2\pi r} - 1 = \frac{R}{r} - 1 \qquad [1]$$

and

$$n_1 = \frac{2\pi R_1}{2\pi r_1} - 1 = \frac{R - \Delta}{r - \Delta} - 1 \qquad [2]$$

if no slip is assumed. It is apparent at once that since $R \neq r$, n is not equal to n_1, and hence slip must occur. The ball must then roll in such a way that the forces due to sliding will balance as shown in Fig. 6. Sliding will occur in opposite directions in the areas marked A and B, and the boundaries between these areas represent the lines of rolling contact.

It is interesting to note that the ratio of the separation of the lines of rolling contact to the major diameter of the ellipse of contact is independent of the shape of the ellipse if it is assumed that the frictional force per unit area is constant and hence, that the areas A and B are equal. The calculated ratio of spread to major

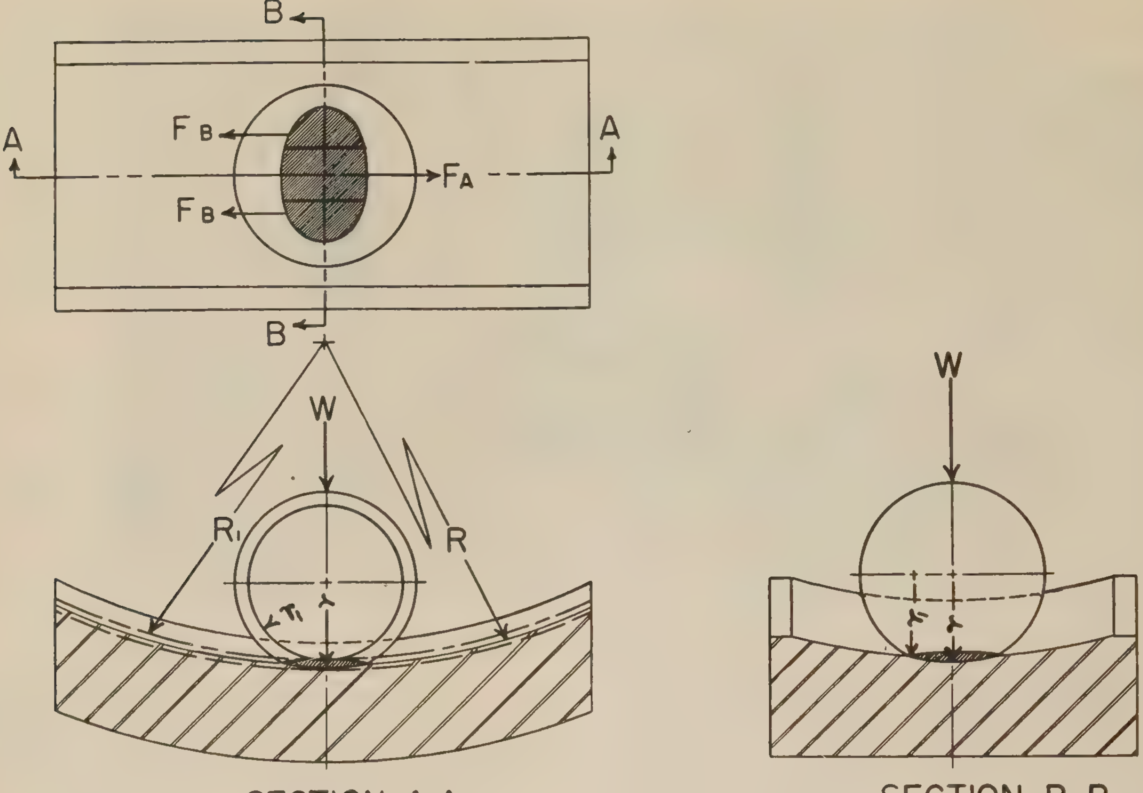

SECTION A-A

SECTION B-B

Fig. 6 Sketch of Ball Bearing Under Radial Load

diameter compares with the ratio measured on the outer race shown in Fig. 4 as follows:

$$\text{Calculated} \ldots\ldots\ 0.405$$

$$\text{Measured } \frac{0.0985}{0.246} = 0.400$$

The bearing shown in Figs. 4 and 5 had a total internal radial clearance of 0.0015 in., and a maximum load per ball of 140 lb. Other pertinent bearing dimensions are as follows:

Radii of outer race ....—1.950 in., —0.397 in.
Radii of inner race .... +1.199 in., —0.387 in.

Application of the Hertz equations[6,7] gives an outer race track width of 0.11 in. for the normal load of 140 lb plus the centrifugal load of 68 lb.

The observed track width of 0.246 in. corresponds to a ball load of about 2100 lb, or 15 times the normal load. The only logical source of a load of this magnitude is from preloading of the bearing caused by expansion of the balls due to the frictional heat. Thus this load was acting only after depletion of the lubricant supply and until the shaft was stopped. Maximum stress beneath the ball in the preloaded condition approaches 400,000 psi which, taken together with the frictional forces, appears ample to cause the spalling or pitting observed. The calculated interference required to create a ball load of 2100 lb is 0.003 in. on each side of the bearing or 0.006 in. total. If it is assumed that it is the balls which heat most rapidly from the friction, a temperature difference of about 800 F between balls and races is estimated. If it is assumed that the balls and inner race both expand, a temperature difference of about 250 F is estimated. The hardness of the balls in the tracked area after test is 61-62 Rockwell C, so that it is doubtful whether more than a thin surface layer was heated severely. The peak outer-race temperatures were about 200 F.

Similar analysis of the No. 306 bearing showed it to have a track width of 0.102 in. corresponding to a ball load of 240 lb. The normal maximum ball load from the applied radial load of 160 lb is 113 lb.

The Course of a Failure

From the experimental observations and the analysis of their meaning, a fairly complete picture may be drawn of the course of a lubrication failure in a ball bearing. The following stages during failure are indicated, although many of the test bearings were not driven to complete failure.

Loss of Lubricant Film. It seems apparent from the minute quantities of oil which lubricate the ball bearings successfully that depletion of this oil supply beyond a certain critical value results in a lubrication failure. There doubtless is some lubricant remaining on the metal surfaces at this stage, but it is not sufficient to separate the high spots on the rubbing surfaces. Experiments with the No. 306 bearing appear to indicate that load and speed influence the quantity of lubricant remaining at failure, since the time of operation on a given small quantity of oil is strongly influenced by load and speed.

Local Heating Due to Friction. This localized heating occurs in the contact areas between the balls and the races as the result of sliding and friction in the absence of oil.

Loss of Radial Play. As a result of the local heating of the surfaces thermal expansion results in removal of the radial play or

---

[6] "Analysis of Stresses and Deflections," by A. B. Jones, New Departure Divison, General Motors Corporation, Bristol, Conn., vols. 1 and 2, 1946.

[7] "Ball and Roller Bearing Engineering," by Arvid Palmgren, SKF Industries, Inc., Philadelphia, Pa., 1945.

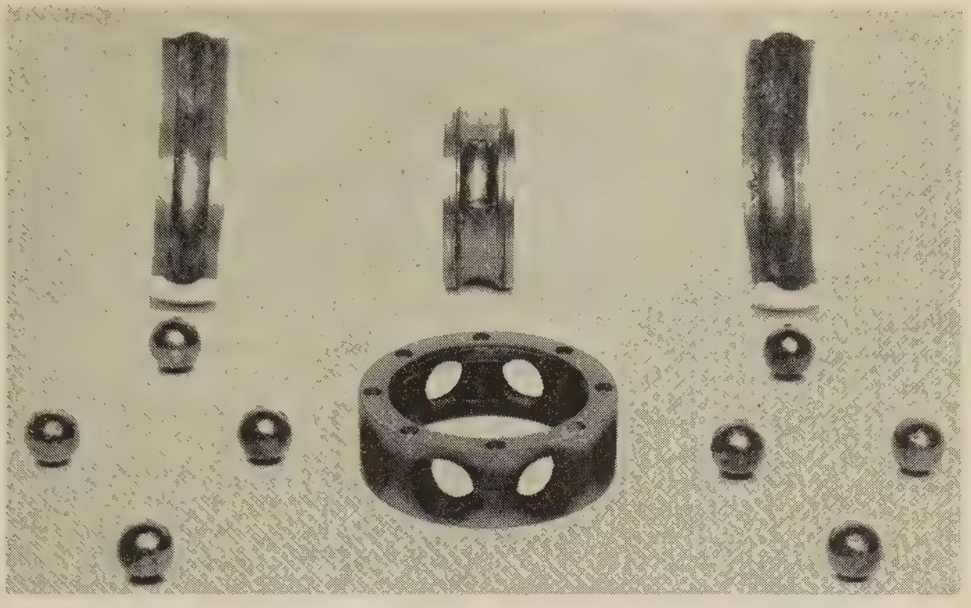

Fig. 7 Bearing Parts After Failure to Ball-Skidding Stage, Showing Indentation of Inner Race Due to Preloading

internal clearance of the bearing. A temperature difference of about 150 F between the balls and the races is sufficient to remove the radial play of 0.0015 in.

Preloading of Bearing. Continued heating beyond the point of zero clearance results in preloading because of "negative clearance." This results in high ball loads and high stresses beneath the contact areas.

Spalling or Pitting of the Contact Surfaces. Pitting appears to start as soon as the lubricant fails and it becomes severe when the preloaded condition is reached. Metal removed from the pits becomes rolled onto the races and balls.

Ball Skidding. Metal rolled beneath the balls causes skidding of one or more balls.

Separator Failure. The high tangential forces on the separator caused by the skidding balls break the separator.

Bearing Jammed. The bearing may jam before or after separator breakage depending upon the amount of inertia and power available in the shaft.

Indentation of Races. When the bearing is examined after a severe failure, i.e., after progression to the three preceding stages, the inner race is found to contain a number of indentations equal to the number of balls (see Fig. 7). This is an indication of the severe preloading at the time of failure.

Discussion

Thomas Barish.[8] The authors' work to determine the actual mechanism of high-speed ball-bearing failures should be of great value in indicating to the ball-bearing manufacturers, some steps that can delay such failures.

The conclusion that the separator does not account for ball-bearing failures at high speeds is true only for certain special conditions; either pure radial load or pure thrust load combined with perfect alignment. The test conditions selected fill these special requirements, but are rarely met in actual practice. Separators account for a large proportion of the field failures, because the contact angle changes around the circumference of the bearing, causing the ball speed to change and jam the separator.

To illustrate how serious and large this effect can be, we take the specific case quoted by the authors as a special test, 300 lb thrust, plus 100 lb radial load (when the cage did fail). The radial load is carried only on the bottom half of the bearing, and the contact angle changes from the top ball to the bottom ball, approximately as shown in Fig. 8. The change in contact angle on the inner race varies the ball speed from 3308 ft per min at the top, to 3172 at the bottom ball—a total change of 134 feet per min or 4.2 per cent.

Furthermore, this effect accumulates over half of the bearing causing an appreciable and dangerous displacement of the ball from its mean position—in this case, about 0.027 in. (Fig. 9[9]). Part of this motion is absorbed by a displacement of the cage, as shown, but this effect cannot be large in high-speed bearings since cages cannot be very loose. The rest of the ball displacement produces cage distortion with resulting severe loads and heating. It is this effect which produces most high-speed failures in the field.

The authors had some difficulty in interpreting the very wide contact area. They deduced a load of 2100 lb per ball[9] (a nomographic chart for making this calculation is given in reference[9]), and attributed it to radial expansion caused by differential heating, the inner ring being hotter than the outer. Such a large load does not seem reasonable. The misapprehension is easily explained: the contact area appeared so wide because it moved.

On the test bearings, the following three conditions existed:

1 The initial bearing with 0.00155 in. looseness (average) contact angle 12.2 deg.

2 Add 300 lb thrust load, contact angle 16.2 deg.

3 Add radial expansion, say, 0.00155 in (85 deg temperature differential) contact angle 7.0 deg.

A radial preload as large as the authors' interpretation would have made the contact practically radial, but it is quite clear

---

[8] Consulting Engineer, Washington, D. C.

[9] "Ball Bearing Troubles," by Thomas Barish, *Product Engineering*, March, 1939.

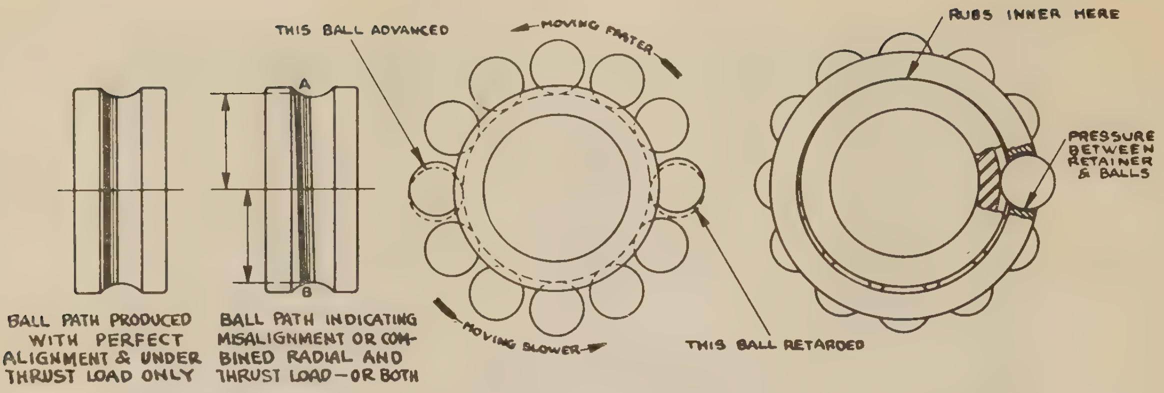
THIS BALL ADVANCED
MOVING FASTER
A
B
RUBS INNER HERE
PRESSURE BETWEEN RETAINER & BALLS
BALL PATH PRODUCED WITH PERFECT ALIGNMENT & UNDER THRUST LOAD ONLY
BALL PATH INDICATING MISALIGNMENT OR COMBINED RADIAL AND THRUST LOAD—OR BOTH
MOVING SLOWER
THIS BALL RETARDED

Fig. 9 Indicating Accumulative Effect of Variation in Contact Angle on Ball Position and on Cage

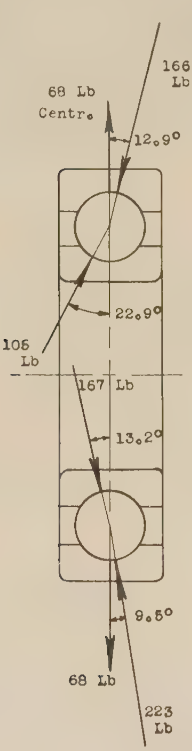

Fig. 8 Variation in Contact Angle From Top Ball to Bottom Under 300 Lb Thrust and 100 Lb Radial Load

from Fig. 4 in the paper that the area being measured was not radial, but at a considerable angle.

Hence most of the race marking in these tests occurred before the final excessive heating of the bearings. However, some heating and resultant contact movement took place during the initial run when the races were marked, or else the contact would not be so wide.

Incidentally, the authors' tests further confirm Poritsky's[10] contention that the balls do not spin in angular contact bearings.

It is still to be proved that an oil film only one molecule thick can be an effective and necessary lubrication between the ball and the race. Lubricating unit pressures of over 200,000 psi do not appear feasible. Perhaps the oil film functioned to improve the heat transfer, rather than as a lubricant. It is suggested that very high pressures and slight movements are better lubricated by such things as "molycote," which should then show better results under the authors' tests.

Much more testing of this valuable type should be undertaken in the near future. Too many machines like gas turbines are being used as testing grounds instead of running the bearings separately under controlled test conditions.

H. T. Morton.[11] The authors amply described a test procedure which creates a lubrication failure of high-speed ball bearings. By stopping the test after various intervals of operation, the progressive figures of failure were observed.

During the writer's years of experience in the examination of bearings which have failed in service due to lack of lubrication, he has also observed similar steps leading to the complete failure of the bearing. Under normal operations the lubricant keeps a film between the ball surface and retainer surface to prevent friction and localized heating at these areas of contact. Likewise, experience requires changes in retainer materials for bearings operated at high speeds.

Under heavy loads or after the balls have expanded due to increase in temperature, the condition shown in Fig. 6 occurs. Here the ellipse of contact is divided into three areas separated by two lines. These lines were especially visible on the sample raceway Mr. Jones had with him at the meeting. These lines represented the position of rolling contact of balls. At all other positions of the ellipse, sliding friction occurred due to the difference in length between r and r_1 of Fig. 6 representing the distance from the point of contact to the axis of rotation of the ball. Thus the lubricant must have sufficient film strength to separate these surfaces or sliding friction will occur, which will increase the ball temperature and the raceway temperature. This increase in temperature will create expansion by heat and decrease of internal radial clearance, as explained by the authors.

It is interesting to note that the authors have computed the width of contact of the balls with the raceways, the stresses and temperatures to create this preload.

The authors also discovered the effect of stopping the bearing while the preload was in effect and plastic flow occurred both on the balls and raceways, leaving indentation in the bearing raceway surface.

Under preload conditions the retainer works all of the time under higher stresses. As a result, early fatigue failure occurs to break the retainers.

The important consideration in bearing service is that when the lubricant fails and the temperature of the bearing lubricant rises, the machine should be stopped immediately.

---

[10] "Sliding Friction of Ball Bearings of the Pivot Type," by H. Poritsky, C. W. Hewlett, Jr., and R. E. Coleman, Jr., *Journal of Applied Mechanics*, Trans. ASME, vol. 69, 1947, pp. A-261–268.

[11] Standards Engineer, The Fafnir Bearing Company, New Britain, Conn.

E. F. Macks and E. E. Bisson.[12] The authors should be complimented upon presenting a paper on bearings which is fundamental in nature.

Inasmuch as this type of failure occurs in low-speed as well as high-speed ball bearings, we feel that the title may be too specific. In this regard, another type of failure which may occur in very high-speed ball bearings, and which has not been mentioned in the paper, is a lubrication failure at the cage locating surface. This type of failure may occur even with adequate lubrication at the points of contact between the balls and races.

The starting speed and rate of accleration are important variables which have not been given. Flat spots on the balls are likely to occur during quick starts, particularly with faulty lubrication; such flat spots may affect the results. Have the authors checked for flat spots on a bearing before it had failed?

Inasmuch as the contact angle and therefore the track width vary with diametral clearance, the observed track width at the time of failure may be somewhat misleading regarding preloads as the balls have not retraced their paths but have gradually worked downward into the groove. Inasmuch as the three sliding and two rolling areas were evident in the failed bearings, the foregoing effect of reduced clearance on contact angle may be overshadowed by the high preloads at the time of failure. What is the author's opinion?

Is it not possible to tell from the tempering colors and hardness of an incipient failure what the ball and inner race maximum temperatures may have been? What have the authors found in this regard?

Authors' Closure

The authors appreciate the comments of the discussers concerning the interpretation of the data in the paper. Mr. Barish has raised some questions which deserve further discussion.

The paper neither states nor implies that the separator does not account for ball-bearing failures at high speeds, but rather that in the event of a "lubrication failure" or failure to supply adequate lubricant to the bearing, separator failure is not the primary cause but rather an end result of localized heating due to friction in the contact areas between balls and races. It was indeed surprising how much punishment this bearing could absorb from misalignment, combined load, and other sources, provided adequate lubrication was supplied. The paper clearly states in the description of special test No. 1, under 300 lb thrust and 100 lb radial load, that a "dry" bearing was used; and, because of the high ball-race friction, failure occurred before full speed was attained by the same process observed in the high-speed failures of very lightly oiled bearings.

There is no difficulty in interpreting the wide contact area, since its width simply serves as a measure of the preload due to localized heating of the balls. For reasons of heat transfer it seems likely that the balls become hotter than either race. Whether the calculated load seems reasonable is a question of judgment in view of the permanent indentations left in the races, as illustrated in Fig. 7. That the contact area is wide because it moved appears highly unlikely for two reasons: (1) because the pitted contact surfaces were not found in the raceways of even scantily lubricated bearings after high-speed runs, and (2) because measurement of the position of the contact area illustrated in Fig. 4 of the paper shows that the contact was nearly radial as Mr. Barish has predicted it should be at the calculated high load.

We believe the evidence is clear that even under the high Hertz stresses, calculated for the contact area between a loaded ball and the raceway, the oil provided as lubricant serves the important function of reducing friction within the contact area. Since the relative motion is small and of short duration, it is possible that oil trapped in surface irregularities, aided by the increase in viscosity due to pressure, explains the beneficial effect.

Lubrication failure at the cage locating surface, as mentioned by Macks and Bisson, has been encountered by the authors in the case of roller bearings having land riding retainers. Undoubtedly similar failures would be encountered in the case of ball bearings constructed to have land riding metal retainers. The rate of acceleration used in these tests was not large—the rotor being brought to full speed in about ten seconds; and at no time were flat spots observed on the balls except after the most severe type of failure when they were obviously caused during failure. The authors have observed so many cases of colors similar to tempering colors arising from the effect of more moderate temperatures on thin oil films on bearing parts that they did not feel that this was a reliable method of judging temperatures. Measurement of hardness in the ball track after an incipient failure using the Rockwell C scale showed no change in hardness. Superficial hardness checks were made.

Bearing testing under controlled laboratory conditions can indeed be more informative than testing in complicated machines, where all too often a failed bearing has progressed so far toward complete destruction that the course of the failure cannot be ascertained. Doubtless it is for this reason that faulty separator lubrication, resulting in separator breakage, has been thought in the past to be the primary result of failure to supply lubricant to a ball bearing, when, in fact, it is the end result of a rapid progression of events originating in friction in the ball-race contact area.

---

[12] Technical Staff, NACA Lewis Flight Propulsion Laboratory, Cleveland, Ohio.

Turbulence in High-Speed Journal Bearings

By D. F. WILCOCK,[1] WEST LYNN, MASS.

Measurements of the operating characteristics of journal bearings up to high surface speeds have revealed abnormalities beyond a certain critical value. A rapid increase in bearing torque, power loss, and oil-film temperature occurs as speed is increased beyond the critical value, while oil flow decreases below normal. These phenomena are attributed to the onset of instability or turbulence in the bearing oil film with an accompanying increase in energy absorption within the film. The experiments were conducted in a newly designed test apparatus capable of driving large bearings at high speeds. Maximum speed attained was 14,700 rpm, or 30,800 fpm, for an 8-in-diam bearing, and 20,000 rpm, or 21,000 fpm, for a 4-in. bearing.

NOMENCLATURE

The following nomenclature is used in the paper:

C = diametral clearance, in.
D = shaft diameter, in.
L = bearing length, in.
N = shaft speed, rpm
P = bearing load, psi
T = torque on bearing, in-lb
Z = absolute viscosity, lb min/in.^{2}
e = shaft eccentricity, in.
g = gravitational constant, in./min^2
ν = kinematic viscosity, in.^{2}/min
ρ = liquid density, lb per cu in.

INTRODUCTION

In the course of an investigation of the operating characteristics of sleeve bearings over a broad range of diameter, clearance, length-to-diameter ratio, and design, anomalous behavior was observed in certain larger clearance bearings when operating at high rotative speeds. It was noted that the friction coefficient under these conditions was considerably higher than would be predicted from the f versus ZN/P curve for the bearing, and that correspondingly high oil-film temperatures were obtained. Turbulence in the oil film was suspected as being responsible for this behavior, since Reynolds numbers over 1000 were estimated.

Some years ago the problem of the stability of a fluid contained between concentric rotating cylinders was treated by G. I. Taylor (1, 2).[2] For the special case, in which the outer cylinder is stationary and the inner cylinder rotates, he was able to calculate the speed at which instability begins in terms of the fluid viscosity, the diameter of the inner cylinder, and the clearance between the cylinders. For the opposite case of a rotating outer cylinder and stationary inner cylinder, the fluid flow was found to be stable to higher speeds. The initial instability for inner-cylinder rotation was predicted mathematically to be in the form of uniform symmetrical vortexes or eddies, and this prediction was borne out by careful, precise experiments. The symmetrical disturbances in the fluid changed to random turbulence as speed was increased above the transition speed.

It is interesting, therefore, to investigate whether the anomalous bearing performance observed at high rotative speeds obeys the relations derived by Taylor and may be ascribed properly to the effects of turbulence. Considerable differences in configuration and conditions exist between a loaded high-speed journal bearing and the annular space between smooth concentric cylinders. Consequently, deviations may be expected in applying the theory for cylinders to journal bearings. Some of the important differences are as follows:

1 Oil grooving in the bearings.
2 Eccentricity of the shaft in the bearing, as a result of the load applied.
3 Variations in oil viscosity throughout the bearing oil film.
4 Small clearance-to-diameter ratios.

The bearings used in this study are made with two longitudinal oil-distribution grooves at either side of the bearing located 90 deg from the load line. Thus, the external cylindrical surface is interrupted twice by oil grooves carefully blended with it. The smallest clearance-to-diameter ratio for the cylinders used by Taylor in his experiments was 0.0271, or 27 mils per in. The bearing tests have been made with much smaller clearance-to-diameter ratios ranging from 1.7 to 4.4 mils per in.

MATHEMATICAL RELATIONS

The essential mathematical relations are presented here without proof or derivation, for which the reader is referred to the original (1, 2). For the case of laminar flow of a fluid between concentric cylinders, the torque may be obtained directly from the definition of viscosity

$$T = \frac{(\text{surface area}) \times (\text{surface velocity}) \times (\text{viscosity}) \times (\text{radius})}{(\text{distance between surfaces})}$$

Neglecting the difference in diameter between bearing and shaft because of the relatively small clearance, and assuming a constant viscosity, this becomes

$$T = \frac{\pi^2 D^3 L N \rho \nu}{gC} \qquad [1]$$

This may be rewritten in the following form in terms of two dimensionless variables

$$\left(\frac{Tg}{\rho N^2 D^4 L}\right) = \frac{\pi^3}{2}\left(\frac{\pi NDC}{2\nu}\right)^{-1} \qquad [2]$$

A log-log plot of

$$\left(\frac{Tg}{\rho N^2 D^4 L}\right) \text{ versus } \left(\frac{\pi NDC}{2\nu}\right)$$

which is defined by Taylor as the Reynolds number, is a straight line with a slope of —45 deg. (It has been plotted in Figs. 6 and 7 as the "theoretical curve" for laminar flow.)

Taylor's criterion for the critical point beyond which instability should occur may be rewritten as

---

[1] Thomson Laboratory, General Electric Company. Mem. ASME.

[2] Numbers in parentheses refer to the Bibliography at the end of the paper.

Contributed by the Research Committee on Lubrication and the Petroleum Division and presented at the Annual Meeting, New York, N. Y., November 27–December 2, 1949, of THE AMERICAN SOCIETY OF MECHANICAL ENGINEERS.

NOTE: Statements and opinions advanced in papers are to be understood as individual expressions of their authors and not those of the Society. Paper No. 49—A-37.

$$\frac{\pi NDC}{2\nu} = \pi^2 \sqrt{\frac{D}{0.0577\,C}} = 41.1 \sqrt{\frac{D}{C}} \ldots\ldots\ldots [3]$$

for the case where C is small[3] compared to D. At Reynolds numbers higher than those given by Equation [3], values of $(Tg)/(\rho N^2 D^4 L)$ higher than those calculated from Equation [2] are expected because of turbulence.

Test Equipment

The experiments were conducted in test equipment designed and constructed in 1946–1947, and shown schematically in Fig. 1. The test bearing is located at the center of the test shaft. This shaft is supported by two pedestal bearings, which are usually smaller in diameter than the test bearing. It is driven through two step-up gears with an over-all ratio of 20:1 by a 200-hp d-c motor. An amplidyne control system is used to adjust the motor speed and to maintain it constant. With this drive, tests may be run at shaft speeds of 250 rpm to 30,000 rpm with full power available from 5000 to 30,000 rpm. Special control circuits permit full power to be used to stop the shaft in the event of a bearing seizure or other emergency.

Load is applied to the test bearing by means of a hydraulic cylinder located beneath it which can apply a maximum load of 133,000 lb. The load is transmitted to the test-bearing housing through a stationary pivot bearing supplied with high-pressure oil from the hydraulic cylinder. The pivot bearing is cylindrical, embracing 85 deg of arc, and contains four oil pockets symmetrically disposed. Oil is fed to each pocket individually through a small tube which restricts the flow and keeps the bearing balanced (3).

The pivot bearing is essentially frictionless and permits free rotation of the test-bearing housing which is restrained only by a torque arm and scale for measuring the torque reaction on the bearing during operation. The torque is measured with a precision of 0.05 ft-lb.

A general view of the installation without the scale is shown in Fig. 2. The control console and some of the oil piping are visible. The test bearing is supplied with filtered oil at controlled temperature and pressure. Each of the longitudinal oil grooves in the test bearing is fed through its own oil line containing a volumetric-type totalizing oil meter for the measurement of oil-flow rates. The pedestal bearings and the gears are supplied with oil from a second system completely independent of the test bearing.

Shaft speed is measured with a precision tachometer generator and meter. Shaft position in the bearing is measured with magnetic strain gages mounted radially to the shaft on the test-bearing housing. Changes in the gap between the gage armature and the shaft change the reactance of the gage coil which is measured in a bridge circuit.

Different size bearings may be mounted in the test-bearing housing and in the pedestals by means of adapters. Fig. 3 shows the installation of a 4-in-diameter bearing in the test-bearing housing. The torque arm and part of the scale may be seen in the background.

The test bearing is usually fitted with a number of thermocouples for measurement of the oil-film temperatures and, at times, is also fitted with pressure taps for the measurement of oil-film pressures. The bearing thermocouples are copper-Copnic and are mounted so that the tips are open to the oil film and flush with the bearing surface. The wires are brought through a short section of two-hole ceramic insulator which is cemented in a close-fitting drilled radial hole. Softening of the cement by the oil is prevented by coating the exposed cemented surfaces with several coats of clear Glyptal cement. Temperatures read with thermocouples installed in the foregoing manner have been from 1 to 2 deg C above those read from adjacent thermocouples embedded in the babbitt metal. The true oil-film temperature is not known, but it is thought that the disturbance of the bearing surface where the thermocouple is inserted causes a local disturbance in the oil film sufficient to circulate oil over the thermocouple bead.

Experimental Results

Four bearings have been run at speeds high enough to exhibit the effects of oil-film instability. Three are 8-in-diam bearings, 4 in. long. The fourth is a 4-in-diam bearing, 4 in. long. Bearing and shaft dimensions are summarized in Table 1. The bearings are of the split cylindrical type shown in Fig. 4, with longitudinal oil-distribution grooves reaching to within $^1/_4$ in. of each end.

Bearing D has 14 thermocouples at the oil-film surface, 10 of them in the lower half. Bearings E, L, and N each had four thermocouples disposed on a circumferential line $^3/_4$ in. from one end of the bearing at 0, 45, 180, and 315 deg from the bottom of the bearing, respectively.

The tests were conducted at a bearing load of 150 psi of projected bearing area and with an oil-inlet temperature of 40 C (104 F) in most cases. Bearings D, E, and L were tested with an oil having a viscosity of 70 centistokes at 100 F. Bearing N was tested with an oil having a 100 F viscosity of 54 centistokes.

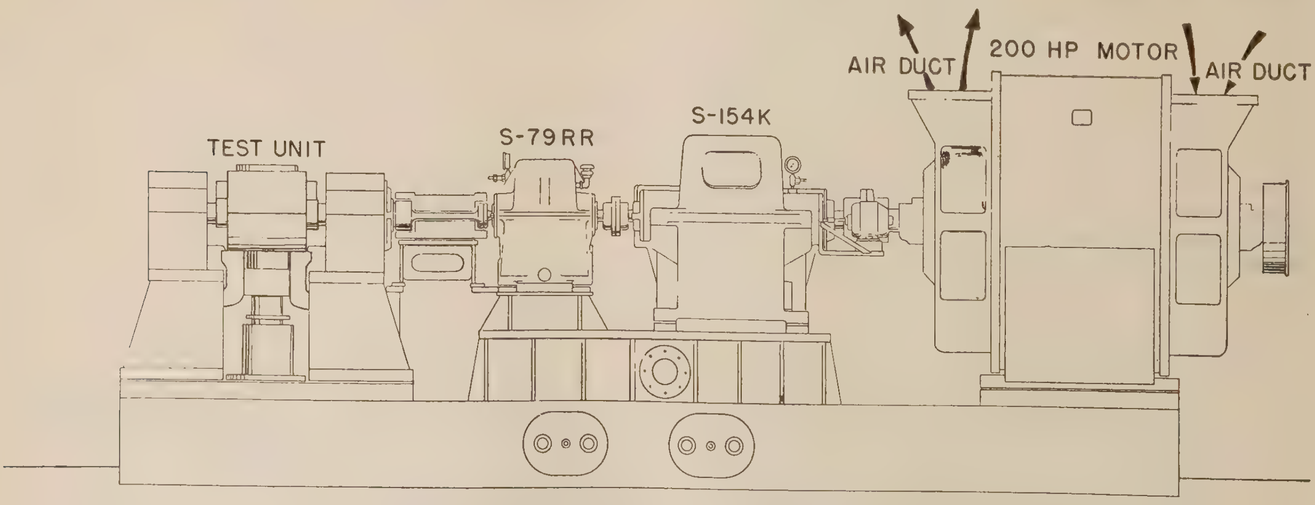

Fig. 1 Schematic Diagram of High-Speed Journal-Bearing Test Stand

---

[3] Reference (2), Equations [3] and [5], p. 558.

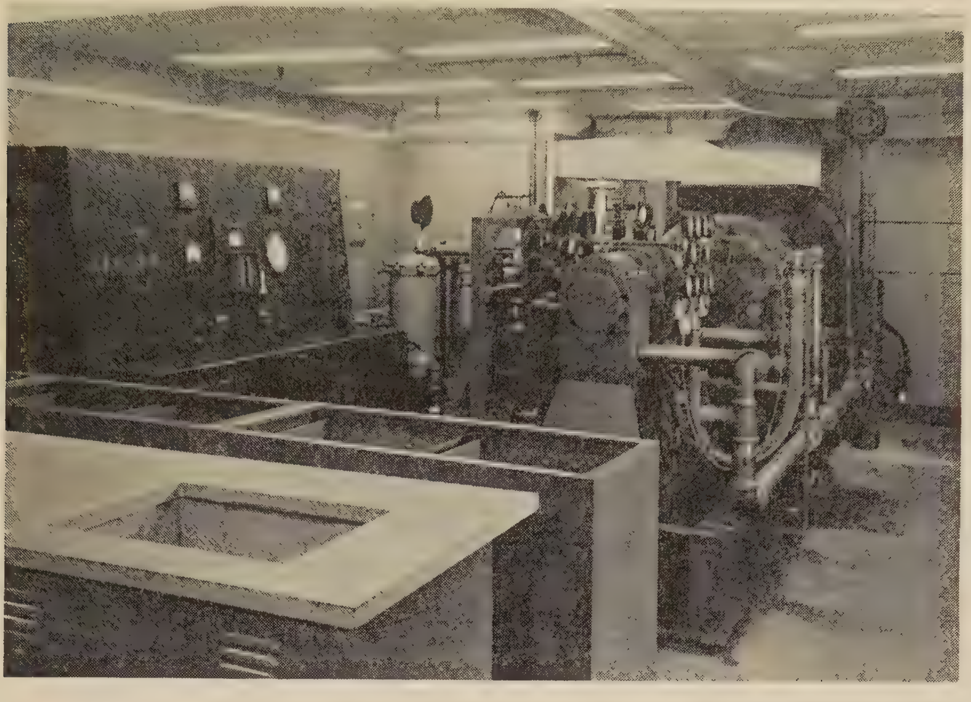

Fig. 2 View of Journal-Bearing Test Stand

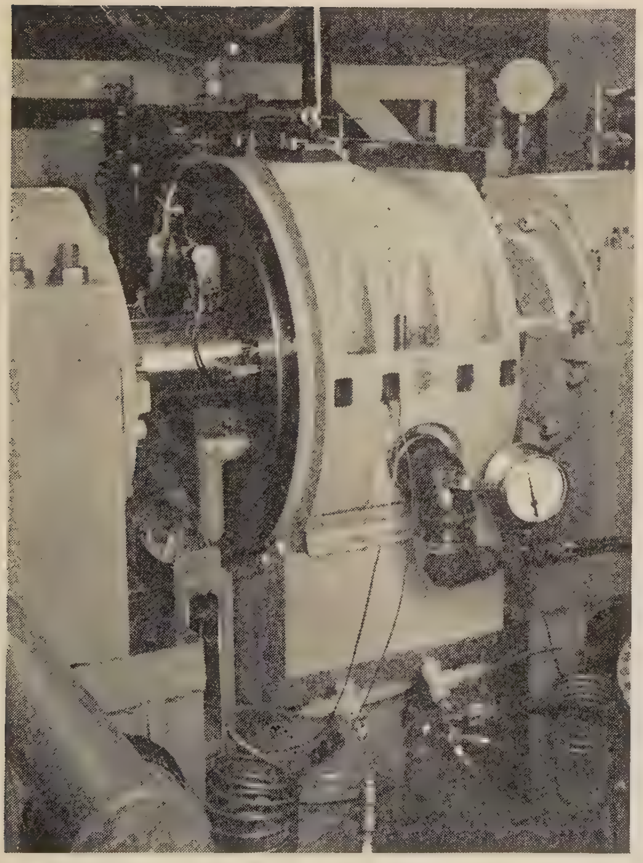

Fig. 3 View of Test-Bearing Housing, Showing Installation of 4-In. × 4-In. Bearing, Magnetic Film Thickness Gages, and Torque Arm

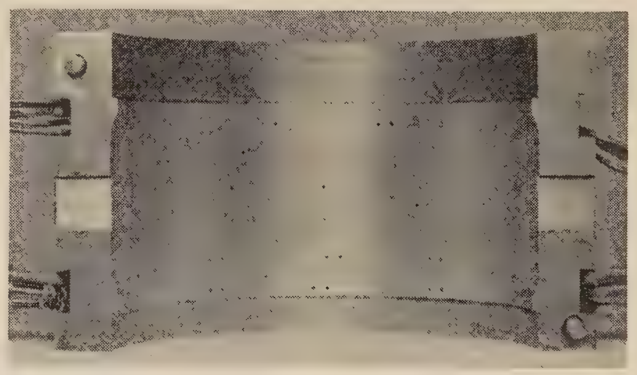

Fig. 4 Typical Test Bearing—Lower Half Only—Showing Shape of Oil-Feed Grooves, Pressure Taps, and Thermocouples

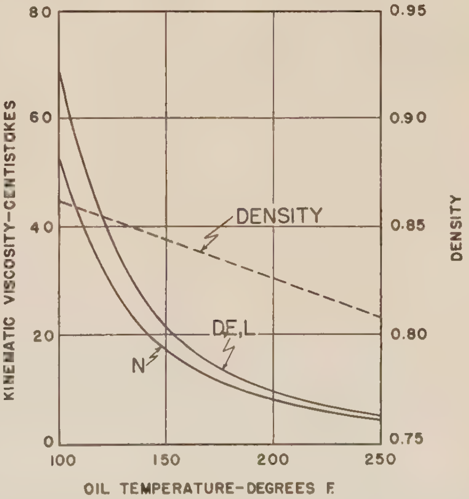

Fig. 5 Viscosities and Densities of Test Oils as a Function of Temperature

TABLE 1 SUMMARY OF BEARING DIMENSIONS

Bearing	Shaft Diameter, Inches	Bearing Bore, Inches* Maximum	Minimum	Average	Bearing Clearance, Inches	Bearing Length, Inches
D	8.0010	8.0148	8.0131	8.0139	0.0129	4
E	8.0000	8.0223	8.0190	8.0200	0.0200	4
L	8.0000	8.0358	8.0335	8.0349	0.0349	4
N	3.9998	4.0166	4.0137	4.0151	0.0153	4

*Measured with bearing clamped in test housing.

TABLE 2 TEST DATA ON 8-IN. × 4-IN. × 0.0129-IN. BEARING D

Run No.	Speed RPM	Shaft Torque ft-lbs	Horsepower	Inlet Oil Temp., °C	Outlet Oil Temp., °C	Max. Obsd. Brg. Temp., °C	Oil Flow GPM
D-12	250	8.4	0.40	39.0	40.7	48.2	0.7
D-11	500	8.95	0.85	39.3	43.3	48.7	1.0
D-45	1,000	10.9	2.1	40.2	46.0	59.8	1.5
D- 5	2,720	17.4	8.9	40.2	57.3	78.0	3.1
D-18	5,000	24.2	23.0	40.5	68.9	84.5	5.3
D-24	7,510	33.3	47.5	42.9	85.1	98.6	7.4
D-54	9,500	42.6	76.9	51.8	109.8	130.2	8.6

TABLE 3 TEST DATA ON 8-IN. × 4-IN. × 0.0200-IN. BEARING E

Run No.	Speed RPM	Shaft Torque ft-lbs	Horsepower	Inlet Oil Temp., °C	Outlet Oil Temp., °C	Max. Obsd. Brg. Temp., °C	Oil Flow GPM
E- 5	500	9.4	0.9	39.4	39.5	42.4	1.7
E- 6	500	8.4	0.8	40.0	41.0	43.4	1.8
E- 4	1,000	11.7	2.2	40.1	44.3	51.2	2.5
E-12	1,000	11.1	2.1	40.1	43.4	50.8	2.5
E- 9	3,000	19.3	11.0	39.8	53.2	75.2	5.4
E- 7	6,000	28.7	32.7	39.8	62.7	88.2	9.6
E-33	6,000	27.5	31.3	39.6	62.9	88.2	9.5
E- 8	9,000	42.6	73.0	43.1	77.7	103.5	13.9
E-51	11,000	61.0	127.0	47.8	99.5	122.4	15.2

The viscosity-temperature curves for the two oils are shown in Fig. 5, together with the density-temperature curve.

The results obtained with the four bearings are given in Tables 2, 3, 4, and 5. Runs D, E, and N using bearings D, E, and N, were made with a constant inlet-oil pressure of 10 psi on both oil-feed grooves. In run L using bearing L, oil was fed only to the groove on the leading or downcoming side of the bearing above 4000 rpm, and modified inlet-oil conditions were permitted as shown in Table 4 because of limitations in the oil-supply system. The oil line to the trailing-edge oil groove was closed above 4000 rpm. The shaft torques are obtained from the measured bearing-torque reactions by correcting for the torque due to the displacement of the shaft in the bearing at right angles to the load.

When the results are plotted in the dimensionless form used by Taylor, the curves, shown in Fig. 6 are obtained for $(Tg)/(\rho N^2 D^4 L)$ versus $(\pi NDC)/(2\nu)$, where the oil viscosity is calculated on the basis of the measured outlet-oil temperature. The vertical arrows indicate the critical values of $(\pi NDC)/(2\nu)$, calculated from

TABLE 4 TEST DATA ON 8-IN. × 4-IN. × 0.0349-IN. BEARING L

Run No.	Speed RPM	Shaft Torque ft-lbs	Horse-power	Inlet Oil Press. PSI	Inlet Oil Temp., °C	Outlet Oil Temp., °C	Max. Obsd. Brg. Temp.	Oil Flow GPM
L- 2	1,000	10.4	2.0	10.0	40.0	41.9	49.9	7.6
L-35	1,000	9.5	1.8	10.0	39.8	41.6	49.7	7.6
L- 8	2,000	13.1	5.0	10.0	39.7	43.4	55.0	10.0
L- 6	3,000	15.8	9.0	3.0	40.5	47.1	51.9	9.7
L-11	4,000	15.3	11.6	3.0	40.2	47.6	72.0	10.8 *
L-12	6,000	18.9	21.6	3.0	40.1	51.8	76.7	12.6 *
L-13	8,000	23.7	36.0	3.0	39.7	57.2	78.0	13.8*
L-14	10,000	29.9	56.8	3.0	39.6	63.5	84.5	15.3*
L-16	12,000	41.6	94.9	3.0	45.8	80.9	99.2	18.2*
L-17	13,000	47.6	118.0	2.0	51.7	92.6	115.5	19.3*
L-19	14,000	53.8	143.0	1.5	52.4	99.6	121.0	19.8*
L-27	14,700	55.7	156.0	0.8	48.3	98.6	124.0	19.2*

*Oil feed to leading edge oil groove only.

TABLE 5 TEST DATA ON 4-IN. × 4-IN. × 0.0153-IN. BEARING N

Run No.	Speed RPM	Shaft Torque ft-lbs	Horsepower	Inlet Oil Temp., °C	Outlet Oil Temp., °C	Max. Obsd. Brg. Temp., °C	Oil Flow GPM
N-10	1,000	1.7	0.3	39.8	43.7	46.4	0.8
N- 2	3,000	3.0	1.7	39.9	48.6	55.5	1.4
N- 4	7,000	4.6	6.1	39.9	55.8	66.0	2.5
N- 7	14,000	7.6	20.1	40.4	74.5	85.4	3.8
N-22	20,000	12.8	48.5	41.9	114.5	115.7	4.0

Taylor's criterion, Equation [3]. It is apparent that runs D, E, and N deviate markedly from the theoretical straight-line relation at values of Reynolds number above the critical. Run L shows a similar effect, but at a critical value considerably higher than calculated. Fig. 7 is a similar plot based on viscosities at the maximum observed bearing temperature. It shows the same marked deviation from the theoretical curve above the critical values of Reynolds number; and, in addition, the straight-line portions are more nearly parallel to the theoretical curve, Equation [2].

Surveys of bearing oil-film temperatures made with bearing D, among others, have shown that the outlet-oil temperature is approximately the same as the average oil-film temperature. Barber and Davenport (4) have made a similar survey on a 2-in-diameter bearing. Consequently, the curves in Fig. 6 represent the bearing behavior based on average oil-film viscosities, while the curves in Fig. 7 refer to bearing behavior in terms of the maximum Reynolds number in the oil film. Further refinements in the calculation of Reynolds number, such as correcting for the effect of shaft eccentricity, do not appear to be warranted, since the measured bearing torque is the summation of the shear resistance over the entire bearing area.

Whether comparison is made on the basis of average or of minimum oil-film viscosity (Fig. 6 or Fig. 7), deviation from the curve representing normal viscous behavior occurs at approximately the point predicted by the Taylor equation. Beyond the critical point, the frictional resistance of the bearing increases rapidly. The critical point for run L occurs at from 2 to 4 times the predicted value, depending upon the method of plot chosen. It is thought that this extension of the normal range may be related to the method of feeding oil only to the leading-edge oil groove rather than to both grooves as in the other runs.

Effects of Turbulence on Bearing Performance

In addition to the "Taylor plot," the presence of oil-film instability, or turbulence, reveals itself in a number of extremely practical effects. It affects power loss, oil-film temperatures, oil-flow rate, shaft eccentricity, and the Sommerfeld plot.

Power loss increases much more rapidly with speed after the critical Reynolds number is exceeded. Fig. 8 shows the relation of horsepower loss to speed. Below the critical point, horsepower varies as the 1.4 power of the speed; above the critical point, horsepower varies as the 2.7 power of the speed.

Oil-film temperatures tend to rise rapidly beyond the critical Reynolds number. Fig. 9 shows the maximum oil-film temperature, in terms of the rise above the inlet-oil temperature, as a function of shaft speed, and illustrates the rapid rise at high speeds.

The oil-flow rate is depressed at speeds above the critical point,

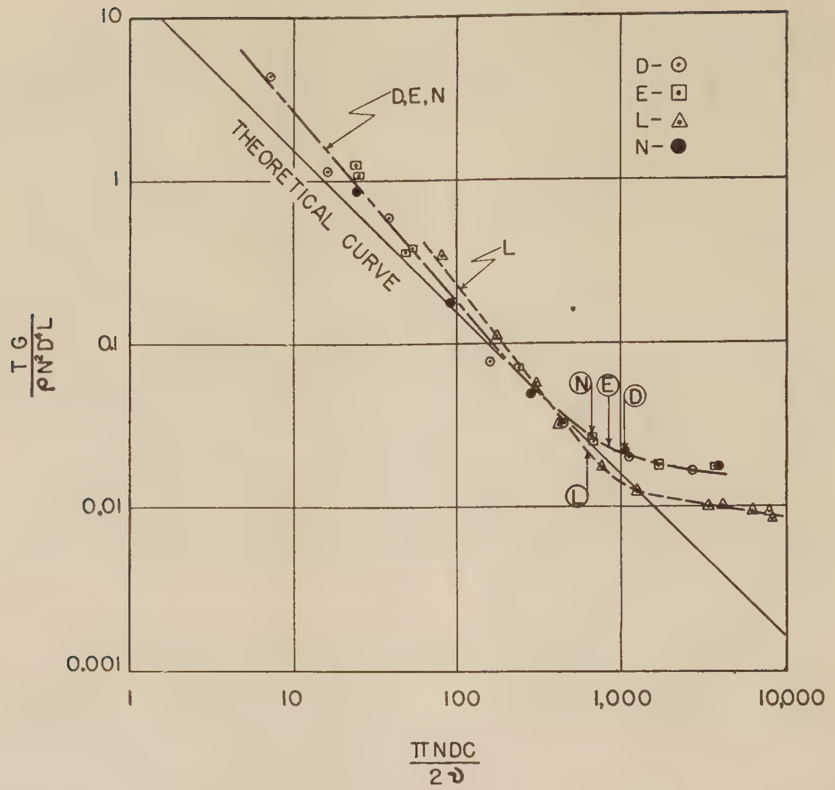

Fig. 6 Taylor Plot Based Upon Viscosities at Outlet-Oil Temperatures
(Vertical arrows indicate calculated transition points between laminar and turbulent flow.)

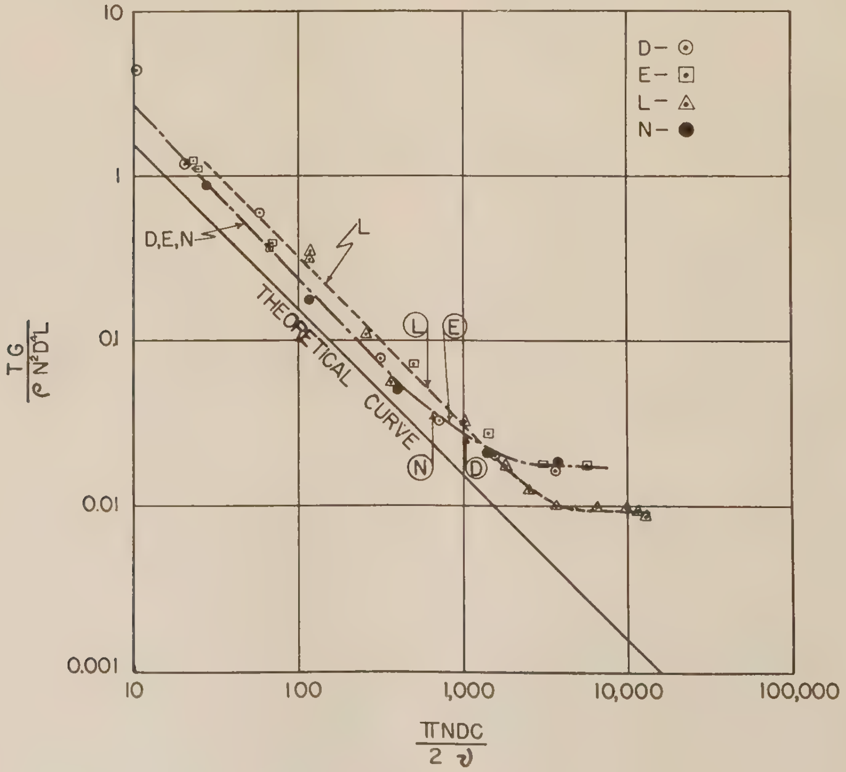

Fig. 7 Taylor Plot Based Upon Viscosities at Maximum Observed Bearing Temperatures
(Vertical arrows indicate calculated transition points between laminar and turbulent flow.)

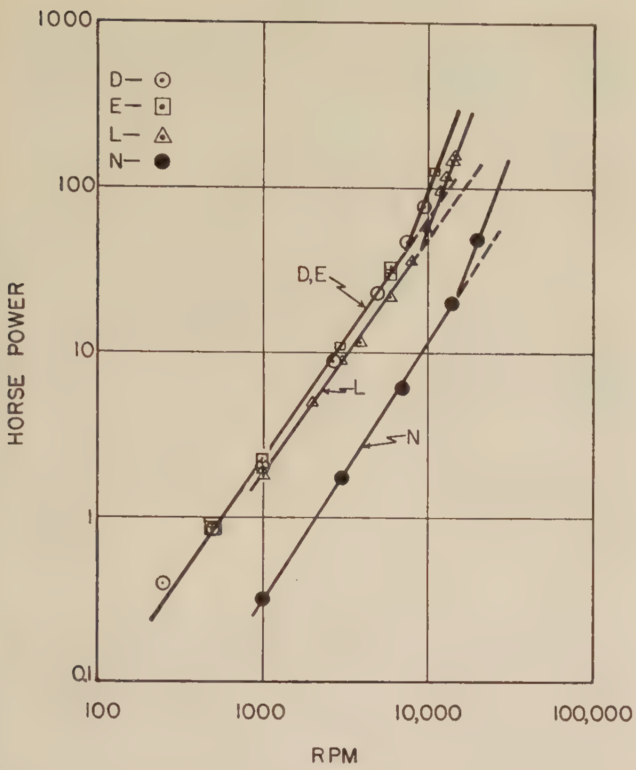

FIG. 8 BEARING POWER LOSS AS FUNCTION OF SPEED

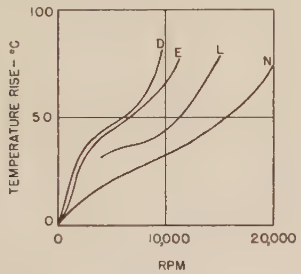

FIG. 9 MAXIMUM BEARING-TEMPERATURE RISE ABOVE INLET-OIL TEMPERATURE AS FUNCTION OF SPEED

as shown in Fig. 10. This occurs in spite of the fact that the higher inlet-oil temperatures occurring in the highest-speed runs should result in increased flow rates. Thus turbulence tends to obstruct oil flow, much as it does in a pipe line. The oil flow in run L is further depressed by the drop in inlet-oil pressure.

The effect of turbulence on shaft eccentricity is unusual and is shown in dimensionless form for runs E and L in Fig. 11 in which eccentricity ratio, $2e/C$, is plotted as a function of the Sommerfeld variable (5), based on the oil viscosity at the outlet-oil temperature. Above the critical Reynolds number, a sharp break in the eccentricity curve is observed. The Sommerfeld number decreases and the eccentricity simultaneously decreases toward the value predicted by the hydrodynamic theory for a complete cylindrical bearing without end leakage. It is presumed that the high eccentricities found in the normal range of operation are due to the effects of end leakage (oil flow) and of the oil-distribution grooves. The onset of turbulence then tends to reduce the effect of these factors.

Turbulence effects are sharply revealed in the Sommerfeld plot for friction factor (5), Fig. 12. The result of oil-film instability is a coefficient of friction greatly increased over the normal value at the same Sommerfeld number.

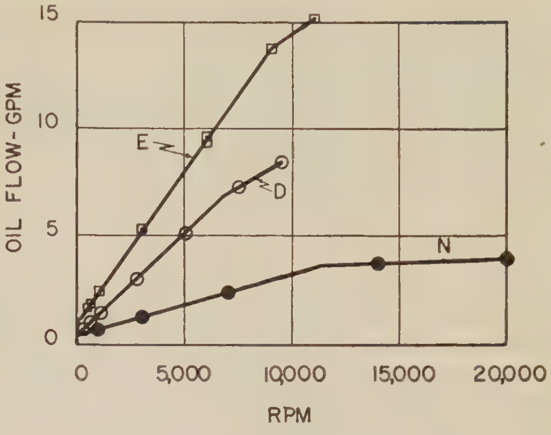

FIG. 10 OIL FLOW THROUGH TEST BEARINGS AS FUNCTION OF SPEED

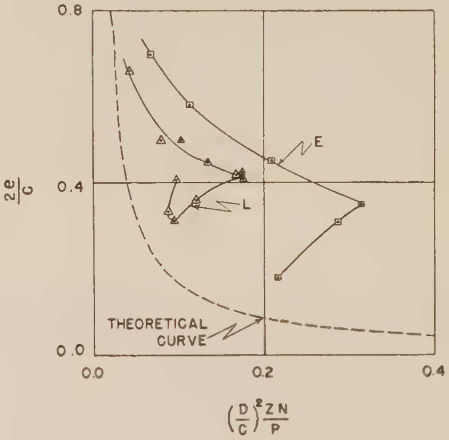

FIG. 11 SHAFT ECCENTRICITY RATIO, $2e/C$, AS FUNCTION OF SOMMERFELD VARIABLE FOR BEARINGS E AND L

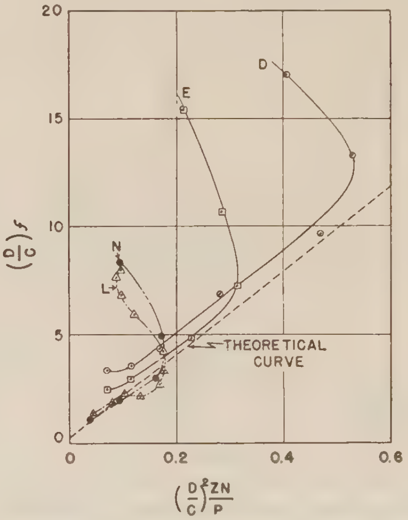

FIG. 12 REDUCED FRICTION COEFFICIENT, $(D/C)F$, AS FUNCTION OF SOMMERFELD VARIABLE

HIGH-SPEED BEARINGS

There is a marked trend today toward higher rotative speeds in new turbine and gear designs. In many cases requirements for shaft stiffness dictate that these speeds be attained with large shaft diameters, i.e., at high surface speeds. Do the experimental and theoretical effects outlined herein indicate a practical upper speed limit for cylindrical bearings?

The interplay of the several factors is complicated. The critical Reynolds number is inversely proportional to $\sqrt{C}$. Consequently, the requirement that a bearing of a given size operate in the normal range may be stated as

$$N < \frac{K\nu}{C^{3/2}}$$

in which K is a numerical constant. Thus the transition speed depends not only on the clearance but also upon the increase in oil flow as clearance is increased, and upon the corresponding increase in oil viscosity as outlet-oil temperature drops. Operation in the turbulent region is more feasible with the lower temperatures accompanying larger clearances, but opposed to this is the problem of machine alignment introduced by large-clearance bearings; for example, the larger clearances required between rotors and stators, and the possible improper meshing of gears. What do the experiments have to say about transition speeds at the critical Reynolds number and about practical top speeds?

The data on the three 8-in. × 4-in. bearings indicate the following relation between clearance and the transition speed at which instability sets in:

	—Approximate transition speed, rpm—	
Clearance	Found	Predicted
D: 0.0129	7000	7500
E: 0.0200	6000	6700
L: 0.0349	8000	5500

The experimental transition speed is obtained from the Sommerfeld plot, but similar values may be obtained from the Taylor plot based on outlet-oil temperature. The predicted values are obtained from the Taylor plot using the calculated critical Reynolds numbers. Bearing in mind that the experimental transition speed for bearing L is high because of the method of oil feed, we see that lower transition speeds may be anticipated as clearances are increased.

The temperatures at the transition speed decrease as the clearance is increased as follows:

	—Approximate temperature, deg C—	
Clearance	Outlet oil	Max bearing
D: 0.0129	82	96
E: 0.0200	63	88
L: 0.0349	57	78

As a result, operation in the turbulent region will be safer at the larger clearances, and the safe top operating speed will increase somewhat as the clearance is increased. Referring to Fig. 9, the speed at which a bearing temperature 70 C (126 F) above inlet-oil temperature is reached is approximately as follows:

Clearance	Speed for 70 C bearing temp rise, rpm	Excess over transition speed, rpm
D: 0.0129	9000	2000
E: 0.0200	10500	4500
L: 0.0349	14000	6000

showing that the invasion of the turbulent speed region may be deeper at larger clearances. Decreasing the oil viscosity would be expected to have similar results, that is, it would decrease the speed at which the turbulent region begins but make possible operation at higher speeds for the same temperature rise.

The results on run L indicate that the region of normal operation may be extended considerably by feeding oil to the leading edge or downcoming side only. Confirmation of this effect of oil-feed method is furnished by the additional data for bearing E at 9000 rpm shown in Table 6. Feeding oil only to the leading edge removed the bearing operation from the turbulent region, reducing the power loss from 73 hp to exactly the value calculated for laminar flow, 50 hp. Feeding oil to the leading edge also reduced the outlet-oil temperature, the maximum observed bearing temperature, and the oil flow. The effect of a similar change in oil feed at speeds below the transition speed is slight.

TABLE 6 EFFECT OF OIL FEED UPON BEARING OPERATION ABOVE CRITICAL REYNOLDS NUMBER

(Bearing E, 9000 rpm, 150 psi load
Critical Reynolds number = 825)

Oil-feed method	Both sides	Leading edge	Trailing edge
Inlet-oil temp, deg C........	43.1	39.5	42.9
Outlet-oil temp, deg C.......	77.7	70.0	89.4
Maximum observed bearing temp, deg C..............	103.5	98.5	106.2
Oil flow, gpm..............	13.9	10.4	8.6
$\frac{\pi NDC}{2\nu}$..................	3110	1290	2270
Power loss, hp.............	73	50	63
Power loss for laminar flow at indicated value of $\frac{\pi NDC}{2\nu}$..................	21	50	28
Type of operation...........	Turbulent	Laminar	Turbulent

Feeding oil to the trailing edge (Table 6), results in much less reduction in the power loss which remains much greater than that calculated for laminar flow in the oil film. This method of feed also results in a decreased oil flow. However, outlet-oil temperature and bearing temperature are higher than when feeding to both grooves.

The beneficial effect of feeding oil only to the leading edge appears to be related to a decreased amount of oil in the upper half when feeding in this manner. Pressure measurements in the upper half of other bearings have indicated negative gage pressures with this type feed at locations which show positive pressures when feeding to both grooves or to the trailing edge. Because of the depressed position of the shaft in the bearing under load, the maximum Reynolds number normally occurs in the upper half where the clearance is largest, and consequently a reduced amount of oil in the upper half will result in less tendency toward turbulence in the bearing.

The depth of the oil-feed grooves doubtless results in the presence of turbulent eddies within them at even moderate speeds. These eddies will cause some slight increase in bearing friction. A. Rumpf (6), in comparing the performance of a cylindrical bearing with one with a circumferential groove in the upper half, has ascribed the increased friction of the latter bearing to turbulence in the circumferential groove. If such a bearing were operated with a restricted oil feed so that this groove did not run full of oil, considerably reduced friction would be expected because of the absence of turbulence.

CONCLUSION

The relation derived by G. I. Taylor for the Reynolds number at which fluid instability will begin between concentric cylinders with the inner cylinder rotating has been applied to the nonconcentric case of a journal bearing under load. With diameter-to-clearance ratios less than one tenth of those used experimentally by Taylor, the existence and location of the predicted critical point have been verified. The transition to turbulent oil-film conditions is evidenced by (*a*) increased power consumption, (*b*) increased bearing temperature, (*c*) reduced oil flow, (*d*) a sharp break in the dimensionless shaft-eccentricity plot, and (*e*) a break in the Sommerfeld friction-factor plot toward higher bearing friction. Feeding oil to the bearing through only the downcoming-side oil groove extends at least twofold the region of laminar oil-film behavior.

ACKNOWLEDGMENT

The assistance of W. Rogers, P. Lyons, and H. Stone in obtaining the experimental data is gratefully acknowledged.

BIBLIOGRAPHY

1 "Stability of a Viscous Liquid Contained Between Two Rotating Cylinders," by G. I. Taylor, Trans. of the Royal Society of London, England, series A, vol. 223, 1923, p. 289.

2 "Fluid Friction Between Rotating Cylinders," by G. I. Taylor, Proceedings of the Royal Society, London, England, series A, vol. 157, 1936, p. 546.

3 "Hydrostatic Lubrication," by D. D. Fuller, *Machine Design*, vol. 19, June, 1947, pp. 110–116; July, pp. 117–122; August, pp. 115–120; and September, pp. 127–131 and 188–190.

4 "Investigation of Journal Bearing Performance," by E. M. Barber and C. C. Davenport, Pennsylvania State College Bull. No. 42.

5 "Lubrication," by A. E. Norton, McGraw-Hill Book Company, Inc., New York, N. Y., 1942, pp. 119–120.

6 "Friction and Temperature Paths in Plain Bearings," by Adolf Rumpf, *VDI Forschungsheft*, Ausgabe B, vol. 9, November-December, 1938, 24 pp.

Discussion

M. D. Hersey.[4] The results of primary interest in this investigation are the confirmation of G. S. Taylor's criterion for turbulence under practical bearing conditions, and the exploration of performance characteristics for an appreciable distance into the turbulent region. There are also many important secondary results extending over the normal speed range which will establish this paper as one of reference value for some years to come.

Another form in which Taylor's criterion may be expressed is

$$N = \frac{\nu}{n^{3/2}} \left(\frac{77}{\mathrm{D}^2}\right)$$

where N denotes the critical speed in thousands of revolutions per minute, D the journal diameter in inches, n the clearance in parts per thousand, and ν the kinematic viscosity in centistokes.

A formula for the occurrence of turbulent motion due to longitudinal flow in the clearance space was derived empirically by Edgar Buckingham (7) which may be written

$$\frac{CS}{\nu} = 2000$$

where S denotes the mean speed of flow through the clearance space toward each end of the bearing, the other quantities being expressed in the same system of units.

In referring to friction coefficients higher than expected from the ZN/P curve, it must be remembered that the correct use of the ZN/P diagram, under conditions where the density of the lubricant can effect its performance, requires a family of curves for constant values of the parameter $\rho N^2 D^2/P$, or its equivalent, see page 84 of reference (8). It might be of interest to plot some of the author's data at the higher speeds in this manner.

Since it is difficult to evaluate the effective film viscosity Z, it may be more convenient to work with the inlet viscosity Z_1. Approximate allowance can then be made for the variation in viscosity at different points in the film by introducing an additional parameter representing the more essential thermal properties of the lubricant, see discussion of the Linn and Irons paper, page 623 of reference (9). This parameter may be written aP/q where a is the temperature coefficient of viscosity at the inlet temperature and q the mean heat capacity of the lubricant per unit volume. A separate family of curves will be required when any great change is made in the parameter p_1/P representing the ratio of inlet pressure to the load per unit area. Once laid out, such curves would be expected to apply to all geometrically similar bearings of whatever size, and to other lubricants besides those actually used in the tests. Two additional parameters are needed when loads are reached involving elastic deformation and the change of viscosity under pressure.

The beneficial effect of feeding oil only to the leading edge suggests that the conditions then prevailing are in some degree those of an externally pressurized bearing (3), and that the tendency for thermal expansion of the cooler entering oil also contributes to the lifting force of the film.

It is recommended that the factor g be omitted from Equation [1] in future publications. As it stands, this equation apparently states that the same operating conditions will create a greater friction torque on Pike's Peak than at West Lynn, Mass., which is plainly false in a physical sense, however accurate it may be made by virtue of specially chosen units. Lord Rayleigh (10) called attention to the practice of many engineers of putting g in their descriptions of phenomena that are in no way influenced by gravity, and leaving it out when it should be in. The aim of his criticism was to set up equations that will not merely serve for slide-rule work, but will convey a true physical picture of what happens.

BIBLIOGRAPHY

7 "Leakage Through Thin Clearance Spaces," by Edgar Buckingham, *Engineering*, vol. 15, 1923, pp. 225–226.

8 "Theory of Lubrication," by M. D. Hersey, John Wiley & Sons, Inc., New York, N. Y., 1936.

9 "Power Losses in High-Speed Journal Bearings," by F. C. Linn and D. E. Irons, Trans. ASME, vol. 63, 1941, pp. 617–629.

10 "The Principle of Similitude," by Lord Rayleigh, *Nature*, vol. 95, 1915, pp. 66–68.

H. Poritsky.[5] Offhand, one would not associate oil flow in bearings with the turbulence, and most of the theory of lubrication phenomena is based on the assumption of laminar flow of oil. The author is therefore to be congratulated on his precise delineation of one field of lubrication phenomena in which turbulent motion prevails.

It is of interest to point out that the turbulence occurring in the space between two cylinders of which the inner one is rotating and the outer one is stationary, first studied by Lord Taylor, is one of the few known cases of fluid motion in which it is actually possible to predict from theory the onset of turbulence. Turbulent fluid flow in a pipe, first studied by O. Reynolds some 90 years ago, has not as yet been fully explained.

The physical reason for the onset of turbulence in the case of an inner rotating cylinder may be visualized as follows. In laminar motion, the fluid particles move in circular paths with velocities varying from zero at the outer stationary cylinder to the speed of rotation at the inner cylinder. Thus the centrifugal force which tends to throw the particles out radially is largest on the inside and decreases to zero on the outside. The situation is completely analogous to a stationary layer of air which is warmed by contact with a heated surface at the bottom (for instance, atmospheric air, heated from the surface of the earth through the energy absorbed from solar radiation), and acquires buoyancy proportional to its temperature rise. When the temperature gradient becomes sufficiently large to overcome viscous resistance, convection currents will tend to get set up. Since the warm, lighter air cannot rise simultaneously everywhere, it is to be expected that circulation will be set up, with the warm air rising at some places and cooler air descending elsewhere. Thus vortexes will be set up. A similar situation occurs in the fluid between a rotating and a stationary cylinder. Taylor's theory actually predicts size of these vortexes, and Taylor verified it by injecting ink in the fluid between glass cylinders. Since he was concerned only with onset of turbulence, and used a linear theory retaining only the first powers of the circulation amplitude, he did not predict the amplitude of the vortexes, nor the increased losses which occur as a result of onset of turbulence.

---

[4] Mechanical Engineer, U. S. Naval Engineering Experiment Station, Annapolis, Maryland. Fellow ASME.

The opinions expressed in this discussion are those of the writer and do not necessarily reflect the views of the Navy Department or of the Naval Service at large.

[5] Consulting Engineer, General Electric Company, Schenectady, N. Y. Mem. ASME.

M. C. Shaw.[6] When one cylinder rotates concentrically relative to another cylinder the motion of the fluid between the cylinders is observed to change its character with the speed of rotation. At relatively low speeds the fluid particles have circular paths, as in ordinary journal bearings which operate at normal speeds. As the speed is increased inertia forces become significant and pairs of ring vortexes are found to appear in the film. As the speed is further increased the orderly vortex motion gives way to turbulence. Interesting photographs of the vortexes formed during the second type of motion have recently been presented by W. W. Hagerty.[7] This type of motion as well as turbulent motion in which there is a random intermingling of stream tubes will give rise to greater friction, temperature rise, etc., than will be obtained with the more usual laminar type of flow.

The experiments described by the author show a significant deviation from the friction characteristics based upon laminar flow with circular streamlines. However, from the data presented, it cannot be determined whether this increase in friction is due to the appearance of vortex pairs or truly turbulent motion. The critical value of Reynolds number given by Equation [3] is for the transition to turbulent motion. Therefore the statement in the conclusions that "... the existence and location of the predicted critical point have been verified" might possibly be too inclusive, since the increase in friction might be due to the onset of vortex motion rather than turbulent motion. In fact, one should expect the initial deviation from the laminar friction curve to be due to vortex motion; and a second rather abrupt increase in friction to accompany the beginning of turbulence.

A series of tests with concentric spheres havebeen reported[8,9,10,11] by French workers which are of interest in connection with this problem. The friction torque was carefully measured when the inner sphere was rotated and the outer sphere was held stationary. At the same time the nature of the motion of the fluid was observed as in Taylor's experiments. It was found that at low rotative speeds the fluid moved in circular paths parallel to the equator, but as the speed was increased vortex pairs appeared due to inertia effects. The fluid in the upper hemisphere was observed to move downward along the moving member, being deflected upward upon reaching the equator and thence flowing along the stationary member. At the same time a circulatory flow was established in the lower hemisphere in the opposite direction. The friction torque was observed to rise abruptly from the value corresponding to the usual flow with circular streamlines with the onset of the vortex motion. The observed increase in torque above that expected for circular stream lines was as high as 46 per cent, all of these tests being performed well below speeds required to give turbulence. Deviation from the usual curves was observed at very much lower speeds with spheres than the values Taylor found for cylinders for comparable values of clearance, diameter, and viscosity. Incidentally, these studies upon concentric spheres now verify the inertia induced circulatory flow postulated by Shaw and Strang[12] to explain the mode of operation of the Hydrosphere.

The tests presented in this paper are for a bearing in which the journal is in motion while the bearing is at rest. In discussing the question of turbulence in the oil film of a high-speed bearing in connection with a paper presented by A. E. Roach at the 1948 Annual Meeting, it was pointed out[13] that even though Taylor observed different critical speeds for turbulence when either the outer or inner cylinders are rotated, this difference in the two critical speeds converges as the clearance-diameter ratio is decreased. By extrapolation the two critical speeds are found to converge to the same value for values of the clearance-diameter ratio usually employed in lubrication. Thus the material given in this paper should also be applicable to high-speed bearings in which the journal is stationary and the bearing surface is in motion.

Author's Closure

The author appreciates the helpful comments which the discussers have given. It is important to be able to delineate the region in which normal bearing operation with laminar oil flow in the bearing film can be expected; and the additional evidence cited will help in this regard.

It is not felt that the effect of feeding oil only to the leading edge in extending the region of laminar flow is due to the conditions mentioned by Mr. Hersey. In fact our measurements indicate that the shaft is riding somewhat lower in the bearing under these conditions, in agreement with Fig. 11. In other words, nonlaminar flow tends to restore the shaft toward the bearing center.

Mr. Hersey's recommendation on the use of the factor g is accepted with thanks. The confusion results from the failure to use a consistent system of units in the discussion.

The term turbulence has been used somewhat loosely, as Dr. Shaw points out, to mean "nonlaminar flow." The experiments indicate a gradual transition from the laminar region, which may be the region of vortex flow. Mr. Taylor's experiments at large clearances show the same type of transition, and in addition, his visual observations showed that beyond the transition region turbulence was experienced.

---

[6] Associate Professor of Mechanical Engineering, Massachusetts Institute of Technology, Cambridge, Mass.

[7] "Use of an Optical Property of Glycerine—Water Solutions to Study Viscous-Fluid-Flow Problems," by W. W. Hagerty, ASME Preprint 49—APM-21.

[8] "Mesure du moment d'un couple par emploi du moteur chronometrique. Application à l'étude de la viscosité," by A. Guillet, Comptes Rendus, vol. 200, 1935, p. 442. "Sur le viscosimètre constitué par une sphere en rotation au sein d'un fluide, by A. Guillet, Comptes Rendus, vol. 200, 1935, p. 1522.

[9] "Contribution à l'étude experimentale de phénomènes anomaux en mecanique des fluides visquex," by M. Jacques Huetz, Comptes Rendus, vol. 223, 1946, p. 534.

"Sur l'existence de plusieurs régimes, où les forces de viscosité sont linéaires en function de la vitesse," by M. Jacques Huetz, Comptes Rendus, vol. 223, 1947, p. 1205.

[10] "Sur le couple de viscosité entre deux sphères concentriques," by M. Aubert and Jean Villey, Comptes Rendus, vol. 224, p. 1271.

[11] "Movement of a Viscous Fluid Between Two Concentric Spheres," by F. Charron, Publications Scientifiques et Techniques du Ministere de L'air, No. 208, 1947, p. 1.

[12] "The Hydrosphere—A New Hydrodynamic Bearing," by M. C. Shaw and C. D. Strang, Jr., *Journal of Applied Mechanics*, Trans. ASME, vol. 70, 1948, pp. 137–145. Discussion, *Journal of Applied Mechanics*, Trans. ASME, vol. 71, 1949, pp. 93–98.

[13] "The Load-Carrying Ability of Hydrodynamic Oil Films," by A. E. Roach, *Mechanical Engineering*, vol. 71, 1949, pp. 293–296 and 326. Discussion by Milton C. Shaw, *Mechanical Engineering*, vol. 71, 1949, pp. 763–764.

Closed-Cycle Gas Turbine

Escher Wyss—AK Development, 1945-1950

By CURT KELLER,[1] ZURICH, SWITZERLAND

In 1945 Ackeret and the author made the first presentation in the United States of the basic theory and results of tests on the closed-cycle gas-turbine process, which had been pioneered by the author's company. Since then the development has progressed rapidly and larger industrial installations have been made. Compressed high-temperature air and other gases, used in closed-cycle turbines, have led to new designs of components and plant layouts. This paper describes new stationary units which will be in operation in the near future and discusses future work and possibilities.

THE gas turbine with a closed externally heated working cycle and variable pressure level is still a young proposal. The first plant of this kind, a test unit at the Escher Wyss works, produced 1000 kw for 7 hr in January, 1940. Early experience with this plant, theory of the cycle, and constructional proposals were covered in a paper (1)[2] presented in 1945.

Since 1945, when necessary materials again became available to Swiss industry, development has been rapid. Further experience has been gained with the test plant, research has gone ahead on individual components, and two large installations are under way. This report supplements the 1945 paper by covering the work of the past 4 years and outlining expected future trends.

In relation to its size, Swiss industry has made a great effort to bring the industrial gas turbine into being. Each firm, relying on its own resources, has taken the risk involved in exploring and developing one of several gas-turbine cycles—open, semiclosed, or closed.

Our work has been mainly with the closed cycle. The advantages we believe to be inherent have been discussed in previous papers (1, 4). They can be summarized as follows: (*a*) Suitability for plants of large size; (*b*) possibility of using solid fuels; (*c*) use of clean air under pressure in working cycle gives advantages in design of rotating machinery and heat exchangers; and (*d*) regulation by variation of pressure level yields good part-load characteristics.

At present, one other firm which has been licensed under the basic patents Escher Wyss holds in most countries: Messrs. John Brown & Co., Ltd., Clydebank, Scotland, as our licensee in Great Britain, is also manufacturing plants of this kind. These will be referred to in this paper.

To avoid splitting our resources (man power as well as funds) we have concentrated first on the most promising projects—plants for central stations, industrial use, and ships (2). We have made only preliminary studies of closed-cycle possibilities for vehicles, locomotives, aircraft, and atomic-energy conversion, which would seem to be a most promising application in the future (4).

Actual designs for the two 12,500-kw plants now under construction are based to a considerable extent upon experience with the 2000-kw shop plant and laboratory tests of components. We have been deliberately cautious in introducing new features and extrapolating from known information. Thus the essentially conservative design of these plants should not be regarded as more than an essential stage of development. Further progress, especially concerning size and simplification of heat-exchange apparatus, air heaters, and the like, as well as further improvements in machine efficiencies, are definitely in sight. Nevertheless, the plants under construction are expected to show a heat rate of 10,000 Btu per kwhr. Every future rise of temperature will yield about three times as much efficiency gain as it would with steam, Fig. 1. Herein lies a major cause for optimism regarding the future application of gas turbines.

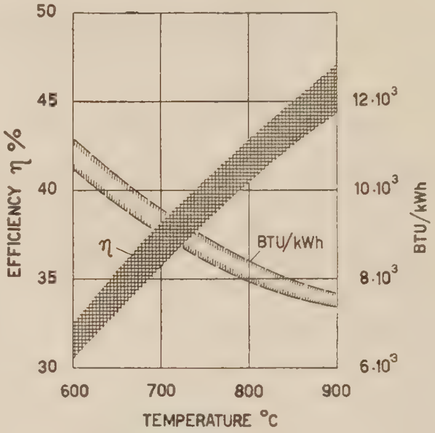

Fig. 1 Approximate Over-All Plant Efficiencies—Based Upon Lower Calorific Values—and Heat Consumption for Closed-Cycle Turbine Installations Depending Upon Working Temperature

(Figures valid for today's constructional possibilities.)

Long-Time Operating Experience With Test Plant

As the 2000-kw test plant is in many respects the basis of our present designs, a review of its 10-year record forms a good starting point. Despite many severe trials, it is still in good condition and ready for further work, Fig. 2.

Total running time (till spring, 1949) is close to 5000 hr. Apart from trial runs, more than 2.5 million kwhr have been delivered to the grid. Official tests (5) were run after about 1000 hr total service, including a first 50-hr nonstop run at 650 C and 1000 kw output in December, 1943. After successful official tests in December, 1944, attention was focused on tests of component parts and especially on regulation, to check theoretical calculations.

In the test plant, the high-pressure turbine drives the compressor at 8000 rpm and the low-pressure turbine drives the generator at 3000 rpm. A gear set couples these two groups and maintains the speed relation. Tests on the pilot plant, without this intermediate gear, proved that with suitable simple regu-

---

[1] Escher Wyss, Ltd. Mem. ASME.

[2] Numbers in parentheses refer to the Bibliography at the end of the paper.

Contributed by the Gas Turbine Power, Power, and Aviation Divisions and presented at the Annual Meeting, New York, N. Y., November 27–December 2, 1949, of The American Society of Mechanical Engineers.

Note: Statements and opinions advanced in papers are to be understood as individual expressions of their authors and not those of the Society. Paper No. 49—A-35.

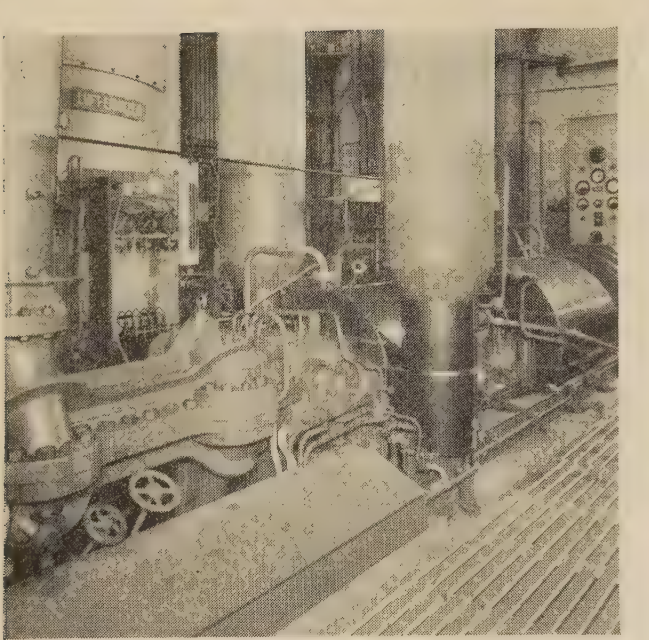

Fig. 2 View of Machine Set of Escher Wyss 2000-Kw Test Plant

(From left to right are shown compressor, high-pressure turbine, low-pressure turbine, generator. Note absence of inlet valve to high-pressure turbine. Vertical air accumulator in background.)

lating devices, the two groups are stable. Thus in most of the coming plant designs, the two turbine groups will run entirely separately.

Scarcity of hydroelectric energy in Switzerland during the past three winters offered the possibility of long nonstop runs, furnishing electricity to the town grid. The energy produced corresponded to the daily need of the Escher Wyss works. The main continuous operating periods were as follows:

First run, ended March, 1947	888 hr
Second run, ended November, 1947	1243 hr
Third run, ended March, 1949	1338 hr

All these were continuous, day and night, without any important interruptions caused by basic failures of the plant. A few short stops of several hours were caused by minor troubles with auxiliaries, electrical equipment, and instruments. We believe this represents a high order of reliability for a plant built for laboratory work, with much temporary auxiliary equipment. During the last long runs, two untrained men operated the plant each shift.

Neither air heater nor machines have experienced detrimental fouling. Air-heater tubes have never been cleaned since the beginning in 1940. Their surfaces are still almost unsoiled. Furnace oil as employed in Switzerland for industrial purposes, and synthetic oil were used. These are not the crudest grades.

Despite direct exposure to flame radiation, tube bundles are still in good order, Fig. 3. Since the beginning, about 250 starts and stops have been made, with corresponding heating and cooling. Nevertheless, over-all efficiency today is not lower than during official tests 4000 hr earlier. Average efficiency of the last 1338-hr run (loads between 650 and 800 kw, temperatures between 620 and 650 C) was 24.2 per cent, based on lower heating value. This corresponds well with the Quiby figure, taking account of temperature corrections. Between the second and third long-time runs, there was no revision or overhaul of machinery. The set was started at the beginning of 1949 in the same condition as at shutdown a year before.

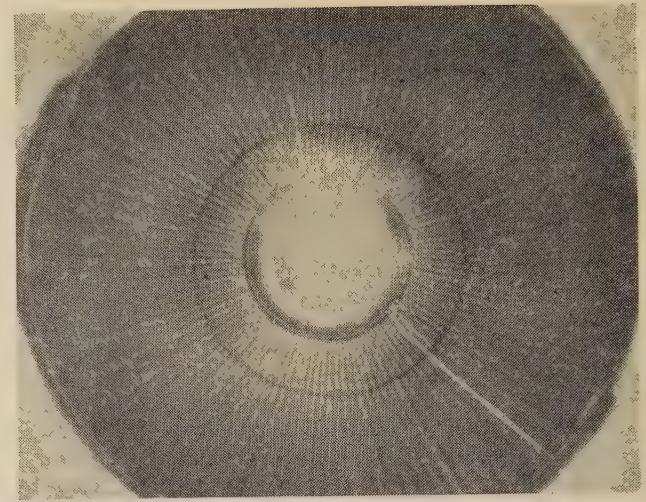

Fig. 3 View Inside Combustion Chamber of Test-Plant Air Heater, Seen From Top Under Operation at One Third Full-Load

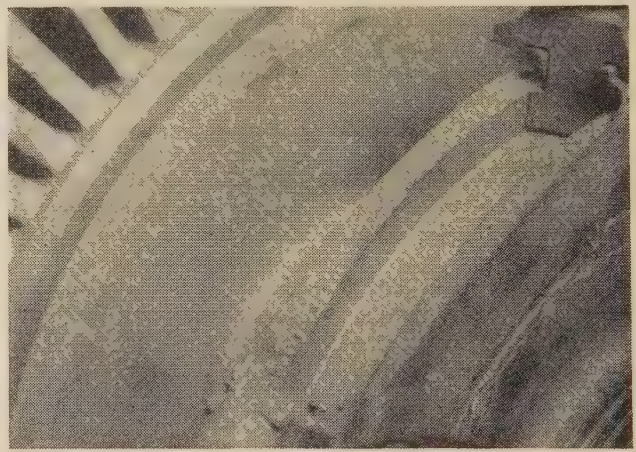

Fig. 4 Broken Rim of First Stage of Experimental Turbine

The worst accident occurred after 1200 hr of running, in December, 1943. The rim of the high-pressure turbine's first stage broke off; rotor and blading were badly damaged, Fig. 4. Close investigation furnished valuable information on the behavior of high-alloy heat-resisting steels. Following older steam-turbine practice, blades were attached to the first disk in a T-groove, not with the "fir-tree" fastening common today. Calculated stress in the outer rim from blade centrifugal forces amounted to about 17,000 psi. Due attention had not been given to rounding-off the T-root, and a sharp notch produced stress concentrations. Actually, a maximum stress of 28,000 to 35,000 psi must have been produced. This corresponds to the value which will cause rupture of this kind of material (Poldi AKRV steel—11.2 per cent Cr, 12.4 per cent Ni, 2.5 per cent Wo) in about 1000 hr. Tests established these values long after our rotor was ordered in 1935. In our new machines stresses are much lower.

The blades, of ATS steel (17.6 per cent Cr, 9.3 per cent Ni, 1 per cent Wo), behaved well. They were bent and twisted but none was broken. Ductility of the material had not suffered during its high-temperature service and there was no embrittlement.

Over the years, compressor design has changed to take advantage of later knowledge. Before putting new rotors into service in the test plant, efficiencies were carefully measured on a special test bed. During the tests an amazingly quick and pronounced drop in rotor efficiency of 3 percentage points was measured after 12 hr, with ambient air taken from a relatively clean workshop.

Such compressor-efficiency drops would influence performance of the whole plant to a considerable extent. In two-stage plants of the kind we build, a 1 per cent compressor-efficiency drop results in 0.5 point loss of efficiency for the entire plant. This is equivalent to about 1.5 per cent rise in fuel consumption. Such detrimental effects of fouling are not encountered when the cycle is fully closed, as the long-time runs of the test plant demonstrate.

Regulation of closed-cycle plants has been explained in earlier publications (6). Practical operation of the test plant has proved that pressure-level variations combined with by-pass connections between high-pressure and low-pressure sections of the circuit can meet the demands usually imposed on steam-turbine plants. This principle was adopted for the 12,500-kw sets. Absence of moving parts, such as regulating valves, spindles, or throttling devices in the high-temperature region, and constant temperatures at each part of the plant for all loads, prove practical assets.

Because of accumulated heat in tubes and walls of the air heater and heat exchanger, combustion regulation need not follow load fluctuations quickly. If combustion rate is not properly adjusted, air temperature changes only relatively slowly. A load change as a consequence of altered temperature conditions will be compensated temporarily by a corresponding modification of pressure level. Fig. 5 shows the small change in pressure level (P/P_0) which is needed to hold plant output constant as turbine-inlet temperature varies. If, for instance, burner interruption causes a sudden drop from 650 to 600 C, a rise of only 12 per cent in pressure level, by releasing cold-storage air from the accumulators to the circuit, restores normal load. Such effects were quite clearly demonstrated in the test plant.

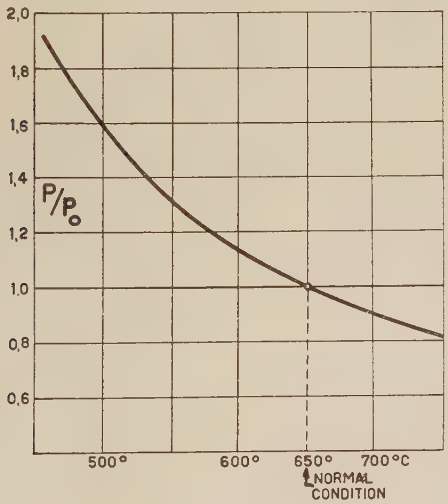

FIG. 5 COMPENSATION OF TEMPERATURE VARIATION BY CHANGING PRESSURE LEVEL

It is impressive, for example, to see that one can change fuel injection for several minutes without appreciable effect on output. Fig. 6 shows results of such demonstrations. Before point A, conditions were constant with normal output N_0, maximum pressure P_0, inlet temperature of 1050 F, and fuel consumption G_0. At point A, load dropped suddenly to about 40 per cent of N_0, and continued for about 10 min, to point B. Pressure level fell, too. With no change in fuel-pump delivery, inlet temperature rose steadily, but at only 10 to 15 F per min. Increase in output from temperature rise was compensated automatically by gradual lowering of circuit pressure brought about automatically by the governing gear.

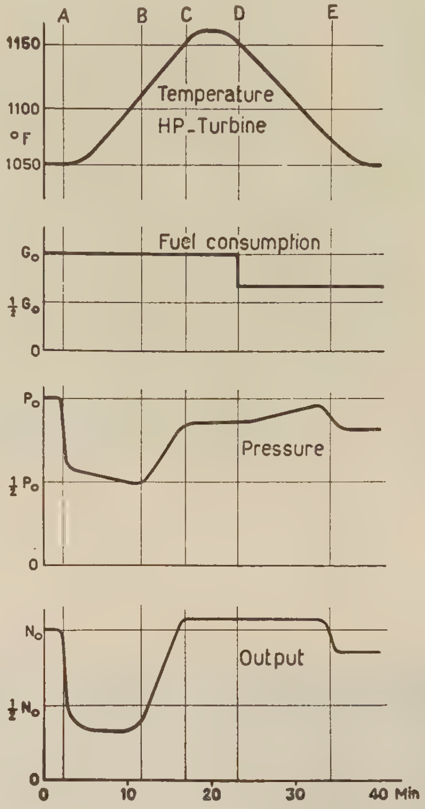

FIG. 6 TEST RESULTS AS TO ACCUMULATING EFFECT AT VARYING FUEL SUPPLY AND LOAD IN EXPERIMENTAL TURBINE

Between points B and C, load increased without an extra supply of fuel. Temperature still rises first as there are inertia effects. At point C load has reached its original value. Fuel supply remains constant to point D. This brings temperature to a maximum value of 1160 F. It then drops again. At point D fuel supply to air heater was suddenly reduced to 65 per cent. Normal output could be secured, in spite of falling turbine temperature, by the automatic pressure compensation (P_0 rose between D and E for another 10 min).

Shutting off fuel supply completely makes an impressive demonstration. With the test plant running at 1000-kw load, shutting oil supply off for a minute or two proves only slightly noticeable at the kilowatt meter. While these characteristics will be less pronounced in bigger plants because they depend on volumes and heat capacity of the installation, they will, in principle, help to make the set insensitive to unforeseen changes

FIRST CLOSED-CYCLE PLANTS FOR CENTRAL STATIONS

At present, three closed-cycle plants are under erection, two for power plants and one for waste-heat use in a gas works. The central-station designs will be considered first, the industrial plant later.

Électricité de France has ordered a 12,500-kw oil-fired set for the St. Denis power station in Paris, Figs. 7 and 8. This plant will start operation late in 1950. Its regulation system enables it to follow load fluctuations independently of the network. This

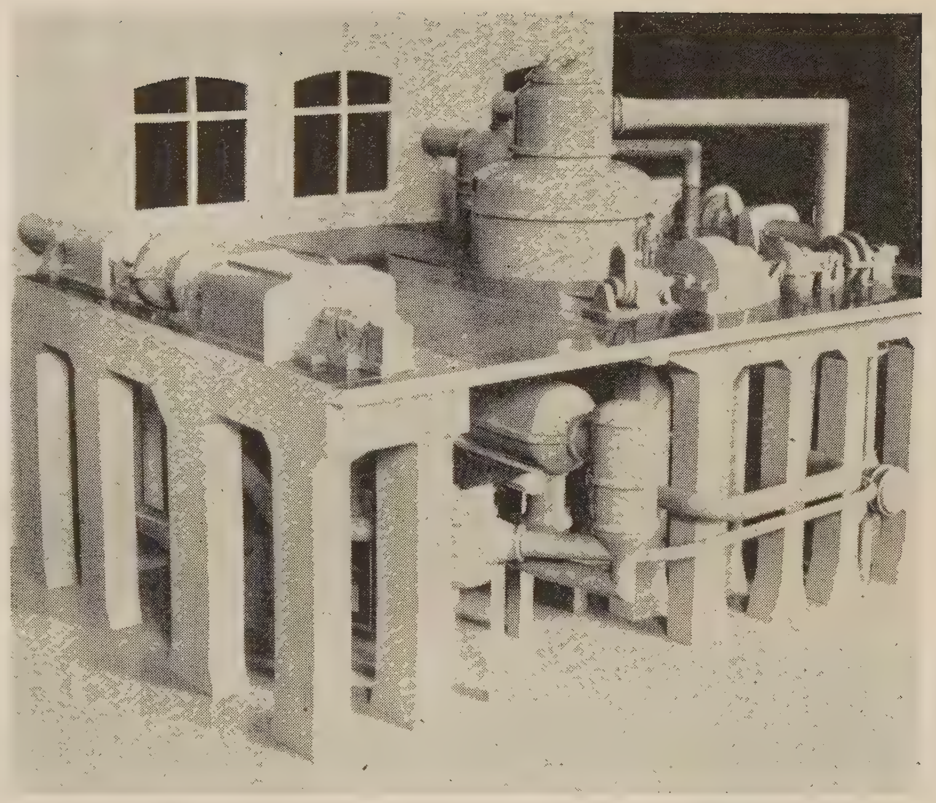

Fig. 7 Model of 12,500-Kw Paris Installation

(At left, generator low-pressure turbine group; at right in foreground, high-pressure turbine-compressor group; center, upper part of air heater.)

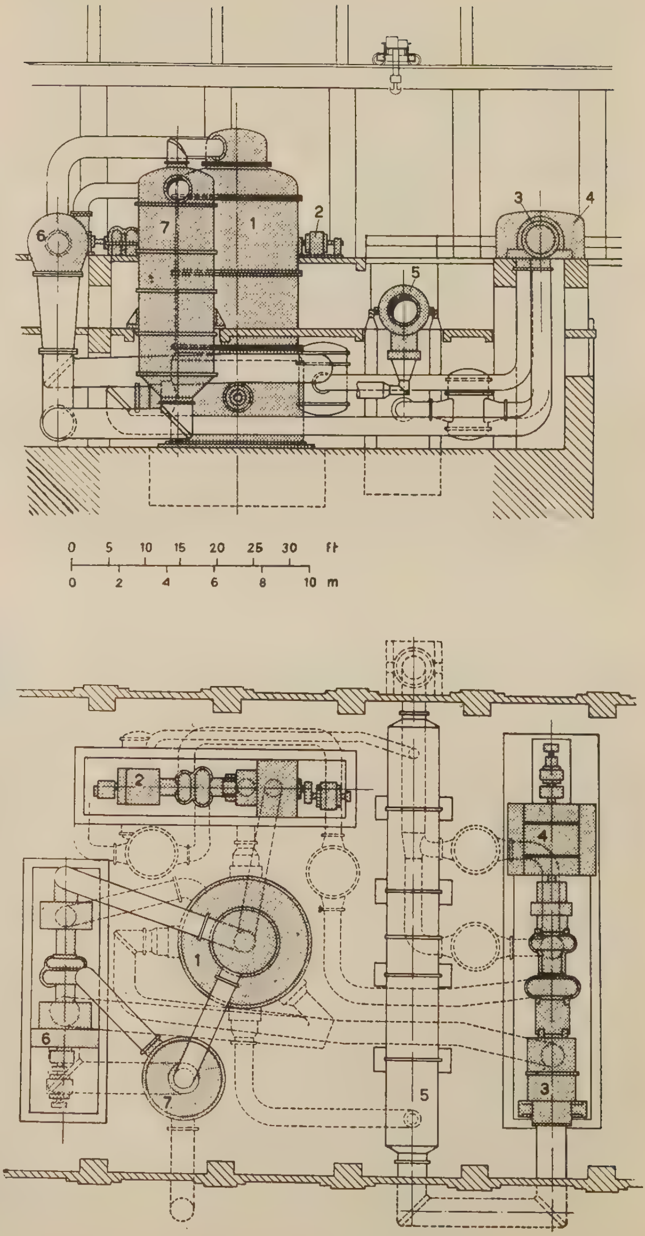

Fig. 8 (*right*) General Layout of Paris Installation

1 Air heater
2 High-pressure turbine-compressor group
3 Low-pressure turbine with low-pressure compressor
4 Generator
5 Heat recuperator
6 Charging set with return gas fan
7 Combustion-air preheater

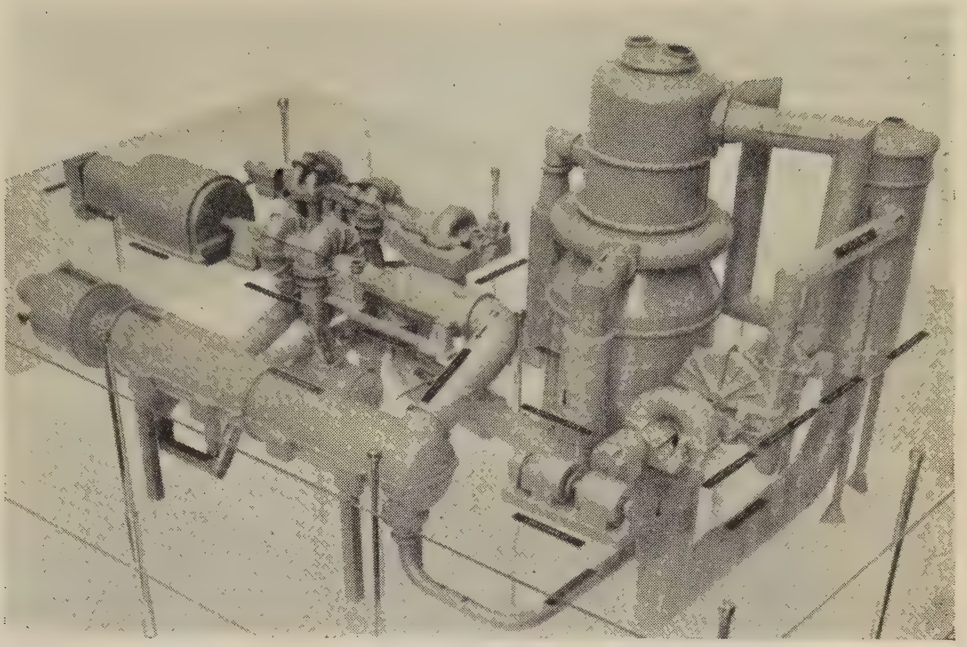

Fig. 9 Model of Dundee Installation
(Seen from right lower corner of Fig. 10.)

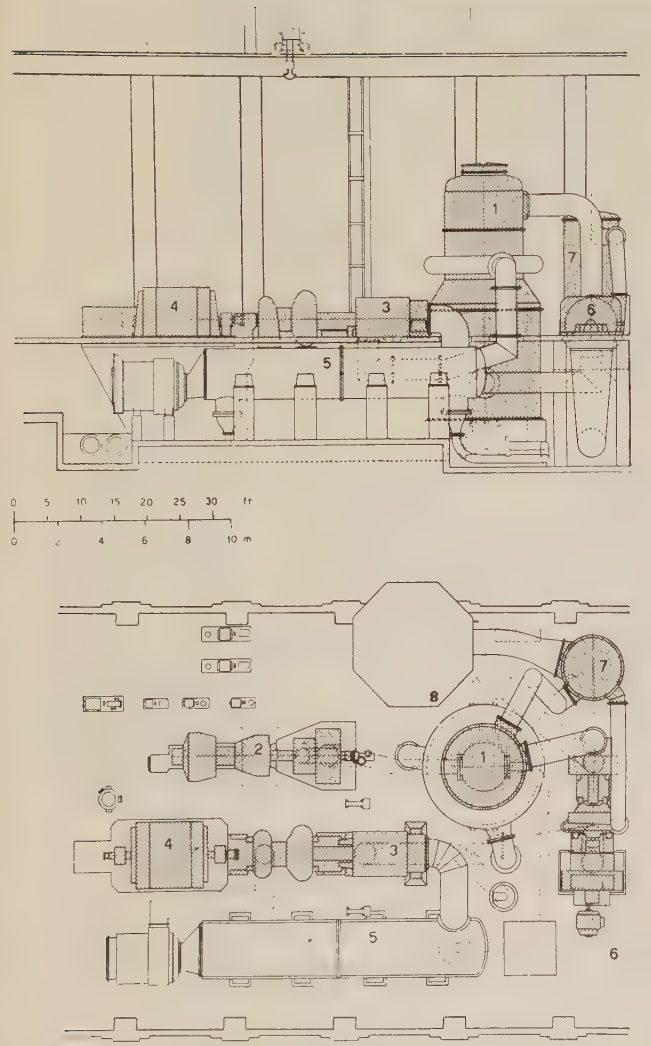

Fig. 10 General Layout of Dundee Installation
(Courtesy of Messrs. John Brown & Co., Ltd., Clydebank, and North of Scotland Hydro-Electric Board; 8, chimney, other numbers same as Fig. 8.)

system works on the principle tried out in the test plant, using cold-storage air for changing pressure level in the circuit. Allowable generator speed variations for different load fluctuations are about the same as in corresponding steam plants. A heat rate of about 10,000 Btu per kwhr is expected. At full load, working data are: Inlet of high-pressure turbine, 750 psia, 665 C; inlet of low-pressure turbine (reheat), 255 psia, 675 C; back pressure, 65 psia.

Layout of equipment was conditioned by a need to utilize given space in the old powerhouse. To provide good accessibility to all parts of this first industrial set, components are separated. This leads to unnecessarily long piping. The air heater stands in the center of the machine group. It extends into the cellar, which is unnecessarily high because the machine floor already existed.

Another 12,500-kw unit is being built by John Brown & Co., for the Carolina Port power station (Dundee) of the North of Scotland Hydro-Electric Board, Figs. 9 and 10. This forms part of the hydro scheme under development in Scotland, and it will operate as a base-load or stand-by plant depending on future needs. Regulation will be effected by pressure-level variation, but, as unforeseen load fluctuations will not occur in the same degree as at Paris, the system is somewhat simpler. No compressed-air accumulators are necessary; auxiliary reciprocating compressors introduce or withdraw air from the circuit. These take care of any eventual leakage also. Main circuit data for Paris and Dundee sets are the same.

This second set had to be fitted into an existing powerhouse also. As Fig. 10 shows, main machines and apparatus could be arranged in parallel, leading to shorter pipe connections. Good accessibility to major units is assured. Foundation height of this installation is less than that of the Paris plant. The two layouts show that a wide variety of machine arrangements is possible. In both cases, no special "boiler" room is foreseen. Machines can be easily dismantled as all inlets are below the machine floors.

If necessary in future plants, the space required can be reduced by combining the different elements. Fig. 11 shows a model of an ideal arrangement for a pulverized-coal-fired plant. The layout differs little from steam practice. Air heater and associated firing equipment would be separated from the machine set and heat exchanger. Since the heater uses no water, it is highly suited to outdoor installation.

On the machine-house ground floor, the regenerator is in line with the low-pressure turbine driving a compressor and generator. All the coolers are at the same level, beside the regenerator. The second floor carries the high-pressure turbine driving a compressor. This arrangement leads to short piping while providing ample space for operation and maintenance. (In Fig. 11, floors are partly omitted to show equipment.)

Description of Main Components

Figs. 12 to 19, inclusive, show some main parts of the 12,500-kw sets during manufacture at the Escher Wyss works. At the time this paper was written, some parts were still unfinished and erection of the power group in Paris was only just beginning.

Small size of the machines is impressive. Fig. 12 shows the high-pressure rotor having an actual output of 14,000 kw—it is only 20 in. diam. Small dimensions lead to comparatively low maximum stresses in blades and rotors. These do not exceed 7500 psi at 8500 rpm and full load. The useful-output turbine of Fig. 14, actually produces 18,500 kw, running at 3000 rpm. Tip diameter amounts to only 42 in.

Turbine and compressor shafts are sealed by compressed air withdrawn from a suitable point of the cycle, and oil sealing toward the ambient air. Fig. 14 shows this sealing arrangement, which proved quite satisfactory in the test plant, at the inlet side of a compressor. Sealing air for turbine shafts arrives at somewhat higher pressure than in the turbine and therefore flows into it, where it also serves to cool the first disk.

Model tests and calculations have been used in a careful study of cooling. Too-cold incoming air gives rise to temperature stresses in the rotor. Therefore, air of suitable higher temperature is used. Cooling effect is high because we work with high-pressure air from the circuit. Approximate temperature dis-

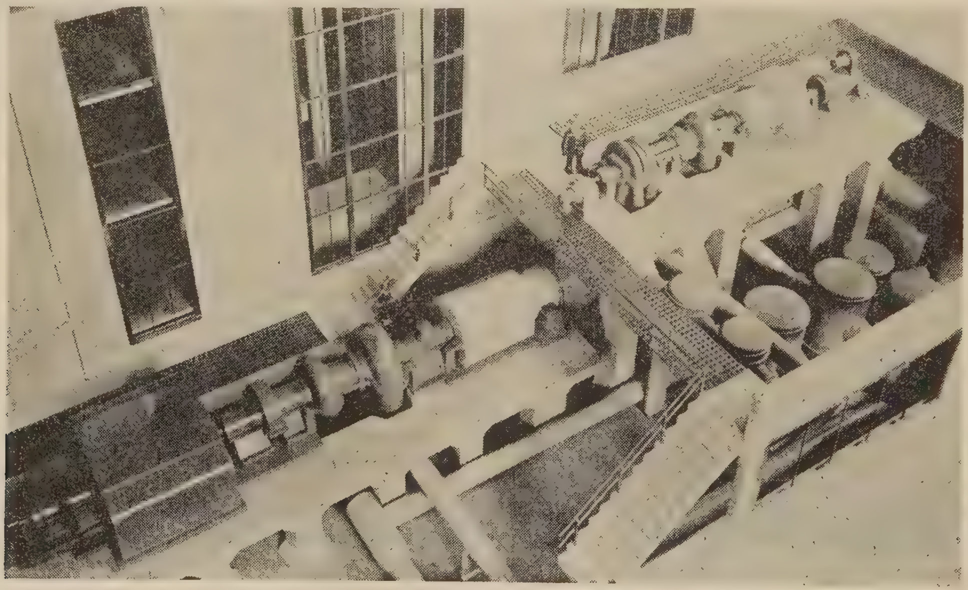

Fig. 11 Ideal Arrangement of Machine Set Showing Floors Partially Removed

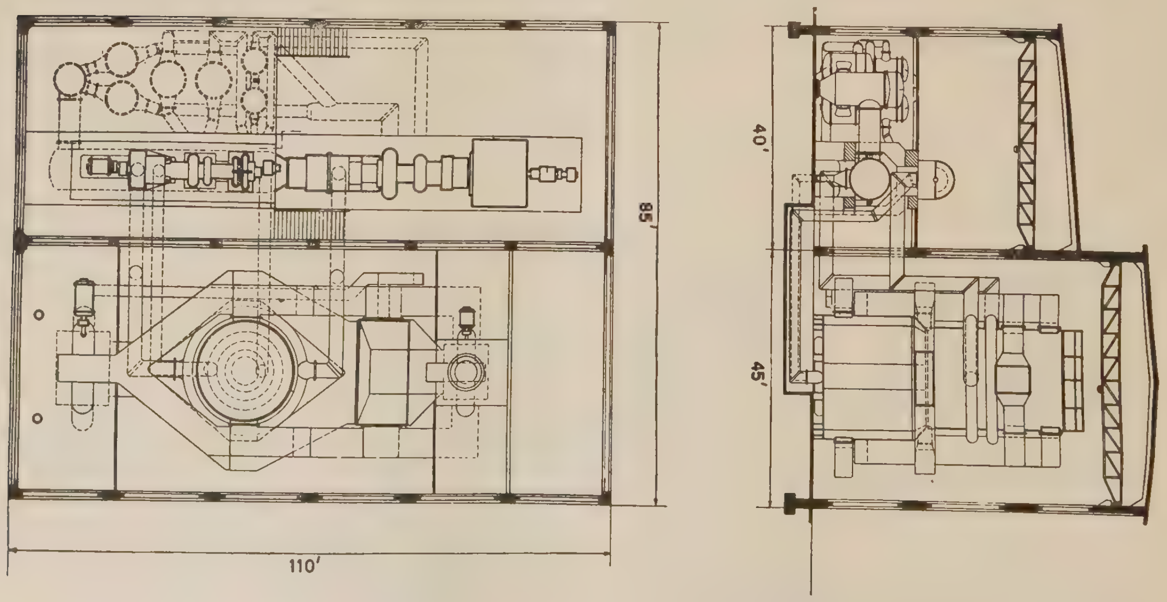

Fig. 11(*a*) Proposed Layout for 12,000-Kw Coal-Fired Plant

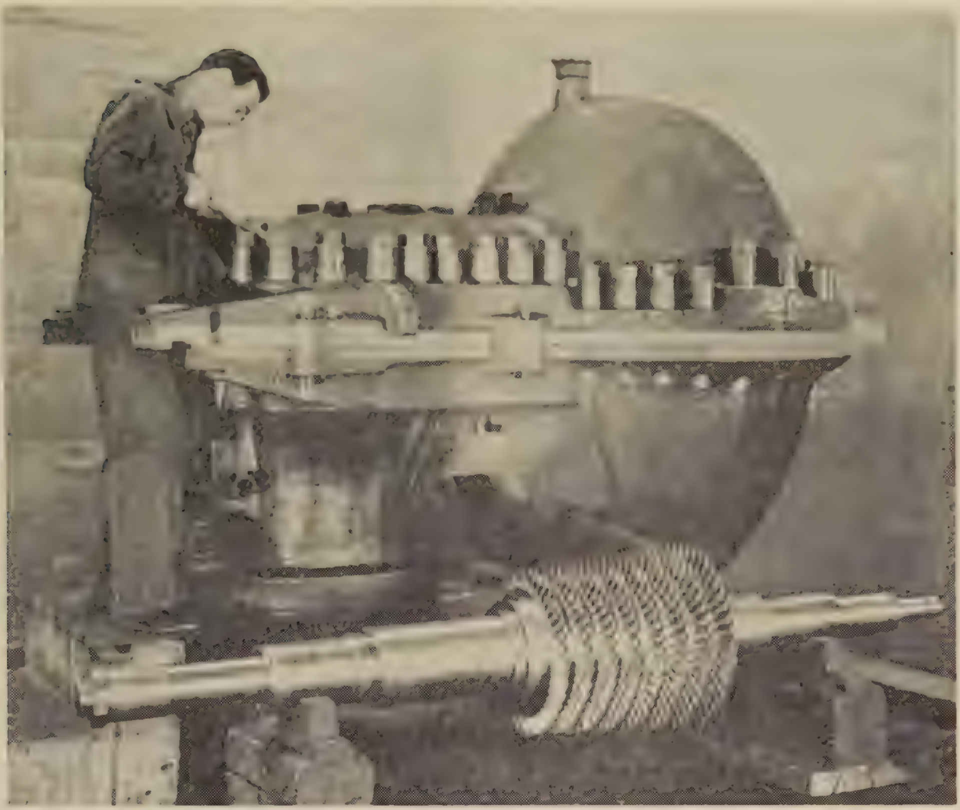

Fig. 12 High-Pressure Turbine Casing and Rotor of Paris Set in Erection Shop
(Rotor output 20,000 hp.)

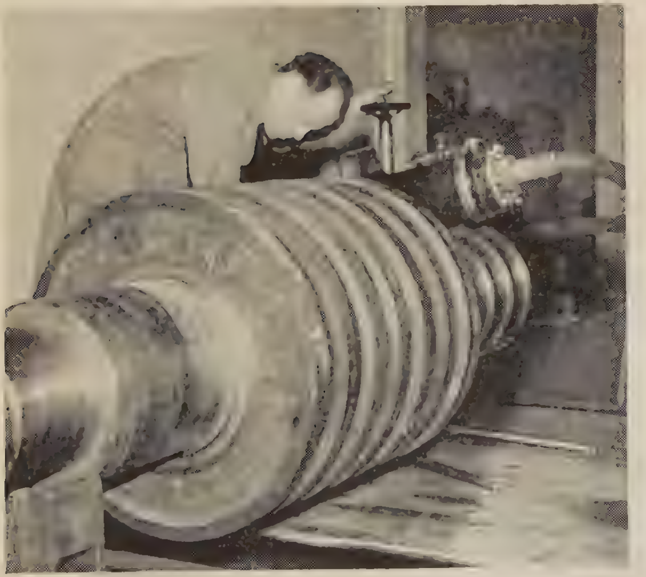

Fig. 13 Rotor of Low-Pressure Turbine of Paris Set Under X-Ray Checking
(Disks are welded on shaft. Rotor output 26,000 hp.)

tribution for the high-pressure turbine is shown in Fig. 15. All temperatures are appreciably lower than maximum temperature of working air.

An electrical analog was used to work out the temperature distribution. Similarity between differential equations for heat flow and an electric field can be used in model tests. Electrical field lines represent temperature distribution. Boundary conditions are represented by different resistances arranged along the border of the model in the electrolyte tank. Fig. 15(a) shows simple test equipment for evaluating temperature of the turbine shaft at certain working conditions.

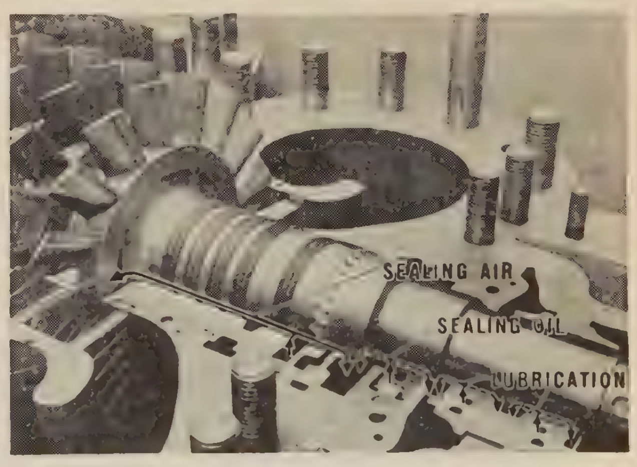

Fig. 14 Combined Labyrinth—Liquid Sealing for Shafts
(Dotted lines = pressure oil; solid lines = pressure air.)

As described previously (1), turbines and high-temperature sections of piping employ double-casing construction, with an intermediate insulating layer. This permits saving heat-resisting material. For instance, casings for both turbines are entirely of normal molybdenum steel as used for steam turbines. Fig. 16 shows the thin inner shell of the low-pressure turbine. The thin wall which leads incoming air to the first guide wheel is per-

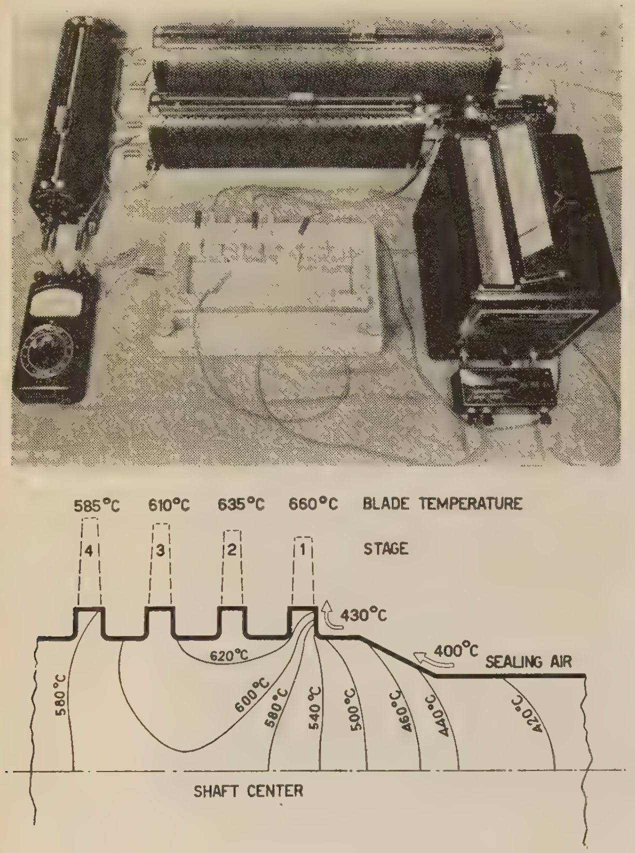

Fig. 15 (*above*) and 15(*a*) (*below*) Device for Evaluating Temperature Distribution in Cooled Machine Parts
(Example for high-pressure-turbine shaft. Wooden model in center of Fig. 15 represents shaft.)

forated so that pressure differences on both sides do not occur when changing load. Absence of any regulating device, such as inlet valves, and lack of distributing chambers facilitate this kind of design.

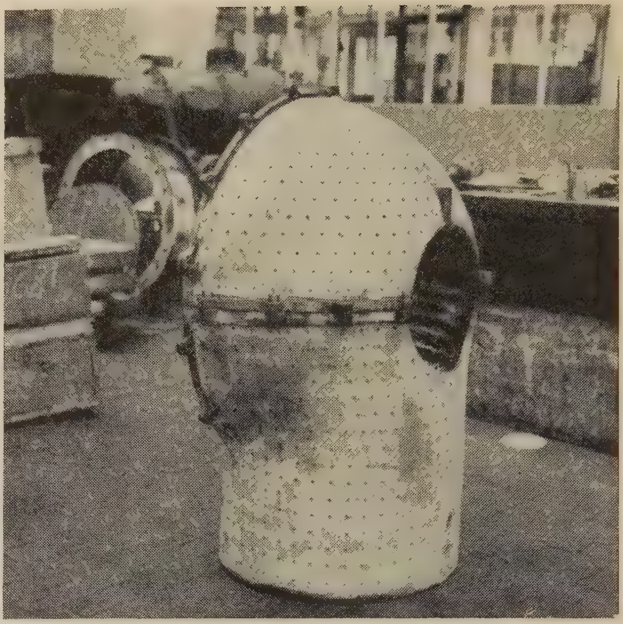

Fig. 16 Inner Inlet Casing of Low-Pressure Turbine

Compression of circuit air from 65 to 210 psig is handled in two stages by axial compressors, and from 210 to 750 psig by a centrifugal compressor, as volumes are already smaller here, Fig. 17. Three intercoolers, Fig. 18, are used. High pressures make dimensions of tube nests relatively small.

Regenerator design is basically the same as in the test plant. Fig. 19 shows the lower half of this counterflow apparatus. Test experience with the old regenerator was quite satisfactory; no soiling of the small tubes occurred. Tubes are normal mild steel. Individual tube nests are welded into conical headers from which a connecting tube of larger diameter leads to the outlet plate.

The bent flexible tubes take up differences in elongation between hot tubes and cold shell.

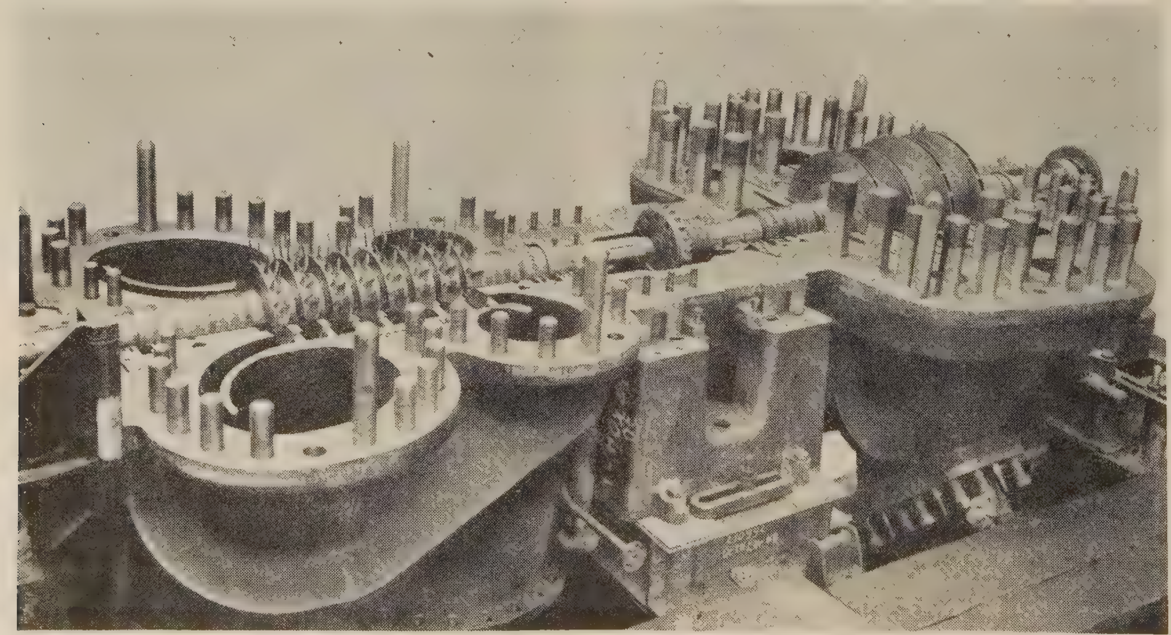

Fig. 17 Second Axial Medium-Pressure Compressor and Radial High-Pressure Compressor for Paris Set

AIR-HEATER DESIGNS

At present, the main difficulty in air-heater design is to choose the best construction out of a great variety of possible solutions, all of which have their pros and cons. In this the development resembles that of the steam boiler. Some of the basic ideas have already been discussed (mainly for oil firing) in previous papers (1). If we compare older designs with today's ideas and experience, we find that much has been gained by simplification.

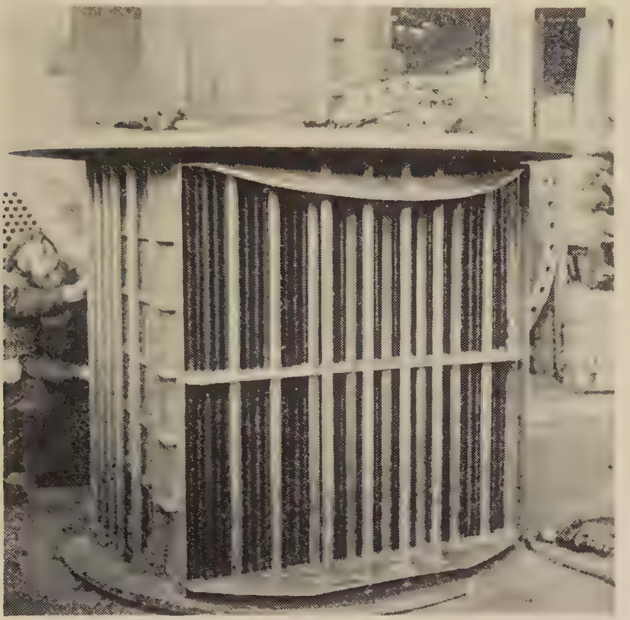

FIG. 18 ONE OF TUBE BUNDLES WITH FINNED TUBES FOR INTERCOOLERS
(Tube nest is enclosed in cylindrical pressure shell.)

As a matter of fact, air-heater questions needed most re-examination in comparison with earlier projects. This is quite natural since the air heater represents an entirely new element. It is one of the most important parts of the closed-cycle plant from the economic aspect and we realize that much of the closed cycle's future depends on air-heater design. In the St. Denis plant, the air heater represents about 30 per cent of the total weight and cost.

Our studies show that great simplifications become apparent as we advance from the rather conservative layouts intentionally adopted in the first units. To appreciate the considerations leading to this choice, we should recall that, in principle, heat can be transferred from fuel to working air through heater surfaces by radiation or convection. Radiation is best in theory; it does not require any pressure drop on the gas side and results in the smallest surfaces.

This kind of heater will be the eventual solution. However, at the time of designing the first industrial plants some years ago, more exact basic information and test figures were available on convection heat transfer. The first Paris air heater is, therefore, a pure convection-type tubular heat exchanger with counterflow layout. Temperature of combustion gas entering the tube nests is only about 1000 C. Recirculated gas mixed with combustion air brings the temperature down.

Further designs based on latest heat-transfer tests have shown that a crossflow convection-type tubular heater yields a great saving in space and weight, the latter being only about 60 per cent as compared with the first type. After securing enough test figures for calculation, this later type of air heater was chosen for the Dundee plant. To reduce heat-transfer surface, pressurized firing is adopted in both cases, as convection transfer coefficient on the gas side rises sharply with pressure. Use of about 45-psia combustion pressure reduces the surface to at least one half that necessary with atmospheric pressure and no radiation. Combustion-gas volumes are also reduced, which leads to smaller piping and fans.

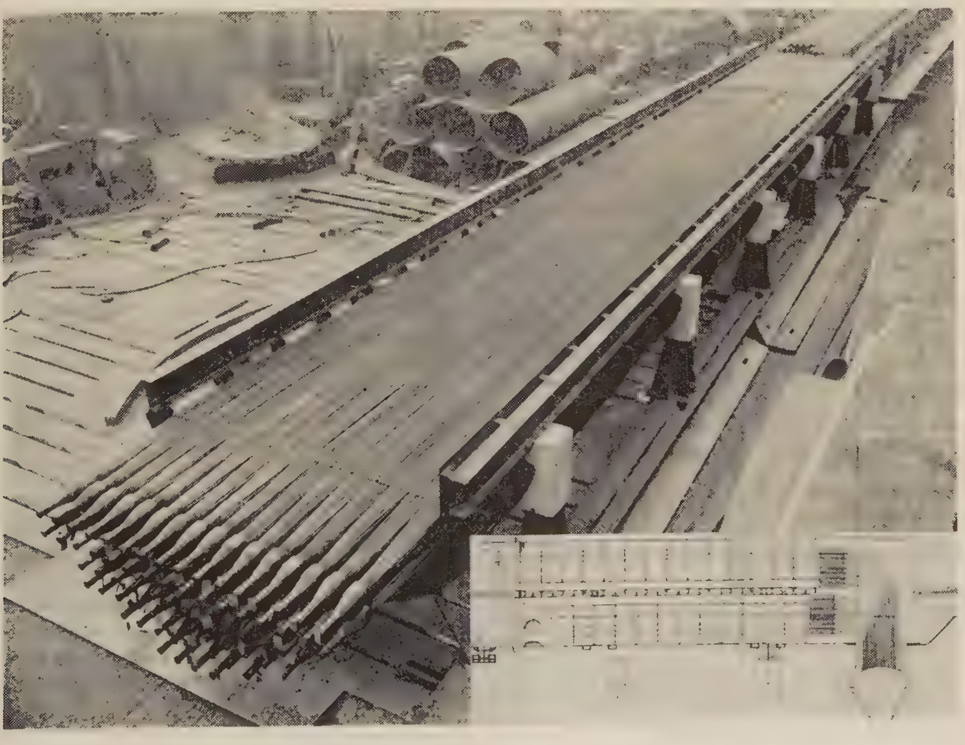

FIG. 19 TUBE BUNDLES FOR PARIS HEAT EXCHANGER
(Tube diameter $^1/_4$ in.)

Greater use of radiation heat permits reducing air-heater surfaces without pressurized combustion. We did not choose this system first because we needed additional information and experience on tubes directly exposed to hot flames. Tests and calculations made in the meantime show that earlier fears about deformation and temperature stresses from unequal heating were overemphasized because assumptions for initial calculations were too primitive. The test-plant air heater, the first ever built, included a radiation-tube wall and encountered none of the expected difficulties in operation, Fig. 3.

A closer study of conditions in radiation tubes with high wall temperatures revealed new phenomena (7). Normal calculations assume heat radiated from combustion space to tube wall coming in over half of the circumference, Fig. 20. Without allowance for heat transfer in a peripheral direction and interradiation to the opposite side of the tube, a rather big temperature difference results for conditions existing in the hottest parts of air-heater tubes.

A more exact calculation shows that, because of circumferential heat flow in the relatively thick tube wall, temperature differences are appreciably smaller than they would be assuming only heat flow perpendicular to the wall. Effect of interradiation of the inner tube surface in leveling up temperature variations can be taken into account quantitatively and proves to be considerable at temperatures above 600 C. Thus final temperature variations and resulting stresses are much smaller in actual cases than they seem at first sight, Fig. 20.

It was logical that early development of air heaters was based on ideas prevailing in boiler practice. We made many studies in this direction but this leads to complicated and costly constructions and readily foreseeable difficulties of expansion and nonuniform temperature distribution. A symmetrical arrangement of tubes around the combustion space helps to avoid local overheating. This point need not be faced to such an extent in boilers. Their wall temperatures are comparatively low, whereas in air heaters poorer heat transfer inside tubes causes metal temperature to approach within as little as 50 C of the temperature of the working medium. Thus no large margin is left for the material.

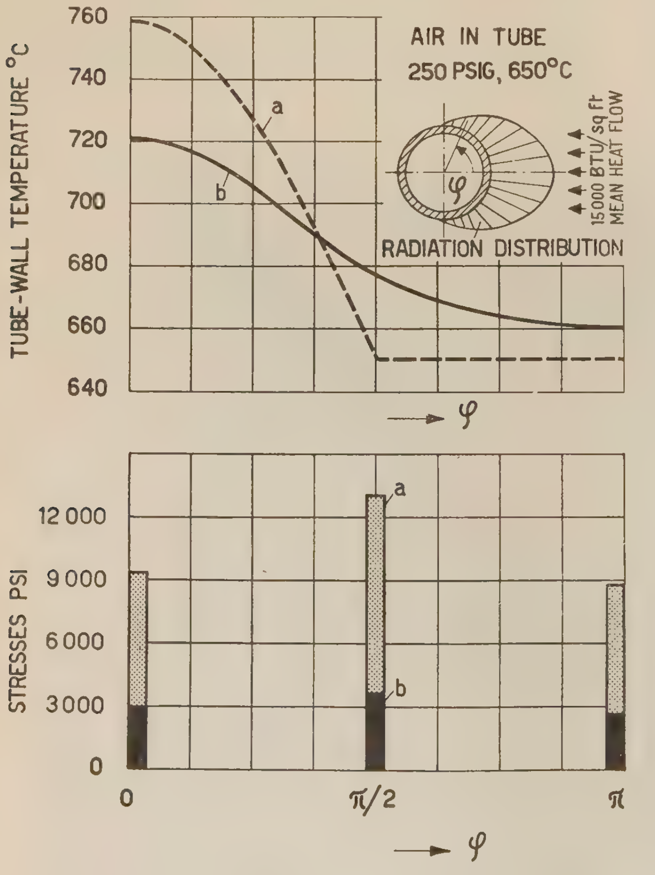

Fig. 20 Example of Temperature and Stress Distribtion in Heater Tubes Exposed to One-Side Radiation

(Curve (*a*) Without circumferential heat transport in wall and without interradiation. Curve (*b*) Actual conditions.)

A symmetrical arrangement which assures uniform admission to the surface is essential. Care must be taken that flame does not reach individual tubes. Many of our newer designs for oil- and gas-fired air heaters, as well as for pulverized-coal firing, are therefore of cylindrical, symmetrical type, with a central combustion chamber. For reheating, high and low-pressure tube systems can be combined suitably in one shell. This avoids losses from long pipe connections.

Figs. 21 to 23, all at the same scale, show the great influence on design and size of choice of basic heat-transfer mechanism. Starting from the conservative counterflow convection air heater, development leads to the crossflow heater. Its main advantage is absence of the many guide walls needed in the counterflow type. Accessibility is good and individual tube bundles can be replaced easily. (All heaters, Figs. 21 to 23, for 12,500-kw sets.)

Adoption of radiation transfer, with atmospheric firing, gives the simplest layout. This air heater should also prove successful for coal firing. As radiation intensity of coal flames is rather high, the mean temperature in the combustion space must be reduced. Therefore we foresee need for recirculating a rather large amount of flue gas. To keep slag-ash particles as far away from the tube wall as possible, recirculated flue gas is blown in along the whole length of the tubes and all around the circumference of the combustion chamber between the spaced tubes. This gas stream blows impurities away from the tube surface and, as it is comparatively cool (500–600 C), it has the additional effect of cooling and granulating ash particles. It can be seen that a pulverized-coal-fired air heater should not differ much in principle and components from units already built.

Cylindrical design permits use of many identical tube serpentines and headers for both high- and low-pressure systems. One design, Fig. 23, is based on figures for combustion rates (20,000 Btu per cu ft per hr) corresponding to those of modern boilers. Maximum wall temperatures and stresses are of the same order as for pressurized oil-fired heaters, and the surface per kw is about the same. This design can be used for solid fuel as well as for oil. With oil-firing, the quantity of flue gas recirculated is reduced. This results in higher combustion-space temperature, compensating for lower radiation intensity of oil flames.

Over-all dimensions of the atmospheric air heater are somewhat bigger than those of the pressurized type, but by no means exceed those of normal boilers. Accessibility and cleaning possibilities are good.

Allowable heat release in the combustion chamber largely determines dimensions of air heaters. Assumptions discussed in the foregoing paragraphs do not differ from normal steam practice. If, in the future, combustion rates can be raised by special burners, this will, as with boilers, result in reduction of size.

Temperatures in air-heater collectors and tubes are the highest in the entire plant. It has been said that these temperatures establish a limit for raising air temperature at the turbine inlet and thus for future higher efficiency of the closed cycle. It should not be overlooked, however, that temperature difference between highest tube-wall temperatures and air-inlet temperature for the turbine is not more than 30–50 C. Life of alloy steels depends on the relation of temperature and axial stress imposed.

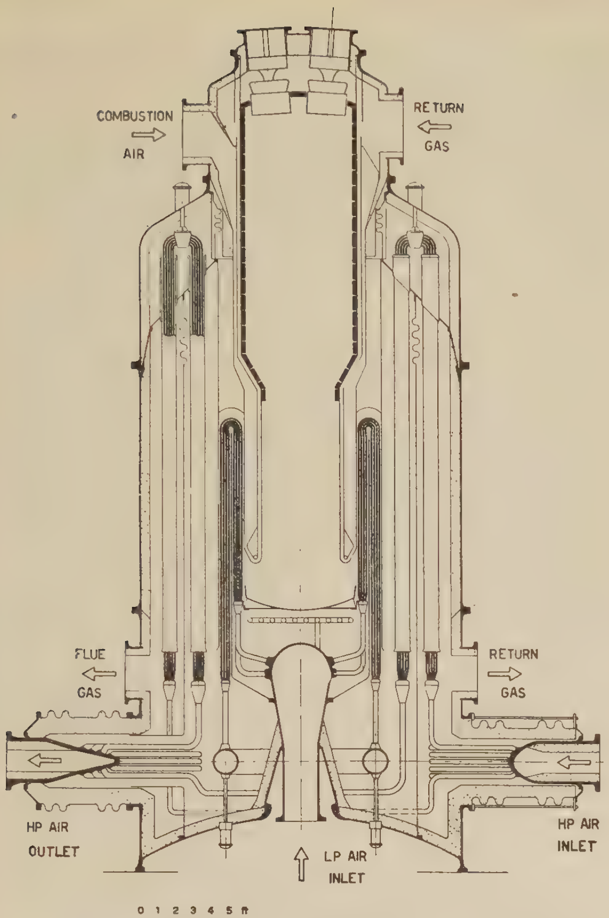

Fig. 21 Counterflow Convection-Type Air Heater for Double Heating

(Pressurized combustion. Individual high-pressure tube bundles are surrounded by cylinders in which combustion gases flow at elevated velocities.)

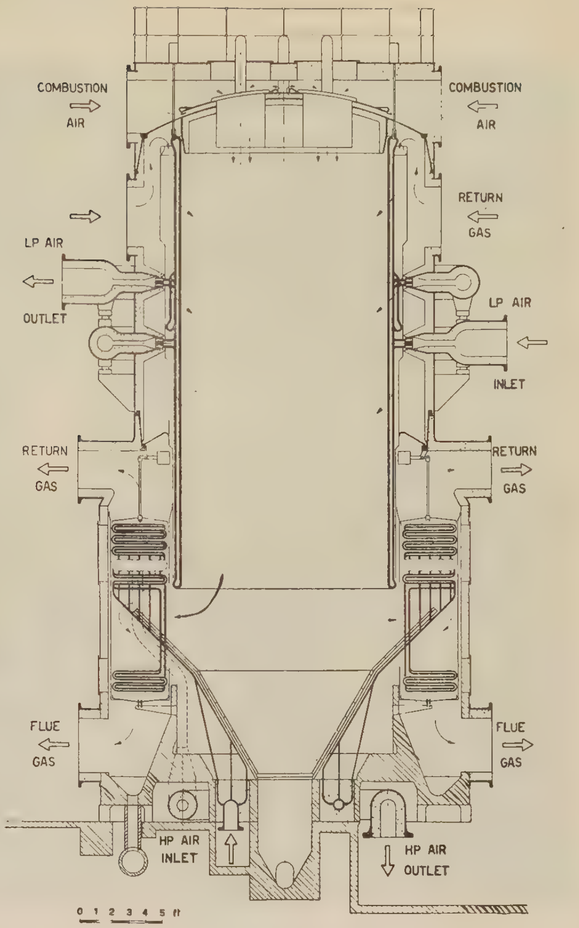

Fig. 23 Radiation-Type Heater With Atmospheric Combustion

(Suitable for pulverized-coal or oil firing.)

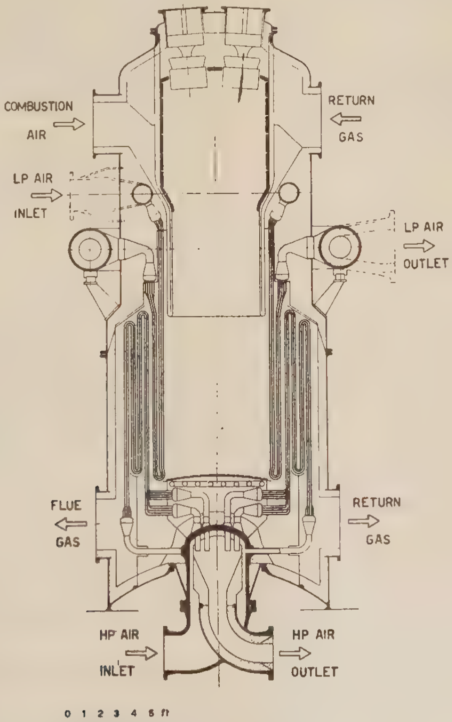

Fig. 22 Crossflow Convection-Type Air Heater for Double Heating

(Pressurized combustion. Double-walled outlet collectors for high-pressure and low-pressure system do not need high-alloy steels.)

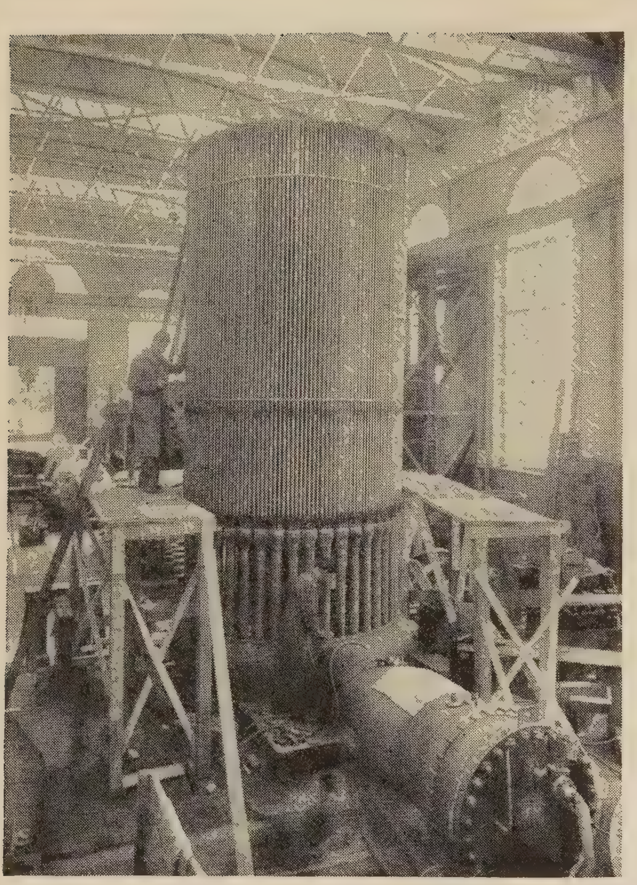

Fig. 24 Low-Pressure Tube System for Paris Air Heater in Course of Pressure Tests
(Tests at Escher Wyss Works.)

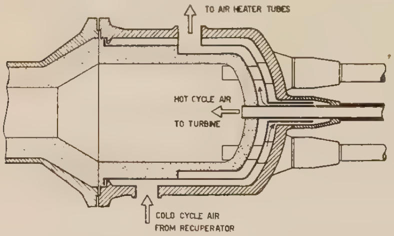

Fig. 25 Double-Shell Air-Cooled Collector for Elevated Working Pressures and Temperatures

Stresses in the air-heater surface can be kept small—between 1500 and 2000 psi. In all the gas-turbine rotors much higher stresses occur. Thus, although temperatures in some heater parts are higher, the safety margin against rupture is at least as large as in other parts of the plant. The rotors limit allowable temperature, not the air heater.

We have developed new means for reducing temperatures of collectors, which can thus be built without high-alloy heat-resisting material. Fig. 25 shows the double-shell principle used in design of the high-pressure outlet collector of the crossflow heater. Inlet and outlet collectors are combined. Relatively cold inlet air to the high-pressure heating system (about 400 C) enters a cylindrical chamber which encircles the outlet. Small pressure difference between inlet chamber and outlet corresponds to pressure drop in the high-pressure tubes. The outer casing is cooled by inlet air and takes up pressure stresses. The thin inner casing, which withstands the high temperature, is virtually not loaded. Incoming cooling air passes first along tube inlets and produces a steady diminution between hot inlet tube wall and cooler collector shell.

Air at the pressures of these closed circuits, up to 750 psi, has a good cooling effect. Heat transfer at this pressure is 20 times as high at normal atmospheric conditions, for the same velocity. Even with a small amount of extraction air, high-temperature parts can be cooled effectively with small air velocities.

Closed-Cycle Turbines for Industrial Use and for Small Outputs

In estimating future possibilities of gas turbines it is a peculiar fact that whatever their kind and size they are compared with large modern steam-turbine units. Yet only in large sizes do steam plants attain thermal efficiencies of 30 per cent or more. For smaller steam units, fuel consumption rises gradually, and for capacities below 10,000 kw an over-all efficiency of 25 per cent represents a good figure (8). It is an important but often overlooked fact that gas turbines can, even now, be built for small outputs with efficiencies nearly as high as for large outputs.

It follows that the field of small and medium-power sets is at present a promising one for gas turbines. As the closed cycle provides freedom in choosing suitable working pressures, and therefore volumes, favorable possibilities for small-output turbines exist. Units of a few hundred to a few thousand kilowatts can work with 150-250 psig top pressure. The dimensions of the machines are by no means too small for maintaining good

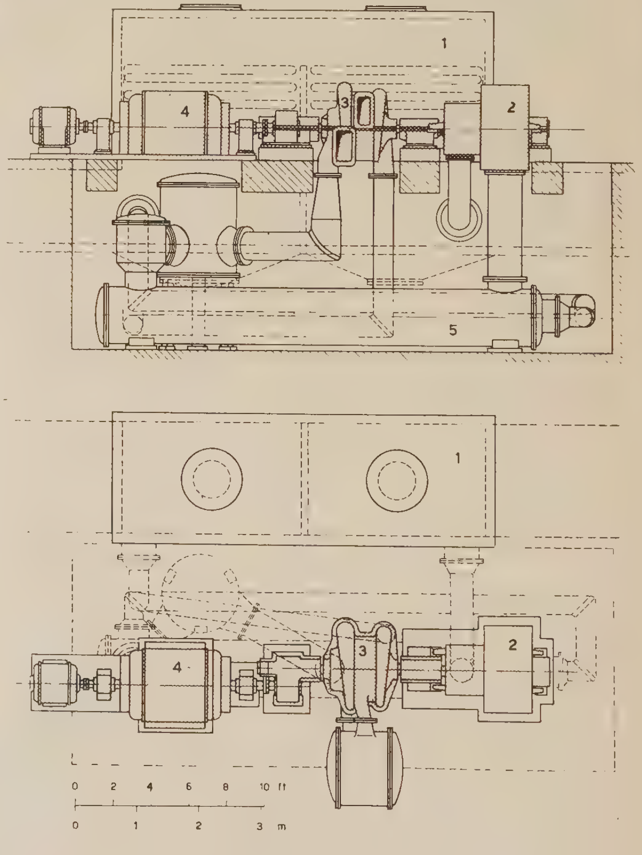

1 Waste-gas air heater
2 Turbine
3 Compressor
4 Generator
5 Heat exchanger

Fig. 26 Layout for 1000-Kw Closed-Cycle Plant for Waste-Heat Recovery
(General arrangement is same as for first 700-kw set of this kind built by John Brown & Co., Ltd., for Coventry gas works. Turbine-inlet pressure about 140 psia, counterpressure about 35 psia.)

efficiencies. The guarantee of lasting cleanliness of the circuit is essential for such small installations, which often work in dirty surroundings.

A striking example of the favorable possibilities of small closed-cycle plants is a waste-heat utilization unit of about 700 kw being built by John Brown and Co., together with Spencer Bonecourt, Ltd., London (6). It is for a gas works.

Studies have shown that a closed-cycle plant offers an economical and reliable way of utilizing heat available in waste gases such as occur in gas works, carbonizing plants, and the steel, chemical, and oil industries. It often occurs that waste heat is available at high temperatures (600–900 C) and low pressures. Heat must be supplied to the working medium of any turbine cycle in an indirect way. Up to now, waste heat was mostly used in boilers to produce steam for engines or turbines. As high-temperature service is not suitable for them and efficiencies of small sets are low, it usually does not pay to produce electrical energy.

The gas turbine changes this picture entirely. In the case just mentioned, one gets about double the electric output when choosing a closed air cycle instead of steam. The air heater can be built very simply as a counterflow tubular heat exchanger. Waste gases with a temperature of 800 C can easily heat working air to 600 C. The exhaust gases of the air heater can still be used to produce process steam.

Taking into account the favorable position of the small-output gas turbine, compared with corresponding steam sets, we have also made projects for simple coal-fired closed-cycle plants down to only 1000–2000 kw net output. The air heater may be of the cylindrical type with atmospheric combustion. Pressures in the working cycle would be 230 psia at the turbine and 60 psia at the suction side of the compressor. Simple expansion in one turbine is proposed, with maximum working temperature of 650 C. The turbine is directly coupled to a two-stage compressor and runs at about 10,000 rpm. Only one intercooler is planned. The generator connects through a reduction gear. The regenerator, of the tube-bundle type, may serve directly as a foundation for the machine set. In the arrangement shown, Fig. 27, shortness of piping is notable. The turbine would have 6 stages with a tip diameter of only 16 in. Depending upon the economic amount of heat-exchanger surface, efficiencies of from 26 to 30 per cent can be expected from this simple plant. These are over-all efficiencies, including all auxiliaries.

Necessary cooling-water quantities can be very small, one fifth to one tenth of those of corresponding steam plants. Sacrificing some fuel economy, closed-cycle plants can also run without water at all, using air cooling for compressor intercoolers.

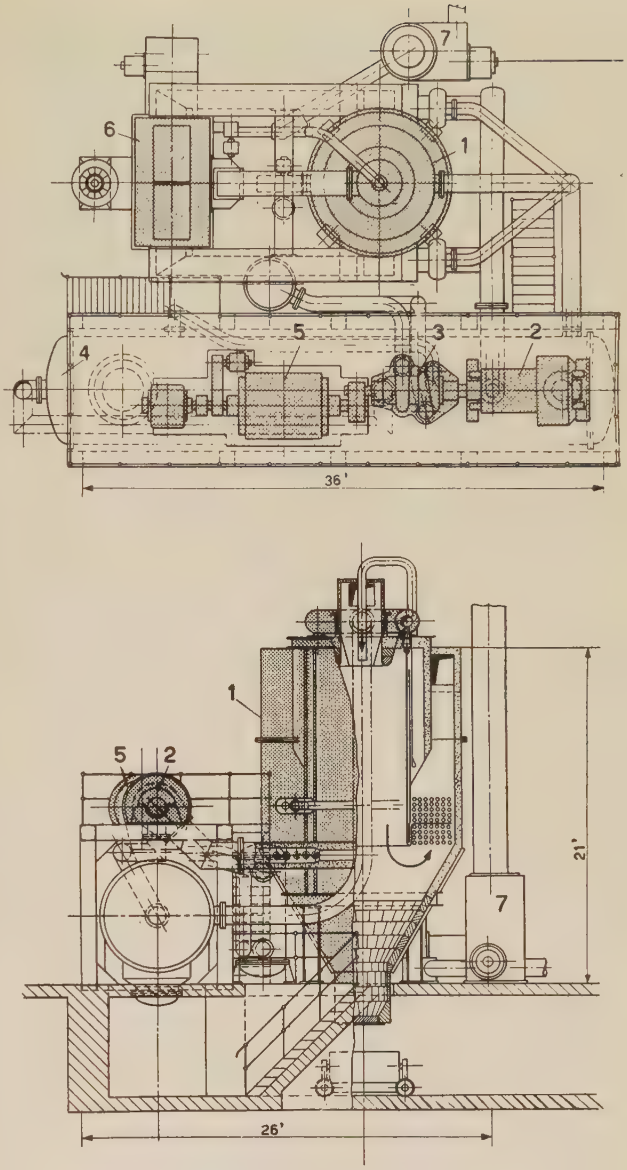

Fig. 27 Project for 1000-Kw Pulverized-Coal-Fired Unit

1 Air heater
2 Turbine
3 Compressor
4 Heat exchanger
5 Generator
6 Combustion-air preheater
7 Coal-handling and preparation equipment

BIBLIOGRAPHY

1 "The Escher Wyss-AK Closed-Cycle Turbine, Its Actual Development and Future Prospects," by Curt Keller, Trans. ASME, vol. 68, 1946, pp. 791–822.

2 For development of naval gas turbines which are not treated in this paper see: "The Gas Turbine as Applied to Marine Propulsion," by T. A. Crowe, *Journal of The Institution of Mechanical Engineers*, London, vol. 157, June, 1948, pp. 103–116.

3 "Applied Atomic Power," by S. C. Smith, A. H. Fox, R. Tom Sawyer, and H. R. Austin, Prentice-Hall, Inc., New York, N. Y., 1946, chapt. 3, p. 141.

4 "An Aerodynamic Thermal Power Plant," by J. Ackeret and C. Keller (in German), *Revue Polytechnique Suisse*, vol. 113, 1939, p. 229.

5 "Compte-Rendue des Essais de la turbine aérodynamique Escher Wyss-AK," by H. Quiby (in French), *Revue Polytechnique Suisse*, vol. 125, 1945, p. 269. English translation in *The Oil Engine*, London, England, November, 1945.

6 "Regulation Theory for Thermal Power Plants Employing a Closed Gas Cycle," by F. Salzmann, Trans. ASME, vol. 69, 1947, pp. 329–335.

7 "A Method of Calculating the Temperature Distribution in Non-Uniformly Heated Tubes," by F. Salzmann; paper presented at the International Congress of Applied Mechanics, London, England, September, 1948.

8 "Technische und Wirtschaftliche Aussichten von Gasturbinen," by F. Münzinger, *Schweizerische Bauzeitung*, vol. 126, 1945, p. 63; "Comparison of Gas and Steam Turbines," *Combustion*, vol. 20, September, 1948, pp. 39–42.

9 "Presidential Address," by Capt. (E) W. Gregson, Proceedings of The Institution of Mechanical Engineers, London, England, vol. 160, 1949, p. 58.

Discussion

P. F. Martinuzzi.[3] The author is to be congratulated on an excellent paper which reports clearly and concisely an important development in the industrial gas-turbine field. It is a great pity that Dr. Keller could not present his paper himself; not only was it impossible to congratulate him and welcome him again, but also the opportunity was lost of extracting further information. The paper is full of tantalizing statements about which further details would be most welcome. The author and Escher Wyss are both to be congratulated on their courage, which is a characteristic of Swiss industry, in undertaking the whole development work described in the paper without outside financial assistance. It may surprise some American readers to learn that the whole Swiss industrial gas-turbine development work, which has been carried on in four different technical directions by four firms, the largest of which has only 8000 workmen, has been financed entirely by the firms themselves without any help from either the government, the military, or any other outside sources. Yet Switzerland is still easily in the lead in industrial gas turbines.

---

[3] Professor of Mechanical Engineering, Cornell University, Ithaca, N. Y. Mem. ASME.

When in 1945 Professor Ackeret and Dr. Keller listed as an advantage of the closed-cycle turbine the fact that the air in the cycle is clean, not much importance was given to this point. Recent unfortunate experiences of other firms, as well as the author's report on compressor efficiency drops when the compressors are run with ambient air, show the importance of this point. Of course these efficiency drops become very noticeable only if the compressor efficiency is really high; if axial compressors can run in a dusty atmosphere without loss of efficiency, this might tend to indicate that the compressors are not as efficient as they should be. The extensive use of centrifugal compressors in the new plants is extremely interesting; these compressors are of course immune from efficiency drops due to impure air. This fact alone justifies their adoption in the charging sets. But it is interesting to see that the high-pressure stage of the main compressor is also centrifugal. Are these centrifugal stages designed on the Oerlikon principle? It is well known that, although Escher Wyss and Oerlikon are independent in their technical staff, they are linked financially. What is the efficiency of these centrifugal stages, and how does it compare with that of the axial stages? The fact that four centrifugal stages are used for a compression ratio of 3.6 to 1 indicates very conservative peripheral velocities; the efficiencies should be excellent. Further details on this point would be extremely welcome. Also some more information is desired on turbine-blading type and efficiency. The fact that 8 stages are used in the high-pressure section for an expansion ratio of about 3, and presumably 7 stages in the low-pressure section for an expansion ratio of 3.9, shows the desire to obtain the highest possible turbine efficiency.

The air heater is the most important component of the closed-cycle gas turbine, and the author is to be congratulated on the many details he has given. If, as is to be hoped, full test data will be published in due course about the Paris and Dundee plants, it will be most interesting to compare the performance of the counterflow and crossflow types. The fact that pressurized firing has been adopted is a distinct advantage; the complication due to the charging set does not seem excessive in view of the reduction in air-heater size (and tube stress); the more so as even the nonpressurized type must have circulation and recirculation fans. Presumably pressurization will be impossible with pulverized-coal firing.

One of the main advantages of the closed-cycle gas turbine is that it constitutes probably the only practical way of burning coal in a gas turbine; certainly the only practical way to burn coal in a high-efficiency gas turbine. At present prices of oil and coal, the cost of running a high-efficiency oil turbine might well be smaller than that of a low-efficiency coal turbine. It will be most interesting to get further details on the proposed 1000-kw pulverized-coal-fired unit described by the author. Is there any chance of its being built soon?

It is difficult to agree with the author on his contention that the turbine blades and not the air-heater tubes represent the most delicate point in the closed-cycle turbine; 30-50 C can make a lot of difference in the creep characteristics of high-temperature alloys. One need only remember the effect that 50 F has had on the Seawaren plant as compared with the Essex plant! And the turbine of a closed-cycle installation is protected from local overheating due to uneven combustion, which sometimes gives trouble in open-cycle types; while the air-heater tubes are very much at the mercy of local overheating. The fact that the air-heater tubes are the most delicate point is implied in Professor Quiby's official test report of the experimental Escher Wyss turbine (5).[4] In these tests the maximum temperature was increased from 687 C to 698 C, when the load was decreased from 2000 to 400 kw; these tests were of course effected at the maximum temperature the machine would stand, in order to show the highest possible efficiency. Now, a decrease in load does not affect, in practice, the turbine stresses, as the turbine peripheral velocity remained constant; but it decreases very substantially the air-heater tube stresses as the pressure in them is reduced about proportionally to the load. Hence the increase in temperature was allowed by the decrease in air-heater tube stress, which, consequently, is the critical point. This is also proved by the fact that, in the reheat turbine, the temperature is 10 C higher than in the high-pressure turbine.

There is no question that the future of the closed-cycle gas turbine depends on the development (or rather, on the lack of development) of alloys or devices which would allow very high temperatures in the turbine. If special alloys, or blade cooling, or a combination of the two should allow turbine temperatures of about 900 C in industrial use, the complication of the closed-cycle turbine and the difficulties that would arise with the air heater would not justify the use of this type of turbine. At those temperatures the efficiency and compactness of the open-cycle type would be unbeatable.

Tremendous sums of money are spent to develop very high-temperature turbines for aircraft uses. The objective is an aircraft turbine running at about 1600 C (3000 F). If such a turbine became available, it would presumably be possible to run an industrial turbine at over 1000 C, and the closed-cycle turbine would be doomed, except for special applications such as atomic energy or waste heat or coal-fired turbines. However, much of the money poured into the development of the high-temperature aircraft turbine works at very low efficiency, owing to military secrecy, changes of plan, duplication of work, and so forth, and a change in the political picture would stop very rapidly the flow of money. So it is quite possible that in the next 10 or 15 years, the temperatures of industrial gas turbines will not go above 800 C. In that event, the closed-cycle gas turbine will certainly have a vast field of application.

The waste-heat turbine described by the author at the end of his paper is a most interesting development. One is rather inclined to think of the closed-cycle turbine as a rather large unit; it is interesting to see that the cycle can be used for small and even very small powers. This is probably rendered possible by the use of centrifugal compressors which maintain their efficiencies even with small flows. This type of waste-heat closed-cycle turbine has the advantage that the efficiency drop in the waste-heat exchanger would apply equally to any other type. Test results on this type will be very interesting also because they would give indications on one of the possible types of closed-cycle turbine for atomic power.

F. Nettel.[5] The progress made by Escher Wyss during the last 5 years is impressive. However, while extensive information was given concerning component design and arrangement, it is difficult to get a clear idea of the cycle actually employed. It would be highly desirable if a T-S diagram with pressures and temperatures at all points would be given. Lacking that, we can guess from the figures that the three intercoolers are evenly spaced over the compression range giving a fairly close approximation of isothermal compression. The plant works over a pressure range from 750 to 65 psi with top temperature 665 C. Reheating takes place to 675 C after expansion to 255 psi, which seems rather late. The high efficiency of this cycle is predicated on a heat exchanger of very high effectiveness and visibly very large dimensions. It is, however, influenced to a similar degree by the sizes of the intercoolers, the aftercooler, and the air preheater for the furnace of the air heater proper, about which hardly any information is given.

---

[4] Reference is to author's bibliography.

[5] Consulting Engineer, Manhasset, L. I., N. Y. Mem. ASME.

In order to compare the closed-cycle plants described with steam plants and other gas-turbine systems, it would be helpful to know the total heating plus cooling surface pro kilowatt plant output of all elements involved. It seems that this figure will be found much higher than the corresponding figure for steam plants, including boiler, superheater, economizer, air heater, condenser, and feedwater heaters. This comparison will be of great import for the economic prospects of the AK plants in this country. The utilities of the United States are primarily interested in plants of from 25,000 kw upwards to 75,000 kw or more which can burn coal. For base-load application, highest efficiency is paramount, provided the installation cost remain at present levels. For peak-load plants, economic considerations often will force low installation cost and, consequently, lower efficiency. Important savings obviously can be made easiest by reducing the size of the heat exchanger and possibly the furnace air preheater.

With decreasing effectiveness (size) of the heat exchanger it remains imperative to obtain the highest cycle efficiency attainable with the chosen size of equipment. To achieve this, it will be necessary to deviate from the "double-isotherm" cycle, i.e., restrict the air intercoolers to the first half of the compression range, thus leaving the second half uncooled. It will also be important not to reheat as late during the expansion as the described plants indicate. These measures bring very substantial efficiency gains, particularly for relatively small heat exchangers, not only for thermodynamic reasons, but also because they reduce the parasitic pressure losses.[6]

While the closed-cycle plant has reached practical application for medium-sized installations using liquid fuels, new problems will arise for large coal-burning plants for which supercharged furnaces are as yet undeveloped. For such conditions, semiclosed plants may have great potentialities, and more information regarding them will help to clarify the issue.

W. T. Sawyer.[7] The author's position as a pioneer in the field of gas-turbine engineering lends special meaning to his review of the progress of the closed-cycle gas-turbine plant during the past 5 years. He was among the very first engineers to recognize the necessity for treating rotating components from the standpoint of aerodynamic theory. The progress of this Escher Wyss plant embodying his approach is accordingly of direct interest to all of us.

It is believed the author may be accused of having been excessively modest in his reference to the effort being made by Swiss industry to bring the industrial gas turbine into being. In proportion to its size and population, Switzerland has clearly made the greatest effort in this regard of any country in the world. Special commendation is due to Swiss industry for undertaking upon its own resources the risk involved in exploring the development of three of the major gas-turbine cycles.

At the time when the author's first paper was presented to this Society in 1945, one of the advantages claimed for the closed cycle, namely, the use of clean air under pressure in working cycles, was perhaps discounted by some of us for lack of factual information regarding the degree of compressor and turbine fouling which would be encountered in practice with other cycles. Subsequent experience which has been reported, particularly with regard to compressor fouling, lends additional weight to this feature. The writer is happy to hear that Escher Wyss considers shipboard plants among the most promising projects and is continuing to concentrate upon them along with other applications. The good full- and part-load fuel economy of this type of plant makes it very attractive for ship propulsion.

By way of emphasis, will the author reaffirm the fact implied in Fig. 1 of the paper, that an air-heater tube-wall temperature of 900 C is today a constructional possibility? Also, does the author associate a diminished operating life with the use of a temperature of this magnitude?

While not taking specific exception to the statement that the gas-turbine rotors and not the air heater limit the allowable temperature in the Escher Wyss plant, one factor in that regard deserves mention, in order to maintain our perspective. The present-day trend toward higher temperatures is clear. Many of us feel that these higher temperatures will be accommodated only by the development of adequate cooling methods. Although current progress promises considerable success with the cooling of hot turbine parts, it is extremely difficult to see how cooling can be applied to the tube walls of an air heater through which heat must be transferred. The air heater, therefore, appears destined to become, if it is not already, the limiting factor for allowable cycle temperatures in the closed cycle.

The present trend toward reduction in content of scarce and expensive materials in high-temperature parts also seems to encounter a stumbling block in the inability to cool the hottest metal parts of the closed cycle—the air-heater tubes. It will be of interest to hear the author's views on this development trend.

Author's Closure

The author unfortunately was prevented from attending the meeting and the discussion when this paper was presented. Therefore, he wishes to express his thanks to Mr. L. N. Rowley, who presented the paper. On a recent visit to the United States, the author had an opportunity to discuss many questions concerning gas turbines. On the occasion of an informal meeting of the ASME Gas Turbine Power Division, in New York on May 25, he dealt with most of the questions put forward in the paper and in the discussions. Therefore, in order to condense the closure, only the most important points will be considered.

Attention is called to the fact that the Ackeret-Keller power plant bears a much closer resemblance to the steam power plant than it does to the open-cycle gas turbine. This should help in our thinking, particularly in the discussion of higher cycle temperatures.

During the recent visit mentioned, the author was greatly impressed with the practical progress in metallurgy and in the development of appropriate designs for gas and steam-turbine components. Successful developments in the chemical industry and its apparatuses for high-temperature service may have a pronounced effect on the design of future caloric machinery. This holds true at least for the closed-cycle plant with its different components such as air heaters, heat exchangers, and coolers. The advanced technical know-how of the chemical industry and its plants will lead to a marked cost reduction. When comparing the technical solution for the closed-cycle plants discussed in the paper presented 5 years ago[8] with what can be done now, the possibility is shown of very great simplification, both in machines and apparatuses.

---

[6] "The Universal Optimum Power Cycle for Elastic Fluid Turbine Power Plants," by J. Kreitner and F. Nettel, Paper No. 47—A-43, abstract published in *Mechanical Engineering*, vol. 70, 1948, p. 355.

[7] Bureau of Ships, Navy Department, Washington, D. C.

In answer to Professor Martinuzzi's questions: The radial-type compressor was selected for the last two stages of compression due to specific speed requirements. This is a typical high-efficiency Escher-Wyss compressor and bears no resemblance to the Oerlikon compressor referred to. This compressor has a capacity of about 8000 cfm, and an adiabatic efficiency of well above 80 per cent at a pressure ratio of slightly less than 2:1. There is a good case for design of the whole high-pressure compressor set as radial machines as we foresee the immediate possibility of achieving an efficiency of 85 per cent, and use of such a radial-flow machine for the high-pressure group will result in a saving in capital cost and space.

The author would like to attempt to clarify the thoughts that exist regarding the limitations of the cycle as governed by the air heater. It is obvious that the temperature of the working air must be lower than that of the air-heater tubes, for otherwise no heat transfer would take place. The difference in temperature between the tube wall and working air can be controlled within precise limits as it is dependent entirely upon the air-side film coefficient and the rate of heat input. It has been our practice to work with not more than 100 deg F temperature difference between tube wall and air. Considerable latitude is offered in the design of the air heater as the life of the tubes is governed by both temperature and the accompanying stress. Thus the type of steel used and the wall thickness can be varied through the heater with the type being dictated by the local temperatures, consideration being given to the oxidizing and scaling requirements and wall thickness, determined by the type of steel and the working temperatures.

Again, it should be stressed that this is a static structure readily susceptible to analysis by anyone skilled in the art. The heater can be designed with the same high-temperature section tube material as that used for turbine blading, and the turbine-blading stress will limit the design. It must be realized that, while the turbine-blading stresses are substantially the same at all loads, due to the fact that the machines are operating at constant speed and temperature, the heater tube-wall stresses are proportional to load. Thus, assuming a load factor of 75 per cent, heater-tube operating stresses are 75 per cent of design value, while turbine-blade operating stresses are substantially 100 per cent of design value.

We will be the first to admit that the design of the air heater has constituted the greater part of our problem as we have had to work without the benefit of the experience engineers in the United States have had in the design of tube stills for the petroleum industry. Years of experience in the operation of such stills have led to a complete understanding of the problems of radiant-heat transmission and the expected life and characteristics of metals under conditions of high temperature and stress. One recent metallurgical contribution to this service is the centrifugally cast pipe for tube stills. Centrifugally cast pipe offers better creep rates at high temperature than drawn pipe, thus opening possibilities of still higher operating temperatures than those currently contemplated. The casting process of tubes also enables use in a much wider range of any desired composition of heat-resisting material which would be difficult to draw.

The position regarding the air heater can be summed up in the statement that American manufacturers can offer air heaters to meet the required service of a 12,500-kw plant at prices of the order of $25 per kw with 6 months delivery.

Professor Martinuzzi and W. T. Sawyer have referred to the possibility of the development of the open-cycle gas turbine to cycle temperatures of the order of 1000 C, in which case they say the closed-cycle system would be doomed. Quite naturally, we do not believe this. In fact the closed-cycle plant at 650 C cycle temperature is here, while an open-cycle plant operating at anything over 800 C is a future possibility. The efficiency of the closed-cycle plant at 650 C is currently some 20 per cent better than the higher temperature open-cycle plant. While cycle temperature is important to obtain high efficiency, it is not the only means. We prefer to trade static heat-transfer surface for high temperature to gain in efficiency and high circuit pressures for temperature in order to reduce machinery size.

It is realized that much theoretical discussion is taking place also in this country dealing with high-temperature schemes. Such schemes look quite attractive on paper, but they are far from practical realization. This is stated only from the standpoint of the power-plant engineers and operators who require a reliable plant of at least 100,000-hr service life. For the next few years 700–750 C will be the upper limit for an economical and safe gas-turbine plant. A future closed-cycle plant with this temperature range should run economically with 8500–9500 Btu-kwhr.

We do not favor the combination of high-temperature working medium with adequate cooling methods. Much complication for practical service would be involved which does not pay. Only a simple plant layout can show economical advantages compared with modern steam sets.

In reply to Mr. Nettel, the cycle arrangement and conditions within the cycle are substantially as given in the previous paper[8] for a double heating plant.

Concerning the questions of different working cycles, mentioned in Mr. Nettel's discussion, as a means of obtaining maximum efficiency, it must be pointed out again that what may seem favorable in theory, often does not bring the expected improvement when put into design. During the last few years we calculated hundreds of different cycles with various data and came to the conclusion that not much can be gained in performance with tricky layouts, but a lot can be lost by this means in simplicity of a plant and sound operation.

With respect to heat-transfer surface, it may be said that these figures are not alone significant for the economics of the AK plant. The total surface per kilowatt depends upon various factors as wanted efficiency, cooling-water quantities, flue-gas temperature of air heater, and naturally, on the design of the various auxiliaries which may be quite manifold. Figures for different plants now under construction will be published later. As the heat exchanger plays an important role in today's gas-turbine designs, the following figures may be useful:

The savings that can be made in reducing the size of the closed-cycle heat exchanger are not as important as would appear from first glance, particularly when one realizes that the heat-exchanger surface required for the closed-cycle plant is 2.8 sq ft per kw for an 88 per cent effectiveness in contrast to about 5 sq ft per kw for existing open-cycle plants where the effectiveness is but 75 per cent. It should also be remembered that an 88 per cent effective regenerator has over $2^1/_2$ times the surface of a 75 per cent effective regenerator.

For those interested in practical operation of open and closed-cycle gas turbine, attention is drawn to a recent publication by J. B. Bucher of John Brown & Company, Ltd., Clydebank.[9]

---

[8] Bibliography (1).

[9] "Experimental Running of Open and Closed-Cycle Gas Turbines," by J. B. Bucher, Transactions of the Institution of Engineers and Shipbuilders, Glasgow, Scotland, vol. 93, part 5, 1949–1950.

A Pyrometer for Measuring Total Temperature in Low-Density Gas Streams

By SIDNEY ALLEN[1] and J. R. HAMM[2]

The need for improved methods of measuring total temperature in low-density moving gas streams has been emphasized by the rapidly increasing use of gas-turbine engines for aircraft propulsion at high altitudes. Recent experience with various types of pyrometers has shown that increased errors of measurement and a reduced rate of response to temperature changes become apparent as the gas density is reduced. A design of suction pyrometer is presented in which sonic gas velocity is maintained over the thermocouple element at all operating conditions, thus insuring the maximum rate of heat transfer to the thermocouple from the gas, and enabling a simple correction for impact error to be applied to the indicated reading in order to derive the total temperature of the gas stream. The rapid rate of response to temperature change obtained with this pyrometer is a fundamental necessity in any control mechanism in which gas temperature is the operating criterion.

Introduction

In actual or simulated high-altitude testing of combustors for aircraft gas-turbine engines, the problems encountered in measuring temperatures in gas streams are greatly accentuated. In these tests the pyrometers are exposed to radiation from the flame, the wall temperatures are rather low, and the gas densities are quite low. Measurement errors of the order of 500 F have been found for bare-wire thermocouple installations in low-pressure combustor-component test rigs, and single shielded thermocouples are not appreciably better. Accurate calibration of thermocouples for this application is not possible because of the indeterminable effects of radiation from the flame and radiation to the walls. This is so because the luminosity of the flame and the temperature of the walls vary widely with location and with test conditions. Even if an approximate calibration were obtained, its application would be so difficult that it would be impractical.

In this paper a type of thermocouple pyrometer is presented in which the errors are reduced to negligible magnitudes or can be evaluated definitely. The paper deals with the reasons for the increase in error in gas-temperature measurement under these conditions, describes the development of a suction pyrometer in which sonic velocity is maintained over the thermocouple element, and presents calibration data and service performance of this instrument.

Analysis of Problem

When a thermocouple, which is located in a combustor and sees the flame, is in equilibrium with its surroundings at a given operating condition, a balance exists between the heat supplied to it by forced convection, and radiation and the heat flowing from the thermocouple to its surroundings by radiation and conduction. This may be written as follows:

Heat received from gas by forced convection
+ heat received from flame by radiation
= heat lost by conduction along the leads
+ heat lost by radiation to surrounding walls
+ heat lost by radiation to surrounding gas.

Expressed algebraically this becomes

$$C_1 \times (G)^n \times (T_g' - T_c) + C_2\,\epsilon'_c(\epsilon_f T_f^4 - \alpha_f T_c^4) = C_3 \frac{dT}{dL} + C_4\,(T_c^4 - T_w^4) + C_5\,(T_c^4 - T_{sg}^4) \quad [1]$$

where C_1, C_2, C_3, C_4, and C_5 are constants for a particular installation and for a given gas, the temperature of which is required. Where also

dT/dL = temperature gradient along the thermocouple lead, deg R per ft
G = mass velocity of gas (ρV)—lb/(sec) (ft^2)
n = exponent varying from, roughly, 0.5 to 0.8, depending upon size and shape of body and direction of flow of gas relative to surface, dimensionless (1)[3]
T_c = thermocouple temperature, deg R
T_f = flame temperature, deg R
T_g' = T_{sg} + some part of temperature equivalent of gas velocity, deg R
T_{sg} = static gas temperature, deg R
T_w = wall temperature, deg R
V = velocity of gas, fps
α_f = absorptivity of flame, dimensionless
ϵ_c = emissivity of thermocouple, dimensionless
ϵ_c' = $(\epsilon_c + 1)/2$, dimensionless
ϵ_f = emissivity of flame, dimensionless
ρ = density of gas, lb per cu ft

Since it is required that T_c should approach as closely as possible to T_g', a consideration of Equation [1] shows that the error terms must be made as small as possible, and the value of G or (ρV) should be made as large as possible.

When the density of the gas stream is reduced, as in the case of gas-turbine combustors operating under simulated high-altitude conditions, where pressures as low as 1 psi may occur, it is evident that the gas velocity over the thermocouple must be increased substantially to offset the effect if the numerical value of (ρV) is to be maintained as large as possible.

Experience has shown that a thermocouple can receive only a part of the equivalent dynamic temperature $(V^2)/(2gJC_p)$ of the gas, from which it is evident that a thermocouple in the gas stream can never indicate the true total temperature of the gas (T_{tg}). In fact, once the radiation and conduction errors in the pyrometer have been made negligible, a further increase in gas velocity may

---

[1] Armstrong Siddeley Motors, Ltd., Coventry, England.

[2] Development Engineer, Aviation Gas Turbine Division, Westinghouse Electric Corporation, Lester, Pa. Jun. ASME.

Contributed by the Gas Turbine Power, Power, and Aviation Divisions and presented at the Annual Meeting, New York, N. Y., November 27–December 2, 1949, of The American Society of Mechanical Engineers.

Note: Statements and opinions advanced in papers are to be understood as individual expressions of their authors and not those of the Society. Paper No. 49—A-66.

[3] Numbers in parentheses refer to Bibliography at end of paper.

result in a reduced value of T_c and hence a greater divergence from the total temperature. However, no objection can be raised to this fact, provided that the error involved can be calculated for any condition under which the pyrometer is required to operate.

This impact error in pyrometry is often expressed in the form of a "temperature-recovery factor" which is given by

$$r = \frac{T_c - T_{sg}}{T_{tg} - T_{sg}} \qquad [2]$$

using the same notation as previously.

The expression $(T_{tg} - T_{sg})$ represents the equivalent dynamic temperature $(V^2/2gJC_p)$ for the gas.

A number of investigators (1, 2, 3) have determined the recovery factors of various types of pyrometer, but in most cases the results are not applicable to routine experimental work because of the indeterminate nature of the actual gas conditions at the thermocouple itself.

This difficulty has been overcome by Dunning (5), who suggested that sonic gas velocity should always be maintained over the thermocouple element. Dunning has shown that under these conditions the relation:

Total temperature (T_{tg}) = 1.02 × indicated temperature of the thermocouple (T_c) is accurate to within $^1/_3$ per cent. (An abstract of Dunning's theory is given in the Appendix.)

Hence the use of sonic gas velocity over the thermocouple element not only enables a simple correction to be applied readily to compensate for the otherwise indeterminate impact error; but in addition, it also provides a maximum value of (ρV) for given conditions of the gas, thus insuring the maximum rate of heat transfer to the thermocouple.

Regarding the methods which can be used to minimize the losses in a pyrometer, there is a wide background of knowledge available, and in this paper only minor refinements to what is now accepted practice are suggested.

The conduction of heat along the thermocouple wire away from the junction can be reduced to a very small order, if not entirely eliminated, by arranging for the gas stream to flow over the bare wires for a certain distance after the junction.

Radiation effects on the thermocouple can be reduced to a minimum by making the thermocouple as small as is consistent with mechanical reliability, and by surrounding it with a shield, the temperature of which is maintained as near as possible to that of the thermocouple itself.

With a single radiation shield round the thermocouple, it is clear that the same arguments concerning heat transfer to the surroundings will be applicable as in the case of the thermocouple itself. Conduction of heat along the shield and radiation of heat to and from the surroundings will be present; and in addition, if the gas velocity over the outside of the shield is low, the conditions for transfer of heat from the surrounding gas to the shield by forced convection will not be optimum. These effects will make the temperature of the inner surface of the shield different from that of the gas and hence affect the thermocouple junction temperature. If this effect is to be eliminated, the logical assumption is that an infinite number of shields will be necessary; but in actual practice it has been shown by Probert (4) that, for the conditions met with in gas-turbine combustion work, two shields are sufficient to reduce the radiation effects on the thermocouple to negligible magnitudes. If two shields are used, it is essential that the gas velocity between the shields should be maintained as high as possible and that the shields should be insulated thermally from each other.

From the foregoing discussion the following basic design features for a pyrometer may be stated:

1 Sonic gas velocity should be maintained over the thermocouple element, which should be made as small as is consistent with mechanical reliability.

2 Isothermal conditions should be maintained along the wires leading away from the junction.

3 Two radiation shields should be provided and be insulated from each other, and the gas velocity in the annular space between them should be maintained as high as possible.

COMMENTS ON EXISTING TYPES OF SUCTION PYROMETERS

Although several of the points mentioned in the previous discussion have been known for an appreciable period, it was not until serious attention was given to the study of combustion problems at high altitudes that the full magnitude of some of the errors involved became apparent. Previous work with high-density gas streams had shown the need for adequate radiation shielding, but with the high rates of heat transfer to the thermocouple under these conditions it was possible for comparatively large conduction losses to remain undetected. As the density of the gas stream is reduced, however, the reduced rate of heat transfer to the thermocouple by forced convection will reveal any conduction losses by an increasingly slow rate of response to change of temperature.

Several types of suction pyrometers had been constructed in which the conduction and radiation effects were considerably reduced, as shown by a more rapid response rate than ordinary stagnation thermocouples. With these pyrometers it was customary to operate with the suction adjusted to give a maximum thermocouple reading. The assumption was made that equilibrium conditions had been reached and that the resultant temperature reading was the true one. No "recovery-factor" correction could be applied since the actual gas conditions at the thermocouple junction could not be defined with certainty.

Fig. 1 shows one of these pyrometers which was developed from a design by Probert. It should be noticed that only one suction point was fitted, although double radiation shields were used. Because of this the gas-flow conditions over the thermocouple were difficult to predict over the comparatively wide range of operating conditions for which the pyrometer was required. Calibration of this pyrometer revealed that it gave substantially correct measurement of temperature down to pressures of the order

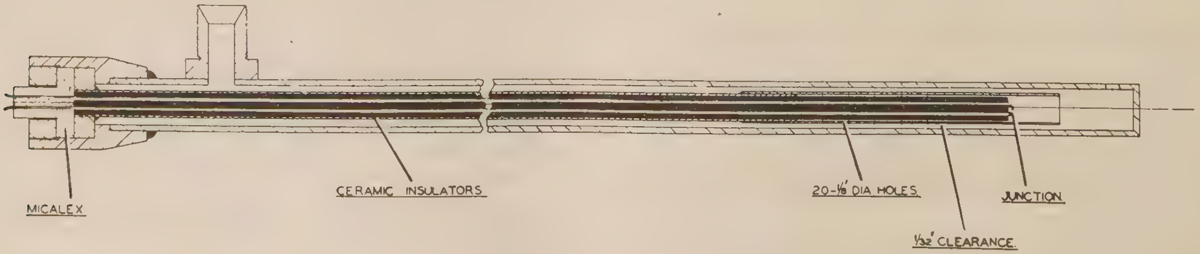

FIG. 1 PROBERT TYPE PYROMETER

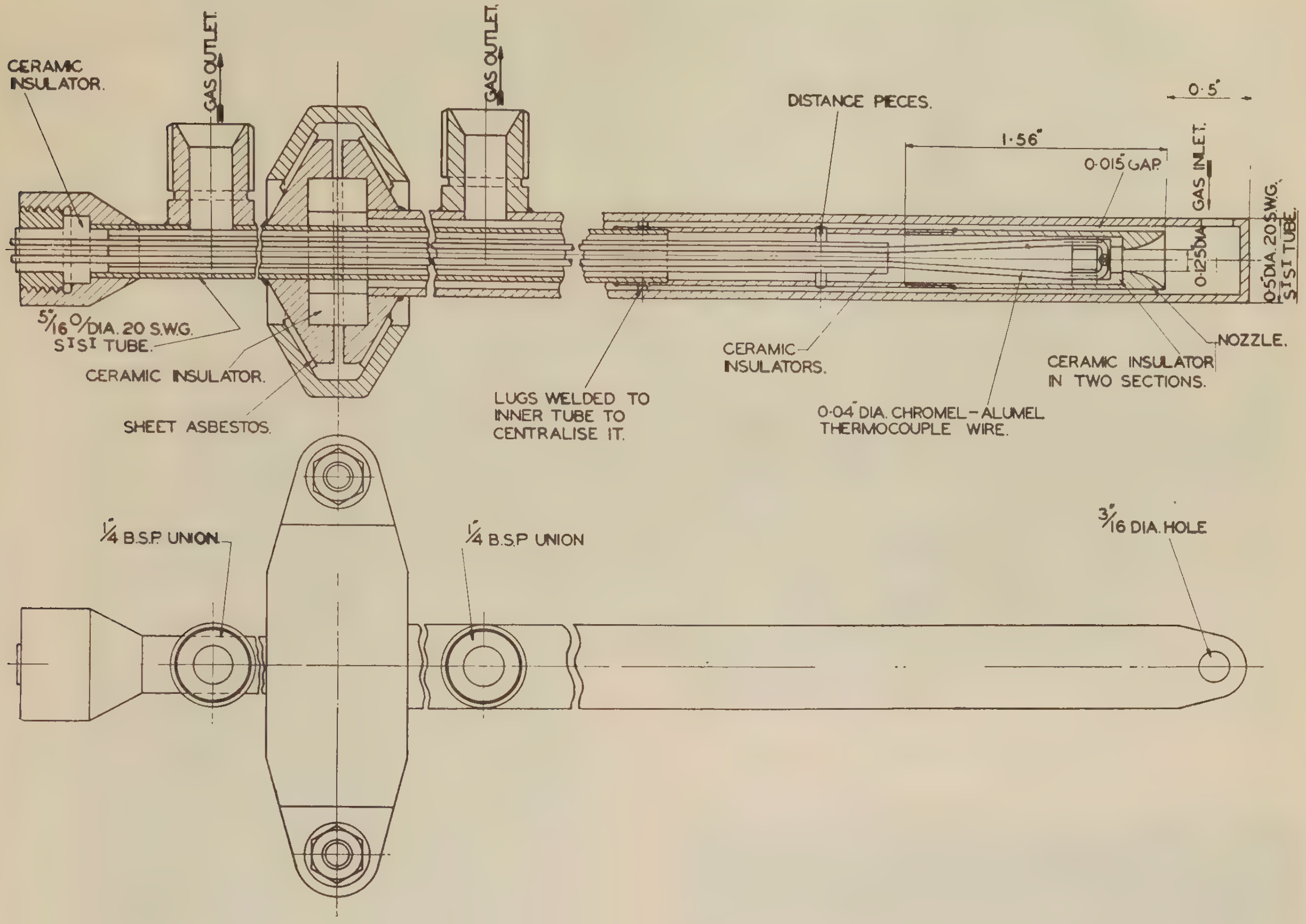

Fig. 2 General Arrangement of Sonic Suction Pyrometer

of 0.75 atm. Below this pressure, errors which increased with reduction in gas density became apparent until at a pressure of 0.3 atm, an error of the order of 5 per cent was evident.

This experience emphasized the need for a pyrometer in which a known correction could be applied to the observed reading for any required operating condition, and in which the conduction and radiation effects would be negligible.

Construction of Sonic Suction Pyrometer

Fig. 2 shows the details of a sonic suction pyrometer which was designed by Armstrong Siddeley Motors, Ltd., in an attempt to fulfill the essential requirements mentioned previously.

Sonic gas velocity over the thermocouple was obtained by placing the junction behind the throat of a convergent nozzle 0.125 in. diam, machined in the end of the inner radiation shield. Care was taken to insure that the junction was situated not more than 1 diam downstream from the nozzle throat, the location being achieved by means of two specially made ceramic insulators placed immediately behind the nozzle. A chromel-alumel butt-welded thermocouple was used, the wire being 0.040 in. diam. Flame or electric-resistance welding was used to form the junction, care being taken to remove any welding "flash" before installation in the pyrometer.

Isothermal conditions in the wires immediately next to the junction were achieved by arranging for the gas to flow over the bare wires downstream of the nozzle for a distance of about 1.5 in., after which the wires were insulated by conventional two-way porcelain insulators which were centralized in the shield by means of a suitably positioned 3-pin "spider." The gas stream was arranged to flow around these insulators to the end of the shield where it was extracted by means of a vacuum pump. The two wires passed through a suitable gland and insulator to a small terminal block.

The outer radiation shield consisted of a heat-resisting steel tube 0.5 in. diam by 20 SWG. The annular clearance between the two shields was adjusted to 0.015 in., and a $^{3}/_{16}$-in-diam entry hole was used. A separate gas connection was provided at the end of the outer shield.

In order that the two shields should be insulated thermally from each other, a tapered flange was welded to each of the shields which were centered and insulated from each other by means of a ceramic bushing through which the inner shield was threaded.

The whole assembly was held together and was rendered gastight by means of a split clamping ring which compressed the two tapered flanges onto the ceramic bushing. Thermal leakage between the clamping ring and the flanges was prevented by means of two asbestos washers inserted between the ring and the flanges.

Figs. 3 and 4 show details of an actual pyrometer, and Fig. 5 shows the assembled pyrometer.

Pyrometer Calibration

A detailed calibration of any type of pyrometer requires a specialized and comparatively elaborate rig. This is especially true when the investigation has to include subatmospheric gas pressures and exposure of the pyrometer to flame radiations. Since no such calibration rig has been available, it has been necessary

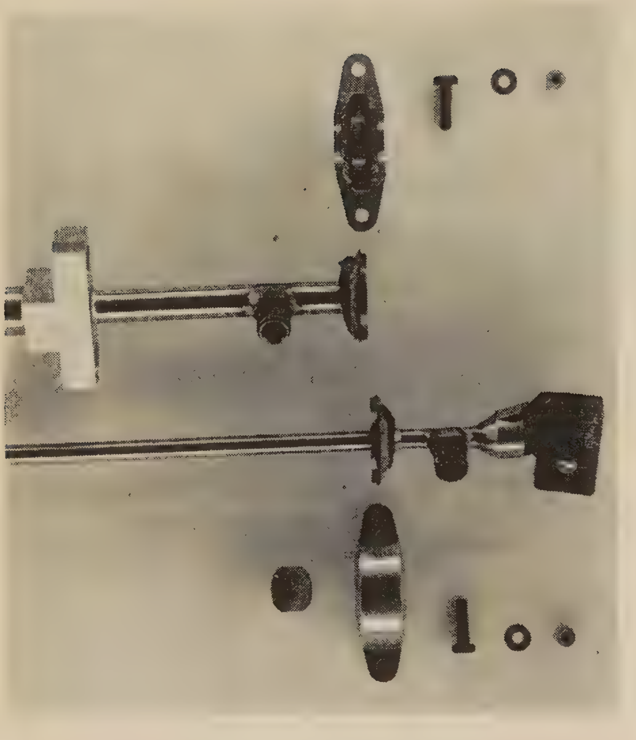

Fig. 3 Sonic Suction Pyrometer Parts

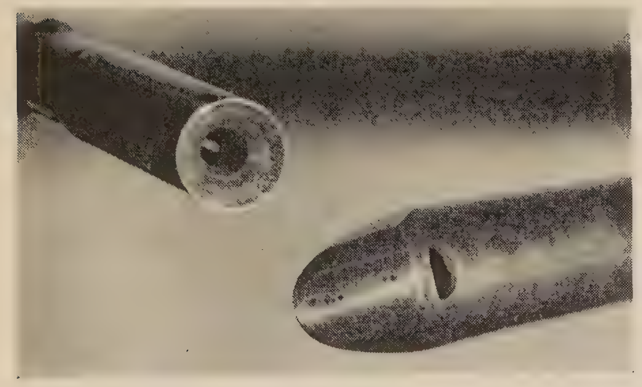

Fig. 4 Sonic Suction Pyrometer Radiation Shields

to use other means to obtain an absolute calibration of the pyrometer at these critical conditions.

After a consideration of various compromise methods of calibration, it was decided that an indirect method of absolute calibration against gas analysis should be adopted, especially as it would be fairly easy to apply this method at subatmospheric pressures where information on the performance of the pyrometer was particularly required.

A gravimetric technique of chemical analysis of combustion products had been developed by Macfarlane at the National Gas Turbine Establishment, England. This is described in detail by Lloyd (6). With care the over-all standard of accuracy of this technique is within 0.5 per cent when used to deduce combustion losses. If, therefore, the combustion efficiency of a combustor could be measured by both gas analysis and a heat balance under exactly reproducible conditions, an indirect assessment of the accuracy of the sonic pyrometer could be made at any desired operating condition. It is clear that this method is dependent upon the reproducibility of test conditions in the combustor. With the standards of accuracy usually encountered in research work of this kind, it was considered that this requirement could be met satisfactorily.

The sonic pyrometer was installed in a water-cooled traversing gear fitted to the outlet end of a gas-turbine combustor which was known to maintain its performance for a considerable period of service. This combustor was being tested at simulated high-altitude engine conditions at the Royal Aircraft Establishment, Farnborough, England, and the initial development and calibration of the pyrometer were carried out there.

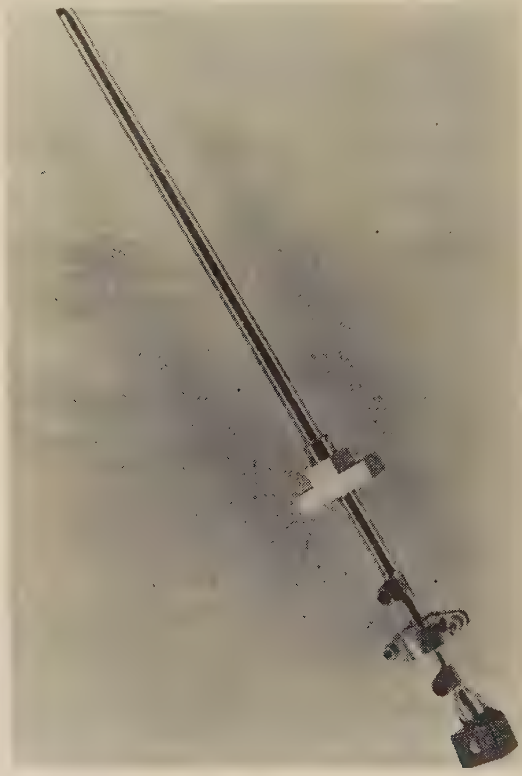

Fig. 5 Sonic Suction Pyrometer Assembled

Fig. 6 shows this test rig. Since the combustion-chamber pressure was always subatmospheric, the gas flow through the pyrometer was induced by means of two rotary vacuum pumps as is shown in the illustration. Pressure taps were located at the outlets of the two radiation shields in order to measure the gas-flow conditions through the pyrometer. These readings were based upon the assumption that there would be negligible pressure loss along the length of the shields. Exact measurement of the pressure drops would have required taps in the throat of the nozzle; this would have meant increased complication and a much larger instrument—a condition which could not be tolerated.

Experience with earlier types of pyrometers had shown the errors in the pyrometer readings to be of an appreciable order at pressures below 0.3 atm. Therefore all initial calibrating tests were carried out with the pressure at the entry to the combustor adjusted to 11 in. Hg abs, this pressure being of particular interest in the combustor test program then being carried out.

The fuel flow to the combustor was adjusted to give a mean gas temperature at the chamber outlet of 1090 F, and the gas flows through the pyrometer were adjusted to give a maximum thermocouple reading. While these conditions were held steady, the exposed cool end of the pyrometer was heated in a flame, but no change in reading was obtained. This indicated that there was sufficient gas flow through the pyrometer to swamp any

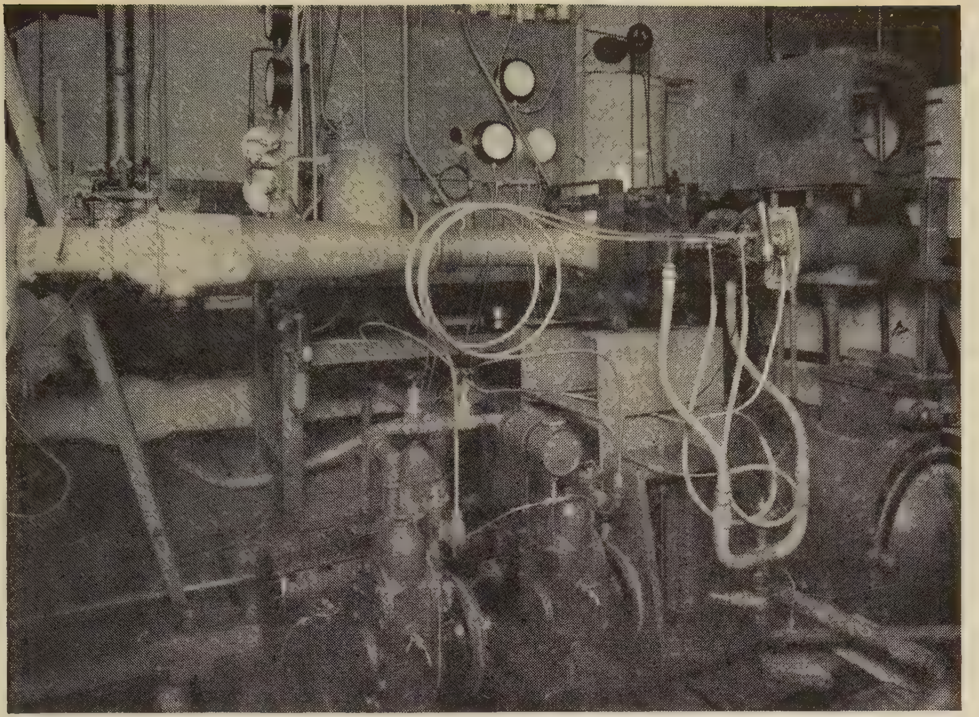

Fig. 6 Pyrometer Test Rig

conduction losses along the leads and shields. The sensitivity to rapid changes in gas temperature was exceptionally good.

Following this, a series of response curves was obtained in order to assess the effectiveness of the radiation shields. It was assumed that the magnitude of the radiation from the thermocouple to the walls was greater than that from the flame to the thermocouple, and therefore a reduction in the radiation to and from the thermocouple would cause an increase in the thermocouple temperature. With the combustion-chamber conditions steady, the full suction available was applied to the inner shield with no gas flowing through the outer shield. The gas flow through the inner shield was then reduced progressively, the steady thermocouple reading being noted in each case, until the gas flow was reduced to zero. This enabled a curve to be drawn showing the variation of thermocouple reading with suction through the pyrometer. The suction on the outer shield was then adjusted so that there was a depression of 1 in. Hg relative to the zero-flow reading on the inner shield. A second response curve was then obtained as before, keeping this depression constant.

Further curves were obtained with increasing gas flows through the outer shield until no further effect on the thermocouple reading was evident.

The family of response curves thus obtained are shown in Fig. 7. This plot shows that all the response curves for the sonic pyrometer are similar in shape and that the maximum thermocouple reading occurs at about the critical pressure drop. Increasing the gas flow through the outer radiation shield results in a vertical displacement of the whole curve, but the difference between successive curves rapidly diminishes and no appreciable difference in reading was obtained once a relative depression of 4 in. Hg was exceeded. No significant reduction in indicated temperature was obtained once the maximum reading was reached. This was due to the fact that the maximum temperature reading was reached at near the critical pressure drop across the nozzle and, consequently, there was no change in velocity at the junction as the pressure drop was further increased. In actual practice, this factor constituted an advantage, since

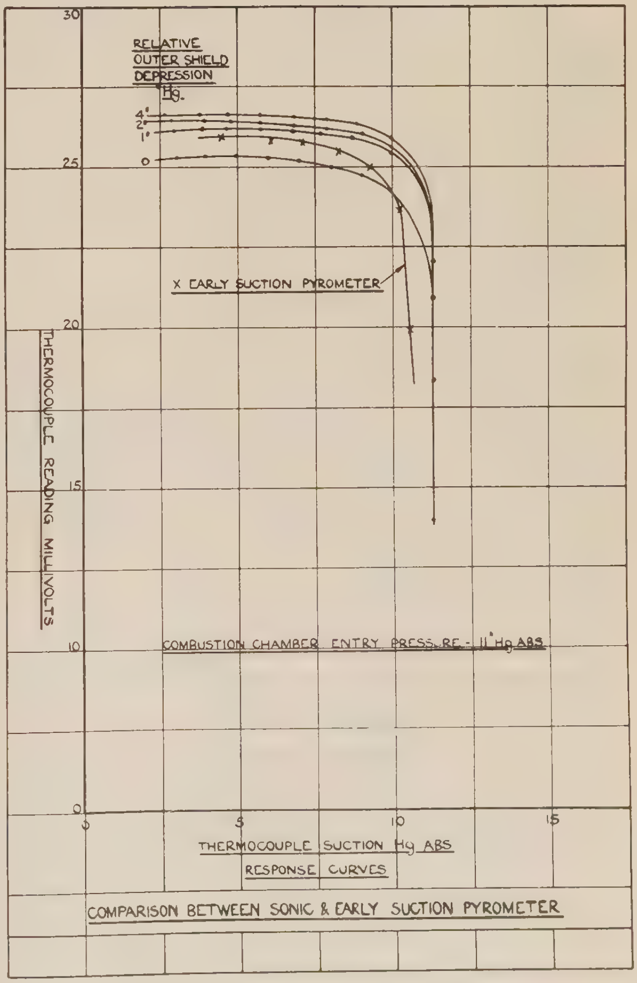

Fig. 7 Response Curves for Pyrometers

elaborate regulation of the suction on the pyrometer became unnecessary once this occurred.

The single response curve obtained with the earlier type of pyrometer under the sonic test conditions is also included in Fig. 7. Whereas the response curve for the sonic pyrometer shows the initial temperature rise to be vertical, that for the early pyrometer exhibits a definite shape. In the Appendix it is shown that the gradient of this initial portion of the curve may be interpreted as a measure of the losses existing in a pyrometer. The smaller the losses in the pyrometer, the more rapidly it reaches a maximum temperature as the gas velocity is increased from zero. Hence the response curves provide a simple qualitative method of assessing initially whether the losses in a pyrometer are appreciable. The maximum reading attained by the early pyrometer is seen to be about 2 per cent lower than that attained by the sonic pyrometer.

To check the absolute accuracy of the sonic pyrometer, a number of combustion-chamber-outlet temperature traverses were made under carefully controlled test conditions, in order to derive the combustion efficiency. Gas analyses of the combustor products were then made using the gravimetric technique mentioned previously (6). Table 1 shows a comparison among the results obtained by gas analysis, from the corrected sonic pyrometer readings, and from readings obtained with the Probert type pyrometer.

TABLE 1 COMPARISON OF TEST RESULTS

	Gas analyses		Sonic pyrometer		Probert type pyrometer	
Entry total pressure, in. Hg abs	11		11		11	
Inlet air temp, deg F ..	113 F		113 F		113 F	
A/F ratio............	52.9	75.2	52.9	75.2	52.9	75.2
Combustion efficiency, per cent...	95.5	94.9	95.3	95.7	90.2	92.6

When the standard of accuracy of the sonic pyrometer is considered, it is shown to give results which are in good agreement with those obtained by gas analysis if the correction suggested by Dunning is applied.

In order to check the thermocouple correction factor of 1.02 given by Dunning, a sonic suction pyrometer was calibrated in an atmospheric-pressure-thermocouple calibration rig at the Westinghouse Research Laboratories. In this test the gas velocity was varied from 150 to 700 fps, and the gas temperature was varied from 1000 to 2000 deg R. The average value for the correction factor for thirteen points was 1.0154. Fig. 8 shows the spread in the correction factor among these thirteen points which is about ± 0.2 per cent. Since there is no discernible trend due to velocity level, it can be assumed that this spread is due to experimental error. Spot checks on a second pyrometer gave substantially the same result.

The use of 1.0154 for the temperature correction factor in the two test points given in Table 1 gives values for efficiency of 94.7 and 94.9, respectively. These values agree with the gas-analysis results as well as do the sonic-pyrometer values which were based upon a correction factor of 1.02.

General Comments

The previous discussion has shown that the design of sonic pyrometer described in this paper is capable of a high order of accuracy of temperature measurement, coupled with a rapid rate of response. These features are evident over a wide range of gas densities, tests having been made at the Armstrong Siddeley Works at pressures varying from about 100 psia down to 2 psia. So far, only laboratory versions of this type of pyrometer have been constructed. Much smaller sizes of instrument are contemplated to meet the need for a small pyrometer, having a rapid response rate, which exists in gas-turbine engines where a measured temperature operates the control mechanism for the engine. For this application a slow response rate may cause hunting and consequent overheating of the engine. The likelihood of this happening would be greater as the operating altitude of the engine is increased.

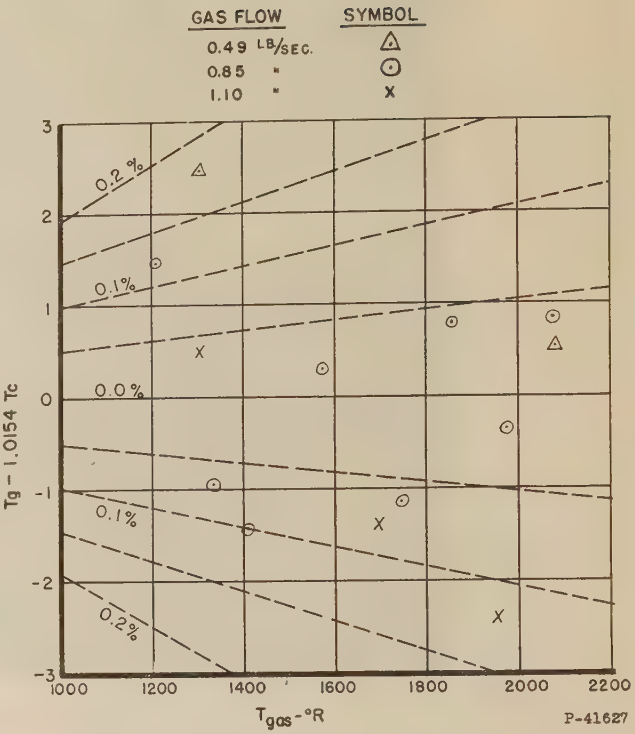

Fig. 8 Calibration of Pyrometer

(Error in sonic suction pyrometer using correction factor of 1.0154.)

The mechanical reliability and the thermoelectric stability of the pyrometer design presented in this paper have proved to be very good. Sonic suction pyrometers have been used for as long as 150 hr without any mechanical problems whatsoever. The accuracy of the pyrometer after 150 hr of operation has been checked and found to be unchanged.

In laboratory tests it has been possible to use the sonic suction pyrometers in any way that ordinary bare-wire thermocouple can be used. They have been used singly for simple temperature traverses, in gangs for traverses of annular passages, and on oscillating multi-instrument rigs for obtaining average temperatures in annular passages.

In general, the need for vacuum lines to the pyrometer has not been a serious disadvantage in laboratory testing, and the relatively high cost of these pyrometers has been justified by the good accuracy and durability obtained.

Conclusions

1 The suction pyrometer employing sonic gas velocity over the thermocouple element incorporates all the essential features shown to be necessary for obtaining an accurate measurement of the total temperature of a moving gas stream for any gas density and enables a simple correction to be applied readily for impact error.

2 In the case of gases met within gas-turbine practice, the correction for impact error is theoretically:

Total temperature of gas (T_{tg}) = 1.02 × indicated temperature of thermocouple (T_c). Actual calibration of two thermocouples gave a correction factor of 1.0154 which differs slightly from the theoretical figure.

3 The sonic pyrometer has a very rapid response to changes of gas temperature, and a simple qualitative check is possible to assess the magnitude of any thermal losses in the pyrometer.

4 Because of its rapid rate of response at low-density conditions, the sonic suction pyrometer has a particular application in the aircraft gas-turbine engine for any control mechanism in which a gas temperature is the operating criterion.

5 The sonic suction pyrometer has proved very satisfactory for gas-turbine combustion work, especially for temperature measurement at very low gas densities.

6 In gas-turbine combustion work the good durability and accuracy of the sonic pyrometer have justified its relatively high cost.

ACKNOWLEDGMENTS

The authors' thanks are due to Mr. R. W. O. Papworth of Armstrong Siddeley Motors, Limited, who was mainly responsible for the design of this pyrometer, to Mr. J. E. P. Dunning of the Royal Aircraft Establishment, who has greatly contributed to the successful development of the sonic pyrometer, and to the managements of Armstrong Siddeley Motors, Limited, and Westinghouse Electric Corporation for permission to publish this paper.

BIBLIOGRAPHY

1 "Measurement of High Temperatures in High-Velocity Gas Streams," by W. J. King, Trans. ASME, vol. 65, 1943, pp. 421–431.

2 "Temperature Measurements in High-Velocity Air Streams," by H. C. Hottel and A. Kalitinsky, *Journal of Applied Mechanics*, Trans. ASME, vol. 12, 1945, pp. A-25–32.

3 "Performance of Butt-Welded Thermocouples in High Velocity Air Streams," by L. O. Olsen, A. I. Dohl, and P. D. Freeze, National Bureau of Standards.

4 "The Measurement of Gas Temperatures in Turbine Engines," by R. P. Probert, *Journal of Scientific Instruments*, vol. 23, April, 1946, pp. 72–77.

5 Unpublished Work, by J. E. P. Dunning.

6 "Determination of Gas-Turbine Combustion-Chamber Efficiency by Chemical Means," by P. Lloyd, Trans. ASME, vol. 70, 1948, pp. 335–341.

7 Unpublished Paper, by P. R. Owen.

Appendix

Additional nomenclature is introduced in the Appendix as follows:

C_p = constant-pressure specific heat, Btu/(lb) (deg F)
C_v = constant-volume specific heat, Btu/(lb) (deg F)
g = acceleration of gravity, ft/sec²
J = Joule's constant, 778 (ft) (lb)/Btu
k = ratio of specific heats, C_p/C_v
P_R = Prandtl number, dimensionless
R = gas constant, ft/deg F
r = recovery factor, dimensionless
V = gas velocity, fps

The following is an abstract from reference (5) on the theory of the sonic pyrometer, as evolved by Dunning:

Using the same notation as previously, we have

$$T_c = T_{sg} + r \cdot \frac{V^2}{2gJC_p} = T_g' \text{ . . . . } [3]$$

Assuming that the radiation and conduction losses are negligible, and that r is a factor depending upon the thermocouple shape and gas conditions; if V is equal to the local velocity of sound

$$V^2 = kgRT_{sg} = \frac{C_p}{C_v} \cdot gJ(C_p - C_v)\, T_{sg}$$

and

$$T_c = T_{sg}\left[1 + r \times \frac{(k-1)}{2}\right]$$

We require the total temperature (T_{tg}) of the gas which is given by

$$T_{tg} = \frac{(k+1)}{2} \cdot T_{sg}$$

from which

$$T_{tg} = \frac{(k+1)}{2 + r(k-1)} \cdot T_c \text{ . . . . } [4]$$

Therefore, if k and r are known, a precise correction can be applied to the thermocouple reading T_c.

German experimental work (7) has shown that the temperature of a cone in a gas stream is in very close agreement with Pohlhausen's formula

$$T_c = T_{sg} + \frac{V^2}{2gJC_p}\left[1 + \left(\frac{U}{V}\right)^2 \times (P_R^{1/2} - 1)\right] \text{ . . . . } [5]$$

where U is the gas velocity near the surface of the cone and V is the gas velocity in the free stream. If Equation [5] can be accepted as holding at Mach number = 1, and the thermocouple is considered as a small cone, then $U \approx V$ and $r = P_R^{1/2}$.

For gases of the composition and temperature range generally met with in combustion work, P_R may be taken to have a constant value of 0.76, making $r = 0.87$.

Equation [4] shows that the nearer r approaches unity, the smaller is the effect of changes in the value of k, and with $r = 0.87$, Equation [4] becomes

$$T_{tg} = 1.021 \times T_c \text{ when } k = 1.4$$

$$T_{tg} = 1.017 \times T_c \text{ when } k = 1.3$$

Therefore, in general, the relationship

$$T_{tg} = 1.02 \times T_c$$

may be used without accepting an error greater than $^1/_3$ per cent.

EFFECT OF HEAT LOSSES ON PYROMETER PERFORMANCE

It is shown in reference (5) that for a given heat loss L in the pyrometer and for constant total conditions of the gas, the indicated temperature T_c will pass through a maximum value as the velocity of the gas over the thermocouple is varied, and that when T_c is a maximum, the following relationship holds

$$L = \frac{K \cdot T_{sg}^{\left(\frac{k}{k-1}\right)} [T_{tg} - T_{sg}]^{3/2}}{\left[\frac{(k+1)}{2} \times T_{sg} - T_{tg}\right]}$$

where K is a constant.

From this it is seen that

When $L = 0$, T_c is a maximum when $T_{sg} = T_{tg}$, i.e., $V = 0$

When $L = \infty$, T_c is a maximum when $T_{sg} = 2/k + 1\ T_{tg}$, i.e., V is sonic

and as L varies from zero to infinity, V increases continuously from zero to sonic to maintain T_c at a value whose locus is the envelope of maximum temperatures.

Hence it is apparent that with an ideal pyrometer, having no losses

$$\frac{dT_c}{dV} \longrightarrow \infty \text{ when } V \text{ is small}$$

Therefore the smaller the losses in a pyrometer, the more rapidly it reaches a maximum temperature as the gas velocity over the thermocouple is increased from zero.

This feature of the suction pyrometer provides a means whereby a rapid qualitative assessment can be made of the losses existing in the pyrometer.

Heat Transfer From an Air Jet to a Plane Plate With Entrainment of Water Vapor From the Environment

By MAX JAKOB,[1] R. L. ROSE,[2] and MAURICE SPIELMAN[3]

This paper presents some experimental results, obtained by discharging hot air from a continuous slot parallel to a plane surface. A method for predicting the distribution of surface temperature, relations for the temperature and vapor pressure in the jet, a common correlation relating heat transfer and mass transfer, considering also the entrainment of environment air by the jet, and a numerical example are given.

NOMENCLATURE

The following nomenclature is used in the paper:

a = vertical height of nozzle opening, ft
$b_j = \dot{m}'' RT_f/(p_j - p_s)$ = local coefficient of mass transfer, ft/hr
C = constant
$h_j = q''/(t_j - t_s)$ = local film coefficient of heat transfer, Btu/hr ft² F
K = constant
k = thermal conductivity, Btu/hr ft F
k_f = thermal conductivity of air at temperature t_f, Btu/hr ft F
m = an exponent
$\dot{m}''$ = local rate of mass flow per unit area (see note a at end of nomenclature), lb$_m$/hr ft²
n = an exponent
$N_{Nu} = h_jx/k_f$ = Nusselt number
$(N_{Nu})_{\text{mod}} = b_jx/\delta$ = modified Nusselt number
$N_p = (p_o - p_j)/(p_j - p_e)$ = partial-pressure ratio
$N_{Pr} = \nu/\alpha$ = Prandtl number
$N_{Re} = v_ox/\nu_o$ = Reynolds number
$N_{Sc} = \nu/\delta$ = Schmidt number
$N_t = (t_o - t_j)/(t_j - t_e)$ = temperature ratio
p_e = partial pressure of water vapor in environment air (room air), lb/sq in.
p_j = smallest observed partial pressure of water vapor measured in jet at distance x from nozzle outlet, lb/sq in.
p_o = partial pressure of water vapor in air at nozzle outlet, lb/sq in.
p_s = partial pressure of water vapor at plate surface, lb/sq in.
q'' = local rate of heat flow per unit area (see note a), Btu/hr ft²
$R = 85.4$ = individual gas constant for water vapor ft-lb$_f$/lb$_m$ F
r = an exponent
s = thickness of test plate, ft
t_b = temperature of bottom surface of plate, deg F (see note b)
t_d = dew-point temperature (used also with additional subscripts, e, j, o, corresponding to environment, jet, and outlet conditions), deg F
t_e = temperature of environment air, deg F
T_f = absolute temperature of air film, deg R (see note b)
$t_f = \frac{1}{2}(t_j + t_s)$ = air-film temperature, deg F
t_j = maximum jet temperature at distance x, deg F
t_o = nozzle-outlet air temperature, deg F
t_s = surface temperature of plate at distance x, deg F
v_o = air velocity at nozzle outlet, ft/sec
x = horizontal distance from nozzle outlet, ft
y = vertical distance from surface, in.
α = thermal diffusivity, sq ft/hr
δ = mass diffusivity, sq ft/hr
$\eta_s = (t_s - t_b)/(t_o - t_b)$ = a temperature ratio
ν = kinematic viscosity of air (used also with subscript o corresponding to outlet condition), sq ft/hr

NOTE: (a) The double prime sign in the symbol refers to unit area and the dot refers to unit time.

(b) Deg F is used for ordinary temperature, deg R for absolute temperature in the Fahrenheit scale; F = R is used for the unit of temperature difference.

INTRODUCTION

The work upon which this paper is based arose from a problem submitted to the War Research Committee of Illinois Institute of Technology[4] by the United States Army Air Forces in 1945.

Ice formation on the inside surface of aircraft windshields had become a serious problem with the introduction of high-altitude pressurized cabin bombers. One of the techniques available for preventing ice formation is that of blowing a jet of heated air over the inside windshield surface. No basic design information, however, was available.

The Republic Aviation Corporation had begun to study the problem before the authors' work started (3, 4, 5, 6).[5] Another experimental study was published later by Zerbe and Selna (7). As in these investigations, a plane heat-flow meter was used for the present measurements. No attempt was made to duplicate frosting conditions on the test plate. It is more convenient to employ higher temperatures and to convert the results to freezing conditions using the principle of similarity.

EQUIPMENT AND OPERATION

Basically, the apparatus simulates a plane windshield by a model

---

[1] Research Professor of Mechanical Engineering, Illinois Institute of Technology, Chicago, Ill. Mem. ASME.

[2] Assistant Professor of Mechanical Engineering, Illinois Institute of Technology. Jun. ASME.

[3] Associate Research Engineer, Illinois Institute of Technology. Jun. ASME.

Contributed by the Heat Transfer Division and presented at the Annual Meeting, New York, N. Y., November 27–December 2, 1949, of THE AMERICAN SOCIETY OF MECHANICAL ENGINEERS.

NOTE: Statements and opinions advanced in papers are to be understood as individual expressions of their authors and not those of the Society. Paper No. 49—A-16.

[4] This work was also used in the MS theses of R. L. Rose (1) and M. Spielman (2).

[5] Numbers in parentheses refer to the Bibliography at the end of the paper.

which is heated by a jet of hot air blown over one surface and cooled on the other side by a stream of water.

Figs. 1 and 2 are views of the major equipment in the laboratory. Filtered air, having passed through a refrigerating dehumidifier (Fig. 2, left background) enters the blower (Fig. 1, right background). Steam can be added to the laboratory air through perforated pipes above the door, Fig. 1, to increase the humidity difference between the jet and environment air. From the blower, the air passes through a duct with electric heaters and baffles, to the slot, from which it is discharged over the test plate, Fig. 3. Duct air temperatures and static pressure were read from three thermocouples and a pressure tap ahead of the slot.

The slot, 17.5 in. wide, variable in height from 0 to 0.75 in. is the outlet of a nozzle having an elliptical profile. Openings 0.25 and 0.50 in. high were used in these tests. The lower edge of the

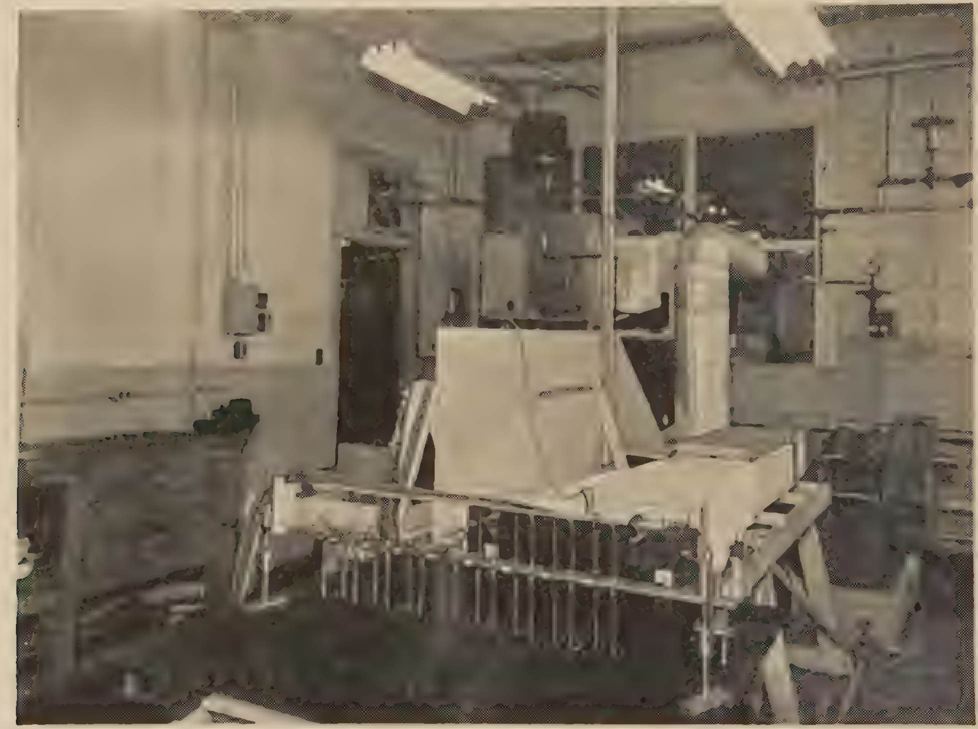

Fig. 1 View of Laboratory, Showing Duct and Test Plate

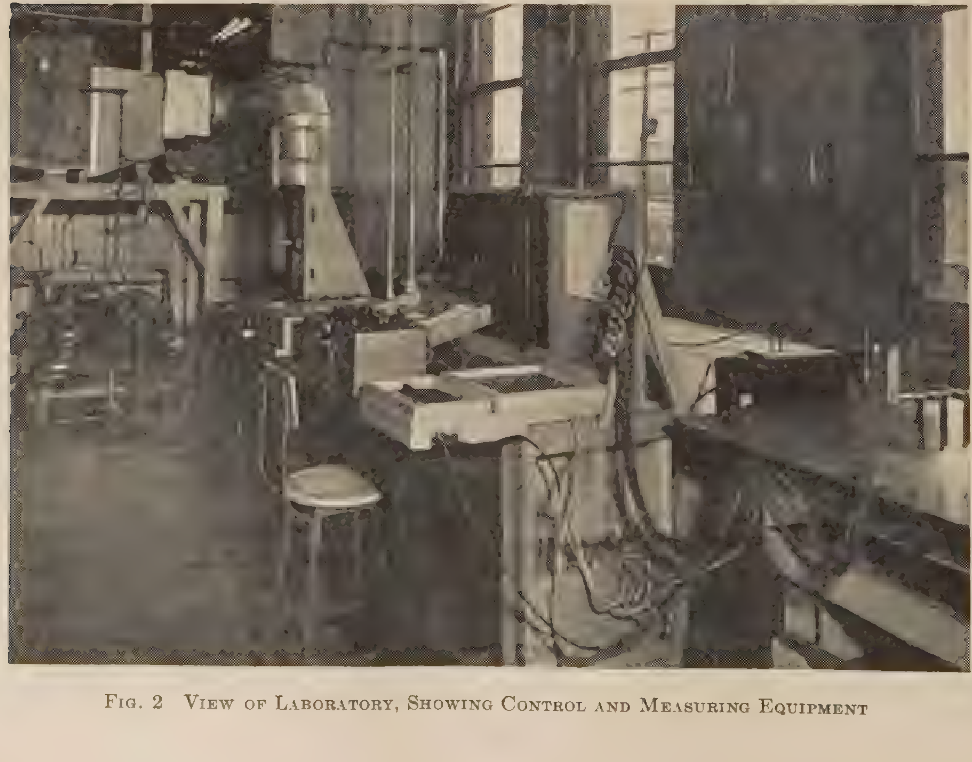

Fig. 2 View of Laboratory, Showing Control and Measuring Equipment

nozzle outlet was 0.25 in. above the starting section of the test plate, the leading edge of which was in contact with the downstream side of the nozzle plate, see Fig. 3. This arrangement has been designated by Republic Aviation Corporation as a blocked nozzle. High-velocity eddies between the jet and the surface of the starting section cause the stream to be forced against the surface, so that the jet behaves essentially as if the starting surface were even with the lower edge of the nozzle opening. This limits entrainment of environment air to one side of the jet.

The test plate, used as a heat-flow meter, is a rectangular slab of Johns-Manville asbestos ebony, 1.53 in. thick, 15 in. wide, and 30 in. long. The thermal conductivity of the plate, measured by the Armour Research Foundation of Illinois Institute of Technology, is 0.484 Btu/hr ft F at 100 deg F.

The starting section, 6 in. long, and two side extensions, 10 in. wide, as well as the outlet for the cooling water, are seen in Fig. 3.

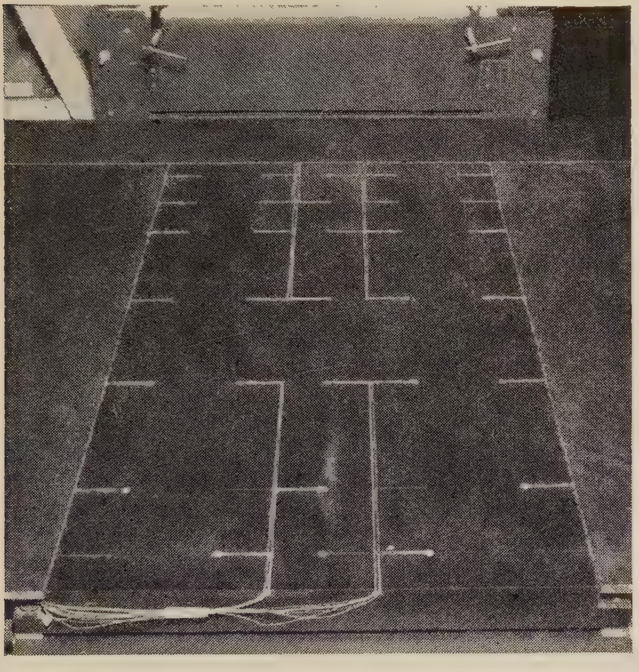

Fig. 3 Test Plate Before Filling Thermocouple Grooves

Thirty surface thermocouples are on the jet side of the plate, and nine are on the water side. Fig. 3 shows the upper side of the plate before filling the grooves containing the wires. The junctions are in the center of 0.25-in-diam by 0.020-in. copper disks recessed in the plate. The wires from the junctions run for at least 1.5 in. parallel to the nozzle outlet, to reduce heat conduction along the wires.

A traverse unit, resembling a rake (foreground, Fig. 1) was used for traverses in three dimensions throughout the jet. Thermocouples and impact tubes are spaced alternately, 1.5 in. apart, across a width of 24 in. parallel to the nozzle outlet, and can be set at various heights above the test surface. Thermocouple readings were corrected for the temperature increase encountered in high-velocity streams (8). The impact tubes, $^3/_{32}$-in-OD brass tubing, were used to measure local velocities in the jet.[6] In addition, they were used as sampling tubes in the tests with dew-point traverses of the jet. For this purpose the tubes across the width of the test plate were connected to a common manifold, and this was led to the dew-point meter.

Three thermocouples, one above and one at each side of the nozzle, were provided for measuring environment air temperatures. A six-point Micromax recorder served to record the duct-air and environment-air temperatures.

Fig. 4 shows details of the dew-point meter used in the jet traverses. This instrument is similar to an automatic indicating meter developed by the University of Chicago Meteorological Laboratories; simpler in design, however, because automatic indicating was not necessary. The main part is a polished silver mirror, against which samples of the air are blown. The mirror button, containing three thermocouples, is cooled from the rear until its exposed surface is clouded by condensation, which occurs at the dew point.

The finned end of the copper rod, seen in Fig. 4, was kept in melting ice. By varying the electrical input to the heating coil, a suitable range of temperatures could be maintained at the mirror surface. The temperature of clouding of the mirror was used as the dew point, because observation of clearing was less accurate.

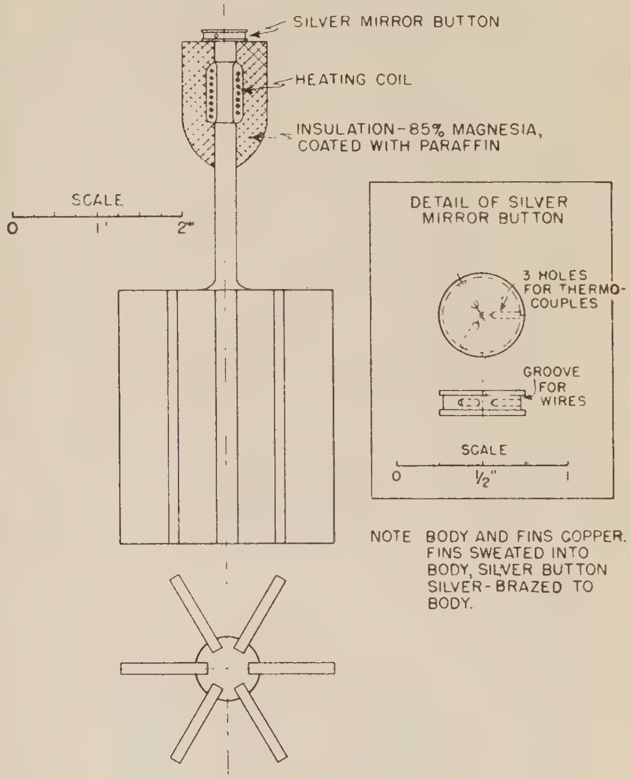
SILVER MIRROR BUTTON
HEATING COIL
INSULATION-85% MAGNESIA, COATED WITH PARAFFIN
SCALE
0
1"
2"
DETAIL OF SILVER MIRROR BUTTON
3 HOLES FOR THERMOCOUPLES
GROOVE FOR WIRES
SCALE
0
1/2"
1
NOTE BODY AND FINS COPPER. FINS SWEATED INTO BODY, SILVER BUTTON SILVER-BRAZED TO BODY.

Fig. 4 Dew-Point Meter

All thermocouples used in the experiments were made of 30-gage copper and constantan wires, enameled and single-cotton covered. The cold junctions were kept in melting ice.

Equilibrium for a test was reached within 1 or 2 hr. A complete test required a full day for two observers. Such a test included velocity, temperature, and sometimes dew-point traverses, at different distances from the nozzle and heights above the plate surface, and measurement of the temperature distribution on the test-plate surface.

Scope of Experiments

A total of 19 tests are reported in this paper. Table 1 sum-

---

[6] Static pressures in similar jets have been reported to exceed the environment pressure by 0.5 per cent of the dynamic pressure (9). This difference was neglected in the calculations.

TABLE 1 SUMMARY OF TEST CONDITIONS

Test no.	Initial jet vel, v_o fps	Initial jet temp, t_o deg F	Bottom surf temp, t_b deg F	Environment temp, t_e deg F	Initial jet dew-pt temp, $t_{d,o}$ deg F	Environment dew-pt temp, $t_{d,e}$ deg F	Traverses
19	53	201	71	87			T V
18	75	202	73	91			T V
17	129	199	71	86			T V
13	129	201	52	80			T V
14	130	203	52	88			
25	132	199	36	85	20	62	T D
29	132	199	39	95	48	72	T V D
26	151	199	37	91	17	64	T D
22	167	80	80	80	49	64	D
28	167	148	38	71	31	62	T D
27	167	248	37	90	17	64	T D
24	168	202	58	94	46	70	T V D
30	169	199	43	98	55	74	T V D
9	176	200	38	75			T V
23	185	79	79	79	49	67	D
11	202	252	49	85			T V
12	203	151	49	86			T V
10	203	201	45	87			T V
21	204	201	60	98	45	77	T D

NOTES: Tests 29 and 30 were made with 0.5 in. nozzle opening, all others with 0.25 in. opening.
Transverse abbreviations:
T, jet temperature
V, jet velocity
D, jet dew point

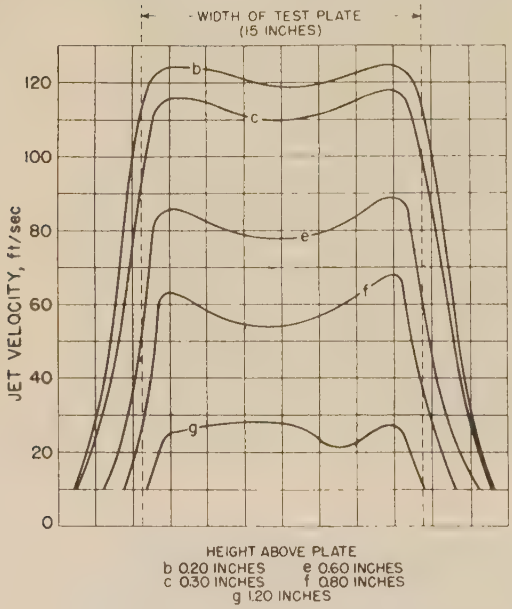

FIG. 5 VELOCITY DISTRIBUTION ACROSS JET, STATION A

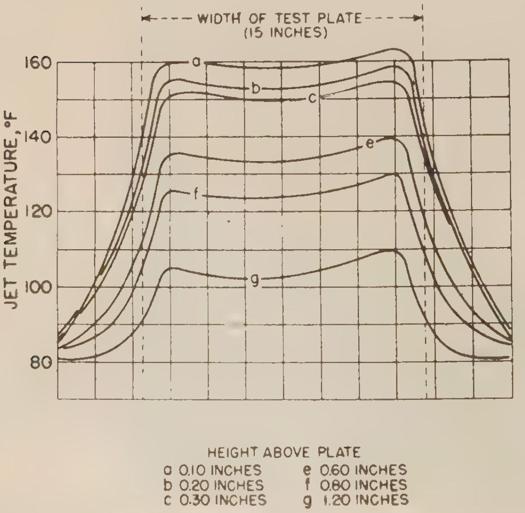

FIG. 6 TEMPERATURE DISTRIBUTION ACROSS JET, STATION A

marizes the measurements and conditions. The 6-in. starting section and the vertical distance of 0.25 in. from the plate surface to the lower edge of the nozzle opening were used in all tests.

All physical properties of air in the calculations were taken from tables of Keenan and Kaye (10).

JET CHARACTERISTICS

Results of typical velocity and temperature traverses across the width of the jet, from test No. 10, are shown in Figs. 5 to 8,

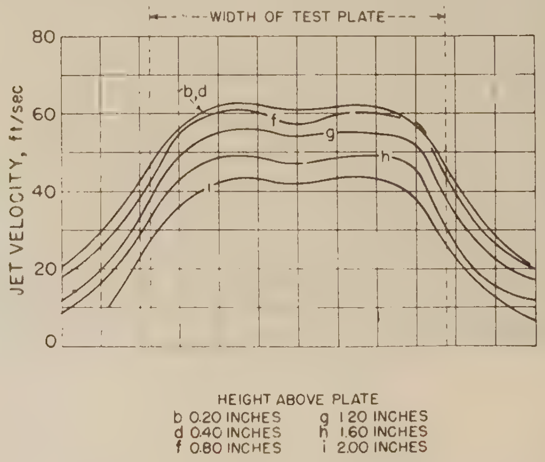

FIG. 7 VELOCITY DISTRIBUTION ACROSS JET, STATION F

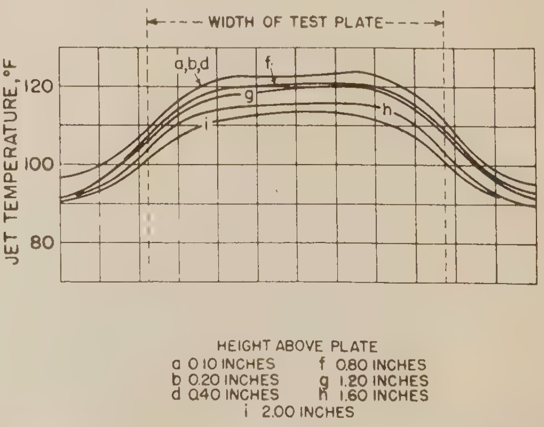

FIG. 8 TEMPERATURE DISTRIBUTION ACROSS JET, STATION F

inclusive. Distances from the nozzle to stations A and F are $x = 0.625$ and 2.625 ft, respectively.

The variations across the width of the test plate, at any height y, are not severe and therefore, in general, only average values were read in the traverses. For this purpose the thermocouples above the test plate were connected in series, and the impact tubes above the plate surface were connected to a common manifold.[7]

Using these averages at the various heights, profiles such as shown in Figs. 9 and 10 were obtained.

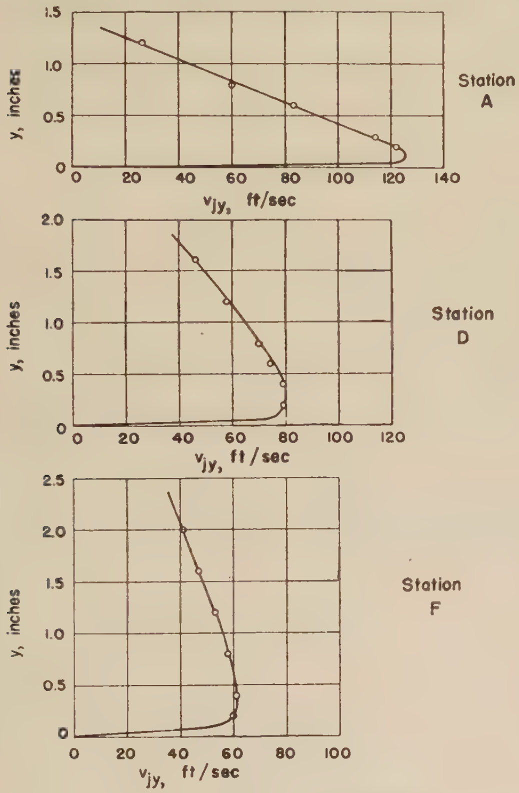

Fig. 9 Jet-Velocity Profiles

The average dew points measured led to vapor-pressure profiles of the type shown in Fig. 11.

It was desired to find the maximum local jet temperature t_j, at any distance from the nozzle because a local coefficient of heat transfer h_j, will be used, based on the temperature difference $t_j - t_s$, where t_s is the plate-surface temperature at any distance from the nozzle. Since the greatest part of the jet cooling is caused by entrainment of environment air, the initial jet temperature t_o and the environment temperature t_e are the main factors in determining the average and the maximum jet temperature at any distance from the nozzle. Therefore a dimensionless temperature ratio may be defined as

$$N_t = \frac{t_o - t_j}{t_j - t_e} \quad \ldots\ldots\ldots\ldots [1]$$

This was found to be a function of the ratio of distance from the nozzle to height of the nozzle opening, x/a, independent of the initial jet temperature and velocity.

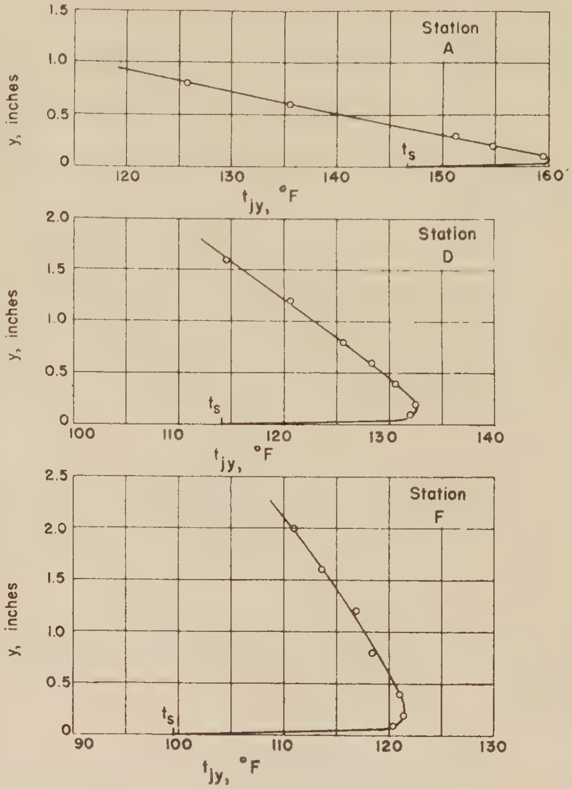

Fig. 10 Jet-Temperature Profiles

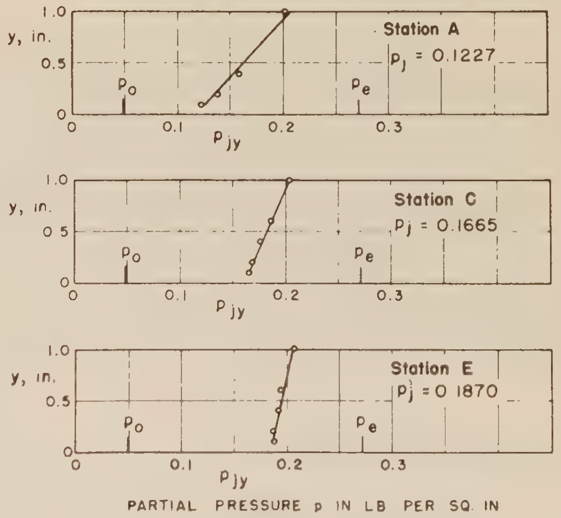

Fig. 11 Jet Partial-Pressure Profiles

Fig. 12 illustrates the variation of N_t with x/a for all tests made with jets of hot air. The test points can be represented by a line corresponding to the equation

$$N_t = 0.055\left(\frac{x}{a} - 12.5\right)^{0.8} \quad \ldots\ldots\ldots\ldots [2]$$

This equation was determined for the following range of conditions

$53 < v_o < 205$ fps, $150 < t_o < 250$ deg F, $71 < t_e < 98$ deg F, and $15 < x/a < 126$.

---

[7] This averaging of pressures is subject to an inherent error, because the average of the square roots of the individual impact pressures should be used for the average velocity. The result of using the multiple connection was compared with the mean of individual measurements on several occasions. The difference was considered to be within the limits of accuracy of the measurements.

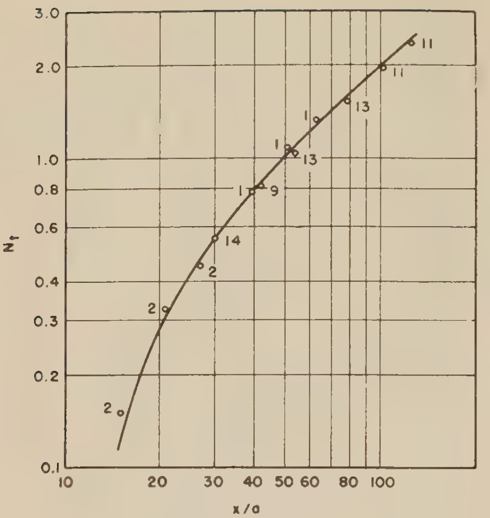

FIG. 12 N_t VERSUS x/a
(Numerals at each point represent number of runs averaged)

For the tests involving humidity differences between the jet and environment air, a similar ratio involving partial pressures can be defined as

$$N_p = \frac{p_o - p_j}{p_j - p_e} \qquad [3]$$

where p_o, p_j, and p_e are the partial pressures of water vapor in the nozzle outlet, jet, and environment, respectively. This will be discussed further in the section on mass transfer.

HEAT TRANSFER

Definitions and Procedure. Fog, or ice formation, may begin on any surface, the temperature of which is at, or below, the dew point of the adjacent air. If the dew point of the air in the jet boundary layer and the surface-temperature distribution are known, the distance from the nozzle at which clouding will begin on a windshield surface can be determined. The surface-temperature distribution may be found, using a local heat-transfer coefficient, h_j. With this in mind, the object of the experiments was to obtain h_j in terms of initial conditions.

For steady state, the heat flow per unit area at any point on the plate surface can be considered either as convection from the jet to the surface

$$q'' = h_j\,(t_j - t_s) \qquad [4]$$

or as conduction through the test plate

$$q'' = \frac{k}{s}\,(t_s - t_b) \qquad [5]$$

Equation [4] defines the local coefficient h_j. The symbols k, s and t_b in Equation [5] stand for thermal conductivity of the test plate material, length of heat-flow path through the plate, and temperature of the bottom surface of the plate, respectively. From Equations [4] and [5],

$$t_s = \frac{h_j t_j + \dfrac{k}{s}\,t_b}{h_j + \dfrac{k}{s}} \qquad [6]$$

This result indicates that t_s can be determined if h_j is known, since t_j can be obtained by means of Equations [1] and [2].

In the tests, q'' was found at each station from the measured surface temperatures and the known values of k and s for the test plate.[8] The measured values of t_b were constant over the entire bottom surface of the plate, due to the large film coefficient between the water stream and the plate. Fig. 13 shows the pattern of isothermal lines on the upper surface of the test plate, from test No. 9. The surface isothermals show a dip at the center of the plate, matching the variation noted in the jet traverses, Figs. 6 and 8.

For test No. 10, the local heat-transfer coefficients were determined and found uniform across the width of the plate. Values of h_j in the following correlation were all based upon the average t_j and t_s for each station.

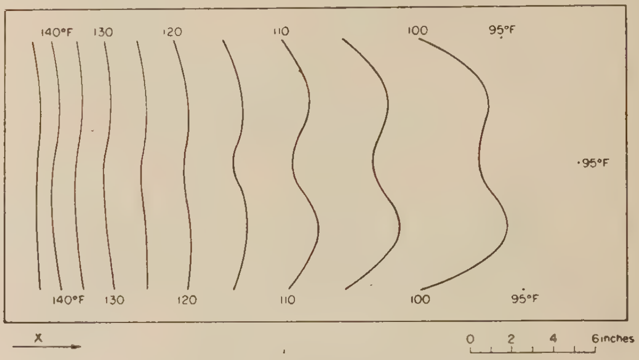

FIG. 13 ISOTHERMALS ON UPPER SURFACE OF TEST PLATE

Correlation of Heat-Transfer Data. The results can be represented by

$$N_{Nu} = C(N_{Re})^m \left(\frac{x}{a}\right)^n \qquad [7]$$

where

$$N_{Nu} = \frac{h_j x}{k_f} \qquad [8]$$

and

$$N_{Re} = \frac{v_o x}{\nu_o} \qquad [9]$$

Subscripts o and f refer to nozzle outlet and film temperature, $t_f = (t_j + t_s)/2$, respectively.

Figs. 14 and 15 show the experimental data for $a = 0.25$ in. and straight lines according to the equation

$$N_{Nu} = K(N_{Re})^{0.8} \qquad [10]$$

where K is an individual constant for each station, which can be expressed as a function of x/a. Considering all tests, Equation [7] becomes

$$N_{Nu} = 0.105\,(N_{Re})^{0.8} \left(\frac{x}{a}\right)^{-0.4} \qquad [11]$$

The range of measurements was

$$134{\cdot}10^3 < N_{Re} < 2.94{\cdot}10^6 \text{ and } 15 < x/a < 126$$

---

[8] The length s, was taken as the distance between the mid-planes of the copper buttons for the surface thermocouples. In the region near the nozzle, the heat flow is not perpendicular to the plate, owing to the temperature variation with length on the upper side. The difference between the true length of path, perpendicular to the isothermal lines in the plate cross section, and the perpendicular distance was determined and found to be negligible.

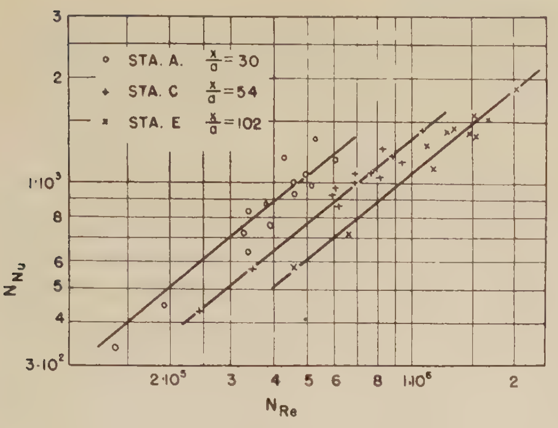

FIG. 14 N_{Nu} VERSUS N_{Re}, STATIONS A, C, AND E

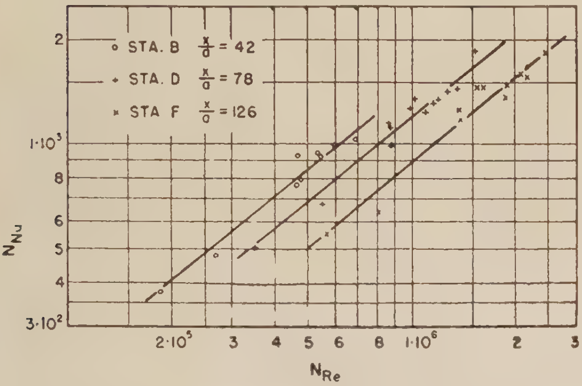

FIG. 15 N_{Nu} VERSUS N_{Re}, STATIONS B, D, and F

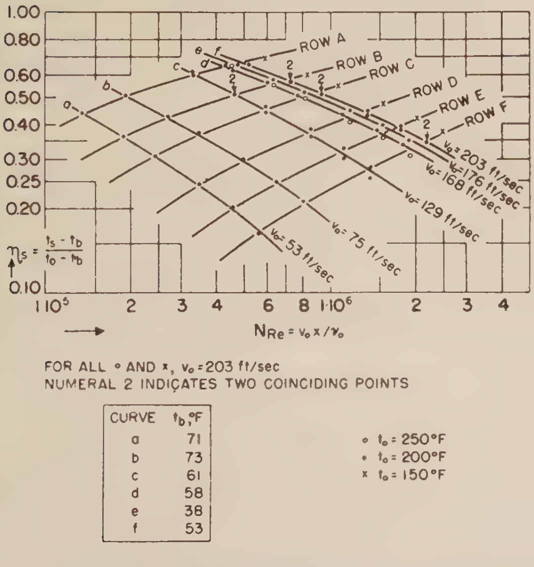

FIG. 16 DIMENSIONLESS REPRESENTATION OF SURFACE-TEMPERATURE PATTERN

Special Graph for Surface Temperature. A graphical representation useful for determining the surface-temperature variation is shown in Fig. 16. A ratio similar to an effectiveness, defined as

$$\eta_s = \frac{t_s - t_b}{t_o - t_b} \quad \ldots\ldots\ldots\ldots\ldots\ldots\ldots\ldots [12]$$

is plotted as a function of Reynolds number, defined in Equation [9]. A given plate unit conductance k/s, initial jet temperature t_o, and bottom surface temperature t_b, determine a family of curves such as Fig. 16, having x and v_o as parameters. The lines on the graph are for tests conducted with t_o = 200 deg F.

It will be noted that increasing v_o has a smaller effect at higher velocities. Hence little would be gained by using initial jet velocities in excess of 160 fps with this nozzle. An increase of t_o tends to shift the lines of constant v_o to the right, the lines of constant x remaining essentially the same.

The coefficient h_j would not be affected greatly by a change in surface temperature and, according to Equation [2], t_j depends only upon t_o, t_e, and x/a. Thus it would be possible to construct a similar family of curves for a different plate material and other initial conditions, using Equations [2], [4], [5], [11], and [12].

MASS TRANSFER

Corresponding to the representation of N_t in Equation [2] and Fig. 12, the results of the vapor-pressure traverses in the jet are shown in Fig. 17, with N_p, defined by Equation [3], as ordinate. Assuming[9] the same influence of x/a as in Equation [2], the points in Fig. 17, are correlated by a curve according to

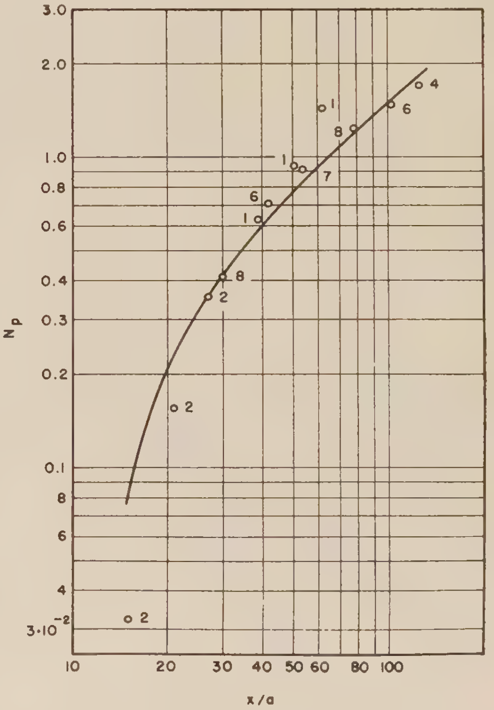

FIG. 17 N_p VERSUS x/a

(Numerals at each point represent number of runs averaged.)

$$N_p = 0.042\left(\frac{x}{a} - 12.5\right)^{0.8} \quad \ldots\ldots\ldots\ldots [13]$$

Figs. 18-A and 18-B are sketches of typical measured profiles. Figure 18-D would represent the case of a jet becoming drier by dilution with dry air from the environment and condensation on the surface. A case similar to D, namely, Fig. 18-C, would represent entrainment of vapor from the environment, combined with evaporation on the surface, both contributing to the humidity of the jet. In the experiments, p was not measured close to the surface. Since no condensation or evaporation occurred at the surface, the curve in Fig. 18-B should not come to a minimum of p_j, but would proceed as a vertical line approaching the surface. This is an inherent lack of similarity.

---

[9] Without this assumption, a somewhat better representation of the points could be obtained.

If the experiments had been undertaken solely for checking the principle of similarity and not mainly for the practical purpose mentioned in the introduction, an arrangement yielding a profile according to C or D would have been chosen. In a continuation of the work, experiments with evaporation are being performed. In the present experiments, that partial pressure which was measured closest to the surface was called p_j, and was assumed to correspond to the maximum jet temperature t_j.

Common Correlation Between Heat Transfer and Mass Transfer

If heat transfer and mass transfer occur separately in geometrically similar fields, and the boundary conditions for each case are alike, the principle of similarity may be applied to predict the behavior of one field from measurements of the other.[10] In the present case, heat and mass transfer, respectively, are represented by

$$N_{Nu} = C\, N_t^{m}\, N_{Re}^{n}\, N_{Pr}^{r} \qquad [14]$$

and

$$(N_{Nu})_{\text{mod}} = C\, N_p^{m}\, N_{Re}^{n}\, N_{Sc}^{r} \qquad [15]$$

where $(N_{Nu})_{\text{mod}} = b_j x/\delta$ is a modified Nusselt number, a coefficient of mass transfer b_j being defined by $\dot{m}'' = b_j(p_j - p_s)/R\,T_f$ (see Nomenclature).

If the fields were perfectly similar,[11] the constants C, m, n, and r should be the same in Equations [14] and [15], giving

$$\frac{(N_{Nu})_{\text{mod}}}{N_{Re}^{n} N_{Sc}^{r}} = \frac{N_{Nu}}{N_{Re}^{n} N_{Pr}^{r}} \left(\frac{N_p}{N_t}\right)^{m} \qquad [16]$$

To check the influence of the simplifications, two "isothermal" experiments of diffusion were performed in analogy to the heat-transfer experiments in which no humidity differences existed. The isothermal tests yielded essentially the same partial-pressure profiles as the nonisothermal diffusion tests. It was also found that the jet-temperature profiles in diffusion and mere heat-transfer tests were practically identical.

Based on this evidence of similarity, a common correlation by means of Equations [14] and [15] was attempted. Taking $n = 0.8$ from Equation [11], and assuming $r = 0.4$, $N_{Pr} = 0.72$ and $N_{Sc} = 0.63$, a trial-and-error method led to $C = 0.0242$ and $m = -0.4$, so that

$$N_{Nu} = 0.0242\, N_t^{-0.40}\, N_{Re}^{0.80}\, N_{Pr}^{0.4} \qquad [17]$$

and

$$(N_{Nu})_{\text{mod}} = 0.0242\, N_p^{-0.40}\, N_{Re}^{0.80}\, N_{Sc}^{0.4} \qquad [18]$$

Fig. 19 shows the common correlation. Either of the groups $N_{Nu}\, N_{Re}^{-0.8}\, N_{Pr}^{-0.4}$ or $(N_{Nu})_{\text{mod}}\, N_{Re}^{-0.8}\, N_{Sc}^{-0.4}$ can be considered as ordinate, depending upon whether N_t or N_p is taken as the abscissa. The straight line represents heat and mass transfer alike.

Comparing Equations [2] and [13] gives

$$N_p = 0.765\, N_t \qquad [19]$$

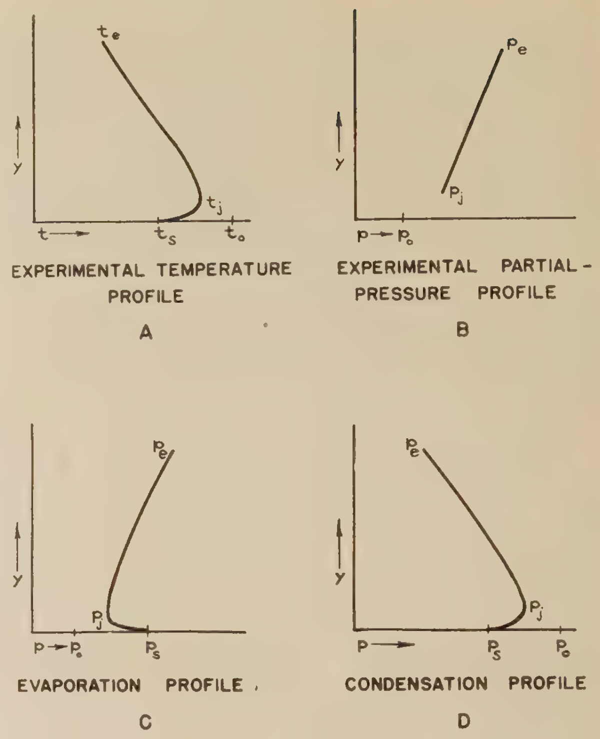

EXPERIMENTAL TEMPERATURE PROFILE
A

EXPERIMENTAL PARTIAL-PRESSURE PROFILE
B

EVAPORATION PROFILE
C

CONDENSATION PROFILE
D

Fig. 18 Comparison of Schematic Profiles

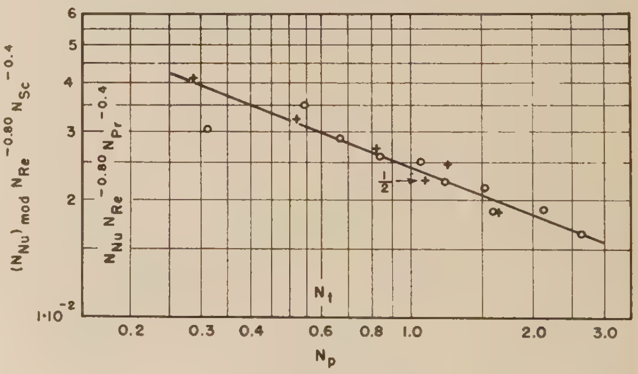

Fig. 19 A Single Correlation for Heat Transfer and Mass Transfer

(Circles represent temperature measurements. Crosses represent partial-pressure measurements. Each point represents the average of eight experimental values except the point marked ½ which represents four experimental values.)

for any x/a. Hence for any fixed value of N_{Re} and x/a

$$(N_{Nu})_{\text{mod}} = 1.05\, N_{Nu} \qquad [20]$$

The difference between N_p and N_t may be caused by the lack of similarity discussed in connection with Fig. 18. In fact, cooling of the jet by the plate, which has no equivalent in the diffusion tests, reduces t_j and therefore makes N_t larger, compared to N_p. The influence upon Equation [20] is smaller, mainly because of the exponent -0.40 in Equations [17] and [18].

Further experiments with evaporation under experimental conditions as described in this paper are now in progress in continuation of our study for the United States Air Forces.

Numerical Example

The following example shows how the experimental results can be applied. An airplane is assumed at such an altitude and speed that the outer windshield surface temperature is —30 deg F. A $^1/_2$-in. windshield is used, having a unit conductance k/s = 5.6 Btu/hr ft^2 F. The defroster discharges air, initially at 150 deg F, 50 fps, parallel to the inner surface, from a continuous $^1/_4$-in. slot. Dry air from the outside is used for defrosting. Cabin pressure is maintained at 20.6 in. Hg abs, equivalent to 10,000-ft altitude. Cabin air temperature is 45 deg F, dew point 40 deg F.

---

[10] Nusselt (11) has also derived equations for both processes occurring simultaneously. Here, his simpler equations for separate fields can be used, since the concentration of water vapor in air is small.

[11] Nusselt mentions that there is a certain lack of similarity between heat-transfer and mass-transfer fields on a heated or cooled surface where no change of phase occurs, since heat but no mass flow crosses the surface.

Assuming a film temperature of 40 deg F, Equation [11] reduces to

$$h_j = 4.93\ (x)^{-0.6} \ldots\ldots\ldots\ldots\ldots\ldots [21]$$

with h_j in Btu/hr ft^2 F and x in ft. This gives the values of h_j in Table 2. The values of N_t and N_p are found from Equations [2] and [13], respectively. Solving Equation [1] gives the values of t_j. Then Equation [6] is solved for t_s.

TABLE 2 VALUES OCCURRING IN CALCULATION OF THE EXAMPLE

x, ft	0.50	1.00	2.00	3.00
h_j from Equation [21] Btu/hr ft^2 F	7.48	4.93	3.25	2.55
N_t from Equation [2]	0.386	0.958	1.89	2.68
N_p from Equation [13]	0.295	0.732	1.45	2.09
t_j from Equation [1], deg F	121	98.7	81.4	73.6
t_s from Equation [6], deg F	56.3	30.4	10.8	2.5
p_j from Equation [3], psia	0.0276	0.0515	0.0718	0.0822
$t_{d,j}$ from Steam Tables, deg F	8.7	20.5	27.2	30.3

From steam tables, p_e = 0.1217 psia. Further, $p_o \approx 0$. Herewith Equation [3] yields the values of p_j. The dew-point temperature $t_{d,j}$ is obtained from the steam tables, as the saturation temperature at vapor pressure p_j for the various x. Condensation or freezing is assumed to begin when $t_{d,j} = t_s$. Under the assumed conditions this occurs at a distance x = 1.25 ft (found by graphical interpolation).

The table shows that $(t_j + t_s)/2$ for x = 1.25 ft is larger than the assumed value of the film temperature t_f = 40 deg F. Using the correct temperature, however, would only change k_f by 2 per cent, i.e., within the accuracy of the equations.

Acknowledgment

The major part of the material in this paper is taken from reports submitted to the United States Air Forces (12). The authors wish to express their appreciation to the Air Materiel Command for permission to publish these data.

BIBLIOGRAPHY

1 "Heat Flow From a Jet Discharged Parallel to a Plane Surface," by R. L. Rose, MS thesis, Illinois Institute of Technology, Chicago, Ill., June, 1948.

2 "Diffusion of Water Vapor From the Atmosphere Through a Jet of Less Humid Air," by M. Spielman, MS thesis, Illinois Institute of Technology, Chicago, Ill., June, 1947.

3 "Heat Transfer and Velocity Distribution Characteristics of a Free Air Jet Discharged From a Narrow Slot and Directed Parallel to a Horizontal Plate," Republic Aviation Corporation, Farmingdale, N. Y., Report ERF-3, 1945.

4 "Heat Transfer and Velocity Distribution Characteristics of a Free Air Jet Discharged From a Narrow Slot and Directed Parallel to a Horizontal Plate—Part II, $^1/_2$ Inch Deep Continuous Slot," Republic Aviation Corporation, Farmingdale, N. Y., Report ERF-3, 1945.

5 "Heat Transfer and Velocity Distribution Characteristics of a Free Air Jet Discharged From Individual Nozzles and Directed Parallel to a Horizontal Plate—Part I, Discontinuous Slots and Specially Designed Nozzles," Republic Aviation Corporation, Farmingdale, N. Y., Report ERF-9, 1946.

6 "Heat Transfer and Velocity Distribution Characteristics of a Free Air Jet Discharged From Individual Nozzles and Directed Parallel to a Horizontal Plate—Part II, Commercial Nozzle, Nozzle 'L,'" Republic Aviation Corporation, Farmingdale, N. Y., Report ERF-9, 1946.

7 "An Empirical Equation for the Coefficient of Heat Transfer to a Flat Surface From a Plane Heated-Air Jet Directed Tangentially to the Surface," by J. Zerbe and J. Selna, National Advisory Committee for Aeronautics, Washington, D. C., Technical Note 1070, 1946.

8 "Temperature Measurements in High-Velocity Air Streams," by H. C. Hottel and A. Kalitinsky, JOURNAL OF APPLIED MECHANICS, Trans. ASME, vol. 67, 1945, p. A-25.

9 "Turbulent Jet Expansion," by E. Forthmann, National Advisory Committee for Aeronautics, Washington, D. C., Technical Memo 789, 1936.

10 "Thermodynamic Properties of Air," by J. H. Keenan and J. Kaye, John Wiley & Sons, Inc., New York, N. Y., 1945.

11 "Heat Transfer, Diffusion and Evaporation" (Title translated), by W. Nusselt, *Zeitschrift für angewandte Mathematik und Mechanik*, vol. 10, 1930, p. 105.

12 "Aircraft Windshield Heating," Report to the Army Air Corps, Illinois Institute of Technology, Chicago, Ill., April 15, 1947.

Pressure Drop and Convective Heat Transfer With Surface Boiling at High Heat Flux; Data for Aniline and n-Butyl Alcohol[1]

By FRANK KREITH[2] AND MARTIN SUMMERFIELD,[3] PASADENA, CALIF.

Heat-transfer coefficients to commercial-grade aniline and n-butyl alcohol have been measured at high rates of heat flux. Data have been obtained for both of the liquids in the heat-flux range from 0.3 to 3 Btu/sq in. sec and in the pressure range from 30 to 400 psia at velocities from 20 to 40 fps. The test section consisted of a $^1/_2$-in-ID stainless-steel tube which was heated electrically.

Nomenclature

The following nomenclature is used in this paper:

A = area, sq in.
C_F = friction coefficient, $\left(\Delta H \dfrac{D}{L} \dfrac{2g}{V^2}\right)$
C_p = specific heat, Btu/lb deg F
D = inside diameter of tube, in.
h = heat-transfer coefficient, Btu/sq in. sec deg F
g = gravitational constant, ft/sec^2
ΔH = pressure drop in head of liquid
j = forced-convection index, $(Nu/Re^{0.8}Pr^{1/3})$
C_H = $(Nu/Re\ Pr) \cdot Pr^{2/3}\ (\mu_W/\mu_B)^{0.14}$
K = thermal conductivity, Btu/ft hr deg F
L = length, in.
Nu = Nusselt modulus, $(hD/K) \times 12$
P = pressure, psia
Pr = Prandtl modulus, $(C_p\mu/K \times 3600\ g)$
ΔP = pressure drop
q = rate of heat flow, Btu per sec
Re = Reynolds modulus $(VD\rho/\mu \times 12)$
T = temperature, deg F
v or V = velocity, fps
w = flow rate, lb per sec
μ = absolute viscosity, lb sec/sq ft
ρ = mass density, (lb/cu ft)/g

Subscripts:

e = entrance
B or F = fluid bulk
HT = heat-transfer condition
iso = isothermal condition
s = saturation
v = vapor
W = wall
x = excess above saturation temperature

Introduction

This presentation is an extension of a previous paper by the same authors (1).[4] In addition to water, the data for which were presented in the preceding paper, new data are presented for aniline and n-butyl alcohol.

Equipment and Experimental Technique

A detailed description of the experimental setup used for the study of heat transfer to liquids at high heat flux has been presented in a previous paper by the authors (1). The test section was a stainless-steel tube 17.5 in. long, 0.587 in. ID, and 0.020 in. wall thickness. This tube served also as a resistance heating element, as it was heated by electric current. The heat flux was regulated by changing the voltage potential across the tube. Measurements were taken of the liquid flow rate, the inlet and outlet temperatures, the pressure, and the frictional pressure loss in the test section. The temperature of the heat-transfer surface-to-liquid interface was calculated from the temperature of the outer tube wall, which was measured at 14 points along the tube by means of thermocouples.

The technique for installing the thermocouples and the derivation of the equation for the temperature distribution in an electrically heated cylinder has been discussed (1). However, in tests with aniline as a coolant, it was found that a deposit formed on the inner tube wall after short periods of operation. Therefore it was necessary to devise a technique for correcting the temperature measurements in order to obtain a true indication of the liquid-to-surface interface temperature.

A standard check test at a flow rate of 4.3 lb per sec, a pressure of 100 psia, and a heat flux of 1.2 Btu/sq in. sec was made with a clean and newly installed tube, and a true liquid-to-wall interface temperature was obtained. The data of this test could be reproduced within ±5 deg F in subsequent tests after cleaning the tube with a rag saturated with clean aniline. A standard test under the foregoing specified conditions of flow, pressure, and heat flux was made before and after each series of tests, which lasted less than 10 min. During this 10-min period, a deposit formed on the inner tube wall which caused, on the average, an outer-wall temperature indication of 30–50 deg F higher than the original test on the clean tube. The build-up of the deposit for short periods of heating was found to be approximately a straight-line function of time, and by plotting temperature increase due to scale versus time for each series of tests, a temperature correction, corresponding to the time interval at which the test data had been obtained, was determined. The correction which had to be applied amounted to less than 5 per cent of the measured temperature, and the accuracy of the temperature of the liquid to surface interface

---

[1] This paper presents the results of one phase of research carried out at the Jet Propulsion Laboratory, California Institute of Technology, under Contract No. W-04-200-ORD-455 sponsored by the U. S. Army Ordnance Department.

[2] Senior Research Engineer, Jet Propulsion Laboratory, California Institute of Technology. Now, Guggenheim Fellow, Department of Aeronautics, Princeton University, Princeton, N. J. Jun. ASME.

[3] Chief, Rockets and Materials Division, Jet Propulsion Laboratory, California Institute of Technology. Now, General Editor, Aeronautics Publication Program, Princeton University. Mem. ASME.

Contributed by the Heat Transfer Division and presented at the Annual Meeting, New York, N. Y., November 27–December 2, 1949, of The American Society of Mechanical Engineers.

Note: Statements and opinions advanced in papers are to be understood as individual expressions of their authors and not those of the Society. Paper No. 49—A-94.

[4] Numbers in parentheses refer to the Bibliography at the end of the paper.

is believed to be at least within ±15 deg F. Reproducible data within ±10 deg F were obtained in tests made on different days with the same test section.

The n-butyl alcohol did not form a deposit on the heating surface, and thus the wall-temperature measurements did not require any corrections. In the test with n-butyl alcohol, the frictional pressure loss was measured with a differential mercury manometer, as well as a differential Barton pressure gage (1).

Each series of tests was made by setting the power level and flow rate, and changing the back pressure by adjusting the control valve on the downstream side of the test section. This technique made possible a maximum number of tests in a minimum time. At least five complete records of all the thermocouples mounted on the outside of the tube were obtained for each test, and steady state was assumed when three or more of the temperature records agreed within 5 deg F. In separate tests it could be shown that the time lag of the heating tube was less than 2–3 sec before coming to equilibrium. Heat balances between the electric power input and the thermal power output check within 2 to 3 per cent for all the tests.

Experimental Results

Heat Transfer to Aniline With Bubble Formation Adjacent to Heating Surface. In the course of the experiments, data were obtained on the heat-transfer characteristics of aniline flowing upward in a stainless-steel tube 0.587 in. ID. The experiments covered the pressure range from 40 to 400 psia, and the heat-flux range from 0.3 to 3 Btu/sq in. sec at velocities of about 20 and 40 fps. The aniline which was used in the experiments was taken from the rocket-fuel supply of this laboratory.

The data presented in this paper have been corrected for deposit build-up and are representative of heat transfer from a surface of known temperature to aniline. The results of the first series of tests are shown in Fig. 1 as plots of wall temperature versus pressure at a constant aniline flow rate for various heat fluxes. It can be seen that as the pressure is reduced, the wall temperature necessary to remove a given heat flux decreases. This phenomenon has been observed previously in heat transfer to water with surface boiling. In the water experiments the decrease in wall temperature with reduction in pressure occurred initially at the saturation temperature of the liquid. The results with the commercial-grade aniline, on the other hand, show that the temperature potential necessary for the removal of a given heat flux begins to decrease at a wall temperature more than 100 deg F below the saturation temperature of pure aniline.

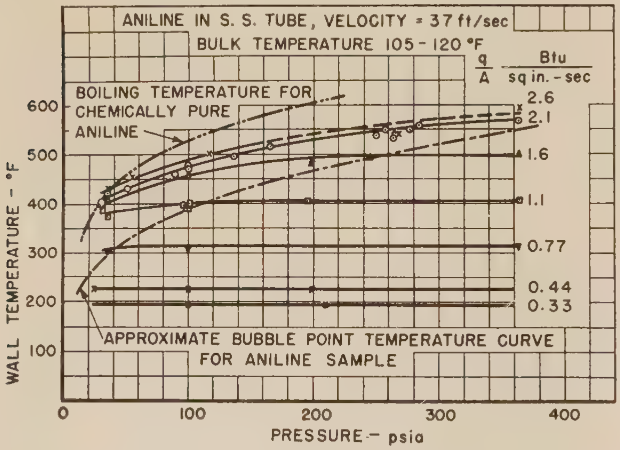

Fig. 1 Wall Temperature Versus Pressure (Aniline)

In the search for an explanation of the occurrence of surface-boiling phenomena at temperatures below the saturation point of the liquid, a plot of friction coefficient C_F and heat-transfer coefficient C_H versus pressure was made at a flow rate of 16 lb/sq in. sec at a heat flux of 2.1 Btu/sq in. sec, Fig. 2. An examination of these curves shows that the friction coefficient, as well as the heat-transfer coefficient, increases as the pressure is reduced. This increase in friction coefficient was believed to be caused by the formation of gas bubbles in the heat-transfer tube. After studying the results of the aniline tests, it was assumed tentatively that some phenomenon similar to surface boiling brought about the phenomena which correspond to the surface-boiling effects in water-cooling. On the assumption that bubble formation was causing an increase in turbulence level and a corresponding increase in heat-transfer coefficient with reduction in pressure, an effective bubble-point curve was estimated from the heat-transfer data presented in Fig. 1; it is superimposed on the same graph.

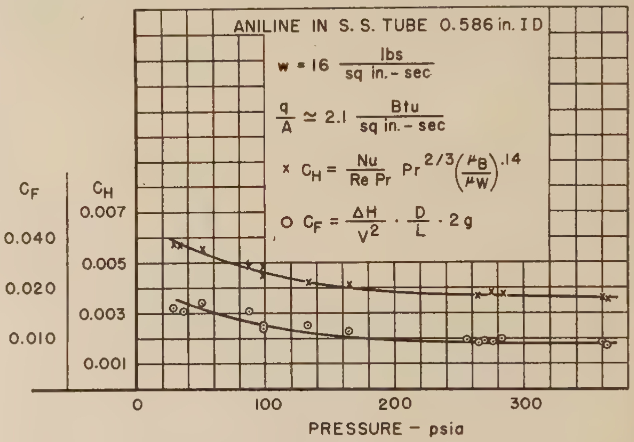

Fig. 2 Heat Transfer and Friction Moduli Versus Pressure (Aniline)

In order to obtain further proof of the bubble-temperature curve, estimated from the heat-transfer characteristics, a sample of the aniline which had been used in the experiments was analyzed for impurities and gas content; also the bubble temperatures were observed visually at reduced pressure in a distillation apparatus. The chemical analysis showed that about 5 per cent of water was dissolved in the aniline, and the experiments on bubble temperatures at reduced pressures indicated that bubble formation occurred at temperatures considerably below the boiling point of pure aniline. It was not feasible, without great expense and effort, to extend the visual observation of bubble temperatures to the pressure range used in the heat-transfer experiments. It was, however, possible to calculate a theoretical bubble temperature for the water-aniline solution at the critical pressure of aniline from Raoult's law.

The bubble temperatures obtained by three independent methods, (*a*) the visually observed bubble temperatures in the low-pressure range, (*b*) the calculated bubble temperature at the critical pressure, and (*c*) the bubble temperatures estimated from the heat-transfer experiment in the intermediate pressure range, are shown on one graph, Fig. 3, as the logarithm of the absolute pressure versus the inverse of the absolute temperature. Over a wide pressure range, all data fall on a smooth and continuous curve and thus lend additional weight to the explanation of the heat-transfer phenomena in terms of bubble formation adjacent to the heat-transfer surface.

The second series of tests was designed to determine the influence of velocity and bulk temperature on heat transfer to

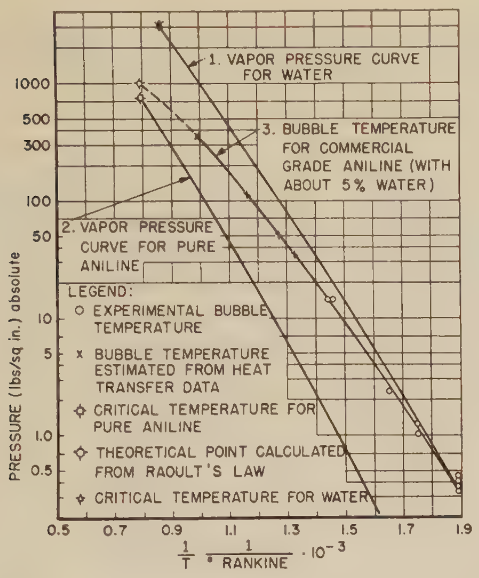

Fig. 3 Bubble-Point Temperature for Commercial-Grade Aniline
(Containing about 5 per cent water.)

aniline for the heat-flux and pressure ranges covered in the tests just described, for which the entrance velocity was about 37 fps. The entrance velocities for the tests in this part of the program were held to about 20 fps, and the bulk temperature ranged from 100 to 170 F. It was found that when the surface temperature exceeds the bubble temperature, the wall temperature is determined primarily by the pressure; the effects of changes in velocity, bulk temperature, and heat flux are small.

A summary of the results of the heat-transfer tests with aniline is presented in graphical form in Fig. 4, and the basic data from the tests is given in Table 1, with important calculated results. The graph in Fig. 4 shows (for an average fluid bulk temperature of 115 deg F) the temperature difference between the surface-to-liquid interface, and the bulk of the aniline necessary to remove heat fluxes from 0.3 to 3 Btu/sq in. sec at pressures of 35, 115, and 365 psia, for velocities of 21 and 37 fps in the pure forced-convection regime, and in the bubble regime. Only a few points were obtained in the transition region, and the curves in this region were faired by comparison with the previous water tests (1). For some of the points the test pressure did not correspond exactly to the pressures chosen for this presentation. In those cases the surface temperature was estimated from data which were obtained in tests at pressures slightly above and below the pressures presented in Fig. 4. For this type of presentation

TABLE 1 HEAT-TRANSFER DATA* FOR TESTS WITH ANILINE
(Corrected for formation of deposit)

Test No.	Temperature		Electric Potential (volts)	Power (watts)	Flow Rate	Heat Flux q/A	T_W	T_B	Re_B	Pressure	f_c	Nu	$\frac{\mu_B}{\mu_W}$	j	V	Δp **	C_f
	Inlet	Outlet															
1	98	116	25.9	40.7	4.32	1.188	394	112	76270	96	0.00421	1067	7.188	0.00390	36.87	8.6	0.0105
2	103	120	25.9	40.7	4.32	1.188	375	114	78820	34	0.00455	1153	6.45	0.00385	36.98	10	0.0121
3	100	118	25.9	40.7	4.32	1.188	403	117	81570	99	0.00415	1052	7.13	0.00338	36.98	9.5	0.0115
4	103	126	31.2	54.5	4.32	1.591	460	116	80630	99	0.00462	1171	8.88	0.00367	36.98	9.5	0.0115
5	101	125	31.2	56.75	4.34	1.657	410	123	88090	34	0.00577	1463	6.78	0.00448	37.27	12	0.0143
6	100	133	36.4	70.5	4.07	2.0586	560	116	75970	284	0.00464	1176	11.92	0.00375	34.84	8	0.0100
7	101	132	36.4	70	4.37	2.044	490	116	81570	134	0.00546	1384	9.78	0.00423	37.41	10.5	0.0125
8	101	133	36.4	72.5	4.32	2.117	460	116	80630	88	0.00615	1559	8.88	0.00488	36.98	12.5	0.0152
9	105	145	36.1	74	4.32	2.161	430	116	80630	51	0.00688	1744	7.91	0.00555	36.98	14	0.0170
10	100	118	25.9	40.7	4.32	1.188	396	110	74640	96	0.00415	1052	7.46	0.00355	36.87	8.6	0.0105
11	103	120	25.9	40.5	4.10	1.183	390	103	67150	29	0.00412	1044	8.100	0.00374	36.58	9.5	0.0118
12	102	127	31.7	57.4	4.32	1.676	458	116	80630	99	0.00490	1242	8.735	0.00418	36.98	9.6	0.0117
13	107.2	133	31.5	59.2	4.32	1.729	389	118	85130	29	0.00640	1622	6.417	0.00516	37.04	12.4	0.0150
14	102	133	36.1	71	4.32	2.073	536	118	83310	265	0.00496	1257	10.795	0.00373	36.98	7.5	0.0091
15	104	136	36.1	71	4.20	2.073	470	122	87500	99	0.00596	1511	8.492	0.00452	36.96	9.7	0.0118
16	108.3	138	36.1	72	4.20	2.102	404	128	93330	29	0.00762	1932	6.209	0.00576	37.08	13.2	0.0159
17	101	118	25.9	39.12	4.32	1.142	398	118	83510	99	0.00401	1016	7.339	0.00384	36.92	8.5	0.0104
18	101	127	36.8	71.4	4.32	2.085	538	122	87690	250	0.00501	1270	10.336	0.00350	37.10	7.7	0.0093
19	103	135	36.8	74.65	4.31	2.180	476	117	84340	99	0.00617	1564	9.247	0.00488	36.90	10	0.0122
20	105	138	36.8	74.3	4.31	2.170	418	123	88140	34	0.00736	1866	6.904	0.00571	37.01	12.5	0.0152
21	101	118	25.9	39.25	4.31	1.146	390	110	74460	98	0.00409	1037	7.231	0.00352	36.78	8.4	0.0103
22	99	122	32.3	55.42	4.24	1.618	482	108	72910	199	0.00434	1100	10.549	0.00358	36.78	7.2	0.0088
23	101	126	32.3	56.42	4.32	1.647	460	118	82530	99	0.00482	1222	8.673	0.00378	36.98	8.8	0.0107
24	101	126	32.3	57.75	4.28	1.686	394	120	83740	29	0.00615	1559	6.694	0.00471	36.70	11	0.0136
25	86	103	25.9	40	4.31	1.168	401	100	64800	98	0.00389	983	8.710	0.00357	36.66	-	-
26	94	110	25.9	40.02	4.32	1.169	406	101	65570	266	0.00390	988	8.629	0.00356	36.75	8.5	0.0105
27	97	137	36.8	74	4.32	2.161	517	116	80630	165	0.00539	1366	10.357	0.00420	36.98	9.5	0.0115
28	93	110	25.9	40.5	4.32	1.183	396	104	68790	98	0.00405	1026	8.095	0.00360	36.81	8	0.0098
29	100	128	36.8	70.3	4.32	2.132	550	114	78820	275	0.00489	1239	12.027	0.00379	36.92	7.5	0.0091
30	86	103	25.9	40	4.32	1.168	398	98	63780	100	0.00389	986	8.871	0.00358	36.69	8.25	0.0102

* Cf. nomenclature for definitions of symbols and units.

** Δp in inches of water $\times 10^{-1}$.

TABLE 1 (*Continued*)

Test No.	Temperature Inlet	Temperature Outlet	Electric Potential (volts)	Power (watts)	Flow Rate	Heat Flux q/A	T_W	T_B	Re_B	Pressure	f_c	Nu	$\frac{\mu_B}{\mu_W}$	j	V	ΔP	C_F
31	92	116	31.2	55	4.32	1.606	494	108	73070	257	0.00416	1054	10.909	0.00342	36.86	7.3	0.0089
32	98	136	36.8	74	4.32	2.161	550	114	78820	256	0.00496	1257	12.027	0.00385	36.92	8.1	0.0099
33	101	117	25.9	39.8	4.32	1.162	405	106	70160	195	0.00389	986	8.197	0.00346	36.81	8.55	0.0105
34	101	119	25.9	40	4.32	1.168	398	108	73310	100	0.00403	1021	7.742	0.00348	36.98	-	-
35	99	138	40	90	4.32	2.628	540	116	81570	269	0.00620	1572	11.026	0.00475	36.98	-	-
36	106	143	40	90	4.32	2.628	500	120	84520	116	0.00692	1754	9.651	0.00525	37.10	-	-
37	110	148	40	90	4.32	2.628	457	122	87690	54	0.00784	1987	8.000	0.00596	37.10	-	-
38	112	150	40	90	4.32	2.628	430	122	87690	34	0.00853	2162	7.273	0.00657	37.10	-	-
39	107	119	20.9	28	4.32	0.7884	310	114	77940	155	0.00402	1018	4.787	0.00358	36.81	-	-
40	103	118	20.9	28	4.32	0.788	305	112	76250	34	0.00408	1034	4.742	0.00366	36.86	-	-
41	103	118	20.9	28	4.32	0.788	310	112	76250	100	0.00398	1009	4.894	0.00355	36.86	-	-
42	94	125	24.8	39.3	2.49	1.1476	417	110	43020	99	0.00374	948	8.103	0.00549	21.25	-	-
43	101	131	24.9	38.8	2.52	1.1330	500	116	47580	262	0.00295	748	9.348	0.00396	21.57	-	-
44	108	140	24.9	40.25	2.51	1.1753	375	128	54340	35	0.00476	1206	5.435	0.00631	21.59	-	-
45	100	120	20	26.1	2.49	0.7621	425	114	44920	250	0.00245	621	8.036	0.00353	21.28	-	-
46	102	124	20	26.1	2.49	0.7621	414	116	47030	115	0.00256	649	7.414	0.00360	21.32	-	-
47	104	125	20	26.4	2.50	0.7709	392	117	47020	40	0.00280	710	6.719	0.00397	21.40	-	-
48	101	139	40	85	4.32	2.5112	546	120	85550	265	0.00589	1493	10.789	0.00433	37.04	7.5	0.0090
49	103	128	32.5	55	4.32	1.606	510	120	85550	264	0.00412	1044	9.762	0.00314	37.04	6.5	0.0076
50	104	137	40	85	4.31	2.5112	508	120	85360	136	0.00647	1640	9.318	0.00488	36.96	9.3	0.0113
51	103	124	32.3	56.1	2.48	1.638	520	116	42690	252	0.00405	1026	10.610	0.00606	21.23	7.1	0.0261
52	103	146	31.2	55	2.48	1.606	450	116	42690	99	0.00481	1219	8.529	0.00742	21.23	9	0.0329
53	106	150	31.2	57	2.48	1.664	386	118	47400	31	0.00621	1574	6.439	0.00898	21.34	-	-
54	104	160	36.8	73.2	2.48	2.137	550	130	54940	291	0.00509	1290	9.733	0.00619	21.30	4.6	0.0168
55	111	163	36.8	75.0	2.48	2.190	480	126	52310	138	0.00619	1569	8.388	0.00794	21.44	-	-
56	114	171	36.8	76	2.48	2.219	435	145	62530	43	0.00765	1939	5.517	0.00943	21.37	7	0.0254
57	87	107	20.9	26.1	2.52	0.7621	432	101	38610	364	0.00230	583	9.815	0.00350	21.44	2.6	0.0094
58	92	120	24.9	38	2.47	1.1096	545	110	42680	365	0.00255	646	12.368	0.00355	21.08	2.6	0.0097
59	99	140	29.8	54	2.48	1.5768	575	120	48530	364	0.00347	879	11.857	0.00450	21.27	2.7	0.0099
60	105	160	34.9	72.3	2.48	2.111	597	122	52370	364	0.00444	1125	12.121	0.00532	21.27	-	-

it was necessary to use a common bulk temperature, and the arithmetic average for all tests of 115 deg F was chosen. Bearing in mind the limitations in the accuracy of wall-temperature measurements (±15 deg F), the graphical presentation of the data in Fig. 4 may be used in design to determine the temperature of the liquid-to-surface interface necessary to remove heat rates up to 3 Btu/sq in. sec.

The conventional heat-transfer coefficient is defined as

$$h = \frac{q/A}{T_W - T_F} \qquad [1]$$

The data presented in Fig. 4 can be evaluated in terms of the heat-transfer coefficient by dividing the ordinate (q/A) by the abscissa ($T_W - T_F$) at any desired heat flux. Calculations of this type show that heat-transfer coefficients 3 to 4 times larger than for pure forced convection can be obtained by reducing the pressure and operating at wall temperatures which permit the formation of bubbles adjacent to the heat-transfer surface.

No flow instabilities were observed in any of the tests with aniline, and no tube failure due to overheating was encountered (1). The stability of operation in cooling a surface at high heat flux with aniline containing small amounts of water is probably aided by the low vapor pressure of the major constituent of the liquid. In such a two-component system, where only a small portion of more volatile liquid is present, the bubbles formed on the heating surface may not be able to exist for any appreciable length of time in the main stream or grow to such a size as to cause violent vibrations when they collapse. Therefore the conditions of the tests were probably not as severe from a cavitation point of view as those with water, and indeed no vibrations were encountered. The maximum bulk temperature of the aniline was 170 F, which is about 100 deg F below the bubble temperature at the test pressure of 34 psia. For this test the wall temperature was about 150 deg F above the bubble point.

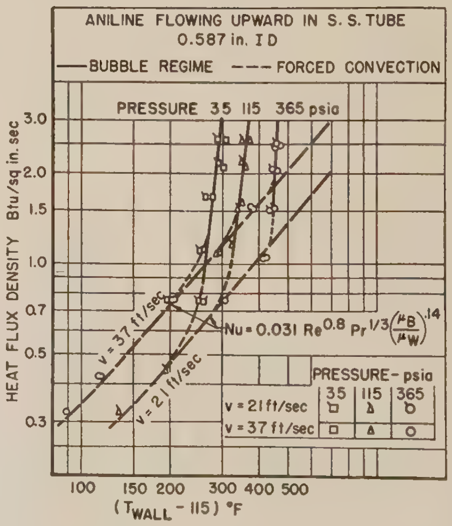

Fig. 4 Heat Flux Versus Temperature Difference (Aniline)

TABLE 1 *(Continued)*

Test No.	Temperature		Electric Potential (volts)	Power (watts)	Flow Rate	Heat Flux q/A	T_W	T_B	Re_B	Pressure	f_c	Nu	$\frac{\mu_B}{\mu_W}$	j	V	ΔP	C_F
	Inlet	Outlet															
61	91	102	15	15.2	2.48	0.4438	300	97	35960	116	0.00219	555	5.657	0.00379	21.03	-	-
62	93	106	15	15.2	2.48	0.4438	300	100	37290	35	0.00222	562	5.455	0.00378	21.06	-	-
63	95	102	15	15.2	4.32	0.4438	225	100	64960	200	0.00355	900	3.462	0.00370	36.69	-	-
64	94	102	15	15.2	4.32	0.4438	227	100	64960	25	0.00349	884	3.484	0.00363	36.69	-	-
65	95	102	12.6	11.2	2.48	0.3270	245	100	37290	250	0.00226	573	3.971	0.00402	21.06	-	-
66	94	100	12.6	11.2	4.32	0.3270	192	100	64960	34	0.00355	900	2.700	0.00358	36.69	-	-
67	100	120	20.9	26	2.48	0.7592	368	110	41770	34	0.00281	747	6.912	0.00433	20.63	3.5	0.0084
68	101	132	25.9	39.8	2.48	1.162	375	118	47380	34	0.00452	1146	6.159	0.00379	21.23	4.7	0.0106
69	102	145	31.2	56.1	2.48	1.638	380	120	48530	34	0.00630	1597	6.103	0.00891	21.27	5.65	0.0125
70	101	112	20.9	26.4	4.32	0.7709	315	110	74620	365	0.00376	953	5.109	0.00339	36.86	-	-
71	101	118	25.9	40	4.32	1.168	410	110	74620	364	0.00389	986	7.966	0.00330	36.86	-	-
72	103	128	31.2	54.4	4.32	1.588	500	112	76250	365	0.00409	1037	10.698	0.00329	36.92	-	-
73	103	135	36.8	72.5	4.32	2.117	573	115	79740	364	0.00462	1171	12.222	0.00354	36.92	-	-
74	103	140	40	84	4.32	2.4508	602	120	85550	364	0.00508	1288	12.813	0.00368	37.04	-	-
75	83	112	25.9	37.7	2.48	1.1096	545	100	37120	364	0.00249	631	14.211	0.00372	21.10	-	-
76	92	120	25.9	38.6	2.48	1.124	483	110	42840	212	0.00301	763	10.444	0.00425	21.16	-	-
77	97	126	25.9	39.1	2.48	1.156	430	115	45770	115	0.00367	930	8.000	0.00520	21.20	-	-
78	101	130	25.9	39.8	2.48	1.168	380	120	49130	34	0.00450	1144	5.857	0.00634	21.27	4.8	0.0108
79	98	130	36.8	72.5	4.32	2.117	560	115	79710	364	0.00476	1206	12.055	0.00366	36.92	-	-
80	93	158	40	85	2.48	2.482	545	110	42840	314	0.00571	1447	12.368	0.00754	21.16	8.1	0.0185
81	102	170	40	89	2.48	2.599	470	125	51630	115	0.00776	1917	7.959	0.01007	21.30	-	-
82	102	171	40	90	2.48	2.628	430	130	53700	34	0.00876	2221	6.818	0.01150	21.37	-	-
83	88	154	40	86	2.48	2.511	570	118	47380	364	0.00556	1409	11.972	0.00725	21.23	-	-
84	98	154	36.8	73.5	2.48	2.140	572	125	52310	367	0.00479	1214	11.000	0.00588	21.30	-	-
85	112	154	31.2	107.5	2.48	1.5695	560	135	58360	362	0.00369	935	9.452	0.00434	21.40	-	-
86	113	140	25.9	76.5	2.48	1.117	540	130	55170	362	0.00272	689	9.481	0.00331	21.37	-	-
87	95	102	-	31.5	4.32	0.4438	229	100	64960	24.5	0.00344	872	3.553	0.00359	36.69	-	-
88	94	100	-	23	4.32	0.3270	195	100	64960	250	0.00344	872	2.769	0.00372	36.69	-	-

In water tests, flow instabilities occurred when the bulk temperature approached the saturation temperature within 80 deg F, and the wall temperature exceeded the saturation temperature by about 55 deg F. In comparing results for both liquids it must be remembered that the boiling point of pure aniline is more than 100 deg F above the bubble point, and the information as to whether the saturation temperature or the bubble-point temperature is important in causing violent cavitation is inconclusive at this date.

It is expected that with pure aniline (without water) the transition from the forced convection to the boiling regime will take place at a higher wall temperature in correspondence with the vapor characteristics of the liquid. As soon as the wall temperature, at a given pressure, exceeds the boiling temperature of the coolant, it is expected that the pressure will determine the heat-transfer surface temperature and changes in flow, bulk temperature, and heat flux will have only a secondary influence similar to the results obtained for pure water and n-butyl alcohol.

The effect of dissolving a more volatile component in a liquid of low vapor pressure on the heat-transfer characteristics is somewhat similar to the effect of dissolved gases as shown by McAdams (2). Working with an electrically heated test section of annular shape, McAdams found that bubble formation and surface-boiling phenomena occurred at lower wall temperature as the air content of the water was increased. These results agree qualitatively with the observations in the present study.

Heat Transfer to n-Butyl Alcohol With Surface Boiling. A summary of the results of the heat-transfer tests with n-butyl alcohol is presented in Fig. 5, and the basic data from the tests are given in Tables 2 and 3, with important calculated results.

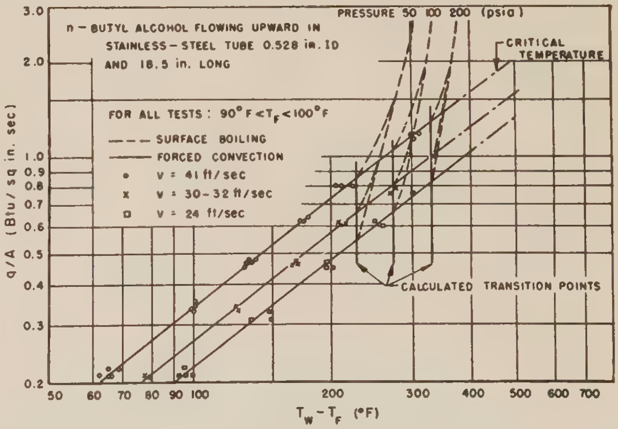

FIG. 5 HEAT FLUX VERSUS TEMPERATURE POTENTIAL FOR n-BUTYL ALCOHOL AT VARIOUS FLOW RATES

The curves show (for an average fluid bulk temperature of 95 F) the temperature potential necessary for the removal of heat fluxes up to 3 Btu/sq in. sec, at pressures of 50, 100, and 200 psia, and for entrance velocities of about 20, 30, and 40 fps. An inspection of the curves in Fig. 5 shows that when the surface temperature exceeds the boiling point of the alcohol, (*a*) substantial increases in heat flux result in only minor increases in the temperature of the heat transfer to liquid surface interface, and (*b*) the temperature of the heat-transfer surface is insensitive to variations of the coolant velocity in the surface-boiling regime.

During one test in the surface-boiling regime, the influence of

TABLE 2 HEAT-TRANSFER AND FRICTION DATA FOR TESTS WITHOUT SURFACE BOILING (n-BUTYL ALCOHOL)

Test No.	w	T_{in}	ΔT	v	q/A Electrical	q/A Thermal	T_W	T_F	h	Re_F x 10^{-3}	Nu	$\frac{\mu_F}{\mu_W}$	$\left(\frac{Nu}{Re^{0.80}Pr^{0.33}}\right)$ x 10^{-2}	ΔP *	$C_{F_{HT}}$	$\frac{C_{F_{iso}}}{C_{F_{HT}}}$
1	3.85	86	11.5	43.1	0.82		298	92	3.74	74.1	991	7.33	4.14			
2	3.85	85	11.4	40.9	0.80	0.77	303	88	3.59	66.1	952	8.10	4.30			
3	3.84	87	16.8	41.0	1.19	1.16	393	95	3.88	73.1	1028	11.81	4.39			
4	3.84	90	11.2	41.0	0.79	0.77	301	93	3.71	71.4	983	7.37	4.25			
5	3.84	97	11.3	40.8	0.79	0.79	314	87	3.48	65.8	922	8.66	4.17			
6	3.83	89	17.0	41.2	1.21	1.21	420	100	3.79	77.6	998	12.70	4.21			
7	3.84	97	6.2	41.2	0.44	0.46	225	100	3.66	77.6	970	4.00	4.02			
8	3.84	92	4.7	41.1	0.33	0.33	189	98	3.63	75.7	962	2.97	4.03			
9	2.79	93	6.6	29.9	0.34	0.33	224	98	2.59	55.0	686	4.10	3.71			
10	2.79	93	9.1	29.9	0.46	0.46	265	100	2.77	56.4	737	5.37	3.94			
11	2.79	94	14.9	30.0	0.78	0.79	375	104	2.91	59.4	769	9.50	4.10			
12	3.85	86	11.1	41.1	0.80	0.80	320	94	3.54	72.3	938	7.23	4.03	7.45	0.0119	1.67
13	3.85	87	16.5	41.2	1.18	1.16	405	98	3.78	75.9	1002	12.13	4.20	6.28	0.0100	1.96
14	3.85	88	11.1	41.1	0.79	0.79	320	96	3.47	74.0	920	7.06	3.91	7.58	0.0121	1.63
15	3.84	92	3.1	41.0	0.22	0.21	163	94.5	3.07	72.2	814	2.35	3.51	10.78	0.0173	1.15
16	3.84	89	4.8	41.0	0.34	0.34	192	92.5	3.39	70.6	899	3.28	3.91	10.02	0.0161	1.24
17	3.84	90	6.8	41.0	0.48	0.47	228	93.8	3.52	71.9	933	4.45	4.02	9.22	0.0149	1.34
18	3.84	94	3.0	41.1	0.21	0.21	164	96	3.09	73.9	819	2.27	3.48	10.84	0.0174	1.14
19	3.84	88	4.8	41.0	0.34	0.33	191	91.2	3.35	69.6	888	3.31	3.90	10.11	0.0162	1.23
20	3.84	91	6.6	41.1	0.47	0.46	226	94.8	3.53	72.2	936	4.34	4.03	9.28	0.0149	1.34
21	3.84	89	3.1	41.0	0.22	0.22	157	91.5	3.27	69.8	867	2.25	3.80	10.88	0.0175	1.15
22	3.84	96	4.7	41.1	0.33	0.33	196	99	3.50	76.6	928	3.12	3.87	10.01	0.0160	1.22
23	3.84	92	6.6	41.1	0.47	0.47	228	96.8	3.60	74.5	954	4.30	4.04	9.24	0.0148	1.33
24	3.84	90	3.0	41.0	0.21	0.21	158	91.8	3.24	70.0	859	2.25	3.76	10.84	0.0175	1.14
25	3.84	91	4.7	41.0	0.33	0.33	191	93.5	3.40	71.6	901	3.22	3.89	10.06	0.0161	1.24
26	3.84	93	6.4	41.1	0.46	0.46	225	97.5	3.59	75.4	952	4.12	4.00	9.30	0.0149	1.32
27	2.22	92	5.3	23.7	0.22	0.22	191	97	2.28	43.2	604	3.05	3.95	3.69	0.0177	1.26
28	2.22	92	7.9	23.8	0.33	0.33	245	95	2.19	42.2	580	5.01	3.85	3.22	0.0154	1.47
29	2.22	90	10.7	23.8	0.44	0.45	290	96	2.33	42.8	618	6.67	4.07	2.83	0.0136	1.65
30	2.22	90	14.4	23.8	0.60	0.62	350	100	2.48	44.9	657	9.09	4.14	2.40	0.0115	1.96

* The units of the frictional pressure loss in Tables 2 and 3 are: inches of mercury minus inches of n-butyl alcohol.

bulk temperature upon the temperature of the heat-transfer surface was investigated. The n-butyl alcohol was circulated at a constant flow rate and at constant pressure, but without being passed through the heat exchanger. This procedure resulted in the bulk temperature of the liquid increasing from a value of 100 deg F to a value which was higher than 200 deg F. The wall-to-liquid interface temperature was unaffected by this increase in the bulk temperature of the liquid and remained constant at 386 deg F, thus proving that in the surface-boiling regime, the temperature of the interface between the liquid and the heat-transfer surface is insensitive to changes in bulk temperature.

In reference (1), the results of the experiments on heat transfer to water, with surface boiling, were correlated by plotting the excess temperature against pressure for constant heat fluxes. The excess temperature was defined as the temperature difference between the wall-to-liquid interface and the boiling point at the pressure of the liquid during the test. The results of the tests with n-butyl alcohol are presented in the same form in Fig. 6 where the excess temperature is plotted against pressure for various heat fluxes. During these tests, the flow rate of the n-butyl alcohol was held constant at 3.85 lb per sec. It can be seen that the excess temperature required to remove a given heat flux at a constant bulk temperature decreases as the pressure increases. A corresponding relationship between excess temperature and pressure exists for water; however, the curves for water have a steeper negative slope than do those for the n-butyl alcohol.

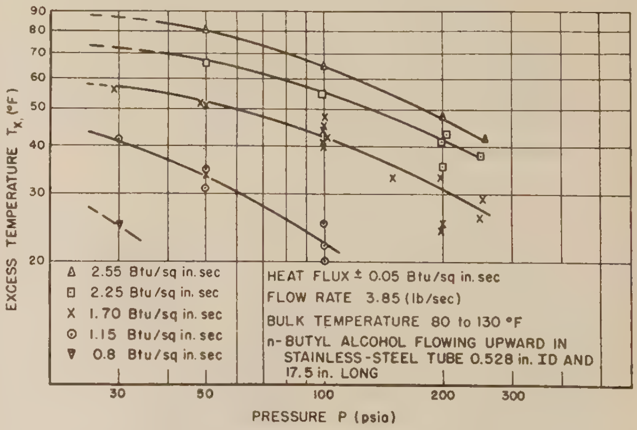

Fig. 6 Excess Temperature Versus Pressure at Various Heat Fluxes With Surface Boiling (n-Butyl Alcohol)

A further comparison of the results obtained from tests using n-butyl alcohol as a coolant with results obtained from tests using water as a coolant is presented in Fig. 7. In this figure the excess temperatures (from Fig. 6), are plotted against heat flux for constant pressures (100 and 25 psia). The results obtained in tests with water at corresponding pressures are superimposed on the same graph.

An inspection of Fig. 7 shows that the general trends of the curves for the n-butyl alcohol agree with trends of the curves for water. However, for the removal of the same heat flux, the n-

TABLE 2 *(Continued)*

Test No.	w	T_{in}	ΔT	v	q/A		T_W	T_F	h	Re_F $\times 10^{-3}$	Nu	$\frac{\mu_F}{\mu_W}$	$\left(\frac{Nu}{Re^{0.80}Pr^{0.33}}\right) \times 10^{-2}$	ΔP	$C_{F_{HT}}$	$\frac{C_{F_{iso}}}{C_{F_{HT}}}$
					Electrical	Thermal										
31	2.22	89	5.1	23.7	0.21	0.21	190	93	2.21	41.3	586	3.18	3.93	3.72	0.0179	1.27
32	2.22	91	7.4	23.8	0.31	0.31	230	97	2.36	43.3	626	4.32	4.10	3.35	0.0161	1.40
33	2.22	87	10.6	23.8	0.43	0.45	298	96	2.24	42.8	594	7.00	3.90	2.82	0.0136	1.65
34	2.22	93	14.2	23.8	0.59	0.60	354	102	2.38	46.0	631	9.07	4.00	2.48	0.0119	1.86
35	2.22	92	5.1	23.7	0.21	0.21	190	95	2.23	42.2	571	3.11	3.78	3.72	0.0179	1.26
36	2.22	89	7.5	23.7	0.31	0.31	238	90	2.12	39.9	562	5.00	3.83	3.32	0.0160	1.43
37	2.22	94	10.5	23.8	0.44	0.47	294	98	2.42	43.8	640	6.72	4.16	2.88	0.0138	1.62
38	2.22	90	5.1	23.7	0.21	0.21	191	90	2.12	39.9	562	3.33	3.83	3.70	0.0178	1.29
39	2.22	90	7.8	23.7	0.32	0.33	242	92	2.19	40.6	580	5.08	3.92	3.25	0.0156	1.46
40	3.84	89	8.7	41.0	0.62	0.63	261	92	3.72	70.3	986	5.74	4.30	8.50	0.0136	1.47
41	3.85	86	9.1	41.0	0.64	0.64	265	90	3.68	69.1	975	6.04	4.29	8.36	0.0134	1.50
42	3.84	88	8.9	41.0	0.63	0.63	264	90	3.62	69.1	960	6.00	4.22	8.49	0.0136	1.48
43	3.84	95	8.7	41.1	0.62	0.63	261	98	3.86	75.7	1023	5.32	4.29	8.52	0.0136	1.45
44	3.85	86	3.2	40.9	0.21	0.21	149	86	3.40	64.8	901	2.19	4.10	10.88	0.0175	1.17
45	3.84	88	4.7	41.0	0.33	0.37	188	88	3.69	66.9	978	3.32	4.32	9.98	0.0161	1.25
46	3.84	92	6.6	41.0	0.47	0.47	221	92	3.61	70.2	957	4.25	4.18	9.25	0.0149	1.34
47	3.85	87	9.1	41.0	0.64	0.63	264	89	3.60	67.6	954	6.13	4.24	8.34	0.0134	1.51
48	2.89	95	3.1	30.9	0.21	0.21	172	95	2.75	54.8	729	2.55	3.81	6.05	0.0171	1.24
49	2.89	92	6.3	30.9	0.34	0.33	213	92	2.72	52.9	721	3.98	3.95	5.51	0.0156	1.37
50	2.89	93	8.5	30.9	0.45	0.46	257	95	2.82	54.9	747	5.43	4.01	4.96	0.0140	1.52
51	2.89	94	11.5	30.9	0.62	0.62	310	92	2.83	52.9	750	7.89	4.11	4.40	0.0125	1.71
52	3.00	92	3.8	32.0	0.21	0.21	170	91	2.72	53.9	721	2.65	3.87	6.72	0.0177	1.20
53	3.01	87	6.2	32.0	0.34	0.34	211	89	2.76	52.7	732	4.07	3.98	6.09	0.0161	1.33
54	3.00	88	8.2	32.0	0.45	0.46	253	90	2.81	53.9	745	5.56	3.99	5.48	0.0145	1.47
55	3.00	92	11.0	32.1	0.62	0.62	305	96	2.98	57.8	790	7.30	4.09	4.85	0.0130	1.61
56	3.00	91	10.9	32.1	0.61	0.61	302	94	2.96	56.4	785	7.35	4.11	4.89	0.0129	1.64
57	2.22	94	17.6	23.9	0.75	0.76	410	108	2.52	49.9	668	10.91	4.07	2.25	0.0106	2.05
58	3.00	89	13.6	32.2	0.76	0.78	353	100	3.08	60.7	816	9.20	4.12	4.40	0.0114	1.81

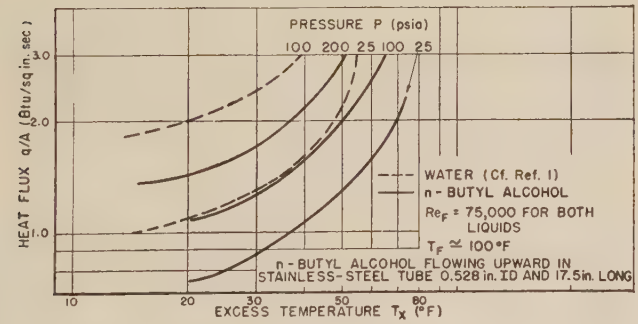

Fig. 7 Heat Flux Versus Excess Temperature for n-Butyl Alcohol and Water

butyl alcohol requires an excess temperature which is about 25 deg F higher than that required when water is used as the coolant. The test sections used for both liquids were of similar dimensions, and the Reynolds number (evaluated at the bulk temperature) was about 75,000 for both liquids. A bulk temperature of about 100 deg F was used during the tests with both of the liquids.

The qualitative remarks presented next are pertinent to the proper use and interpretation of the data on heat transfer with surface boiling. Because the bulk temperature was nearly constant during the tests, the degree of subcooling of the bulk of the liquid was not the same in tests at different pressures. Even though the bulk temperature or degree of subcooling has no effect upon the wall temperature in the fully developed surface-boiling regime, the point of transition from the pure forced-convection regime to the surface-boiling regime is dependent upon the bulk temperature and pressure of the liquid. Thus at a higher bulk temperature, the transition will occur at a lower heat flux, and vice versa. The heat flux at transition can be calculated for a given bulk temperature and pressure by the following equations

$$(q/A)_{\text{trans}} = 0.034 \frac{K}{D} Re^{0.8} Pr^{1/3} \left(\frac{\mu_F}{\mu_W}\right)^{0.1} (T_S - T_F)$$

for n-butyl alcohol......[2]

$$(q/A)_{\text{trans}} = 0.027 \frac{K}{D} Re^{0.8} Pr^{1/3} \left(\frac{\mu_F}{\mu_W}\right)^{0.14} (T_S - T_F)$$

for water......[3]

Before using the curves applicable only to heat transfer with surface boiling, it is necessary to determine first whether or not the surface temperature (for the pressure, flow conditions, and heat flux under consideration) exceeds the boiling temperature T_S of the coolant.

It has been shown (2) that the exact point of transition from forced-convection heat transfer to surface-boiling heat transfer is influenced by the amount of dissolved gases or impurities in the liquid. When a degassed liquid is used as the coolant, the surface temperature may exceed the boiling point by as much as 20 deg F before bubbles begin to form. On the other hand, if a large amount of gas is dissolved in the coolant, bubble formation may occur at a surface temperature below the saturation temperature. For this reason, the curves in Fig. 7 are not extended to excess temperatures of less than 10 deg F.

In previous tests with water, the heat flux that could be re-

TABLE 3 HEAT TRANSFER AND FRICTIONAL PRESSURE-LOSS DATA FOR TESTS IN SURFACE BOILING REGIME (n-BUTYL ALCOHOL)

Test No.	v	T_{in}	ΔT	q/A Electrical*	q/A Thermal**	P	T_w	T_X	ΔP
1	3.84	93	--	1.50	--	68	371	35	
2	3.85	78	22.5	1.59	1.59	200	451	26	
3	3.85	80	16.4	1.17	1.15	50	348	31	
4	3.85	86	23.5	1.66	1.68	50	351	34	
5	3.86	75	23.4	1.63	1.68	200	450	25	
6	3.85	86	--	2.17	--	200	460	35	
7	3.84	89	29.7	2.17	2.13	250	482	38	
8	3.83	103	29.8	2.23	2.22	205	470	43	
9	3.84	91	23.1	1.66	1.67	250	470	26	
10	3.84	98	23.1	1.69	1.69	197	448	24	
11	3.83	103	23.5	1.66	1.74	150	432	33	
12	3.84	90	23.0	1.67	1.66	254	476	29	
13	3.89	95	23.7	1.72	1.73	102	407	42	
14	3.83	99	24.1	1.74	1.77	50	370	53	
15	3.83	101	24.1	1.74	1.77	29	340	56	
16	3.84	92	35.3	2.52	2.58	255	489	42	
17	3.84	96	34.9	2.59	2.57	200	473	48	
18	3.85	81	22.2	1.60	1.58	199	457	33	5.83
19	3.85	86	30.2	2.17	2.19	200	465	41	6.55
20	3.84	92	33.5	2.52	2.45	200	472	48	7.26
21	3.85	87	16.1	1.16	1.14	100	385	22	6.92
22	3.85	87	24.0	1.69	1.72	99	405	41	7.20
23	3.85	85	31.1	2.23	2.24	99	418	55	7.91
24	3.85	85	11.2	0.79	0.79	50	319	2	7.52
25	3.84	87	16.7	1.19	1.20	50	352	35	7.59
26	3.85	87	24.3	1.72	1.74	50	366	49	8.35
27	3.84	89	31.0	2.29	2.28	50	383	66	9.36
28	3.81	79	11.2	0.82	0.78	30	310	25	7.68
29	3.85	85	16.5	1.17	1.17	30	327	42	8.35
30	2.22	90	14.7	0.62	0.62	50	318	1	2.83
31	2.22	91	10.7	0.44	0.45	30	290	5	2.89
32	2.22	90	14.5	0.64	0.63	30	296	11	3.20
33	2.89	94	11.6	0.63	0.65	30	294	9	4.72
34	3.00	90	11.5	0.64	0.63	30	296	11	5.02
35	2.22	87	26.7	1.12	1.13	199	433	9	2.38
36	2.22	90	18.2	0.74	0.77	100	370	6	2.62
37	2.22	89	27.2	1.15	1.16	100	392	28	2.95
38	2.22	86	18.8	0.78	0.79	50	328	11	3.10
39	2.22	90	27.2	1.15	1.18	50	349	32	3.54
40	2.22	88	19.0	0.79	0.80	30	300	15	3.51
41	2.22	86	28.4	1.19	1.19	30	323	38	3.94
42	3.00	89	20.2	1.14	1.14	200	434	9	3.96
43	3.00	88	20.0	1.13	1.16	100	376	12	4.64
44	3.00	90	14.0	0.78	0.78	50	320	3	5.01
45	3.00	86	20.7	1.17	1.18	50	350	33	5.51
46	3.00	89	14.0	0.78	0.79	30	299	14	5.60
47	3.00	88	20.9	1.18	1.19	30	324	39	6.12
48	3.00	90	29.3	1.66	1.64	200	456	31	4.30
49	3.00	92	29.4	1.68	1.70	100	403	39	5.13
50	3.00	98	30.1	1.75	1.70	50	372	55	5.66
51	2.27	95	39.1	1.69	1.70	100	410	46	3.36
52	2.23	102	39.6	1.73	1.74	50	377	60	4.16
53	3.02	91	14.0	0.79	0.80	30	321	36	5.40
54	3.84	99	22.2	1.67	1.63	100	404	40	7.59
55	3.84	92	--	1.79	--	100	408	44	7.74
56	3.84	94	--	1.19	--	100	389	25	6.98
57	3.84	97	--	1.72	--	100	412	48	7.64
58	3.84	93	--	1.22	--	100	384	20	7.00
59	3.84	99	--	1.70	--	100	409	45	7.90
60	3.00	95	--	2.20	--	200	470	45	4.88
61	3.00	90	39.0	2.23	2.24	100	420	56	5.78
62	2.22	93	51.1	2.20	2.20	200	473	48	3.27
63	2.22	94	51.4	2.23	2.24	100	417	53	3.95
64	3.00	95	39.3	2.26	2.28	50	384	67	6.82
65	3.82	103	34.2	2.54	2.56	200	--	--	7.56
66	3.84	89	16.3	1.17	1.16	200	--	--	6.62
67	3.84	90	22.6	1.64	1.63	200	--	--	6.42
68	3.84	89	23.1	1.67	1.66	100	--	--	7.51
69	3.84	98	24.0	1.69	1.75	50	--	--	8.85
70	3.84	99	30.6	2.27	2.27	50	--	--	9.92
71	3.82	101	35.2	2.63	2.62	50	398	81	10.50
72	3.84	90	35.1	2.60	2.57	100	429	65	8.84
73	2.22	89	59.4	2.57	2.56	200	477	52	3.65

*q/A = (kilowatts)/(1.054 · A_{HT}).

**q/A = (c_p * ΔT)/(A_{HT}).

moved by forced convection with surface boiling was limited by burnouts of the tube (1, 2). It is believed that these burnouts were caused by flow instabilities due to growth and collapse of vapor bubbles. No burnouts (such as had been encountered when water was used as the coolant) occurred in the tests with n-butyl alcohol. However, during several tests at heat fluxes above 2 Btu/sq in. sec, the stainless-steel tubular test section developed almost invisible longitudinal cracks. These cracks are believed to have been caused by metal fatigue, possible because of vibrations induced by the growth and collapse of bubbles within the test section.

Heat Transfer by Forced Convection Without Surface Boiling (Aniline, n-Butyl Alcohol, Water). The results of the tests in which the wall temperature remained below the bubble or boiling temperature of the coolant liquid are shown in Fig. 8. The data are presented as a plot of the dimensionless index $Nu/(Re^{0.8}Pr^{1/3})$ versus the ratio of the viscosity at the bulk temperature to the viscosity at the wall temperature. This type of presentation was chosen because, at the high heat fluxes used in the experiments, a very steep temperature gradient exists adjacent to the heat-transfer surface; this temperature gradient causes an appreciable variation in the viscosity of the liquid and it is known (3, 4) that the variation in viscosity influences the heat-transfer process. The experimental results for aniline and n-butyl alcohol are correlated within ±10 per cent by

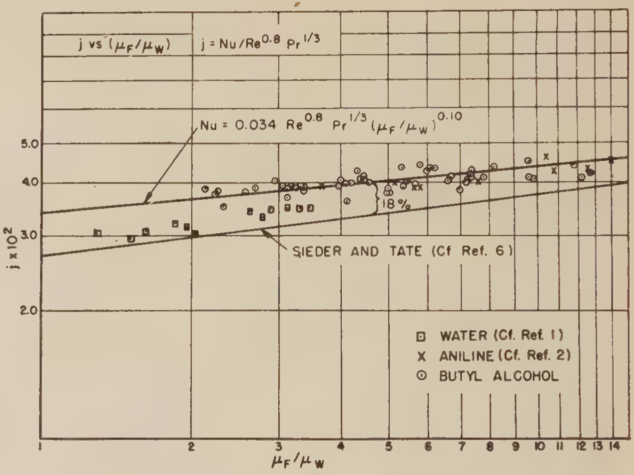

FIG. 8 CORRELATION OF PURE FORCED-CONVECTION DATA

$$Nu = 0.034\, Re^{0.8}\, Pr^{1/3}\, (\mu_F/\mu_W)^{0.10} \qquad [4]$$

Sieder and Tate (3) have examined the results of a large number of experiments on heat transfer to liquids at low heat fluxes and for best correlation of the experimental results derived the following equation

$$Nu = 0.027\, Re^{0.8}\, Pr^{1/3}\, (\mu_F/\mu_W)^{0.14} \qquad [5]$$

The results of experiments by Sherwood and Petrie on heat transfer from a tube to n-butyl alcohol (15) at heat fluxes below 0.2 Btu/sq in. sec were in agreement with Equation [5].

An inspection of Fig. 8 shows that while the data for water (1) fall within the experimental accuracy on a line representing the Sieder and Tate equation, the results for n-butyl alcohol and aniline show Nusselt moduli which are from 15 to 25 per cent higher than would be predicted by Equation [5]. However, the precision to which the forced-convection data for the latter two liquids were correlated was subject to uncertainties because no precise data for the physical properties of the liquids were available for the full range of temperature and pressure covered in the experiments. In particular, there exists some uncertainty regarding the thermal conductivity of the liquids. When more reliable information on the thermal conductivity of aniline and n-butyl alcohol becomes available, the results of the heat-transfer tests can be re-evaluated. The physical properties for aniline and n-butyl alcohol, used in the reduction of the experimental results, were taken from the references given in the following tabulation:

	C_p	ρ	μ	P_v
Aniline	5	5	5,6	5
n-Butyl alcohol	7	8	9	10

The thermal conductivities were assumed to be independent of temperature, and the values which were used in reducing the data are given as follows:

Aniline, $K = 0.1$ (ref. 11)
n-Butyl alcohol, $K = 0.095$ (ref. 12)

It is interesting to note, Fig. 5, that the maximum heat flux which can be removed by pure forced convection with liquid n-butyl alcohol at a velocity of 24 fps is about 1.15 Btu/in.^{2} sec. (More than twice this heat flux has been removed with surface boiling.) At this heat flux the surface temperature reaches the critical temperature. In general, the thermal conductivity of a fluid in the gaseous state is very much smaller (about one tenth) than the conductivity of the same fluid in the liquid state. Therefore the curves in Fig. 5 should not be extrapolated to temperatures and pressures higher than critical.

The heat-transfer results obtained from tests in the nonboiling forced-convection regime were also compared with the momentum transfer (as measured by the frictional pressure loss) following the technique of the von Kármán analogy theory (16). No satisfactory agreement was obtained (the experimental *Nu* moduli, when extrapolated to zero heat flux, were about 50 per cent higher than would be predicted by the analogy). The reason for this discrepancy is not apparent at this time.

Frictional Pressure Loss With Heat Transfer. The effect of heat transfer upon the frictional pressure loss was studied quantitatively with n-butyl alcohol only. (During the period in which the aniline tests were performed, there was no differential manometer connected across the test section, and the frictional pressure loss in the aniline tests was measured with a differential Barton pressure gage. The results are qualitatively in agreement with those presented for n-butyl alcohol in this paper.)

The frictional pressure drop as a function of heat flux is shown in Figs. 9, 10, and 11, for entrance velocities of 23, 31, and 41 fps at four different pressures. From an inspection of these curves it can be seen that the frictional pressure loss initially decreases (for a given flow rate of coolant liquid) with an increase in heat flux. This decrease continues until boiling begins adjacent to the heat-transfer surface. After surface boiling has begun, then the pressure loss increases with any increase in heat flux. In the surface-boiling regime the frictional pressure loss (at constant heat flux, bulk temperature, and flow rate) increases also with a decrease in pressure. This result appears reasonable, since boiling is more vigorous at lower pressures. In none of the tests did the pressure loss with heat transfer exceed the isothermal value at the same liquid flow rate.

In initial tests the isothermal friction factor was measured in the Reynolds-number range from 25,000 to 70,000. Friction factors were correlated within ±1 per cent by the following equation, and are in agreement with accepted values within 2 per cent (14)

$$C_F = 0.265\, Re^{-0.23} \qquad [6]$$

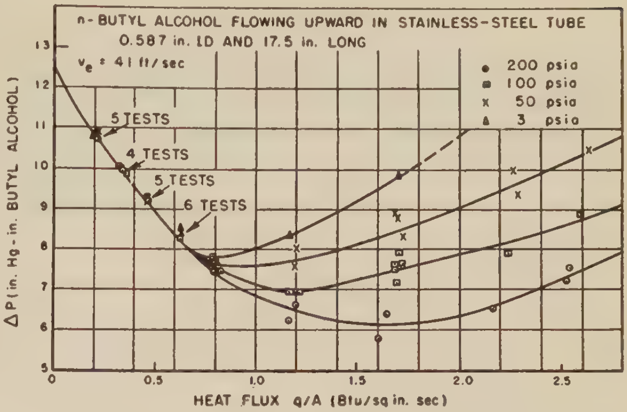

Fig. 9 Effect of Heat Flux on Frictional Pressure Loss (V_e = 41 fps.)

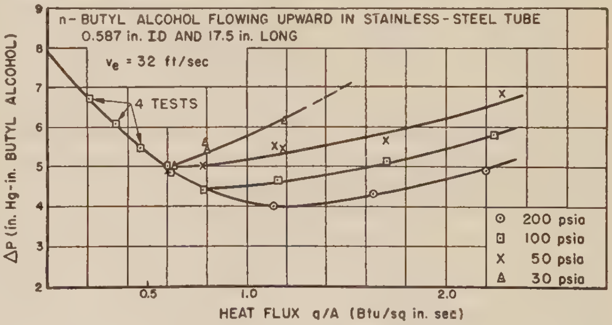

Fig. 10 Effect of Heat Flux on Frictional Pressure Loss (V_e = 31 fps)

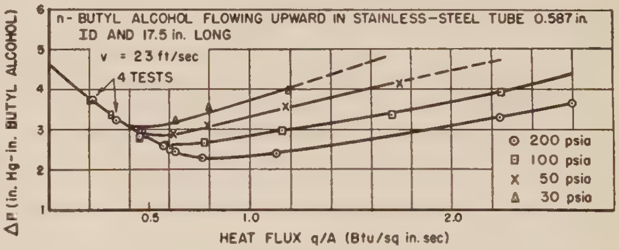

Fig. 11 Effect of Heat Flux on Frictional Pressure Loss (V_e = 23 fps)

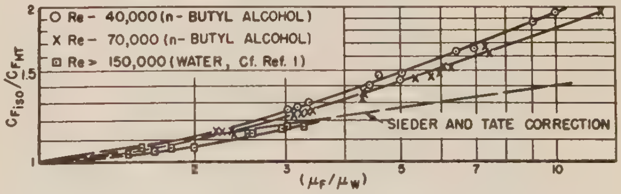

Fig. 12 Ratio of Heat-Transfer (Nonboiling) Friction Coefficient to Isothermal Friction Coefficient Versus Ratio of Viscosity at Bulk Temperature to Viscosity at Wall Temperature

For nonboiling heat-transfer conditions, the results on the frictional pressure drop with heat transfer are correlated by plotting the ratio of the isothermal friction coefficient to the heat-transfer friction coefficient (both evaluated at the same bulk Reynolds number) against the ratio of the viscosity at bulk temperature to the viscosity at the wall temperature, Fig. 12. These results will be studied further. However, it can be stated at this time that evaluation of the Reynolds number at a temperature equal to or slightly below the temperature of the heat-transfer surface will result in a friction coefficient under heat-transfer conditions close to the experimentally observed value.

CONCLUSIONS

1 Experimental results have been obtained on heat transfer from a stainless-steel tube to a 96 per cent aniline, 4 per cent water, solution and to n-butyl alcohol in the heat-flux range from 0.3 to 3 Btu/sq in. sec, over a pressure range from 40 to 400 psi for velocities ranging from 20 to 40 fps. The results of the tests are summarized in Figs. 5 and 6 which show (for average fluid bulk temperatures) the temperature potential necessary for the removal of given heat fluxes in the forced-convection and boiling or bubble regime.

2 The temperature of the heat-transfer surface is insensitive to changes in velocity, heat flux, and bulk temperature when it exceeds either the bubble temperature (aniline) or the boiling temperature (n-butyl alcohol) of the coolant liquid. The controlling factor of the surface temperature in the bubble or boiling regime is the system pressure. These phenomena are similar to results obtained previously in heat transfer to water with surface boiling.

3 In the pure forced-convection regime, the results for aniline and n-butyl alcohol were correlated by the following equation

$$Nu = 0.034\ Re^{0.8}\ Pr^{1/3} \left(\frac{\mu_B}{\mu_W} \right)^{0.10}$$

4 No instabilities of flow or breakdown of the heat transfer with subsequent failure of the heating tube were encountered in any of the tests with aniline at bulk temperatures up to 170 F.

5 The beneficial characteristics of surface-boiling in heat transfer (i.e., higher heat-transfer efficiency) can be obtained with a coolant of low vapor pressure at temperatures below its boiling point by dissolving a more volatile component of low solubility in the main constituent. This technique may have application in heat-transfer devices other than rockets, especially in the chemical industry and power plants of the future.

6 The frictional pressure loss decreases (for a given flow rate of coolant liquid) with an increase in heat flux. After surface-boiling has begun, then the pressure loss increases with any increase in heat flux. Even in the bubble or boiling regime the heat-transfer pressure loss was less than the isothermal pressure loss for the same flow rate.

7 Friction coefficient for heat-transfer conditions can be approximated by evaluating the Reynolds number at a temperature slightly below the heat-transfer surface temperature. It would be desirable to predict heat-transfer friction coefficient from theoretical considerations; work along this line should be encouraged.

BIBLIOGRAPHY

1 "Heat Transfer to Water at High Flux Densities With and Without Surface Boiling," by Frank Kreith and Martin Summerfield, Trans. ASME, vol. 71, 1949, pp. 805–815.

2 "Heat Transfer at High Rates to Water With Surface Boiling," by W. H. McAdams, J. N. Addoms, and W. E. Kennel, Report ANL-4268. Argonne National Laboratory, Massachusetts Institute of Technology, Cambridge, Mass., December, 1948.

3 "Heat Transfer and Pressure Drop of Liquids in Tubes," by E. N. Sieder and G. E. Tate, *Industrial and Engineering Chemistry*, vol. 28, 1936, pp. 1429–1436.

4 "Remarks on the Analogy Between Heat Transfer and Momentum Transfer," by L. M. K. Boelter, R. C. Martinelli, and F. Jonassen, Trans. ASME, vol. 63, 1941, pp. 447–455.

5 "Some Studies of the Reaction of Aniline and Orthotoluidine With Red Fuming Nitric Acid," by E. W. Hough, J. M. Green, and B. H. Sage, Report No. 1–14. Pasadena, Calif.; Jet Propulsion Laboratory, April 20, 1943.

6 "Correlating Viscosity and Vapor Pressure of Liquids," by D. F. Othmer and J. W. Conwell, *Industrial and Engineering Chemistry*, vol. 37, 1945, pp. 1112–1115.

7 "International Critical Tables," McGraw Hill Book Company, Inc., New York, N. Y., vol. 5, 1933, p. 108.

8 Ibid., vol. 3, pp. 27–33.

9 Ibid., vol. 7, p. 215.

10 Ibid., vol. 3, p. 219.

11 "Thermal Conductivities of Certain Liquids," by G. W. C. Kaye and W. F. Higgins, Proceedings of the Royal Society of London, vol. A117, 1928, p. 459.

12 "International Critical Tables," McGraw Hill Book Company, Inc., New York, N. Y., vol. 7, 1933, p. 228.

13 Eleventh Informal Monthly Report of M.I.T., Project DIC 1-6489 for period August 18 to September 18, 1947, by W. H. McAdams, Massachusetts Institute of Technology, Cambridge, Mass., Sept. 25, 1947.

14 "Friction Factors for Pipe Flow," by F. L. Moody, Trans. ASME, vol. 66, 1944, pp. 671–684.

15 "Heat Transmission to Liquids Flowing in Pipes," by T. K. Sherwood and J. M. Petrie, *Industrial and Engineering Chemistry*, vol. 24, 1932, p. 736.

16 "The Analogy Between Fluid Friction and Heat Transfer," by Th. von Kármán, Trans. ASME, vol. 61, 1939, pp. 705–710.

Discussion

O. P. BERGELIN.[5] Local boiling can be extremely useful in certain cases of heat transfer and certainly deserves more attention than it has received in the past. In this paper, as well as in previous papers on the subject, the authors have made valuable contributions in this field. In looking over their results, the high rates of heat transfer, which are shown to be available through local boiling, appear so attractive that perhaps it would be advisable to emphasize the dangers and disadvantages that might occur when applying local boiling to the process industries. One major disadvantage is the severe conditions to which the heating surface is subjected. The vibrations caused by collapsing bubbles may cause mechanical failure of thin-walled tubes, and the rates of corrosion under local boiling conditions are as yet unknown. Until more information is available it might be wise to restrict local boiling to heavy-walled ducts, such as passages through engine blocks, or to equipment where a short life is permissible. In those cases where the upper temperature level is above the melting point of the duct wall, there is also the danger of burnout if the liquid velocity becomes so low that an insulating vapor blanket can form over the heat-transfer surface. Surface roughness may enhance vapor blanketing and must be investigated before local boiling conditions can be predicted with assurance.

The data reported for pressure drop show a relatively small increase in pressure drop due to local boiling. One might expect a much larger effect because of the increase in wall shear caused by surface "roughness," due to bubbles and to the increase in liquid velocity as a result of the volume occupied by the bubbles. Moreover, all bubbles which become detached from the surface will be accelerated to some velocity before they disappear in the liquid stream. Can it be that enough bubbles collapse away from the surface to form a relatively thick layer of high-temperature fluid near the surface and thus lower the wall shear in spite of the disturbances at the surface? Temperature and velocity traverses as well as visual observation probably will be needed to clarify the mechanism of flow near the surface during local boiling.

CLOSURE

The authors wish to acknowledge with appreciation the discussion by Professor Bergelin. The comments on the limitations of surface-boiling heat transfer are well to keep in mind when attempting to utilize this technique for practical application.

Regarding the question whether or not bubbles collapse away from the surface, the authors agree with Professor Bergelin that additional work will be necessary before a definite answer can be given. Preliminary work along the lines suggested in the discussion has been performed by means of photographic observations, and some of the results have been presented in two recent papers (17, 18). These photographic studies are being continued at present. To date no data on temperature and velocity traverses have been obtained, according to the authors' knowledge. In addition to these experiments, a determination of the increase in turbulence caused by surface boiling would help to clarify the mechanism of flow in surface boiling and aid in a quantitative analysis.

---

[5] University of Delaware, Newark, Del.

REFERENCES

17 "Photographic Study of Bubble Formation in Heat Transfer to Subcooled Water," by Fred C. Gunther and Frank Kreith, Heat Transfer and Fluid Mechanics Institute, June 22–24, 1949, ASME Publication.

18 "A Study of the Mechanism of Boiling Heat Transfer," by Warren M. Rohsenow and John A. Clark," Massachusetts Institute of Technology, 1949.

Heat Transfer and Fluid Friction During Viscous Flow Across Banks of Tubes—III

A Study of Tube Spacing and Tube Size

By O. P. BERGELIN,[1] G. A. BROWN,[2] H. L. HULL,[3] AND F. W. SULLIVAN[4]

In the course of a research program on tubular heat exchangers, pressure-drop and heat-transfer data are reported for heating and cooling a medium-viscosity oil flowing across banks of vertical tubes in seven test exchangers. The apparatus variables include equilateral triangle, in-line square, and staggered square arrangements; tube sizes of $^3/_8$ in. and $^3/_4$ in. OD; and pitch ratios of 1.25 and 1.50. The results are shown both in simple plots of pressure drop and coefficient of heat transfer versus the rate of flow, and in generalized correlations. Tentative correlations are provided for friction and heat transfer which bring the data for these seven tube banks somewhat closer together than previous correlations. In a comparison of the heat-transfer coefficient versus pumping-power loss per unit surface area, the smaller diameter tubes at the smaller pitch ratio give the best performance.

NOMENCLATURE

The following nomenclature is used in the paper:

A_F = shell-side friction area, sq ft
A_H = outside surface area of tubes, sq ft
c = heat capacity, Btu/(lb)(deg F)
D_s = minimum clearance between tubes, ft (except where otherwise indicated)
D_i = inside diameter of tube, in.
D_t = outside diameter of tube, ft (except where otherwise indicated)
D_v = volumetric hydraulic diameter $\dfrac{4 \times \text{free volume}}{\text{exposed area of tubes}}$, ft
d = tube core diameter, in.
E = pumping-power loss per unit heat-transfer area, (ft)(lb force)/(hr)(sq ft)
f_{Cs} = friction factor, defined by $f_{Cs} = \dfrac{2\Delta p g_c \rho_f D_v}{4{G_m}^2 L}$, dimensionless
f_{Ct} = friction factor, defined by $f_{Ct} = \dfrac{2\Delta p g_c \rho}{4{G_m}^2 N}$, dimensionless
f_G = friction factor, defined by
$$\frac{f_G}{2} = \frac{\Delta p g_c \rho D_v}{{G_m}^2 L}\left(\frac{\mu}{\mu_s}\right)^{0.14}\left(\frac{S_T}{D_v}\right)^{0.4}\left(\frac{S_T}{S_L'}\right)^{0.6}, \text{ dimensionless}$$
G_m = mass velocity through minimum cross section, lb/(hr)(sq ft)
g_c = conversion factor, 4.18×10^8 (mass lb)(ft)/(force lb)(hr)^2
h = surface coefficient of heat transfer based on outside surface area of tubes, Btu/(hr)(sq ft)(deg F)
j = heat-transfer factor, $j = \left(\dfrac{h}{cG_m}\right)\left(\dfrac{c\mu}{k}\right)^{2/3}\left(\dfrac{\mu_s}{\mu}\right)^{0.14}$, dimensionless
k = thermal conductivity, Btu/(hr)(ft)(deg F)
L = length of tube bank, $L = nS_L$, ft
m = exponent of $\dfrac{\mu}{\mu_s}$, dimensionless
N = number of major restrictions encountered in flow through the bank (equivalent to n, where S_m occurs in transverse openings; equivalent to $n - 1$ where S_m occurs in diagonal openings), dimensionless
N_{Re} = Reynolds number $\dfrac{D_v G_m}{\mu}$, dimensionless
n = number of tube rows in direction of flow, dimensionless
P = pitch, defined as minimum center-to-center distance between adjacent tubes (in case of staggered square arrangements pitch is measured along a line 45 deg from direction of flow), ft
p = pressure, psf
S_L = longitudinal pitch, distance between center lines of adjacent transverse rows, ft
S_L' = longitudinal pitch, center-to-center distance from a tube in transverse row to nearest tube outside of that row, ft
S_m = shell-side minimum flow area, sq ft
S_T = transverse pitch, center-to-center distance between tubes in a transverse row, ft
S_w = total annulus flow area, sq ft
W = mass rate of flow, lb per hr
μ = absolute viscosity at average bulk temperature, lb/(hr)(ft)
μ_f = absolute viscosity at film temperature, lb/(hr)(ft)
μ_s = absolute viscosity at tube-surface temperature, lb/(hr)(ft)
ρ = density at average bulk temperature, lb per cu ft
ρ_f = density at film temperature, lb per cu ft
τ_0 = frictional resistance per unit tube-surface area, psf

INTRODUCTION

It has long been known that the size and spacing of tubes in a tube bank will affect the rate of heat transfer and the friction between the fluids and the tubes. Data have been published by a number of investigators for turbulent flow of gases past

---

[1] Associate Professor, Department of Chemical Engineering, University of Delaware, Newark, Del.

[2] Research Fellow in Chemical Engineering, University of Delaware.

[3] Research Fellow in Chemical Engineering, University of Delaware. Present address, E. I. du Pont de Nemours and Company, Wilmington, Del.

[4] Research Fellow in Chemical Engineering, University of Delaware.

Contributed by the Heat Transfer Division and presented at the Annual Meeting, New York, N. Y., November 27–December 2, 1949, of THE AMERICAN SOCIETY OF MECHANICAL ENGINEERS.

NOTE: Statements and opinions advanced in papers are to be understood as individual expressions of their authors and not those of the Society. Paper No. 49—A-87.

tubes of various sizes in tube banks over a wide range of tube spacings, the most extensive work in this field being that of Huge and Pierson with the later correlation of their data by Grimison (1).[5] However, there are few data available for fluids in viscous flow through tube banks, and the correlations which have been proposed for this case have been based upon the data of Sieder and Scott (2), covering only one tube size, one tube arrangement, and two tube spacings. It therefore appeared desirable to obtain additional data upon the effect of tube size and spacing in the region of viscous flow.

In a previous paper (3), results were presented for flow under isothermal and cooling conditions for three tube arrangements having $^3/_8$-in. tubes spaced on a 1.25 pitch ratio. (Pitch ratio is here defined as the ratio of the pitch P to the tube diameter D_t.) The present paper includes data on flow through the original three tube banks, isothermally and with heating and cooling, as well as similar data for four additional tube banks. The new tube banks consist of an equilateral-triangle arrangement with $^3/_8$-in. tubes on a 1.50 pitch ratio, an in-line square arrangement with $^3/_8$-in. tubes on a 1.50 pitch ratio, an in-line square arrangement with $^3/_4$-in. tubes on a 1.25 pitch ratio, and a staggered square arrangement with $^3/_4$-in. tubes on a 1.25 pitch ratio. These combinations of tube-bank dimensions were selected to cover the range of greatest interest for the case of viscous flow. All seven tube banks are shown in tube-sheet layouts in Fig. 1.

The work discussed in this paper is part of a comprehensive program on flow across tube banks that will deal with variation in fluid properties as well as variation in the dimensions of the tube bank. While the characteristics of tube bundles for simple crossflow are fairly well covered by the seven models discussed in this paper, only relatively minor variations in physical properties of the fluid have been treated thus far. The program will be continued using a heavier oil and possibly later a gas so that a wide range of Reynolds numbers and wide variation between tube-wall and bulk temperatures can be investigated. Along with this study of simple crossflow exchangers, a systematic study of flow and leakage around baffles will be carried out. In this way it is hoped conclusions from the data on the simple units can be extended to the analysis of commercial heat exchangers.

Equipment and Procedure

The equipment and procedures have been described in previous papers (3, 4), and detailed descriptions are available in a current research bulletin (5). Therefore only a brief description of the new exchangers and current operating procedures will be given here. The dimensions of the seven exchangers are summarized in Table 1 and the tube layouts are presented in Fig. 1. Although it was desired that the exchangers be identical except for variation of the dimensions under study, it was found that some other characteristics necessarily would have to vary, in this case the number of rows of tubes, the shell-side minimum flow area, and the exposed surface, as shown in Table 1.

A highly refined turbine oil, Gulfcrest "E," having a viscosity of 525 SUV at 100 F has been used for all tests. A table of physical properties of this oil is given in a previous paper (4). The exchangers are located with the tubes vertical, and during both heating and cooling runs, water is passed at constant high velocity upward through the tubes, with the resulting water-film coefficients of heat transfer in the range of 1000 to 2000 Btu/(hr) (sq ft) (deg F). Cores are used inside the tubes to reduce the

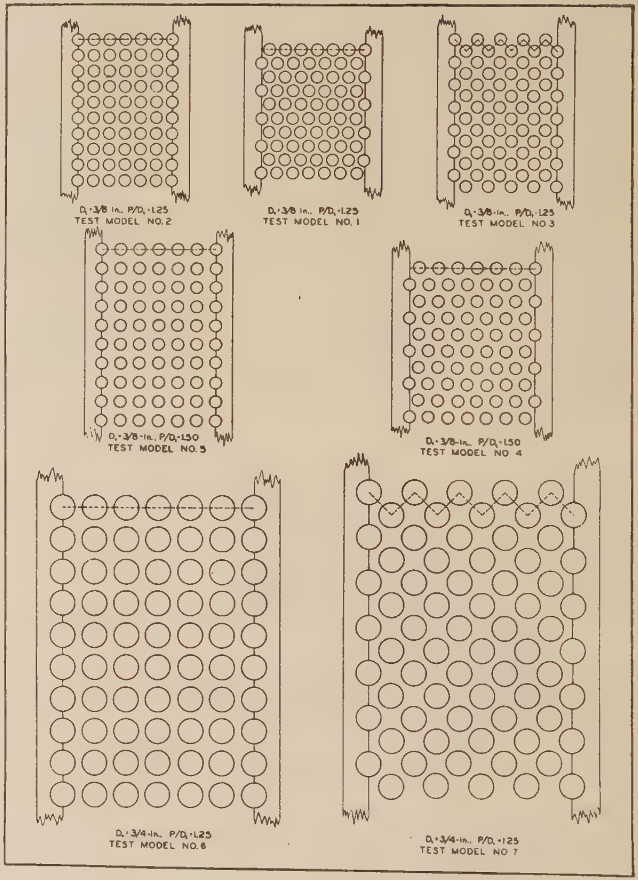

Fig. 1 Tube Layouts
(See Table 1 for dimensions.)

TABLE 1 HEAT-EXCHANGER DIMENSIONS AND CONSTANTS

Model number	1	2	3	4	5	6	7
Tube arrangement	Triangular	In-line square	Staggered square	Triangular	In-line square	In-line square	Staggered square
Outside tube diameter, D_t, in.	0.375	0.375	0.375	0.375	0.375	0.750	0.750
Minimum tube clearance, D_c, in.	0.094	0.094	0.094	0.188	0.188	0.188	0.188
Exposed tube length, in.	6.0	6.0	6.0	6.0	6.0	6.0	6.0
Number of copper tubes	70	70	70	70	70	70	70
Equivalent exposed tubes	65	60	63	65	60	60	63
Volumetric hydraulic diam, D_v, ft	0.0225	0.0309	0.0309	0.0463	0.0582	0.0619	0.0619
Min flow area, S_m, sq ft	0.0254	0.0234	0.0352	0.0508	0.0469	0.0469	0.0703
Number of tube rows, n	10	10	14	10	10	10	14
Number of contractions, N	10	10	13	10	10	10	13
Heat-transfer area, A_H, sq ft	3.19	2.94	3.09	3.19	2.94	5.89	6.18
Friction area, A_F, sq ft	3.44	3.10	3.36	3.57	3.24	6.38	6.91
Pitch ratio, P/D_t	1.25	1.25	1.25	1.50	1.50	1.25	1.25
S_L/D_t	1.08	1.25	0.883	1.30	1.50	1.25	0.883
S_L'/D_t	1.25	1.25	1.25	1.50	1.50	1.25	1.25
S_T/D_t	1.25	1.25	1.77	1.50	1.50	1.25	1.77
Length of tube bank, L, ft	0.338	0.391	0.387	0.406	0.469	0.781	0.773
Inside tube diameter, D_i, in.	0.277	0.277	0.277	0.277	0.277	0.620	0.620
Tube core diameter, d, in.	0.188	0.188	0.188	0.188	0.188	0.562	0.562
Annulus ratio, D_i/d	1.48	1.48	1.48	1.48	1.48	1.10	1.10
Total annulus area, S_w, sq ft	0.0158	0.0158	0.0158	0.0158	0.0158	0.0263	0.0263

---

[5] Numbers in parentheses refer to Bibliography at end of paper.

amount of water and thus increase the temperature change of the water stream. Standardized test runs, made with each unit upon installation and repeated as the final run, have shown that no appreciable fouling occurred during the period of testing. Heat balances of less than ±5 per cent deviation were obtained for all runs reported except those at very low oil velocities when the temperature change of the water stream became too low to give reliable heat balances. The heat load was calculated from the oil stream in these cases, and it is believed that the accuracy of these data is nearly comparable to those taken at higher oil velocities.

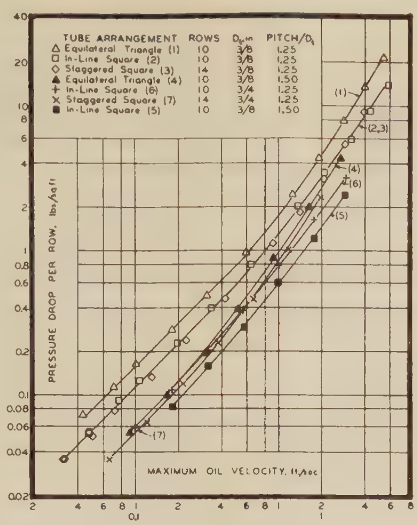

Fig. 2 Pressure Drop per Row During Isothermal Flow of Oil at 175 F for Seven Tube Banks

(Flow normal to vertical tubes. Gulfcrest "E" oil, viscosity 17 centipoises at 175 F.)

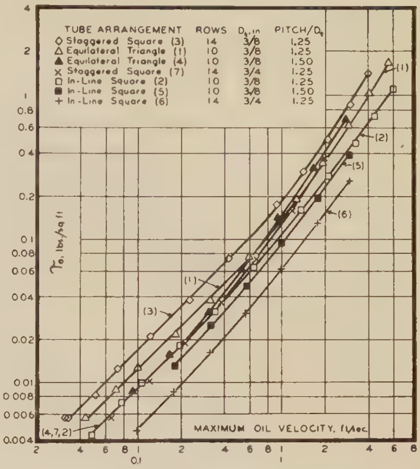

Fig. 3 Frictional Resistance per Unit Area of Tube Surface During Isothermal Flow of Oil at 175 F for Seven Tube Banks

(Flow normal to vertical tubes. Gulfcrest "E" oil, viscosity 17 centipoises at 175 F.)

Results

The experimental results are presented graphically both as simple plots of pressure drop and coefficient of heat transfer versus rate of flow and in generalized correlations. The experimental data and calculated results are too voluminous for inclusion in this paper but are presented in a current Engineering Experiment Station Bulletin (5).

Discussion of Results

Effect of Tube Spacing—Friction. The pressure drop per row of tubes for isothermal flow at 175 F is shown in Fig. 2 as a function of the linear oil velocity through the minimum cross-sectional area for flow. It can be seen that the data fall roughly into two groups, with the upper group, as indicated by the two top lines, representing the smaller tube size and the smaller clearance between tubes. The lower band of data represents the two arrangements of smaller tubes on the 1.50 pitch ratio, and the two arrangements of larger tubes on the 1.25 pitch ratio. In the latter four cases the minimum clearance between tubes is just double that of the upper band of data, the minimum clearance being 0.188 in. as compared to 0.094 in. At the lower oil velocities the upper group of curves has a slope of unity, indicating viscous flow. The slopes of the lower group approach unity at low velocities but do not maintain this slope over any appreciable range.

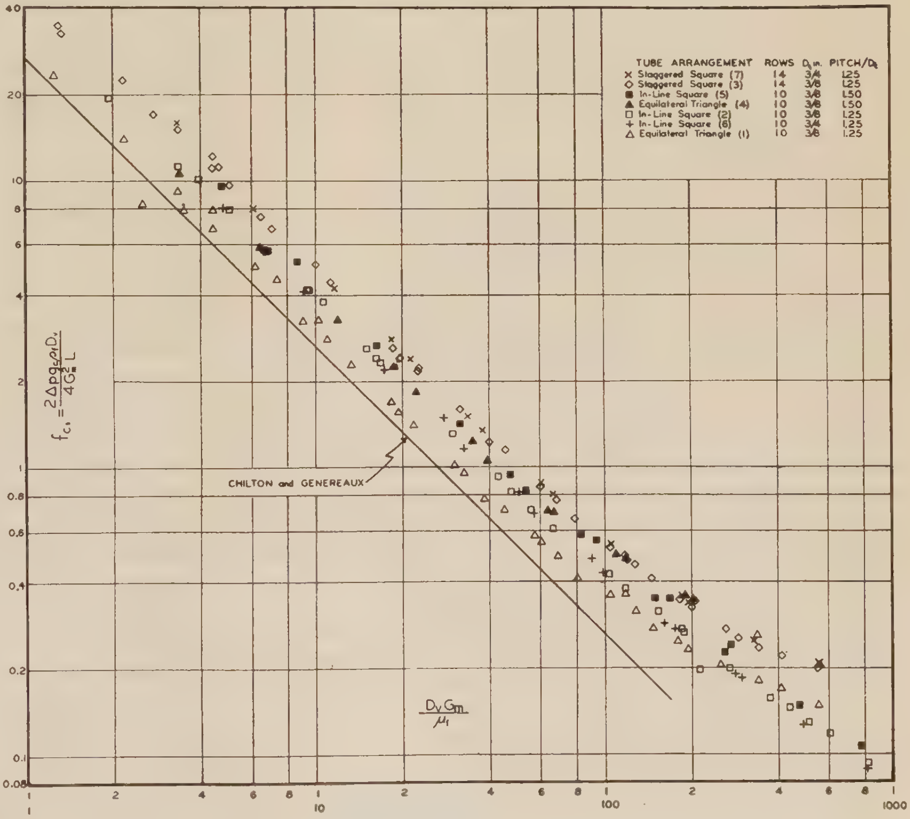

Fig. 4 Friction-Factor Correlation by Method of Chilton and Genereaux for Viscous Flow

(Isothermal flow normal to vertical tubes. Average bulk oil temperatures 125, 150, 175 F. Gulfcrest "E" oil, viscosity 49 centipoises at 125 F, 28 centipoises at 150 F, and 17 centipoises at 175 F. It should be noted that the line of Chilton and Genereaux is based upon data from two equilateral-triangle arrangements with 1.25 and 1.59 pitch ratios using 3/4-in. tubes.)

The friction data are also shown in Fig. 3 as frictional resistance per unit tube-surface area which is a term more directly comparable with coefficients of heat transfer, since the latter refer to tube-surface area. The spread of data is about the same as for Fig. 2, although the order of the different models is somewhat changed.

Another comparison of the pressure-drop data for the two spacings is given in Fig. 4 where a friction factor is calculated and plotted versus Reynolds number in the manner proposed by Chilton and Genereaux (6). By this representation the two arrangements with the 1.50 pitch ratio lie 10 to 40 per cent above

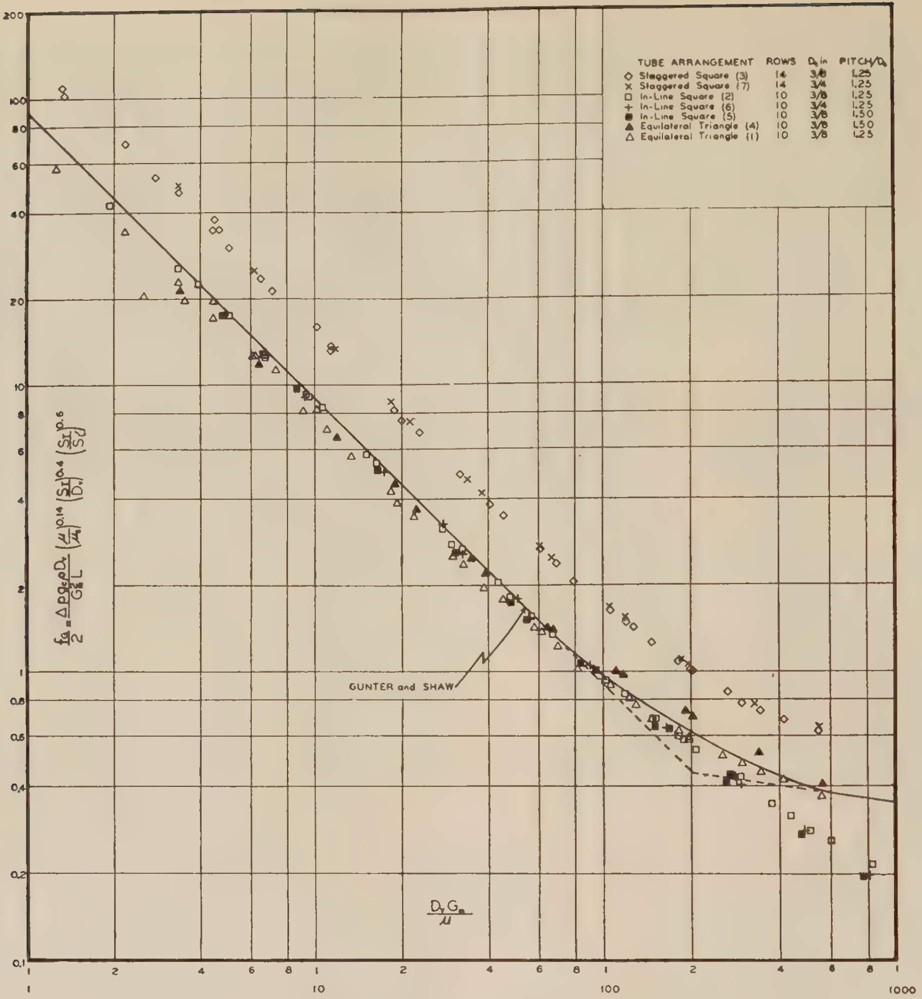

FIG. 5 FRICTION-FACTOR CORRELATION BY METHOD OF GUNTER AND SHAW

(Isothermal flow normal to vertical tubes. Average bulk oil temperatures 125, 150, 175 F. Gulfcrest "E" oil, viscosity 49 centipoises at 125 F, 28 centipoises at 150 F, and 17 centipoises at 175 F.)

their counterparts with 1.25 pitch ratio, so this representation does not allow suitably for changes in pitch. At Reynolds numbers greater than about 200, turbulence probably appears in varying degree in the different tube banks, and a clear separation of the in-line from the staggered arrangements is shown. Tube spacing does not appear to affect this separation of the data from these two general types of tube arrangements.

When the data are presented in the manner proposed by Gunter and Shaw (7), as shown in Fig. 5, there appears to be a somewhat better correlation of the effect of tube spacing, but this method does not bring the staggered square arrangement into agreement with the others. However, separate lines might be utilized for correlating the different types of arrangements.

Heat Transfer. The effect of tube spacing upon the coefficient of heat transfer, shown in Fig. 6, indicates that increasing the tube spacing results in somewhat lower heat-transfer coefficients, although the effect becomes less pronounced in the region of partial turbulence. This trend is also shown in the upper section of Fig. 7 where a j-factor with viscosity correction is plotted versus a Reynolds number based upon the tube diameter. In this figure the data represent both heating and cooling of the oil at average bulk temperature levels of 125, 150, and 175 F. The spread of the data shows that the effects of temperature variation between the tube wall and the body of the oil stream are not allowed for completely by this method of representation. It is interesting to note that the spread is greater for the in-line arrangements with the greater minimum tube clearance than for the other tube banks. This possibly may be due to free convection, but if so, a similar spread should be observed for the other arrangements with wide clearance between tubes.

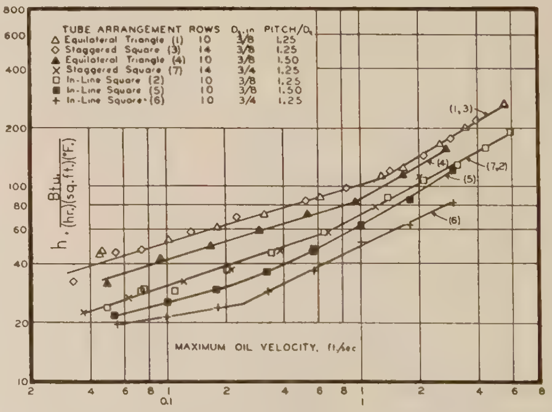

FIG. 6 OIL-FILM COEFFICENTS OF HEAT TRANSFER FOR SEVEN TUBE BANKS

(Flow normal to vertical tubes. Average bulk oil temperature 175 F. Tube-surface temperature range 101–113 F. Gulfcrest "E" oil, viscosity 98 centipoises at 100 F, 64 centipoises at 115 F, and 17 centipoises at 175 F.)

Heat Transfer Versus Pumping Power. In order to show the effect of spacing upon both friction and heat transfer, the heat-transfer coefficient is shown in Fig. 8 versus the power loss per unit surface area. The triangular arrangement with the 1.25 pitch ratio has approximately 25 per cent greater heat-transfer coefficients than the same arrangement on a 1.50 pitch ratio at given power losses. The increase is not so pronounced with the in-line square arrangements where the exchangers with the smaller pitch ratio give about 5 per cent greater heat transfer than those with the larger pitch ratio. In both cases the effect of spacing tends to decrease as turbulence appears.

The Effect of Tube Size—Friction. From Figs. 2 and 3 it can be seen that doubling the tube size reduces the pressure drop per row of tubes and the surface friction, respectively, by approximately 50 per cent when the pitch ratio is maintained constant. Doubling the tube size while maintaining the same minimum clearance between tubes increases the pressure drop by about 30 per cent, probably due to the longer flow path per row. When the pressure drop is expressed in terms of friction factors, as defined by Chilton and Genereaux, Fig. 4 shows that the large-tube data agree very well with the small-tube data for both the in-line and staggered square tube banks although the two arrangements do not coincide. The same is true for the Gunter and Shaw method as plotted in Fig. 5, so it may be said that both methods adequately allow for variation in tube size, although they do not allow for changes in spacing.

Heat Transfer. Fig. 6 shows that an increase in tube size causes an appreciable decrease in the coefficient of heat transfer. When the data are plotted in Fig. 7 as j-factor versus Reynolds number, the large- and small-tube data fall together, so that, for each arrangement, a single line is justifiable for representing both tube sizes. A spreading of the data for the in-line square arrangement again is noticeable and appears to be a characteristic of the wider clearance between tubes. A definite change of slope is also noticeable in the data for the in-line arrangement in the transition zone over the range of Reynolds numbers of 60 to 150. Motion pictures (8) of flow through sections of tube banks show that flow through an in-line square bank is somewhat similar to

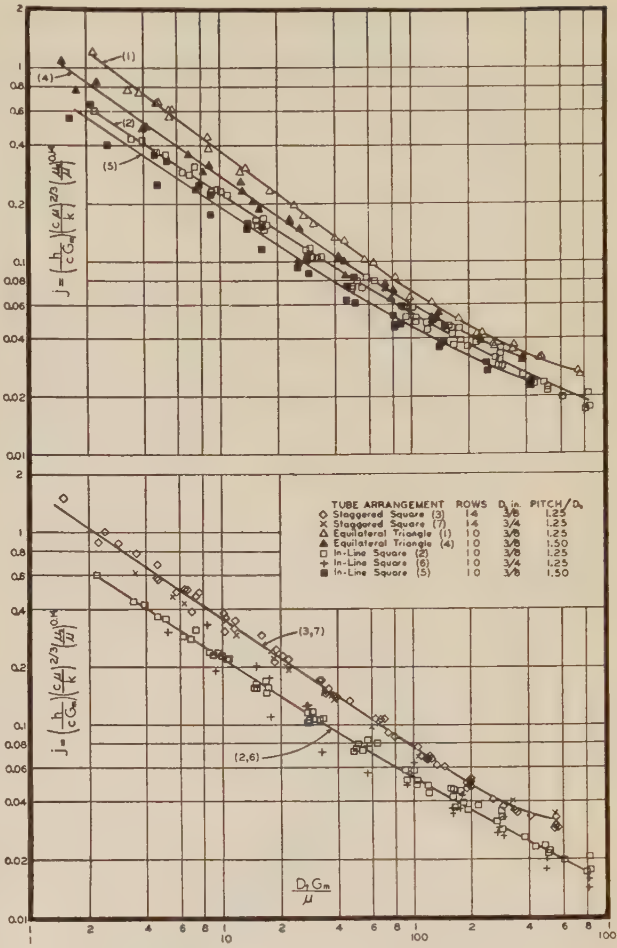

FIG. 7 HEAT-TRANSFER FACTOR j FOR SEVEN TUBE BANKS

(Flow normal to vertical tubes at average bulk oil temperatures of 125, 150, and 175 F. Both heating and cooling. Gulfcrest "E" oil, viscosity 49 centipoises at 125 F, 28 centipoises at 150 F, and 17 centipoises at 175 F.)

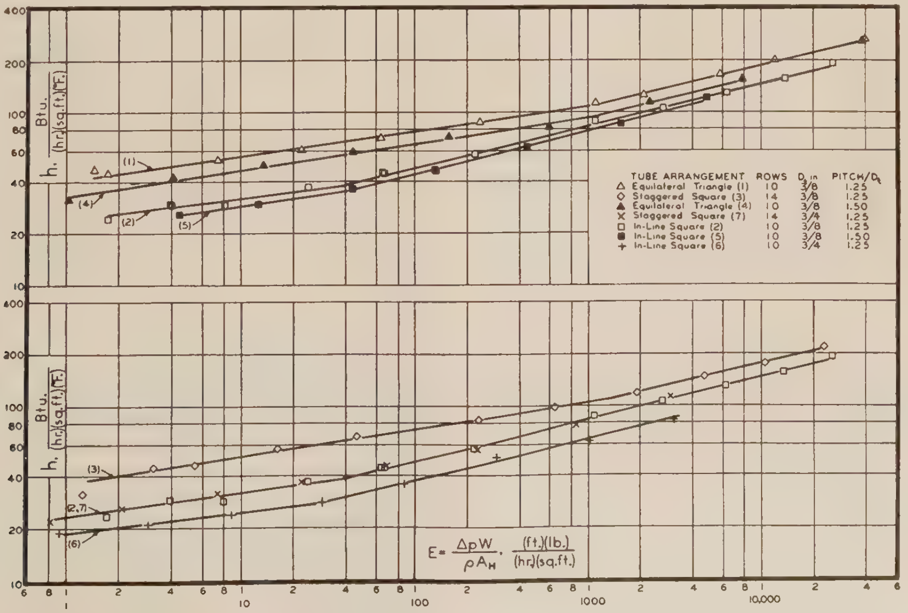

FIG. 8 COMPARISON OF HEAT-TRANSFER AND POWER REQUIREMENTS FOR SEVEN TUBE BANKS

(Flow normal to vertical tubes. Average bulk oil temperature 175 F. Tube-surface temperature range 101–113 F. Gulfcrest "E" oil, viscosity 98 centipoises at 100 F, 64 centipoises at 115 F, and 17 centipoises at 175 F.)

flow through a straight channel and therefore the increase in the rate of heat transfer which has been observed inside pipes in the transition zone may occur also to a lesser degree with in-line tube banks.

Heat Transfer Versus Pumping Power. Fig. 8, the plot of heat-transfer coefficients versus pumping power, clearly shows that when the pitch ratio is kept constant the small tubes provide from 20 to 50 per cent greater heat transfer at a given power loss per unit surface area than the large tubes.

Pressure Drop During Nonisothermal Flow. Although the foregoing discussions of pressure drop have dealt only with isothermal flow, the conclusions may be applied to flow through tube banks during heating or cooling if a suitable relation can be found to correlate the heating and cooling results with the isothermal data. A complete study of this problem has not yet been made, but it is possible that an analysis along the lines followed by Boelter and associates (9) for viscous flow inside pipes may prove successful. For the present, however, the use of an empirical factor $\left(\frac{\mu}{\mu_s}\right)^m$, similar to one proposed in a previous paper, is suggested. The extent of deviation during nonisothermal flow may be seen in Fig. 9 in which heating and cooling pressure-drop data are plotted for model 3. While in the previous paper the data were limited to cooling conditions for three tube banks, the present study includes heating data for all exchangers except model 1, as well as cooling data for all seven exchangers. The divergence of the pressure-drop lines seen in Fig. 9 for various $\frac{\mu}{\mu_s}$ ratios in model 3 is believed to be due principally to the viscosity gradient between the oil at the tube wall and in the center of the stream, rather than nonuniformity of flow throughout the tube bank during cooling at low velocity as previously suspected. The apparent systematic trend of the data from the cooling into the heating zone indicates that the deviation is essentially a viscosity-gradient effect.

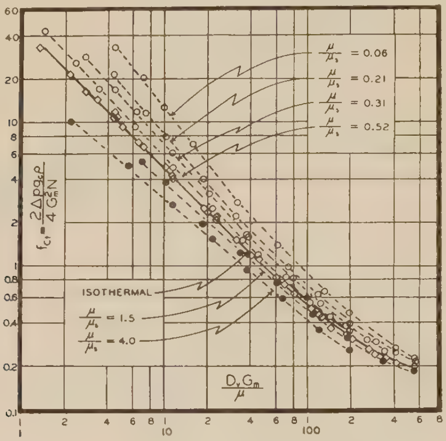

FIG. 9 VARIATION OF FRICTION FACTOR WITH HEATING AND COOLING

(Flow normal to 3/8-in-OD vertical tubes, model 3, staggered-square tube arrangement on 15/32-in. centers. Gulfcrest "E" oil, viscosity 49 centipoises at 125 F, 28 centipoises at 150 F, and 17 centipoises at 175 F.)

In developing a correction factor for such deviations, the exponents required for $\frac{\mu}{\mu_s}$ in order to bring the nonisothermal data in agreement with the isothermal data are plotted in Fig. 10 versus the Reynolds number. The scattering of the data is considerable but is not troublesome, since the exponent applies only a second-order correction. A straight line with the equation $m = 0.57\, N_{Re}^{-0.25}$ shown in the figure is suggested for representing the $\frac{\mu}{\mu_s}$ exponent over a range of Reynolds numbers from 1 to 300. The results of using this line to correct the data in Fig. 9 are shown in Fig. 11, and the resulting excellent agreement bears out the satisfactory nature of the correction term. This correction is equally satisfactory for the data from the other six tube banks.

Further Correlations. The isothermal pressure-drop data plotted in Figs. 4 and 5 show that neither the well-established Chilton and Genereaux method nor the more recent proposal of Gunter and Shaw allows completely for variation of tube-bank characteristics. On the whole, the Gunter and Shaw method appears better in the viscous region but, in the transition region, the in-line data deviate markedly, while the staggered square arrangements deviate from the other arrangements over the entire range. This method can be utilized, however, if a separate line is used for the staggered square arrangement. It is interesting to note that for the seven tube banks under consideration a much better correlation is obtained by interchanging S_T and S_L', which places the staggered square arrangements within 5 per cent of the proposed line of Gunter and Shaw. No other data are available to check the generality of this procedure, but a similar observation was made by Jameson (10) for turbulent flow past finned tubes.

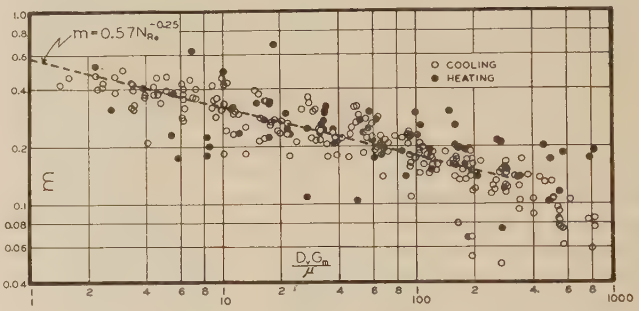

FIG. 10 EXPONENT m FOR VISCOSITY CORRECTION OF FRICTION FACTOR

(Flow normal to vertical tubes at average bulk oil temperatures of 125, 150, and 175 F. Both heating and cooling for seven tube banks. Gulfcrest "E" oil, viscosity 49 centipoises at 125 F, 28 centipoises at 150 F, and 17 centipoises at 175 F.)

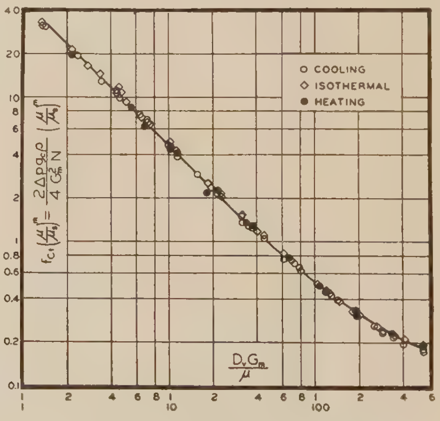

FIG. 11 FRICTION FACTORS FOR HEATING AND COOLING CORRECTED WITH VISCOSITY RATIO

(Flow normal to 3/8-in-OD vertical tubes, model 3, staggered-square tube arrangement on 15/32-in. centers. Gulfcrest "E" oil, viscosity 49 centipoises at 125 F, 28 centipoises at 150 F, and 17 centipoises at 175 F.)

In view of the plans to obtain more experimental data, no exhaustive attempt has been made to obtain the best possible

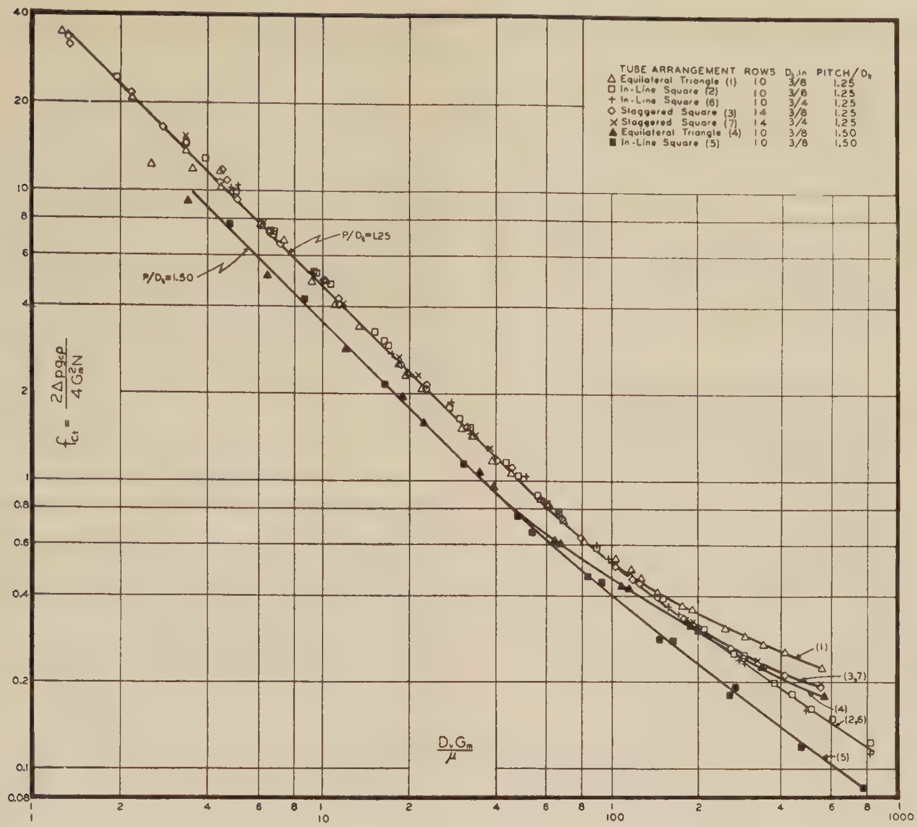

Fig. 12 Tentative Friction-Factor Representation
(Isothermal flow normal to vertical tubes. Average bulk oil temperatures 125, 150, 175 F. Gulfcrest "E" oil, viscosity 49 centipoises at 125 F, 28 centipoises at 150 F, and 17 centipoises at 175 F.)

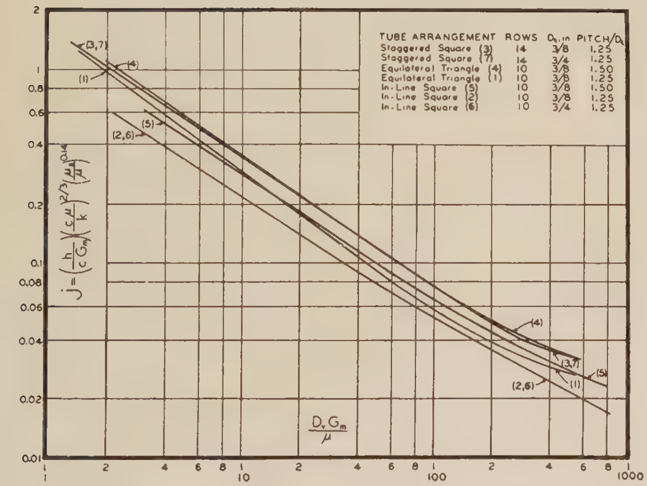

Fig. 13 Tentative Heat-Transfer Representation
(Flow normal to vertical tubes at average bulk oil temperatures of 125, 150, and 175 F. Both heating and cooling. Gulfcrest "E" oil, viscosity 49 centipoises at 125 F, 28 centipoises at 150 F, and 17 centipoises at 175 F.)

correlation with the data now available. On the other hand, it has been found that a relatively simple form of correlation brings the friction data considerably closer together than previous methods in the literature. This method involves plotting as ordinate

$$2\Delta P g_c \rho / 4 G_m^2 N$$

which was used by Chilton and Genereaux for turbulent flow versus $D_v G_m/\mu$ as shown in Fig. 12. Apparently different tube sizes and arrangements are brought together, but pitch ratio remains a parameter.

Similarly, for heat transfer, a final correlation will await further data, but it has been found that if the j-factor is plotted versus the Reynolds number using the volumetric hydraulic diameter D_v, instead of the tube diameter D_t, the data are brought closer together as shown in Fig. 13. The correction of $\left(\frac{\mu}{\mu_s}\right)^{0.14}$ for viscosity gradient, which was originally used by Sieder and Tate (11) for flow inside tubes, is used here as an approximation until additional data permit a further refinement.

It should be kept in mind that the conclusions presented in this paper are based upon data from simple crossflow exchangers and probably cannot be expected to apply without considerable modification to baffled exchangers where leakage around baffles, parallel flow, and nonuniformity of flow are important and must be given consideration.

Conclusions

Data from the present study show the following:

1 When the pitch is increased for a given arrangement and tube size:

(*a*) At constant velocity, the pressure drop is lower (Fig. 2).

(*b*) At constant velocity, the coefficient of heat transfer is lower (Fig. 6).

(*c*) At constant pumping-power loss, the coefficient of heat transfer is slightly lower (Fig. 8).

2 When the tube diameter is increased for a given arrangement and a constant pitch ratio:

(*a*) At constant velocity, the pressure drop is lower (Fig. 2).

(*b*) At constant velocity, the coefficient of heat transfer is lower (Fig. 6).

(*c*) At a constant pumping-power loss, the coefficient of heat transfer is considerably lower (Fig. 8).

3 The highest coefficients of heat transfer were obtained with the smaller tube sizes and the smaller tube pitches in the staggered arrangements.

4 A modification of the method of Chilton and Genereaux, utilizing the volumetric equivalent diameter, gives the best correlation of the pressure drop for viscous flow across the seven tube banks tested, although separate lines are found for the two pitch ratios. A variable exponent on the ratio of $\frac{\mu}{\mu_s}$ is suitable to correlate the nonisothermal pressure-drop data.

5 The use of the volumetric equivalent diameter in the Reynolds number gives a somewhat better correlation of the heat-transfer data than does the use of tube diameter.

ACKNOWLEDGMENT

The authors acknowledge the suggestions on design of the apparatus and on the program of study by the Special Advisory Committee of the Heat Transfer Division, which is sponsoring this co-operative research project. The committee at the time of the work was composed of W. H. McAdams, chairman; S. Kopp; W. N. McCurdy, Jr.; A. C. Mueller; B. E. Short; W. H. Thompson; T. Tinker; and P. R. Trumpler. The help of A. Wurster in the design and construction of the test units was invaluable. Assistance in interpretation and presentation of data was given by A. P. Colburn; Research Fellow W. E. Meece aided in the experimental work. Funds and equipment were kindly furnished by the Tubular Exchanger Manufacturer's Association, The American Petroleum Institute, Andale Company, Davis Engineering Company, Downingtown Iron Works, du Pont Company, Standard Oil Development Company, and York Ice Machinery Company. The oil was provided by the Gulf Oil Company.

BIBLIOGRAPHY

1 "Experimental Investigation of the Influence of Tube Arrangement on Convection Heat Transfer and Flow Resistance in Cross Flow of Gases Over Tube Banks," by O. L. Pierson, Trans. ASME, vol. 59, 1937, pp. 563–572. See also papers by E. C. Huge, pp. 573–581, and E. D. Grimison, pp. 583–594, and discussion, vol. 60, 1938, pp. 381–391.

2 "Fluid Friction at Parallel and Right Angles to Tubes and Tube Bundles," by E. N. Sieder and N. A. Scott, Jr., ASME unpublished paper No. 83, 1932.

3 "A Study of Tube Arrangements in Unbaffled Tubular Heat Exchangers," by O. P. Bergelin, E. S. Davis, and H. L. Hull, Trans. ASME, vol. 71, 1949, pp. 369–374.

4 "Heat Transfer and Fluid Friction During Viscous Flow Across Banks of Tubes," by G. A. Omohundro, O. P. Bergelin, and A. P. Colburn, Trans. ASME, vol. 71, 1949, pp. 27–34.

5 "Heat Transfer and Fluid Friction During Flow Across Banks of Tubes," by O. P. Bergelin, A. P. Colburn, and H. L. Hull, University of Delaware Engineering Experimental Station, Bulletin No. 2, 1950.

6 "Pressure Drop Across Tube Banks," by T. H. Chilton and R. P. Genereaux, Trans. AIChE, vol. 29, 1933, pp. 161–173.

7 "A General Correlation of Friction Factors for Various Types of Surfaces in Crossflow," by A. Y. Gunter and W. A. Shaw, Trans. ASME, vol. 67, 1945, pp. 643–660.

8 "Flow Across Tube Banks," a 400 ft., 16 mm. film available upon request from the Department of Chemical Engineering, University of Delaware, Newark, Del.

9 "Heat Transfer and Pressure Drop for a Fluid Flowing in the Viscous Region Through a Vertical Pipe," by R. C. Martinelli, C. J. Southwell, G. Alves, H. L. Craig, E. B. Weinberg, N. F. Lansing, and L. M. K. Boelter, Trans. AIChE, vol. 38, 1942, pp. 493–530.

10 Discussion by S. L. Jameson to "A General Correlation of Friction Factors for Various Types of Surfaces in Crossflow," by A. Y. Gunter and W. A. Shaw, Trans. ASME, vol. 67, 1945, pp. 658–659.

11 "Heat Transfer and Pressure Drop of Liquids in Pipes," by E. N. Sieder and G. E. Tate, *Industrial and Engineering Chemistry*, vol. 28, 1936, pp. 1429–1435.

Experimental Evaluation of Human Shape Factors With Respect to Floor Areas

BY F. W. HUTCHINSON,[1] BERKELEY, CALIF.

Results are presented for the shape factor of an average standing person with respect to energy in the form of heat received from a floor area. The use of shape factors is essential in determining conditions of comfort in a heated or cooled enclosure.

INTRODUCTION

THE establishment of conditions of comfort in a heated or cooled enclosure requires realization of a stable heat balance between the occupant and his surroundings. By a stable balance is meant one which provides a practically fixed net rate of heat loss from the occupant, irrespective of his position (as standing, sitting, or reclining), and irrespective of his location within the room. If room air temperature were uniform and if all inside surfaces of the enclosure were at the same temperature, there would be no difficulty in maintaining a stable balance, but in an enclosure where some surfaces (as windows) may be warmer in summer and colder in winter whereas others (as radiant panels) may be colder in summer and warmer in winter, the difficulty of stabilizing the occupant's rate of heat loss may be very great.

As an extreme case, visualize a room with large single-glass windows heated on a cloudy midwinter day by means of a small fireplace; obviously, the occupant will be too warm if he stands very near the fireplace, and too cold if he stands very near the windows. At one or more points in such a room conditions of comfort would necessarily exist, but the heating system would be considered unsatisfactory, and the occupant would experience marked instability with respect to his rate of heat loss.

Engineering evaluation of stability requires establishing a heat balance on the occupant and investigating the manner in which individual terms of that balance vary with position or location of the occupant. Since, for any fixed-load condition that may be acting on the enclosure the air and surface temperatures normally will remain fixed with respect to time, it follows that the major factor affecting stability will be changes in the geometry of the system (consisting of occupant and surroundings) which occur as the occupant alters his position or moves around in the enclosure. All such geometrical changes appear in the equations for radiant transfer between the occupant and the various surfaces of the room, each such surface possessing a shape factor with respect to the occupant which, in itself, expresses the fraction of energy received by that surface of the total radiant energy emitted by the occupant. Conversely the fraction of radiation emitted by a surface which strikes the occupant (prior to reflection) is said to be the shape factor of the occupant F_{os}, with respect to the surface; in equation form

$$F_{os} = \frac{1}{A_s} \int_{A_0} \int_{A_s} \frac{\cos \phi_0 \cos \phi_s dA_0 dA_s}{\pi (r_{os})^2} \quad \text{........} \quad [1]$$

where

F_{os} = shape factor of occupant with respect to energy received from surface A_s, or fraction of energy emitted by A_s which is received by occupant

r_{os} = distance between center of surfaces A_0 and A_s

ϕ_0 = angle between r_{os} and normal to center of A_0

ϕ_s = angle between r_{os} and normal to center of A_s

The mathematical problem of carrying out a double integration over the complex surface of the human body is, for practical purposes, insurmountable. Thus experimental methods must be used for evaluation of Equation [1]. The intent of this paper is to present complete results from such an experimental investigation for the particular case of an "average" occupant with respect to points, infinitesimal areas, or finite areas on the floor. A similar study[2] has dealt with human shape factors with respect to infinitesimal and finite areas in the wall or ceiling. The earlier study was for an occupant in either standing or sitting position whereas the present paper presents results only for the standing position.

EXPERIMENTAL PROCEDURE

The test procedure used in this research was practically identical with that which has been reported in detail in an earlier study.[2] The subject was a clothed dummy representing an "average" man 5 ft 10 in. in height and weighing 165 lb. The dummy was dressed in a two-piece suit, was in standing position, and had both arms at its sides. Shape factors were obtained by using a mechanical integrator of the type proposed by Hottel[3] and developed by Boelter[4] and associates.

Previous experience[2] had shown that the full-face shape factor of a standing subject is practically the same whether the subject is facing forward or backward, and that complete shape-factor curves for any facing direction could be readily and accurately determined by interpolation and extrapolation from experimental data for full face and for semiprofile. Accordingly, the dummy was placed in a fixed position on the test floor and a line drawn in the facing direction, another line being drawn making a 45-deg angle with the facing direction. Shape factors were then determined at intervals of 1 ft out along each of these lines to a distance of 18 ft from the dummy. In obtaining shape factors the mechanical integrator was placed at each of the designated points on the floor and a light beam from the integrator used to trace the outline of the dummy. Corresponding to each closed curve traced by the light beam, the integrator would draw a

---

[1] Professor of Mechanical Engineering, University of California.

Contributed by the Heat Transfer Division and presented at the Spring Meeting, Washington, D. C., April 12–14, 1950, of THE AMERICAN SOCIETY OF MECHANICAL ENGINEERS.

NOTE: Statements and opinions advanced in papers are to be understood as individual expressions of their authors and not those of the Society. Manuscript received at ASME Headquarters, November 1, 1949. Paper No. 50—S-4.

[2] "Optimum Surface Distribution in Panel Heating and Cooling Systems," by V. F. Raber and F. W. Hutchinson, Trans. ASHVE, vol. 50, 1944, pp. 231–257.

[3] "Radiant Heat Transmission," by H. C. Hottel, *Mechanical Engineering*, vol. 52, 1930, pp. 699–704.

[4] "A Mechanical Integrator for the Determination of the Illumination From Diffuse Surface Sources," by V. H. Cherry, D. D. Davis, and L. M. K. Boelter, Trans. Illuminating Engineering Society, vol. 34, 1939, pp. 1085–1092.

closed pencil curve; the area of the pencil curve divided by a constant of the integrator was then taken as the shape factor of the dummy with respect to energy emitted from the point on the floor at which the integrator was then located.

Shape factors were redetermined at each station at least three times and never less than the number of times necessary to assure ability to reproduce the same result.

Experimental Results

Table 1 presents a summary of all experimental data. The maximum shape factor of the occupant with respect to a point on the floor is seen to occur when that point is 2 ft out along the line in which the occupant is facing; at this point the value of 0.0851 indicates that 8.5 per cent of the energy emitted from the infinitesimal area surrounding the point (providing this area emits diffuse radiation) will strike the occupant. The reduction in shape factor as the occupant moves closer to the point than 2 ft can be attributed to the rapid decrease in the cosine of ϕ_s. The decrease as the occupant moves farther from the point than 2 ft is primarily due to the increasing value of r_{os}, but partially to the increase in ϕ_0; these two factors far more than offset the decrease in ϕ_s.

TABLE 1 EXPERIMENTAL TEST DATA

Distance from the dummy, ft	Front view		Semiprofile view	
	Integrator reading, sq in.	Shape factor[a]	Integrator reading, sq in.	Shape factor[a]
1	5.10	0.065	4.65	0.0593
2	6.68	0.0851	5.45	0.0695
3	4.30	0.058	2.75	0.0350
4	2.42	0.0309	2.05	0.0261
5	1.54	0.0196	1.35	0.0172
6	1.20	0.0153	1.11	0.0140
7	0.82	0.01045	0.72	0.0092
8	0.50	0.00637	0.50	0.00636
9	0.46	0.00586	0.45	0.00572
10	0.40	0.00510	0.35	0.00445
11	0.29	0.00370	0.22	0.00280
12	0.27	0.00344	0.20	0.00235
13	0.25	0.00319	0.12	0.00153
14	0.25	0.00319	0.10	0.001265
15	0.22	0.00281	0.08	0.00102
16	0.15	0.00191	0.07	0.000892
17	0.08	0.00102	0.06	0.000765
18	0.06	0.000765	0.05	0.000637

---

[a] The shape factor is equal to the experimentally determined integrator area divided by the area of the base circle of the integrator; for the particular mechanical integrator used in this research the constant value of the base circle area was 78.5 sq in.

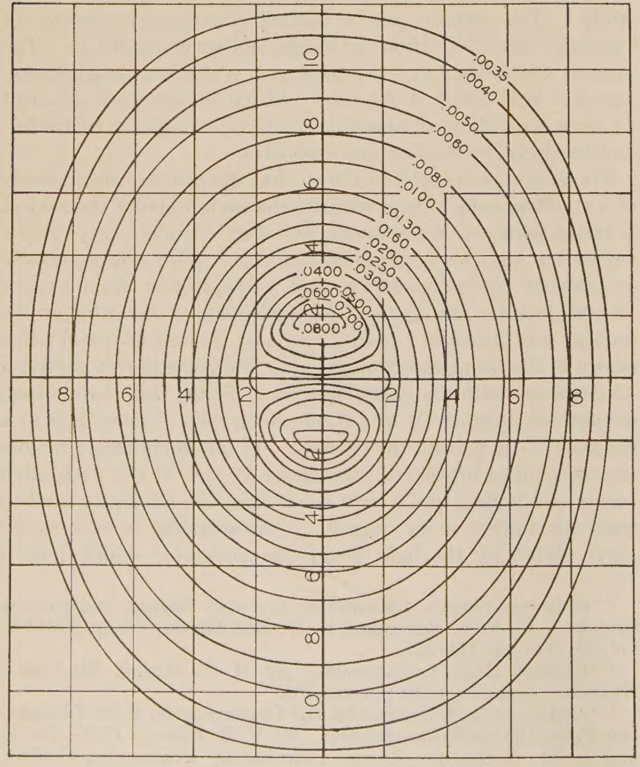

Fig. 1

The results show that floor areas more than 5 ft from the occupant emit less than 2 per cent of their energy in a direction such that it will be received by a perfectly absorbing (black body) occupant. Areas more than 7 ft away provide less than 1 per cent direct radiant transfer, whereas areas more distant than 10 ft provide less than $^1/_2$ per cent direct radiant transfer. For equal distances from the occupant, points along the semiprofile transmit 10 per cent to 15 per cent less energy to the occupant than do corresponding points (or rather infinitesimal areas) along the line corresponding to a full-face view.

Fig. 1 is a plot obtained by interpolation and extrapolation of the experimental results given in Table 1. In this figure the occupant is considered to be standing at the center of co-ordinates and facing either toward the top or the bottom (front and rear views being taken as symmetrical) of the figure. Thus the scale along the Y-axis indicates distance in feet in front of, or behind the occupant, whereas the scale along the X-axis indicates distance in feet to the right or left (again, symmetry is assumed for the full-profile views) of the occupant. Therefore the curves in Fig. 1 are iso-shape factor lines, and the number shown on each such curve is numerically equal to the fraction of energy leaving any infinitesimal floor area along that curve which would be directly absorbed by the occupant if his emissivity were unity.

For an occupant so dressed that his emissivity is less than unity, the shape factor as given would have to be multiplied by the emissivity of the occupant in order to obtain the fraction of energy that would be absorbed of that leaving the floor surface. As an example, note that from an infinitesimal floor area located 6 ft to the right and 7 ft ahead of the occupant, the shape factor would be 0.0050, hence $^1/_2$ per cent of the energy leaving such an area would be received by the (black body) occupant. Although this shape factor has been stated for an infinitesimal area, it would be equally applicable to any finite area over which the average of point shape factors had the same numerical value.

Application of Results

In practice, interest is almost wholly centered on radiant transfer between the occupant and some moderate-sized area as a window, heated panel, or an unheated but uniform surface, such as an exterior wall, floor, ceiling, or inside partition. In such cases the shape factor of the occupant with respect to energy received from the surface in question can be taken as the average (not the sum) of shape factors with respect to the small finite areas which make up the larger surface. The smaller the finite areas become the greater will be the accuracy of the averaged over-all shape factor, but the greater, too, will be the effort required to obtain an average value.

As an approximation which is adequate for usual engineering purposes, it is suggested that within a radius of 4 ft of the occupant, the unit area be taken as 1 sq ft, whereas, at greater distances, a satisfactory unit area will be one which is square and 2 ft on the side. For areas larger than 8 ft × 8 ft, with the occupant located at the center, adequate accuracy would thus be attained by dividing the inner 4-ft × 4-ft area of one quadrant into four unit areas of 1 sq ft each, and dividing any additional part of this one quadrant into 2-ft × 2-ft unit areas. Note that for a centrally located occupant, the shape factor for any one quadrant (provided the occupant is facing one of the sides) will be numerically equal to the shape factor of the occupant with respect to energy received from the entire area. For arrangements of occupant and panel which are nonsymmetrical, all unit areas of the panel must be used rather than those of a single quadrant.

Example. Consider a room 11 ft × 11 ft which is to be heated and cooled by means of a 3-ft × 3-ft floor panel which is to be centered at the center of the floor, the sides of the panel running parallel to the sides of the room. The shape factor of the occupant with respect to energy received from the panel is desired for a case in which the occupant is standing parallel with a wall at a position in the room 2 ft in from each of two walls.

Solution. Draw on tracing paper a plan of the room, with panel, to the same scale as that of Fig. 1. On this tracing divide the 3-ft × 3-ft panel into 9 equal unit areas and indicate by point O the position of the occupant on the tracing. Now superimpose the tracing on Fig. 1 (refer to Fig. 2), so that point O of the tracing is at the center of co-ordinates of Fig. 1, and the facing direction of the occupant corresponds on both tracing and on Fig. 1. It is now possible to read directly, or obtain by interpolation, the shape factor at the center of each of the 9 unit areas. Referring to Fig. 2, and reading these shape factors from left to right and from top to bottom, we obtain the over-all shape factor of the occupant with respect to energy received from the entire panel as

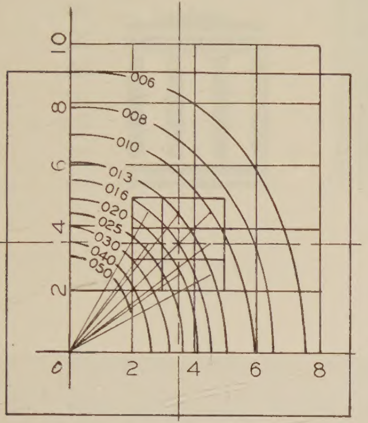

FIG. 2

$$F_{os} = (0.016 + 0.013 + 0.010 + 0.024 + 0.016 + 0.012 + 0.029 + 0.020 + 0.013)/9 = 0.017 = 1.7 \text{ per cent}$$

Thus 1.7 per cent of the energy emitted by the diffuse panel would be absorbed by an occupant at the stated position, provided his clothing was such that he possessed unit emissivity.

CONCLUSION

Results have been presented for the shape factor of an average standing person with respect to energy received from a floor area. Similar results for standing and sitting persons with respect to energy from wall and ceiling areas are already available in the literature.[2] Representations of the earlier data in a form similar to that of Fig. 1 are also available in other publications.[5] The use of shape factors of this type is needed for exact studies of stability of comfort conditions in a room that is heated or cooled by radiant or partially radiant means, or for stability studies in a convection-heated room in which single-glass or other surfaces reach equilibrium temperatures lower than the room air temperature.

---

[5] "Panel Heating and Cooling Analysis," by B. F. Raber and F. W. Hutchinson, John Wiley & Sons, Inc., New York, N. Y., 1947.